

OTIC FILE COPY

(2)

AD-A215 076

AAMRL-TR-89-027  
NMRI-89-58



**PROCEEDINGS OF THE  
17TH CONFERENCE  
ON TOXICOLOGY —  
3-5 NOVEMBER 1987**

**NSI TECHNOLOGY SERVICES CORPORATION  
101 WOODMAN DRIVE, SUITE 12  
DAYTON, OH 45431**

**DTIC  
ELECTE  
NOV 27 1989  
S B D**

**SEPTEMBER 1989**

**INTERIM REPORT FOR THE PERIOD 3-5 NOVEMBER 1987**

Approved for public release; distribution is unlimited.

**HARRY G. ARMSTRONG AEROSPACE MEDICAL RESEARCH LABORATORY  
HUMAN SYSTEMS DIVISION  
AIR FORCE SYSTEMS COMMAND  
WRIGHT-PATTERSON AIR FORCE BASE, OHIO 45433-6573**

**89 11 22 068**

## NOTICES

When U S Government drawings, specifications, or other data are used for any purpose other than a definitely related Government procurement operation, the Government thereby incurs no responsibility nor any obligation whatsoever, and the fact that the Government may have formulated, furnished, or in any way supplied the said drawings, specifications, or other data, is not to be regarded by implication or otherwise, as in any manner licensing the holder or any other person or corporation, or conveying any rights or permission to manufacture, use, or sell any patented invention that may in any way be related thereto.

Please do not request copies of this report from the Harry G. Armstrong Aerospace Medical Research Laboratory. Additional copies may be purchased from:

National Technical Information Service  
5285 Port Royal Road  
Springfield, Virginia 22161

Federal Government agencies and their contractors registered with Defense Technical Information Center should direct requests for copies of this report to:

Defense Technical Information Center  
Cameron Station  
Alexandria, Virginia 22314

## TECHNICAL REVIEW AND APPROVAL

AAMRL-TR-89-027

The experiments reported herein were conducted according to the "Guide for the Care and Use of Laboratory Animals," Institute of Laboratory Animal Resources, National Research Council.

This report has been reviewed by the Office of Public Affairs (PA) and is releasable to the National Technical Information Service (NTIS). At NTIS, it will be available to the general public, including foreign nations.

This technical report has been reviewed and is approved for publication.

FOR THE COMMANDER



MICHAEL B. BALLINGER, Lt Col, USAF, BSC  
Chief, Toxic Hazards Division  
Harry G. Armstrong Aerospace Medical Research Laboratory

UNCLASSIFIED

SECURITY CLASSIFICATION OF THIS PAGE

REPORT DOCUMENTATION PAGE				Form Approved OMB No. 0704-0188	
1a. REPORT SECURITY CLASSIFICATION UNCLASSIFIED			1b. RESTRICTIVE MARKINGS		
2a. SECURITY CLASSIFICATION AUTHORITY			3. DISTRIBUTION / AVAILABILITY OF REPORT Approved for public release; distribution is unlimited		
2b. DECLASSIFICATION / DOWNGRADING SCHEDULE					
4. PERFORMING ORGANIZATION REPORT NUMBER(S)			5. MONITORING ORGANIZATION REPORT NUMBER(S) AAMRL-TR-89-027 NMRI-89-58		
6a. NAME OF PERFORMING ORGANIZATION NSI Technology Services, Corp		6b. OFFICE SYMBOL (If applicable)	7a. NAME OF MONITORING ORGANIZATION AAMRL, Toxic Hazards Division		
6c. ADDRESS (City, State, and ZIP Code) 101 Woodman Drive, Suite 12 Dayton, OH 45431			7b. ADDRESS (City, State, and ZIP Code) HSD, AFSC Wright-Patterson AFB, Ohio 45433		
8a. NAME OF FUNDING / SPONSORING ORGANIZATION		8b. OFFICE SYMBOL (If applicable)	9. PROCUREMENT INSTRUMENT IDENTIFICATION NUMBER F33615-85-C-0532		
8c. ADDRESS (City, State, and ZIP Code)			10. SOURCE OF FUNDING NUMBERS		
			PROGRAM ELEMENT NO 62202F	PROJECT NO 6302	TASK NO 00
					WORK UNIT ACCESSION NO. 01
11. TITLE (Include Security Classification) Proceedings of the 17th Conference on Toxicology, 3, 4, 5 November 1987					
12. PERSONAL AUTHOR(S)					
13a. TYPE OF REPORT Conference Proceedings		13b. TIME COVERED FROM Nov87 TO Nov87		14. DATE OF REPORT (Year, Month, Day) September 1989	
				15. PAGE COUNT 422	
16. SUPPLEMENTARY NOTATION					
17. COSATI CODES			18. SUBJECT TERMS (Continue on reverse if necessary and identify by block number)		
FIELD	GROUP	SUB-GROUP			
06	01		acetone biological models		
06	11		acetylcholinesterase inhibition cancer		
			behavior cancer modeling		
19. ABSTRACT (Continue on reverse if necessary and identify by block number)					
<p>This series of manuscripts from the 17th Conference on Toxicology addresses critical research and development issues for quantitatively assessing the health risks associated with various occupational and environmental exposures. To meet the needs of the Department of Defense, these contributions focus on the current knowledge of quantitative methods in toxicology especially as applied to military systems or military operations. These manuscripts present state-of-the-art methodologies that will improve our ability to develop objective indices of toxicity keeping in mind that the ultimate purpose is to predict expected human toxicity.</p>					
20. DISTRIBUTION / AVAILABILITY OF ABSTRACT <input checked="" type="checkbox"/> UNCLASSIFIED/UNLIMITED <input type="checkbox"/> SAME AS RPT <input type="checkbox"/> DTIC USERS			21. ABSTRACT SECURITY CLASSIFICATION		
22a. NAME OF RESPONSIBLE INDIVIDUAL Michael B. Ballinger, Lt Col, USAF, BSC			22b. TELEPHONE (Include Area Code) (513) 255-3916		22c. OFFICE SYMBOL AAMRL/TH

18. Subject Terms Continued...

carcinogenesis  
cis-Diamminedichloroplatinum(II) (DDP)  
cisplatin  
computer-assisted toxicity prediction  
computer models  
computer simulation  
dibenzo-p-dioxins  
diurnal rhythms  
ethanol  
extrapolation modeling  
flow cytometry  
forced-choice paradigm  
halogenated epoxides  
halogenated olefins  
hematopoietic stem cells  
initiation  
intermittent schedules of reinforcement  
lactation  
methyl ethyl ketone  
methylene chloride  
motor function  
multistage models  
neurobehavioral testing  
neurotoxicology  
nickel  
operant conditioning  
oxotremorine  
pattern recognition  
percutaneous absorption  
pharmacodynamic model  
physiologically-based pharmacokinetics  
promotion  
propylene glycol dinitrate  
psychophysics  
quantitative structure-activity relations  
quantitative structure-property relations  
radiation  
rating paradigm  
response paradigm  
risk assessment  
saccharin  
tremor  
tributyltin  
yes-no paradigm

## PREFACE

The 17th Conference on Toxicology was held in Dayton, Ohio, on 3-5 November 1987. The conference was sponsored by Northrop Services, Inc. - Environmental Sciences (NSI-ES), under the terms of Contract No. F33615-85-C-0532 with the Harry G. Armstrong Aerospace Medical Research Laboratory (AAMRL) Human Systems Division, Air Force Systems Command, Wright-Patterson Air Force Base, Ohio; and the Naval Medical Research Institute Toxicology Detachment (NMRI/TD), Wright-Patterson Air Force Base, Ohio.

Dr. Melvin E. Andersen, Toxic Hazards Division, AAMRL, served as Conference Chairman, and Deborah Ussery-Baumrucker, NSI-ES, was Conference Coordinator. Lois Doncaster, NSI-ES-THRU, provided administrative support in Dayton.

<b>Accession For</b>	
NTIS GRA&I	<input checked="checked" type="checkbox"/>
DTIC TAB	<input type="checkbox"/>
Unannounced	<input type="checkbox"/>
Justification	
By _____	
Distribution/	
Availability Codes	
Dist	Avail and/or Special
A-1	

## TABLE OF CONTENTS

	PAGE
OPENING REMARKS ..... Colonel Charles P. Hatsell	5
WELCOME ADDRESS ..... Major General Fredric F. Doppelt	6
INTRODUCTORY ADDRESS ..... Dr. Melvin E. Andersen	9
SESSION I – OCCUPATIONAL TOXICOLOGY ..... Colonel Bruce J. Poitras	13
COMPUTER-BASED NEUROBEHAVIORAL EVALUATION SYSTEM FOR OCCUPATIONAL AND ENVIRONMENTAL EPIDEMIOLOGY ..... Dr. Richard E. Letz	14
ASPECTS OF BIOLOGICAL MONITORING OF EXPOSURE TO GLYCOL ETHERS ..... Dr. Gunnar Johanson	15
AN INHALATION DISTRIBUTION MODEL FOR THE LACTATING MOTHER AND NURSING CHILD ..... Major Michael L. Shelley	32
EFFECTS OF SHORT DURATION EXPOSURES TO ACETONE AND METHYL ETHYL KETONE ..... Dr. Robert B. Dick	40
A REVIEW OF PROPYLENE GLYCOL DINITRATE TOXICOLOGY AND EPIDEMIOLOGY ... Dr. Samuel A. Forman	60
SESSION II – PHARMACOKINETICS AND EXPERIMENTAL DESIGN ..... Dr. Daniel B. Menzel	75
PLANNING AND USING PB-PK MODELS: AN INTEGRATED INHALATION AND DISTRIBUTION MODEL FOR NICKEL ..... Dr. Daniel B. Menzel	76
A PHYSIOLOGICALLY BASED MODEL OF SKELETAL GROWTH IN THE RAT ..... Dr. Ellen J. O'Flaherty	94

# TABLE OF CONTENTS (Continued)

	PAGE
INCORPORATION OF <i>IN VITRO</i> ENZYME DATA INTO THE PB-PK MODEL FOR METHYLENE CHLORIDE: IMPLICATIONS FOR RISK ASSESSMENT .....	106
Dr. Richard H. Reitz	
RESEARCH NEEDS AND ADVANCES IN INHALATION DOSIMETRY IDENTIFIED THROUGH THE USE OF MATHEMATICAL DOSIMETRY MODELS OF OZONE .....	126
Dr. Frederick J. Miller	
CISPLATIN PHARMACOKINETICS: APPLICATIONS OF A PHYSIOLOGICAL MODEL .....	143
Dr. Fred F. Farris	
SESSION III - BIOEFFECTS MODELING .....	166
Dr. Rory B. Conolly	
BIOLOGICALLY MOTIVATED TWO-STAGE MODEL FOR CANCER RISK ASSESSMENT ...	167
Dr. Suresh H. Moolgavkar	
CELL GROWTH DYNAMICS IN LONG-TERM BLADDER CARCINOGENESIS .....	180
Dr. Samuel M. Cohen	
MODELING OF RECEPTOR-MEDIATED PHARMACODYNAMICS OF PREDNISONE IN THE RAT .....	204
Dr. William J. Jusko	
A PHARMACODYNAMIC MODEL FOR SOMAN IN THE RAT .....	205
Mr. Donald M. Maxwell	
PHARMACOKINETICS, BIOCHEMICAL MECHANISM AND MUTATION ACCUMULATION: A COMPREHENSIVE MODEL OF CHEMICAL CARCINOGENESIS .....	220
Dr. Rory B. Conolly	
SESSION IV - EMERGING TECHNIQUES .....	232
Major Michael J. Parnell	
FLOW CYTOMETRIC ANALYSIS OF THE CELLULAR TOXICITY OF TRIBUTYL TIN .....	233
Dr. Robert M. Zucker	

## TABLE OF CONTENTS (Continued)

	PAGE
FLOW CYTOMETRY TECHNIQUES IN RADIATION BIOLOGY .....	252
Dr. Kenneth F. McCarthy	
MODELING THE TISSUE SOLUBILITIES AND METABOLIC RATE CONSTANT OF HALOGENATED METHANES, ETHANES, AND ETHYLENES .....	267
Mr. Michael L. Gargas	
COMPUTATIONAL APPROACHES TO THE IDENTIFICATION OF SUSPECT TOXIC MOLECULES .....	293
Dr. Peter Politzer	
QSAR APPROACHES TO PREDICTING TOXICITY .....	315
Dr. William J. Dunn, III	
SESSION V - QUANTITATIVE METHODS FOR BEHAVIORAL TOXICOLOGY .....	323
Major James R. Cooper	
QUANTITATIVE PERSPECTIVES ON BEHAVIORAL TOXICOLOGY .....	324
Dr. Bernard Weiss	
QUANTIFICATION OF MOTOR FUNCTION IN TOXICOLOGY .....	333
Dr. M. Christopher Newland	
QUANTITATIVE SENSORY ASSESSMENT IN TOXICOLOGY AND OCCUPATIONAL MEDICINE: APPLICATIONS, THEORY, AND CRITICAL APPRAISAL .....	359
Dr. Jacques P.J. Maurissen	
QUANTITATION OF NATURALISTIC BEHAVIORS .....	385
Dr. Hugh L. Evans	
QUANTIFICATION OF OPERANT BEHAVIOR .....	400
Dr. Deborah C. Rice	
CLOSING REMARKS .....	418
Dr. Melvin E. Andersen	

## OPENING REMARKS

Colonel Charles P. Hatsell, USAF, MC

Commander, H.G. Armstrong Aerospace Medical Research Laboratory

Wright-Patterson Air Force Base, Ohio

General Doppelt, our guests, welcome to Dayton, OH. Welcome to the 17th Annual Conference on Toxicology. As you know, it is jointly sponsored by AAMRL and NMRI. I am not going to say too much more except to tell you a little about AAMRL. As you know, toxicology is one of our three missions areas; the other two are biodynamics and human engineering.

The research at Wright-Patterson Air Force Base mainly falls under the Aeronautical Systems Division. We are under the Human Systems Division (HSD), headquartered at Brooks Air Force Base, and it is important to keep that in mind. We deal with the human aspects of the man and the machine along with our sister organizations headquartered at Brooks Air Force Base.

HSD is commanded by Major General Fredric F. Doppelt. He has been with the research and development side of the Air Force for some time. I believe I met him first in the late '70s, and he brings to HSD quite a diverse background, including having been a past commander of AAMRL. He is a physical phenomenologist and a flight surgeon. I would now like to introduce General Doppelt who will tell us more about the Human Systems Division and why it exists.

## WELCOME ADDRESS

Major General Fredric F. Doppelt, USAF, MC

Commander, Human Systems Division

Brooks Air Force Base, Texas

Good morning, Ladies and Gentlemen. I am pleased once again to have the opportunity of welcoming you to the annual Conference on Toxicology on behalf of the Air Force and our newly reorganized Human Systems Division (HSD).

Because of the rapidly changing technological world in which we live, it is important to understand the need for proper management of hazardous materials during weapon systems development and acquisition.

Such an understanding is paramount to protect and defend our way of life. We in the Human Systems Division are the advocates for the man-machine interface in the Air Force. The Human Systems Division has five laboratories – USAFSAM, AFHRL, AFOEHL, AAMRL, and AFDTL. Each laboratory has a key role in the acquisition process as we head into the 21st century. Our host today, the Harry G. Armstrong Aerospace Medical Research Laboratory, with our sister service, the Naval Medical Research Institute, are keenly aware of toxicology's role in the assessment of toxic hazards to the man-machine interface. Four components of the HSD organization share equal roles in facing the challenges that toxic materials management has levied.

Today's conference focuses on the role of quantitative toxicology in assessing toxic risk. This conference is emphasizing the "quantitative structure-activity relationship" of chemicals and compounds.

Our focus is on the military environment. Into this environment we introduce the concept of "modeling," which uses existing knowledge to make risk assessments of new chemical compounds and materials before they are utilized in future weapon systems. I urge you, as toxicologists, to consider the benefits of developing expanded models to allow those tasked with weapon systems acquisition greater confidence to make selection decisions. This is especially critical in the initial phases of weapon system acquisition and in the management of hazardous waste by-products.

In acquisition, the decision-making process involves a series of trade-offs. We do not always gain clear, positive, acceptable, and risk-free benefits. If we rush into development of weapon systems on the basis of technology alone, we may be disregarding the lessons of history. As recently as WWII, the nations at war rushed headlong to gain technological superiority. We produced many

new compounds and materials that now, four decades later, reside in potentially hazardous dumpsites throughout the country. Hazardous waste management as just described is the worst possible scenario. We simply cannot repeat this mistake! I challenge you today to get involved and help prevent events like this from ever occurring again. At the very outset of weapon systems development, we must have the expertise in place to assess the toxicity or potential toxicity of materials being considered in weapon systems. With adequate knowledge and forethought, we can make intelligent choices. Given product A and product B, we can choose the more efficacious. Let's consider A as the more toxic but, at the same time, the more desirable in terms of shelf life, producibility, reliability, maintainability, and operability. We can choose product A over the less toxic product B based on knowledge gained through research and modeling. We have gained by the use of models a technological edge and have curtailed the risk associated with product A. We must design our management system to allow for the safe incorporation of hazardous materials to be incorporated safely into the life cycle cost model of products under consideration for future weapon systems and acquisition. In the final analysis we gain both superiority and the technological edge by being highly selective in our use of compounds and materials in weapons acquisition. We are not restricted to the total consideration of a substance's toxicity - we can manage it, preventing its deleterious effects. Through hazardous waste management we can prevent, neutralize, or contain the potential hazardous risk of a product or its by-products, giving us informed choices. By this process we can best use our limited resources. We can consider alternative resources of a toxic nature should our present supply be curtailed through confrontation or conflict.

Performing animal study assessments on the expanding inventory of products being produced today is neither feasible nor practical. As you may be aware, animal studies tend to be qualitative in nature. They are observational and difficult to assess. This is one of the reasons you have gathered this week to explore more the quantitative aspects of your discipline. In the week ahead you will discuss computer modeling to extrapolate the hazards of analogs in cases where it is neither feasible nor economical to use the animal model.

In the Air Force's bold venture known as Forecast-II, we are designing and beginning to implement systems that will be commonplace in the year 2000. Many of the propellants and materials of this venture are starting to arrive in our inventory today. As these new substances arrive, they will require scientists and engineers to be fully knowledgeable in the associated health effects and potential risks associated with the use of these materials. It is imperative that hazardous material management be at the front end of weapon systems development and acquisition. This will insure the integration of existing knowledge on the toxicity and risk of these materials. This nation's survival may be determined by the knowledge and expertise shared in meetings like this one today. My closing points are to emphasize once more a new direction in our thinking.

- To think about the total picture more – to see the forest and not just its individual trees;
- To design into our research the concept of hazardous materials and waste management;
- To think of new and innovative ways of analyzing toxic hazards by models and expanding these models to include life cycle cost of the material or substance being studied;
- To realize that the more we know about a substance, the more latitude it gives the military in using it should the need arise, despite its toxic nature.

With the knowledge gained today, we do much toward rendering our environment a pollution-free zone. Systems and materials can be used that would have never gotten off the drawing board for their potentially hazardous nature, because we will know how to manage the risk associated with their use.

## Introductory Address

Dr. Melvin E. Andersen

H.G. Armstrong Aerospace  
Medical Research Laboratory  
Toxic Hazards Division  
Wright-Patterson Air Force Base, Ohio

Conference Chairman

Thank you very much, General Doppelt, for that accurate accounting of the goals of our conference.

The USAF toxicology program at the Toxic Hazards Division is really not unlike many large-scale occupational toxicology programs in the United States. It was developed some 25 years ago, and much of the efforts in the early years was put into the development of facilities to do toxicology testing. In our case, we built an exquisite set of large, 28 m<sup>3</sup> inhalation exposure chambers called Thomas Domes. They were designed, fabricated, and installed, and we learned how to operate them. What we had then was a very good system to discover what chemicals do to test animals. One of the difficulties, of course, was that we wanted to know what these chemicals might do to human beings. We could intoxicate animals by a variety of routes of exposure with a whole variety of chemicals, but still not really know what to expect if human beings were exposed. This deficiency was recognized in most toxicology laboratories early on and efforts were made to become more thoughtful about what approaches we could use to more accurately predict human response based on animal experiments.

Long before I arrived in Dayton there were efforts being made to answer these questions about what toxicity findings in animals might mean for exposed humans. These efforts started in a program that was developed to look at chemical disposition (i.e., pharmacokinetics); a program whose first champions were Dr. Ken Back, Dr. Vern Carter, and Ms. Marilyn George. This program focused on the issue of how quantitative information on chemical disposition would be used to better understand chemical toxicity in exposed people.

This early work was directed toward understanding how chemical disposition changed with concentration or with dose route, always being careful that the experiments in the laboratory were not done under totally unrealistic exposure conditions. On a local level, this initiative reflected the development of a quantitative consciousness that was pervading the toxicology testing community as a whole in the late 1970s. Since then, there has been a rather natural evolution of this concept of quantitative toxicology, and as with an evolutionary process of any type, there has also been a continuing redefinition of quantitative toxicology.

The first major aspect of quantitative toxicology is related to chemical disposition in the body; i.e., to pharmacokinetics. You need to know how much active chemical reaches target tissues. For extrapolation, you also need to know how a chemical causes an effect and whether the mechanisms are likely to be the same in human tissues. The advantage of defining dose with a quantitative approach to chemical disposition is that it allows you to extrapolate beyond the experimental conditions and predict tissue dose for other exposure scenarios or in other species.

Even when you know everything about chemical disposition, you still need to know how that chemical causes an effect in a particular tissue. That is the area of bioeffects modeling. We are going to discuss chemical disposition this afternoon in a session on pharmacokinetics and experimental design. Tomorrow morning we have a session on pharmacodynamics – the modeling of the effects of chemicals on biological systems. The emphasis in pharmacodynamics is in how the chemical's presence produces changes in the system that ultimately result in toxicity. This area is called pharmacodynamics (PD) and is less well developed compared to the disposition (pharmacokinetic) studies, probably because it is a more difficult area. PD models require increased sophistication in our understanding of basic biological processes. That understanding is coming about now, and we can start to make tentative descriptions of how the presence of chemicals in tissues causes particular effects.

This work in biodisposition and in pharmacodynamic modeling relies heavily on computers. We have a poster for this conference. It emphasizes the fact that the ability to handle data in a quantitative way, whether it is biodisposition data or pharmacodynamics effect data, is changing the way we conduct the business of toxicology. As part of the conference, we have a computer demonstration scheduled where five scientists will present aspects of computer modeling in toxicology. The same individuals will be here tomorrow evening during a poster session, and there will be a chance to talk to them at some length about their work.

General Doppelt talked about the problem of the long lead time required to do comprehensive toxicology testing. He mentioned the large-scale animal studies, detailed pathological observations, accumulation of data, statistical analysis, and then the collation of the entire report. This type of work will always be with us and will always be necessary; the question is the scale to which it will be necessary. Many of us who work in quantitative toxicology hope the development of computational-based methods will make the job of designing experiments easier, will help us design better experiments, and will make the job of interpreting these experiments for their human relevance more straightforward. These improvements would reduce the number of required experiments and reduce the numbers of animals involved. We could then predict outcomes of experiments so the process of experimental design, toxicity testing, and retesting can be streamlined. Other approaches

also hold promise for more rapid accumulation of information on potential toxic effects of new chemicals.

One area of investigation that is discussed in this conference is quantitative structure-activity modeling. In this area it is hoped that studying many different chemicals will allow us to make some predictions of the toxicity of untested chemicals based on chemical structures or other physical chemical properties of tested materials. In this area we have a session on quantitative structure - activity relationship, which also is a new field where many different methods are being examined to predict the likely outcome of toxicity tests.

There is yet another aspect of quantitation that I do not want to leave out. That is, how can we reliably collect data in a quantitative way? Our last session is a discussion of quantitative techniques in behavioral toxicology, a field that we tend to think of as being very subjective. To make decisions on priority for testing and classifying materials in terms of potency, we have to develop ways to quantify various types of toxicity in all fields of toxicology.

To return to the beginning, the first session today is on occupational toxicology. Occupational toxicology, as you heard from General Doppelt, is really our primary function here in Dayton. Our job is to make sure that chemicals are not going to have adverse effects on Air Force work populations or, in some cases, non-Air Force populations that may come in contact with chemicals used in Air Force operations. We have to remember that these human populations are our ultimate interest.

I told you that we are doing quantitative toxicology because we need to have ways to predict beyond the experiments in the laboratory to suggest what might happen to humans. In some cases, we know what happens in humans. We have access to information from occupational environments or information from controlled human exposure conditions. These results can be used to estimate the likelihood of toxicity in inadvertently exposed humans. The topic of our first session is Occupational Toxicology where human experience with chemicals is discussed directly.

My last remarks are in the form of a story. My apologies to those of you in the audience who may have heard me tell this story before. This is a story of asking questions and of doing scientific research. The story goes something like this. There was a toxicology meeting held in Dayton. One afternoon, the conference participants were allowed the afternoon off to do as they pleased. So they got together in little cliques. Our audience here has different groups represented. We have friends from industrial toxicology laboratories, co-workers in other Department of Defense laboratories, and representatives from academic institutions throughout the country. I urge you to co-mingle, but I recognize the need for all human communities to form cliques, and this is what happened at the toxicology meeting. One group, in this case the academic toxicologists, decided they would go on a picnic in a nice, broad, grassy field. Another group, the regulatory toxicologists, decided that they

would go out and rent hot air balloons for the day. Everyone went off and was having a good time. Before long, though, the regulatory toxicologists were lost. (This is not a parable, it is a story.) As they were floating along, they saw the picnickers and decided to call out to get some help. They called out to the academic group on the ground saying, "Hello, can you tell us where we are?" The group of academicians on the ground got together to hold a committee meeting, and they appointed a spokesman. The spokesman called out (actually the balloons were almost out of sight by then), "Yes, you are 35 feet above the ground in a hot air balloon." The regulatory toxicologists in the balloon looked around disgustedly and said, "It is just like those academic toxicologists: The information is absolutely correct, late, and entirely useless." The people on the ground heard that. One turned to another and said, "Well, if that is not the answer they wanted, why did they ask that question?"

One of the important aspects of doing modeling of any kind, quantitative modeling to describe pharmacokinetics or to describe pharmacodynamics, is to improve our ability to develop objective indices of toxicity and to ask better questions, the right questions. We need to pursue experimental data not for its own sake but because it has value in some larger perspective. We have to always keep in mind that our ultimate purpose is not to study animal toxicity but to predict expected human toxicity based on results in test animals or on limited observations in exposed human populations. With these remarks we will now begin our first session on Occupational Toxicology.

**SESSION I**

**OCCUPATIONAL TOXICOLOGY**

**Colonel Bruce J. Poitrast, Chairman**

**COMPUTER-BASED NEUROBEHAVIORAL EVALUATION SYSTEM FOR OCCUPATIONAL AND  
ENVIRONMENTAL EPIDEMIOLOGY**

**Richard E. Letz**

**The Mount Sinai Medical Center**

**New York, NY**

**Manuscript Not Submitted**

## ASPECTS OF BIOLOGICAL MONITORING OF EXPOSURE TO GLYCOL ETHERS

Gunnar Johanson

*National Institute of Occupational Health, S-171 84 Solna, Sweden*

### ABSTRACT

Glycol ethers are frequently used as solvents, detergents, and emulsifiers alone or as components in industrial and consumer products. The monomethyl and monoethyl ethers of ethylene glycol, and their acetate esters, are teratogenic and embryotoxic and cause testicular damage in laboratory animals, while the monobutyl ether causes hemolysis of the red blood cells. The adverse effects are attributed to the acid metabolites methoxy-, ethoxy- and butoxyacetic acid, respectively. The glycol ethers may readily enter the body by inhalation as well as dermal uptake. Biological monitoring of exposure to glycol ethers has therefore been suggested. This presentation reviews physical properties, occurrence, analysis, toxicity, and toxicokinetics of the most common glycol ethers and then discusses toxicokinetic aspects of biological monitoring. The effect of physical exercise and the relative importance of respiratory and percutaneous absorption of the internal exposure to glycol ethers are illustrated. Monitoring the acid metabolite in urine is suggested as the best index of exposure. Intra- and inter-individual variability, dose dependent toxicokinetics, and metabolic induction and inhibition are examples of possible sources of error in the estimation of internal exposure from the urinary excretion of acid metabolite.

### INTRODUCTION

Glycol ethers are used in industry and in consumer products for a wide variety of purposes. They are often used as solvents for cellulose esters, dyes, resins, lacquers, varnishes, and stains. They also are present in varnish removers, cleaning solutions, products for treatment of leathers and textiles and in jet fuel as a deicing additive. The favorable solvent properties and evaporation rates of the glycol ethers make them very useful for coating purposes. In particular, EGEAc and EGEE (see Table 1 for abbreviations) are often used as solvents in paints and lacquers used, for example, in car painting, silk screen printing, and leather manufacturing. Other glycol ethers such as EGBE, PGME, and diEGBE are often present as minor components in water-based paints, glues, and cleansing agents. In many of the products containing glycol ethers, toluene, xylene, ethanol, propanol, or butanol also are present [1].

The glycol ethers are colorless liquids with slight odor. They are completely miscible with water and have high solvent activities. The vapor pressures and evaporation rates are generally low and decrease with increasing length of the alkyl chain. In accordance with the high water solubility and low vapor pressure, the liquid/air partition coefficients of the glycol ethers are extremely high. Some physico-chemical properties are listed in Table 2.

TABLE 1. SYNONYMS AND ABBREVIATIONS OF GLYCOL ETHERS AND METABOLITES APPEARING IN THIS PAPER

Ethers	Abbreviations	Synonyms
Ethylene glycol monomethyl ether	EGME	2-Methoxyethanol
Ethylene glycol monomethyl acetate	EGMAc	2-Methoxyethyl acetate
Ethylene glycol monoethyl ether	EGEE	2-Ethoxyethanol
Ethylene glycol monoethyl ether acetate	EGEA <sub>c</sub>	2-Ethoxyethyl acetate
Ethylene glycol monoisopropyl ether	EGPE	2-Isopropoxyethanol
Ethylene glycol monoisopropyl ether acetate	EGPA <sub>c</sub>	2-Isopropoxyethyl acetate
Ethylene glycol monobutyl ether	EGBE	2-Butoxyethanol
Ethylene glycol monobutyl ether acetate	EGBA <sub>c</sub>	2-Butoxyethyl acetate
Propylene glycol monomethyl ether	PGME	1-Methoxy-2-propanol
Diethylene glycol monoethyl ether	diEGEE	2-(2-Ethoxyethoxy)ethanol
Dipropylene glycol monomethyl ether	diPGME	1-(2-Methoxy-2-methylethoxy)-2-propanol
<i>metabolites</i>	MAA	Methoxyacetic acid
	EAA	Ethoxyacetic acid
	PAA	Isopropoxyacetic acid
	BAA	Butoxyacetic acid

TABLE 2. PHYSICAL AND CHEMICAL PROPERTIES OF SOME GLYCOL ETHERS

Properties	EGME	EGMA <sub>c</sub>	EGEE	EGEA <sub>c</sub>	EGBE	EGBA <sub>c</sub>	PGME
Molecular weight	76	118	90	132	118	160	90
Boiling point (°C) [7]	124	137-152	135	145-165	171	186-194	120
Relative evaporation rate ( <i>n</i> -butyl acetate = 1) [42]	0.5	0.3	0.3	0.2	0.07	—	0.7
Level in saturated air (%) (25°C) [7]	1.28	0.31-0.60	0.76	0.21-0.27	0.093	—	1.55
Conversion factor (ppm - mg/m <sup>3</sup> ) (25°C, 101.3 kPa) [7]	3.11	4.83	3.68	5.40	4.83	6.54	3.68
Water/air partition coefficient [38]	35869	—	23069	3822	7051	—	12280
Oil/air partition coefficient [38]	529	—	962	4860	5446	—	696

The acute toxicity of the glycol ethers is low. Regarding subacute effects, however, several studies have shown that EGME, EGMAc, EGEE, and EGEAc are embryotoxic and teratogenic and cause testicular damage in laboratory animals. The reproductive effects were observed at exposure levels close to former threshold limit values (TLV). These observations have urged the American Conference of Governmental Industrial Hygienists (ACGIH) and legislating authorities in various countries to adopt lower exposure limits (Table 3). EGBE and EGBAc show no reproductive toxicity, the critical effect probably being hemolysis of red blood cells. All the ethylene glycol ethers disturb the hemopoiesis and the blood picture at low doses. The adverse effects have been attributed to the corresponding acid metabolites (MAA, EAA, and BAA) [2-5].

TABLE 3. ADOPTED HYGIENIC EXPOSURE LIMITS TO THE GLYCOL ETHERS IN PPM  
(TIME-WEIGHTED AVERAGES)

	EGME	EGMAc	EGEE	EGEAc	EGPE	EGBE	EGBAc	PGME	diPGME
USA, ACGIH [43]	5	5	5	5	25	25	25	100	-
West Germany, MAK [44]	5	5	20	20	-	20	20	100	100
Sweden [45]	10	10	20	20	-	20	-	-	-

There are few reports in the literature on workplace levels of glycol ethers. In a recent survey [6], ethylene glycol ethers were detected in 10% of 2654 air samples collected from various establishments in northern Belgium. Most exposure levels were below the TLVs (Figure 1). However, a great variability was noted even within the same establishment, and occasionally very high levels were recorded. The highest values measured were 330 ppm, 150 ppm, and 370 ppm for EGEE, EGEAc, and EGBE, respectively. The glycol ethers were frequently present in air samples from printing, painting, and car repair installations. Other solvents were present in almost all samples. The findings frequently included aromatic, 6-9 carbon aliphatic and cyclic hydrocarbons, alcohols, ketones, and esters. Similar results were obtained in a survey performed by OSHA in the United States [2]. The occurrence in industrial and consumers products in Sweden [1] is also in agreement with these surveys.

In the following sections, toxicokinetics, analysis, and biomonitoring of glycol ethers are discussed. Main attention is paid to the ethylene glycol ethers EGME, EGMAc, EGEE, EGEAc, and EGBE. These belong to the most widely used glycol ethers and probably present the major health hazards in this group of solvents. The propylene glycol ether PGME is included for comparison. PGME has been proposed as a substitute for some of the ethylene glycol ethers.

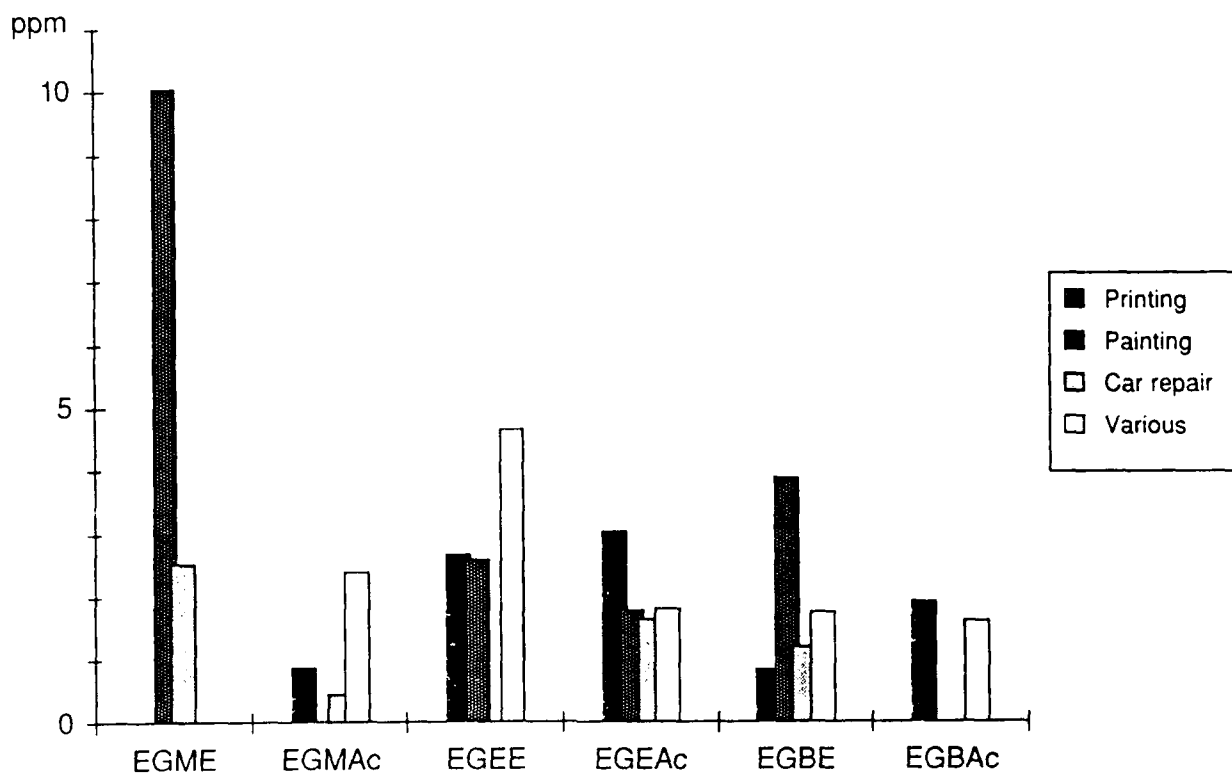


Figure 1. Average levels (geometric mean) of ethylene glycol ethers in the air, measured in industrial establishments in northern Belgium 1983-1985. The graph is based on data from Veulemans et al. [5].

#### TOXICOKINETICS AND METABOLISM

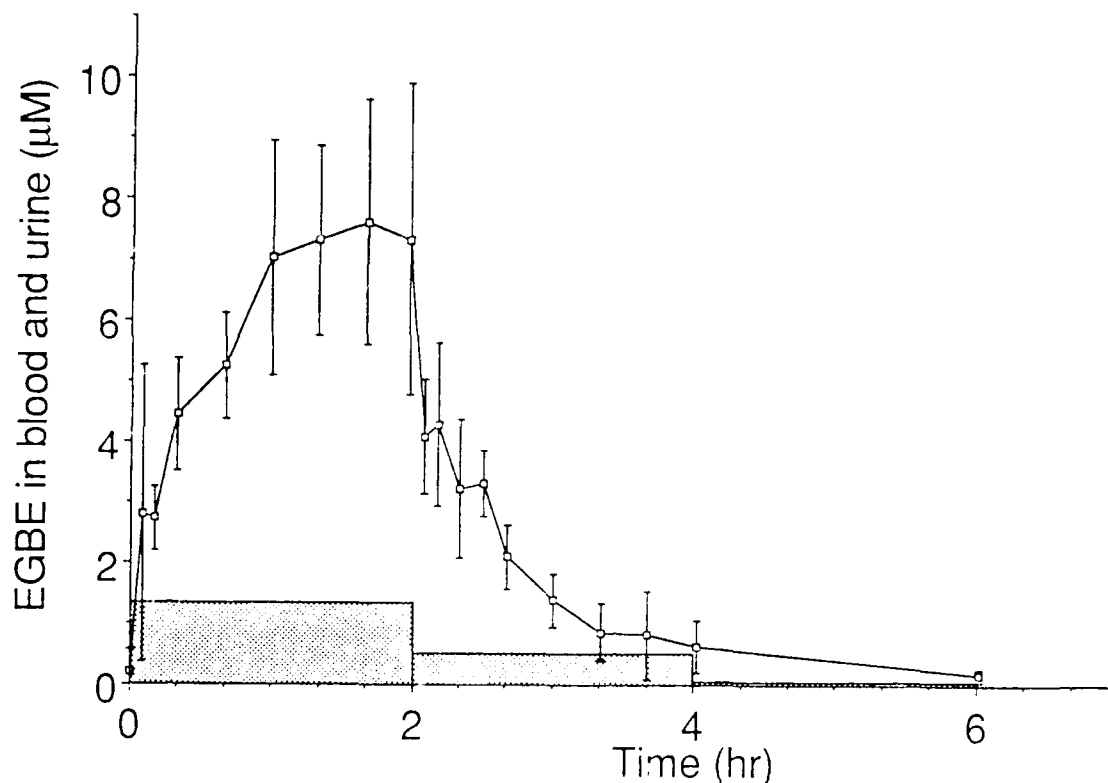
The glycol ethers are available for systemic uptake by all routes of exposure. Gastrointestinal uptake is evidenced in animals by toxic effects and urinary metabolites recorded after oral administration, and in man by toxic or even fatal effects after ingestion [2,3,4,7,8]. After oral intake of diEGEE, 68% of the dose was recovered as the acid metabolite in urine [9]. In the absence of additional human data a high oral availability of the glycol ethers must be assumed.

Uptake of glycol ethers via the respiratory route has been measured both in man and in animal. The relative respiratory uptake of EGEE, EGEAc, and EGBE ranged from 53 to 64% in man [10-12]. Similar results were obtained with EGEAc and EGPAc in beagle dogs [13].

Dermal uptake of glycol ethers has been manifested as toxic effects in animals as well as in man [2,3,4,7]. Absorption of EGBE has been demonstrated *in vitro* with human, mini pig, and rat skin [14,15] and *in vivo* in man and guinea pig [16-18]. The uptake of EGBE was enhanced when the glycol ether was presented in water solution [18]. The permeability of isolated human epidermis to glycol ethers increased in the order EGBE, EGEE, PGME, and EGME [15]. Dermal uptake rates of EGEAc and EGPAc have been determined *in vivo* in beagle dogs [13].

Only EGBE has been detected in human blood at occupationally relevant doses. The concentration of EGBE in blood measured during inhalation exposure at the TLV (Figure 2) or dermal exposure of four fingers to neat solvent was in the low micromolar range [12,17]. The low apparent

volume of distribution (70% of bw), short blood half-life (40 min) and high apparent blood clearance (1.2 L/min) suggest that EGBE is not accumulated in man.



**Figure 2.** Average concentrations of EGBE in the blood (squares) and urine (shaded) from seven men during and after a 2-h exposure to EGBE at 20 ppm. The men performed light work (50 W) during the exposure. The vertical bars indicate one standard deviation. Redrawn from Johanson et al. [12].

A half-life of 2.4 h and a blood clearance of 3.1 mL/min/kg bw were observed in rats exposed to PGME at 300 ppm for 6 h [10]. At higher exposure levels the half-life of PGME was prolonged and the clearance reduced, indicating saturation kinetics.

Exhalation accounted for less than 0.4% of the body uptake after exposure to EGEE [10]. Similar results were obtained with EGEAc [11]. The low percentage is in accordance with a very rapid post-exposure decline in the concentration of EGEE and EGEAc in expired breath. A rapid post-exposure decay in exhaled air also was noted in men after exposure to PGME [20]. The rapid decay probably reflects washout from the respiratory epithelium, while the contribution of glycol ether from the systemic circulation should be minimal considering the extremely high blood/air partition coefficients (Table 2).

The unmetabolized glycol ether appears to be excreted in urine to a very limited degree. In men exposed to EGBE at 20 ppm for 2 h, the average half-life of EGBE in urine was 1.4 h and the urinary recovery less than 0.03% of the uptake [12]. No parent compound was detected in animal experiments even after high doses of EGME, EGEE, or EGPE [21-23]. Following an oral dose of  $^{14}\text{C}$ -PGME to rats, 1-2% was excreted as unchanged PGME in urine [23].

The glycol ether acetate esters (EGMAc, EGEEAc, etc.) are rapidly converted to the corresponding glycol ethers (EGME, EGEE) by esterases present in the nasal mucosa, liver, kidneys, lungs, and blood [24]. Hence, exposure to the acetate ester should be expected to mimic exposure to the corresponding glycol ether regarding toxic effects as well as metabolite pattern.

A major metabolic pathway of the ethylene glycol ethers is oxidation of the hydroxy group yielding the corresponding alkoxyacetic acid. BAA was found in blood from rats after dermal application of EGBE [14], and MAA in maternal plasma and embryo homogenate after a high intraperitoneal dose of EGME [25]. In addition, MAA, EAA, PAA, and BAA have all been found in urine from experimental animals or humans exposed to the corresponding glycol ether or glycol ether acetate [12,17,22,23,26-31]. The possible acid metabolite of diEGEE, 2-(2-ethoxyethoxy)acetic acid, was found in urine samples from several patients, the source of exposure being unknown [9].

In men exposed to 20-ppm EGBE for 2 h, 17-55% of the estimated inhaled dose was excreted as BAA within 24 h (Figure 3). The excretion rate increased for 5 h and then declined with a half-life of 4 h (Figure 4) [12]. Men exposed to 5-ppm EGEE or EGEEAc for 4 h excreted  $23 \pm 6\%$  or  $22 \pm 1\%$  (mean  $\pm$  S.D.) of the inhaled dose as EAA within 42 h. A maximum in the excretion rate was reached 3-4 h after the end of the exposure. The estimated half-life of the excretion rate was 21-24 h [27,28]. In a field study with women occupationally exposed to EGEE and EGEEAc (6 h/d, 5 days/week), the half-life of the urinary excretion rate of EAA was estimated to 1-2 days [31].

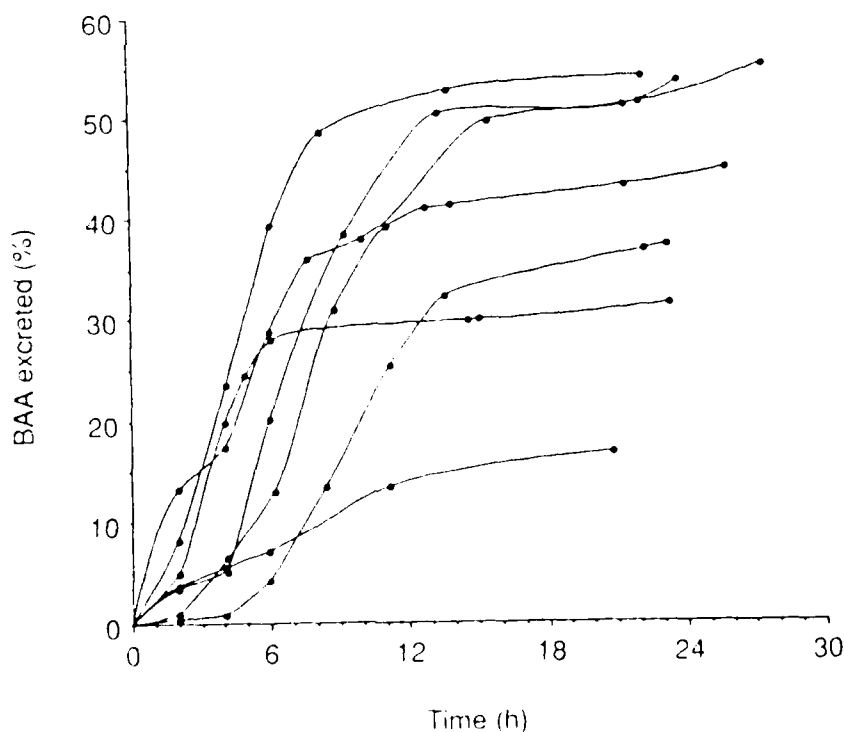
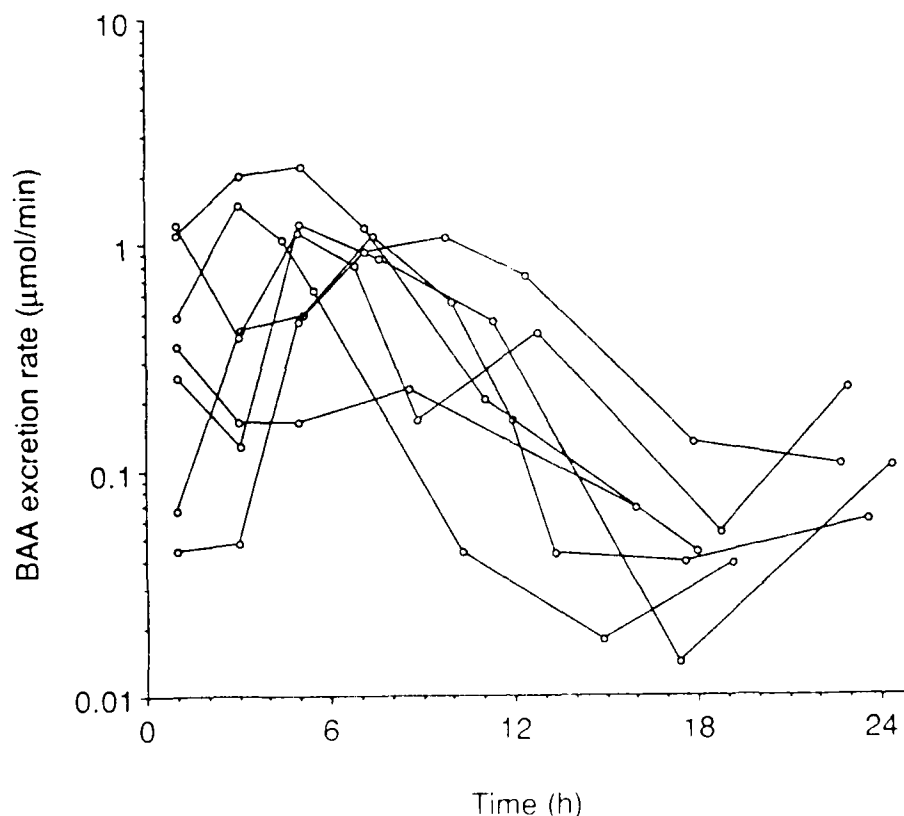


Figure 3. Cumulative excretion of BAA in the urine from seven men following a 2-h exposure to EGBE at 20 ppm. The excretion is expressed as a percentage of the total uptake of EGBE. Redrawn from Johanson et al. [12].



**Figure 4.** Excretion rate of BAA in the urine from seven men following a 2-h exposure to EGBE at 20 ppm. Redrawn from Johanson et al. [12].

The glycine conjugate of EAA was found in rat urine after exposure to EGEE [21,29]. Similarly, the glycine conjugate of PAA was found in the urine of dogs and rats exposed to EGPE [22]. However, no glycine conjugate of MAA was found in rats exposed to EGME [23]. No reports from human exposure are available that would indicate formation of the glycine conjugate.

In two patients who had ingested about 100 mL of EGME, the clinical picture showed similarities with that of poisoning with ethylene glycol and methanol [8]. In one of them, calcium oxalate was found in the urine, indicating cleavage of the ether bond to yield ethylene glycol that is subsequently oxidized to oxalic acid. However, other reports are negative with respect to these metabolites in human urine. In one subject of two dermally exposed to EGME, a tendency of increased urinary excretion of methanol was seen [32]. Animal experiments with isotope-labelled EGME and EGEE [21,23] indicate that the exhaled carbon dioxide must derive from the ethylene glycol portion of the parent molecules. Thus, although not found in blood or urine, ethylene glycol may be an intermediary metabolite in the formation of carbon dioxide from EGME and EGEE. Ethylene glycol, but no oxalic acid, was found in the urine of rats dosed with EGPE, indicating cleavage of the ether bond in the molecule [22]. Crystals of calcium oxalate were observed in the urine of dogs exposed to high concentrations of 800-ppm EGME, EGEE (800 ppm), or EGBE (400 ppm) [33].

In contrast to the ethylene glycol ethers, PGME, being a secondary alcohol, cannot be oxidized to a corresponding acid. Oral doses to rats yielded propylene glycol as well as unchanged PGME, and

glucuronic acid and sulfate conjugates in the urine [23]. After exposure of rats to PGME, vapor propylene glycol was detected in the blood indicating cleavage of the ether bond [19].

#### ANALYSIS IN BIOLOGICAL SPECIMENS

EGME, EGEE, AND EGBE were analyzed by head space gas chromatography (GC) with flame ionization detection (FID) at millimolar levels in blood from rats exposed to high doses [34]. An unspecified GC method involving gas liquid equilibration was used to detect EGME at millimolar levels in blood from dermally exposed men [32]. GC-FID methods were used to analyze PGME and its metabolite propylene glycol in blood from rats. The limit of detection was 40  $\mu$ M (3  $\mu$ g/g) [19]. EGBE below 100  $\mu$ M was quantified by GC-FID in ethyl acetate extracts of rat liver perfusate [35]. A method based on derivatization of toluene extracts with pentafluorobenzoyl chloride followed by GC with electron capture detection (ECD) was used to quantify EGBE in blood and urine from man and guinea pig. The detection limit in blood was approximately 0.1  $\mu$ M [12,16-18]. This method may be used also for EGEE but not EGME in its present form (unpublished observation).

BAA in plasma ultrafiltrate from rats was measured down to approximately 100  $\mu$ M by high performance liquid chromatography (HPLC) with UV detection [14].

Both GC and HPLC methods have been used successfully to detect the acid metabolite in urine. Methylation with diazomethane followed by GC-FID has been used to analyze MAA, EAA, and BAA in human urine [27,28,30,31,36]. The reported detection limits were 2  $\mu$ M for MAA and 0.7  $\mu$ M for EAA [36]. Silylation with N,O-bis(trimethylsilyl)-trifluoroacetamide followed by GC-FID was used to detect EAA and N-ethoxyacetyl glycine in rat urine [29]. Extractive alkylation with pentafluorobenzyl bromide was used prior to GC-FID analysis of MAA, EAA, and BAA. The detection limits were reported to be 140  $\mu$ M for MAA and 50  $\mu$ M for EAA [37], while levels down to approximately 50  $\mu$ M were measured in human urine [12]. The sensitivity may be improved by modifying the method for GC-ECD (unpublished observation).

#### ASPECTS OF BIOLOGICAL MONITORING

##### *Effect of physical exercise*

Because of the high water/air and blood/air partition coefficients of the glycol ethers their respiratory uptake is mainly limited by the supply from the ambient air, that is, the pulmonary (or alveolar) ventilation [38]. As increased work load results in increased pulmonary ventilation, increased respiratory uptake and elevated blood levels of glycol ether are expected. Simulated curves illustrating the effect of work load on blood levels of EGBE during inhalation exposure are shown in Figure 5. The relative respiratory uptake of EGBE was assumed to be constant at 60%. At heavy work loads (100 and 150 W) the liver blood flow is reduced, resulting in a reduced metabolic clearance and

further elevated blood levels. Inhalation experiments with EGEE in man showed that the relative uptake increases from 63 to 70 and 71% when the work load is changed from rest to 30 and 60 W, respectively [10]. Similar results were obtained for EGEEAc [11]. These results suggest that the uptake of the glycol ethers is determined to a large extent by the alveolar ventilation. The alveolar ventilation is about two thirds of the pulmonary ventilation at rest, and the fraction increases at increased work loads. Thus, the assumption of a constant relative uptake of EGBE of 60% in the simulation study may have resulted in slightly underestimated respiratory uptake and blood levels at heavy work loads.

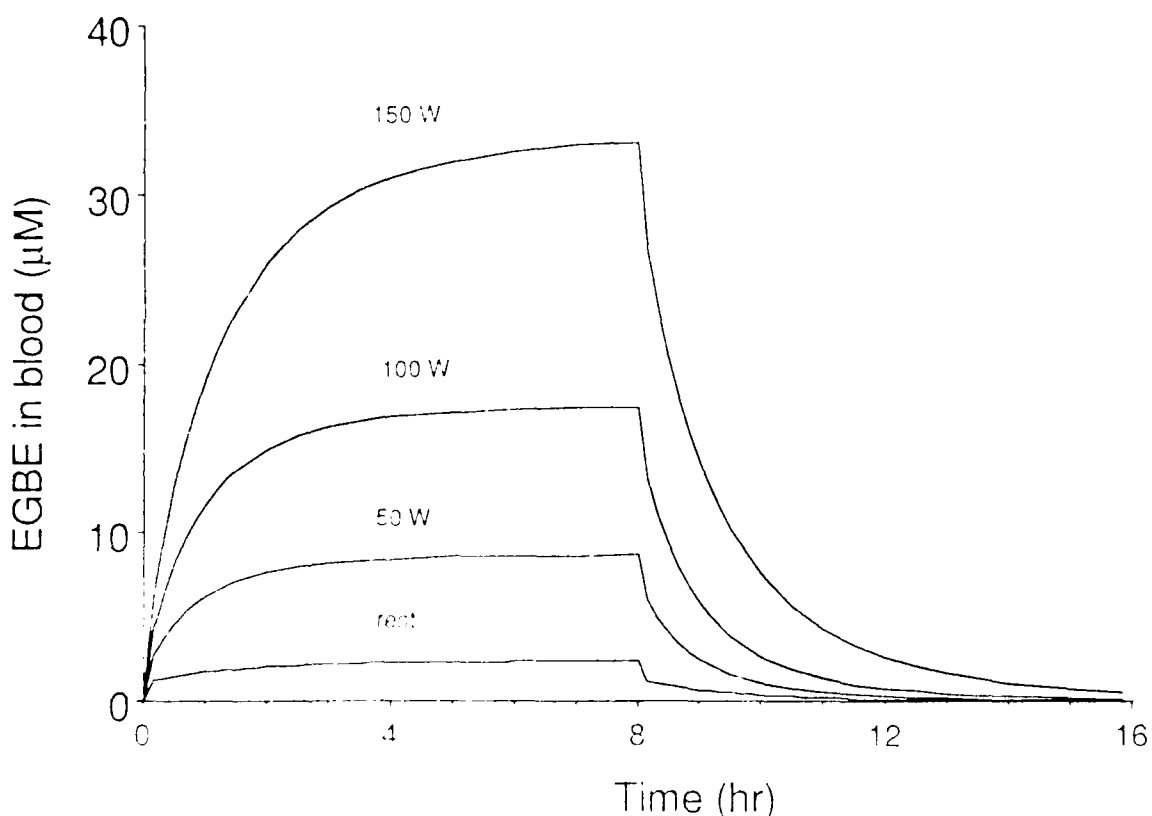


Figure 5. Effect of physical exercise on the blood concentration profile of EGBE in man simulated in a physiologically based pharmacokinetic model. The conditions were inhalation exposure to EGBE at 20 ppm for 8 h, followed by 8 h of no exposure, during rest, light (50 W), moderate (100 W), and heavy (150 W) work. Redrawn from Johanson [46] where more details on the model are given.

#### Respiratory versus skin uptake

It is of interest to compare the relative importance of respiratory and dermal exposure. Figure 6 shows such an attempt. The dermal uptake rate was calculated as *in vitro* dermal uptake rate per unit area times exposed area. An area of 50 cm<sup>2</sup> of the skin was assumed to be continuously exposed to undiluted solvent. While *in vivo* and *in vitro* data on the percutaneous uptake rates of glycol ethers appear to be in agreement, the *in vitro* uptake rates in human epidermis were used

because data were available for several glycol ethers. The respiratory uptake rate was calculated as relative uptake times concentration in air times pulmonary ventilation. Exposure either at the ACGIH TLV level or at 1% of the saturation level at room temperature was assumed. The 1% approach was used because the ambient air concentration of a solvent often may be related to its vapor pressure and evaporation rate rather than its TLV. The pulmonary ventilation was set to 10 L/min and the relative uptake to 60% for all glycol ethers. Figure 6 illustrates that dermal exposure to glycol ethers may be of great importance when liquids are handled. This is a most important argument for biological monitoring because ambient air concentration measurements do not take skin absorption into account.

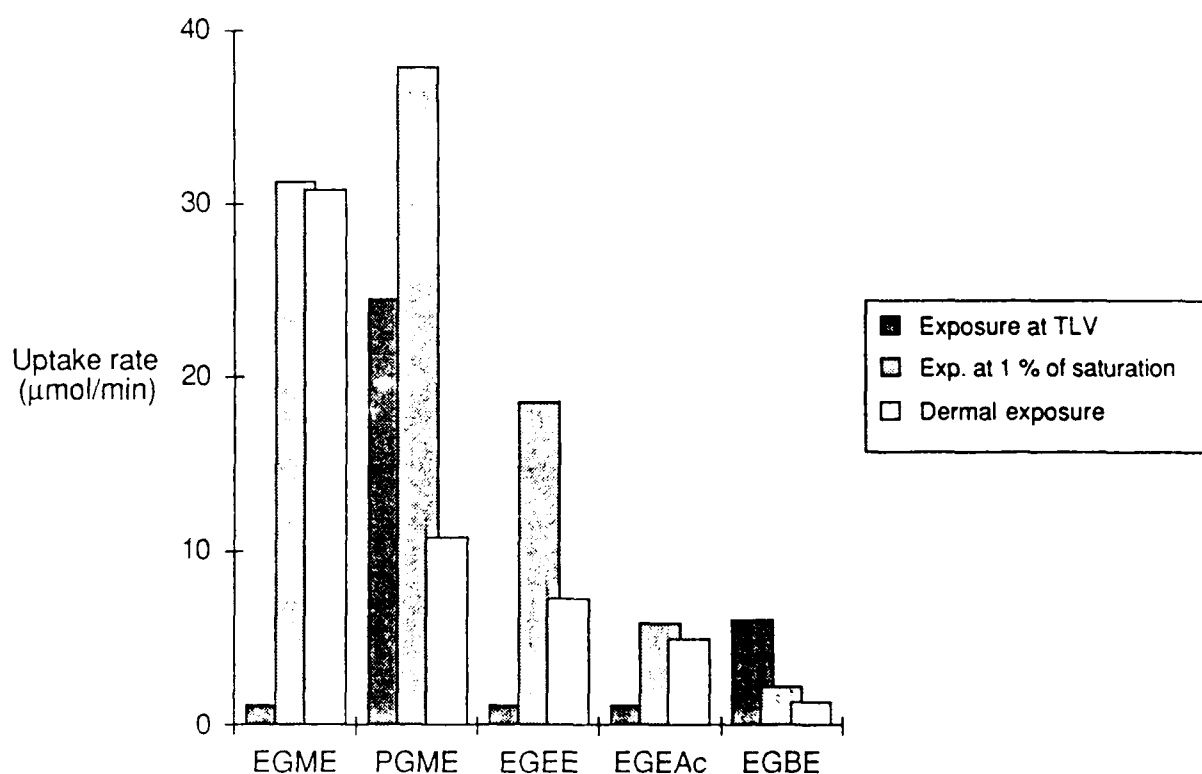


Figure 6. Theoretical inhalation uptake of glycol ether during exposure to vapor at the TLVs adopted by ACGIH (Table III) or at 1% of the saturation concentration at room temperature (Table II) compared to theoretical percutaneous absorption during skin exposure to liquid solvent. The values were calculated assuming a pulmonary ventilation of 10 L/min and a relative respiratory uptake of 60%, and by scaling from *in vitro* experiments [16] with separated epidermis to a skin area of 50 cm<sup>2</sup>.

#### Choice of parameter for biological monitoring

A rapid decay in the concentration in exhaled air has been observed for EGEE, EGEAc, and PGME in man as cited earlier. Similarly, the levels of EGBE in blood and urine decline rapidly. Thus, biomonitoring of the parent ethylene glycol ether in expired breath, blood, or urine appears less

suitable as such levels mainly reflect the exposure during and immediately prior to sampling. However, the secondary alcohol PGME is not as subject to metabolic degradation and may therefore be a candidate for monitoring in blood or urine samples.

On the basis of inhalation experiments with EGBE, it is reasonable to assume that the levels of glycol ether in blood and urine will be in the low micromolar range after occupational exposure. Such low levels require sophisticated analytical methods.

Of the acid metabolites, MAA and BAA have been detected in blood, but only in experimental animals at millimolar levels after high doses. Thus, at the moment no method appears to be available that would permit the use of the acid metabolite in blood for biological monitoring.

In conclusion, short half-lives, low concentrations, and lack of methods disfavor the use of the parent glycol ether in expired breath, blood, or urine, or of the acid metabolite in blood as a biological exposure index.

In contrast, the excretion of acid metabolite in urine appears to be very suitable as an index of exposure to ethylene glycol ethers for several reasons.

1. The acid metabolites MAA, EAA, and BAA are not normally present in human urine [12,30,36].
2. Following exposure to EGEE, EGEEAc, or EGBE around the TLVs, EAA, and BAA reach high (millimolar) levels in the urine [12,27,28].
3. The acid metabolites appear to be closely related to the major hazards of the glycol ethers. The urinary excretion of the acid metabolite probably reflects its concentration at the target sites, and thus the health hazard, better than ambient air levels or absorbed dose of glycol ether.
4. The half-life of the excretion of acid metabolite in urine is long, 1-2 days for EAA [27,28,31] and 3-4 h for BAA [12,17]. Hence, occasional exposure peaks may be reflected in the urinary excretion of acid metabolite, whereas they may be overlooked in air monitoring due to limited sampling time or sampling area.
5. Collection of urine is simple to perform.

An investigation using biological monitoring of exposure to glycol ethers has recently been published. Veulemans et al. [31] investigated the excretion of EAA in the urine of five women working with silk screen printing. The women were exposed to a mean combined concentration of 4-ppm EGEE and EGEEAc. The possibility of skin exposure during the investigation period was reduced by the use of gloves. The urinary excretion of EAA showed a clear increase over the week, and EAA was still detectable after 12 days of non-exposure. The half-life of EAA excretion was estimated to 1-2 days. A high correlation ( $r = 0.92$ ) was found between average exposure over the week and the EAA excretion at the end of the week. The regression equation suggests that one week (5 days, full shift)

of occupational exposure to EGEE or EGEEAc at 5 ppm corresponds to  $150 \pm 35$  mg EAA/g creatinine in urine.

#### ***Possible sources of error in biological monitoring of glycol ethers***

The field work conducted by Veulemans and colleagues is encouraging although a limited number of subjects were studied. However, a number of potential sources of error have to be investigated before a more secure quantitative relationship between exposure to glycol ethers and urinary metabolites can be established. Some of these will be discussed below.

The concentration as well as the excretion rate of BAA in urine of seven men following controlled short-term exposure to EGBE varied approximately tenfold at any given time ([12] and Figure 4). The cumulated excretion of BAA during 24 h varied by a factor of three (Figure 3). These observations indicate a limitation to the use of BAA in urine as an exposure index.

Intra-individual variations in excretion rate may be caused, for example, by changes in hepatic blood flow, metabolic rate, renal blood flow, diuresis, and renal excretion efficiency. These factors may be influenced by physical exercise, food intake, ambient temperature, and time of day, although no data on such influences were found in the literature on glycol ethers. A tendency of circadian variation in EAA excretion was seen in the field study by Veulemans et al. [31] in that the level of EAA was often higher in the preshift urine samples collected in the morning than in the postshift samples. A similar tendency may be present in the excretion of BAA (Figure 4).

Inter-individual variations in excretion of acid metabolites may be congenital or related to body constitution, personal habits (e.g., smoking, dietary factors, ethanol consumption) or illness that will influence the metabolism, distribution, and excretion. Sex differences in the metabolism of PGME in rats have been observed [19].

The metabolism of a foreign substance in the body may be induced by the substance itself, as shown for PGME in the rat [19], or by other xenobiotics. In contrast, the metabolism may be inhibited by simultaneous exposure to xenobiotics. Aliphatic alcohols are of special interest both because they are widely used and because they share a common metabolic pathway with the ethylene glycol ethers. When pregnant rats were exposed to EGEE and ethanol early in gestation, the behavioral and neurochemical effects of EGEE in the offspring were reduced. In contrast, coexposure later in pregnancy potentiated the effects of EGEE [39]. Both *in vivo* and *in vitro* experiments show that ethanol markedly inhibits the elimination of EGME, EGEE, and EGBE in rats [34, 35]. No effect of inhaled EGME on the elimination of ingested ethanol was seen in man [40]. The low dose of EGME as compared to ethanol may explain the lack of effect. However, equimolar doses of ethanol and EGME, EGEE, or EGBE given to rats resulted in marked inhibition of the elimination of glycol ether but no inhibition of ethanol elimination [34]. Thus it appears that the oxidative metabolism has a higher

preference for ethanol than for glycol ethers. Similar results have been obtained *in vitro* with human liver alcohol dehydrogenase [41].

Further, the uptake, metabolism, or excretion may be dose dependent. A small but unusual concentration dependence in the relative respiratory uptake of EGEEAc was seen in man, in that the uptake increased from 53% at 2.6 ppm to 57% at 5.2 ppm and 62% at 9.3 ppm [11]. Dose-dependent Michaelis-Menten kinetics in the elimination of EGBE were observed in the perfused rat liver. The maximum elimination rate ( $V_{max}$ ) averaged  $0.7 \mu\text{mol}/\text{min}/\text{g}$  liver and the apparent Michaelis constant ( $K_m$ ) was 9.2 mM [35]. In rats intraperitoneally dosed with EGEE (10 mmol/kg bw), blood levels consistent with metabolic saturation were seen with a maximum metabolic rate of approximately 5 mmol/h/kg bw corresponding to  $2 \mu\text{mol}/\text{min}/\text{g}$  liver. In rats dosed with EGBE (2.5 mmol/kg bw) the corresponding values were 3.6 mmol/h/kg bw and  $1.5 \mu\text{mol}/\text{min}/\text{g}$  liver (my interpretation from Figure 1 in [34]). Exposure to EGEE and EGBE at their TLVs results in respiratory uptake rates of approximately 1 and  $5 \mu\text{mol}/\text{h}/\text{kg}$  bw (calculated as in Figure 6). These values are approximately doubled at light work loads but are still about two orders of magnitude lower than the estimated maximum elimination rates in rats. Thus, if extrapolation from rat to man is allowed, dose-dependent metabolism of EGEE and EGBE appears to be of minor concern in the work place with the possible exception of extensive skin exposure.

The situation may be different for PGME. In rats exposed at 300 to 3000 ppm, a marked concentration dependence in blood levels and disappearance rates of PGME was seen, indicating saturation kinetics. The blood concentration's failing to plateau during exposure, even at 300 ppm, is indicative of saturated metabolism [19]. The zero-order elimination rate in rats exposed at 3000 ppm was approximately  $60 \mu\text{g}/\text{h}/\text{g}$  bw, corresponding to  $0.7 \text{ mmol}/\text{h}/\text{kg}$  bw, which is about 35 times higher than the respiratory uptake rate in men exposed at the TLV calculated as in Figure 6. Assuming the metabolic rate to be proportional to body area rather than body weight, the difference is reduced to a factor of 7. In this case, extrapolation from rat to man indicates that saturation kinetics may occur after occupational exposure.

Monitoring acid metabolite in the urine may be appropriate even if the uptake or metabolism of the glycol ether is influenced by saturation kinetics, xenobiotics, or other factors. The amount of acid metabolite in the urine then will not be linearly correlated to the absorbed dose but may still be well correlated to the concentration of active metabolite in the target sites, and thus related to the potential toxicity. At least this would be expected if the distribution and excretion kinetics of the metabolite were linear. However, the acid metabolites of the glycol ethers – being carboxylic acids – may bind to plasma proteins. In addition, they may be excreted in urine by active tubular secretion.

Both of these two processes are known to be saturable, although no information was found in the literature on glycol ethers in this matter.

## CONCLUSIONS

Percutaneous uptake may play a major role in occupational exposure to glycol ethers. This is an important argument for biological monitoring because ambient air concentration measurements do not take skin absorption into account. The large influence of work load on the respiratory uptake and the possibility of occasional high peaks of glycol ether in ambient air are additional arguments for biological monitoring.

Several factors, such as the toxicokinetic profile, analytical methods, and ease of sampling, indicate that analysis of the corresponding acid metabolite in urine is an appropriate way of monitoring exposure to ethylene glycol ethers. The influence of work load as well as the possibility of skin uptake must be taken into account when comparing exposure levels of glycol vapor to urinary excretion of acid metabolite at the work place. Intra- and inter-individual differences in excretion kinetics must be investigated more closely. The toxicokinetics of the glycol ethers may be dose dependent. Finally, exposure to other xenobiotics may influence the excretion kinetics of the acid metabolite by induction or inhibition of the metabolism, for example. These factors should not be overlooked when establishing quantitative relationships.

## ACKNOWLEDGMENTS

I wish to express my gratitude to Dr. M. Byfält Nordqvist for valuable discussions during the elaboration of the manuscript.

## REFERENCES

- 1 Johanson, G. and Rick, U. (1986) Occurrence of glycol ethers in chemical products in Sweden. Arbetskyddsstyrelsen, Solna, Sweden, Arbete och Hälsa 13 (in Swedish with English summary).
- 2 European Chemical Industry Ecology and Toxicology Centre. (1985) The Toxicology of Glycol Ethers and Its Relevance to Man: An up-dating of ECETOC Technical Report No. 4, Technical Report No. 17, Brussels, Belgium.
- 3 Gudbergsson, H. (1985) Nordic expert group for documentation of occupational exposure limits, ethylene glycol monoethers, and their acetates. Arbetskyddsstyrelsen, Solna, Sweden, Arbete och Hälsa 35 (in Swedish with English summary).
- 4 Illing, H.P.A. and Tinkler, J.J.B. (1985) Toxicity review 10, Glycol ethers. Her Majesty's Stationery Office, London, Great Britain.
- 5 Kalf, G.F., Post, G.B., and Snyder, R. (1987) Solvent toxicology: Recent advances in the toxicology of benzene, the glycol ethers, and carbon tetrachloride. Annu. Rev. Pharmacol. Toxicol. 27, 399-427.

- 6 Veulemans, H., Groeseneken, D., Masschelein, R., and van Vlem, E. (1987) Survey of ethylene glycol ether exposures in Belgian industries and workshops. *Am. Ind. Hyg. Assoc. J.* 48, 671-676.
- 7 Rowe, V.K. and Wolf, M.A. (1982) Derivatives of glycols. In: G.D. Clayton and F.E. Clayton (eds), *Patty's Industrial Hygiene and Toxicology*, Vol. 2C, John Wiley & Sons, New York, NY, pp. 36-41.
- 8 Nitter-Hauge, S. (1970) Poisoning with ethylene glycol monomethyl ether, report of two cases. *Acta Med. Scand.* 188, 277-280.
- 9 Kamerling, J.P., Duran, M., Bruinvis, L., Ketting, D., Wadman, S.K., deGroot, C.J. and Hommes, F.A. (1977) (2-Ethoxyethoxy) acetic acid: An unusual compound found in the gas chromatographic analysis of urinary organic acids. *Clin. Chim. Acta* 77, 397-405.
- 10 Groeseneken, D., Veulemans, H., and Masschelein, R. (1986) Respiratory uptake and elimination of ethylene glycol monoethyl ether after experimental human exposure. *Br. J. Ind. Med.* 43, 544-549.
- 11 Groeseneken, D., Veulemans, H., Masschelein, R., and van Vlem, E. (1987) Pulmonary absorption and elimination of ethylene glycol monoethyl ether acetate in man. *Br. J. Ind. Med.* 44, 309-316.
- 12 Johanson, G., Kronborg, H., Näslund, P.H., and Byfält Nordqvist, M. (1986) Toxicokinetics of inhaled 2-butoxyethanol (ethylene glycol monobutyl ether) in man. *Scand. J. Work. Environ. Health* 12, 594-602.
- 13 Guest, D., Hamilton, M.L., Deisinger, P.J., and DiVincenzo, G.D. (1984) Pulmonary and percutaneous absorption of 2-propoxyethyl acetate and 2-ethoxyethyl acetate in beagle dogs. *Environ. Health Perspect.* 57, 177-183.
- 14 Bartnik, F.G., Reddy, A.K., Klecak, G., Zimmermann, V., Hostynek, J.J., and Kunstler, K. Percutaneous absorption, metabolism, and hemolytic activity of n-butoxyethanol. *Fundam. Appl. Toxicol.* 8, 59-70.
- 15 Dugard, P.H., Walker, M., Mawdsley, S.J., and Scott, R.C. (1984) Absorption of some glycol ethers through human skin in vitro. *Environ. Health Perspect.* 57, 193-197.
- 16 Johanson, G. and Fernström, P. (1986) Percutaneous uptake rate of 2-butoxyethanol in the guinea pig. *Scand. J. Work Environ. Health* 12, 499-503.
- 17 Johanson, G., Boman, A., and Dynésius, B. (1988) Percutaneous absorption of 2-butoxyethanol in man. *Scand. J. Work Environ. Health* 14, 101-109.
- 18 Johanson, G. and Fernström, P. (1988) Influence of water on the percutaneous absorption of 2-butoxyethanol in guinea pigs. *Scand. J. Work Environ. Health* 14, 95-100.
- 19 Morgott, D.A. and Nolan, R.J. (1987) Nonlinear kinetics of inhaled propylene glycol monomethyl ether in Fischer 344 rats following single and repeated exposures. *Toxicol. Appl. Pharmacol.* 89, 19-28.
- 20 Stewart, R.D., Baretta, E.D., Dodd, H.C., and Torkelson, T.R. (1970) Experimental human exposure to vapor of propylene glycol monomethyl ether. *Arch. Environ. Health* 20, 218-223.

- 21 Cheever, K.L., Plotnick, H.B., Richards, D.E., and Weigel, W.W. (1984) Metabolism and excretion of 2-ethoxyethanol in the adult male rat. *Environ. Health Perspect.* 57, 241-248.
- 22 Hutson, D.H. and Pickering, B.A. (1971) The metabolism of isopropyl oxitol in rat and dog. *Xenobiotica* 1, 105-119.
- 23 Miller, R.R., Hermann, E.A., Langvardt, P.W., McKenna, M.J., and Schwetz, B.A. (1983) Comparative metabolism and disposition of ethylene glycol monomethyl ether and propylene glycol monomethyl ether in male rats. *Toxicol. Appl. Pharmacol.* 67, 229-237.
- 24 Stott, W.T. and McKenna, M.J. (1985) Hydrolysis of several glycol ether acetates and acrylate esters by nasal mucosal carboxylesterase in vitro. *Fundam. Appl. Toxicol.* 5, 399-404.
- 25 Scott, W.J., Jr., Nau, H., Wittfoht, W., and Merker, H.J. (1987) Ventral duplication of the autopod: Chemical induction by methoxyacetic acid in rat embryos. *Development* 99, 127-136.
- 26 Carpenter, C.P., Pozzani, U.C., Weil, C.S., Nair, J.H., Keck, G.A., and Smyth, H.F., Jr. (1956) The toxicity of butyl cellosolve solvent. *Arch. Ind. Health* 14, 114-131.
- 27 Groeseneken, D., Veulemans, H., and Masschelein, R. (1986) Urinary excretion of ethoxyacetic acid after experimental human exposure to ethylene glycol monoethyl ether. *Br. J. Ind. Med.* 43, 615-619.
- 28 Groeseneken, D., Veulemans, H., Masschelein, R., and van Vlem, E. (1987) Ethoxyacetic acid: A metabolite of ethylene glycol monoethyl ether acetate. *Br. J. Ind. Med.* 44, 488-493.
- 29 Jönsson, A.K., Pedersen, J., and Steen, G. (1982) Ethoxyacetic acid and N-ethoxyacetyl glycine: Metabolites of ethoxyethanol (ethylcellosolve) in rats. *Acta Pharmacol. Toxicol. (Copenh.)* 50, 358-362.
- 30 Jönsson, A.K. and Steen, G. (1978) n-Butoxyacetic acid, a urinary metabolite from inhaled n-butoxyethanol (butylcellosolve). *Acta Pharmacol. Toxicol. (Copenh.)* 42, 354-356.
- 31 Veulemans, H., Groeseneken, D., Masschelein, R., and van Vlem, E. (1987) Field study of the urinary excretion of ethoxyacetic acid during repeated daily exposure to the ethyl ether of ethylene glycol and ethyl ether of ethylene glycol acetate. *Scand. J. Work. Environ. Health* 13, 239-242.
- 32 Nakaaki, K., Fukabori, S., and Tada, O. (1980) An experimental study on percutaneous absorption of some organic solvents. *J. Sci. Labour* 12, 1-9.
- 33 Werner, H.W., Mitchell, J.L., Miller, J.W., and von Oettingen, W.F. (1943) The acute toxicity of vapors of several monoalkyl ethers of ethylene glycol. *J. Ind. Hyg. Toxicol.* 4, 157-163.
- 34 Römer, K.G., Balge, F., and Freundt, K.J. (1985) Ethanol-induced accumulation of ethylene glycol monoalkyl ethers in rats. *Drug. Chem. Toxicol.* 8, 255-264.
- 35 Johanson, G., Wallén, M., and Byfalt Nordqvist, M. (1986) Elimination kinetics of 2-butoxyethanol in the perfused rat liver - dose dependence and effect of ethanol. *Toxicol. Appl. Pharmacol.* 83, 315-320.

- 36 Groeseneken, D., van Vlem, E., Veulemans, H., and Masschelein, R. (1986) Gas chromatographic determination of methoxyacetic and ethoxyacetic acid in urine. *Br. J. Ind. Med.* 43, 62-65.
- 37 Smallwood, A.W., DeBord, K.E., and Lowry, L.K. (1984) Analyses of ethylene glycol monoalkyl ethers and their proposed metabolites in blood and urine. *Environ. Health Perspect.* 57, 249-253.
- 38 Johanson, G. and Dynésius, B. (In Press) Liquid/air partition coefficients of six commonly used glycol ethers. *Br. J. Ind. Med.*
- 39 Nelson, B.K., Brightwell, W.S., Setzer, J.V., and O'Donohue, T.L. (1984) Reproductive toxicity of the industrial solvent 2-ethoxyethanol in rats and interactive effects of ethanol. *Environ. Health Perspect.* 57, 255-259.
- 40 Pedersen, L.M., Nielsen, G.D., and Cohr, K.H. (1980) Alcohol elimination rate after inhalation of oxitol (2-ethoxyethanol). *Z. Rechtsmed.* 85, 199-203.
- 41 Blair, A.H. and Vallee, B.L. (1966) Some catalytic properties of human liver alcohol dehydrogenase. *Biochemistry* 6, 2026-2034.
- 42 Smith, R.L. (1984) Review of glycol ether and glycol ether ester solvents used in the coating industry. *Environ. Health Perspect.* 57, 1-4.
- 43 American Conference of Governmental Industrial Hygienists. (1986) Threshold limit values of chemical substances in the work environment adopted by ACGIH. Cincinnati, OH.
- 44 Deutsche Forschungsgemeinschaft (1986) Maximale Arbeitsplatzkonzentrationen und Biologische Arbeitsstofftoleranzwerte, VCH, Weinheim, F.R. Germany.
- 45 Arbetarskyddsstyrelsens författningssamling 12 (1987) Hygieniska gränsvärden, Svenskt Tryck, Stockholm, Sweden.
- 46 Johanson, G. (1986) Physiologically based pharmacokinetic modeling of inhaled 2-butoxyethanol in man. *Toxicol. Lett.* 34, 23-31.

## AN INHALATION DISTRIBUTION MODEL FOR THE LACTATING MOTHER AND NURSING CHILD

Michael L. Shelley, Melvin E. Andersen, and Jeffrey W. Fisher

*Harry G. Armstrong Aerospace Medical Research Laboratory, Wright-Patterson AFB, OH*

### SUMMARY

A rule-of-thumb methodology is presented to assist in assessing risk to a nursing child due to the mother's occupational inhalation exposure. The method represents an example of the use of physiologically based pharmacokinetic modeling using state-of-the-art computational techniques. A computer model is developed to describe distribution of non-metabolized, inhaled contaminants into a mother/child system as a function of the contaminant's blood:air and octanol:water partition coefficients. Risk is assessed in terms of the area under the blood concentration vs. time curve of the exposure chemical. Since low partition values yield low risk for the nursing child and high values yield high risk, the model is exercised over a range of intermediate values (blood:air = [2, 25]; octanol:water = [100, 1500]). Results are thus applicable to chemicals for which the mother's dose is a strong factor in estimating the child's risk. The most notable observation is that, for the range of partition values used, this model never predicts a risk for the child greater than 25% of that of the mother. An equation is provided (based on model results) that expresses the child's risk as a fraction of the mother's risk.

### INTRODUCTION

The increasing number of women in the workplace has raised new issues in the area of safe workplace exposure criteria. One such issue involves workplace exposure of the lactating mother and risk to the nursing child due to chemicals in the milk. Uncertainties involve more than simply the possibility of increased sensitivity in the newborn. Quantifying the infant's exposure from the mother's breathing zone air concentration involves a chemical distribution and transport description employing physiological parameters that are sparsely represented in the literature. Occupational physicians often feel compelled to recommend removal of the nursing mother from the work environment due to lack of data concerning risk to the child. The present work employs mathematical simulation to describe the distribution of a chemical from the mother's breathing zone during a work shift to a child on a 24-h nursing schedule. The purpose is to elucidate trends in distribution to the child based on physicochemical characteristics of the exposure chemical (i.e., partition coefficients into tissues). The chemical's metabolism is not included in this preliminary model.

## MATERIALS AND METHODS

### Model Description

A system of mass balance equations was constructed using the conceptual model shown in Figure 1. Physiologically based toxicokinetic principles were employed using realistic ventilation rates, tissue volumes, and blood flows to tissue groups, as well as estimated rates of milk production and partitioning of chemical to milk. A chemical enters the system by alveolar equilibration with blood flow in the mother during a work shift and exits by both mother and child exhalation. The child receives a chemical dose by direct transfer of bulk milk from the mother's mammary compartment to the child's gastrointestinal (GI) track according to the nursing schedule and the concentration in the mother's milk compartment at the time of nursing. GI absorption of chemical by the infant is assumed to be instantaneous with a bioavailability of 1.0. Risk is expressed in terms of the area under the blood concentration vs. time curve (AUCB), which is analogous to an effective dose at a given point in time (an index of potential to express a toxic effect). Thus, the child's risk may be stated in terms of a fraction of the mother's risk (whatever the mother's risk may be for a particular chemical). That is, the relative risk to the child (RRC) is expressed by the following equation.

$$RRC = AUCB (Child) / AUCB (Mother)$$

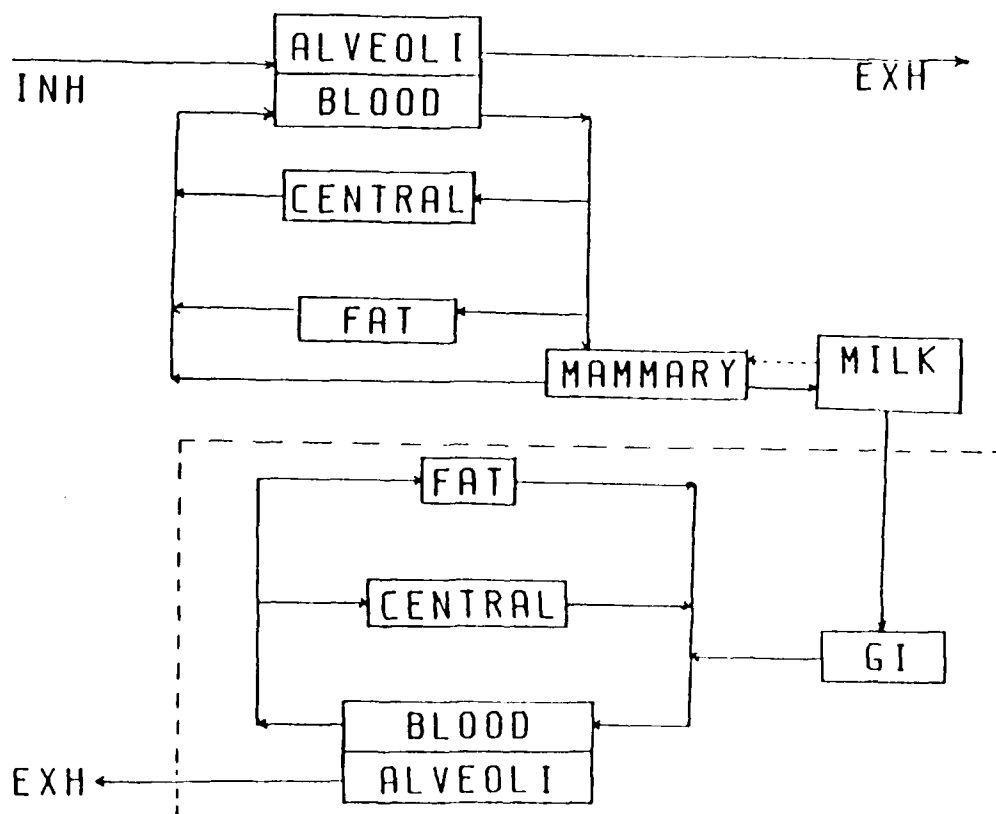


Figure 1. Conceptual model of a mother/nursing child distribution system.

Figure 2 shows the model predictions of AUCB for mother and child illustrating a 9-hour work shift and a  $3\frac{1}{2}$ -h nursing schedule. An RRC value of 0.5 would indicate that the child's risk is one-half that of the mother's for the described exposure and nursing scenario. Loss of chemical by metabolism and urinary excretion depends on specific metabolic pathways and thus is not included in this generic distribution model. Consequently, transfer of a toxic metabolite from the mother to the child is not described. However, in the case of short-lived, reactive metabolites, this potential for toxicity in either the mother or the child should be proportional to the AUCB for each.

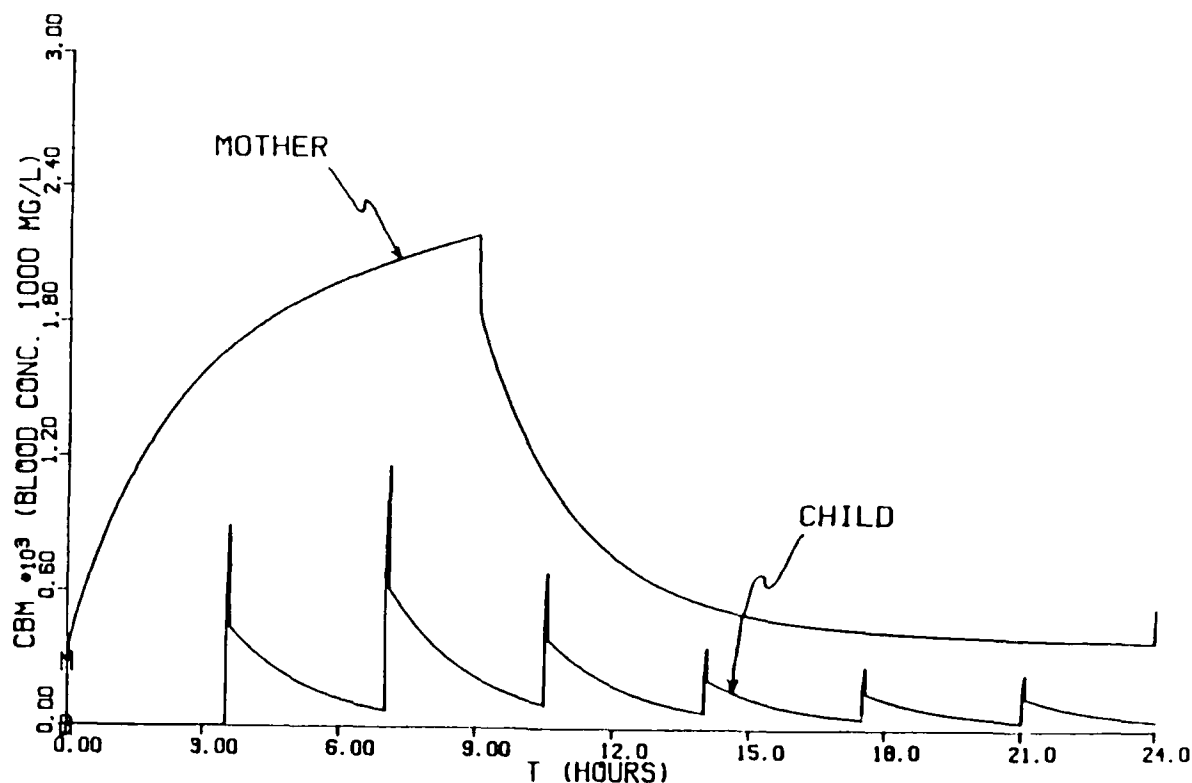


Figure 2. Blood concentration vs. time curve for 9-h workshift and  $3\frac{1}{2}$  h nursing schedule. ( $P_{B:A} = 25$ ;  $P_{O:W} = 1500$ ).

Using the model described above, the child's risk relative to the mother's risk is expressed under the following critical assumptions.

1. The mother's exposure is by inhalation only.
2. Distribution is described sufficiently by considering central and fat tissue groups and a third mammary/milk compartment in the mother.
3. Absorption of chemical in the child's GI tract is 100%.

4. Loss of chemical by metabolism and urinary excretion is neglected in both mother and child.
5. The child's relative risk is represented accurately by the ratio of child's to mother's AUCB.

The blood:air partition coefficient is entered directly into the model. Fat:blood and milk:blood partition coefficients are calculated from the more common octanol:water partition coefficient according to the following expressions.

$$P_{fat:blood} = 70.9 \log(P_{oct:water}) - 127.0$$

$$P_{milk:blood} = 0.04 P_{fat:blood} + 0.96 (1.0)$$

The first equation is derived empirically from literature partition coefficient data [1,2,3]. The second equation is based on the assumption of 4% fat content in human milk. The model thus exercises a defined exposure/nursing scenario with input values of blood:air and octanol:water partition coefficients. Ranges of values used in the model were  $P_{B:A}$  (2, 25) and  $P_{O:W}$  (100, 1500). These values are typical of organic chemicals of inhalation concern in the workplace. Low  $P_{O:W}$  chemicals do not readily distribute to adipose tissue and are fairly quickly eliminated, presenting little hazard to the child. High  $P_{O:W}$  chemicals are stored readily in adipose tissue and partition easily to milk, resulting in long-term release from tissue and distribution to the child for high infant risk [4]. The values used in this model are intermediate in range and thus represent chemicals for which the mother's dose is a strong factor in estimating the child's risk. Simulation was performed using Advance Continuous Simulation Language (ACSL) by Mitchell and Gauthier, and Statistical Analysis System (SAS) was used for the plotting and curve fitting of model results.

## RESULTS AND DISCUSSION

The results demonstrate a clear upward trend in RRC with increasing values of  $P_{B:A}$  and  $P_{O:W}$ , as illustrated in Figures 3 and 4 which are plots of model results. Figure 3 demonstrates a linear relationship of child's relative risk to the blood:air partition coefficient. This is easily explained since  $P_{B:A}$  directly controls the rate of the child's elimination by exhalation. The effect of  $P_{O:W}$ , as shown in Figure 4, is not as straightforward since it controls the amount of chemical distributed to milk and the amount distributed to the child's fat tissue and subsequently released back into distribution. The most notable observation is that for the range of partition values used, this model never predicts a risk for the child greater than 25% of that of the mother.

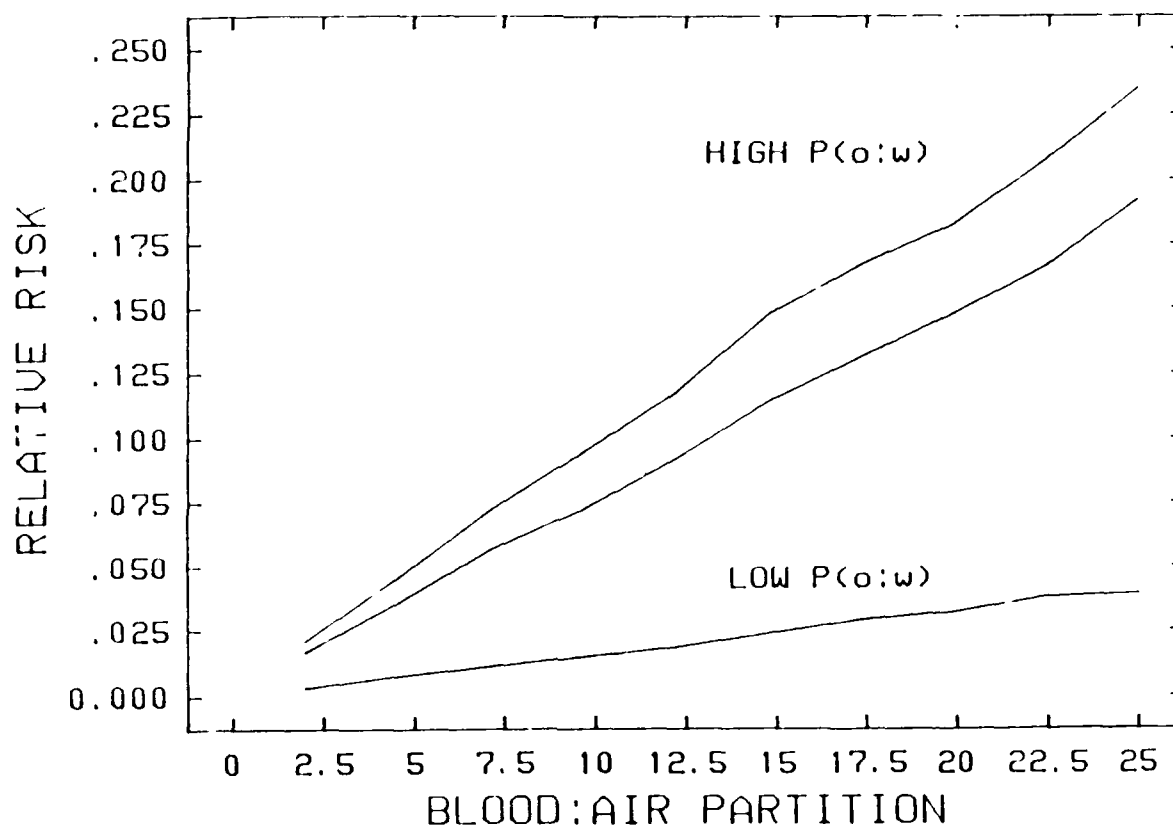


Figure 3. Child's relative risk (compared to mother's risk) vs. blood:air partition coefficient for  $P_{o:w}$  values of 100, 722, and 1500.

Sensitivity analyses were performed to determine physiological factors that significantly influenced model results. The duration of a single nursing had little effect until the duration was reduced to 5 min. Since most of the milk volume is in fact taken up early in a nursing session, 5 min was used as the nursing duration in the model. Blood flow to the child's fat tissue demonstrated a definite inverse relationship to the child's risk, particularly in the case of high  $P_{o:w}$ . The value used in the model was approximately one-half that estimated in the literature to influence model results toward the conservative side. Both the volume of milk per feeding and the fat content of the milk are directly related to the child's risk. The literature value of 4% milk-fat was used since variation from human to human should be small. Milk volume per feeding was double that of the literature average value to conservatively account for variation. All other physiological factors which were components of the model did not significantly influence model results when varied over a reasonable range.

Of particular concern was the model description of chemical loading of the mother's milk compartment. Transport mechanisms between mammary tissue and bulk milk are not clearly established in the literature. Therefore, two separate models were exercised: (1) model "A" which controlled milk concentration by continual equilibration with mammary blood flow, and (2) model "B" which accumulated chemical in the milk based on mammary tissue concentration at the time of

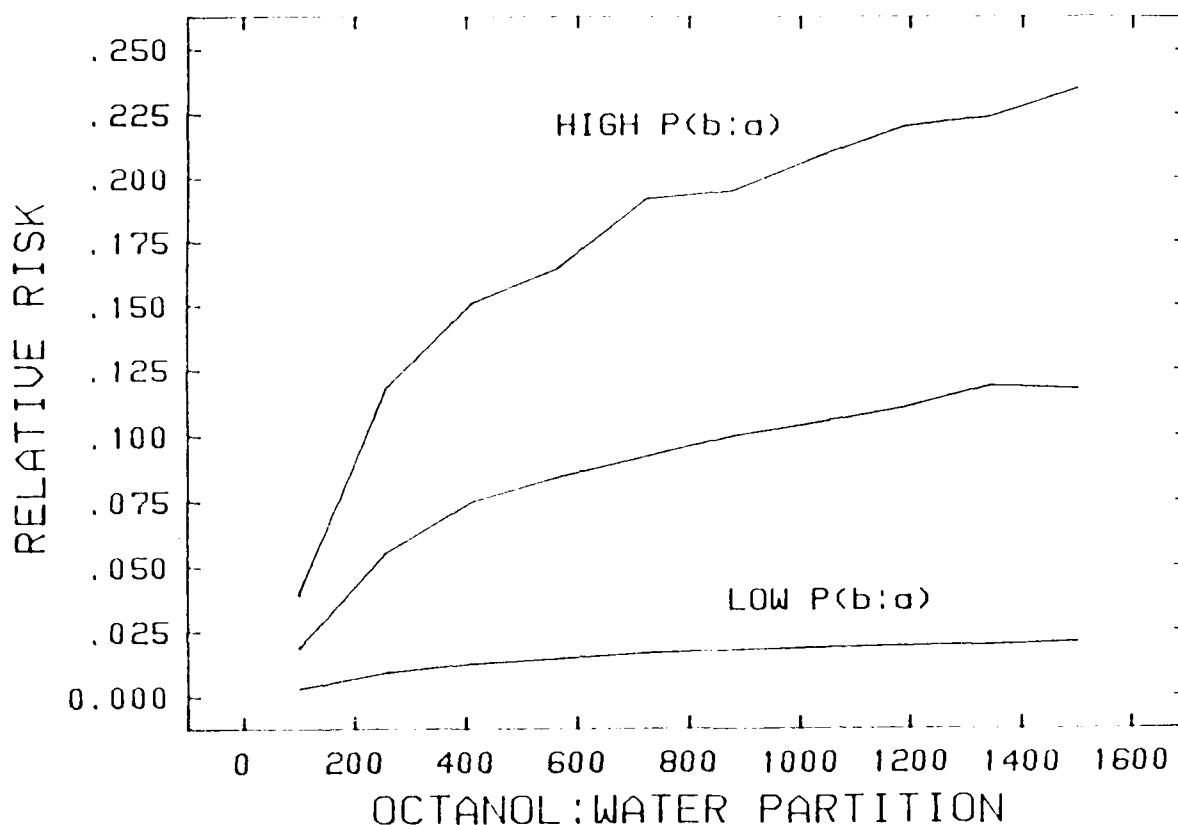


Figure 4. Child's relative risk (compared to mother's risk) vs. octanol:water partition coefficient for  $P_{b:A}$  values of 2, 12, and 25.

milk production. In the latter case, milk concentration reflects the mother's history of blood concentration rather than current blood concentration and thus always lags behind milk concentration predicted by the former model. That is, during the mother's work exposure, milk concentration is lower than in the former model and higher after exposure, as illustrated in Figure 5. Results from each model were essentially the same, apparently due to this compensation effect.

Finally, the effect of altering the mother's work schedule was studied. Results showed that increasing the work shift from 8 h to 12 h increased the child's relative risk by only 0.1. However, after only one shift exposure, the child's relative risk continued to rise days after the single exposure. This is due to a gradual releasing of stored chemical from the mother to a child having a much smaller volume of distribution. Thus, chemical accumulation over multiple workshifts is suggested. Employing daily workshifts and exercising the model over an extended period, it was shown that the child's relative risk increased and approached an asymptotic value, 90% of that value being reached in approximately two months. Therefore, the model used to generate the final results shown in Figures 3 and 4 employs a continuous 9-h work shift, 7 days/week, for 2 months. The child nurses every  $3\frac{1}{2}$  h.

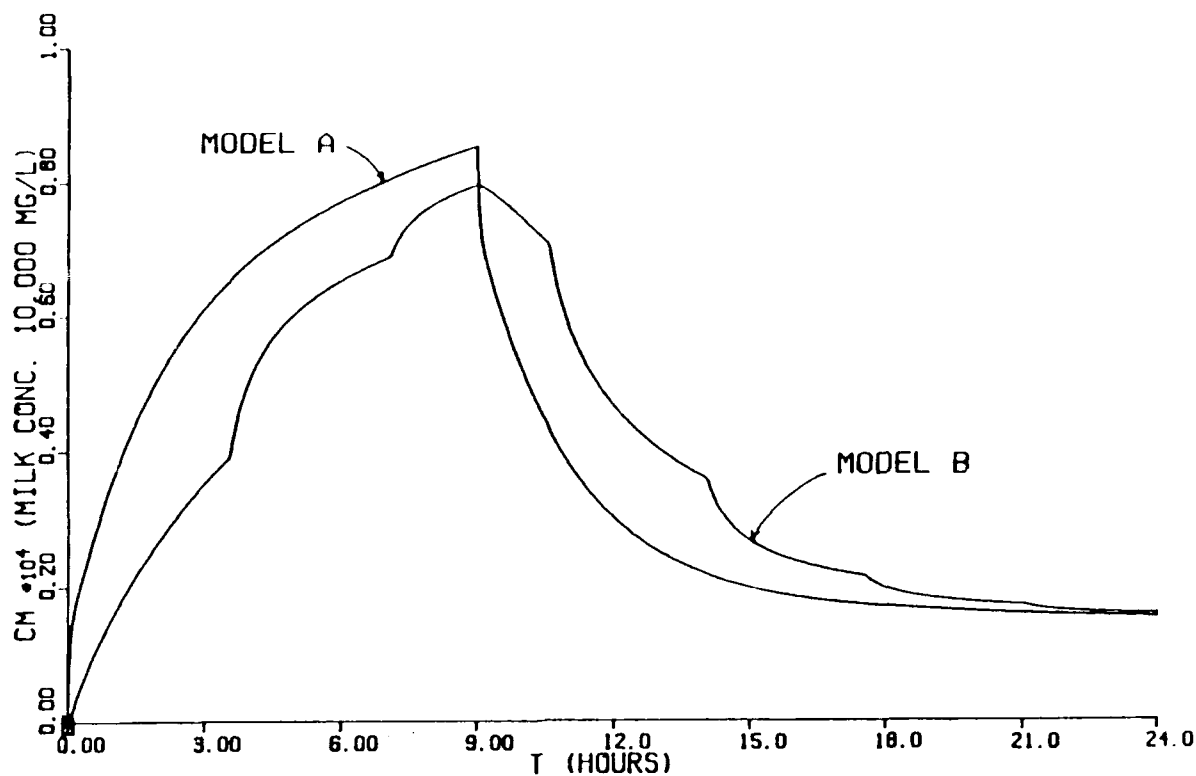


Figure 5. Milk concentration vs. time curve for two separate models describing alternative mechanisms for the loading of chemical into milk: (1) continual equilibration with mammary blood flow (model A); and (2) accumulation according to mammary tissue concentration at the time of incremental milk production (model B).

To interpret these findings in terms of guidelines for potential field use, an equation was derived empirically from model results, expressing the child's relative risk in terms of the chemical's blood:air and octanol:water partition coefficients as follows.

$$RRC = 2.5 \times 10^{-4} P_{B:A} P_{O:W}$$

The equation is, of course, limited to the range of values and model assumptions specified above.

## REFERENCES

- 1 Banerjee, S., Yalkowsky, S.H. and Valvani, S.C. (1980) Water solubility and octanol/water partition coefficients of organics. Limitations of the solubility-partition coefficient correlation. Environ. Sci. Tech. 14, 1227-1229.
- 2 Chiou, C.T., Freed, V.H., Schmedding, D.W. and Kohnert, R.L. (1977) Partition coefficient and bioaccumulation of selected organic chemicals. Environ. Sci. Tech. 11, 475-478.
- 3 Gargas, M.L., Andersen, M.E. and Clewell, H.J. (1986) A physiologically based simulation approach for determining metabolic constants from gas uptake data. Toxicol. Appl. Pharmacol. 86, 341-352.
- 4 Poitras, B.J., Keller, W.C., and Elves, R.G. (1985) A Guide to the Estimation of the Hazard Presented by Chemicals in Human Milk. USAF Occupational and Environmental Health Laboratory Report No. 85-185C0111LCE, Brooks AFB, TX.

## EFFECTS OF SHORT DURATION EXPOSURES TO ACETONE AND METHYL ETHYL KETONE

Robert B. Dick<sup>a</sup>, William D. Brown<sup>a</sup>, James V. Setzera<sup>a</sup>, Bobby J. Taylor<sup>a</sup>, and Rakesh Shukla<sup>b</sup>

<sup>a</sup>*U.S. Department of Health and Human Services, Public Health Service, Centers for Disease Control, National Institute for Occupational Safety and Health, Division of Biomedical and Behavioral Science, Cincinnati, OH, and* <sup>b</sup>*Biostatistics-Epidemiology Laboratory, Department of Environmental Health, University of Cincinnati Medical Center, Cincinnati, OH*

### SUMMARY

Workers are commonly exposed to mixtures or combinations of chemical agents, and these mixtures often consist of solvents. One group of solvents that has been extensively studied for its neurotoxic properties has been the ketones. However, previous research has focused on neuropathies produced by extended exposures and not on the simple pharmacokinetics or the reversible CNS effects from short duration exposures. In this research, 137 volunteers were recruited and tested for neurobehavioral performance changes and biochemical indicators during and after a short-duration (4-h) exposure to either acetone at 250 ppm, methyl ethyl ketone (MEK) at 200 ppm, acetone at 125 ppm with MEK at 100 ppm, or a chemical-placebo. Ethanol (95%-0.84 mL/kg) was used as a positive control. Testing took place in an environmental chamber with four test stations. The computer-controlled test regimen took 10 h, and several measures were collected: (1) biochemical measurements of venous blood and alveolar breath; (2) psychomotor tests of choice reaction time, visual vigilance, dual task (auditory tone discrimination and tracking), and memory scanning; (3) one sensorimotor (postural sway) test; and, (4) one psychological (Profile of Mood States [POMS]) test. Blood and breath concentrations during and after exposure did not demonstrate any interaction between the two solvents, nor were statistically significant sex differences present during uptake or elimination. The 250-ppm acetone exposure produced small but statistically significant differences from controls in two measures of the auditory tone discrimination task, and on the anger-hostility scale (males only) of the POMS test. The other chemical exposure conditions, MEK at 200 ppm and combination MEK with acetone, produced no consistent statistically significant results, which suggest there was no potentiation of the acetone effects with the co-exposure to MEK or vice versa under these test conditions. Ethanol at 0.07 to 0.08% blood alcohol concentrations (BAC) caused significant decrements on both the auditory tone and tracking tests in the dual task.

### INTRODUCTION

In the daily work setting, individuals are often exposed to combinations of industrial chemicals. Exposures can occur during manufacturing processes (adhesives, plastics, chemicals), degreasing operations, paintings, coatings, and drycleaning [1]. Often, the exposures contain concentrations of several volatile solvents, which could pose potential health risks for workers. The purpose of this

research was to study a combination exposure from the same chemical group, test for possible neurobehavioral effects, and profile the biochemical measurements of venous blood and alveolar breath. The chemical group chosen was the ketones, of which several billion pounds are produced annually. Two members of this class, acetone and methyl ethyl ketone (MEK), were selected for study. The selection was based upon their frequency of occurrence in the NIOSH Health Hazard Evaluation (HHE) reports and MEK's property of potentiating certain neurotoxic effects of other ketones (methyl *n*-butyl ketone) [2,3].

The primary routes of exposure from acetone and MEK are inhalation and skin contact, with the former being the most common due to the volatility of most ketones at room temperature. Principal toxic effects from exposure are (progressively) eye, nose, and throat irritation; headache; nausea; vertigo; incoordination; central nervous system (CNS) depression; narcosis; and, with extremely high exposures, cardiorespiratory failure [4]. Neurobehavioral studies involving only single, short-duration exposures to acetone and MEK have been reported in the literature. The studies are not numerous, although some marginal effects have been reported at levels below the OSHA-PEL [5]. Table 1 summarizes these few studies.

TABLE 1. HUMAN STUDIES WITH NEUROBEHAVIORAL EXPOSURES TO KETONES

Report	Chemical	Exposure		Tests	Results
		Conc.	Duration		
Matsushita et al. (14)	Acetone	500 ppm	6h/d for 6d	Simple RT	10% increase
		250 ppm	6h/d for 6d	Simple RT	5% increase
Nakaaki (18)	Acetone	170-690 ppm	4h	Time est.	inc. > 450 ppm
	MEK	90-270 ppm	4h	Time est.	no change
Dick et al. [15]	MEK	200 ppm	4h	Choice RT	no sig. dif.
				Vis.-Vig.	no sig. dif.
				Pattern Recog.	no sig. dif.

In the present study, single exposures to acetone (250 ppm) and MEK (200 ppm) followed the NIOSH-recommended exposure limits (RELs) [6]. Combination exposures (acetone 125 ppm/MEK 200 ppm) followed the OSHA additivity formula [5]. All exposures occurred in a simulated 8-h workday, and neurobehavioral and biochemical measurements were taken before, during, and after exposures.

## MATERIALS AND METHODS

One hundred thirty-seven participants were tested over a 1-year period. They ranged in age from 18 to 32, and were required to pass a physical exam. Pre-existing medical conditions (viz., pregnancy, diabetes, hypertension) or evidence of recent or chronic drug/alcohol use (verified by urinalysis and breathanalysis) were grounds for exclusion from testing or subsequent data analysis. Six subjects were eliminated only from the psychomotor and psychological data analysis because of suspected marijuana usage (9-carboxy THC confirmed by GC/MS > 50 ng/mL), and one subject was eliminated from all data analysis for excessive ethanol (BAC > .03). Usable data also are reduced through equipment failures, which caused some imbalance in the number of subjects in the various conditions (see Table 2).

TABLE 2. NUMBER OF SUBJECTS IN EACH TREATMENT CONDITION BY SEX AND CHEMICAL AND SUBJECTS RATINGS OF THEIR EXPOSURE<sup>a</sup>

Condition	Male		Female		Total	
	N	% <sup>b</sup>	N	% <sup>b</sup>	N	% <sup>b</sup>
Acetone - 250 ppm	11 (11)	100	11 (9)	82	22 (20)	91
Acetone-125/MEK - 200 ppm	8 (8)	100	11 (10)	91	19 (18)	95
MEK - 200 ppm	12 (10)	83	13 (7)	54	25 (17)	68
Chemical-Placebo	11 (11)	100	10 (6)	60	21 (17)	81
Ethanol	9 (9)	100	11 (10)	91	20 (19)	95
Ethanol-Placebo	11 (4)	36	11 (4)	36	22 (8)	36
Total	62 (53)	85	66 (45)	68	129 (99)	77

<sup>a</sup> Number in parentheses refers to the number of subjects who reported they were exposed to a chemical or who reported they had a drink containing ethanol.

<sup>b</sup> percent of subjects reporting they were exposed or had ingested a drink containing ethanol.

### Experimental design and procedures

The experiment was a mixed model (split-plot factorial) design, with subjects treated as a random factor. There were 6 separate treatment conditions, but the chemical and ethanol conditions were analyzed separately because of route of administration (inhalation vs ingestion) differences. The treatment conditions were (1) acetone-250 ppm, (2) MEK-200 ppm, (3) acetone-125 ppm/MEK-100 ppm, (4) chemical-placebo, (5) 95% ethanol-0.84 mL/kg, and, (6) ethanol-placebo. Subjects were assigned to one of the treatment conditions following a forced randomization scheme. The two requirements were to test equal numbers of males and females in each group and that subjects be at least 21 years of age for the ethanol conditions. Two placebo groups were used, one as a control for the chemical conditions and the other as an ethanol control. Ethanol was used as a treatment

condition to verify test sensitivity and for magnitude of effect comparisons. The chemical-placebo consisted of short (2 min), 25-ppm exposures of an acetone/MEK mixture presented twice during the 4-h exposure period. The ethanol-placebo was the ethanol drink mixture without ethanol. Table 2 shows the number of subjects in each treatment condition and their self report ratings of what their exposure/ingestion was.

Experimental sessions were conducted double blind (subjects and experimenter). Testing procedures were in accordance with the guidelines of the NIOSH Human Subjects Review Board and the ethical principles of the American Psychological Association. Volunteers were paid \$135 for their participation and were required to be drug free (except for medication approved by the medical officer) and to abstain from alcohol for 24 h prior to the 2 days of testing. Testing and exposures took place at 1 of 4 test stations inside an Environmental Chamber (Forma-Scientific) with interior dimensions of 2.5 m wide by 5.3 m long by 2.2 m high. Test stations were configured with a Hewlett-Packard 1311B video display terminal (VDT), a laboratory-made reaction time panel, 1 cylindrical microswitch (Switchcraft E-19), 2 box-mounted toggle switches (Switchcraft 41306), earphones (Realistic Pro-IIA), and a pressure-type joystick (Measurement Systems 735DC).

The testing regimen began with a 2-h practice session on the afternoon before the exposure day and ended with a 2 1/2-h test session the day following exposures. Exposure day testing took 8 h and was divided into four 2-h test periods. The 4-h exposure, which occurred in the middle 2 periods, was continuous, except for body burden sampling. The test periods were labeled as Pre: 1-2 h, Exp: 3-4 h, Exp: 5-6 h, Post: 7-8 h, and Post: 23-24 h. The Post: 23-24 h period was used to assess potential learning and exposure carry-over effects. Exposure testing commenced at 8 a.m., with lunch breaks at one-half hour prior to the Exp: 3-4 h period and at the end of the Exp: 5-6 h period. Five breath samples and 4 blood samples were collected from each subject over the 3-day test session. During the 4-h exposure session, blood samples were staggered with one-half of the subjects giving a sample at 2 h and the others at 4 h. Figure 1 displays the test regimen, showing the times of the blood and breath samples.

Subjects were tested for 10 h with the neurobehavioral tests described below. In each 2-h test period, approximately 32 measurements were used for purposes of analysis. These measurements were derived from 4 psychomotor tests, 1 sensorimotor test, and 1 psychological test. These tests are labeled in Figure 1, along with their order of appearance and time of administration. Included in the test regimen was an eyeblink reflex test that will be reported in a separate paper. While the actual testing of subjects took 1 year, control over seasonal effects was accomplished through randomization. In any 3-month period, the 6 treatment conditions occurred at least once.

Period	Day 1	Day 2				Day 3			
	Practice	Pre 1-2 h	Exp 3-4 h	Exp 5-6 h	Post 7-8 h	Post 23-24 h			
Vis-Vig	████	████	████	████	████	████			
Dual Task	████	████	████	████	████	████			
Eye Blink		████		████	████	████			
CRT	████	████	████	████	████	████			
Sternberg	████	████	████	████	████	████			
Sway	████	████	████	████	████	████			
POMS					████	████			
<hr/>									
Blood	████		████	████	████	████			
Breath	████	████	████	████	████	████			
Misc.	Consent Form	Lunch	Lunch		Med Check	Release			
Time		0745	0953	1250	1440	1608	1700	0800	1030

Figure 1. Test regimen (neurobehavioral performance tests were presented in order from top to bottom).

#### Performance tests

All tests, with the exception of the mood test, were administered to subjects in the environmental chamber. An IBM Series I was used for the computer-controlled tests except the postural sway test, which used a Northstar Horizon computer. Software was both user-developed and proprietary.

Subjects were administered tests at the same time, and the order of test presentation was the same in each period and succeeding periods. However, trial order within a test was different for each subject, and the trial order changed with each successive administration of the same test. All subjects were required to reach criterion levels or they received a set number of practice trials on the psychomotor tests during the 2-h practice session the day before exposure and testing. Speed and

accuracy were equally emphasized in the instructions for all the psychomotor tasks. Only brief descriptions of the tests follow.<sup>a</sup>

**Visual-vigilance.** This test was a non-memory type computerized version of the Mackworth Clock Test [7]. Centered on the VDT screen were 30 spokes radiating from a central hub, and computerized graphics created the appearance of a moving clock hand jumping from one spoke to the next. Movement speed was 60 jumps/min, with the critical signal (i.e., the one to be detected) being a jump of 2 spokes (24°). The test ran 36 min and there were 28 double jumps (critical events). Time (msec) to correct responses and number of correct and incorrect responses were recorded for analysis purposes.

**Dual task.** This task ran for 30 min and encompassed single presentations of an auditory tone discrimination task and a compensatory tracking task, followed by the simultaneous presentation (dual) of both tasks. Each test segment took 10 min, and there was a 1-min rest between the single and dual tasks. The auditory tone test required the detection of a 760-Hz tone from a series of 750-Hz tones.

In the compensatory tracking task, subjects used a pressure-type joystick to reposition the moving arrow underneath the stationary arrow. Three sine wave forcing functions created tracking task difficulty levels (hard, medium, easy). The tracking error measurement computed was a 1-min average modulus mean error at each level.

In the dual task presentation, the auditory tone discrimination test was paired with the tracking task. Tracking error, time (msec) to correct responses and correct and incorrect responses were recorded.

**Choice reaction time test.** Arrayed on a 16 x 25-cm response panel in a semicircular pattern were 8 momentary push-button switches with red translucent covers. Centered at the bottom of the panel was a single green button. Subjects kept the green button depressed at all times, removing it only when a red button was lit. There were 80 trials, and 2 reaction times (release time and movement time) were calculated on each trial.

**Memory scanning.** This test was a computerized version of the Sternberg Short Term memory scanning test [8]. Subjects were presented 90 trials (lists) of numbers and each trial consisted of either 2, 4, or 6 digits (monosyllable digits 1-9). Following successive presentation of each trial, another single digit (probe digit) appeared. During this time subjects responded (yes or no) whether or not

---

<sup>a</sup> This manuscript represents the condensation of two separate manuscripts, one prepared by the first author and one prepared by the second author. Each of these manuscripts has been submitted to separate journals for publication and present the research findings in much greater detail than is covered in this manuscript. The article relevant to the blood and breath analysis has been published in *Journal of Occupational Medicine* (1987), 29(11), 877-883. The article relevant to the neurobehavioral effects is scheduled to be published in the *British Journal of Industrial Medicine*.

the probe digit matched a number in the previously presented list. A varied set procedure was used (each trial presented a different list of digits to be remembered). For data analysis purposes, 6 mean reaction times for each set size (list length) and probe type (yes or no) were used.

**Postural sway (steadiness) test.** A measure of postural steadiness was used to determine whether chemical exposures would affect any CNS processes controlling body posture. A computerized biomechanics platform system manufactured by Advanced Mechanical Technology, Inc., (AMTI) was used for testing. Two 30-sec samples, one with eyes closed and one with eyes open, were recorded during every 2-h test period. Data were collected at the rate of 10 samples/sec.

**Profile of mood states (POMS).** This test measures 6 mood or affective states from a factor-analyzed inventory. The test is derived from research by McNair et al. [9]. The 6 affective states measured are tension-anxiety, depression-dejection, anger-hostility, vigor-activity, fatigue-inertia, and confusion-bewilderment. Subjects were instructed to "include their feelings during the past week including today" (1-week POMS) in filling out the test, and it was scored using the "college norm" profile sheet.

#### ***Atmosphere generation and body burden measurement***

Atmospheres were generated by drawing acetone and MEK, 99.43% and 99.46% pure, respectively, from a reservoir through a dual high pressure metering pump (Eldex-Model AA) into a 2 L, three-vertical-neck mixing flask. Chamber airflows provided 2 fresh air changes per hour, with a constant temperature of  $22 \pm 1^\circ\text{C}$  and humidity of  $50 \pm 5\%$ . Chamber atmospheres were sampled from ports calibrated to agree with the subjects' breathing zones at each of the 4 test stations. The atmospheres were monitored by 2 methods: (1) continuous monitoring via Miran 1A infrared analyzers (850 nm) using an Apple IIe computer to control sampling and record readings, and (2) monitoring at 30-min intervals by gas chromatography (Perkin-Elmer 3920). Table 3 summarizes the chamber concentrations by sampling times using data from the infrared analyzers.

Breath samples were collected from subjects immediately upon exit from the chamber in 5-L mylar sampling bags using a 30-sec breath-holding method. The samples were analyzed within 15 min. Blood samples were collected from the antecubital vein upon exit from the chamber in 5-mL heparinized glass tubes and analyzed within 24 h. Analysis was performed by gas-liquid chromatography using the head space technique.

TABLE 3. CHAMBER CONCENTRATIONS FOR CHEMICAL EXPOSURE CONDITIONS

Condition Measure	Average Sample Measurements <sup>a</sup>				
	Hour 1	Hour 2	Hour 3	Hour 4	4 h Mean
Acetone-250 ppm Exposures <sup>b</sup> = 9					
Mean	204.6 ppm	250 ppm	245.2 ppm	249.4 ppm	237.4 ppm
S.D.	17.6 ppm	4.3 ppm	3.9 ppm	4.3 ppm	4.4 ppm
Methyl Ethyl Ketone-200 ppm Exposures = 8					
Mean	155.1 ppm	197.0 ppm	194.5 ppm	198.5 ppm	186.3 ppm
S.D.	26.3 ppm	4.7 ppm	9.4 ppm	6.7 ppm	4.8 ppm
Combination - Acetone and Methyl Ethyl Ketone Exposures = 8					
Acetone-125 ppm					
Mean	100.5 ppm	120.7 ppm	118.4 ppm	121.2 ppm	115.2 ppm
S.D.	17.2 ppm	11.7 ppm	7.9 ppm	3.2 ppm	5.6 ppm
Methyl Ethyl Ketone 100 ppm					
Mean	72.6 ppm	94.6 ppm	91.6 ppm	93.3 ppm	88.1 ppm
S.D.	13.2 ppm	9.7 ppm	9.9 ppm	13.0 ppm	9.3 ppm

<sup>a</sup> S.D. = Standard deviation.<sup>b</sup> Exposures refer to the number of times this treatment condition was run.**Ethanol administration**

Ethanol was administered in a cocktail that contained 0.84 mL/kg 95% ethanol, combined with 100 mL quinine water, 75 cm<sup>3</sup> of orange juice, two drops of tobasco sauce, and crushed ice. Additional quinine and orange juice replaced ethanol in the placebo cocktail.

**RESULTS****Blood and breath analysis**

The results of the blood and breath analysis are presented in Figures 2 and 3 and in Table 4. Sample sizes in Table 4 represent usable blood and breath samples from only the chemical and ethanol conditions. Endogenous concentrations of acetone were detected in most of the pre-exposure blood and breath samples from subjects. Pre-exposure blood concentrations averaged 1.9 µg/mL (S.D. = 1.0), and breath concentrations averaged 0.3 ppm (S.D. = 0.7) for the chemical control group. The other treatment groups showed minor but not significant variations from the

control group. Pre-exposure breath levels of ethanol were detected in trace amounts (see Table 4) in a few subjects. MEK was not detected in any pre-exposure blood or breath samples.

Steady-state breath levels of 8 to 12% for acetone and 5 to 6% for MEK of the chamber concentration were obtained at the 2-h sample period. Steady-state levels for blood were not reached for either chemical within the 4-h exposure period, although the slope of the uptake curve for MEK was less pronounced than the acetone uptake curve. Significant correlation coefficients were obtained between blood and breath measurements for both chemicals. For MEK, it was 0.78 ( $p < 0.001$ ) and for acetone it was 0.61 ( $p < 0.001$ ).

Although graphically (Figures 2 and 3) the results show a consistent trend toward lower blood concentrations in females than males for both solvents, statistically significant differences were not consistently obtained. Statistical significance was only evident in the acetone/MEK combination exposure with the 2-h sample (Kruskal-Wallis = 4.05,  $p = 0.04$ ) and 90-min post-exposure sample (Kruskal-Wallis = 4.47,  $p = 0.03$ ).

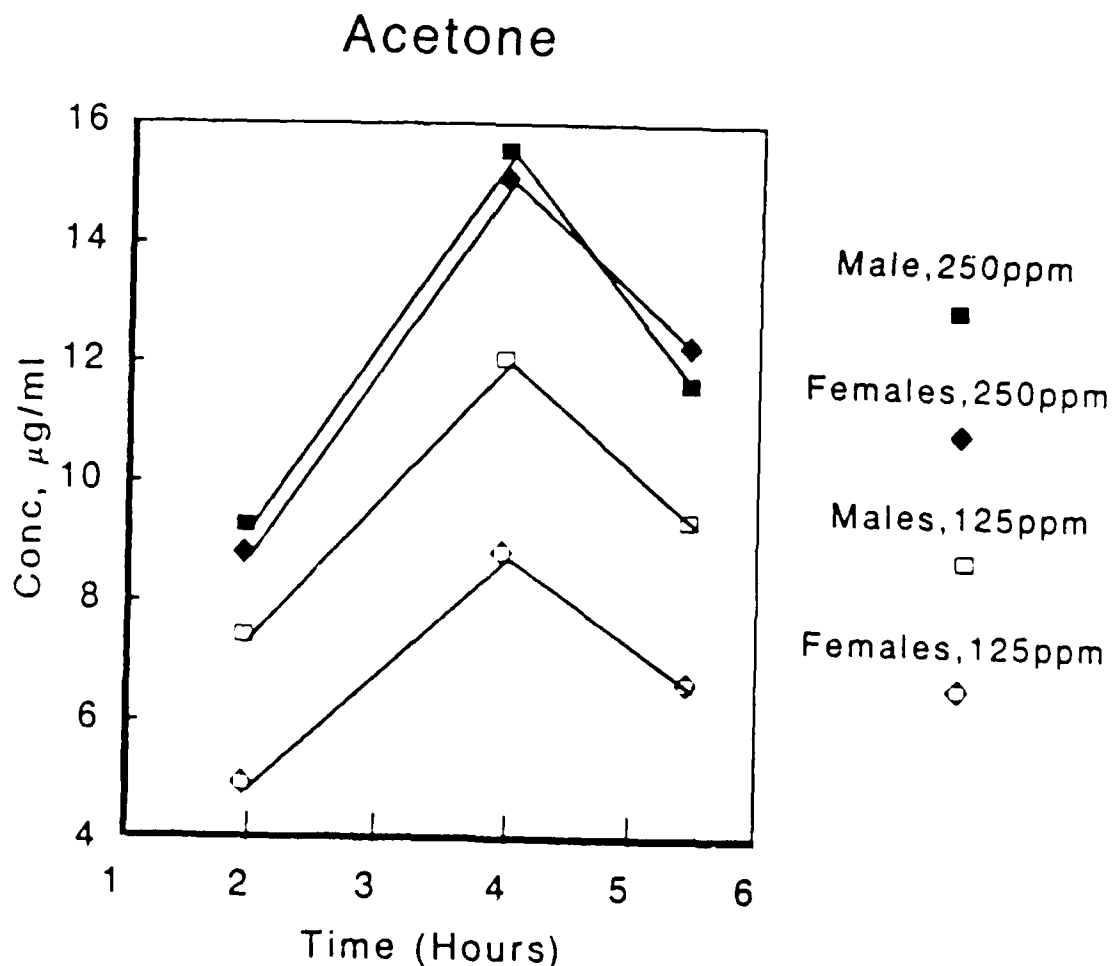


Figure 2. Acetone concentrations in venous blood during and after 4-h inhalation exposures. Time begins with onset of exposure. Data points are means.

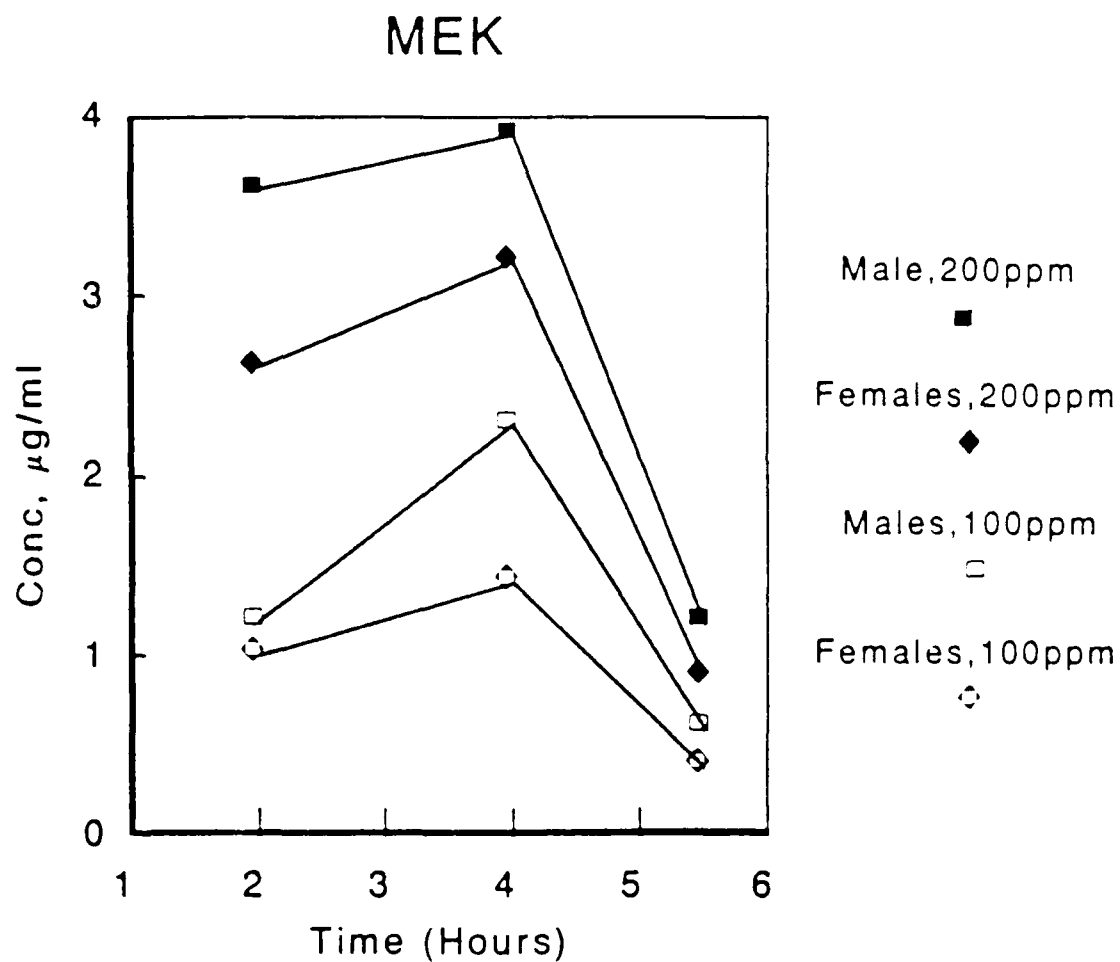


Figure 3. Methyl ethyl ketone (MEK) concentrations in venous blood during and after 4-h inhalation exposures. Time begins with onset of exposure. Data points are means.

TABLE 4. BLOOD AND BREATH CONCENTRATIONS

Condition	Blood Concentration (µg/mL or w/v%) <sup>a</sup>				
	Pre	2 h	4 h	1.5 h Post	20 h Post
Acetone - 250 ppm N <sup>b</sup> = 22					
Mean	2.0	9.0	15.3	11.9	1.5
S.D.	2.0	2.0	2.9	2.6	1.0
MEK - 200 ppm N = 26					
Mean	ND <sup>c</sup>	3.1	3.5	1.0	ND <sup>c</sup>
S.D.		1.1	1.5	0.6	

(continued)

TABLE 4. (Continued)

Condition	Blood Concentration ( $\mu\text{g/mL}$ or $\text{w/v}\%$ ) <sup>a</sup>				
	Pre	2 h	4 h	1.5 h Post	20 h Post
Acetone - 125 ppm N = 22					
Mean	1.9	6.2	10.4	8.0	1.6
S.D.	1.0	1.8	2.4	2.1	1.3
MEK - 100 ppm N = 22					
Mean	ND <sup>c</sup>	1.1	1.9	0.5	ND <sup>c</sup>
S.D.		0.3	0.9	0.3	
Ethanol <sup>d</sup> - 0.84 mL/kg N = 21					
Mean	<0.002	0.062	No Sample	0.0072	<0.001
S.D.		0.01		0.007	
Condition	Breath Concentration (ppm)				
	Pre	2 h	4 h	1.5 h Post	20 h Post
Acetone - 250 ppm N = 22					
Mean	0.4	21.5	25.8	12.8	0.6
S.D.	0.6	4.4	4.0	2.9	0.8
MEK - 200 ppm N = 26					
Mean	ND <sup>c</sup>	11.4	11.9	0.7	ND <sup>c</sup>
S.D.		3.0	3.0	1.1	
Acetone - 125 ppm N = 22					
Mean	0.3	12.9	15.3	8.0	0.6
S.D.	0.7	3.3	2.7	2.4	0.8
MEK - 100 ppm N = 22					
Mean	ND <sup>c</sup>	5.1	5.3	0.7	ND <sup>c</sup>
S.D.		2.9	1.9	1.3	
Ethanol <sup>d</sup> - 0.84 mL/kg N = 21					
Mean	<.01	179.1	85.8	19.0	<.01
S.D.		28.3	38.1	16.4	

<sup>a</sup> Values are means and standard deviations (S.D.) of the tested chemicals and correspond to the treatment condition. Sample times are from the beginning of exposure or ingestion of ethanol, except for the pre-exposure samples. Pre-exposure blood samples were taken on the day previous to exposure and pre-exposure breath samples were taken the morning of exposure. All subjects were tested for ethanol, MEK, and acetone. Pre- and post-acetone values for the non-acetone exposed groups corresponded to the control values reported for the chemical control group. Likewise, MEK and ethanol values for the other groups were non-detectable (ND).

<sup>b</sup> N = number of subjects

<sup>c</sup> 100% of values below detectable limits

<sup>d</sup> Ethanol values are given in  $\text{w/v}\%$ , which corresponds to percent blood alcohol concentration. Ethanol normally peaks 1 h after ingestion, however, the values in the table are from samples 2 h after ingestion. Assuming a standard 15  $\text{mg}\%/\text{h}$  elimination, peak values averaged higher.

For the analysis of all blood sample results involving chemical exposures, pre-exposure acetone values were subtracted from exposure sample values because there were significant sex differences in pre-exposure blood concentrations. Females had lower concentrations than males (Kruskal-Wallis = 4.45,  $p = 0.035$ ). Blood and breath ethanol measurements corresponded to our predicted values and are summarized in Table 4.

### **Behavioral performance measurements**

SAS version 5.15 [11] programs were used to analyze the data. The performance measurements were analyzed using multivariate analyses of variance (MANOVAs) of difference scores, with the chemical groups analyzed separately from the ethanol groups. The MANOVA test statistic reported is the Wilks' Lambda, and statistically significant results were determined using the Hummel-Sligo procedure [12]. With this procedure, significance is necessary on both the multivariate and univariate analysis at a predetermined alpha (0.05) for rejection of the null hypothesis. For measurements that demonstrated significance using this procedure, least-squares means (LSM) comparisons were used to identify treatment group differences on an *a priori* basis. The only comparisons considered were the placebo groups versus their respective treatment groups for the same test period. The above described approach was taken to minimize the experiment-wise (type I) error rate, while still retaining enough statistical power to detect treatment effects. However, the possibility of a spurious significant finding cannot be completely eliminated.

Initial analysis of all the behavioral tests indicated that performance test results from males and females were qualitatively and statistically not different. As a result, except for the POMS test which has shown sex differences on some of the factor scores [9], the sexes were combined for analysis. Preliminary analyses also revealed that tracking task difficulty in the dual task did not interact with the treatment condition, so the difficulty factor was dropped from further analyses. Only 2 tests, the choice reaction time test and the memory scanning test, showed learning effects over time.

For the chemical treatment groups, only the acetone-exposed group showed statistically significant differences from controls that indicated a possible treatment effect. These differences were evident only in the dual task and on the POMS test. In the dual task, only the MANOVA for the auditory tone discrimination task in single presentation revealed significant changes [ $F(9, 197) = 2.52, p < 0.009$ ]. Subsequent univariate analyses showed significant effects on response time ( $p < 0.05$ ) and false alarm percent ( $p < 0.33$ ). Chemical treatment group LSM comparisons with controls showed significant differences only with the acetone group for response time in the Exp:3-4 h period ( $p < 0.002$ ) and in the post:7-8 h period ( $p < 0.006$ ). Response time increases from baseline averaged 12% and 11% over controls for the only two significant test periods. All chemical treatment groups differed significantly from the control group on false alarm percent in all 3 test periods ( $p < 0.007$  to  $0.05$ ), but the acetone group was the most dramatically divergent. Averaging scores across all 3 test periods, the acetone group's false alarm increased by 4%, whereas the control group

decreased 16%. The other two chemical groups, acetone/MEK and MEK, both decreased like the control group, but by a lesser magnitude (4-5%). These differences between the groups more clearly indicate a chemical effect for the acetone group only. Figure 4 graphically shows these results with the corresponding venous blood measurements for each chemical group.

### Auditory Tone – Single Presentation Response Time, False Alarm % and Venous Blood Levels

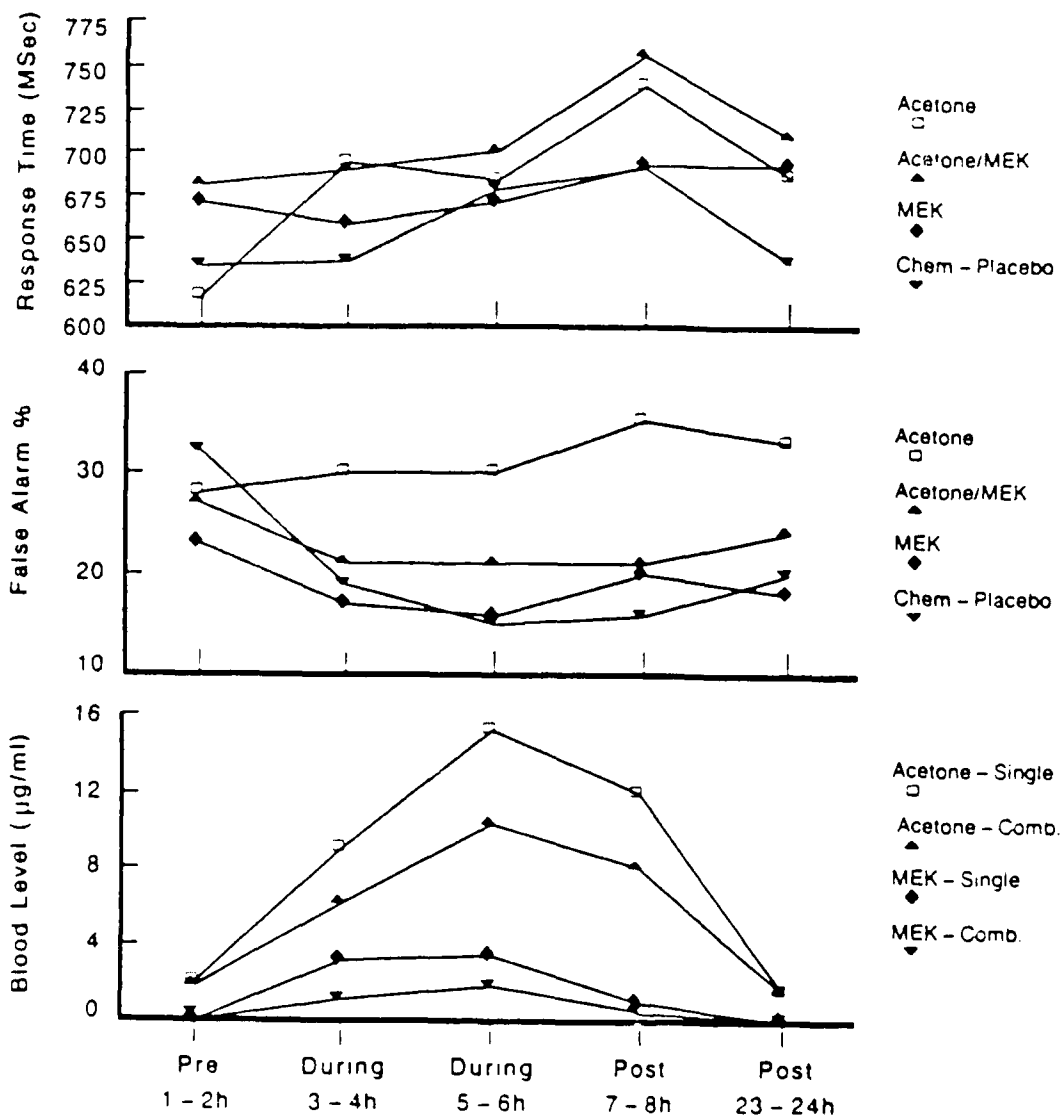


Figure 4. Response time, false alarm percent rate on the auditory tone discrimination task (single presentation) and venous blood levels for each chemical condition.

The POMs test showed no significant chemical main effects, but there was a significant chemical X sex interaction [ $F(18,207) = 1.76, p < 0.03$ ]. The only significant univariate was on the anger-hostility scale ( $p < 0.02$ ). Condition X sex LSM comparisons revealed the effect was significant only for males exposed to acetone ( $p < .001$ ).

In the ethanol group's analyses, the dual task measurements in both single and dual presentation showed several statistically significant differences. In addition, the false alarm rate in the visual-vigilance test was increased over controls, but at a significance level (0.058) slightly above the chosen alpha cutoff. In the auditory tone discrimination task, ethanol effects were present in single presentation [MANOVA, condition  $F(3,38) = 6.39, p < 0.001$ ]. Ethanol also produced significant MANOVAs in dual presentation (auditory tone and tracking) for condition [ $F(4,37) = 4.79, p < 0.003$ ] and condition X period [ $F(8,152) = 2.02, p < 0.048$ ]. Ethanol effects were present on all response variables in the auditory tone single presentation, but only for response times and percent correct hits in the auditory tone dual presentation. Single auditory tone presentation results averaged across the 3 periods for the ethanol group showed a 10% increase in response time, a 12% decrease in correct hits, and a 10% decrease in false alarm percent over controls for comparable periods. In dual presentations, significant effects from univariate analysis ( $p < 0.05$  to  $p < 0.001$ ) occurred with response times, percent correct hits, and tracking error. The significant (LSMs) effects were in the 2 exposure periods for response times and tracking errors and in all 3 periods for percent correct hits. Increases averaged about 14% for response time in the 2 exposure periods compared to only a 2% increase for controls. Tracking error scores increased 23% for the ethanol group in the 2 periods, while controls only increased 2 to 3%. Correct hits averaged a 13% drop for exposed vs. a 2% increase for controls across all three periods. Figures 5 and 6 depict the effects of ethanol on the dual task.

Other tests, such as choice reaction time, postural sway, and memory scanning, did not reveal any statistically significant differences in the chemical conditions. Ethanol did show some marginal effects on the choice reaction time test and in some of the postural sway tests (0.09 MANOVA). The CRT results were improved movement time in the post:7-8 h period only. Postural sway measurements of area, length, and velocity of sway showed increases in the ethanol group over the corresponding ethanol control group. The POMS test was unaffected by ethanol.

## DUAL TASK

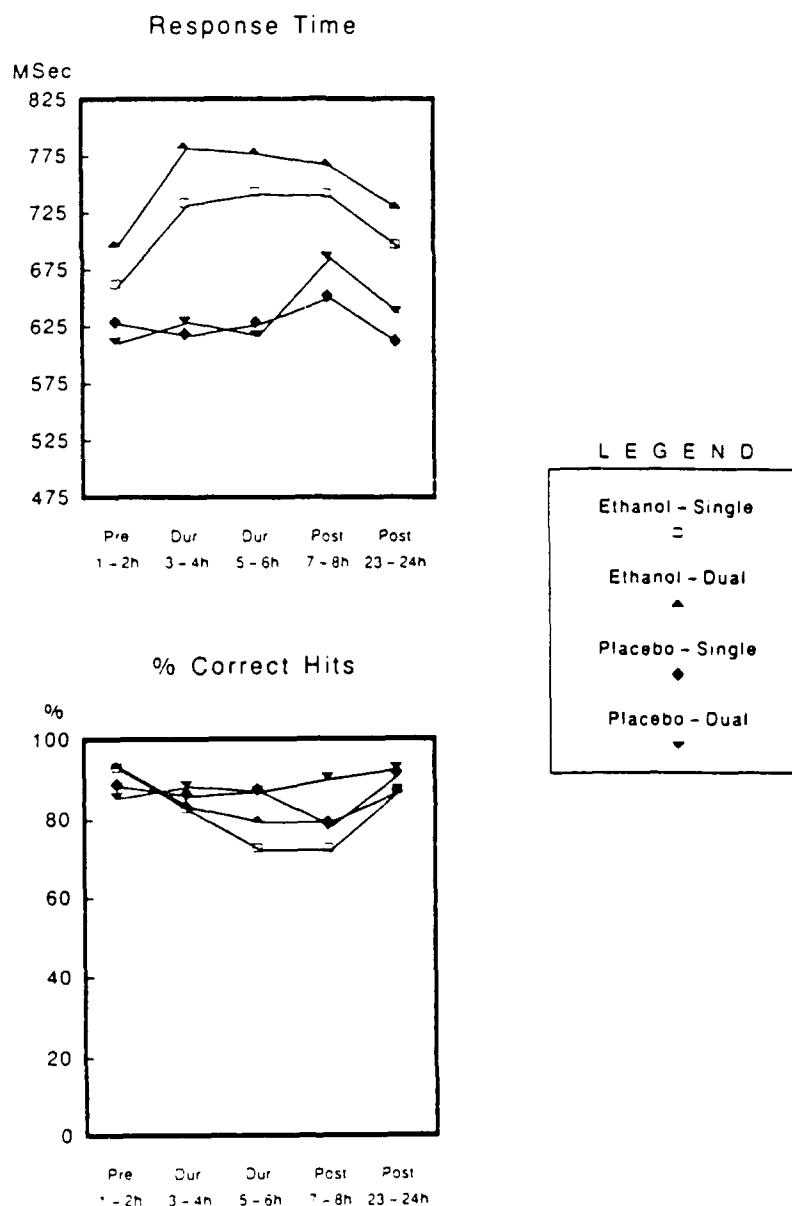


Figure 5. Ethanol response measurements for the dual task (response time and percent correct hits). Data points are group means.

### DISCUSSION

The biochemical indicators for blood and breath, which are summarized in Table 4, indicate that the desired body burden levels were obtained. In the 4-h exposure used in this study, the average blood concentrations of acetone and MEK continued to rise, although less so for MEK than acetone. The slopes also were very consistent when single exposures were contrasted with combination exposures. This probably indicates the lack of any significant metabolic interaction with

these 2 chemicals at the tested exposure concentration and duration. The acetone blood level results are in agreement with two previous studies [13,14], although some extrapolation is necessary. MEK blood levels were in agreement with our previous work [15]. Alveolar breath samples had generally reached steady-state levels by the 2-h sample, stabilizing at 8 to 12% of the exposure concentration for acetone and 5 to 6% for MEK. These results are consistent with research involving acetone [16] and with a previous study in our laboratory on MEK [15].

## DUAL TASK

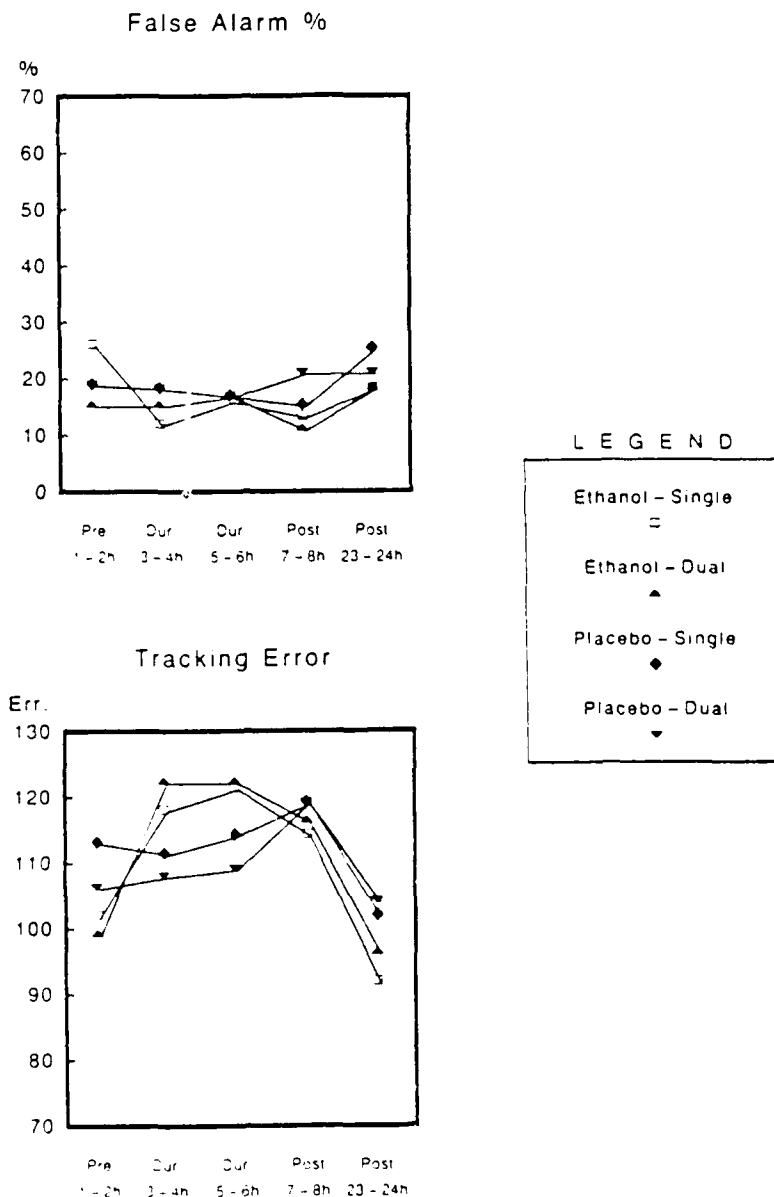


Figure 6. Ethanol response measurements for the dual task (false alarm percent and tracking error). Data points are group means.

The limited number of blood samples obtained from each subject prevents the accurate calculation of an overall elimination half-life. However, if first-order kinetics is assumed, the estimated half-lives for MEK and acetone are 49 min and 3.9 h, respectively. With some speculation, individuals exposed to these solvents for up to 8 h in a normal workday might have residual body burden concentrations of acetone the next day, but MEK should have been completely eliminated. Our present study showed no significant increases of acetone over endogenous levels the morning after exposure. A study by Matsushita et al. [14], using a 6-h exposure duration for 6 consecutive days, did show a residual build-up with a 500-ppm exposure concentration. In that study, the 250-ppm concentration did not show any build-up over the 6-day exposure. Results from our study showed no detectable levels of MEK in the blood or breath the morning following exposure, and more than half of the subjects had non-detectable levels of MEK in the breath samples taken 90 min post-exposure.

While not statistically confirmed by the results in this study, there is the strong suggestion of sex differences in the uptake of acetone and MEK. Examination of Figures 2 and 3 tend to show lower uptake curves for females than males. The differences were only statistically significant in the combination exposure to acetone (125 ppm) and only when corrected for sex differences in baseline acetone blood concentrations. Small sample sizes precluded the use of more powerful statistical tests, thereby limiting the interpretation of these results.

Neurobehavioral performance test results indicated some mild, but detectable, effects caused by one of the chemical treatment conditions in the auditory tone discrimination task, and in one scale on the POMS test. The results were only significant with the single acetone exposure to 250 ppm. In the auditory tone discrimination test (single presentation), the acetone-exposed group had increases in response time to correct hits and in the false alarm percent rate. When compared to the other chemical groups, the acetone group scores on the false alarm rate reached a plateau and did not improve. Similar delays in test score improvement with an acetone exposure were shown by the Matsushita et al. [14] 6-day exposure experiment. With the POMS test, the statistically significant difference occurred only for males on the anger-hostility scale. With the large number of statistical tests calculated in this study, and with no consistent trend indicated on the POMS test, this is one finding that may be due to chance.

Ethanol caused statistically significant differences from controls on all auditory tone discrimination measures in the single presentation mode, and on all measures except false alarm percent in the dual presentation mode. The other test in the dual task, tracking, was only affected by ethanol in dual presentation. This latter result is consistent with other dual task research involving

ethanol [17]. Although not significant at the predetermined alpha of .05, the visual-vigilance test ( $p = 0.058$ ) and some postural sway measures ( $p = 0.09$ ) suggest ethanol effects.

The strength of the acetone effects should be interpreted cautiously. Statistically significant results occurred in only one of the neurobehavioral tests (the dual task), and on only one scale of the POMS test. The measurable differences were only on 2 of the several neurobehavioral measures analyzed. For the 2 performance measures affected (dual task-response time and false alarm percent), the decrements compared to the control group were roughly 11-12%. Notably, significant performance decrements from exposures to acetone occurred with some consistency throughout the 2 exposure periods and even into the Post:7-8 h period. The results also paralleled the blood concentrations for acetone (see Figure 4), which rose throughout the 4-h exposure and were still close to the 2-h sample 90 min after cessation of exposure. The other chemical groups did not have blood concentrations this high, although the combination exposure behaved similarly because of the presence of acetone.

In summary, some small but statistically significant effects were detected during and after a 4-h exposure to 250-ppm acetone. The performance decrements from the acetone treatment were not as dramatic as an ethanol ingestion, which caused more severe decrements on the psychomotor tests. Performance changes from the acetone exposures demonstrated some persistence and paralleled the venous blood levels of acetone, indicating that tolerance did not develop. The results from this study agree with an earlier report by Matsushita et al. [14] that also found some mild decrements in psychomotor performance with 250-ppm exposures to acetone. Acetone is considered to be one of the less toxic solvents and currently has a relatively high OSHA-PEL of 1000 ppm [6]. The findings in this study suggest that further research may be necessary to determine whether exposures to acetone in concentrations approaching 1000 ppm for at least 4 h may produce more distinct CNS performance decrements.

Exposures to 200-ppm MEK showed no interpretable statistically significant results. Furthermore, there were no significant interaction effects with the combination exposure of acetone (125 ppm) and MEK (100 ppm) for either the neurobehavioral or biochemical measures at the concentrations tested in this study.

#### ACKNOWLEDGMENTS

The following individuals contributed significantly to the outcome of the study: Jay Kiemme, M.D.; Richard L. Hawks, Ph.D.; Amit Bhattacharya, Ph.D.; Randy Smith, M.S.; Pam Schumacher; Margaret Regan.

## REFERENCES

- 1 Curtis M.F. and Keller, L.W. (1987) Exposure issues in the evaluation of solvent effects: Report of the workshop session on exposure issues. In: J.M. Cranmer and L. Goldberg (Eds.), *Proceedings of the Workshop on Neurobehavioral Effects of Solvents*. Neurotoxicology 7(4), 5-24.
- 2 Saida, K., Mendell, J.R., and Weiss, H.S. (1976) Peripheral nerve changes induced by methyl *n*-butyl ketone and potentiation by methyl ethyl ketone. *J. Neuropath. Exp. Neurol.* 35, 207-225.
- 3 Spencer, P.S., Schaumberg, H.H., Sabri, M.I., and Veronesi, B. (1980) The enlarging view of hexacarbon neurotoxicity. *CRC Crit. Rev. Toxicol.* 7, 279-356.
- 4 Krasavage, W.J., O'Donoghue, J.L., and DiVincenzo, G.D. (1982) Ketones. In: G.D. Clayton and F.E. Clayton (Eds.), *Patty's Industrial Hygiene and Toxicology*, John Wiley & Sons, New York, pp. 4709-4800.
- 5 Code of Federal Regulations 29 CFR 1910.1000, Table Z-1, Z-2 (June 1981) U.S. Printing Office, Washington, DC.
- 6 U.S. Department of Health and Human Services, Public Health Service, Centers for Disease Control. (Sept. 26, 1986) NIOSH. Recommendations for Occupational Safety and Health Standards. *Morbidity and Mortality Weekly Report-Suppl.* 35(1s).
- 7 Mackworth, N.H. (1961) Research on the measurement of human performance. In: H.W. Sinaika (Ed.), *Selected Papers on Human Factors in the Design and Use of Control Systems*, Dover, New York, pp. 174-331.
- 8 Sternberg, S. (1975) Memory scanning: New findings and current controversies. *Q. J. Exp. Psychol.* 27, 1-32.
- 9 McNair, D.M., Lorr, M., and Droppleman, L.F. (1981) EITS manual for the profile of mood states, Educational and Industrial Testing Service, San Diego, CA.
- 10 Jones, R.H., Elliott, M.F., Cadigan, J.B., and Gaensler, E.A. (1958). The relationship between alveolar and blood carbon monoxide concentrations during breath-holding: Simple estimate of CoHB saturation. *J. Lab. Clin. Med.* 51, 553-564.
- 11 SAS Institute Inc. (1985) SAS User's Guide: Statistics, Version 5 Edition. SAS Institute Inc., Cary, NC.
- 12 Barker, H.R. and Barker, R.M. (1984) Multivariate analysis of variance (MANOVA). University of Alabama Press, Alabama University, Tuscaloosa.
- 13 Wigaeus, E., Holm, S., and Astrand, I. (1981) Exposure to acetone: Uptake and elimination in man. *Scand. J. Work Environ. Health* 7, 84-94.
- 14 Matsushita, T., Goshima, E., Miyakaki, H., Maeda, K., Takeuchi, Y., and Inoue, T. (1979) Experimental studies for determining the MAC value of acetone. 2. Biological reactions in the "six-day exposure" to acetone. *Sangyo Igaku*, 11(10), 507-515.

- 15 Dick, R.B., Setzer, J.V., Wait, R., Hayden, M.B., Taylor, B.J., Tolos, B., and Putz-Anderson, V. (1984) Effects of acute exposure of toluene and methyl ethyl ketone on psychomotor performance. *Int. Arch. Occup. Environ. Health*, 54, 91-109.
- 16 Tada, O., Nakaaki, K., and Fukabori, S. (1972) An experimental study on acetone and methyl ethyl ketone concentrations in urine and expired air after exposure to those vapors. *J. Sci. Labour* 48(6), 305-336.
- 17 Moskowitz, H. (1973) Psychological tests and drugs. *Pharmakopsychiat* 6, 114-126.
- 18 Nakaaki, K. (1974) An experimental study on the effect of exposure to organic solvent vapor in human subjects. *J. Labour. Sci.* 50(21), 89-96.

## A REVIEW OF PROPYLENE GLYCOL DINITRATE TOXICOLOGY AND EPIDEMIOLOGY

Samuel A. Forman

*Ivorydale Technical Center, Procter and Gamble Company, 5299 Spring Grove Avenue, Cincinnati, OH*

The views presented are those of the author and do not represent the official position of the United States Naval Medical Command or the Department of the Navy.

### SUMMARY

Propylene glycol dinitrate (PGDN) is a rapidly metabolized, nitrated ester explosive propellant with acute cardiovascular effects at lower levels of exposure and methemoglobinemia and vascular collapse at higher ones. Exposure can be by dermal or inhalation routes. Toxicology has played an important role in setting workplace-permissible exposure limits, which have been limited by vascular headaches and subtle, transient decrements in central nervous system performance. Less well characterized is the etiology of excess, long-term cardiac morbidity in PGDN-exposed workers. Human central nervous system degeneration and links to infectious diseases are unsubstantiated concerns.

### INTRODUCTION

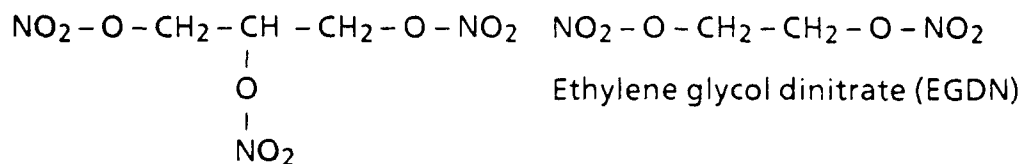
#### *Properties*

Propylene glycol dinitrate (PGDN) is a nitrated ester explosive similar to ethylene glycol dinitrate (see Figure 1). It is a colorless liquid with a density of 1.4 g/ml, a boiling point of 92°C, and is sparingly water soluble at 0.13 g/100 ml water. Its vapor pressure is 0.07 mm Hg at 22.5°C. PGDN synonyms include methylnitroglycol, propanediol dinitrate, propylene glycol dinitrate, and dinitrate propylene glycol. It is most frequently used in the military propellant, Otto Fuel II. Named after its inventor, Otto Reitlinger, Otto Fuel II is approximately 75% PGDN; more than 20% di-*n*-butyl sebacate, a desensitizer; and the balance is 2-nitrophenylamine, a stabilizer. It is an oily, reddish-orange liquid with a distinctive odor. Due to its low vapor pressure and pharmacologic activity, PGDN is the fuel's principal component from a toxicologic and exposure standpoint.

#### *Acute animal studies*

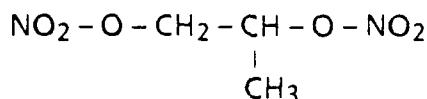
Preliminary toxicology work related to PGDN was done in the 1960s. Kylin et al. [1] studied the acute toxicologic parameters of PGDN, ethylene glycol dinitrate (EGDN), and nitroglycerin (NTG) both *in vivo* and *in vitro*. The LD<sub>50</sub> was determined in one strain of albino female mice by intraperitoneal injection of a 2% solution of each compound in a 10% soy oil emulsion. Twenty mice, averaging 20 g, were dosed in each group. There were 5 dose levels set at logarithmic increments. Controls received the pure soy emulsion. LD<sub>50</sub> determinations revealed PGDN at 930 mg/kg (800 - 1075, 95%

confidence interval), EGDN at 800 mg/kg (661 - 964), and NTG at 194 mg/kg (164 - 228). NTG was about four times as toxic to mice as the other two nitrated esters. Mode of death differed for NTG. Mice exposed to NTG expired within 1 h of injection and suffered convulsions. Expiring animals in the groups exposed to PGDN and EGDN did not exhibit pre-morbid convulsions and most exceeded 1 h to demise.



Ethylene glycol dinitrate (EGDN)

Glyceryl trinitrate (Nitroglycerin)



Propylene glycol dinitrate (PGDN)  
Use: Torpedo propellant -- Otto fuel II



Triethylene glycol dinitrate (TEGDN)  
Use: Proposed torpedo propellant -- NOSET - A

**Fig. 1 Chemical structure of nitrate esters. (Reproduced from Horvath et al. [9] by permission.)**

Kylin et al. [1] also studied blood elimination in 2.5-kg rabbits. Each compound was injected as a single dose of 1 mg/kg body weight in one femoral vein, while serial arterial and venous samples were taken on the contralateral side. Samples were assayed for each compound by gas chromatography. At 1 min, 15% of injected PGDN was found in arterial blood and 3 to 5% in venous samples. At the same time, EGDN and NTG were found to be at almost 30% of initial concentrations. By 2 min, the rates of elimination for PGDN, EGDN, and NTG were the same. This is an extremely rapid breakdown, exhibiting first order kinetics with only slight differences among PGDN, EGDN, and NTG (Figure 2).

In the same report, Kylin et al. [1] reported on *in vitro* metabolism. There were no notable differences in whole blood or liver homogenate among the exposed subjects. In a reduced glutathione solution, there was breakdown of NTG, but not of PGDN or EGDN, a situation suggesting a difference in metabolism for NTG.

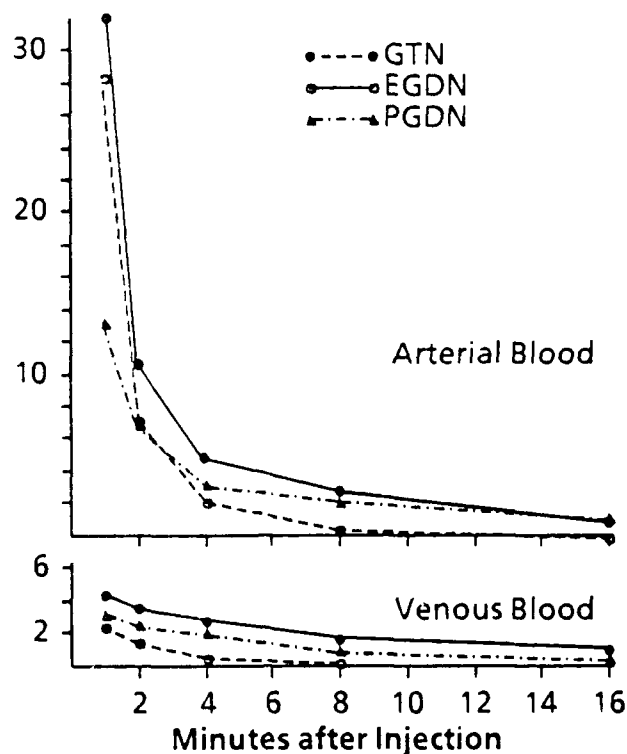


Fig. 2 Rabbit *in vivo* elimination of three nitrate ester explosives followed in arterial and venous blood following injection. (Reproduced from Kylin et al. [1] by permission.)

Further studies were guided by PGDN's similarity to other nitrated esters, with their associated human vasodilatory actions via transdermal, buccal, intravenous, or inhalation exposures and allegations of workplace headaches, hypotension, methemoglobinemia, post-exposure angina pectoris, and sudden death [2].

Clark and Lichtfield [3] extended acute toxicology observations to several animal species. Lethal doses and skin penetration, as well as methemoglobin formation, blood pressure response, and metabolites were studied following acute exposure. LD<sub>50</sub> determinations were made with a 10% PGDN solution in corn oil delivered orally or subcutaneously in 200 to 250-g rats, 20 to 35-g Alderly-Park albino mice, or 2.0 to 4.0-kg cats. PGDN was less toxic when administered orally than subcutaneously. Cats were twice as sensitive as rats, which in turn were twice as sensitive as mice (Table 1). The LD<sub>50</sub> dose in rats resulted in almost complete conversion of hemoglobin to methemoglobin, with lower conversion rates at lower doses (Figure 3). Death was likely due to anoxia. Methemoglobin levels were not measured in the mice or cats, but pre-morbid signs were consistent with methemoglobinemia in these species as well.

TABLE 1. ACUTE LD<sub>50</sub> OF PGDN IN VARIOUS ANIMAL SPECIES.

Species	Sex	Route of Administration	LD <sub>50</sub> and 95% Confidence Interval (mg/kg)
Rat	F	Oral	1190 (970-1460)
Rat	F	Subcutaneous	463 (428-500)
Rat	M	Subcutaneous	524 (474-580)
Mouse	F	Subcutaneous	1208 (1125-1285)
Cat	F	Subcutaneous	200-300

(Reproduced from Clark and Lichtfield [3] by permission)

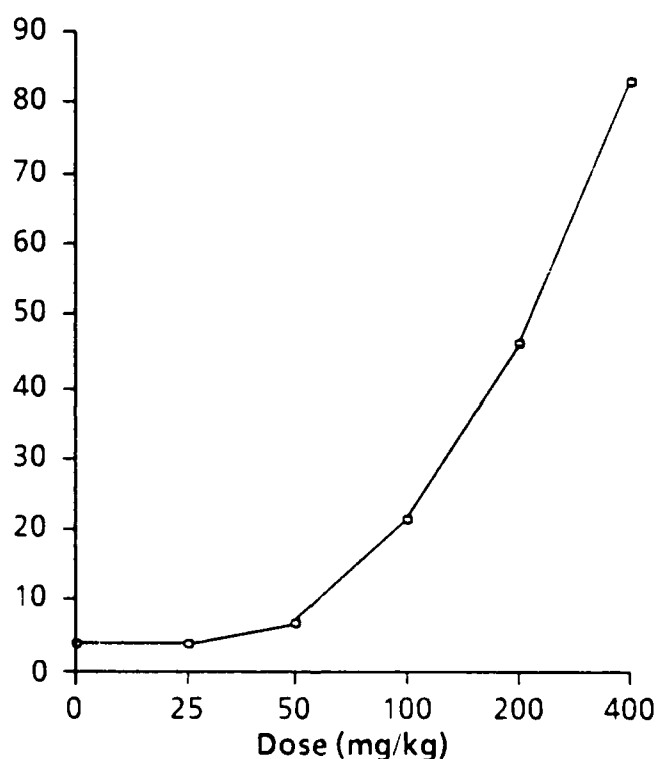


Fig. 3 Methemoglobin dose-response curve after subcutaneous injection of PGDN in the rat. Each point is the mean of two experiments. (Reproduced from Clark and Litchfield [3] by permission.)

Blood pressure effects were recorded from cannulized femoral arteries in anesthetized rats following subcutaneous injection of PGDN. Maximal falls in blood pressure occurred within 30 min after injection (Figure 4). Small responses were seen at 5 mg/kg dose, with small incremental effects occurring above 40 mg/kg (Figure 5). Topically applied PGDN at 50 mg/kg resulted in a 7-mm Hg blood pressure fall, an equivalent effect to the 5 mg/kg injection. The authors inferred that at least 10% of topically administered PGDN penetrated the rat cutaneously.

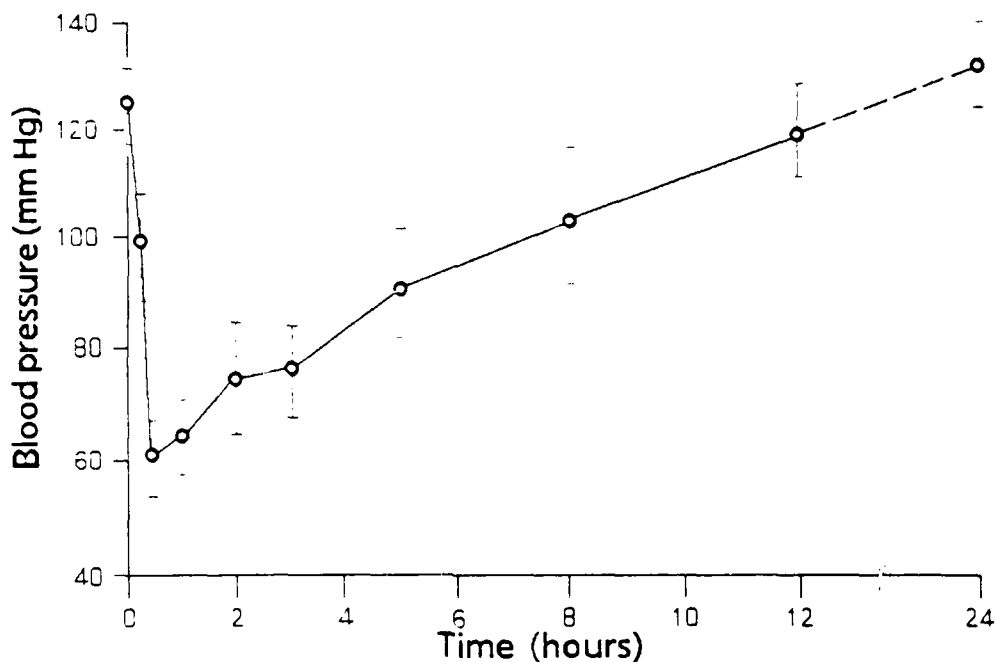


Fig. 4 Blood pressure changes and the blood levels of PGDN, inorganic nitrate, and inorganic nitrite following the subcutaneous injection of 65 mg/kg PGDN in the rat. Each point is the mean of five estimations. The mean coefficients of variation of the points on the curves are 27% for PGDN, 26% for nitrate, and 25% for nitrite. (Reproduced from Clark and Litchfield [3] by permission.)

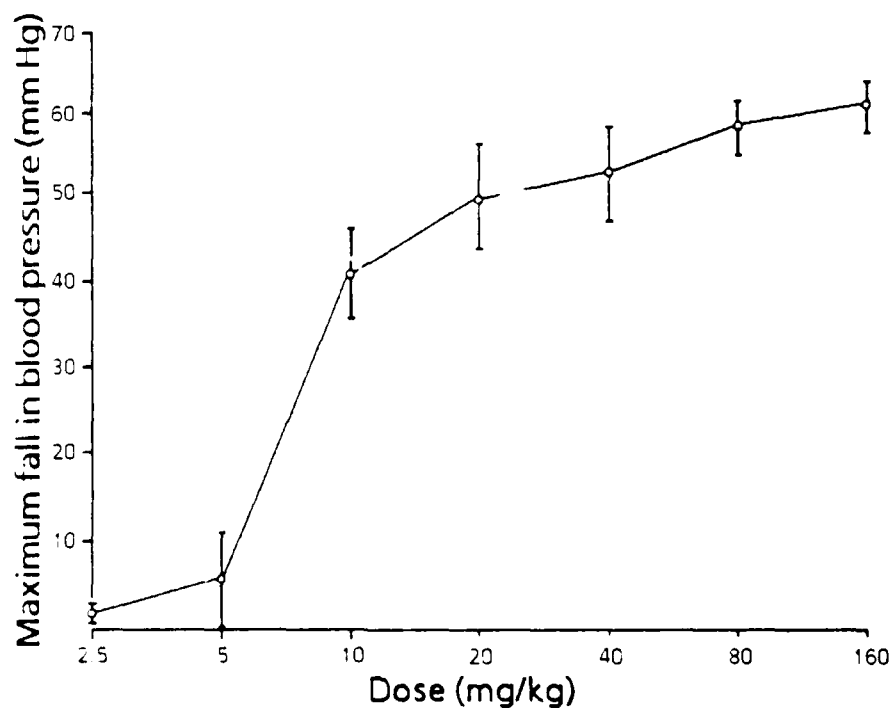


Fig. 5 Mean arterial blood pressure dose-response curve after subcutaneous injection of PGDN in the rat. (Reproduced from Clark and Litchfield [3] by permission.)

*In vitro* metabolic studies revealed metabolism in the blood takes place in the erythrocytes and by 3 h yields mostly propylene glycol 2-mononitrate (PGMN-2) and inorganic nitrate, with the remainder being PGMN-1 isomer and unmetabolized PGDN. Fifty percent of the PGDN is broken down in the first hour and 50% of the remainder in the subsequent hour. PGMN-2 was also the predominant metabolite *in vivo*. Inorganic nitrate was the major metabolite in 24-h urinary excretion, accounting for 56% of the original injection.

These investigators found little to distinguish PGDN metabolism from that of EGDN [4]. Both are rapidly broken down in the circulation to a mononitrate, an inorganic nitrate, and a nitrite. The mononitrates are, in turn, metabolized and excreted as inorganic nitrate. The authors attributed the arterial blood pressure lowering to arteriolar and venous dilation, similar to that noted with NTG. Since the effect is maximal when PGDN concentration is highest, the PGDN most likely acts directly on the blood pressure.

Jones et al. [5] investigated animal dermal and inhalation toxicology, because human exposures would include munition workers exposed through breathing and topical contact. Rabbit skin applications were made daily for a 20-day subacute study. At 1 mg/kg, there was reversible erythema and no signs of systemic effect. At 2 mg/kg, the rabbits appeared weak, slightly cyanotic, and had rapid, shallow breathing. At 4 mg/kg, 13 of 14 animals were dead by the fifth application. Methemoglobin was measured at 34.5% at death. Autopsies showed an overall weight loss and dark, blue-gray internal organs.

PGDN combustion products include carbon monoxide and cyanide gas. Acutely toxic at low levels, these gases have caused concern for possible accidental ignition in enclosed spaces. The toxicology of combustion products is well known and outside the scope of this review.

#### ***Subchronic animal studies***

Jones et al. [5] also conducted continuous (24 h/day) inhalation chamber studies in 4 animal species for 90 days. Fifteen NMRI/O Sprague-Dawley (SD)-derived rats of both sexes, 15 NMRI (ASH) Princeton or FTD/Hartley-derived guinea pigs of both sexes, 9 male squirrel monkeys (*Saimiri sciureus*), and 2 male beagle dogs were dosed in each of 3 exposure levels. PGDN exposures  $\pm$  standard deviation were  $67 \pm 8$ ,  $108 \pm 11$ , and  $236 \pm 24$  mg/m<sup>3</sup> of air. Weight gain was similar for all animal groups. At 67 mg/m<sup>3</sup>, the dogs had hepatic hemosiderin deposition in sinusoids, bile canaliculi, and Kupfer cells. Similar pigment was found in renal proximal convoluted tubules. At 108 mg/m<sup>3</sup>, guinea pigs showed foci of pulmonary hemorrhage. Monkeys and dogs showed hepatic and renal iron-positive granules.

Heavy iron-positive deposits, vacuolar change, and focal necrosis were present in the livers, spleens, and kidneys of dogs and monkeys at 236-mg/m<sup>3</sup> exposures. Similar changes occurred in

female rats and in 4 of 9 monkeys. Percent methemoglobin values were measured in the 236-mg/m<sup>3</sup> exposure groups. Peak values of about 20% were found in dogs and monkeys at week 2, while rats and guinea pigs had much lower values. Monkeys had increased serum urea nitrogen and decreased alkaline phosphatase at 108 mg/m<sup>3</sup> and 236 mg/m<sup>3</sup>, suggesting the possibility of renal damage. Dogs showed marked decreases in hemoglobin and hematocrit at the highest exposure levels. Four monkeys, trained to perform a visual discrimination test, showed no changes in behavior patterns after a 90-day continuous exposure to 262 mg/m<sup>3</sup>.

Based on their animal work and anecdotal industrial observations, Jones et al. [5] recommended a PGDN limit of 1.2 mg/m<sup>3</sup> as a permissible human exposure limit for a 40-h work week. The U.S. Navy adopted an exposure guideline of 1.3 mg/m<sup>3</sup>, or 0.2 ppm, as a ceiling concentration.

### ***Mutagenesis***

Concerns with potential mutagenic or teratogenic health effects accompanied military and industrial PGDN use. Mutagenic assays utilized Otto Fuel II [6]. Negative results were found in the Ames Salmonella assay with or without liver microsomal activation, sister chromatid exchange in L5178Y mouse lymphoma cells, mouse bone marrow cytogenetic analysis, and mouse-dominant lethal assay. The material was mutagenic in the mouse lymphoma forward-mutation assay, but only under conditions directly toxic to cells.

### ***Acute human exposures***

Concern shifted to potential human effects that could not be assayed by animal work and to long-term human outcomes [7]. Stewart et al. [8] exposed human volunteers in a controlled environment chamber to PGDN vapors at 0.2 mg/m<sup>3</sup> (0.03 ppm), 0.65 mg/m<sup>3</sup> (0.1 ppm), 1.3 mg/m<sup>3</sup> (0.2 ppm), 2.3 mg/m<sup>3</sup> (0.35 ppm), 3.25 mg/m<sup>3</sup> (0.5 ppm), and 9.75 mg/m<sup>3</sup> (1.5 ppm) for single or daily exposures of various time periods (Table 2). Seventeen male volunteers ages 22 to 25 years participated.

At the 0.65 mg/m<sup>3</sup> exposure level, two subjects had mild headaches. At 1.3 mg/m<sup>3</sup>, 7 of 9 people had headaches, and most could detect the odor for just 5 min. There was an alteration in visual evoked response (VER). On repeat exposures, the headaches decreased dramatically.

At 2.3 mg/m<sup>3</sup>, the transient odor detection was again found. All subjects exposed for more than 2 h suffered headaches. VER morphology changes were the only objective decrement.

TABLE 2. HUMAN RESPONSE TO AIRBORNE PGDN EXPOSURES AT 0.01 TO 1.5 PPM FOR 1 OR MORE HOURS  
TO SINGLE AND REPEAT DAILY EXPOSURES

RESPONSE TO PGDN EXPOSURE

Group	0.01-0.03 ppm			0.1 ppm			0.21-0.26 ppm			Repeated exposure to 0.2-0.3 ppm					0.33-0.37 ppm			0.47-0.51 ppm			1.2-1.5 ppm		
	1 h 4 h 8 h			1 h 4 h 8 h			1 h 2 h 8 h			Day Day Day Day Day					1 hr 2 h 8 h			1 h 2 h 7.3 h			1 h 3.2 h		
	1 h	4 h	8 h	1 h	4 h	8 h	1 h	2 h	8 h	2	3	4	5	9	1 hr	2 h	8 h	1 h	2 h	7.3 h	1 h	3.2 h	
No. of subjects	2	3	3	2	3	3	3	3	12	9	9	9	9	9	3	3	3	3	3	3	2	6	
No. detecting odor	0	0	0	0	0	0	2	3	2	0	3	1	3	3	1	2	2	1	1	2	2	6	
No. developing mild headache	0	1	0	0	1	1	0	2	5	3	3	0	1	1	0	3	1	1	2	0	0	0	
No. developing severe headache	0	0	0	0	0	0	0	0	6	0	0	0	0	0	0	0	2	0	1	3	2	6	
No. developing eye irritation	0	0	0	0	0	0	0	0	1	0	0	0	0	0	0	1	0	0	0	0	2	6	

(Reproduced from Stewart et al [8] by permission)

The odor was more pronounced at a 3.25-mg/m<sup>3</sup> exposure. Progressive throbbing headaches were noted by 7 of 9 people. After 6 h, 1 person was dizzy and nauseated. By 8 h, 3 had abnormal Romberg and heel-to-toe neurologic tests. The same 3 had narrowed pulse pressures with a 12 mm Hg increase in diastolic pressure. With the exception of VER, no other changes were noted.

At the 9.75-mg/m<sup>3</sup> exposure level, all 8 subjects could detect an odor and all developed headaches. All had eye irritations by 40 min of exposure. Headaches were so severe that exposure was stopped at 3 h, though all symptoms resolved in the subsequent 8 h.

None of these exposures elevated blood nitrate or methemoglobin levels. After 1 h at 9.75 mg/m<sup>3</sup>, expired breath showed 20 to 35 ppb PGDN and serum levels were below the 5-ppb limit of detection.

The most striking feature of the VER was its cumulative effect with daily repeat exposures. There was no biochemical or hematologic evidence of target organ damage in the studied exposure ranges. This study showed pharmacological activity, including headaches and VER changes, at and below the workplace exposure guideline then in effect.

#### ***Chronic human exposures***

Horvath et al. [9] studied 87 Naval employees chronically exposed to PGDN in the form of Otto Fuel II and a smaller number of controls. The PGDN-exposed group noted acute headaches and nasal congestion of presumed vascular origin, but no chronic cardiovascular or neurotoxicity disorders. Following an acute exposure, subjects experienced a decline in saccade velocity and delay time: quantifiable oculomotor functions under central nervous system control (Table 3). This occurred after airborne exposures below the Threshold Limit Value of 0.2 ppm (1.3 mg/m<sup>3</sup>), and was a factor in the decision by the American Conference of Governmental Industrial Hygienists to reduce its exposure guideline to .32 mg/m<sup>3</sup> (0.05 ppm) [10]. The saccade velocity and delay decrements were not seen in the chronically exposed workers.

#### ***Epidemiology***

Safe industrial work with PGDN has been a goal of much of the animal and laboratory research. Epidemiologic approaches to workplace use permits a view of human health experience under actual PGDN use conditions. Helmkamp et al. [11] approximated relative incidence rates by calculating odds ratios for cardiovascular and neurologic diagnoses incriminated in previous research with EGDN and NTG. These diagnoses were from International Classification of Diseases (ICD-8) coded inpatient hospitalizations and deaths recorded for (1) Naval torpedomen munition workers qualified to repair PGDN weapons (TM exposed), (2) comparable workers not using PGDN, and (3) an unrelated group of sailors involved in weapons guidance. The study period was from 1966 through 1979. Analysis

**TABLE 3. RESULTS OF OCULOMOTOR AND QUANTITATIVE ATAXIA TESTS BEFORE AND AFTER AN ACUTE OCCUPATIONAL EXPOSURE (Turnaround-TA)**

	Before TA <sup>a</sup> (N = 29)	After TA <sup>a</sup> (N = 29)	Difference	Probability <sup>b</sup>
Saccade maximum velocity (degrees/sec)	516.6 ± 92.1	479.3 ± 99.6	37.3	p < 0.05
Saccade accuracy (%)	87.9 ± 10.0	85.2 ± 9.3	2.7	NS <sup>c</sup>
Saccade delay time (msec)	202.5 ± 22.7	208.9 ± 23.7	-6.4	p < 0.05
Smooth pursuit index	7.2 ± 4.5	7.6 ± 4.2	-0.4	NS
SR (sec)	210.9 ± 59.6	225.9 ± 43.7	-15.0	NS
SOLEC-R (sec)	107.1 ± 49.2	113.9 ± 48.5	-6.8	NS
SOLEC-L (sec)	108.3 ± 49.7	117.7 ± 45.2	-9.4	p < 0.05
WOFEC (steps)	28.1 ± 4.1	26.3 ± 7.0	1.8	NS

<sup>a</sup> Mean ± standard deviation and difference.

<sup>b</sup> Paired t-test, two-tailed

<sup>c</sup> Not significant at p > 0.05

(Reproduced from Horvath et al. [9] by permission)

concentrated on acute myocardial infarctions, angina pectoris, and cardiac arrhythmias. There were too few cases to analyze for other outcomes and few PGDN-exposed workers prior to 1970. Mean age for incident 1970 to 1979 cases was comparable among all groups. PGDN-exposed workers had an elevated odds ratio of 2.52 for cardiovascular hospitalizations compared to similar control sailors, and 4.03 when compared to non-munition worker controls (Table 4) over the 1970 to 1979 time period.

**TABLE 4. CALCULATION OF ODDS RATIOS AND CONFIDENCE INTERVALS FOR TORPEDOMEN POTENTIALLY PGDN-EXPOSED (TM EXPOSED) AND NON-EXPOSED TORPEDOMEN (TM CONTROL) AND FIRE CONTROL TECHNICIANS (FT) TO OTTO FUEL II**

Comparison Group	Observation Period	Odds Ratio	95% Confidence Interval
TM Exposed vs TM Control	1970-1974	2.66	0.78, 9.04
	1975-1979	2.71	0.97, 7.60
	1970-1979	2.52	1.16, 5.48
TM Exposed vs FT	1970-1974	3.69	1.12, 12.20
	1975-1979	5.25	1.92, 14.34
	1970-1979	4.03	1.89, 8.59
TM Control vs FT	1970-1974	1.37	0.75, 2.50
	1975-1979	1.92	0.93, 3.94
	1970-1979	1.59	1.00, 2.53

(Reproduced from Heimkamp et al. [11] by permission)

The same U.S. Naval cohorts and outcomes were studied in more depth by Forman [12]. Because the earlier association of excess cardiac morbidity was based on small case numbers, they reduced several potential methodologic sources of error in order to increase confidence in the validity of the findings. Cases were included only if directly confirmed from hospitalization records. Age-adjusted incidence rates were calculated directly, instead of the previous approximation from odds ratios. Cohort age, race, and sex characteristics were determined among the 1,352 PGDN-exposed, 14,336 non-exposed munition workers, and 29,129 non-munition controls. Known cardiovascular risk factors, including smoking, family history, obesity, hyperlipidemia, hypertension, diabetes, and gout (Table 5) were determined for cases in all groups. Elevated rates (Table 6) and significantly elevated relative risks (Table 7) of myocardial infarction and angina pectoris together were shown in the PGDN-exposed workers. This work is interesting in several respects. It represents the actual experience of a complete cohort of PGDN workers over a decade. There were no suspicious neurological diseases found. None had the classic nitroglycerin-associated history of angina pectoris and sudden death occurring following leaving an exposed workplace. Two of the exposed angina cases had no coronary atheromatous disease on angiography, a finding suggesting vasospastic etiology associated with PGDN exposure in these cases. Though cases were relatively few, the authors suggested continued caution in PGDN use as reflected in adherence to exposure guidelines and periodic medical examinations.

### ***Human teratogenesis***

The Naval Health Research Center investigated pregnancy outcomes in women Naval munitions workers because a growing number of women were exposed to PGDN in torpedo repair work (unpublished Letter 3900 dated March 13, 1986). From 1980 to 1983, spontaneous abortions among all female torpedomen munitions workers were the same or lower as compared to hospital employees and all other Naval women. There were no spontaneous abortions among the few PGDN-exposed pregnant women (Table 8).

Anecdotal and unsubstantiated concerns linking human disease to PGDN have circulated from time to time. Among them are central nervous system degenerative disease and AIDS.

Central nervous system degeneration was linked by one Naval veteran to his work with Otto Fuel II. Work by Horvath et al. [9] with chronically exposed Naval munitions workers found no evidence of long-term central nervous system effects. It is difficult to speculate on a mechanism for such an outcome, given a compound whose PGDN-active component has a half-life of minutes.

TABLE 5. CHARACTERISTICS OF INCIDENT MYOCARDIAL INFARCTION, ANGINA PECTORIS, AND CARDIAC ARRHYTHMIA CASES IN PGDN-EXPOSED AND CONTROL COHORTS, 1970-1979

Diagnosis	Cohort	Total Cases	Average Age (range)	Race Cauc/Black	Risk Factors <sup>a</sup>							Avg. risk factors per case
					Smoking	FH	Obesity	Lipids	HT	DM	Gout	
Myocardial infarction	TM Exposed	4	37 (33-41)	4/0	4	1	0	2	1	2	0	2.5
Myocardial infarction	TM Control	16	41 (30-55)	16/0	14	6	6	6	8	1	2	2.7
Myocardial infarction	FT Control	16	38 (23-53)	16/0	13	3	7	5	1	0	0	1.8
Angina pectoris	TM Exposed	2 <sup>b</sup>	31 (28-35)	2/0	0	1	1	0	0	0	0	1.0
Angina pectoris	TM Control	5	37 (30-45)	3/2	5	2	0	0	2	0	0	1.8
Angina pectoris	FT Control	6	35 (30-38)	6/0	5	3	2	2	1	0	0	2.2
Cardiac arrhythmias	TM Exposed	1 <sup>b</sup>	35	1/0	1	1	0	0	0	0	0	2.0
Cardiac arrhythmias	TM Control	7	26 (19-37)	7/0	5	0	2	0	0	0	0	1.0
Cardiac arrhythmias	FT Control	16	33 (21-54)	16/0	8	2	4	1	1	2	0	1.1

<sup>a</sup> Cardiac risk factors: HT, hypertension; FH, family history; Lipids, hyperlipidemia; obesity, exogenous; DM, adult onset diabetes mellitus

<sup>b</sup> Includes a case first symptomatic when associated with PGDN work  
(Reproduced from Forman et al. [12] by permission)

TABLE 6. FREQUENCIES AND AGE-ADJUSTED INCIDENCE RATES PER 10,000 FOR SELECTED CARDIAC DIAGNOSES AMONG PGDN-EXPOSED AND CONTROL COHORTS, 1970-1979

Diagnosis	TM Exposed <sup>a</sup> Freq. Rate		TM Control <sup>b</sup> Freq. Rate		FT Control <sup>b</sup> Freq. Rate	
Myocardial infarction	4	18.0	16	8.1	16	6.9
Angina pectoris	2	9.8	5	2.6	6	2.6
Cardiac arrhythmias	1	5.1	7	4.9	16	6.4

<sup>a</sup> PGDN-exposed torpedomen, TM exposed

<sup>b</sup> Control groups are non-exposed torpedomen, TM controls, and weapons guidance technicians, FT controls.

(Reproduced from Forman et al. [12] by permission)

TABLE 7. RELATIVE RISK FOR SELECTED CARDIAC DIAGNOSES AMONG PGDN-EXPOSED AND CONTROL COHORTS, 1970-1979

Diagnosis	TM-Exposed: TM Control <sup>b</sup>  Relative Risk (95% C.I.) <sup>c</sup>	TM-Exposed: FT Control <sup>b</sup>  Relative Risk (95% C.I.)	TM Control: FT Control <sup>b</sup>  Relative Risk (95% C.I.)
Myocardial infarction	2.22 (0.74, 6.72)	2.61 <sup>d</sup> (1.33, 5.14)	1.17 (0.99, 1.42)
Angina pectoris	3.77 (0.43, 32.11)	3.77 <sup>d</sup> (1.01, 14.10)	1.00 (0.99, 1.02)
Myocardial infarction and angina pectoris	2.60 <sup>d</sup> (1.11, 6.12)	2.93 <sup>d</sup> (1.71, 5.03)	1.13 <sup>d</sup> (1.01, 1.31)

<sup>a</sup> PGDN-exposed torpedomen, TM exposed

<sup>b</sup> Control groups are non-exposed torpedomen, TM controls, and weapons guidance technicians, FT controls.

<sup>c</sup> 95% confidence interval.

<sup>d</sup> Statistically significant at  $p < .05$  level.

(Reproduced from Forman et al. [12] by permission)

TABLE 8. PREGNANCY OUTCOMES BY NAVY OCCUPATIONAL GROUP, 1980-83

Enlisted Group	Percent Spontaneous Abortions <sup>a</sup>	Percent Induced Abortions <sup>a</sup>	Percent Total Abortions <sup>a</sup>	Total Pregnant
TMs - PGDN-exposed <sup>b</sup>	0	0	0	5
TMs - unexposed <sup>c</sup>	7.0	0	7.0	43
Hospital Corpsman <sup>d</sup>	9.2	0.7	9.9	1,124
All others <sup>e</sup>	8.5	0.6	9.1	5,814
Total	8.6	0.6	9.2	6,986

<sup>a</sup> Number of abortions/number of pregnancies  $\times 100$

<sup>b</sup> Torpedomen mates (TM) are potentially exposed to PGDN in the form of Otto Fuel II while repairing a specific weapon system.

<sup>c</sup> Torpedomen mates, TM, unexposed are all other female torpedomen/munitions workers.

<sup>d</sup> Hospital Corpsman are enlisted female medical care workers.

<sup>e</sup> All others are all other uniformed Navy enlisted female members.

(Reproduced from Naval Health Research Center Letter 3300 dated March 13, 1986, by permission)

A link of PGDN to AIDS is another unsubstantiated area. Isobutyl nitrate has been used by some homosexuals to produce a transiently altered mental state and relaxed anal sphincter tone. Mirvish and Haverkos [13] and Haverkos et al. [14] have speculated that short-acting nitrate usage in people infected with the AIDS virus is a cofactor to Kaposi's sarcoma induction. As a short-acting nitrate, PGDN has also come under suspicion. Among Naval PGDN munitions workers, no excess in AIDS incidence has been noted as compared to other occupational activities. The investigators believe the nitrate-AIDS linkage implausible on etiologic grounds, with the isobutyl nitrate exposure a likely confounding variable of intravenous drug abuse or concomitant infections.

## REFERENCES

- 1 Kylin, B., England, A., Ehrner-Samuel, H., Yllner, S. (1964) A comparative study on the toxicology of nitroglycerine, nitroglycol and propylene glycol dinitrate. Proceedings of the Fifteenth International Occupational Health Conference. Vienna, 3, pp. 191-195.
- 2 Fine, L.J. (1983) Occupational heart disease. In: W.N. Rom (Ed.), Environmental and Occupational Medicine. Little, Brown and Company, Boston, pp. 360-361.
- 3 Clark, D.G. and Lichtfield, M.H. (1969) The toxicology, metabolism, and pharmacologic properties of propylene glycol 1,2 dinitrate. Toxicol. Appl. Pharmacol. 15, 175-184.
- 4 Clark, D.G. and Lichtfield, M.H. (1967) Metabolism of ethylene glycol dinitrate and its influence on the blood pressure of the rat. Br. J. Ind. Med. 24, 320-325.
- 5 Jones, R.A., Strickland, J.A., Siegal, J. (1972) Toxicity of propylene glycol 1,2 dinitrate in experimental animals. Toxicol. Appl. Pharmacol. 22, 128-137.
- 6 U.S. Navy. (1979) Mutagenicity evaluation of Otto Fuel. Genetics Assay 3738, Litton Bionetics, Inc., Boston, MA.
- 7 Rivera J.C. (1974) Otto Fuel II: Health hazards and precautions. U.S. Navy Medicine. 63 (1), 7-10.
- 8 Stewart, R.D., Peterson, J.E., Newton, P.E., Hake, C.L., Hosko, M.J., Lebrun, A.J., and Lawton, G.M. (1974) Experimental human exposure to propylene glycol dinitrate. Toxicol. Appl. Pharmacol. 30, 377-395.
- 9 Horvath, E.P., Ilka, R.A., Boyd, J., and Markham, T. (1981) Evaluation of the neurophysiologic effects of 1,2 propylene glycol dinitrate by quantitative ataxia and oculomotor function tests. Am. J. Ind. Med. 2, 365-378.
- 10 American Conference of Governmental Industrial Hygienists. (1986) Propylene glycol dinitrate. In: Documentation of the Threshold Limit Values and Biological Exposure indices, Fifth Ed., Cincinnati, OH, pp. 502-503.
- 11 Helmkamp, J.C., Forman, S.A., McNally, M.S., and Bone, C.M. (1984) Morbidity and mortality associated with exposure to Otto Fuel II in the U.S. Navy 1966-1979. Report 84-35, U.S. Naval Health Research Center, San Diego, CA.

- 12 Forman, S.A., Helmkamp, J.C., and Bone, C.M. (1987) Cardiac morbidity and mortality associated with occupational exposure to 1,2 propylene glycol dinitrate. *J. Occup. Med.* 29(5), 445-450.
- 13 Mirvish S.S. and Haverkos, H.W. (1987) Butyl nitrite in the induction of Kaposi's sarcoma in AIDS. *N. Engl. J. Med. (Letter)* 317, 25:1603.
- 14 Haverkos, H.W., Pinsky, P.F., Drotman, D.P., and Bregman, D.J. (1985) Disease manifestation among homosexual men with acquired immunodeficiency syndrome: A possible role of nitrites in Kaposi's sarcoma. *Sexually Transmitted Diseases* 12, 203-208.

**SESSION II**

**PHARMACOKINETICS AND EXPERIMENTAL DESIGN**

**Dr. Daniel B. Menzel, Chairman**

## PLANNING AND USING PB-PK MODELS: AN INTEGRATED INHALATION AND DISTRIBUTION MODEL FOR NICKEL

Daniel B. Menzel

*Duke University Medical Center, Departments of Pharmacology and Medicine, Comprehensive Cancer Center, Durham, NC*

### SUMMARY

A general method is presented for the use of mathematical modeling in the design, execution, and interpretation of toxicology experiments. To illustrate the use of mathematical modeling toxicology, a case study is presented of how a dosimetry model for inhaled nickel was developed for use in cancer risk estimation. A physiologically based pharmacokinetic (PB-PK) dosimetry model is used to plan animal experiments and to extrapolate nickel kinetics from animals to humans. These data are then used to estimate human lung cancer risks from human exposure to nickel aerosols. To achieve this goal, a PB-PK dosimetry model for the lung was integrated with a PB-PK dosimetry model for the internal organs. Nickel removal from the lung was found to be saturable and to follow Michaelis-Menten kinetics. The PB-PK lung dosimetry model was used to design both short-term (single) and long-term (multiple intermittent) exposures needed to validate selected parameters ( $K_m$  and  $V_{max}$ ) of the lung dosimetry model. A constant infusion experiment was planned using the PB-PK modeling approach to measure the distribution and elimination of intravenously administered nickel. The two PB-PK models were integrated to estimate the fate of nickel after inhalation and are being used to plan experiments for other routes of exposure such as ingestion of drinking water and dermal contact. The integrated model has been used to calculate a human cancer risk estimate in combination with short-term genotoxic experiments. Using PB-PK models in toxicology, as illustrated here, conserves experimental animals, aids in understanding new physiological phenomena (such as saturable clearance from the lung), incorporates *in vitro* tests with *in vivo* experiments, and provides a means of extrapolation to human health risks from multiple routes of exposure. Introducing the concepts of mathematical modeling into toxicity experiments at the beginning of the experiments improves the usefulness of the experiments in risk estimation. PB-PK models are suggested as a new basis for experimental design in toxicology.

### INTRODUCTION

Mathematical modeling is a powerful tool that can be applied to many aspects of toxicology. Mathematical modeling requires an explicit statement of the goals and objective of the study and a precise definition of the relation between experimental variables and the experimentally determined results. By its very nature, the application of mathematical modeling focuses thought and experimentation on quantitative relations. The application of mathematical modeling to the

quantitative distribution of nickel in the body is presented as a case study of how mathematical modeling can aid in experimental design in toxicology. Through this case study, we hope that PB-PK models can be recognized as powerful yet easily understood tools for planning toxicity experiments designed to lead ultimately to human health risk estimates [1].

Nickel is a known human carcinogen and occurs widely in the environment [2]. Nickel smelting and refining workers have experienced nasal and lung tumors [2]. Production of similar tumors in animals has not been reported, but a wide variety of genotoxic endpoints have been reported for nickel emphasizing the carcinogenic hazard of nickel [2]. Humans are exposed to nickel by inhalation, ingestion, and dermal contact. The human hazard from environmental exposure to nickel involves several different media as routes of exposure. The amount of nickel reaching the body differs widely from these diverse routes of exposure. To quantitate the human health hazard from alternative routes of exposure, a mathematical model of the disposition of nickel upon inhalation and ingestion is being developed.

Inhalation exposure of the urban population is mainly attributed to nickel aerosols from the combustion of fossil fuels that contain nickel. About 60  $\mu\text{g}$  nickel/ $\text{m}^3$  occur in the urban atmosphere [2]. Cigarette smoke also contains nickel, leading to both passive and intentional inhalation exposure through tobacco smoke. About 2  $\mu\text{g}$  nickel is present in a cigarette; the amount of nickel in environmental tobacco smoke has not been reported. Workers are exposed to respirable aerosols of nickel during the mining, smelting, refining, and industrial use of nickel. The nickel electroplating industry represents the simplest form of nickel industrial inhalation exposure. The present threshold limit value for soluble nickel salts is 100  $\mu\text{g}/\text{m}^3$ , but values greater than the threshold limit value may be encountered during brief work periods. Nickel is present in its chemical form as soluble nickel salts. Urban exposure and cigarette smoking also represent principally soluble nickel exposures because of the acidic nature of the aerosols resulting from the oxidation of nitrogen to nitrous and nitric acids and sulfur to sulfuric acid in the atmosphere. The nickel content of stack emissions of oil-fired power plants is 60 to 100% water soluble, suggesting that nickel occurs mostly as nickel nitrate or sulfate. Nickel oxides are thus probably converted easily to the corresponding nickelous salt after combustion (mostly nickelous nitrate and sulfate) [2].

Nickel also can be consumed in foods and beverages. Foods contain nickel through environmental contamination by fallout of fossil fuel combustion products and nickel naturally occurring in soils. Foods and beverages processed in nickel-containing vessels also are contaminated with nickel. Groundwater and drinking water contamination with nickel provides an additional source of environmental nickel [2].

To assess the carcinogenic potential of nickel, multiple routes of exposure should be evaluated. While inhalation presents the greatest hazard to the respiratory tract and results in nasal and respiratory tumors in workers [2], the overall nickel burden from all sources may present a more significant hazard to other organs such as the kidneys. The ultimate goal of our studies is to assess the hazards of nickel to all organs from all sources of exposures. To do so, we have chosen the use of PB-PK modeling as a means of describing the dose of nickel to specific organs from given exposure scenarios. The PB-PK models also aid in experimental design and reduction in the numbers of experimental animals needed to accomplish the goal of predicting the human health hazard from environmental nickel. PB-PK models also provide a vehicle for integration of *in vitro* tests into *in vivo* extrapolations to humans [3].

## METHODS

Male Sprague-Dawley rats were exposed to nickel aerosols [4,5,6] in a head-only exposure system to diminish contamination of the fur [5]. Submicron-sized particles were used to enhance the deposition of nickel in the pulmonary region of the lung. Soluble salts of nickel (chloride, nitrate, and sulfate) were used. The kinetic behavior of all forms of nickel were essentially the same. Gaseous nickel, as in nickel subsulfite, or slowly soluble forms of nickel, as in nickel oxide, may behave differently. The kinetic behavior of the mixture of nickel salts present in the urban atmosphere as *nickel nitrate and sulfate is not likely to differ much from the results presented here for nickel chloride.*

The removal of nickel from the respiratory tract was determined by analysis of whole lungs at time intervals after single or repeated exposures to nickel. The nasopharyngeal burden of nickel was estimated by a retrograde lavage of the nasopharyngeal region.

The distribution of nickel to the organs of the body was estimated by using a constant intravenous infusion of nickel chloride after administration of a bolus loading dose [6]. All determinations were done at steady state as measured by constant concentrations in blood and urine. The extraction ratio of nickel from the blood to individual organs was calculated from the ratio of blood nickel to organ nickel.

Simulations were carried out using an IBM PC-AT computer or a DECVAX 11/750 computer. The simulations were carried out using two programs. The first program simulated the nickel removal from the respiratory tract according to Michaelis-Menten or saturable type kinetics.<sup>a</sup> The estimated blood concentrations resulting from an exposure were then used as the input for the blood nickel concentrations in a conventional PB-PK flow-limited multicompartmental model. These programs

---

<sup>a</sup> The lung dosimetry and internal organ dosimetry models can be used through the computational facilities of the Toxicology Information Network of the Duke National Biomedical Simulation Resource. Qualified scientists may write for application to Mr. J. R. Boger, II, TOXIN Administrator, Duke University Medical Center, P.O. Box 1813, Durham, NC 27710, USA.

were custom written in the C language and are available through the Toxicology Information Network (TOXIN).

## RESULTS

### *Experimental planning with PB-PK modeling*

The method developed for using PB-PK models in experimental planning is shown in Figure 1. The process is reiterative. The critical steps in developing an experimental plan are the definition of the goals of the project and the anticipated results. An explicit statement of the goal of the project is essential. Until an explicit statement can be made, mathematical relations cannot be defined. Once the goals are stated, the choice of a mathematical modeling solution can be made. An arbitrary choice was made to use PB-PK modeling. While other types of models are available, PB-PK models have distinct advantages. PB-PK models incorporate the known physiology and anatomy of the experimental animal into the model. They use the wealth of information available about physiological processes to be incorporated directly into the model. Known differences in anatomy and physiology between species are more easily accounted for by this approach. Extrapolation to humans from a wide variety of animal species can be more confidently and easily accomplished by direct substitution of human parameters for those of the experimental animal.

## Program Design for PB-PK Modeling

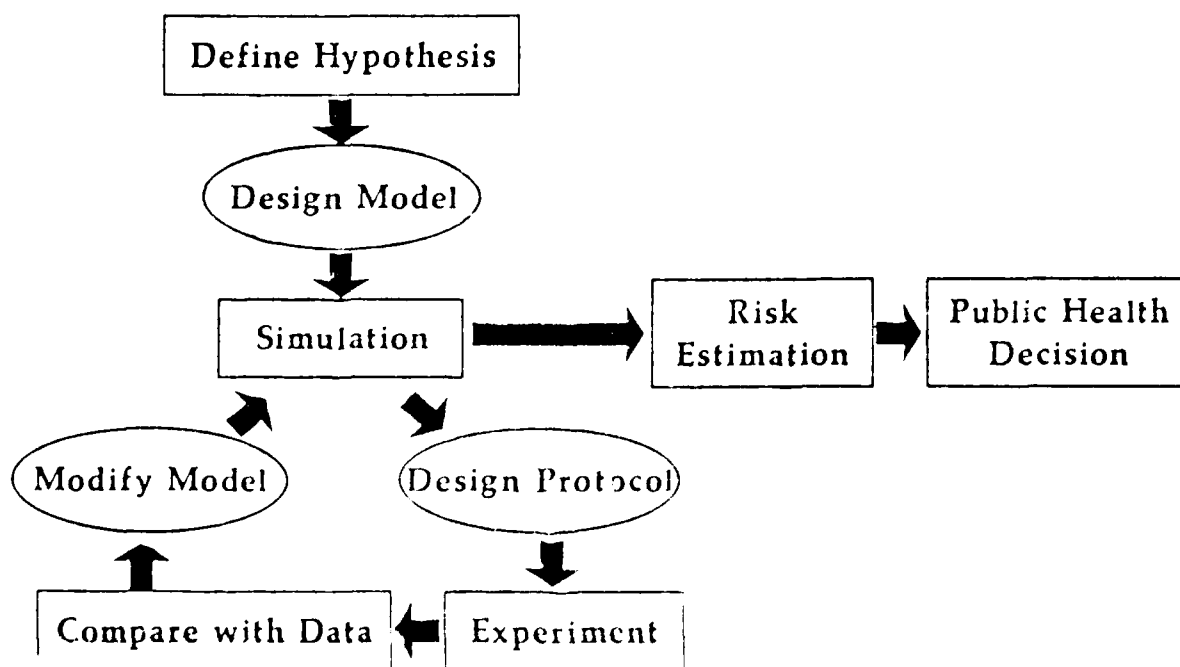


Figure 1. A schematic representation of the steps followed in using mathematical models in toxicity experiments for risk analysis.

The integration of the lung dosimetry model and the multicompartamental model of nickel distribution in the body conceptually follows the scheme in Figure 2. In order for the dosimetry models to be applicable to humans exposed under a number of different conditions, the respiratory tract characteristics of humans must be taken into consideration. The aerodynamic properties of the aerosol determine to a large extent the regional deposition of the aerosol. Several deposition efficiency curves based on aerosol particle size have been developed [7] based on either nose or mouth breathing. Unlike rodents, humans must breathe through their mouths during exercise or to accomplish significant work (e.g. exercise at a level needed to accomplish normal activities other than resting). Deposition efficiencies are markedly influenced by mouth and nose breathing. Thus, clearance to the blood and lymph is described by the physiological parameters determined in lung clearance experiments. The distribution of nickel to the internal organs of the body and elimination of nickel are simulated by the multicompartamental model developed separately.

## **Integrating Inhalation Exposure and Body Organ Distribution Models**

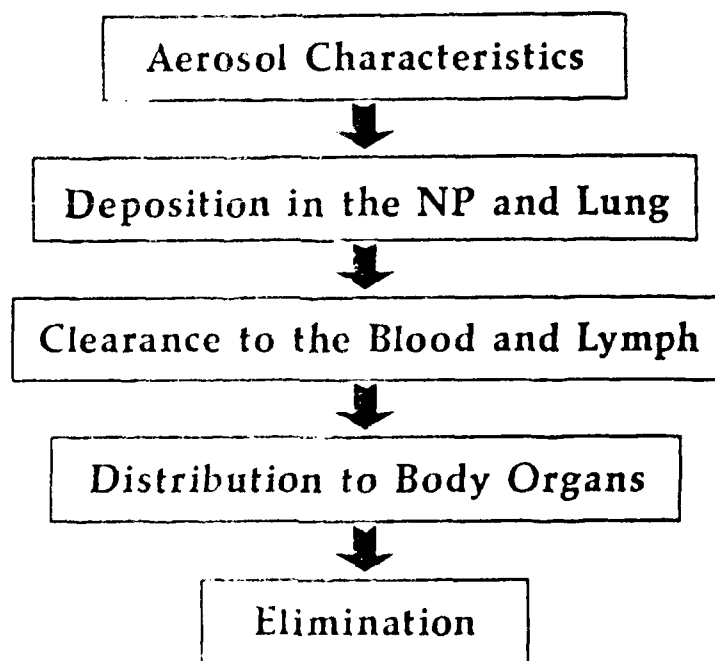


Figure 2. A schematic representation of the steps leading from an integration of inhalation and internal organ PB-PK dosimetry models. The physical characteristics of an aerosol are used to predict the amount of the aerosol deposited in a region of toxicological interest. A PB-PK lung dosimetry model is used to predict the blood burden of the toxicant leaving the lungs. The distribution of the toxicant to the internal organs, its metabolism, and excretion are predicted by an internal PB-PK dosimetry model. Integration of PB-PK models describing the route of entry kinetics with PB-PK models describing organ burdens provides a means of relating multiple sources of exposure to health effects.

Rarely are biological experiments so original that the experimenter has no idea of the result. Rather, most biological experiments are built upon prior experience. Insoluble particle clearance from the lungs is known to follow first-order kinetics [9]. Using the literature, an estimate of the first-order clearance of nickel from the lung was used as the initial estimate to plan sampling points. The preliminary data clearly departed from any combination of multiple first-order rates or a single first-order rate. We hypothesized that the downward curving relationship of lung burden with time shown in Figure 3 resulted from a saturable process [4,6,9,10]. We found no combination of first-order rates that could produce the downward curving relationship or concentration dependence for the removal rate with increasing time after exposure. Using initial data, an estimate of the two kinetic parameters defining a saturable process,  $K_m$  and  $V_{max}$  in Michaelis-Menten kinetics, were used to describe the time course of the nickel lung burden. The  $K_m$  and  $V_{max}$  differed with single exposures of naive animals as compared with that found for repeated exposures (Table 1). The fractional deposition of the aerosol is also important in defining the initial lung burden before clearance. The values calculated from the nickel lung burden immediately after exposure and the clearance rates are also given in Table 1. The solid line in Figure 4 is for the optimized final parameters obtained from multiple experiments [3].

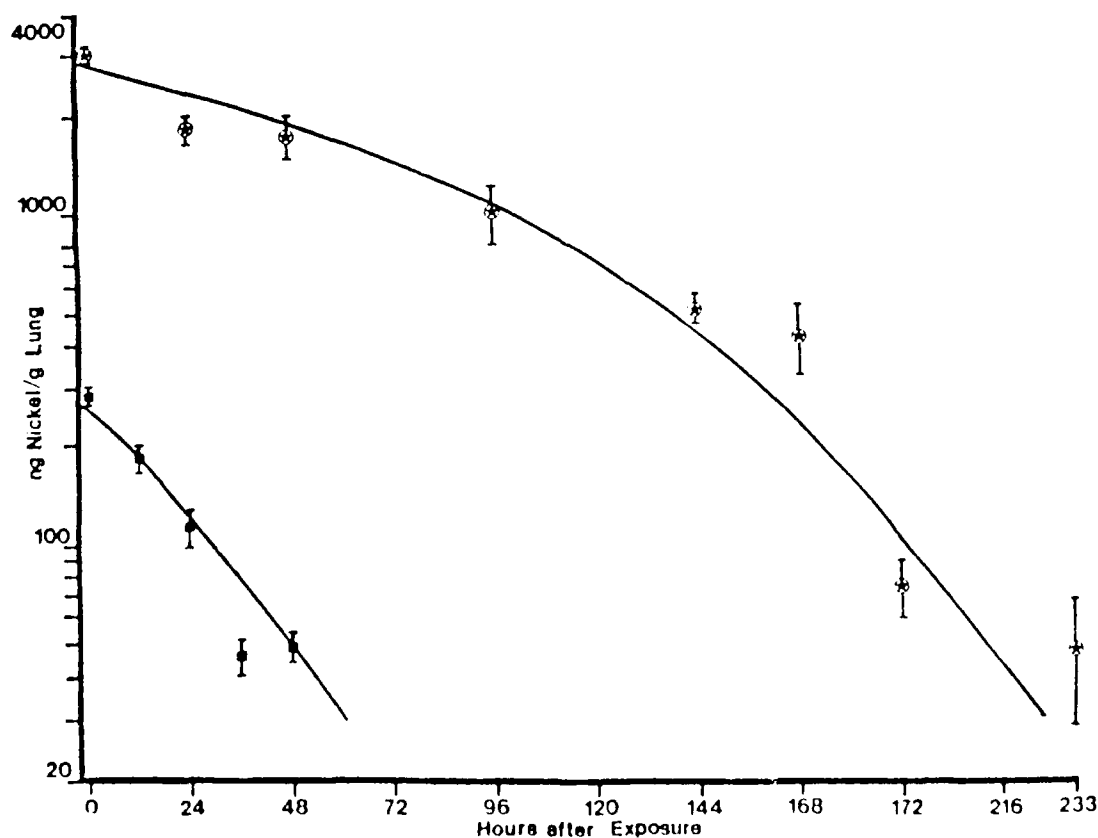


Figure 3. Rat lung nickel burdens following single 2-h exposures. The points represent the mean nickel values found in whole rat lungs after exposure to 126 and 1208  $\mu\text{g nickel}/\text{m}^3$ . Vertical bars represent the standard deviation of the mean. The solid line represents the nonlinear regression fit to the data. Taken from Menzel et al. [10].

TABLE 1. LUNG CLEARANCE MODEL PARAMETERS FOR RATS

Exposure Scenario	$K_m$ (ng/g lung)	$V_{max}$ (ng/g lung/h)	Fractional Deposition (%)
Acute	894	31.3	10.7
Repeated	1,380	34.6	6.9

Values are taken from Menzel et al. [3]

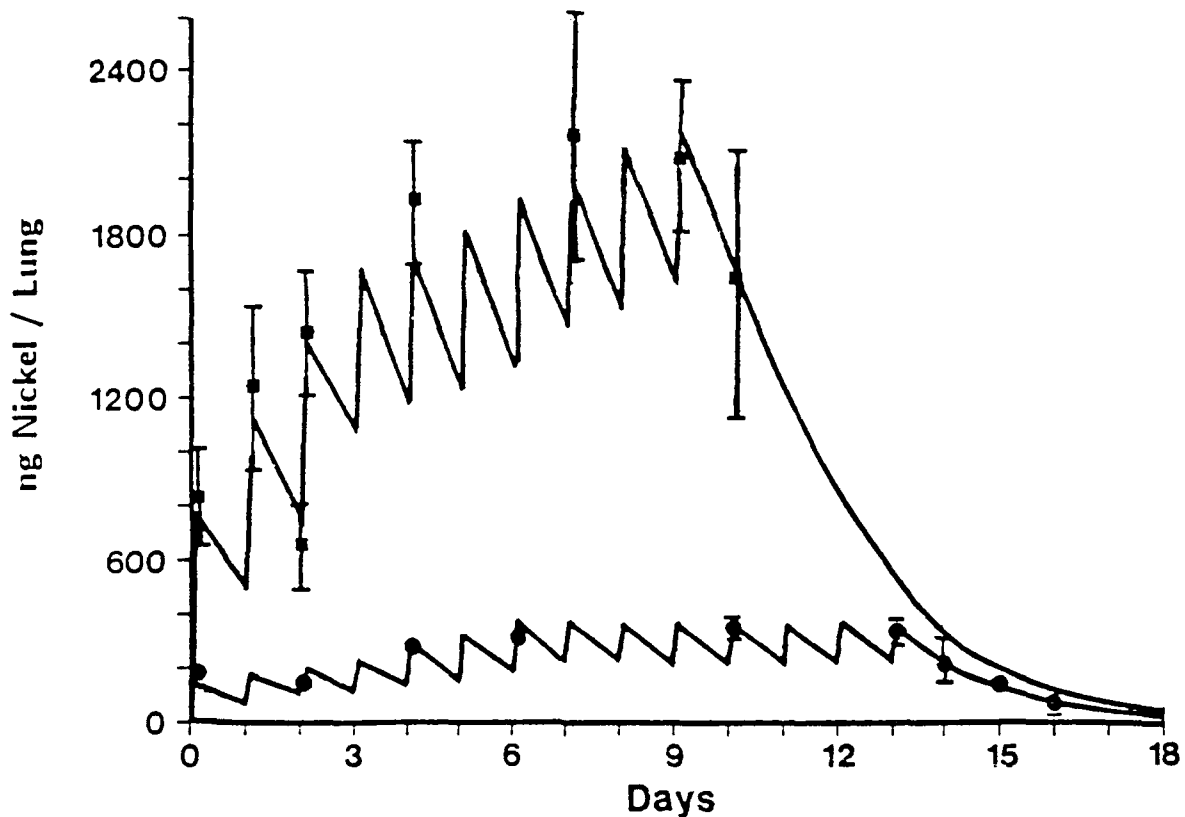


Figure 4. Rat lung nickel burdens following repeated daily exposures to a nickel aerosol. The solid lines represent the predicted lung burdens calculated from the PB-PK lung dosimetry model for nickel. The solid circles and squares represent values of lung nickel determined experimentally with the standard deviation around the mean given as vertical lines. Taken from Menzel et al. [3].

$K_m$  is defined as the concentration at which half the maximum rate of clearance occurs, while  $V_{max}$  is defined as the maximum rate of clearance for the whole lung. Finding that the data were well simulated by such a relationship suggested that nickel clearance from the lung occurred via an ion channel or equivalent carrier mechanism [9].

Recognition of the saturable nature of nickel clearance from the lung was important to subsequent experimental plans. Definition of  $V_{max}$  is critical, so experiments were designed to select an exposure concentration as close as possible to the estimated  $V_{max}$  to determine whether a steady state occurred [4]. Figure 4 illustrates that a steady state could be attained at an exposure

concentration below the  $V_{max}$ , but that ever increasing lung burdens occurred at concentrations above the  $V_{max}$ .

Note that the sampling points were selected to detect the maximum and minimum of the excursions in lung nickel burdens during repeated exposures. A single exposure model developed in the prior cycle of reiteration (see Figure 1) was used to guide the selection of these sampling times.

#### ***Developing a whole-body PB-PK model for nonvolatile chemicals***

The nonvolatile nature of nickel salts presented an experimental challenge to the development of the PB-PK model. The distribution of chemicals between blood and organs is referred to as the extraction coefficient. The extraction coefficient of volatile chemicals can be measured experimentally by determining the chemical concentration in the gas phase or headspace over a homogenate of the organ or blood [1]. The partition coefficient between the chemical and blood can be calculated easily. Nonvolatile chemical distribution between blood and organs is more difficult to determine. The distribution coefficient can be determined by an equilibrium dialysis experiment using organ homogenates. Such an experiment, however, ignores the possible interaction of structure with distribution. Ions, such as nickel, may be accumulated by energy-dependent systems. An alternative approach suggested from the PB-PK model is to determine the organ-to-blood distribution of nickel in the blood at steady state.

Using an infusion pump, the blood nickel concentration was brought to steady state as indicated by a steady value of blood and urine nickel. The ratio of blood nickel to organ nickel was determined at the time of steady state. To expedite reaching steady state, the size of a bolus intravenous dose was calculated from a preliminary PB-PK model. While the extraction ratio varied between organs as shown in Figure 5, the extraction ratios for all organs were independent of concentration [6].

A flow-limited multicompartmental model, as depicted in Figure 6, simulated well a bolus i.v. injection of nickel chloride. A simulation and experimental data from a bolus injection of nickel are shown in Figure 7 for the lung and kidney. The steady-state-measured values of the organ extraction ratios thus estimate well the extraction coefficients occurring during the dynamic changes of a bolus dose.

In Figure 8, the kidney and lung nickel concentrations are shown for a single 2-h exposure to 300  $\mu\text{g}$  nickel/ $\text{m}^3$  inhalation exposure. These results were obtained by using the lung clearance model to describe the blood nickel curve with time. The blood nickel curve was then used in the multicompartmental model of Figure 6 to describe the kidney and lung nickel curves.

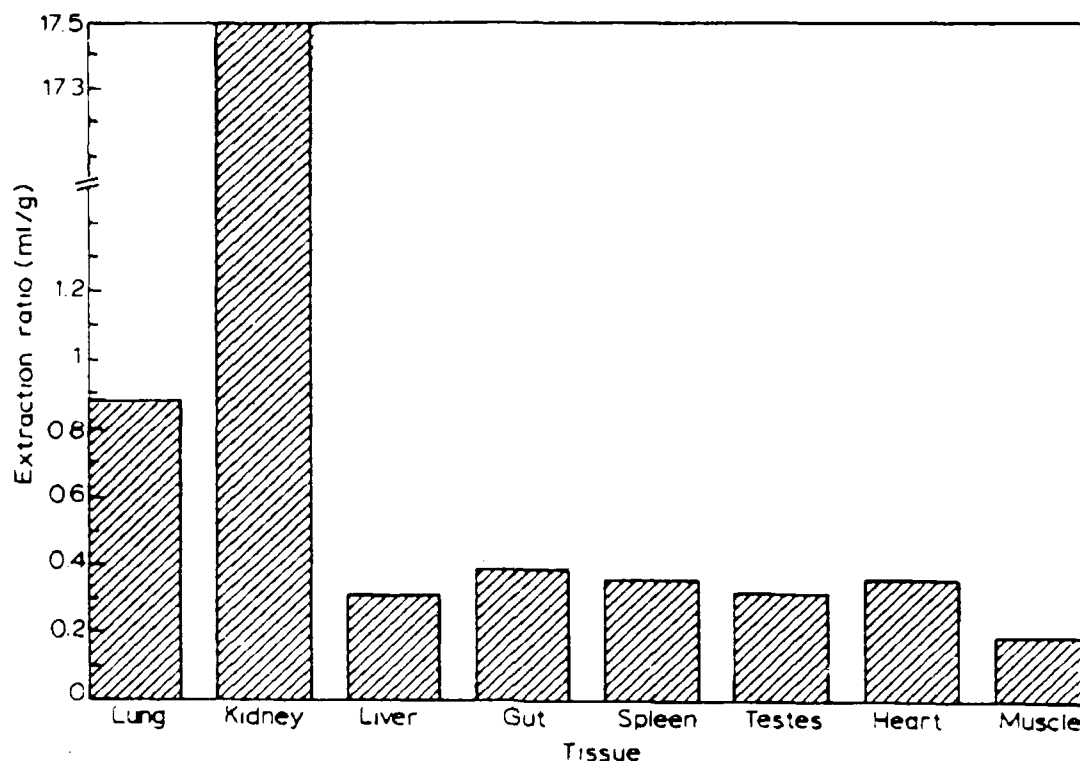


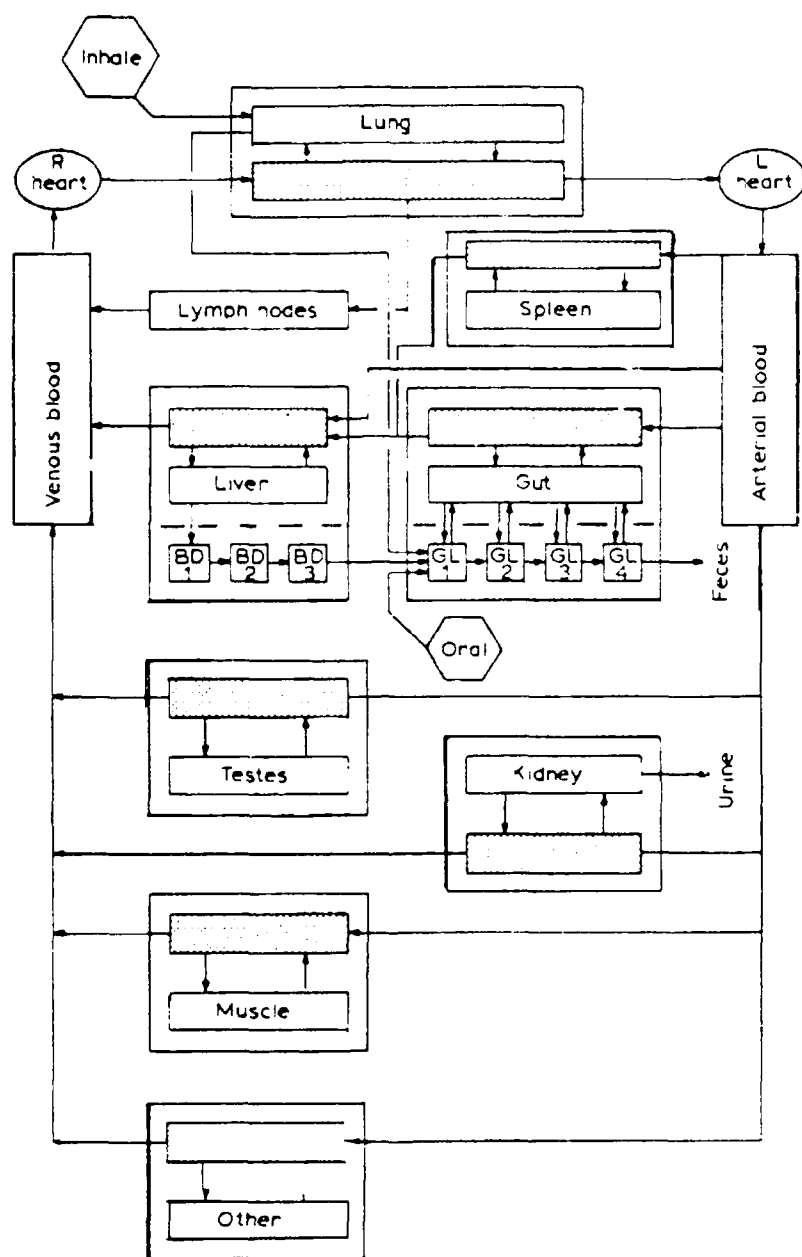
Figure 5. Nickel organ extraction ratios determined at a nickel steady-state concentration. The blood and organ nickel concentrations were determined after reaching a steady-state concentration of nickel by a bolus loading dose followed by constant intravenous infusion.

## DISCUSSION

### *Mathematical modeling as a guide to toxicology research planning*

Toxicity experiments are expensive and time consuming. The urgency for information on the toxicity of chemicals reinforces the need to design experiments to provide the most reliable information in the shortest time at the lowest costs. Increasing the efficiency of toxicity experiments will also reduce the need for experimental animals and conserve this resource. The ultimate criterion for judging experimental designs in toxicology should, however, be how well the final information can be used in predicting human health effects.

Current cancer bioassays assume that the incidence of tumors produced by chemicals will be low and that the maximum tolerable dose is required for a reliable tumor incidence to be detected. A linear relationship between dose and tumor incidence is also assumed. Definition of dose-response relationships by relating exposure concentrations to the lung and organ dose is a major objective of the study described here. Our objective was to develop a dosimetry model for future use in risk assessment. Mathematical models relating the dose to effect can be developed by the same experimental design as shown in Figure 1. The critical step in the process is the definition of the problem.



**Figure 6.** A schematic of a flow-limited physiologically based model of the distribution of nickel to the internal organs. Each of the boxes represents an organ defined in terms of its anatomical size. Each organ consists of two compartments, a capillary blood compartment and an internal compartment. The organs are connected by blood whose flow relationships are defined by the physiological distribution of blood to the organs. Elimination is defined according to the clearance of nickel from that organ. The model is specified for each species by the correct anatomical and physiological data set. Nickel clearance to the bile occurs in humans but not in rats. Taken from Menzel [1].

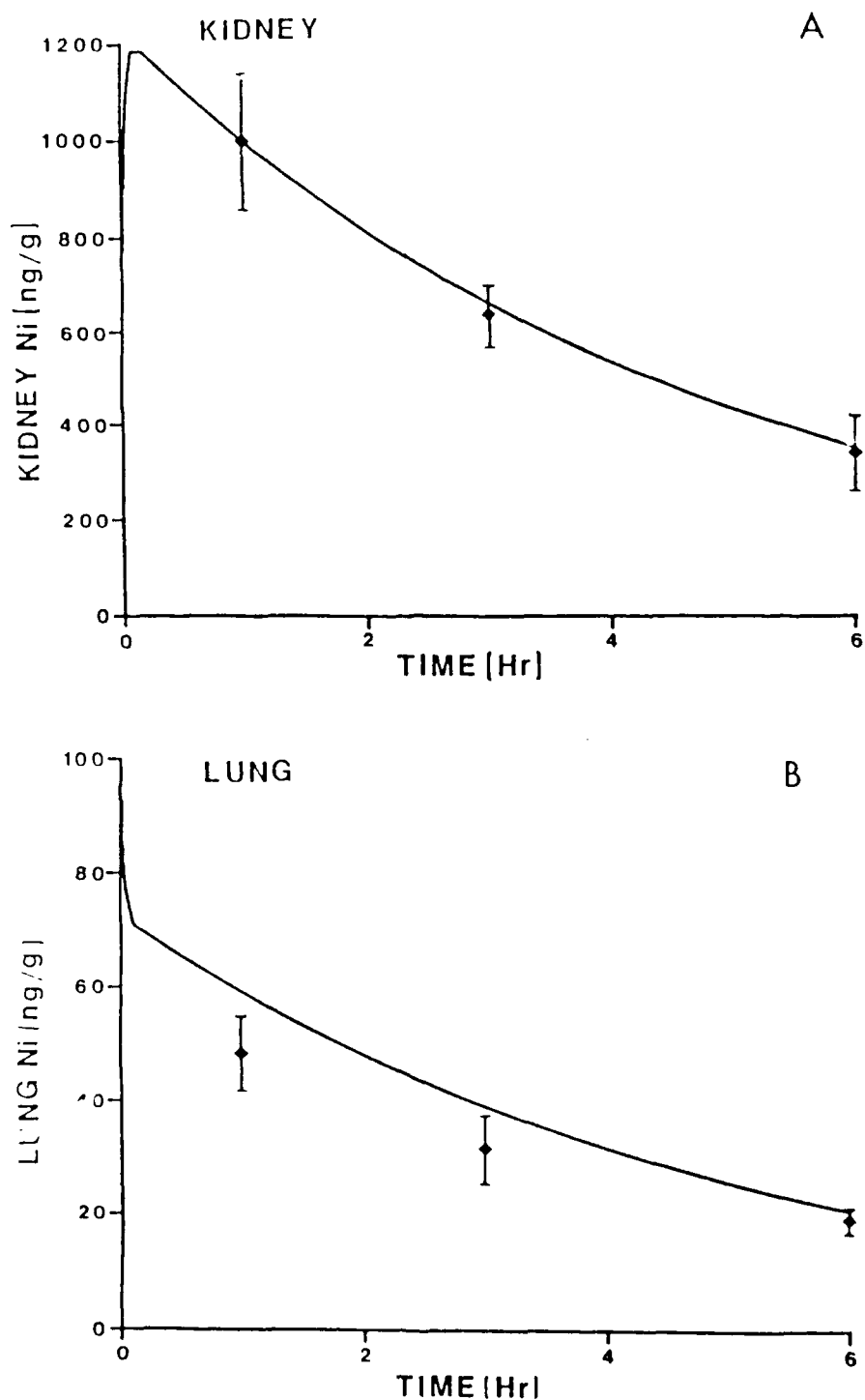
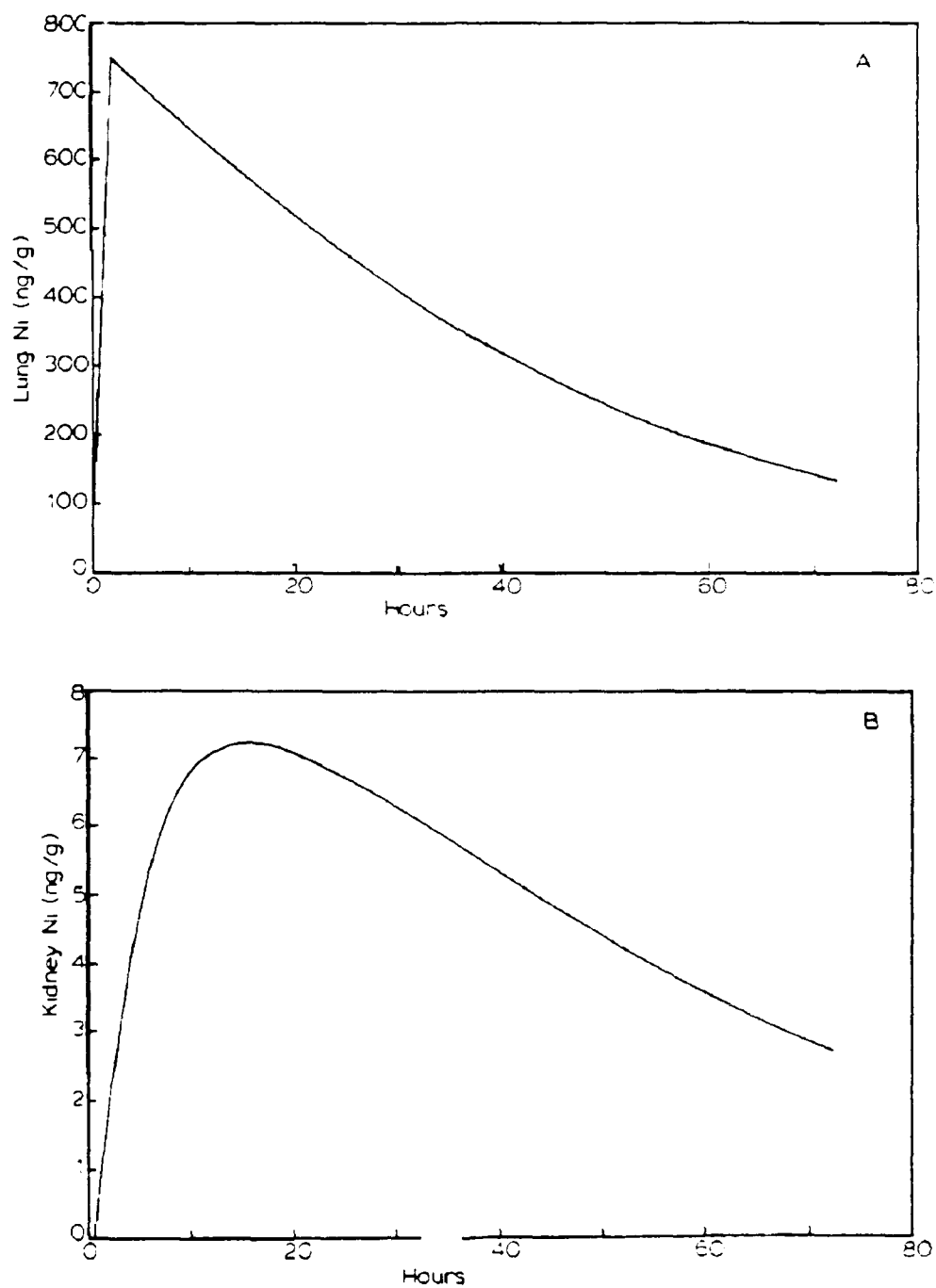


Figure 7. Measured and simulated kidney and lung nickel burdens from a single bolus injection. A. Kidney Burden. B. Lung Nickel Burdens. A single i.v. injection of 45  $\mu\text{g/kg}$  nickel chloride was given. The solid points represent the mean values with the standard deviation shown as the vertical bars. The solid lines represent the simulated time course of nickel.



**Figure 8.** An example of simulated organ nickel burdens from the inhalation of a nickel aerosol. **A.** Lung Burden. **B.** Kidney Burden. The nickel organ burdens of a rat are simulated after inhalation of  $300 \mu\text{g}/\text{m}^3$  of nickel chloride.

Definition of dose is not as simple as it may seem. The multicompartmental and lung clearance models illustrate that the distribution of nickel is far more complex than one might assume from graphic analysis of the data. Dose as defined as the organ nickel burden is a dynamic function of the exposure concentration. Dose also could be defined as the intracellular nickel concentration or as the concentration at the site of action. For genotoxic endpoints, dose could be defined as the nuclear nickel concentration. The dosimetry model presented here provides a beginning estimate of the organ burden, which can be developed further into more molecular concepts of dose as the mechanism of toxicity of nickel is understood.

The mathematical model can undergo further improvement by reiteration through the cycle of hypothesis, modeling, and testing of the model (Figure 1) to develop a dynamic relation between exposure and toxic effect (toxicodynamic). Elsewhere we will report an attempt to use the nickel dosimetry model with a short-term test of nickel genotoxicity to estimate nickel cancer risks [3]. Such an effort is a crude beginning toward a toxicodynamic model.

#### ***Lung nickel clearance follows saturable kinetics***

The observation that soluble nickel deposited as an aerosol was not removed from the lung by a first-order process could not have been anticipated *a priori*. Once saturation of lung clearance was recognized as an explanation for the downward curving nature and concentration dependence of lung nickel burdens with time, a mathematical simulation was formulated that guided further experimentation. In the case of nickel, the analytical method of atomic absorption spectrophotometry used to measure lung and organ burdens proved to be the slowest step in the completion of experiments. This, together with our desire to minimize the use of experimental animals, led us to simulate a variety of exposure conditions to determine whether the anticipated nickel lung burdens would be detected reliably by our atomic absorption method. The preliminary experiments assuming a first-order type of nickel lung clearance gave us a good idea of the variation expected from the exposure system and differences in rat respiration as well as analytical error [5]. The experimental design to determine whether saturation occurred with higher exposure levels also was tested to see if the anticipated results (Michaelis-Menten type of kinetics) could be differentiated statistically from a first-order clearance rate. The major statistical test was to show that the slopes of the clearance curves differed from each other. The extreme values are shown in Figure 3. The differences in the intermediate clearance curves are more subtle. If the clearance was due to a first-order process, the slopes of the clearance curves should be identical and independent of the lung burden.

Given the limited number of animals that could be exposed and analyzed, the simulation suggested that the clearance relationship for single exposures of naive animals could be determined

b) repeated experiments exposing small groups of rats over time. The sample size was fixed and an attempt to balance the sample size between different exposure concentrations and times.

stexposure was made. An equal number of unexposed and initial lung burden samples were taken to adjust for variations in initial lung burden and variations with calendar time in the overall sample.

The model suggested two critical questions: (1) Was the clearance rate dependent on the lung burden at all times after exposure and at all exposure concentrations (i.e., initial lung burdens)? and (2) Could the analytical method combined with the variations in lung burden due to the exposure method (head only, [5]) detect these differences with statistical reliability?

These questions lead to refinement of the head-only exposure system to provide a linear initial lung and nasopharyngeal burden with concentration and duration of exposure [5]. Without meeting these requirements, the experiments were unlikely to be able to test the hypothesis of a saturable lung clearance of nickel.

The lung clearance model also leads us to the multiple-exposure experiment [4] to test for an estimated value of  $V_{max}$  (Figure 4). The power of combining the mathematical model with conventional statistical analysis can be appreciated from Figure 4. Many inhalation experiments, especially aerosol exposures in a head- or nose-only exposure apparatus, are conducted for short times and repeated daily throughout the week. Despite the best design of the apparatus, rodents exposed by head- or nose-only methods are stressed by the necessary confinement. By using the simulation based on single exposures of naive rats, the sampling points of the repeated exposure were selected to detect an approach to steady-state nickel lung burden. Sampling at the maximum and minimum excursion of the nickel lung burden following exposures provided validation of the assumed zero-order deposition of the nickel aerosol and the Michaelis-Menten type of clearance following exposure. The model also adjusted for clearance during exposure so that the lung burdens immediately after exposure could be used as an additional validation of both the deposition and clearance rates. A more conventional analysis and experimental design at fixed sampling times would not have detected this fine structure in the lung nickel burden with time but would have treated the variation in lung burden as statistical variations, not biological events. The deposition rate would have been underestimated by a simple plot of the percent of the lung burden remaining vs. time by as much as 12%. The underestimation occurs because clearance during the exposure period is not accounted for by this common graphical method.

Most importantly, Figure 4 shows that exposure at aerosol concentrations leading to lung burdens above the  $V_{max}$  lead to increasing lung burdens throughout the course of the experiment. The upper exposure concentration exceeded the estimated  $V_{max}$  while the lower exposure concentrations fell below the estimated  $V_{max}$ . One could vary the exposure concentration until the

maximum exposure concentration at which a steady-state lung burden was observed is found. This design would be time consuming and wasteful of animals. The present modeling approach eliminates such empirical experimentation.

Maximum tolerable dose is a concept used extensively in carcinogen bioassays. The incidence of tumors is thought to be infrequent in experimentally exposed animals; thus the chances of finding a tumor are enhanced by selecting the maximum dose allowing long-term survival of the animals. A maximum tolerable dose is often selected on the basis of preliminary experiments as the dose that only produces some general physiological effect, such as no more than 10% loss in body weight. If a maximum tolerable dose were to be selected that exceeded the  $V_{max}$ , the relation between exposure concentration and the lung burden (as a target organ dose) would be obscured without knowledge of the lung clearance model. Cancer risk estimates are difficult to make if the experiment leads to changing target organ concentrations. Through the use of the lung clearance model, experimental conditions could be selected to maintain a steady-state value, thus making cancer rate calculations much simpler. Maximum tolerable dose should be replaced by dose values selected on the basis of more physiological considerations, such as the rate of metabolism, clearance, and elimination from the body. Use of this physiological approach to fixing dose levels also applies to organic chemicals. The PB-PK model of methylene chloride [11] could have been used for fixing the doses used in the mouse and rat cancer bioassay to obvious advantages.

Replacement of empirical methods in toxicology by more physiologically sound experimental approaches seems more complex, but the consequent use of the data from such experiments is clearer and more easily understood than approaches such as the maximum tolerable dose method. As short-term tests become more refined and wide-spread, the use of mathematical models in conjunction with such tests will lead to a better appreciation of the biological significance of the short-term test results.

The experimental demonstration in Figure 4 of the predicted steady-state lung nickel burden from the single exposure value also validated the modeling approach. The uncertainty with the  $V_{max}$  and  $K_m$  values is difficult to determine, however, from this experimental design. Caution should be used when extrapolating these constants because of the statistical problem of estimating the variation in  $K_m$  independent of  $V_{max}$  (see Menzel et al. [10] for a discussion of the problem of separating the variation in  $K_m$  from that in  $V_{max}$ ).

#### ***Combining the lung clearance model with a distributive model***

Humans are exposed to many environmental chemicals through more than one route of exposure. As a known human carcinogen in the respiratory tract, nickel inhalation is a major public health concern. Humans are also exposed to nickel through food, beverages, and drinking water.

Non-inhalation routes of exposure may also lead to toxic effects, including cancer, elsewhere in the body. The lung clearance model is an example of a route of exposure dosimetry model that can be combined with a multicompartmental model to predict organ concentrations from a given exposure scenario. It is important to incorporate the nonlinearity inherent in the saturable nature of nickel clearance into estimates of the body burdens of nickel likely to occur from inhalation exposure. A dosimetry model similar to that developed for inhalation can be constructed for ingestion exposure. Current internal organ dosimetry models for volatile chemicals [11] assume a linear relation between inhaled and blood concentration of chemical. Complex mathematical models exist for reactive gases such as ozone [12], which can be adapted to enhance volatile organic chemical models by correcting the inhaled dose for different species.

### ***Relating dosimetry models to human health risks***

Conceiving a mathematical model of an experiment and using the model to plan experiments is clearly shown by this example to lead to a wealth of data not easily recognized or understood through conventional experimental design. The PB-PK model chosen here has an added advantage of providing a systematic and defensible means of extrapolating the animal dosimetry model to humans.

The scheme of Figure 2 can be applied to calculate human lung burdens. The physical characteristics of the aerosol determine where particles are deposited in the lung [8]. A great deal of information is known about the regional deposition of particles in human lungs so that data from animal exposures can be corrected for the particle size of aerosols to which humans are actually exposed. EPA [7] provides curves for particle deposition efficiency by mouth- or nose-breathing humans. Human lung burdens can then be inserted into lung clearance models as described here. Genotoxic effects [13] and intracellular concentrations of toxicants [14] measured *in vitro* can be used for cancer risk estimates under actual human exposure scenarios [3,9,10].

The mathematical model approach has many strengths, but the most important is its requirement that careful thought be given to any experiment to define quantitatively the relationships hypothesized by the experiment. The ultimate goal cannot be lost from view by this approach. Much of the fragmentation now apparent in the toxicology literature (which has led to conflicting health risks estimated for chemicals, could be eliminated by the use of mathematical models. Building and solving mathematical models is not difficult and even can be accomplished with microcomputers. Simulation control languages for computers guide the toxicologist through the process (see Menzel et al. [15] for a discussion of the resources available for modeling toxicology experiments). The reliability of such predictions of human health risks should be investigated actively. The reliability may be tested as future PB-PK models or other mathematical simulations are

integrated into epidemiological studies. Nickel may be one of these chemicals whereby epidemiological studies of human cancer rates can be compared with the model predictions.

#### ACKNOWLEDGMENTS

The authors would like to thank Drs. C. R. Shoaf and R. L. Wolpert for their collaboration throughout the project. The generous technical assistance of Mr. John R. Boger, III, in carrying out the modeling effort made this work possible. Drs. J. A. Graham, F. J. Miller, Ted Martonen, and John Overton of EPA helped with the aerosol dosimetry concepts and provided encouragement for the project. Drs. M. E. Andersen, H. Clewell, and R. Reitz provided helpful comments and inspiration. Grants from the National Institutes of Health, ES07031, CA14236, and RR01693, provided support for the experimental program. A grant from the International Life Sciences Institute, Risk Science Institute provided support for the modeling effort.

#### REFERENCES

- 1 Menzel, D.B. (1987) Physiological pharmacokinetic modeling. *Environ. Sci. Technol.* 27, 324-350.
- 2 U.S. EPA (1985) Health Assessment Document for Nickel, U.S. EPA, Washington, DC.
- 3 Menzel, D.B., Burke, A.M., Shoaf, C.R., Wolpert, R.L., and Boger, J.R., III. (1988) Integration of pharmacokinetic and genotoxicity damage to assessment of nickel exposure risks. *The Toxicologist* 8, 193.
- 4 Menzel, D.B., Deal, D.L., Tayyeb, M.I., Wolpert, R.L., Boger, J.R., III, Shoaf, C.R., Sandy, J., Wilkinson, K., and Francovitch, R.J. (1987) Pharmacokinetic modeling of the lung burden from repeated inhalation of nickel aerosols. *Toxicol. Lett.* 38, 33-42.
- 5 Francovitch, R.J., Deal, D.L., Tayyeb, M.I., Wolpert, R.L., Boger, J.R., III, Valentini, J.E., and Menzel, D.B. (1987) A head only exposure system for controlled exposures of small rodents. *Toxicol. Lett.* 38, 19-32.
- 6 Francovitch, R.J., Shoaf, C.R., Tayyeb, M.I., and Menzel, D.B. (In Press) Modeling nickel dosimetry from kinetic measurements in rats. *Fundam. Appl. Toxicol.*
- 7 U.S. EPA (1982) Air Quality Criteria for Particulate Matter and Sulfur Oxides. U.S. EPA, Research Triangle Park, NC.
- 8 Menzel, D.B. and Amdur, M.O. (1986) The response of the respiratory system in toxicology. In: C.D. Klaassen, M.O. Amdur, and J. Doull (Eds.), *The Basic Science of Poisons*, Macmillan, New York, pp. 330-358.
- 9 Menzel, D.B. and Wolpert, R.L. (1986) Chemical carcinogenesis and toxicity models: Matching complexity to objectives. *Bull. Math. Biol.* 48, 293-307.
- 10 Menzel, D.B., Wolpert, R.L., Shoaf, C.R., and Deal, D.L. (1986) Predicting human lung burdens of soluble nickel salts. In: S.D. Lee (Ed.), *Aerosols: Research, Risk Assessment, and Control Policies*. Lewis Publishers Inc., Chelsea, MI, pp. 637-648.

- 11 Andersen, M.E., Clewell, H.J., Gargas, M.L., Smith, F.A., and Reitz, R.H. (1987) Physiologically based pharmacokinetics and the risk assessment process for methylene chloride. *Toxicol. Appl. Pharmacol.* 87, 185-205.
- 12 Miller, F.J., Overton, J.H., Jr., Jaskot, R.H., and Menzel, D.B. (1985) A model of the regional uptake of gaseous pollutants in the lung. I. The sensitivity of the uptake of ozone in the human lung to lower respiratory tract secretions and exercise. *Toxicol. Appl. Pharmacol.* 79, 11-27.
- 13 Burke, A.M., Shoaf, C.R., and Menzel, D.B. (1988) Nickel genotoxicity in the Type II alveolar epithelial cell. *The Toxicologist* 8, 16.
- 14 Saito, K. and Menzel, D.B. (1986) Accumulation and efflux of nickel from cultured pneumocytes. *Tohoku J. Exper. Med.* 148, 295-302.
- 15 Menzel, D.B., Wolpert, R.L., Boger, J.R., III, and Kootsey, J.M. (1987) Resources available for simulation in toxicology, specialized computers, generalized software, and communication networks. *Safe Drinking Water and Health*, Vol. 6, National Academy of Science Press, Washington, DC, pp. 229-250.

## A PHYSIOLOGICALLY BASED MODEL OF SKELETAL GROWTH IN THE RAT

Ellen J. O'Flaherty

*Department of Environmental Health, University of Cincinnati College of Medicine, Cincinnati, OH*

### SUMMARY

A model of the growing small animal skeleton has been developed. The model accurately reproduces a variety of different kinds of measurements made at different ages in different species, as well as reproducing a precise and detailed series of measurements in the growing guinea pig. Of the multiple mechanisms responsible for transfer of bone-seeking elements from blood to bone and back again, several are quantitatively insignificant on a skeletal scale. Surface (rapid) exchange, diffuse (slow) exchange, and accretion of new bone during growth are the principal determinants of skeletal metabolism. Bone blood flow can probably be satisfactorily modeled as a combination of a basal flow rate plus an increment that is directly proportional to formation rate of new bone.

### INTRODUCTION

Physiologically based pharmacokinetic (PB-PK) models developed for low-molecular weight hydrocarbons generally leave about 9% of the body unperfused. This fraction includes the bone, which contains the bulk of the adult body burden of lead, as well as other bone-seeking elements. The bone is both a reservoir for and a source of persistent exposure to bone-seeking elements.

Growth and behavioral effects of lead exposure in infants and young children are a focus of current lead-related research activity [1,2]. The consequences of extended workplace exposure to lead are of continuing interest [3], and possible shifts in body distribution of lead that might accompany osteoporotic changes later in life have recently emerged as a potential concern [4]. A PB-PK model of lead disposition would provide the basis for biologically reasonable predictions of lead body burden and of the rate of return of lead from bone to other possible target tissues as functions of age and of duration and timing of exposure.

A PB-PK model for bone-seeking elements will differ from models for low-molecular weight hydrocarbons in several fundamental ways. Because of the long residence time of these elements in bone, bone growth and aging must be taken into consideration. Bone metabolic activity is closely associated with bone growth, bone blood flow rate, and with certain of the several mechanisms responsible for uptake and release of bone-seeking elements. Finally, the bone is not a homogeneously mixed compartment with respect to some of these processes nor is it even a single compartment. Rapid exchange occurs, for example, within a subcompartment of bone while diffuse exchange takes place throughout all the bone mineral.

## THE COMPOSITION OF THE SKELETON

The skeleton can be considered to be composed of bone and of marrow/vascular space. Bone may be subdivided into cortical and trabecular bone. Because bone is not fully mineralized at birth, its density is variable with age; but, as will be shown, the density of mature bone is essentially invariant across species. Marrow, which may be either red (hematopoietic) or yellow (fatty), has a density close to 1.00 g/cm<sup>3</sup>. The relative volumes of bone and marrow/vascular space that compose the mature skeleton are different in different species, so that the density of the skeleton is both age- and species-dependent.

While cortical and trabecular bone are structurally distinct, physicochemically they are essentially the same. From the standpoint of modeling the disposition of bone-seeking elements, the most important distinction between cortical and trabecular bone is that the surface-to-volume ratio of trabecular bone is much greater than that of cortical bone. The skeleton consists of 80% cortical bone and 20% trabecular bone by weight (Table 1). The human data in Table 1, which form a part of the basis for the skeleton of Reference Man [5], were obtained by morphologic analysis; the dog data were obtained by separating and ashing the bone tissue types. With the notable exception of the vertebrae and perhaps the fibula, the human values are closely comparable to the values reported for the beagle. This equivalence, of course, reflects the comparable fractional weights of trabecular and cortical bone in the human and beagle skeletons; because, however, one set of values was calculated by weight of bone ash and the other by weight of whole bone, it also reflects the equivalence in mineral density in mature bone of various species.

Living bone consists of water, a volatile inorganic fraction, organic material (collagen plus small amounts of complex, functionally specialized chemicals) and a mineral fraction, or ash. The densities and fractional volumes of cortical and trabecular bone from four species are given in Table 2. The small density differences between cortical and trabecular bone are seen to be due almost entirely to a slight difference in ash content, which is almost exactly matched by the difference in water content; organic material occupies the same fractional volume in both bone types. The remarkable constancy of mature marrow-free bone across species is also clearly apparent.

From the densities in Table 2 and the independent measurements of ash, collagen, and marrow-free dry bone densities [6,7,8], the densities of the critical skeletal components can be estimated as follows: water, 1.0 g/cm<sup>3</sup>; fully mineralized marrow-free bone, 1.9 g/cm<sup>3</sup>; fully mineralized marrow-free dry bone, 2.3 g/cm<sup>3</sup>; and bone mineral, 3.0 g/cm<sup>3</sup>. Bone mineral density is exactly three times the density of water.

TABLE 1. WEIGHTS AND PERCENTAGES OF INORGANIC ASH FROM DOG AND HUMAN BONE

Bone	Trabecular Ash (g)	Cortical Ash (g)	Trabecular Ash, % of Whole Bone Ash <sup>a</sup>	Human Estimates: Trabecular Bone, % of Whole Bone <sup>b</sup>
Ribs	8.17	7.86	50.9	
Vertebrae	6.09	32.72	15.7	73
Feet <sup>c</sup>	1.62	21.56	7.0	5
Humerus	1.57	4.94	24.1	20
Mandible + teeth	0.87	11.81	6.9	
Femur	2.14	4.76	31.5	33
Scapula	0.39	3.48	10.1	
Pelvic girdle (1/2)	1.22	4.47	21.4	
Fibula	0.06	0.54	10.0	24
Radius	0.33	2.95	10.0	16
Ulna	0.48	2.73	14.9	13
Tibia	1.34	4.50	23.0	26
Cranium <sup>d</sup>	4.98	44.84	10.0	5
All else <sup>e</sup>	9.13	41.06	18.6	
<b>Total</b>	<b>38.39</b>	<b>188.22</b>	<b>17.0</b>	<b>20</b>

<sup>a</sup> Gong [34]

<sup>b</sup> Johnson [35]

<sup>c</sup> Carpals, metacarpals, tarsals, metatarsals, and phalanges of one front and one hind paw.

<sup>d</sup> Upper mandible plus its teeth (10% of cranium weight) included.

<sup>e</sup> One-half lower mandible plus its teeth, opposing humerus, femur, scapula, radius, fibula, ulna, tibia, one-half pelvic girdle, and all other small bones not listed separately.

TABLE 2. FRACTIONAL VOLUMES AND DENSITIES OF MARROW-FREE BONE AND ITS FRACTIONS (GONG ET AL. [34])

Animal	Water	Organic	Volatile Inorganic	Ash	Ash + Organic	Marrow-Free Bone
Fractional volume, cm <sup>3</sup> /cm <sup>3</sup> marrow-free bone						
Trabecular bone						
Steer	.281	.342	.042	.335	.677	1.00
Dog	.288	.345	.042	.326	.671	1.00
Monkey	.271	.361	.040	.329	.690	1.00
Human	.270	.349	.042	.339	.688	1.00
Cortical bone						
Steer	.252	.336	.046	.366	.702	1.00
Dog	.223	.363	.046	.368	.731	1.00
Monkey	.237	.337	.047	.382	.719	1.00
Human	.239	.338	.046	.377	.715	1.00

TABLE 2. Continued.

Animal	Water	Organic	Volatile Inorganic	Ash	Ash + Organic	Marrow- Free Bone
Weight, g/cm <sup>3</sup> marrow-free bone						
Trabecular bone						
Steer	.281	.514	.072	1.067	1.581	1.934
Dog	.292	.507	.070	1.049	1.556	1.918
Monkey	.271	.514	.068	1.011	1.525	1.864
Human	.270	.497	.071	1.076	1.573	1.914
Cortical bone						
Steer	.252	.486	.078	1.178	1.664	1.994
Dog	.223	.519	.078	1.175	1.694	1.995
Monkey	.239	.487	.081	1.228	1.715	2.035
Human	.237	.476	.078	1.182	1.658	1.973

The composition of the mature small animal skeleton is given in Table 3. It is a composite of data from a large number of studies and a variety of disciplines. Contributing information includes skeletal density determinations, estimates of porosity and ash weight measurements, and direct assays of marrow and bone weights and volumes using marrow replacement techniques. The mature small animal skeleton, according to this model, is 53% marrow-free bone and 47% marrow/vascular space by volume. Its density is 1.47 g/cm<sup>3</sup>. The marrow-free bone of the model is about 25% water and 70% dry bone by volume, with 5% volatile inorganic material by volume. Total skeletal water is 41.5% by weight, of which 22.2% by weight is in the bone and 77.8% by weight is in the marrow/vascular space.

TABLE 3. WEIGHTS, VOLUMES, AND DENSITIES OF THE ADULT SMALL ANIMAL SKELETON AND ITS FRACTIONS (PER 100 g BODY WEIGHT)

	Water	Mineral	Marrow-Free Dry Bone	Marrow-Free Free Bone	Marrow	Skeleton
Weight (g)	0.57	2.35	3.5	4.2	2.0	6.2
Density (g/cm <sup>3</sup> )	1.0	3.0	2.23	1.89	1.0	1.47
Volume (cm <sup>3</sup> )	0.57	0.78	1.57	2.23	2.0	4.23

The growing skeleton can be constructed by working back from the mature to the immature skeleton, following guidelines based on one set of data and two assumptions. The data are measurements of skeletal ash in growing rats [9]. The first assumption is that skeletal density during growth reproduces the shape of the dependence of body calcium concentration on age. Since more than 99% of total body calcium is in the skeleton, it is reasonable to equate whole-body calcium with

bone calcium. The second assumption is that the process of mineralization replaces water volume for volume during bone maturation. It was shown by Hammett [10] that during skeletal growth with accompanying increase in mineral density, the increase in fractional mineral weight of the skeleton is very nearly matched by a decline in fractional water weight; the relative weight of the organic plus volatile inorganic fraction remains almost constant. Thus, the process of mineralization displaces an equal volume of water having a weight one-third that of the replacing mineral. As a starting point for development of the model of the growing skeleton, the total skeletal water of the adult rat (250 g) is allocated to marrow and to marrow-free bone in accordance with the model of Table 3: 0.778 by weight of the total water of the mature small animal skeleton is in the marrow/vascular space.

Based on the data of Pickering et al. [9], the assumption is that the process of mineralization replaces water volume for volume during bone maturation and that skeletal density increases as whole-body calcium concentration; thus, the growing skeleton can be constructed. The result is approximated by the set of equations given in Table 4.

**TABLE 4. THE GROWING RAT SKELETON**

---

Ash Weight, g = 0.01075* (BW, g) 1.18
Weight of marrow-free bone, g = 0.03392* (BW, g) 1.06
Weight of skeleton, g = 0.08183* (BW, g) .97
Weight of marrow, g = volume of marrow, cm <sup>3</sup> = 0.02397* (BW, g) 1.01

---

The predictions of the equations describing skeletal growth can be compared to actual growth measurements of several different kinds. A detailed examination of the ash weights of bones of 225 rats, 15 to 170 days old, gave log-log plots of bone ash weight vs. body weight having slopes of 1.2 to 1.3 for most bones [11]. These observations duplicated the results of an earlier study of Zucker and Zucker [12] on femoral growth rate in more than 1000 rats, 2 to 750 days old, in which the slope of the log-log plot of ash weight vs. body weight was found to be about 1.3.

Hudson [13], in a meticulous and extensive series of measurements of guinea pig marrow volumes and marrow-free bone weights, found that marrow volume increased approximately as the 0.5 power of body weight, while marrow-free bone weight was proportional to the 1.045 power of body weight.

Currey and Butler [14] showed that bone ash, as g/g marrow-free dry bone, increased slightly with age in humans, from 0.5998 in a 2-year-old child to 0.64 to 0.66 in adults. The model presented here gives an ash content of 0.533 g/g marrow-free dry bone at birth, increasing to 0.667 g/g at maturity. The comparable values for adult bone are consistent with the constancy of bone across

species, while the low value for newborn rat bone reflects a real difference in degree of mineralization of bone in the very young rat and the young child. Mineralization of the rat skeleton does not begin until 2 to 3 days before birth, and the process continues rapidly after birth.

### MECHANISMS OF ENTRY INTO BONE

The model in Figure 1 allows estimation of the volume of bone in the maturing skeleton as a function of age. The processes by which lead or other bone-seeking elements enter and leave this bone volume will be considered next.

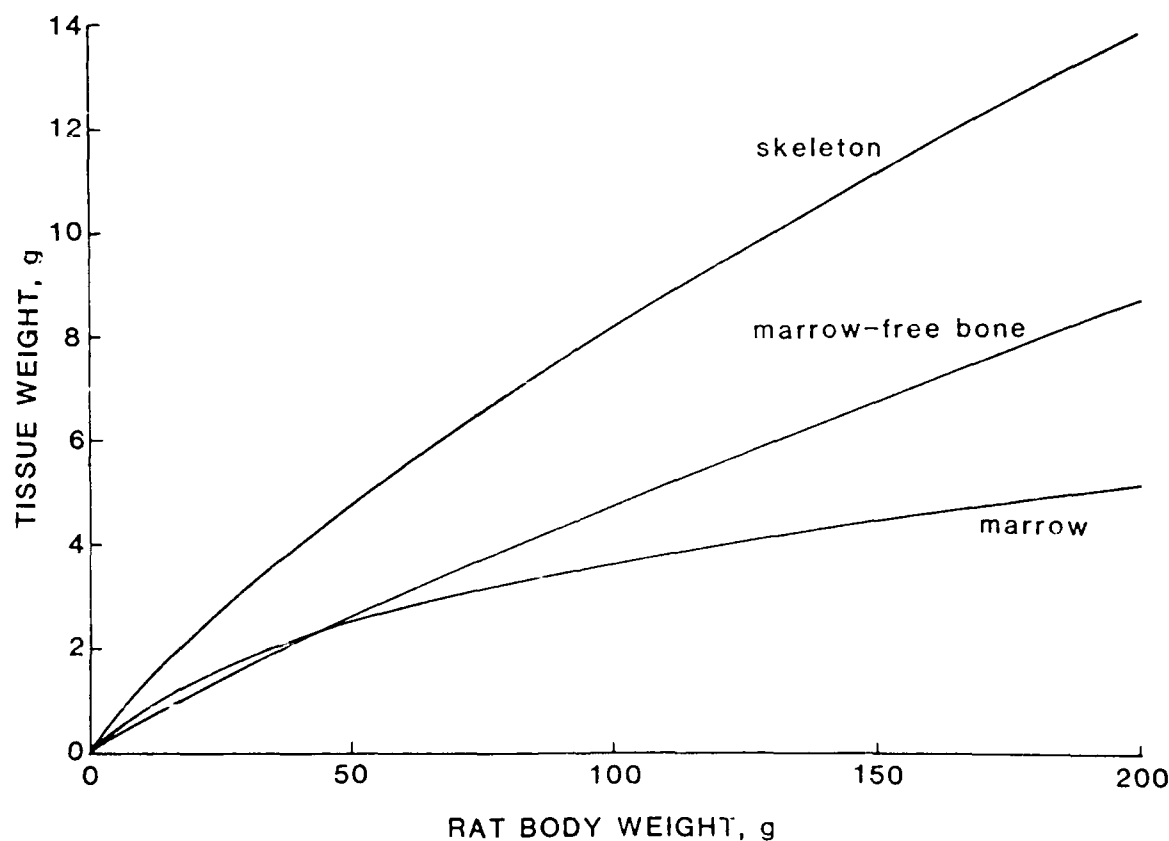


Figure 1. Model of the total and fractional weights of the maturing rat skeleton.

When a calcium tracer is introduced into the blood, it is taken up into the bone by parallel processes that are frequently grouped into three classes: accretion, resorption, and exchange. Accretion includes both apposition, or formation of new bone, and continuing mineralization (secondary mineralization) of previously formed but incompletely mineralized bone. Apposition results in the increase of bone volume, while secondary mineralization results in the increase of bone density. Apposition is the dominant feature of skeletal metabolism in the neonatal and young animal. It incorporates calcium tracers into the newly formed bone at the specific activity of the

plasma, so that it is capable of bringing about skeletal uptake of large quantities of such tracers. Secondary mineralization commonly leads to localized tracer densities approximately 50% greater than the density of adjacent bone [15]; densities several times the density of adjacent bone may be observed [16].

The contribution of these focal volumes of higher tracer density to the specific activity of whole bone is not large, at least in adulthood. Marshall et al. [17] observed rates of .004% per day of new mineral deposition due to new bone formation and secondary mineralization in cortical bone of two adult dogs, and of 0.12% per day in cortical bone of a third dog. In a fourth adult dog, bone formation rate calculated by means of fluorescence labeling of active bone-forming surfaces was found to be 0.07 to 0.08% per day in cortical bone from the midshafts of the femur and the humerus [18]. In the same dog, tracer uptake estimated by a kinetic technique that includes all unidirectional uptake of tracer at 5 days (by formation of new bone, secondary mineralization, and diffuse exchange) was 0.21% per day in the midshaft of the femur [18]. Since diffuse exchange accounts for about one-half of the persistent calcium tracer uptake in adult dogs, it appears that even in the relatively metabolically inactive cortical bone of the adult dog, secondary mineralization is responsible for only a small fraction of total skeletal mineral uptake. In actively growing bone, secondary mineralization is even less important. Bone formation rates estimated by fluorescence labeling in the midshafts of the femur and humerus of a 3- to 4-month-old puppy were 1.7% per day and 1.3% per day, respectively, while the kinetic technique gave a value of 1.4% per day for uptake at 5 days by new bone formation, secondary mineralization, and diffuse exchange in the midshaft of the femur [18].

Resorption is the reverse of apposition. It is the simultaneous removal of both bone mineral and the supporting collagen matrix and is an integral part of bone modeling or remodeling. Resorption is relatively unimportant as a mechanism for return of calcium tracers from bone to blood of adult dogs and humans. The same evidence that supports the dominance of diffuse exchange in tracer loss from bone also demonstrates the inability of resorption to account for this loss. Resorption, like secondary mineralization, is an order of magnitude too low to be quantitatively significant as a determinant of metabolism at the level of the whole mature skeleton. Resorption in the growing animal is relatively more important. Modeling and remodeling of bone take place throughout the growth period, as means of forming and reshaping the skeleton to the changing structural and kinetic requirements of the growing body.

Exchange of calcium tracers with bone mineral is also composed of two distinguishable processes: surface (or rapid) exchange and diffuse (or slow) exchange. Surface exchange of plasma and bone mineral takes place at all bone surfaces in intimate contact with blood [19]. It extends to a depth of microns or less, depending on species [20], and accounts for 0.4 to 0.6% of total bone

volume in humans [19,21,22]. The residence times of calcium tracers participating in surface exchange are of the order of minutes to hours. Because of its magnitude and rapidity, surface exchange is capable of accounting fully for the exchangeable calcium of the body.

In contrast to the rapidly exchanging surface calcium compartment, diffuse exchange is slow. Because equilibrium is reached so slowly, the magnitude of diffuse labeling increases with length of exposure to a calcium tracer and is closely related to total body burden [23]. In adults of several species, diffuse label accounts for about one-half the total label after a single brief exposure [15,24]. The rate of diffuse uptake decreases during growth, but less rapidly than accretion rate [18], so that the diffuse component of distribution of a calcium radiotracer in bone is expected to be relatively more important in animals whose exposures occur at older ages.

Four observations suggest that the rate of loss of a calcium tracer from the whole skeleton is determined, after the first few days, by the diffuse exchange process. First, the rates of loss of diffuse activity and of average activity from bone are the same [24,25], suggesting that loss of tracer from "hot spots" of active bone formation at a time of high plasma-specific activity takes place at the same relative rate as loss from the diffuse distribution. Second, the diffuse distribution remains consistently uniform long after a single administration of calcium tracer [24]. Third, repeated sampling of bone from a single dog has shown that loss by exchange could account for the total measured loss of  $^{226}\text{Ra}$  administered as a tracer [25]. Finally, it has been calculated that the rate of return of  $^{85}\text{Sr}$  from mature human bone is an order of magnitude greater than estimates of bone formation rate [26]. Since bone mass is essentially in a steady-state in the adult human, return must be largely by exchange.

#### **BLOOD FLOW RATES TO BONE**

After defining the processes by which bone-seeking elements enter and leave the bone, it is of interest to consider the rates at which these elements are presented to the bone; that is, the flow rates of blood through bone.

Early estimates of bone blood flow rates were almost all lower than what are now known to be reasonable values. Many of these estimates were based on measurements of fractional extraction of bone-seeking elements such as  $^{45}\text{Ca}$ ,  $^{85}\text{Sr}$ , or  $^{18}\text{F}$ . This technique gives estimates that are less than actual bone perfusion rates of extraction if the tracer by bone is assumed to be complete when it is not. It has been shown by a number of investigators that extraction of bone-seeking tracers is not only incomplete but is also dependent on blood flow within the physiologic range. Because bone blood flow is regionally variable, fractional extraction of tracers is regionally variable as well [27].

Use of a radiolabeled microsphere technique, in which the microspheres have been shown to lodge in the capillary network during their first pass through a tissue without occluding blood flow

through the tissue, has established that the magnitude of bone blood flow is much larger than it was previously believed to be and that it is variable from bone to bone and from region to region within a single bone. Bone blood flow rate is highest in trabecular bone and hematopoietic marrow, and lowest in cortical bone. In dogs, it has been shown to range from a low of around 2 mL/min/100-g bone in cortical bone (midshaft) of the femur and tibia of adults [28,29] to a high of about 200 mL/min/100-g bone at the metaphyseal side of the proximal growth plate of the femur of the neonate [29].

It is reasonable to postulate that bone blood flow rate should be related to the metabolic activity of the bone region being supplied. Several observations [30,31] support this hypothesis. It is possible to compare regional bone blood flows and bone accretion rates directly by drawing on the data of Schnitzer et al. [29] for regional flow rates in immature (4-month-old) and mature (more than 2-year-old) dogs, and on the data of Lee et al. [18] for the kinetically determined 5-day uptake rates in a 3- to 4-month-old puppy and a mature dog believed to be between 1 and 2 years old.

These data are plotted in Table 5 for matched regions of bone selected from the two studies. Because bone blood flow measurements were made to volumes of bone that were smaller and more precisely located than the segments of bone identified in the kinetic study, for some of the matched regions a range of flow rates is associated with a single kinetic uptake rate. The outlier in Table 5 is the proximal shaft of the mature femur. With the exception of this bone region, bone blood flow and accretion rate are directly related to one another, with an intercept suggesting that bone blood flow rate would be about 2 mL/min/100-g bone if bone accretion rate were zero.

TABLE 5. ACCRETION RATE AND BONE BLOOD FLOW RATE IN DOGS

	Accretion Rate, %/day <sup>a</sup>	Bone Blood Flow Rate, mL/min/100 g <sup>b</sup>
Immature dog (4-mo.-old)		
Femur-proximal shaft	1.9	10-18
midshaft	1.4	9
distal shaft	2.3	13-16
Tibia-whole	2.7	15.4
Mature dog (>2-yr.-old)		
Femur-proximal shaft	.26	8-12
midshaft	.21	3
distal shaft	.43	4-6
Tibia-whole	.57	5.2

<sup>a</sup> Lee et al. [18]

<sup>b</sup> Schnitzer et al. [29]

Total skeletal blood flow in the mature rat is about 3% of cardiac output. It does not appear to diminish with aging, although blood flow to specific bones or bone regions may do so [32,33]

## REFERENCES

- 1 Shukla, R., Bornschein, R.L., Dietrich, K.N., Mitchell, T., Grote, J., Berger, O., Hammond, P.B., and Succop, P.A. (1987) Effects of fetal and early postnatal lead exposure on child's growth in stature. Proceedings of the Sixth International Conference on Heavy Metals in the Environment, New Orleans, S.E. Lindberg and T.C. Hutchinson, (Eds.), Vol. 1, CEP Consultants, Edinburgh.
- 2 Dietrich, K.N., Krafft, K.M., Bier, M., Bornschein, R.L., Naraine, S., and Succop, P.A. (1987) Early effects of fetal lead exposure: developmental findings at 6 months. Proceedings of the Sixth International Conference on Heavy Metals in the Environment, New Orleans, S.E. Lindberg, and T.C. Hutchinson (Eds.), Vol. 1, CEP Consultants Edinburgh.
- 3 O'Flaherty, E.J. (1986) The rate of decline of blood lead in lead industry workers during medical removal: The effect of job tenure. *Fund. Appl. Toxicol.* 6, 372-380.
- 4 Silbergeld, E.K. and Schwartz, J. (1987) Lead and osteoporosis: mobilization of bone lead in postmenopausal women and possible etiologic role in bone demineralization. Proceedings of the Sixth International Conference on Heavy Metals in the Environment, New Orleans, S.E. Lindberg and T.C. Hutchinson (Eds.), Vol. 1, CEP Consultants, Edinburgh.
- 5 ICRP Publication Number 23: Report of the task group on reference man. (1975) Pergamon Press, Oxford, England.
- 6 Bear, R.S. (1956) The structure of collagen molecules and fibrils. *J. Biophys. Biochem. Cytol.* 2363-2368.
- 7 Mueller, K.H., Trias, A., and Ray, R.D. (1966) Bone density and composition. *J. Bone Joint Surg.* 48A, 140-148.
- 8 Robinson, R.A. (1975) Physicochemical structure of bone. *Clin. Orthoped.* 112, 263-315.
- 9 Pickering, D.E., Foran, R.F., Scott, K.G., and Crane, J.T. (1956) Chemical growth dynamics of the skeleton in the immature rat. *Am. J. Dis. Children.* 92, 276-283.
- 10 Hammett, F.S. (1925) A biochemical study of bone growth. I. Changes in the ash, organic matter, and water during growth (mus Norvegicus albinus). *J. Biol. Chem.* 64, 409-428.
- 11 Weikel, J.H., Bonner, J.F., and Neuman, W.F. (1955) Skeletal growth of the rat. *Proc. Soc. Exp. Biol. Med.* 88, 122-124.
- 12 Zucker, T.F. and Zucker, L.M. (1946) Bone growth in the rat as related to age and body weight. *Am. J. Physiol.* 146, 585-599.
- 13 Hudson, G. (1958) Bone marrow volume in guinea-pig. *J. Anat.* 92, 150-161.
- 14 Currey, J.D. and Butler, G. (1975) The mechanical properties of bone tissue in children. *J. Bone Joint Surg.* 57A, 810-814.

- 15 Marshall, J.H., Rowland, R.E., and Jowsey, J. (1959) Microscopic metabolism of calcium in bone V. The paradox of diffuse activity and long-term exchange. *Radiat. Res.* 10, 258-270.
- 16 Rowland, R.E. (1963) Some aspects of human bone metabolism deduced from studies of radium cases. *Clin. Orthop.* 28, 193-203.
- 17 Marshall, J.H., Jowsey, J., and Rowland, R.E. (1959) Microscopic metabolism of calcium in bone IV. Ca45 deposition and growth rate in canine osteons. *Radiat. Res.* 10, 243-257.
- 18 Lee, W.R., Marshall, J.H., and Sissons, H.A. (1964) Calcium accretion and bone formation in dogs. An experimental comparison between the results of Ca45 kinetic analysis and tetracycline labelling. *J. Bone Joint Surg.* 47B, 157-180.
- 19 Rowland, R.E. (1966) Exchangeable bone calcium. *Clin. Orthop.* 49, 233-248.
- 20 Groer P.G. and Marshall, J.H. (1973) Mechanism of calcium exchange at bone surfaces. *Calc. Tiss. Res.* 12, 175-192.
- 21 Bauer, G.C.H., Carlsson A., and Lindquist B. (1957) Bone salt metabolism in humans studied by means of radiocalcium. *Acta Med. Scand.* 158, 143-151.
- 22 Bronner, F., Richelle, L.J., Saville, P.D., Nicholas, J.A., and Cobb, J.R. (1963) Quantitation of calcium metabolism in postmenopausal osteoporosis and in scoliosis. *J. Clin. Invest.* 42, 898-908.
- 23 Rowland, R.E. and Marshall, J.H. (1959) Radium in human bone: The dose in microscopic volumes of bone. *Radiat. Res.* 11, 299-313.
- 24 Rowland, R.E. (1960) The deposition and the removal of radium in bone by a long-term exchange process. *Clin. Orthop.* 17, 146-153.
- 25 Rowland, R.E. (1961) Microscopic metabolism of Ra226 in canine bone and its bearing on the radiation dosimetry of internally deposited alkaline earths. *Radiat. Res.* 15, 126-137.
- 26 Shimmins, J. and Smith, D.A. (1966) Estimation of bone mineral transfer rate by the measurement of long-term retention of Sr85. *Metabolism* 15:436-15443.
- 27 Tothill, P., Hooper, G., McCarthy, I.D., and Hughes, S.P.F. (1985) The variation with flow-rate of the extraction of bone-seeking tracers in recirculation experiments. *Calc. Tiss. Int.* 37, 312-317.
- 28 Tondevoid, E. and Bulow, J. (1984) Microsphere determined regional bone blood flow in conscious dogs at rest and long time muscular exercise. In: Arlet, J., R.P. Ficat and D.S. Hungerford (Eds.), *Bone Circulation*, Williams and Wilkins, Baltimore, pp. 175-177.
- 29 Schnitzer, J.E., McKinstry, P., Light, T.R., and Ogden, J.A. (1982) Quantitation of regional chondroosseous circulation in canine tibia and femur. *Am. J. Physiol.* 282, H365-H375.
- 30 Sim, F.H. and Kelly, P.J. (1970) Relationship of bone remodeling, oxygen consumption, and blood flow in bone. *J. Bone Joint Surg.* 52A, 1377-1389.
- 31 Whiteside, L.A., Simmons, D.J., and Lesker, P.A. (1977) Comparison of regional bone blood flow in areas with differing osteoblastic activity in the rabbit tibia. *Clin. Orthop. Rel. Res.* 124, 267-270.

- 32 Hruza, Z. and Wachtlova, M. (1969) Diminution of bone blood flow and capillary network in rats during aging. *J. Gerontol.* 24, 315-320.
- 33 MacFherson, J.N. and Tothill, P. (1978) Bone blood flow and age in the rat. *Clin. Sci. Molec. Med.* 54, 111-113.
- 34 Gong, J.K., Arnold, J.S., and Cohn, S.H. (1964) Composition of trabecular and cortical bone. *Anat. Rec.* 149, 325-331.
- 35 Johnson, L.C. (1964) In: H.M. Frost (Ed.), *Bone Biodynamics*. Little, Brown & Co., Boston, pp. 543-654.

## INCORPORATION OF *IN VITRO* ENZYME DATA INTO THE PB-PK MODEL FOR METHYLENE CHLORIDE: IMPLICATIONS FOR RISK ASSESSMENT

R.H. Reitz<sup>a</sup>, A.L. Mendrala<sup>a</sup>, C.N. Park<sup>a</sup>, M.E. Andersen<sup>b</sup>, and F. P. Guengerich<sup>c</sup>

<sup>a</sup> *Dow Chemical Company, Health and Environmental Sciences, Midland, MI*, <sup>b</sup>*Wright Patterson Air Force Base, Armstrong Aerospace Medical Research Laboratory, Dayton, OH*, <sup>c</sup>*Vanderbilt University, Department of Biochemistry, Nashville, TN*

### SUMMARY

Physiologically based pharmacokinetic (PB-PK) models provide a mechanism for reducing the uncertainty inherent in extrapolating the results of animal toxicity tests to man. This paper discusses a technique for incorporating data from *in vitro* studies of xenobiotic metabolism into *in vivo* PB-PK models. Methylene chloride (CH<sub>2</sub>Cl<sub>2</sub>) is used as an example, and carcinogenic risk estimates incorporating PB-PK principles are presented.

### INTRODUCTION

Human beings are exposed to many chemicals, natural and synthetic. To assess whether those chemicals are likely to produce adverse effects in human populations, toxicity tests are conducted in laboratory animals. Inherent in this procedure is the assumption that laboratory animals are reasonable surrogates for humans; that is, most materials that fail to produce adverse effects in animals will not produce adverse effects in human populations. However, significant differences usually exist between the conditions prevailing in laboratory tests and those encountered by humans.

Animals used in laboratory tests come from carefully bred homogeneous strains and are carefully screened to be free of disease. At the start of the test, all the animals are young adults. For practical reasons, small groups are used, and a limited number of doses are evaluated. Doses are usually high, and chemicals are administered by the most experimentally convenient route.

In contrast, human populations are heterogeneous and contain healthy and diseased individuals of all ages. Human exposures typically involve doses much lower than those employed in the animal tests and frequently occur through one or more routes different than the animal studies.

Therefore, a variety of extrapolations are necessary in order to estimate human hazard from animal studies. Each extrapolation introduces uncertainty into the final risk assessment. Physiologically based pharmacokinetic models are useful for reducing some of this uncertainty because they take into account actual physiological properties of the various species, compound-specific partitioning of the chemical between tissues and blood, and concentration-dependent rates of metabolism. PB-PK models are particularly useful for high dose/low dose extrapolations, dose route extrapolations, and interspecies extrapolations.

We have reported a procedure for incorporating the techniques of PB-PK modeling into the risk assessment for  $\text{CH}_2\text{Cl}_2$  [1]. A PB-PK model was developed providing quantitative descriptions of the rates of metabolism and levels of  $\text{CH}_2\text{Cl}_2$  in various organs of four mammalian species (mouse, hamster, rat, and human). The model was validated by comparing computer simulations with experimental data gathered in mice, rats, and humans. Levels of reactive metabolites produced in target tissues were correlated with tumor incidences in two chronic bioassays of  $\text{CH}_2\text{Cl}_2$  in the  $\text{B}_6\text{C}_3\text{F}_1$  mouse [2,3]. Finally, relevant measures of tissue dose were calculated for use in a pharmacokinetically based risk assessment.

Development of this PB-PK model required the acquisition of three types of model parameters: (1) physiological constants, (2) partition coefficients, and (3) metabolic rate constants. Physiological parameters for the various species were available from the scientific literature [4,5,6], and partition coefficients were determined experimentally at Wright Patterson Air Force Base (WPAFB) according to the procedures of Sato and Nakajima [7].

*In vivo* gas uptake studies conducted at WPAFB, according to the method of Gargas et al. [8] were used to estimate metabolic rate constants for two pathways of  $\text{CH}_2\text{Cl}_2$  metabolism in animals [1]. These pathways involve oxidation of  $\text{CH}_2\text{Cl}_2$  by cytochrome P450-dependent enzymes (mixed function oxidase [MFO]) [9] and conjugation of  $\text{CH}_2\text{Cl}_2$  with glutathione by glutathione-S-transferase enzymes (GST) [10]. Metabolic rate constants for the MFO pathway in humans were derived from measurements of carboxyhemoglobin, exhaled carbon monoxide, and  $\text{CH}_2\text{Cl}_2$  uptake in human volunteers exposed to either 100 or 350 ppm of  $\text{CH}_2\text{Cl}_2$  at the Dow Chemical Company [1].

However, there were no *in vivo* data available for direct calculation of the rate constants for the GST pathway in humans. Since MFO enzymes have a higher affinity for  $\text{CH}_2\text{Cl}_2$  than the GST enzymes [11], most of the metabolism of  $\text{CH}_2\text{Cl}_2$  occurs through MFO at low concentrations. Therefore, the human studies of  $\text{CH}_2\text{Cl}_2$  metabolism (which all used relatively low concentrations of  $\text{CH}_2\text{Cl}_2$ ) are not appropriate for estimating the rate of metabolism by the GST pathway. Consequently, the rate constants for the GST pathway were estimated by allometric scaling of the *in vivo* rate constants for GST metabolism in animals [1]. Although allometric scaling has been used by others for estimating metabolic rates in different species [12], it was clear that data supporting the validity of such scaling for  $\text{CH}_2\text{Cl}_2$  would be valuable.

Additional experiments to estimate the value of the metabolic rate constants for the GST pathway in humans have now been conducted. These experiments involved *in vitro* measurements of the glutathione-dependent metabolism of  $\text{CH}_2\text{Cl}_2$  in tissue samples from humans as well as tissue samples from Fischer 344 (F-344) rats,  $\text{B}_6\text{C}_3\text{F}_1$  mice, and Syrian Golden hamsters. Similar procedures were employed to make *in vitro* measurements of the rate of oxidation of  $\text{CH}_2\text{Cl}_2$  by the MFO

enzymes, and the reliability of the *in vitro* to *in vivo* extrapolation was assessed by comparing observed *in vivo* rates of MFO metabolism with those predicted from the *in vitro* data. This paper will describe the methods employed to collect the *in vitro* data and show how they may be incorporated into PB-PK risk assessments for  $\text{CH}_2\text{Cl}_2$ .

## METHODS

### *Test materials*

Spectroscopic grade  $\text{CH}_2\text{Cl}_2$  (>99.9% purity) was obtained from Fisher Chemical Co.  $\text{CH}_2^{36}\text{Cl}_2$  (0.5 mCi/mmol) was synthesized by New England Nuclear (Boston, MA). This material was checked for radiochemical purity by gas chromatography/mass spectrometry prior to use and was found to be 95.0%  $\text{CH}_2^{36}\text{Cl}_2$ , with small amounts of  $\text{CH}_3^{36}\text{Cl}$  (0.6%) and  $\text{CH}^{36}\text{Cl}_3$  (2.8%) identified as minor impurities.

### *Preparation of enzymes*

Cytosolic and microsomal fractions of lungs and livers were prepared from male F-344 rats,  $\text{B}_6\text{C}_3\text{F}_1$  mice, Syrian Golden hamsters, and tissues of otherwise healthy human accident victims selected for organ transplantation through the Nashville Regional Organ Procurement Agency, Nashville, TN. Tissues were removed from animals or humans and small pieces were rapidly frozen either by immersion in liquid nitrogen (humans) or with dry ice (animals). Soluble enzymes (cytosol) and particulate enzymes (microsomes) were prepared as described elsewhere [13-18].

Samples of human liver from four different individuals were processed individually. Availability of human lung samples was limited, so lung samples from two individuals were pooled (approximately 8g total tissue weight) for the enzyme preparations from human lung. (None of the lung samples were from the same individuals as the liver samples.)

### *Assay of MFO*

Incubations (30 min, 37°C) were conducted in 5.0-mL vials sealed with Teflon<sup>®</sup>-coated rubber septa (4.0 mL headspace). The vials contained an NADPH regenerating system in addition to phosphate buffer (pH 7.4) and  $\text{CH}_2\text{Cl}_2$ . At the end of incubation, the contents of the vial were transferred to a glass tube containing 0.5 mL of a solution of 2%  $\text{Na}_2\text{CO}_3$  and 1%  $\text{NaCl}$  as well as 3.0 mL of unlabeled  $\text{CH}_2\text{Cl}_2$ , and were vortexed vigorously for 10 sec. Centrifugation served to separate the unreacted substrate (in the organic layer) from the water-soluble  $^{36}\text{Cl}^-$  ion formed by enzyme reaction.

### Assay of GST

Incubations (30 min, 37°C) were conducted in 1.8-mL glass vials sealed with Teflon<sup>3</sup>-coated rubber septa (<0.1 mL headspace). Each incubation contained (in addition to CH<sub>2</sub>Cl<sub>2</sub>) potassium phosphate buffer (50 to 100 mM, pH 7.4) and reduced glutathione (10 mM). <sup>36</sup>Cl<sup>-</sup> ion was separated from the unreacted CH<sub>2</sub>Cl<sub>2</sub> as outlined for the MFO assay.

## RESULTS

### MFO enzymes

A series of incubations with microsomes prepared from liver were conducted at CH<sub>2</sub>Cl<sub>2</sub> concentrations varying from 1 mM to 10 mM. The reaction rates observed (nanomoles/min/milligram of protein) are listed in Table 1. The highest rates of oxidation were observed in the hamster liver microsomes, with slightly lower rates in the mouse liver microsomes. Lower rates were observed in rat and human liver microsomes (Table 1).

TABLE 1. REACTION RATE (nmoles/min/mg protein)<sup>a</sup>

Conc. (mM)	Mouse	Rat	Hamster	Human (HL-99)	Human (HL-109)
MFO Assays (Liver)					
1.00	5.87 <sup>b</sup>	2.40 <sup>b</sup>	7.18 <sup>b</sup>	1.49	1.66 <sup>b</sup>
1.23	6.52 <sup>b</sup>	2.42 <sup>b</sup>	8.16 <sup>b</sup>	1.85	2.06 <sup>b</sup>
1.64	7.18 <sup>b</sup>	2.93 <sup>b</sup>	8.54 <sup>b</sup>	2.09	2.26 <sup>b</sup>
2.60	9.02 <sup>b</sup>	3.44 <sup>b</sup>	11.02 <sup>b</sup>	2.28	2.87 <sup>b</sup>
5.00	11.40 <sup>b</sup>	4.10 <sup>b</sup>	14.47 <sup>b</sup>	3.34	4.46 <sup>b</sup>
10.00	14.40 <sup>b</sup>	4.91 <sup>b</sup>	18.18 <sup>b</sup>	4.58	4.80 <sup>b</sup>
MFO Assays (Lung)					
5.00	4.62	0.16	0.99	<0.1 <sup>c</sup>	—
GST Assays (Liver)					
6.7	4.77	0.75	0.182	—	—
10.0	7.24	1.11	0.307	—	—
12.5	9.92	1.36	0.383	1.53	1.28
16.7	12.3	2.08	0.482	1.95	1.66
25.0	18.5	3.19	0.76	2.58	2.24

TABLE 1. Continued.

Conc. (mM)	Mouse	Rat	Hamster	Human (HL-99)	Human (HL-109)
50.0	33.2	6.17	1.24	3.95	3.51
100.0	48.6	12.1	2.64	4.74	3.94
GST Assays (Lung)					
40.0	7.3	1.0	0.0	0.37	—

a Enzyme activities (GST and MFO) observed at various concentrations of  $\text{CH}_2\text{Cl}_2$  with enzymes prepared from liver tissue of male B6C3F<sub>1</sub> mice, F-344 rats, Syrian Golden hamsters, and humans. All values are reported as nmoles product formed/min/mg protein.

b Mean value from two independent experiments.

c Pooled human lung samples, no activity observed at detection limit of 0.05 to 0.1 nmoles/min/mg protein.

Microsomes prepared from lung tissues in the various species were assayed at a single substrate concentration: 5 mM  $\text{CH}_2\text{Cl}_2$ . Microsomes from mouse lungs were much more active than microsomes from the lungs of the other species (Table 1). No MFO activity was detected in pooled samples of human lung microsomes, with a detection limit of approximately 0.1 nmole/min/mg protein.

Double reciprocal plots (1/Velocity vs. 1/Substrate; Lineweaver and Burk [19]) of the results obtained with liver microsomes are presented in Figure 1a (B<sub>6</sub>C<sub>3</sub>F<sub>1</sub> mice), Figure 1b (F-344 rats), Figure 1c (Syrian Golden hamsters), and Figure 1d (human sample HL-99). Kinetic data for three other human liver samples were analyzed but are not shown.

Values of  $K_m$  (the affinity constant) and  $V_{max}$  (the maximum rate of the enzyme reaction) were determined by computer optimization (method of least squares) of the data listed in Table 1. The results ( $\pm$  standard deviation) are listed in Table 2. The values of  $K_m$  were almost identical in the seven sets of liver microsomes analyzed, ranging from 0.92 mM (Human-105) to 2.8 mM (Human-109). However, the values of  $V_{max}$  in the various species differed significantly. The highest values of  $V_{max}$  were observed in microsomes from hamster liver ( $V_{max}$  = 20.8), with lower rates in mice ( $V_{max}$  = 15.9), rats ( $V_{max}$  = 5.39), and humans (range = 1.5-13.0, mean  $V_{max}$  = 6.5).

### GST Enzymes

Assays of GST in cytosol prepared from the livers of the various species were conducted at  $\text{CH}_2\text{Cl}_2$  concentrations from 6.7 mM to 100 mM. (The limited solubility of  $\text{CH}_2\text{Cl}_2$  in water prevented testing concentrations higher than 100 mM.) Enzymes prepared from mouse liver contained the highest levels of the GST enzyme (Table 1). Tissues from the rat liver contained intermediate levels of GST, while tissues from the hamster and human livers contained the lowest levels of GST (Table 1).

Cytosol preparations from the lungs of the different species were assayed at a single substrate concentration: 40 mM  $\text{CH}_2\text{Cl}_2$ . The highest levels of GST activity in lung tissue were observed in the

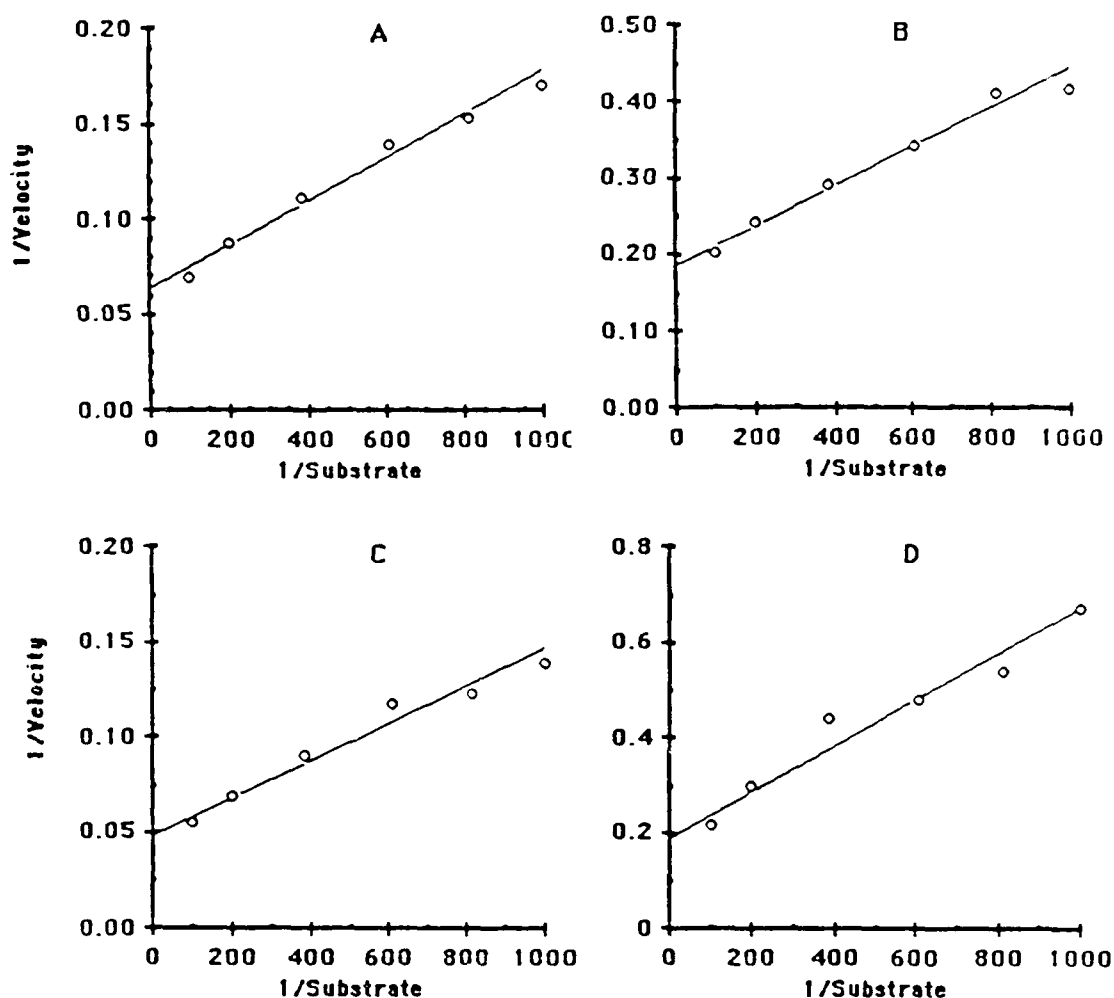


Figure 1. Lineweaver-Burk plots (1/velocity vs. 1/substrate concentration) of the concentration dependence of MFO activity in microsomes prepared from various species. Concentrations of  $\text{CH}_2\text{Cl}_2$  in the incubation mixture varied from 1 mM to 10 mM, and the incubations also contained 50 mmoles potassium phosphate buffer (pH 7.4), 10 mmoles glucose-6-phosphate, 0.5 mmoles NADP + , -1 Unit of glucose-6-phosphate dehydrogenase,  $\text{CH}_2^{36}\text{Cl}_2$ , and 1 to 2 mg of microsomal protein in a total volume of 1.0 mL. Plots are shown for (A) mouse microsomes, (B) rat microsomes, (C) hamster microsomes, and (D) human microsomes prepared from liver #99.

mouse. The rat lung had intermediate activity, and the lowest activity was observed in cytosol prepared from human and hamster lungs. GST activity was not detectable in cytosol from hamster lungs (detection limit approximately 0.2 nmole/min/mg protein), but a low level of GST activity was detected in cytosol prepared from human lungs. Cytosol prepared from lung was less active than cytosol prepared from liver in all species studied (Table 1).

Double reciprocal plots of GST activity were prepared for the four species studied (mouse, Figure 2a; rat, Figure 2b; hamster, Figure 2c; and human, Figure 2d). Examination of these plots

suggested that the  $K_m$ 's were much higher than the  $K_m$  for MFO activity. The  $K_m$ 's obtained by computer optimization of data collected with human and mouse tissues were 44 and 137 mM, respectively (Table 2). Computer optimization failed to find a satisfactory "solution" for  $K_m$  and  $V_{max}$  with enzyme preparations from rat and hamsters, but examination of the double reciprocal plots (Figures 2b, 2c) suggested that the  $K_m$  was much higher than 100 mM.

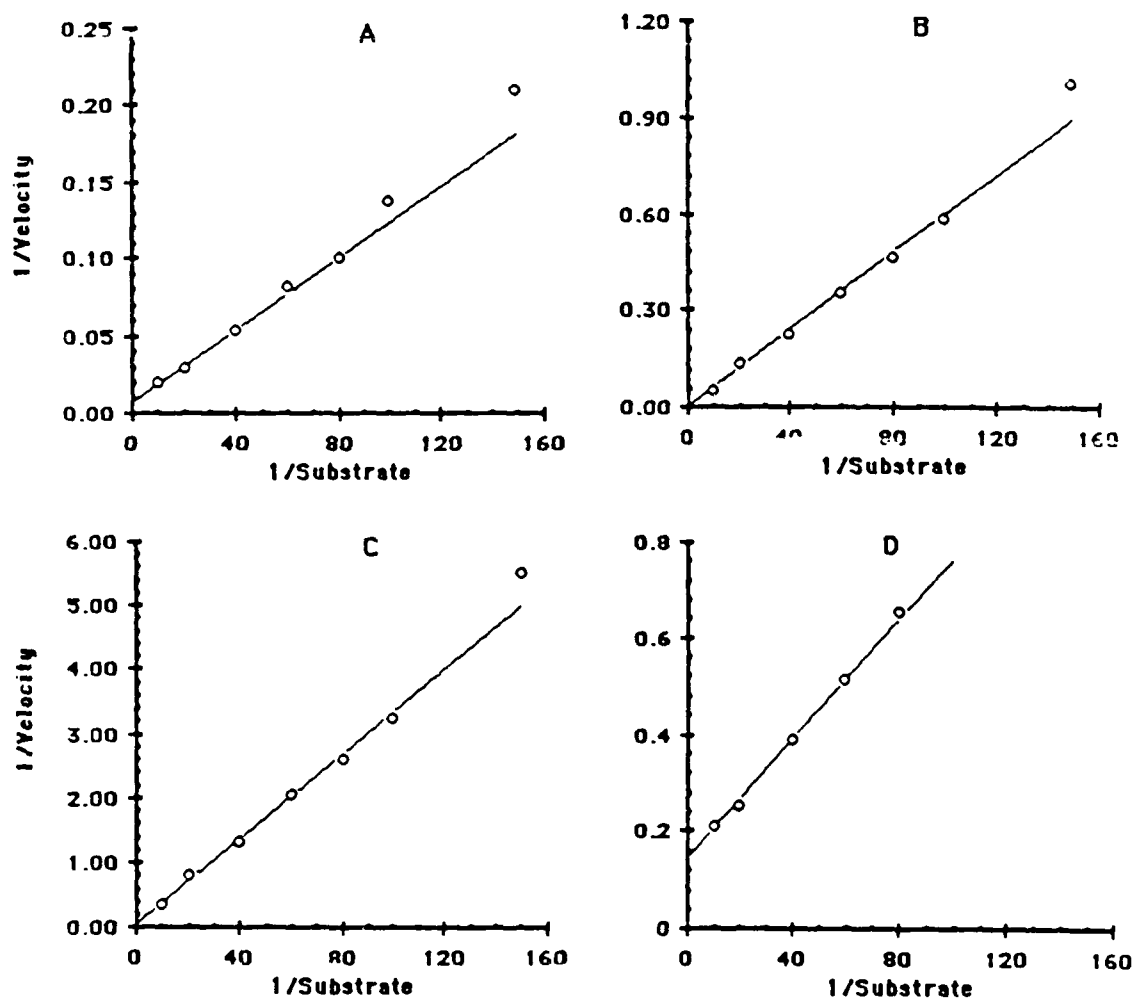


Figure 2. Lineweaver-Burk plots (1/velocity vs. 1/substrate concentration) of the concentration dependence of GST activity in cytosols prepared from various species. Concentrations of  $\text{CH}_2\text{Cl}_2$  in the incubation mixture varied from 6.7 mM to 100 mM, and the incubations also contained 8 mM glutathione, and 60 mM phosphate buffer (pH = 7.4). Plots are shown for (A) mouse cytosol, (B) rat cytosol, (C) hamster cytosol, and (D) human cytosol prepared from liver #99.

TABLE 2. KINETIC CONSTANTS<sup>a</sup>

Species	N	K <sub>m</sub> (mM)	V <sub>max</sub> (nmoles product formed / min. mg prot.)
MFO Assays			
Mouse	12	1.84 ± 0.33	15.90 ± 1.10
Rat	12	1.42 ± 0.74	5.39 ± 0.94
Hamster	12	2.07 ± 0.30	20.80 ± 1.15
Human-99	6	2.57 ± 2.17	5.27 ± 1.85
Human-103	6	1.95 ± 5.24	1.53 ± 1.56
Human-105	6	0.92 ± 0.29	13.00 ± 1.13
Human-109	6	2.82 ± 1.47	6.24 ± 1.39
GST Assays			
Mouse	5	137 ± 21	118.2 ± 14.4
Rat	5	N.S. <sup>b</sup>	N.S. <sup>a</sup>
Hamster	5	N.S. <sup>b</sup>	N.S. <sup>a</sup>
Human-99	5	43.8 ± 4.5	7.05 ± 0.44
Human-109	5	44.1 ± 8.1	6.04 ± 0.67

<sup>a</sup> Kinetic constants obtained from *in vitro* experiments with GST and MFO assays in enzyme preparations from the livers of male B6C3F1 mice, F-344 rats, Syrian Golden hamsters, and humans. Constants were obtained by relative least squares weighting using the SimuSolv<sup>®</sup> computer program. Values reported are the best estimate ± the standard deviation of the estimate as calculated by the computer program.

<sup>b</sup> Data collected but no acceptable solution obtained during computer optimization.

## DISCUSSION

### MFO enzymes

The *in vivo* values of V<sub>max</sub> and K<sub>m</sub> for MFO reported by Andersen et al. [1] were converted to rates of metabolism per gram of liver tissue (V<sub>max</sub>1) by dividing the *in vivo* V<sub>max</sub> for the whole animal by the grams of liver tissue per animal (Table 3). Liver sizes for the three species of animals were estimated from historical data collected at the Dow Chemical Company (Table 3). *In vivo* rates of metabolism in liver tissue (assuming that the liver is the primary site of metabolism in the animal) were calculated for a concentration in the linear portion of the velocity vs. concentration curve (1 μM or 10<sup>-6</sup> molar) according to the Michaelis-Menten equation:

$$\text{Rate} = \frac{V_{\max} * \text{Conc}}{K_m + \text{Conc}} \quad (1)$$

and are listed in row 5 of Table 3 (with units of nanomoles/gram liver/hour). This calculated rate of *in vivo* metabolism was divided by the rate of metabolism observed in *in vitro* experiments at a concentration of 1 mM (a concentration that was also in the nearly linear portion of the *in vitro* velocity vs. substrate curve), and the ratio of the two activities is listed in row 7 of Table 3.

TABLE 3. COMPARISON OF MFO ACTIVITY CALCULATED FROM *IN VIVO* EXPERIMENTS AND *IN VITRO* ENZYME ASSAYS<sup>a</sup>

	Mouse	Rat	Hamster	Human
Body Wt (g)	34.5	233.0	140.0	70,000
Liver Wt (g)	1.84	5.41	4.34	2198
V <sub>max</sub> 1 (nmoles/g/hr)	6700	3260	5560	637
K <sub>m</sub> (μM)	4.66	9.08	7.64	6.83
Calc (nmoles/g/hr)	1180	324	644	81.4
Obs (nmoles/mg/hr)	352	144	431	31-433
Ratio (Calc/Obs)	3.36	2.25	1.49	0.2-2.6
Mean Ratio		2.37		1.13
		± 0.94		± 1.04

<sup>a</sup> Rates of *in vivo* metabolism are calculated from the reference of Andersen et al. [1] by converting V<sub>max</sub> (mg/h/animal) to V<sub>max</sub>1 (nmoles/gram liver/h), K<sub>m</sub> from mg/liter to mmoles/liter and solving the Michaelis Menten equation with a concentration of 1 μM. *In vitro* rates are given as nmoles converted/h/mg microsomal protein.

The ratio of the *in vivo* and *in vitro* activities is reasonably consistent across the three animal species (mouse = 3.36, rat = 2.25, hamster = 1.49). This suggests that the *in vitro* and *in vivo* results are proportional to each other in spite of the obvious variations in assay conditions (e.g., cofactor concentrations, ionic strength, oxygen tension, substrate concentrations, etc).

*In vitro* measurements of MFO activity in microsomes prepared from human livers revealed considerably more variation than was present in microsomes prepared from the animal species. In addition to the two samples of human liver microsomes reported in Table 1, two additional samples of microsomes were assayed: HL-103 and HL-105. One of these, HL-103, had about one-fourth the activity observed in HL-99 and HL-109, and the other, HL-105, had about twice as much activity as HL-99 and HL-109. Therefore, variations in the level of MFO in human tissues spanned almost one order of magnitude. However, the mean ratio of *in vivo* to *in vitro* activity in human liver microsomes ( $1.13 \pm 1.04$ ) was fairly close to the mean ratio observed in the animal liver microsomes ( $2.37 \pm 0.94$ ), and this comparison provides support for the concept of incorporating *in vitro* enzyme data into the *in vivo* PB-PK model for CH<sub>2</sub>Cl<sub>2</sub>.

### GST enzymes

Saturation of MFO occurred *in vivo* during exposure to concentrations of 300 to 500 ppm CH<sub>2</sub>Cl<sub>2</sub> [1]. *In vitro* K<sub>m</sub>'s for MFO activity were in the range of 1 to 2 mM CH<sub>2</sub>Cl<sub>2</sub> (Table 2). Since the *in vitro* K<sub>m</sub>'s for GST in animal tissues were at least two orders of magnitude higher than the K<sub>m</sub>'s for MFO (Table 2), it appears unlikely that saturation of GST *in vivo* would occur at concentrations of CH<sub>2</sub>Cl<sub>2</sub> roughly one order of magnitude higher than those causing saturation of MFO *in vivo*.

Consequently, the *in vitro* studies reported here are consistent with the description of GST metabolism as a first order pathway as described by Andersen et al. [1]. The rate of GST reaction ( $dAM2/dt$ ) in this paper was calculated according to the equation

$$\frac{dAM2}{dt} = (KF) (Conc) (Vol) \quad (2)$$

where

$KF$  = first order rate constant,

$Conc$  = concentration of  $CH_2Cl_2$  in venous blood leaving the liver, and

$Vol$  = size of the liver in liters.

This equation is equivalent to a simplified form of the Michaelis-Menten equation

$$\frac{dAM2}{dt} = \frac{(V_{max})(Conc)(Vol)}{(K_m + Conc)} \sim \frac{V_{max}}{K_m} (Conc)(Vol) \quad (3)$$

when  $V_{max}$  has units of milligram/hour/liter of tissue and  $Conc$  is small relative to  $K_m$ . Thus, the constant  $KF$  in equation 2 is Equivalent to the expression  $V_{max}/K_m$  in equation 3. Assuming that a liter of liver from each species contains roughly equal amounts of cytosolic protein (so that the volume term drops out of the equation), we can rearrange equation 2 to solve for  $KF$  as follows:

$$KF = (K_1) \frac{dAM2/dt}{Conc} = (K_2) \frac{Velocity}{Substrate} \quad (4)$$

where  $KF$  is equal to a proportionality constant times the rate of the enzyme reaction divided by the substrate concentration (V/S ratio). Equation (4) can be written in the same form for either the *in vivo* reaction or the *in vitro* reaction; only the proportionality constant is different ( $K_1$  or  $K_2$ ). Since the *in vivo*  $KF$  and the *in vitro* V/S ratio are known with reasonable accuracy for the  $B_6C_3F_1$  mice, the value of  $K_2$  can be obtained by dividing  $KF$  by the V/S ratio, and then used to calculate the *in vivo*  $KF$  in any species for which an *in vitro* V/S ratio is known.

V/S ratios for GST activity in cytosol prepared from the livers of  $B_6C_3F_1$  mice, F-344 rats, Syrian Golden hamsters, and human livers were determined by dividing the *in vitro* reaction velocities for GST in Table 1 (columns 2 through 6) by the substrate concentration (column 1, Table 1). The V/S ratio was essentially constant up to 25 mM in all species, but declined at concentrations of 50 mM or higher in the human liver samples. Consequently, the average V/S ratio for concentrations less than 50 mM in a given species (Table 4, column 1) was used in these calculations. Values of the *in vivo* rate constant  $KF$  calculated for rats, hamsters, and humans, using mouse data as a reference point, are listed in column 2 of Table 4.

The estimated value of  $KF$  for humans obtained by this procedure (0.43) was very close to that which Andersen et al. [1] obtained by allometric scaling of the mouse data (0.53; Table 4, column 3). The value of  $KF$  for rats (0.63) was somewhat lower than that estimated by Andersen et al. [1] in gas

TABLE 4. METABOLIC RATE CONSTANTS.<sup>a</sup>

	V/S	Calc KF	Orig KF	A1	A2
Mouse	741.4 ± 31.1	4.01 <sup>b</sup>	4.01 <sup>b</sup>	0.405	0.28
Rat	116.9 ± 8.6	0.63	2.21	0.039	0.14
Hamster	29.6 ± 1.5	0.16	1.51	0.068	0.10
Human	105.6 ± 12.0	0.43 <sup>c</sup>	0.53	0.0014	0.18

a. Calculation of metabolic rate constants for use in the PB-PK model of Andersen et al. [1]. Column 1 contains the velocity to substrate ratio (V/S). Column 2 contains the value of KF calculated from the *in vitro* studies as outlined in the text. Column 3 lists the value of KF cited by Andersen et al. [1] for their PB-PK model. (The value of KF cited by Andersen et al. [1] is used as a reference point for calculating the *in vivo* rate constants in the rat, hamster, and human.) Columns 4 and 5 show the relative specific activities of MFO (A1) and GST (A2) in enzyme preparations from the various species.

b. Used as a reference point for the other values.

c. Value multiplied by 0.75 to correct for the fact that only three of the four human liver samples had detectable activity.

uptake experiments (2.21), and the value of *KF* in hamsters (0.16) was almost an order of magnitude less than the value that Andersen et al. [1] derived from gas uptake (1.51). It seems likely that the rather large discrepancy in the hamster constants is related to an inherent limitation of the gas uptake procedure from which the *in vivo* constant was estimated.

The gas uptake technique depends upon measuring overall rates of loss of CH<sub>2</sub>Cl<sub>2</sub> from the chamber [8]. Consequently, uncertainty in the values of rate constants estimated with this procedure increases when one of the two pathways is much more active than the other.

In the mouse, the ratio of GST to MFO activity, measured at substrate concentrations of 6.7 and 5.0 mM CH<sub>2</sub>Cl<sub>2</sub>, respectively, was 0.420 (Table 1). Consequently, the gas uptake procedure should give reasonable accuracy in estimating both the GST and MFO rate constants. In contrast, the ratio of GST to MFO activity in hamsters was only 0.013, and large errors in the estimation of *in vivo* GST rate constants are possible (although estimation of *in vivo* MFO rate constants by gas uptake should be reliable in this species). Clearly the values for *KF* estimated from gas uptake studies in mice will be the most reliable, the values estimated from gas uptake studies in rats somewhat less reliable, and the values for *KF* in the hamster studies will contain the highest levels of uncertainty.

#### **Correlation of *in vitro* results with animal bioassays**

High incidences of malignant lung and liver tumors have been observed in B<sub>6</sub>C<sub>3</sub>F<sub>1</sub> mice exposed to high concentrations of CH<sub>2</sub>Cl<sub>2</sub> vapor [2]. However, increased levels of lung and liver tumors were

not seen in F-344 rats and Syrian Golden hamsters exposed to similar levels of  $\text{CH}_2\text{Cl}_2$  vapor [2,20], and exposure of  $\text{B}_6\text{C}_3\text{F}_1$  mice to  $\text{CH}_2\text{Cl}_2$  in drinking water also failed to induce a tumorigenic response [3]. Andersen et al. [1] have suggested that the reactive metabolites derived from conjugation of  $\text{CH}_2\text{Cl}_2$  with glutathione are likely to be responsible for the tumorigenic activity of  $\text{CH}_2\text{Cl}_2$  in the  $\text{B}_6\text{C}_3\text{F}_1$  mouse, and the PB-PK model allows us to calculate levels of these metabolite(s) in the target tissues of the various species in either inhalation or drinking water studies to determine whether there is a correlation between GST activity and tumorigenicity.

Under the conditions of the NTP inhalation bioassay, the dose (in milligram equivalents of GST metabolites formed per day per liter of tissue) to lung and liver tissues of the  $\text{B}_6\text{C}_3\text{F}_1$  mouse was 482 and 1670, respectively (Table 5). Under the conditions of the NCA drinking water bioassay in this same strain, the dose to lung and liver tissues was only 2.2 and 16, respectively. This result correlates well with the observed tumor frequencies in the two bioassays: malignant tumors of lung and liver tissue were observed following inhalation exposure, but no significant changes in lung or liver tumor frequencies were observed in the drinking water study [2,3].

TABLE 5. GLUTATHIONE CONJUGATE<sup>a</sup>

Species	Dose	Route	Lung	Liver
Mouse	4000 <sup>b</sup>	Inh	482	1670
Mouse	250 <sup>c</sup>	Water	2.2	16.0
Rat	4000 <sup>b</sup>	Inh	96	677
Hamster	3500 <sup>b</sup>	Inh	17.1	167

a. Average amounts of glutathione conjugate (in mg equivalents of  $\text{CH}_2\text{Cl}_2$ ) produced in target tissues per 24 hr per liter of tissue in various species during inhalation exposures (6 hr/day, 5 days/week, 96-week, 104-week study) or drinking water exposures (24 hr/day). Concentrations in the inhalation exposures are in ppm, and doses in the drinking water study are in mg/kg/day.

b. Dose in ppm of  $\text{CH}_2\text{Cl}_2$ .

c. Dose in mg/kg/day in drinking water.

The dose of GST metabolites to lung and liver tissue in the rat following inhalation exposure (4000 ppm) to  $\text{CH}_2\text{Cl}_2$  was three- to fivefold lower than in the mouse exposed to 4000 ppm (Table 5). The rat failed to show a significant increase in the levels of lung and/or liver tumors, although an increase in the number of benign mammary tumors was noted in this species [2,20]. The dose of GST metabolites to lung and liver tissue in the hamster exposed to 3500 ppm  $\text{CH}_2\text{Cl}_2$  was 11- to 31-fold lower than in the mouse (Table 5). Hamsters exposed to  $\text{CH}_2\text{Cl}_2$  failed to show significant increases in any type of tumor at any site [20]. Thus there appears to be a reasonable correlation between the *in vivo* activity of GST in the various species and their sensitivity to  $\text{CH}_2\text{Cl}_2$ .

### **Human risk estimations**

Quantitative risk assessments (QRAs) cannot provide precise estimates of human risk due to the empirical nature of the models. Furthermore, as a policy decision, QRA procedures have been designed to be protective of public health through inclusion of conservative assumptions wherever uncertainty exists. Consequently, as currently practiced, QRA provides estimates of the "plausible upper bounds" on risk. Actual risks are unknown, and in many instances may be as low as zero.

Nevertheless, QRA plays a useful role in hazard evaluations by providing an objective mechanism for "ranking" materials thought to pose a carcinogenic risk to man. This allows limited societal resources to be directed toward those materials that probably pose the greatest risk to human populations.

QRA may also provide a mechanism for definitive action in some cases. For example, if a material is thought to have carcinogenic potential, but QRA suggests that even under the most pessimistic assumptions, the risk to human populations will be less than some very small number (e.g.,  $10^{-5}$ ), then use of that substance in commerce need not be regulated (i.e., the *de minimus* approach).

Within this framework, the PB-PK model can now be used to formulate human cancer risk estimations. Formulation of the risk estimation involves the following steps.

1. Selection of appropriate animal bioassay data.
2. Calculation of the delivered dose to the target organ(s) under conditions that produced tumors in animals.
3. Fitting tumor incidence and delivered dose data to one or more empirical dose-response models for carcinogenesis.
4. Defining human exposure conditions of interest and calculating the delivered dose to corresponding organs of humans under those particular conditions.
5. Estimating upper bounds on human risk from the dose-response model previously fitted to animal bioassay/target organ delivered dose data.

This process differs from that used by default when pharmacokinetic data on delivered dose are not available. In the absence of pharmacokinetic data, delivered dose is considered to be proportional to nominal dose throughout the entire exposure range. Extrapolation from animal to human is performed by assuming that equipotent doses are expressed in milligram of chemical per unit of surface area in the various species. The latter process always assumes that humans are more sensitive to a given dose of test chemical (in milligram per kilogram per day) than rodents because of the lower surface area to volume ratio (humans are assumed to be five- to sixfold more sensitive than rats and 13-fold more sensitive than mice).

Following the default procedure for  $\text{CH}_2\text{Cl}_2$  (without use of PB-PK data), Singh et al. [21] estimated that the lifetime risk for continuous exposure to a concentration of  $1 \mu\text{g}/\text{m}^3$   $\text{CH}_2\text{Cl}_2$  in inhaled air was  $4.1 \times 10^{-6}$ <sup>a</sup>. This estimate was presented as a "plausible upper limit" on risk, along with the qualifier that "...the true value is unknown and may be as low as zero." The uncertainty and upper limit aspect of this assessment reflect the fact that a series of conservative assumptions were made in the face of scientific uncertainty, including uncertainty as to the magnitude of the delivered dose. Development of a unified PB-PK model for  $\text{CH}_2\text{Cl}_2$  permitted the reduction of uncertainty in the original risk estimation through replacement of default assumptions with results from the PB-PK model [1].

Delivered doses for the female  $\text{B}_6\text{C}_3\text{F}_1$  mice in the drinking water and inhalation chronic bioassays [2,3] were calculated with the PB-PK model of Andersen et al. [1] and are summarized in Table 6. Model parameters used by Andersen et al. [1] were employed for these calculations with the exception of  $KF$  (the metabolic rate constant for the GST pathway) and the proportionality constants  $A1$  and  $A2$  (which give the relative levels of GST in lung and liver tissue).  $A1$  and  $A2$  were calculated from the data presented in Table 1 of this report, and  $KF$  was calculated as outlined earlier (Table 4). Tumor incidences in treated and control groups of female mice in these studies also are summarized in Table 6 [2,3]. (In the interest of brevity, data from male mice are not presented since these gave estimates of risk similar to those derived from female mice.)

Once delivered dose had been calculated, it was necessary to choose a dose-response model to describe the animal responses. The choice of the appropriate high dose to low dose model has been the subject of considerable discussion (e.g., see Brown [23]). Some models, including the linearized multi-stage (LMS) model, impose conservative assumptions on the QRA process (in this case by forcing the model to be linear at low doses). Other models, such as the Probit model, make fewer assumptions about the shape of the dose-response curve. The LMS has been widely used by regulatory agencies because of the feeling that the estimates produced by this model are very unlikely to underpredict the true risk. However, current regulatory practice generally includes presentation of a range of risks estimated from other models as well.

Consequently, the delivered dose data were fit to four different dose response models currently used by the toxicological community. The models chosen were (1) the LMS, (2) the Probit Model, (3) the Weibull Model, and (4) the Logit Model. All of the models predict excess risk (ExRisk) as a function of administered dose, except the Probit model which predicts the probit of the excess risk

---

<sup>a</sup>  $4.1 \times 10^{-6}$  was the original "unit risk" for  $\text{CH}_2\text{Cl}_2$  in the EPA document of 1985, but this estimate has subsequently been lowered based on use of PB-PK modeling [22]

TABLE 6. CANCER DOSE RESPONSE MODELS<sup>a</sup>

Nominal Dose	PB-PK (Lung)	PB-PK (Liver)	Lung Tumors	Liver Tumors
MOUSE: Drinking Water				
0 mg/kg	0.0	0.0	5/100	6/100
60 mg/kg	0.395	3.00	3/100	4/99
125 mg/kg	0.902	6.77	1/50	2/50
185 mg/kg	1.46	10.8	3/50	5/50
250 mg/kg	2.19	16.0	4/50	3/50
MOUSE: Inhalation				
0 ppm	0.0	0.0	3/50	3/50
2000 ppm	321	785	30/48	16/48
4000 ppm	482	1670	41/48	40/48
HUMAN: Occupational Exposure				
1 ppm	$5.36 \times 10^{-5}$	$8.61 \times 10^{-5}$	-	-
2 ppm	$1.07 \times 10^{-4}$	$1.73 \times 10^{-4}$	-	-
5 ppm	$2.69 \times 10^{-4}$	$4.38 \times 10^{-4}$	-	-
10 ppm	$5.40 \times 10^{-4}$	$8.94 \times 10^{-4}$	-	-
20 ppm	$1.09 \times 10^{-3}$	$1.86 \times 10^{-3}$	-	-
50 ppm	$2.80 \times 10^{-3}$	$5.34 \times 10^{-3}$	-	-
100 ppm	$5.98 \times 10^{-3}$	$1.37 \times 10^{-2}$	-	-
HUMAN: Continuous Inhalation				
1 $\mu\text{g}/\text{m}^3$	$6.16 \times 10^{-6}$	$9.87 \times 10^{-6}$	-	-
HUMAN: Drinking Water				
1 $\mu\text{g}/\text{L}$	$4.26 \times 10^{-7}$	$3.66 \times 10^{-6}$	-	-

<sup>a</sup> The "internal dose" calculated by the PB-PK model is in average mg equivalents of  $\text{CH}_2\text{Cl}_2$  metabolized by the GST pathway/day/liter volume of tissue. The values reported for mice are for exposures of 6 h/day, 5 days/week, corrected for the fraction of a lifetime (96/102) that animals were exposed. Values reported for humans are for one year of occupational exposure, 6 h/day, 5 days/week, corrected for the fraction of the year (48/52) that humans are in the workplace.

ExRisk is defined as the excess lifetime risk resulting from the independent effect of the chemical exposure in question and can be expressed as

$$\text{ExRisk} = \frac{(\text{TumFr} - \text{BckGrnd})}{(1.0 - \text{BckGrnd})} \quad (5)$$

In this equation, TumFr is the tumor frequency observed in the treated groups and BckGrnd is the tumor frequency observed in control groups. The mathematical forms of the four dose response

models are given for the LMS model [Equation (6)]<sup>b</sup>, the Logit model [Equation (7)], the Weibull model [Equation (8)], and the Probit model [Equation (9)].

$$ExRisk = A * Dose \quad (6)$$

$$ExRisk = \frac{1}{1 + EXP(-A - B * LN(Dose))} \quad (7)$$

$$ExRisk = 1 - EXP[-A * (Dose)^B] \quad (8)$$

$$Probit = A + B * LN(Dose) \quad (9)$$

Constants for these equations were derived by computer optimization of the tumor incidences and PB-PK doses from Table 6. All of the treated and control female mice from the two studies (500 animals) were used in the analysis. The values of the constants obtained from these optimizations are listed in Table 7.

TABLE 7. CONSTANTS<sup>a</sup>

Independent Background	Background	A	B
LMS - Lung	0.0453	0.00495	-
LMS - Liver	0.0550	0.00685	-
Logit - Lung	0.0473	-8.788	1.696
Logit - Liver	0.0576	-22.258	3.207
Weibull - Lung	0.0434	-5.072	0.922
Weibull - Liver	0.0576	-15.27	2.132
Probit - Lung	0.0475	-5.303	1.024
Probit - Liver	0.0576	-13.555	1.952

<sup>a</sup> Constants obtained when computerized optimizations were used to fit four dose-response models - LMS, Logit, Weibull, and Probit - to the PB-PK dose and tumor incidence for female mice (given in Table VI). These constants can be used with the equations in the text to estimate excess risk for a given PB-PK dose.

The models can now be used to estimate the risk for any exposure condition within the scope of the PB-PK model. To illustrate this, three specific exposure scenarios were evaluated: (1) lifetime exposure to 1 µg/m<sup>3</sup> CH<sub>2</sub>Cl<sub>2</sub> in the atmosphere (EPA's standard Unit Risk condition), (2) lifetime consumption of 2 L/day of water containing 1 µg CH<sub>2</sub>Cl<sub>2</sub>/L, and (3) one year's occupational exposure to CH<sub>2</sub>Cl<sub>2</sub> at the proposed Threshold Limit Value (TLV, 50 ppm). The PB-PK doses equivalent to these exposures are listed in Table 6.

Low dose risk estimates obtained with the Logit, Weibull, and Probit models may vary depending upon assumptions made about the additivity or independence of the background tumors. Since the LMS model assumes an additive background, this consideration does not apply to this model. The question of whether to use independent or additive backgrounds is a difficult one, and is beyond the scope of this paper. However, the effect of incorporating pharmacokinetic data into the risk estimation can be visualized without resolving this question.

The LMS model, which assumes an additive background, generally gave the highest estimates of low dose risk for a given dose of  $\text{CH}_2\text{Cl}_2$  (Table 8). Low dose risk estimates from the other three models were similar to the risk estimates from the LMS when additive backgrounds were assumed (data not shown). However, when independent backgrounds were assumed, the four models give very different predictions of low dose risk (shown in Table 8). Although each model gave an excellent description of the observable data from the two bioassays, the models differed by 5 to 15 orders of magnitude in predicted risk for the exposure conditions depicted in Table 8.

The effect of incorporating pharmacokinetic principles into the risk assessment process may be visualized by comparing the total risk (lung + liver) predicted by the LMS model. Under conditions of continuous inhalation of  $1 \mu\text{g}/\text{m}^3$ , the LMS predicted an upper bound risk of  $4.1 \times 10^{-6}$  for lifetime exposure [21] when administered dose was used instead of delivered dose. However, use of a pharmacokinetically calculated delivered dose predicted a risk more than two orders of magnitude lower:  $3.7 \times 10^{-8}$  (Table 8).

There are two components of this difference. The first is the nonlinearity in the activity of the metabolic pathways. The primary metabolic pathway (MFO) becomes saturated at high exposure concentrations of  $\text{CH}_2\text{Cl}_2$ , and a disproportionate increase in the activity of the secondary toxic pathway (GST) occurs. The second component has to do with calculation of species-specific doses rather than generic surface area "corrections." Humans possess relatively lower levels of the enzyme(s) responsible for  $\text{CH}_2\text{Cl}_2$  toxicity, and at equivalent tissue concentrations of  $\text{CH}_2\text{Cl}_2$  will generate lower levels of the toxic GST metabolite.

At the same time, it needs to be pointed out that use of a PB-PK model in QRA does not always result in estimation of lower risks for humans than the default procedures mentioned earlier. For instance, if a test chemical were directly toxic and were inactivated by metabolic enzymes, then a PB-PK model would predict more risk to humans than rodents because of the lower levels of detoxifying enzymes in this species. Similarly, if toxicity resulted from reactive metabolite(s)

---

<sup>b</sup> The LMS model is first fit in the form of an exponential polynomial, and then the upper 95% confidence level on the linear term is calculated to give the low dose form shown in Eq. (6)

TABLE 8. EXCESS RISKS FOR INHALATION, WATER CONSUMPTION AND OCCUPATIONAL EXPOSURE<sup>a</sup>

	Inhal 1 $\mu\text{g}/\text{m}^3$	Water 1 $\mu\text{g}/\text{liter}$	Occup. 50 ppm
Risk of Lung Tumor			
LMS (w/P-K)	$3.0 \times 10^{-8}$	$2.1 \times 10^{-9}$	$1.4 \times 10^{-5}$
Logit	$2.1 \times 10^{-13}$	$2.3 \times 10^{-15}$	$7.0 \times 10^{-9}$
Weibull	$9.8 \times 10^{-8}$	$8.4 \times 10^{-9}$	$2.8 \times 10^{-5}$
Probit	$< 10^{-15}$	$< 10^{-15}$	$< 10^{-15}$
Geo. Mean	$2.8 \times 10^{-11}$	$2.5 \times 10^{-12}$	$7.2 \times 10^{-9}$
Risk of Liver Tumor			
LMS (w/P-K)	$6.8 \times 10^{-9}$	$2.5 \times 10^{-9}$	$3.7 \times 10^{-6}$
Logit	$2.1 \times 10^{-26}$	$8.8 \times 10^{-28}$	$1.2 \times 10^{-17}$
Weibull	$< 10^{-17}$	$< 10^{-17}$	$< 10^{-17}$
Probit	$< 10^{-15}$	$< 10^{-15}$	$< 10^{-15}$
Geo. Mean	$3.5 \times 10^{-17}$	$1.2 \times 10^{-17}$	$2.6 \times 10^{-14}$
Total Risk (Lung + Liver)			
LMS (w/o P-K) <sup>b</sup>	$4.1 \times 10^{-6}$		
LMS (w/ P-K)	$3.7 \times 10^{-8}$	$4.6 \times 10^{-9}$	$1.8 \times 10^{-5}$
Logit	$2.1 \times 10^{-13}$	$2.3 \times 10^{-15}$	$7.0 \times 10^{-9}$
Weibull	$9.8 \times 10^{-8}$	$8.4 \times 10^{-9}$	$2.8 \times 10^{-5}$
Probit	$< 10^{-15}$	$< 10^{-15}$	$< 10^{-15}$
Geo. Mean	$2.9 \times 10^{-11}$	$3.1 \times 10^{-12}$	$7.7 \times 10^{-9}$

<sup>a</sup> Excess risks calculated by four dose-response models under three specific exposure conditions: (1) continuous inhalation of 1  $\mu\text{g}/\text{m}^3$  in air for a lifetime, (2) consumption of 2 liters of water/day containing 1  $\mu\text{g}/\text{liter}$  for a lifetime, and (3) occupational exposure (6 h/day, 5 days/week, 48 weeks/year) to  $\text{CH}_2\text{Cl}_2$  at 50 ppm for one year. The four models are: LMS, Logit, Weibull, and Probit. Models are structured with the nonadditive background.

<sup>b</sup> Singh et al. [21] estimated the risk of developing either a lung or liver tumor, but did not estimate the risk of developing only a lung tumor or only a liver tumor

produced by a saturable process, then low dose risk extrapolated from high, saturating doses by a PB-PK model could be more than predicted by linear extrapolations.

In summary, development of a PB-PK for  $\text{CH}_2\text{Cl}_2$ , and subsequent incorporation of *in vitro* enzyme studies, has provided a valuable tool for improving risk estimations for  $\text{CH}_2\text{Cl}_2$ . The model permitted identification of a probable mechanism of carcinogenesis for  $\text{CH}_2\text{Cl}_2$ , provided a consistent explanation for the differences between chronic bioassays of  $\text{CH}_2\text{Cl}_2$  in different species and by different routes, and provided a quantitative basis for evaluating the effect of two competing metabolic pathways upon the production of the putative toxic metabolite *in situ* at various doses. We believe that risk estimations that incorporate these principles will prove significantly more reliable than risk estimations that do not consider pharmacokinetics.

## ACKNOWLEDGMENTS

The authors would like to thank Dr. Daniel Krewski (Health Protection Branch, Canada) and Dr. Murray Cohn (Consumer Products Safety Commission) for their expert assistance in fitting the PB-PK delivered dose data to the various cancer dose-response models.

## REFERENCES

- 1 Andersen, M.E., Clewell H.J., III, Gargas, M.L., Smith F.A., and Reitz R.H. (1987) Physiologically based pharmacokinetics and the risk assessment process for methylene chloride. *Toxicol. Appl. Pharm.* 87, 185-205.
- 2 National Toxicology Program (NTP) (1985) NTP Technical Report on the Toxicology and Carcinogenesis Studies of Dichloromethane in F-344/N Rats and B6C3F1 Mice (Inhalation Studies). NTP-TR-306 (board draft).
- 3 Serota, D., Ulland, B., and Carlborg, F. (1984) Hazelton Chronic Oral Study in Mice. Food Solvents Workshop I: Methylene Chloride, March 8-9, Bethesda, MD.
- 4 Caster, W. O., Poncelet, J., Simon, A. B., and Armstrong, W. D. (1956) Tissue weights of the rat. I. normal values determined by dissection and chemical methods. *Proc. Soc. Exp. Biol. Med.* 91, 122-126.
- 5 Davis, N. R. and Mapleson, W. W. (1981). Structure and quantification of a physiological model of the distribution of injected agents and inhaled anaesthetics. *Br. J. Anaesth.* 53, 399-404.
- 6 International Commission on Radiation Protection (1975) Report of the task group on Reference Man. In: W.S. Snyder, M.J. Cook, E.S. Nasset, L.R. Karhausen, G.P. Howells, I.H. Tipton (Eds.), ICRP Publication 23, (W. S. Snyder et al., Eds.), Pergamon Press, New York.
- 7 Sato, A. and Nakajima, T. (1979) Partition coefficients of some aromatic hydrocarbons and ketones in water, blood, and oil. *Brit. J. Ind. Med.* 36, 231-234.
- 8 Gargas, M.L. and Andersen, M.E. (1988) A gas phase technique for determining the kinetic constants of chemical metabolism in the rat. *Toxicologist* 8, 112.
- 9 Kubic, V.L., Anders, M.W., Engel, R.R., Barlow, C.H., and Caughey, W.S. (1974) Metabolism of dihalomethanes to carbon monoxide. I. *In vivo* studies. *Drug. Metab. Dispos.* 2, 53-57.
- 10 Ahmed, A.E. and Anders, M.W. (1976) Metabolism of dihalomethanes to formaldehyde and inorganic halide. I. *In vitro* studies. *Drug. Metab. Dispos.* 4, 357-361.
- 11 Gargas, M.L., Clewell, H.J. and Andersen, M.E. (1986) Metabolism of inhaled dihalomethanes *in vivo*: differentiation of kinetic constants for two independent pathways. *Toxicol. Appl. Pharmacol.* 82, 211-223.
- 12 Lindstedt, S.L. (1987) Allometry: Body size constraints in animal design. In: National Research Council of the National Academy of Sciences, *Pharmacokinetic in Risk Assessment, Drinking Water and Health*, Vol. 8, National Academy Press, Washington, DC, pp 65-79.

- 13 Beaune, P., Kremers, P.G., Kaminsky, L.W., DeGraeve, J., and Guengerich, F.P. (1986) Comparison of monooxygenase activities and cytochrome P-450 isozyme concentrations in human liver microsomes. *Drug Metab. Disp.* 14, 437-442.
- 14 Bocker, R.H. and Guengerich, F.P. (1986) Oxidation of 4-aryl- and 4-alkyl-substituted 2,6-dimethyl-3,5-bis(alkoxycarbonyl)-1,4-dihydropyridines by human liver microsomes and immunochemical evidence for the involvement of a form of cytochrome P-450. *J. Med. Chem.* 29, 1596-1603.
- 15 Hall, S.D., Guengerich, F.P., Branch, R.A., and Wilkinson, G.R. (1987) Characterization and inhibition of mephenytoin 4-hydroxylase in human liver microsomes. *J. Pharmacol. Exp. Ther.* 240, 216-222.
- 16 Knodell, R.G., Hall, S.D., Winkington, G.R., and Guengerich, F.P. (1987) Hepatic metabolism of tolbutamide: *in vivo* characterization of the form of cytochrome P-450 involved in methyl hydroxylation and relationship to *in vivo* disposition. *J. Pharmacol. Exp. Ther.* 241, 1112-1119.
- 17 Guengerich, F.P., Martin, M.V., Beaune, P.H., Kremers, P., Wolff, T., and Waxman, D.J. (1986) Characterization of rat and human liver microsomal cytochrome P-450 forms involved in nifedipine oxidation, a prototype for genetic polymorphism in oxidative drug metabolism. *J. Biol. Chem.* 261, 5051-5060.
- 18 Guengerich, F.P., Muller-Enoch, D., and Blair, I.A. (1986) Oxidation of quinidine by human liver cytochrome P-450. *Mol. Pharmacol.* 30, 287-295.
- 19 Lineweaver, H. and Burk, D. (1934) The determination of enzyme dissociation constants. *J. Amer. Chem. Soc.* 56, 658-666.
- 20 Burek, J.D., Nitschke, K.D., Bell, T.J., Wackerle, D.L., Childs, R.C., Beyer, J.D., Dittenber, D.A., Rampy, L.W., and McKenna, M.J. (1984). Methylene chloride: A 2-year inhalation toxicity and oncogenicity study in rats and hamsters. *Fund. Appl. Toxicol.* 4, 30-47.
- 21 Singh, D.V., Spitzer, H.L., and White, P.D. (1985). Addendum to the health assessment document for dichloromethane (methylene chloride). Updated carcinogenicity assessment of dichloromethane. EPA/600/8-82/004F.
- 22 Blancato, J.N., Hopkins, J., and Rhomberg, L. (1987) Update to the health assessment document and addendum for dichloromethane (methylene chloride): Pharmacokinetics, mechanism of action, and epidemiology. External Review Draft, EPA/600/8-87/030A.
- 23 Brown, C.C. (1983) Learning about toxicity in humans from studies on animals. *Chemtech* 13, 6.

## RESEARCH NEEDS AND ADVANCES IN INHALATION DOSIMETRY IDENTIFIED THROUGH THE USE OF MATHEMATICAL DOSIMETRY MODELS OF OZONE

Frederick J. Miller and Judith A. Graham

*Health Effects Research Laboratory, U.S. Environmental Protection Agency,  
Research Triangle Park, NC*

### SUMMARY

Knowledge of the quantitative relationship between exposure concentration and delivered dose (i.e., dosimetry) is a fundamental starting point in the evaluation of the toxicity of chemicals, not only for intra- and interspecies comparisons but also for designing experiments that elucidate mechanisms of action and that identify issues or research areas for further study. To these ends a mathematical, lower respiratory tract dosimetry model for gases has been developed which, when linked to experimentally determined upper respiratory tract removal of a gas, can be used for dosimetric extrapolations between one test condition and a theoretical condition (e.g., animal-to-man, child-to-adult, dosimetric extrapolation). This paper, using an ozone ( $O_3$ ) dosimetry model as an example, describes (1) the results of sensitivity analyses that have identified variables that can significantly influence the precision of model predicted doses, (2) research progress in improving the precision of those highly sensitive variables, and (3) approaches being used to validate the model. Results from studies of upper respiratory tract removal of  $O_3$  in animals and humans are used as inputs into the mathematical model of the lower respiratory tract to illustrate applications of dosimetric extrapolations.

### INTRODUCTION

With the increasing international focus on health risk assessments, many deficiencies in supporting knowledge have become apparent. They can be broadly characterized as lack of data on a given chemical or mixture or lack of knowledge to interpret existing health effects data in quantitative risk terms. Dosimetry modeling, herein defined as modeling the relationship between an exposure and the dose delivered to the target, is critically important and central to solving both problems. When assessing the risk of a chemical, knowing the human dose-response is crucial. However, it is not possible to study each relevant exposure scenario in humans and measure each resultant dose and effect for numerous chemicals. Rather, it is necessary to perform definitive studies, most often in animals, that then can be extrapolated to humans and to relevant exposure scenarios.

Dosimetry modeling can assist in designing an experiment that is more definitive. For newly developed as well as historical data, dosimetry modeling can be used to extrapolate dose from the test animal to humans. Although species sensitivity to a given dose also has a major influence on

extrapolation of effective concentrations, quantitative dosimetric extrapolation would enable a substantial advancement in risk assessments based on animal toxicological data. For example, if interspecies dose equivalence were known and human equivalent dose calculated and compared to ambient exposure, then the risk could be more quantitatively defined.

Mathematical dosimetry models also can be useful in extrapolating from human to human by providing estimates of the dose of the compound responsible for the biological effect under consideration. Separation of factors that influence dose-response from actual concentration-response effects increases the quantification of risk assessment. For example, if the young are more responsive to a chemical than adults, is this due to differences in dosimetry or innate sensitivity differences?

On a broader scale, once we better understand the dose-response it should be possible to study and model other environmental factors that influence the toxicological outcome simply by virtue of dosimetric changes. For example, with knowledge of the dose-response of a chemical, the influence of various levels of exercise on dose could be modeled, enabling better interpretation of risk factors. Given the importance of dosimetry models, it is essential that they be as quantitative as possible, as well as realistic, validated, and of use in predicting what can happen in unobserved circumstances. Achieving this requires a multidisciplinary and extensive research program.

The purpose of this paper is to describe research progress on previously identified needs [1], as well as new needs that are crucial to the realization of advanced quantitative dosimetry models for pulmonary toxicity modeling of inhaled chemicals. New applications of the dosimetry model for toxicological evaluations also are presented. Although an O<sub>3</sub> dosimetry model is used as a basis for the following discussion, many of the research findings have generic applicability to other inhaled chemical dosimetry models.

Uptake in both the upper and the lower respiratory tract are considered, but from different perspectives. Upper respiratory tract (URT) uptake is examined solely from experimental data since this region is accessible to direct measurement; lower respiratory tract (LRT) uptake is examined using a mathematical model that is based on theoretical and experimental factors. Merging of the two components yields an integrated approach for examining respiratory tract dosimetry. These components, as well as applications of the model, will be discussed separately.

#### **UPPER RESPIRATORY TRACT REMOVAL OF OZONE**

Removal of an inhaled gas in the URT serves to lessen the dose and, hence, the insult to the LRT tissues. The anatomy of the URT is exceedingly complex and is not as amenable to mathematical modeling as is the LRT. However, its accessibility to probes to measure gas concentration make experimental studies feasible. Such research provides values that serve as tracheal concentration

input values for mathematical modeling of LRT uptake. It is apparent that a research area that can be identified involves the URT removal of gases under various modes of breathing and level of activity. Approaches used are dependent on the species of interest; indirect procedures based on total respiratory tract uptake may be necessary for small animals, whereas for larger species, including man, more direct measurements can be made.

To address these issues for  $O_3$ , experimental studies have been conducted in humans by Gerrity and co-workers [2] and in rats by Wiester et al. [3]. Using a probe at the posterior pharynx, Gerrity et al. [4] measured  $O_3$  removal efficiencies in extra- and intrathoracic airways of human as a function of three  $O_3$  concentrations, three modes of breathing (nose only, mouth only, and oronasal), and two respiratory frequencies. They found that breathing frequency had an effect on extra- and intrathoracic removal of  $O_3$  (i.e., less  $O_3$  removed at faster breathing rate). Nasopharyngeal removal was not influenced by  $O_3$  concentration, but removal in the LRT was. Mode of breathing also affected removal. These influences on  $O_3$  removal efficiency, although statistically significant, were small. The average nasopharyngeal removal under all conditions was approximately 40%; the mean LRT removal efficiency was 91% of the  $O_3$  delivered to the LRT; for the total respiratory tract, the removal was approximately 95%.

Experimental studies of total respiratory tract uptake of  $O_3$  in three strains of rats [3,5] and guinea pigs [3] have been conducted. In the unanesthetized animals,  $O_3$  uptake was calculated by a fractional deposition technique during a 1-h  $O_3$  exposure. The percent uptake of  $O_3$  in the total respiratory tract was 47%; there was no statistically significant difference between the strains of rats or between rats and guinea pigs. The percent uptake was independent of  $O_3$  concentration for up to 1 ppm  $O_3$ . Gerrity [2] modified the model of Aharonson et al. [6] for uptake in the head so that fractional uptake could be examined as a function of unidirectional flow rates, nasopharyngeal surface area, and various allometric equations for a given mammalian species. Preliminary computations (Drs. John Overton and Gary Hatch, U.S. EPA, personal communication) using isotope ratio mass spectroscopy data in nonlinear compartmental analyses suggest that uptake in the head of the rat may be about 23%. This value is in good agreement with what the model of Gerrity [2] would predict. The reader is referred to the section "Applications of Dosimetry Models" for an illustration of how these types of experimental data are utilized in pulmonary dosimetry models for interspecies comparisons of toxicological results.

#### **LOWER RESPIRATORY TRACT MODEL**

Although a mathematical model can incorporate numerous variables as factors, the values of each variable have varying ranges of uncertainty depending on available data. Moreover, various simplifying assumptions are often needed to render the modeling problem tractable from a

mathematical viewpoint. The reader is referred elsewhere [7,8] for a detailed discussion of the partial differential equations and other formulae, assumptions, numerical methods, and such that have been utilized in formulating a dosimetry model for  $O_3$ . Basically, for any given location in the LRT at any point in the breathing cycle, the simulation model accounts for  $O_3$  transport in the lumen and airspaces, as well as chemical reactions and transport in the liquid layers lining the LRT, in the tissue, and in the blood. The simulation model requires specifying anatomical data (e.g., airway lengths, diameters, and number) as well as physiological data (e.g., tidal volume and breathing frequency) for the animal species or human lung being modeled. Additionally, physicochemical data relating to the solubility of  $O_3$  in biological fluids and the reaction of  $O_3$  with various biological constituents are needed. It is important to note that the dosimetry model is physiologically based, as opposed to reflecting an empirically oriented curve-fitting approach.

Because it is not feasible to obtain precise values for every anatomical, physiological, and physicochemical variable for each species, sensitivity analyses have been performed to determine which variables have a dominant influence on the LRT model results. Such analyses [7,8] have shown that lung morphometry, mucus thickness, and mucus -  $O_3$  chemical reactions result in large impacts on dosimetry. While other variables are also important, at the present time reducing uncertainties in the above cited areas is most crucial to improving model precision. Progress in pursuit of these improvements is discussed below.

#### ***Interspecies morphometric data***

Morphometric data (i.e., numbers, lengths, diameters, and radii) are needed for the tracheobronchial and pulmonary airways to serve as inputs to mathematical models that solve the differential equations governing gas transport in the airways. Often the representation of the airways is a series of cylindrical tubes with some kind of bifurcation pattern. Various anatomical models exist for humans [9,10,11,12], rats [13,14], and guinea pigs [13,15]. Major differences can exist among these various anatomical models, even within a single species, with respect to the estimates of the number of airways, lengths, etc. It is important to note that most of the anatomical models cited above were derived from replica lung casts so that little information was available from relationships on pulmonary acinar structure. An example of how the choice of anatomical model can affect the prediction of the  $O_3$  dose is illustrated in Figure 1. Plotted are net and tissue dose profiles vs. zone, order, or generation (depending on the anatomical model) for the guinea pig and for the rat. Although the curves shown in Figure 1 are qualitatively similar, it should be noted that tissue dose is plotted on a logarithmic scale so that quantitative estimates of tissue dose obtained using the various anatomical models differ substantially.

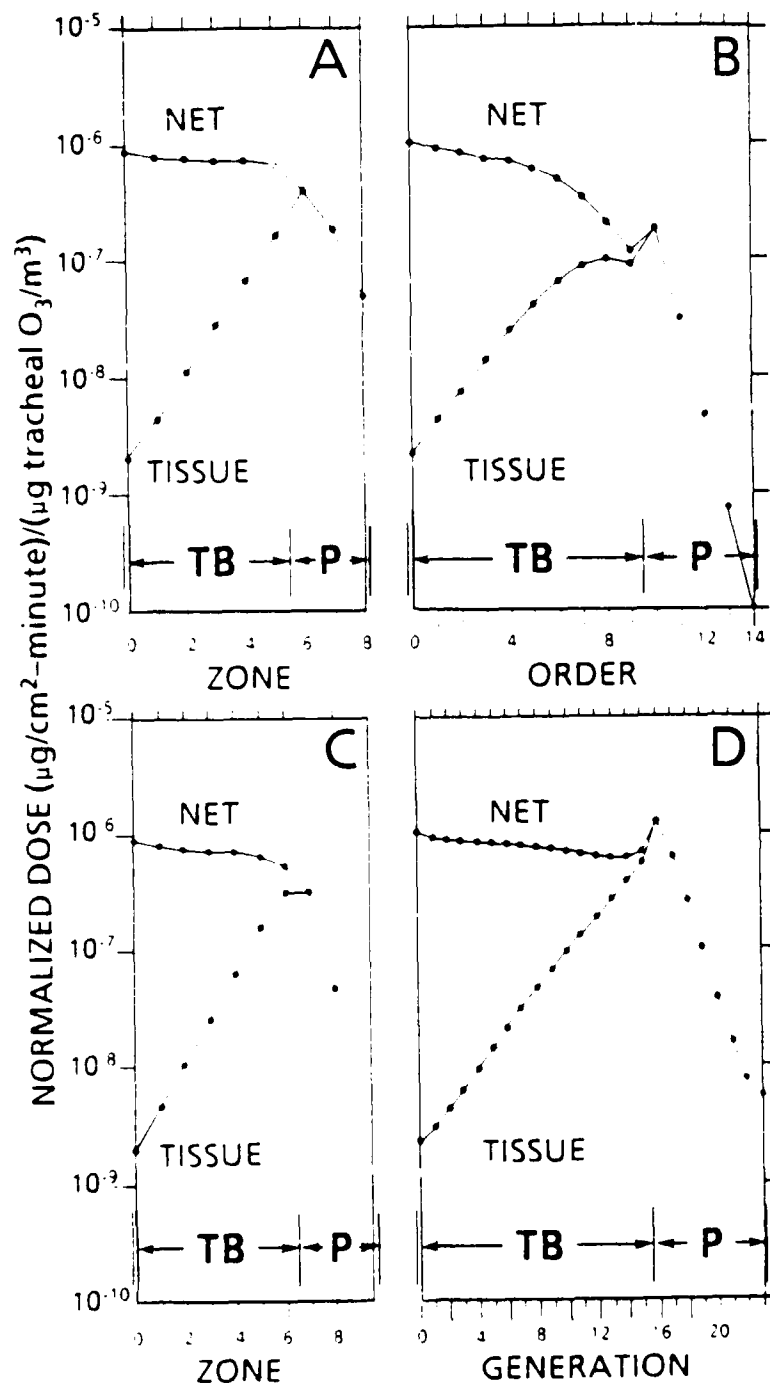


Figure 1. Normalized simulated net and tissue dose profiles. (A) Dose vs. zone, Klimont (1973) anatomical model for guinea pig, VT = 2.53 mL, f = 56.6 BPM. (B) Dose vs. order, Schreider and Hutchens (1980) anatomical model for guinea pig, VT = 2.4 mL, f = 77 BPM. (C) Dose vs. zone, Klimont (1973) anatomical model for rat, VT = 0.7 mL, f = 144 BPM. (D) Dose vs. generation, Yeh et al. (1979) anatomical model for the rat, VT = 1.84 mL, f = 105 BPM. TB = tracheobronchial region (mucus lined), P = pulmonary region (surfactant lined). The dose has been normalized to the input tracheal concentration to enable comparisons. The net dose is the sum of the liquid, tissue, and blood compartments. Multiply figure values by tracheal concentration (mg/m<sup>3</sup>) to obtain dose in mg/cm<sup>2</sup>/min for any given tracheal concentration. SOURCE: Overton et al. [8].

Ultimately, it is desirable that dosimetry can be predicted on a micro-regional scale. The importance of this is illustrated by results of Overton et al. [8] who modeled, in rats, the tissue dose of  $O_3$  to the first alveolated generation because this is the site of the primary lung lesion [16,17,18]. They found that the tissue dose decreases as path length increases, with the right diaphragmatic lobe receiving a lower dose than the right apical lobe. The morphometric data [14] used in this analysis averages path lengths within each lobe. If appropriate morphometric data were available on individual path lengths within each lobe, dosimetric models would better predict relevant dose (i.e., dose to the actual target site) and total dose to the lung since the average value derived from highly extensive and quantitative methods eventually used in a dosimetric equation would be far more precise. Such improvements would also offer opportunities to measure health effects in the lung at ambient levels of exposure due to increased sensitivity of data analyses.

Most inhalation toxicology research ( $O_3$  being a notable exception) uses high exposure levels relative to ambient exposure levels, making high-to-low extrapolations necessary. However, since the science of such extrapolations is in its infancy, it is more useful to perform research for which it is not necessary. Often, variability of an effect increases as dose of a chemical increases. Increased variability makes it less likely that statistical differences between exposed and control groups can be determined. In the future, interanimal variability may be reduced by utilizing ventilatory (breathing frequency and tidal volume) data and dosimetry models to compute an "exposure dose" to be used in the statistical analyses. This could lead to a reduction in experimental error, thereby increasing the likelihood of finding significant biological responses to inhaled pollutants.

Additionally, if microtoxicologic procedures, particularly in the area of lung morphometry, can be coupled with microdosimetry, it is likely that intraanimal variability also can be decreased. For example, Barry et al. [19] examined four acini in each  $O_3$ -exposed rat. Although they demonstrated an overall effect due to  $O_3$  exposure, large and increasing variability in response occurred with increased  $O_3$  exposure among the four acini. Differences in dose to those acini could probably account for much of the variability since Mercer and Crapo [20] have demonstrated a tenfold variation in inspired air to various acini in the left lung of the rat. If intra-animal dose variations could be accounted for in such instances, it eventually may be possible to use fewer experimental animals in toxicological studies since high and low exposure assessment may be done within the same animal.

To achieve the improved morphometric information, studies are being conducted by Drs. James Crapo, Robert Mercer, and colleagues at the Duke University Center for Extrapolation Modeling in Durham, NC. These investigators are using three-dimensional lung reconstruction techniques in conjunction with improved computer-enhanced digitization and three-dimensional graphics to study the pulmonary acinar structure of various laboratory animals and human. Aside from the improved morphometric data, such as is contained in Mercer and Crapo [20] for the acinus of

the rat, new insights are being gained on structure-function relationships in the lung, gas flow distribution properties, and the distribution of target cells. When this information is incorporated into future dosimetry models for  $O_3$  and other pollutants, more accurate dosimetric extrapolations and judgments can be made concerning the animal toxicological results and their significance for human exposure.

#### ***Interspecies liquid lining layer data***

The liquid lining refers to the thin film of mucus that lines the tracheobronchial airways or to the even thinner layer of surfactant that covers pulmonary airways. Quantitative data on the biochemical composition of these layers, their thickness, and the nature of the reactions between the constituents of these layers and  $O_3$  are needed in dosimetry models to quantitate the distribution of dose to the tissue in specific airway generations. Given the paucity of data on these variables in both laboratory animals and humans, Miller et al. [7] performed sensitivity analyses to establish which liquid lining layer parameters most affect delivered dose, thereby establishing a framework for biological experiments that can supply necessary data.

The sensitivity of net and tissue dose of  $O_3$  to variations in the thickness of the liquid lining was examined by Miller et al. [7] and is illustrated in Figure 2. Various thickness schemes were chosen that bracket the lower and upper values reported experimentally. Although these sensitivity analyses are for the human lung, much of the experimental thickness data is based upon animal studies. The net dose curves (A', B', C'), which reflect total absorption and are the sum of all compartmental (i.e., liquid lining, tissue, and blood) doses, are much less dependent on the thickness of the mucous layer compared to the tissue dose curves (A, B, C). Predicted tissue doses of  $O_3$  can vary by three orders of magnitude in the trachea, with net dose remaining essentially unchanged (Figure 2). Proceeding distally in the lung, the effect of the choice of thickness value has a large influence on predicted tissue dose until the pulmonary region of the lung is reached. Other analyses [7], in which the surfactant thickness is reduced in the respiratory bronchioles, lead to tissue dose changes on the order of a factor of three. This indicates that surfactant thickness may play an important role in absorption by acting as a resistance element and thus protecting underlying tissue.

It became apparent that improved data on the thickness of the liquid lining layers were required in view of the kinds of variability in dosimetry related to the ranges of literature values. Such studies currently are being performed by Dr. James Crapo and colleagues at the Duke University Center for Extrapolation Modeling. Using a combination of vascular and airway fixation procedures to preserve the integrity of the mucous layer, a number of different locations within the tracheobronchial tree of the rat are being studied.

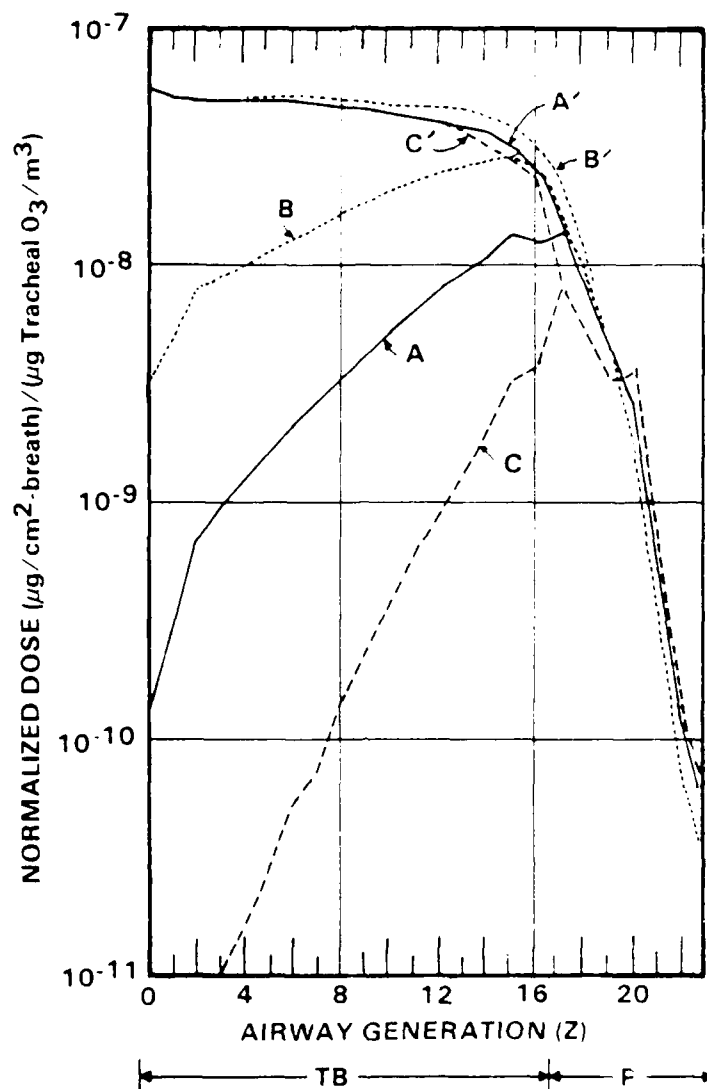


Figure 2. The effect of liquid compartment thickness schemes on  $O_3$  tissue dose (curves A, B, and C) and on the corresponding net dose ( $A'$ ,  $B'$ , and  $C'$ ). Curves A and  $A'$ : reference curves, thickness scheme A. Curves B and  $B'$ : thickness scheme B (one-half thickness of scheme A). Curves C and  $C'$ : thickness scheme C (twice thickness of scheme A). TB = tracheobronchial region (mucous lined); P = pulmonary region (surfactant lined). Multiply figure values by tracheal concentration ( $mg/m^3$ ) to obtain dose ( $mg/cm^2$  per breath). SOURCE: Miller et al. [7].

As noted earlier, in order to mathematically model generation-specific doses of  $O_3$ , quantitative information on the biochemical composition of the liquid lining layer is required to calculate rate constants for the reaction of  $O_3$ . Unfortunately, much of the information available in the literature on the biochemical composition of the lung and its secretions is qualitative, rather than quantitative. In mathematical modeling conducted thus far, the biochemical composition data primarily have been obtained from various studies in humans (see Miller et al. [7] for review). Concentration values of unsaturated fatty acids, major reactants for  $O_3$ , rat lung tissue and whole

blood can be derived using data from Clements [21] and Sanders [22] and from data from Orban et al. [23], respectively. The effective pseudo-first-order chemical rate constant used in the mathematical formulation is the product of the second-order rate constant and the effective molar concentration of the reacting biochemical constituents. In a comparative sense, more is known about the stoichiometry of the reactions that are being modeled than is known about the molar concentrations in some of the animal species and in some of the model compartments (see Miller et al. [7] for review). A sensitivity analysis of the contribution of mucus reaction rate constants had results similar to those for mucus thickness [7]. In the tracheobronchial region, the dose was quite sensitive to reaction rate constants. Also, as the rate constant was increased, the peak tissue dose shifted distally from the 15th to the 17th generation.

Given these sensitivity analyses, quantitative data on the biochemical composition of the mucous layer in various regions of the tracheobronchial tree in both humans and laboratory animals is a major area of needed investigation. Studies are being conducted by Dr. Cheng and colleagues at the University of North Carolina at Chapel Hill that focus on developing microanalytical procedures that will allow quantitation of airway secretions at specific anatomical sites in the rat lung. Components in airway secretions to be measured include urea, amino acids, hydroxyproline, hydroxylysine, desmosine, fatty acids, albumin, and mucin. Ozone-induced alterations in these components also will be measured to evaluate whether  $O_3$  exposure will alter  $O_3$  uptake over the course of an exposure, resulting in the need for adjustment factors.

#### ***Approaches for dosimetry model validation***

Use of a mathematical dosimetry model to integrate toxicological results for estimation of human toxicity is facilitated when the mathematical model is applicable to a wide range of exposure scenarios and target regions. If a mathematical model can be validated in multiple animal species and more limited evaluations made in human studies, the extensiveness to which the mathematical model can be applied in analyzing delivered dose from various human activity patterns is greatly increased.

Experimental validation studies with highly reactive gases such as  $O_3$  are difficult to perform, especially when it is of interest to determine regional doses. Methodological approaches are complicated even further when the radioactive form has an exceedingly short half-life, such as is the case for  $O_3$  where the longest living isotope has a half-life of only 124 sec. However, recent scientific advances in use of a stable isotope of oxygen ( $^{18}O$ ) and single photon emission computed tomography enable the problem to be addressed.

An isotope of oxygen ( $^{18}O$ ) can be used to generate  $^{18}O_3$  for exposures and to examine the relative enrichment of  $^{18}O$  in tissues using isotope ratio mass spectrometry [24,25]. Excess  $^{18}O$  is detectable in the lungs and respiratory tract of mice, rats, and rabbits breathing 1.0 ppm  $^{18}O_3$  for 1 h

[24, and Santrock, J., Hatch, G.E., Slade, R., and Hayes, J.M. (Submitted)] Absorption and disappearance of oxygen-18 in lung tissue from mice allowed to breathe 1-1ppm  $^{18}\text{O}_3$ . Studies are in progress that compare the dose of  $\text{O}_3$  to rats, monkeys, and humans breathing similar concentrations of  $^{18}\text{O}_3$  [26,27]. Hatch and colleagues expose rats to  $^{18}\text{O}_3$  and use a classical body burden approach to determine the compartments enriched in  $^{18}\text{O}$ . At present, the compartments being measured for mass balance are the head (to represent the URT), the LRT, liver, blood, and remaining tissues and carcass. This will permit evaluation of the proportional uptake of the URT vs. LRT. The respiratory tract of the rat is also being dissected, insofar as technically possible, to obtain percentage uptake for the nasopharyngeal epithelium, the trachea, the main airways of the lung, and the remaining parenchyma. Human studies with  $^{18}\text{O}_3$ , in collaboration with Dr. Hillel Koren of the Health Effects Research Laboratory, EPA, will measure  $^{18}\text{O}$  present in macromolecular fractions of lung lavage fluid and alveolar macrophages. Resultant data will be compared to similar measurements being made in rats. Primate studies are being conducted in collaboration with Dr. Charles Plopper at the University of California, Davis. These studies use approaches similar to those for humans, except that microdissection and determination of  $^{18}\text{O}$  in the trachea and all regions of the airways of the primate lung will enable better evaluation of measured vs. theoretical regional doses. The toxicological results of the primate studies also will be correlated to these dosimetric findings.

Another promising research area involves the use of single photon emission computed tomography to examine the real time distribution of uptake of  $\text{O}_3$  in the lung. Studies are being performed by Dr. Coleman and colleagues through the Duke University Center for Extrapolation Modeling to validate mathematical dosimetry model predictions of tissue dose. Since the same region scanned in an imaging study can be compared with anatomically matched morphometric data obtained by lung reconstruction methods, these approaches should eventually enable making microdosimetric and microtoxicological comparisons.

#### **APPLICATIONS OF DOSIMETRY MODELS**

Knowledge of dose at the target site is fundamental to quantitation of risk, particularly when the data being considered are from animal studies and one wishes to infer the relevance of the data to the likelihood of similar effects occurring in man. The ability to convert concentration-response curves to dose-response curves is integral for making intra- and interspecies comparisons of toxicological results more quantitative. Obviously, there is a need for the availability of dosimetry models that can provide a description of the uptake and temporal redistribution of inhaled compounds throughout the body. For the purpose of illustrating potential applications of dosimetry models, inter- and intraspecies examples will be discussed

### ***Interspecies dosimetric applications***

Hatch et al. [28] exposed various animal species (rabbits, guinea pigs, rats, hamsters, and mice) for 4 h to 0, 0.2, 0.5, 1.0, or 2.0 ppm O<sub>3</sub>. As a sensitive indicator of pulmonary edema, the accumulation of protein in lavage fluid 18 to 20 h after cessation of exposure was measured. Statistically significant increases over control were first found at 0.2 ppm O<sub>3</sub> for guinea pigs, 0.5 ppm O<sub>3</sub> for mice, and 1.0 ppm O<sub>3</sub> for other animal species.

How do these results compare when interspecies differences in dose are taken into account and what are their possible implications for human exposures? Since detailed morphometric data are not available for the hamster and the mouse, the following section will only include the data of Hatch et al. [28] for rats, guinea pigs, and rabbits. Utilizing an estimate of 20% uptake for these animal species in the URT and a value of 40% for human (based on Gerrity et al. [4] and Miller et al. [29]), the amount of O<sub>3</sub> delivered to pulmonary tissue over the 4-h exposure period was estimated. Dose estimates were adjusted for body weight differences to facilitate examining possible species differences in sensitivity to O<sub>3</sub> and to speculate on their implications for human exposure.

Their analyses indicated that in rats and rabbits the first significantly elevated level of protein corresponds to a pulmonary tissue dose of around 80 ng O<sub>3</sub>/g body weight. In contrast, the first significant elevation of protein in guinea pigs is associated with about 12 to 13 ng O<sub>3</sub>/g body weight. Thus, for equivalent pulmonary tissue doses, rats and rabbits are not as sensitive as guinea pigs. For the typical intermittent heavy exercise protocol used with human subjects, individuals exposed for 2 h to about 0.2 ppm O<sub>3</sub> are predicted to receive a pulmonary dose of 12 to 13 ng O<sub>3</sub>/g body weight [29]. Exposure to 0.4 ppm O<sub>3</sub> is predicted to result in about 23 ng O<sub>3</sub>/g body weight for humans. If the innate sensitivity of humans to O<sub>3</sub> is similar to the guinea pig, one would expect to be able to demonstrate edema in humans at or above about 0.2 ppm O<sub>3</sub> using the above-cited type of exercise protocol. In contrast, if innate sensitivity of humans is more like the rat or rabbit, one would not expect to be able to detect edema at O<sub>3</sub> levels near those found in ambient air. Recent data [30] on albumin increases in bronchoalveolar lavage fluid from human subjects exposed to 0.4 ppm O<sub>3</sub> for 2 h while exercising would tend to indicate that humans are more responsive than the rat to O<sub>3</sub> for this endpoint. Exposure studies at lower O<sub>3</sub> levels are needed to help clarify this conjecture.

### ***Intraspecies dosimetric applications***

Quantitative understanding of what factors contribute to individual differences in concentration-dose relationships can enable an expanded interpretation of a given human study to situations not measured and can increase the sensitivity of detecting an effect. Within a human clinical study, the range of responses of individuals exposed to O<sub>3</sub> can be large; for example, the decrease in forced expiratory volume at 1 sec can range from 0 to 45% [31]. Given the variation in URT

removal observed in the studies of Gerrity et al. [4], wherein removal efficiency can vary from 20 to 80% among individuals, investigators in the Clinical Research Branch of EPA's Health Effects Research Laboratory are conducting studies to determine the degree to which decrements in pulmonary function might be correlated with individual differences in URT or LRT removal of  $O_3$ , thereby contributing to the variability of responses. It can be hypothesized that differences in innate sensitivity also occur. Separating out innate sensitivity from dosimetric influences can target future research to better identify and characterize subpopulations at greater risk. Thusfar, Gerrity and McDonnell [32] have presented some results for correlations of uptake with ventilatory parameters, such as demonstrating that  $O_3$  uptake efficiency of the LRT is significantly, positively correlated with changes in tidal volume; however, the extent that changes or variation in URT and LRT uptake correlate with changes in pulmonary function measurements is still under investigation.

If exercise levels are adjusted to compensate for differences in body size between children and adults, these groups appear to be equally responsive to the effects of  $O_3$  exposure on pulmonary function [33]. However, the question arises as to whether this adjustment in minute ventilation is a valid approach to normalization, resulting in comparable tissue doses between children and adults in various regions of the LRT. This issue has been examined by Miller and Overton [34] by modeling LRT dose for the mean ages (9.9 and 22.5 yrs) used in the McDonnell et al. [31,33] studies. During both quiet breathing and heavy exercise, LRT dose patterns are predicted to be essentially the same for both age groups. Hence, innate sensitivity differences to  $O_3$  probably can be ruled out for the children and adults studied by McDonnell et al. [31,33]. It should be noted that substantial  $O_3$  dosimetric differences are predicted for infants compared to adults [34].

## DISCUSSION

Although  $O_3$  modeling has been used as an example of advancements being made in dosimetry, many of the fundamental elements are applicable to other gases, as well as particles. The procedures developed to measure total and URT removal of  $O_3$  in rats and humans can be used with other gases, eliminating the need to invest a major effort in devising the optimal apparatus, and such. However, rather than merely applying the method to a long list of gases, it would be preferable to use it to develop principles of URT removal of gases that could be used in the creation of a mathematical model of the URT that can be linked to the LRT model. What factors influence removal? Several can be expected such as minute ventilation, but to what degree do frequency of breathing and tidal volume have a weighted influence? What physiochemical properties of the gas significantly affect removal and, therefore, must be measured before the mathematical model can be applied to a novel situation?

At the present time, the mathematical model of the LRT has the broadest utility to gases. Relatively few of the model variables are chemical-specific. These variables are the effective diffusion and solubility coefficients, as well as expressions for the stoichiometry of reactions of the pollutant with biological constituents. Already, Overton [35] has applied the dosimetry model of the LRT to styrene and the theoretical results correlated well with the human experimental data of Ramsey and Andersen [36]. Studies with other gases that have properties amenable to sensitive tracer techniques also offer opportunities for model validation. However, given the importance of the public health issues for  $O_3$ ,  $O_3$ -specific validation is still required.

Future research to improve the LRT gas dosimetry model is of obvious benefit to that model, but much of the research also will improve particulate dosimetry models. For example, at bifurcations there are "hot spots" of enhanced deposition that cannot be predicted if the lung is viewed as a long, straight tube. Luminal dimensions and branching angles have a weighted impact on regional deposition of particles at bifurcations. As with gases, microdosimetry coupled with microtoxicology has high value to toxicology and risk assessment of particles and this can only be accomplished with full knowledge of the morphometry of the LRT. Mucus thickness and biochemistry also influence particle deposition to and clearance from the tissue, depending on the physiochemistry of the particle. A primary example is for sulfuric acid. Quantitatively, what buffers are in the mucus and to what degree do they influence the hydrogen ion dose to the tissue?

The use of physiologically based dosimetry models will continue to increase in the coming years with applications spanning the gamut of activities involved in the risk assessment process. Figure 3 is a schematic of major phases involved in risk characterization which, when coupled with exposure assessment, yields risk assessment. Figure 3 illustrates the multiple feedback loops and the central nature of a physiologically based dosimetry model. The model, when applied to the literature, enables exposure concentration, time of exposure, and resultant responses of multiple species to be normalized to a predicted dose response. Adding considerations of species sensitivity yields either an estimate of human toxicity or the identification of research gaps. Using the physiologically based dosimetry model will improve the design of experiments to fill these gaps, thereby enhancing the literature data base feeding through the system to achieve more quantitative estimates of human toxicity and hence risk characterization.

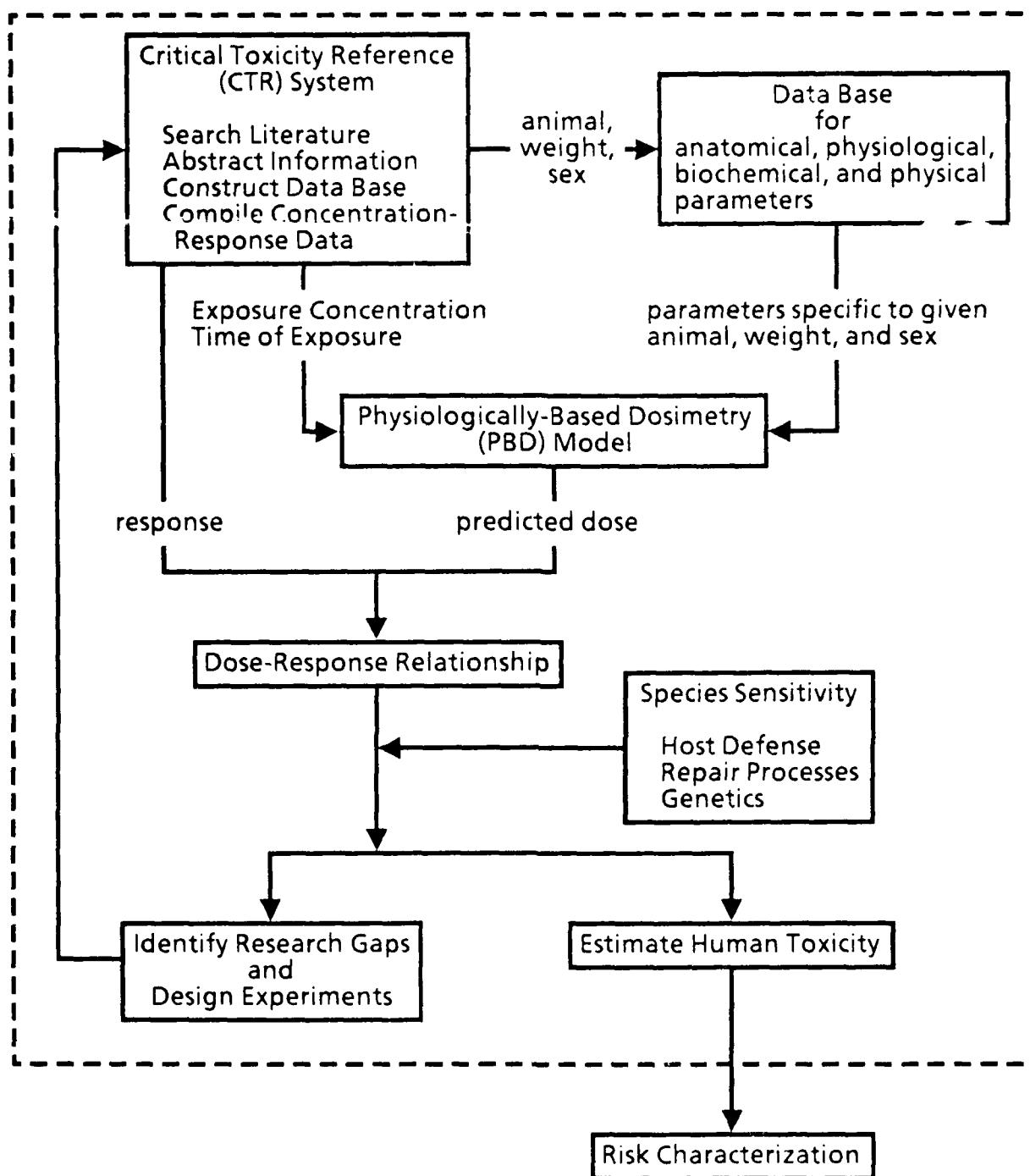


Figure 3. A schematic of the elements of an integrated physiologically based dosimetry modeling approach to estimating human toxicity. A byproduct of the approach is a mechanism that identifies research gaps and leads to further experimentation. SOURCE: Miller et al. [37].

## REFERENCES

- 1 Miller, F.J., Graham, J.A., and Overton, J.H., Jr. (1983) General Considerations for Developing Pulmonary Extrapolation Models. In: Proceedings of the 13th Annual Conference on Environmental Toxicology. AFAMRL-TR-82-101, Dayton, OH, pp. 178-208.
- 2 Gerrity, T.R. (In Press) Nasopharyngeal Uptake of Ozone in Humans and Animals. In: Proceedings of Extrapolation Modeling of Inhaled Particles and Gases: Lung Dosimetry. Durham, NC.
- 3 Wiester, M.J., Tepper, J.S., King, M.E., Menache, M.G., and Costa, D.L. (In Press) Comparative study of ozone (O<sub>3</sub>) uptake in three strains of rats and in the guinea pig. J. Toxicol. Appl. Pharmacol. 96, 140-146.
- 4 Gerrity, T.R., Weaver, R.A., Bernsten, J., House, D.E., and O'Neil, J.J. (In Press) Extrathoracic and Intrathoracic removal of ozone in tidal breathing humans. J. Appl. Physiol.
- 5 Wiester, M.J., Williams, T.B., King, M.E., Menache, M.G., and Miller, F.J. (1987) Ozone uptake in awake Sprague-Dawley rats. Toxicol. Appl. Pharmacol. 89, 429-437.
- 6 Aharonson, E.F., Menkes, H., Gurtner, G., Swift, D.L., and Proctor, D.F. (1974) Effect of respiratory airflow rate on removal of soluble vapors by the nose. J. Appl. Physiol. 37, 654-657.
- 7 Miller, F.J., Overton, J.H., Jr., Jaskot, R.H., and Menzel, D.B. (1985) A model of the regional uptake of gaseous pollutants in the lung. I. The sensitivity of the uptake of ozone in the human lung to lower respiratory tract secretions and exercise. Toxicol. Appl. Pharmacol. 79, 11-27.
- 8 Overton, J.H., Graham, R.C., and Miller, F.J. (1987) A model of the regional uptake of gaseous pollutants in the lungs: II. The sensitivity of ozone uptake in laboratory animal lungs to anatomical and ventilatory parameters. Toxicol. Appl. Pharmacol. 88, 418-432.
- 9 Landal, H.D. (1950) On the removal of airborne droplets by the human respiratory tract. I. The lung. Bull. Math. Biophys. 12, 43-56.
- 10 Weibel, E.R. (1963) Morphometry of the Human Lung. Academic Press, New York.
- 11 Horsfield, K. and Cumming, G. (1968) Morphology of the bronchial tree of man. J. Appl. Physiol. 24, 373-383.
- 12 Raabe, O.G., Yeh, H.C., Schum G.M., and Phalen, R.F. (1976) Tracheobronchial Morphometry: Human, Dog, Rat, Hamster. LF-53, Lovelace Foundation for Medical Education and Research, Albuquerque, NM.
- 13 Kliment, V. (1973) Similarity and dimensional analysis, evaluation of aerosol deposition in the lungs of laboratory animals and man. Folia Morphol. (Warsaw) 21, 59-64.
- 14 Yeh, H.C., Schum, G.M., and Duggan, M.T. (1979) Anatomic models of the tracheobronchial and pulmonary regions of the rat. Anat. Rec. 195, 483-492.
- 15 Schreider, J.P. and Hutchens, J.O. (1980) Morphology of the guinea pig respiratory tract. Anat. Rec. 196, 313-321.

- 16 Freeman, G., Stephens, R.J., Coffin, D.L., and Stara, J.F. (1973) Changes in dog's lungs after long-term exposure to ozone. *Arch. Environ. Health* 26, 209-216.
- 17 Plopper, C.G., Chow, C. K., Dungworth, D.L., and Tyler, W.S. (1979) Pulmonary alterations in rats exposed to 0.2 and 0.1 ppm ozone: A correlated morphological and biochemical study. *Arch. Environ. Health* 34, 390-395.
- 18 Castleman, W.L., Dungworth, D.L., Schwartz, L.W., and Tyler, W.S. (1980) Acute respiratory bronchiolitis: An ultrastructural and autoradiographic study of epithelial cell injury and renewal in rhesus monkeys exposed to ozone. *Amer. J. Pathol.* 98, 811-840.
- 19 Barry, B.E., Miller, F.J., and Crapo, J.D. (1985) Effects of inhalation of 0.12 and 0.25 parts per million ozone on the proximal alveolar region of juvenile and adult rats. *Lab. Invest.* 53, 692-704.
- 20 Mercer, R.R. and Crapo, J.D. (1987) Three-dimensional reconstruction of the rat acinus. *J. Appl. Physiol.* 63, 785-794.
- 21 Clements, J.A. (1971) Comparative lipid chemistry of lungs. *Arch. Intern. Med.* 127, 387-389.
- 22 Sanders, R.L. (1982) The chemical composition of the lung. In: P.M. Farrell (Ed.), *Lung Development: Biological and Clinical Perspectives*, Academic Press, New York, pp. 179-192.
- 23 Orban, E., Maderspach, A., and Tomori, E. (1980) Triton WR-1339 induced changes in fatty acid composition of serum lipids in rats. *Biochem. Pharmacol.* 79, 2879-2882.
- 24 Hatch, G. E. and Aissa, M. (1987) Determination of Absorbed Dose of Ozone (O<sub>3</sub>) in Animals and Humans Using Stable Isotope (Oxygen-18) Tracing. Technical Paper 87-99.2, Air Pollution Control Association 80th Annual Meeting, New York, NY, June 21-26.
- 25 Santrock J. and Hayes, J.M. (1987) Adaptation of the Unterzaucher procedure for determination of oxygen-18 in organic substances. *Anal. Chem.* 59, 119-127.
- 26 Hatch, G.E., Aissa, M., Wiester, M.J., and Overton, J.H. (1988) Respiratory Tract Dosimetry of (18)O-Labeled Ozone in Rats: Implications for a Rat-Human Extrapolation of Ozone Dose. In: *Atmospheric Ozone Research and Its Policy Implications. Proc. Third U.S.-Dutch Symposium, Nijmegen, The Netherlands, May 8-13.*
- 27 Hatch, G.E., Koren, H., and Aissa, M. (In Press) A model for comparison of animal and human alveolar dose and toxic effect of inhaled ozone. *Health Physics.*
- 28 Hatch, G.E., Slade, R., Stead A.G., and Graham, J.A. (1986) Species comparison of acute inhalation toxicity of ozone and phosgene. *J. Toxicol. Environ. Health* 19, 43-53.
- 29 Miller, F.J., Overton, J.H., Jr., Gerrity, T.R., and Graham, R.C. (1987) Interspecies Dosimetry of Reactive Gases. Presented at the Design in Interpretation of Inhalation Studies and Their Use in Risk Assessment Symposium, Hanover, Federal Republic of Germany, March 23-27.
- 30 Koren, H.S., Devlin, R.B., Graham, D.E., Mann, R., and McDonnell, W.F. (1988) The Inflammatory Response in Human Lung Exposed to Ambient Levels of Ozone. In: *Atmospheric Ozone Research and Policy Implications. Proc. Third U.S.-Dutch Symposium, Nijmegen, The Netherlands, May 8-13.*

- 31 McDonnell, W.F., Horstman, D.H., Hazucha, M.J., Seal, E., Haak, E.D., Salaam, S.A., and House, D.E. (1983) Pulmonary effects of ozone exposure during exercise: Dose-response characteristics. *J. Appl. Physiol.: Respirat. Environ. Exercise Physiol.* 54, 1345-1352.
- 32 Gerrity, T.R. and McDonnell, W.F. (1988) Do Functional Changes Correlate with the Airway Removal Efficiency of Ozone? In: *Atmospheric Ozone Research and Its Policy Implications. Proc. Third U.S.-Dutch Symposium, Nijmegen, The Netherlands, May 8-13.*
- 33 McDonnell, W.F., Chapman, R.S., Horstman, D.H., Leigh, M.W., and Abdul-Salaam, S. (1985) A comparison of the responses of children and adults to acute ozone exposure. In: S.D. Lee (Ed.), *Evaluation of the Scientific Basis for Ozone/Oxidants Standards, Air Pollution Control Association, Pittsburgh*, pp. 317-328.
- 34 Miller, F.J. and Overton, J.H. (1988) Critical Issues in Intra- and Interspecies Dosimetry of Ozone. In: *Atmospheric Ozone Research and Policy Implications. Proc. Third U.S.-Dutch Symposium, Nijmegen, The Netherlands, May 8-13.*
- 35 Overton, J.H. (1988) Respiratory Tract Dosimetry Modeling of Air Toxics. In: *Atmospheric Ozone Research and Its Policy Implications. Proc. of U.S.-Dutch Expert Workshop on Air Toxics. Amersfoort, The Netherlands, May 16-18, 1988.*
- 36 Ramsey, J.C. and Andersen, M.E. (1984) A physiologically based description of the inhalation pharmacokinetics of styrene in rats and humans. *Toxicol. Appl. Pharmacol.* 73, 159-175.
- 37 Miller, F.J., Overton, J.H., Smolko, E.D., Graham, R.C., and Menzel, D.B. (1987) Hazard Assessment Using an Integrated Physiologically-Based Dosimetry Modeling Approach: Ozone. In: *Pharmacokinetics in Risk Assessment/Drinking Water and Health, Vol. 8, National Academy Press, Washington, DC*, pp. 353-368.

## CISPLATIN PHARMACOKINETICS: APPLICATIONS OF A PHYSIOLOGICAL MODEL

Fred F. Farrisa, Robert L. Dedrickb, and Franklin G. Kingc

*aSoutheastern College of Pharmaceutical Sciences, North Miami Beach, FL, bBiomedical Engineering and Instrumentation Branch, Division of Research Services, National Institutes of Health, Bethesda, MD, and cDepartment of Chemical Engineering, North Carolina A&T State University, Greensboro, NC*

### SUMMARY

A physiological pharmacokinetic model for the disposition of the antineoplastic drug *cis*-diamminedichloroplatinum(II) (cisplatin or DDP) in several mammalian species is reviewed. The significance of the model's key parameters and of their interspecies relationships is discussed. Methods for estimating two of these parameters (the rate constants for formation of the fixed and mobile metabolites) from *in vitro* experiments are presented. Fixed and mobile metabolites are formed by the irreversible binding of cisplatin to macromolecules and low molecular weight nucleophiles, respectively. Use of the model to simulate and predict the pharmacokinetic behavior of cisplatin and its metabolites in different animal species following intravenous and intraperitoneal administration is illustrated. Fixed metabolite formation rate constants can be used in conjunction with mass transport parameters to estimate tissue exposures to cisplatin following systemic or regional drug administration. The model logically can serve as the basis for a pharmacodynamic model that incorporates cisplatin reactions with DNA. The model also provides a means for comparing the pharmacokinetic characteristics of cisplatin analogs and for assisting in rational analog development.

### INTRODUCTION

For years, empirically based pharmacokinetic models have served as valuable predictive tools for the pharmacologist and toxicologist [1,2]. One of the keys to the success of these models is their relative simplicity. Empirical models can be developed with minimal regard for the mechanistic aspects of drug disposition because their key parameters are usually determined by curve-fitting experimental data [3]; and once developed, these models require relatively little input data and computational sophistication. Such models provide a clearly defined, quantitatively based means for making predictive estimates of systemic concentrations for many drugs and toxins [2,4]. The factors that lead to the simplicity of these models, however, also diminish their versatility. If the focus of a model is to be mechanistic, or if information is desired that is not attainable from a purely empirical model, then a different approach is required.

Physiological pharmacokinetics transcends many of the limitations of classical compartmental models by describing absorption and disposition in terms of identifiable anatomical spaces, as well as

physiological and biochemical processes [5,6,7]. Physiological models can be used to simulate a variety of events for almost any chemical species, including the disposition of drugs for which classical models are often applied. However, the time and effort required to develop physiological models, and the computational complexity involved in their use, can be considerable. Thus, for many drugs there may be little incentive to develop a physiological model when a simpler, classical model will suffice. One of the strengths of physiologically based models is that they can provide information and insight regarding a host of pharmacokinetic phenomena [6,7,8,9]. Physiological models also provide a means of incorporating data derived from *in vitro* experiments and from observations made on different animal species [9,10,11]. The present paper demonstrates some of the uses of a physiological pharmacokinetic model. The discussion centers around a model developed originally to simulate the disposition of the antineoplastic agent cis-diamminedichloroplatinum(II), also known as cisplatin or DDP (12,13). The model and its development are reviewed, and the model's key parameters and some of their interspecies relationships are discussed. The paper then focuses on ways that the model can be used to gain new information about the pharmacology of cisplatin and some related drugs.

## MODEL DESIGN

The details of this model and results of its simulations for several animal species, including humans, have been presented elsewhere [12,13], and no attempt will be made to repeat them *in toto*. The model's key points are presented here.

### *Development of model equations*

The model is based on two simplifying assumptions: (1) drug transport is flow-limited, and (2) each organ or tissue is modeled as a lumped compartment. Those compartments included in the model and their interrelationships are shown in the flow diagram in Figure 1. Each of the compartments modeled represents a major site of platinum (Pt) accumulation and/or elimination. The carcass compartment includes all tissues not otherwise incorporated into the model such as bone, fat, and small organs.

When cisplatin is placed in an aqueous environment, such as the body, water molecules can displace the chloride ions to produce aquated complexes. Both the parent drug and the aquated species can react to form metabolites. Despite the fact that the two species may react at different rates, both reactions can be described with a single rate constant by applying a simple quasi-steady state approximation to the aquated complex. Thus, although the model accounts for reactions of the aquated species, these reactions are kinetically lumped with those of cisplatin.

Current evidence indicates that cisplatin binds very tightly, possibly irreversibly, to low molecular weight nucleophiles and nucleophilic sites on macromolecules to give mobile and fixed

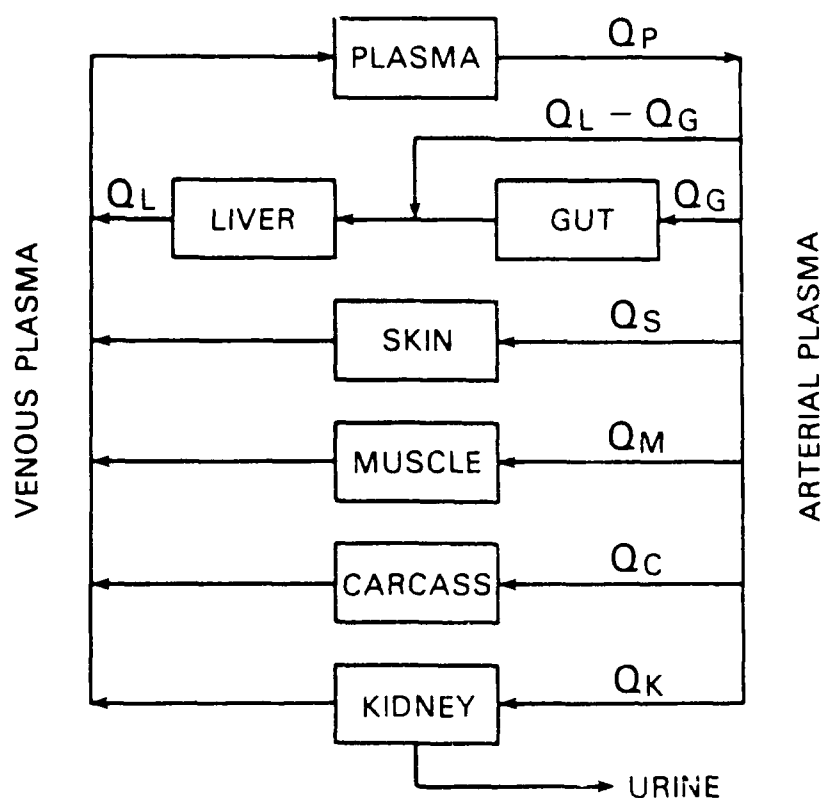


Figure 1. Compartmental flow diagram for the pharmacokinetic model for cisplatin. Here  $Q_i$  represents the plasma flow rate, in milliliters per minute, through the liver (L), gut (G), skin (S), muscle (M), carcass (C), kidney (K), and cardiac output (P) [13].

metabolites, respectively. Both metabolites represent lumped species in the model. The mobile metabolite is any Pt-containing species (other than the parent drug) that easily can traverse cell membranes. This metabolite moves readily between compartments and is assumed to follow flow-limited kinetics. Platinum that is bound irreversibly to macromolecules represents the fixed metabolite. Because protein is quantitatively the dominant form of macromolecule in all tissues, the fixed metabolite is assumed to be primarily Pt bound to proteins. The fixed metabolite is confined to the compartment where it is formed. The only way that Pt bound as a fixed metabolite can be eliminated from a compartment is via catabolism of the Pt-macromolecule complex to give a mobile metabolite. Since both fixed and mobile metabolites are formed by direct reaction with binding sites within tissues, their formation rates are tissue-specific.

Urinary excretion is the major route of Pt elimination following cisplatin administration in all animal species studied. Experiments have shown that urinary Pt is comprised of both the parent drug and the mobile metabolite. In some animal species, 50% or more of the original Pt dose may be excreted in the first 24 h following cisplatin administration. Urinary excretion is modeled as a linear process. Renal clearance values for both cisplatin and the mobile metabolite are assumed to be

identical and correspond to the glomerular filtration rate (GFR) for the particular animal species being modeled. Elimination of Pt via bile is small and is neglected. Figure 2 delineates, in schematic form, the biotransformation and elimination pathways in the model.

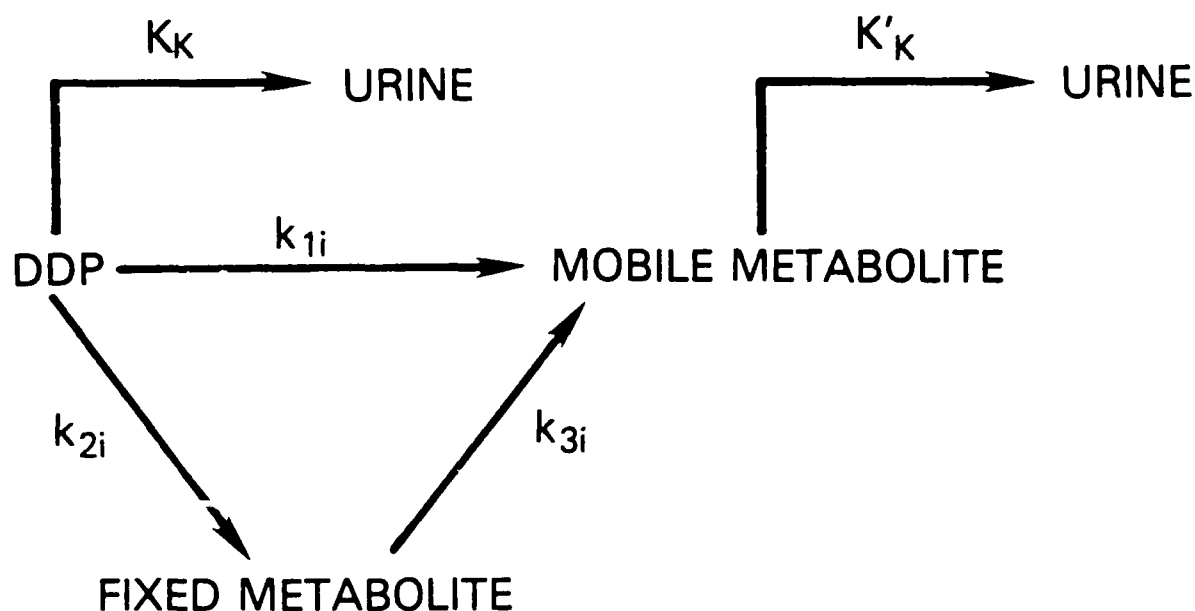


Figure 2. Schematic representation of the biotransformation and elimination pathways of Pt complexes used in the cisplatin model. The meaning of each parameter is defined in the text [13].

The basic tenets of the model are expressed in a series of differential mass balance equations. A separate equation is written for each kinetically unique chemical species in each model compartment. Twenty-one equations are required to model the three kinetically distinct species (cisplatin, fixed metabolite, and mobile metabolite) that exist in each of the seven compartments. In addition, two more equations are needed to describe urinary excretion of Pt as the parent drug and as the mobile metabolite. Each equation is composed of a series of mathematical terms, each term representing a specific influx, efflux, biotransformation, or elimination process. For example, the mass balance for cisplatin in the kidney is given in Eq. (1).

$$V_K dC_K/dt = Q_K C_P - Q_K C_K / R_K - k_{2K} C_K V_K - k_{1K} C_K V_K - K_K C_P \quad (1)$$

where:

$V_K$  = kidney volume

$Q_K$  = plasma flow rate to the kidney

$C_K$  = cisplatin concentration in the kidney

$C_P$  = cisplatin concentration in the plasma

$R_K$  = equilibrium distribution ratio (kidney to plasma concentration ratio) for cisplatin

$k_{1K}$  = rate constant for the biotransformation of cisplatin to mobile metabolite in kidney (mobile metabolite formation rate constant)

$k_{2K}$  = rate constant for the biotransformation of cisplatin to fixed metabolite in kidney (fixed metabolite formation rate constant or protein-binding rate constant)

$K_K$  = renal clearance of cisplatin

The physical significance of the terms on the right side of Eq. (1) are, from left to right, the rates of cisplatin influx into the kidney the from plasma, cisplatin efflux from kidney to plasma, cisplatin loss in kidney via conversion to fixed metabolite, cisplatin loss via conversion to mobile metabolite, and cisplatin excretion in the urine.

The mass balances for mobile and fixed metabolites in the kidney are given in Eqs. (2) and (3), respectively.

$$V_K dC'_K/dt = Q_K C'_P - Q_K C'_K/R'_K + k_{1K} C_K V_K + k_{2K} C''_K V_K - K'_K C'_P \quad (2)$$

$$V_K dC''_K/dt = k_{2K} C_K V_K - k_{3K} C''_K V_K \quad (3)$$

where:

$k_{3K}$  = rate constant for the biotransformation of fixed to mobile metabolite in the kidney (protein turnover rate constant)

Other parameters in Eqs. (2) and (3) are similar to those defined for Eq. (1), but the singly primed characters represent values for the mobile metabolite and doubly primed characters designate fixed metabolite parameters. The meaning of the terms in Eqs. (2) and (3) also are similar to those in Eq. (1). The mass balance expression for fixed metabolite [Eq.(3)] is less complex than Eqs. (1) and (2) because fixed Pt cannot move between compartments and is not excreted.

Once all parameters are estimated, the 23 equations are solved simultaneously to determine the time-dependent concentrations for each kinetic species in each compartment and for the cumulative urinary excretions of cisplatin and its mobile metabolite.

### **Parameter estimation and significance**

Before the mass balance equations can be solved, values must first be assigned to all equation parameters. The total number of parameters required for a physiological model is often large (45 in the present case). Fortunately, some parameters such as compartment volumes and plasma flow rates are independent of the chemical species being modeled. Values for these anatomical and physiological parameters were obtained directly from the literature or by appropriate scaling of literature values.

The equilibrium distribution ratio ( $R$  in the above equations) is a very important parameter in physiological models. It is the ratio of drug concentration in a tissue or compartment to the drug concentration in the venous plasma exiting that compartment [14,15]. Because both cisplatin and the mobile metabolite presumably distribute only to the aqueous phase of each compartment,  $R$  is assumed to equal unity in all cases. The renal clearance of cisplatin is taken to equal GFR because experiments have shown this to be a reasonable approximation in all animal species studied. Renal clearance of the mobile metabolite is assumed to be the same as that of cisplatin. Interspecies variations of GFR (as indicated by insulin and creatinine clearances) in mammals follow a well-defined allometric relationship [16] of the following form:

$$y = \alpha W^b \quad (4)$$

where  $y$  is the clearance value,  $W$  is the animal's body weight, and  $\alpha$  and  $b$  are empirically determined constants. This equation allows the estimation of GFR in mammals for which data are unavailable.

Table 1 summarizes the anatomic and physiological parameters used to model cisplatin pharmacokinetic behavior in the rat, rabbit, dog, and human.

TABLE 1. ANATOMIC AND PHYSIOLOGIC PARAMETERS FOR CISPLATIN

	Rat	Rabbit	Dog	Man
Compartment volume (mL)				
Plasma	9.5	90	410	3,000
Liver	8.8	130	400	1,350
Gut	11.6	155	400	2,100
Kidney	2.0	20	50	280
Muscle	106.0	1,740	4,600	35,000
Skin	36.9	450	1,600	12,600
Carcass	34.0	260	2,540	15,670
Whole animal (g)	211.0	3,000	10,000	70,000
Compartment flow rate (mL/min)				
Plasma	30.3	323	589	3,000
Liver (hepatic artery)	1.3	13	44	100
Gut	5.6	84	124	700
Kidney	5.3	52	75	700
Muscle	3.2	56	115	420
Skin	2.1	31	66	175
Carcass	12.2	87	165	905

(continued)

TABLE 1. (Continued)

	Rat	Rabbit	Dog	Man
Clearance (mL/min)				
Renal	1.1	19	50	100
(cisplatin and mobile metabolite)				

(Table adapted from King et al. [13])

Fixed metabolite is formed when cisplatin binds irreversibly to nucleophilic sites on macromolecules. This corresponds macroscopically to cisplatin binding to proteins, because these are the dominant macromolecules in all tissues. The rate of this binding process is estimable in plasma by measuring the loss of ultrafilterable Pt from an *in vitro* incubation mixture containing the parent drug. The results of such a study in rabbit plasma are shown in Figure 3. The first-order rate constant determined from this plot is  $0.0043 \text{ min}^{-1}$ .

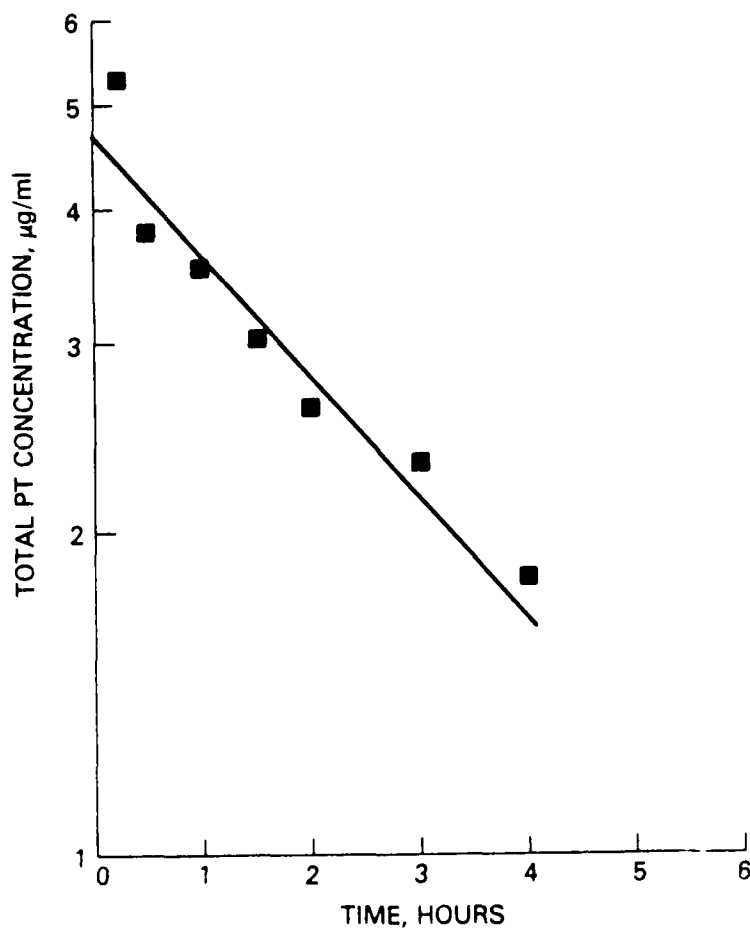


Figure 3. Concentration of total Pt in rabbit plasma ultrafiltrate as a function of *in vitro* incubation time. The initial concentration of cisplatin was  $5.0 \text{ µg/mL}$ . [13]

Fixed metabolite formation rate constants derived from similar incubation studies in rat, dog, and human plasma are summarized in Table 2. Because experimentally determined rate constants for binding of cisplatin to macromolecules in tissues other than plasma were unavailable, fixed metabolite formation rate constants for compartments other than plasma were estimated indirectly. Initial estimates were made by multiplying the experimentally determined protein-binding rate constant for plasma times the ratio of the Pt concentration in the tissue of interest to the Pt concentration in plasma at intermediate times after dosing. These initial estimates then were adjusted (by no more than 10% in most cases) to obtain better agreement between the experimental data and the simulations. Column 2 of Table 2 lists the fixed metabolite formation rate constants used in the model for the three experimental animals and man.

Estimates of mobile metabolite formation rate constants were based on the assumption that cisplatin binds to available sites on small and large molecules with equal avidity. Thus, the relative rates of formation of fixed and mobile metabolites within a compartment reflect the statistical availabilities of macromolecular nucleophilic sites and low molecular weight nucleophiles, respectively. The details associated with the calculation of these rate constants have been presented elsewhere [12,13]. Column 3 of Table 2 summarizes the values of the mobile metabolite formation rate constants used in the model.

An important feature of the data in Table 2 is the small degree of interspecies variability seen in both the fixed and mobile metabolite formation rate constants. The rate constants for the formation of fixed metabolite for plasma, for example, are almost identical for all species except rabbit. For other tissues, only rarely do the values for a given constant vary by more than a factor of 2 among the 3 species of experimental animals. The uniformity of these values among species results presumably from the fact that cisplatin metabolite formation occurs by direct binding of the drug to nucleophilic sites within tissues and not from an enzymatically mediated process. These results are of practical importance because they indicate that the drug's binding characteristics are similar in each of the animal species examined.

Once bound in the form of fixed metabolite, Pt release from a compartment is controlled by the rate of catabolism of that compartment's macromolecules (primarily proteins) to form mobile metabolite. The compartment-specific rate constants associated with this catabolism process in rats, rabbits, dogs, and humans are listed in column 4 of Table 2. Notice that these rate constants, unlike those for metabolite formation, vary considerably among species for a given tissue. In fact, interspecies protein turnover in mammals is known to follow an allometric relationship identical in form to Eq (4) [17,18]. We used this equation to estimate the rate of protein turnover when experimental values were unavailable.

TABLE 2. RATE CONSTANTS FOR THE BIOTRANSFORMATION OF CISPLATIN

Species/Compartment	Fixed Metabolite* Formation ( $k_{2i}$ )	Mobile Metabolite* Formation ( $k_{1i}$ )	Protein* Turnover ( $k_{3i}$ )
Rat (0.211 kg)			
Plasma	820	25	35.0
Liver	3,280	1,570	18.7
Gut	1,400	350	21.5
Kidney	9,020	722	7.8
Muscle	410	139	8.4
Skin	5,330	1,330	14.0
Carcass	820	205	17.6
Rabbit			
Plasma	430	13	10.0
Liver	1,720	825	5.0
Gut	790	195	9.0
Kidney	5,630	450	6.0
Muscle	430	146	5.6
Skin	1,560	390	6.5
Carcass	430	108	4.4
Dog			
Plasma	608	18	7.5
Liver	4,250	2,040	6.9
Gut	1,250	313	12.0
Kidney	14,250	1,140	5.8
Muscle	600	204	7.6
Skin	7,150	1,790	8.8
Carcass	608	152	8.3
Human (70 kg)			
Plasma	740	22	6.0
Liver	3,400	1,630	5.1
Gut	1,200	300	8.5
Kidney	10,800	860	4.8
Muscle	500	178	4.5
Skin	5,300	1,325	4.1
Carcass	740	185	5.9

\* All values are expressed in units of  $\text{min}^{-1} \times 10^5$   
 (Tables adapted from King et al. [13])

### Model applications

#### Disposition simulations

The model has been used to simulate the disposition of cisplatin and its metabolites in several tissues following intravenous (iv) administration in the rat, rabbit, dog, and human [12,13].

Figure 4 compares model simulations [13] with experimentally determined concentrations [19] of total Pt in six compartments following an iv dose of 2 mg/kg of cisplatin to rabbits. These simulations illustrate how the model can be used to gain information about the drug in compartments that are normally inaccessible to sampling. Corresponding simulations can be made for any animal species to which the model is applied.

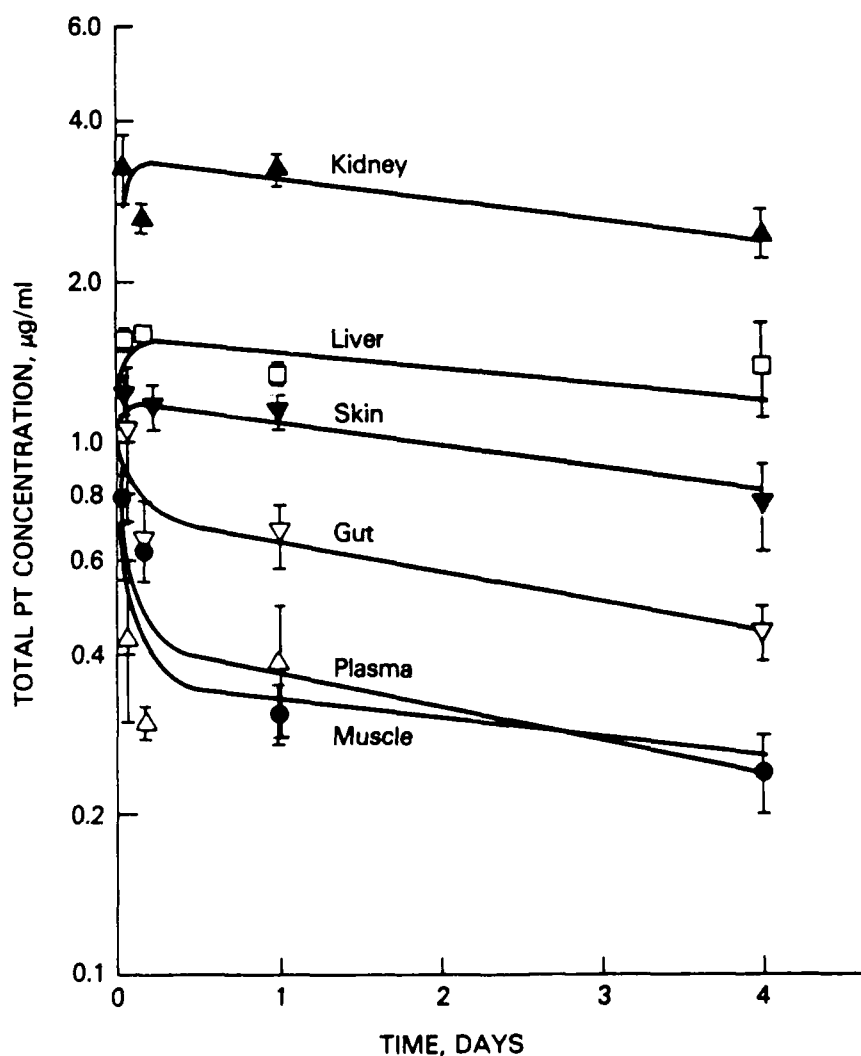


Figure 4. Model simulations compared with experimental data from rabbits for total Pt concentration following a 2 mg/kg iv dose of cisplatin. The points represent the mean  $\pm$  standard deviation (SD) of experimental data from 3 rabbits. In this and the following figures the solid lines represent model simulations [13].

In Figure 5, model simulations [13] are compared with experimental data [20] for the different Pt-containing species in human plasma following iv bolus administration of cisplatin. The figure clearly demonstrates that cisplatin becomes a minority species relatively soon after it is administered. This result occurs in all compartments modeled, although the exact rate of cisplatin disappearance is tissue-specific. For situations where measurement of metabolite concentrations is experimentally difficult or impossible, the model provides a means of simulating these concentrations.

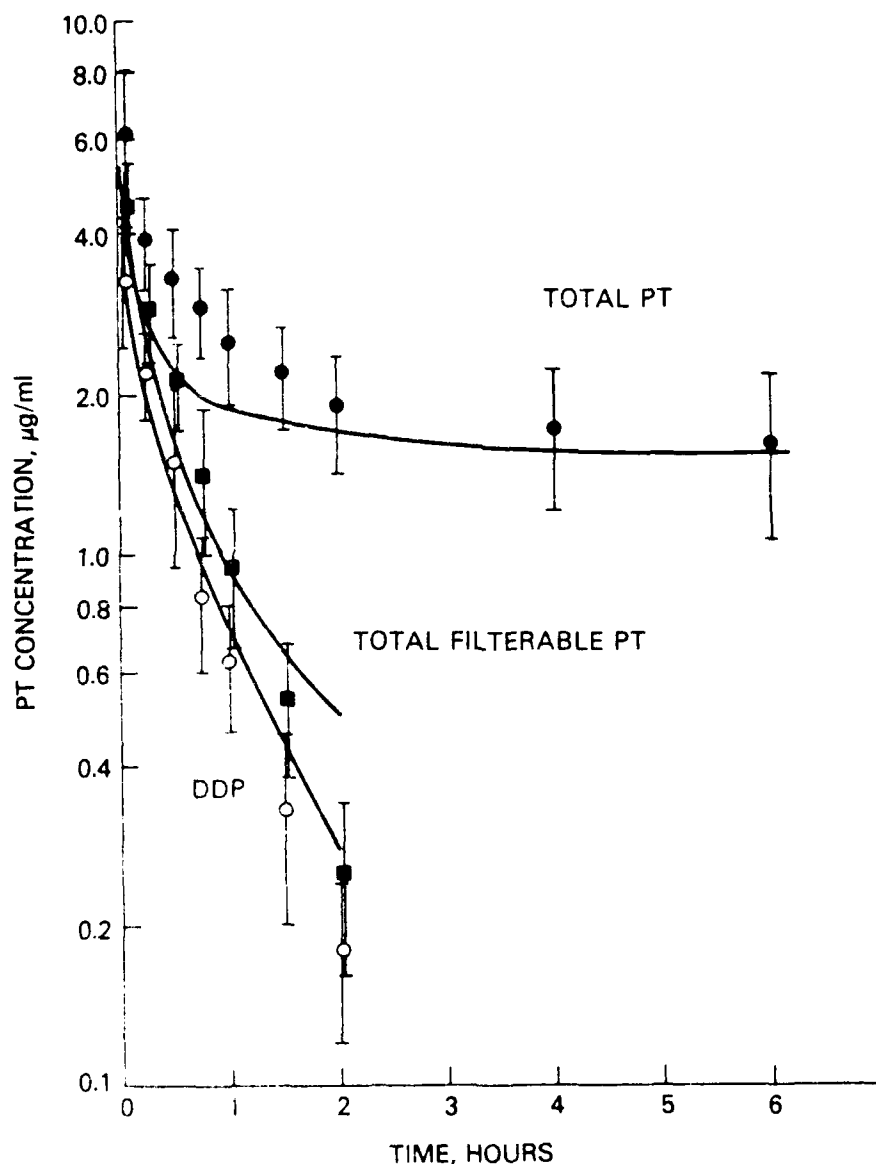


Figure 5. Model simulations compared with experimental data for Pt-containing species in human plasma following an iv dose of 100 mg/m<sup>2</sup> of cisplatin. Each point represents the mean  $\pm$  SD for 5 to 6 patients [13].

The model also has been used to predict the disposition of cisplatin and its metabolites when the route of administration is other than that used for model validation. For example, King et al. [13] predicted total Pt concentrations in plasma following intraperitoneal (ip) administration of cisplatin in dogs. Figure 6 compares these predictions with experimental data following a 3 mg/kg ip dose of the parent drug [21]. These predictions assume an absorption rate constant of  $0.008 \text{ min}^{-1}$  for cisplatin from the peritoneal cavity; otherwise the model parameters are identical to those used to simulate iv administration.

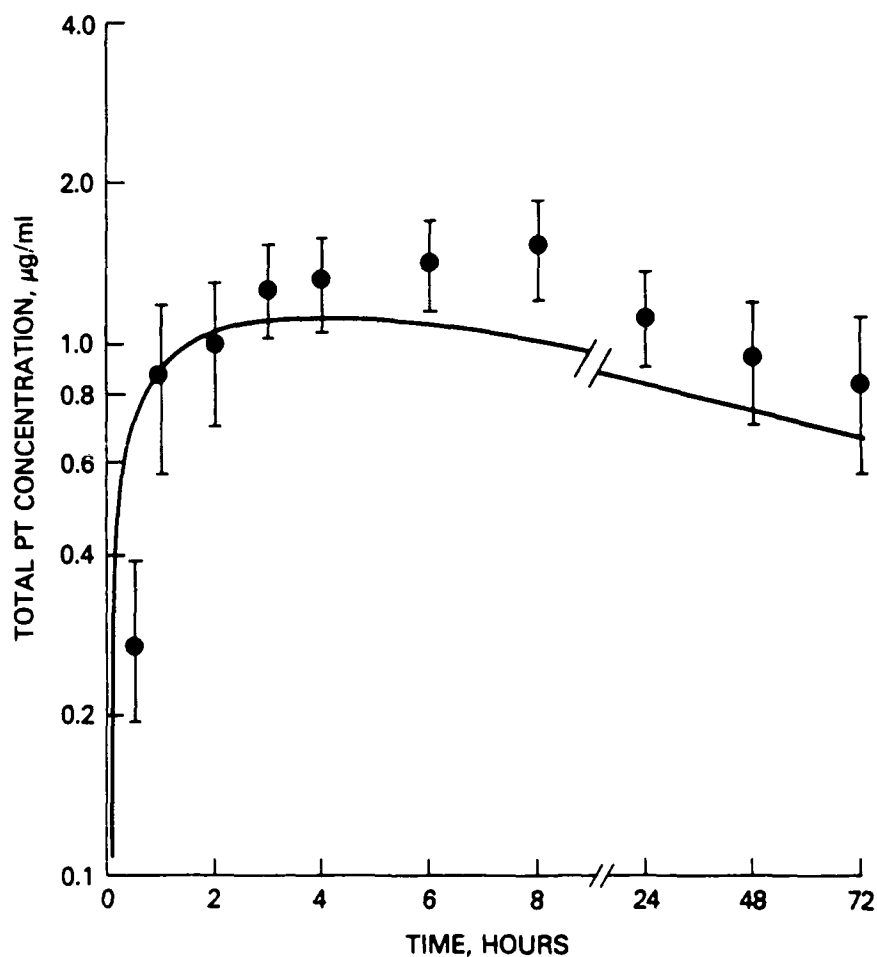


Figure 6. Model predictions compared with experimental data for total Pt concentration in dog plasma following a 3 mg/kg i.p. dose of cisplatin. Each point represents the mean  $\pm$  SD for 11 dogs [13].

The model should be applicable to almost any mammalian species, even those for which model parameters are difficult to measure experimentally. In the previous section on parameter estimation, six classes of parameters were identified: (1) anatomic and physiologic, (2) equilibrium distribution coefficients, (3) renal clearances, (4) fixed metabolite formation rate constants, (5) mobile metabolite formation rate constants, and (6) fixed to mobile metabolite biotransformation (protein turnover)

rate constants. All of these parameters are known and available, or can be estimated. Anatomic and physiologic values, including renal clearances (GFR), are available in the literature or can be estimated from appropriate allometric equations, and the distribution coefficients are assumed to be unity in all cases. Of the three different sets of rate constants, those describing the formation of both fixed and mobile metabolites usually appear to be similar for a given compartment across species. An average of the values given for the three species of experimental animals in Table 2 is probably a reasonable estimate of these parameters in other animal species. Finally, the protein turnover rate constant can be estimated allometrically from Eq. (4). The model also provides a means for assessing the effects of altered physiological states on the disposition of cisplatin. For example, the effects of altered renal function or protein metabolism can be analyzed by modifying the appropriate parameters.

#### ***In vitro estimation of metabolite formation rate constants***

The fixed metabolite formation rate constants for all model compartments, except plasma, were estimated initially from the Pt concentrations in the appropriate tissue relative to those in plasma. Estimates of the mobile metabolite formation rate constants were based on assumptions made about the relative availability of protein versus non-protein nucleophilic binding sites within tissues. The assumptions used in estimating both sets of constants appear sound, and the overall success of the model's simulations is reassuring. Nevertheless, experimental confirmation of these rate constants is desirable and could provide valuable information regarding the nature and kinetics of the metabolic processes. Because of the nonenzymatic nature of the cisplatin/nucleophile interaction, *in vitro* studies are a logical approach to estimating these constants. The logic of this approach is supported by the fact that the metabolites formed during *in vitro* incubation of cisplatin in plasma are identical to those found in this tissue following *in vivo* administration of the drug [22]. If the experimentally determined rate constants are to be applicable directly to the model, then the *in vitro* system must contain all tissue components that are important for drug-binding. This need can be fulfilled most directly by using systems containing the whole tissue.

One such system is isolated organ perfusion. The kinetic treatment of such a system depends on how the experiment is designed. If the perfusate is recirculated between the tissue and a reservoir, then the perfusion system can be described mathematically as a simple two-compartment model [23] where the rate of cisplatin disappearance from the perfusate is determined by the rate of metabolite formation in the organ. If the perfusate is pumped from, but not recirculated to, the reservoir, then the difference in cisplatin concentrations between the perfusate entering and leaving the organ (at steady state with respect to cisplatin) can be used to define the extraction ratio [23]. The metabolite formation rate constants for the perfused organ then can be calculated from these results.

A second experimental approach involves incubating cisplatin *in vitro* with whole tissue homogenates. Siddik et al. [24] used this method to measure the relative binding rates of cisplatin and carboplatin to liver, kidney, and plasma proteins in rats and mice. The drugs were incubated at 37°C in tissue homogenates and plasma that had been diluted with buffer to a final protein concentration of 10 mg/mL. Aliquots were removed periodically and the proteins were precipitated by addition of trichloroacetic acid (TCA). The half-lives for TCA-soluble Pt in the cisplatin incubations were reported to be 11.6 h, 6.8 h, and 7.6 h for rat plasma, liver, and kidney, respectively. If we assume that plasma normally contains about 7% protein [25] and that liver and kidney each contain approximately 20% protein [18,26], then fixed metabolite formation constants can be estimated from the *in vitro* half-life data. The rate constants estimated from these half-life data are 0.007 min<sup>-1</sup>, 0.034 min<sup>-1</sup>, and 0.030 min<sup>-1</sup> for plasma, liver, and kidney, respectively. The fixed metabolite formation rate constants used for these same tissues in the model were 0.0082 min<sup>-1</sup>, 0.033 min<sup>-1</sup>, and 0.09 min<sup>-1</sup>, respectively. The agreement between the constants for plasma and liver are good, but there is a threefold discrepancy between the two kidney constants. The precise reason for this discrepancy is unknown.

The homogenate incubation technique discussed above should be applicable to most tissues. It also is simple enough that minor experimental modifications, such as using ultrafiltration instead of TCA precipitation to separate mobile Pt (cisplatin and mobile metabolite) from fixed Pt, can be easily incorporated. Also, by using the appropriate analytical methods, for example, HPLC [27,28], the rate of mobile metabolite formation can be estimated from its appearance in the filtrate (or soluble fraction).

A third method of estimating the metabolite formation rate constants involves *in vitro* incubation of isolated tissue cells in a cisplatin-containing medium. A variety of enzymatic and non-enzymatic methods are available for the disaggregation of tissues to form isolated cells [29]. Lin et al. [30] have used isolated cell suspensions to measure the uptake of ethoxybenzamide into rat liver cells. To study cisplatin binding, sample acquisition and analysis would be similar to that used in the homogenate incubation method discussed above. Cell viability is often a concern when isolated cells are used [29], but this may be less critical when studying reactions that are not enzymatically mediated.

An alternative to the above methods is the use of diluted cytoplasm as the *in vitro* incubation medium. However, because such systems contain no cell membranes, they provide information solely about the Pt-binding properties of intracellular components.

To measure the rate constants associated with the binding of cisplatin to specific macromolecular sites or to individual nucleophiles, direct incubation is again an appropriate

technique. Several such studies have been conducted with proteins and polypeptides [28,31], and low molecular weight nucleophiles [32]. Most of these studies have not been sufficiently detailed to allow a complete kinetic analysis. More detailed binding studies involving isolated nucleophiles and proteins might yield information that would allow formulation of the model in terms of more fundamental principles.

### **Estimation of tissue exposure**

The irreversible binding of cisplatin to macromolecules and low molecular weight nucleophiles to form metabolites produces a sink effect within each compartment. This effect can diminish a compartment's exposure to cisplatin compared to the exposure received by the arterial plasma. The significance of this diminution depends on the rate of mass transport of the drug into the compartment and the rate of metabolite formation. Although both mobile and fixed metabolites are formed in all compartments, the rate of fixed metabolite formation is more rapid and produces the dominant effect. It can be shown that the exposure (as defined by the area under the concentration-time curve for the parent drug, AUC) received by a flow-limited compartment, following systemic cisplatin administration, can be estimated from Eq. (5).

$$AUC_T = AUC_p (q/[q + k_{2i}]) \quad (5)$$

where:

- $AUC_i$  = area under the concentration-time curve for compartment  $i$
- $AUC_p$  = area under the concentration-time curve for arterial plasma
- $q$  = plasma flow-rate per unit tissue volume
- $k_{2i}$  = fixed metabolite formation rate constant for compartment  $i$

An analogous equation [Eq. (6)] has been shown to hold for a membrane-limited compartment [33].

$$AUC_T = AUC_p (pa/[pa + k_{2i}]) \quad (6)$$

where:

- $p$  = capillary permeability
- $\alpha$  = capillary surface area per unit tissue volume

The rate of drug delivery to a compartment is dependent on the mass transport parameters,  $q$  or  $pa$ . For compartments where the mass transport parameter is large compared with the reaction rate constant,  $k_{2i}$ , the exposure to the compartment is approximately equal to that of the arterial plasma. For compartments where  $k_{2i}$  is comparable to  $pa$  or  $q$ , exposure to the compartment will be diminished compared to that of the arterial plasma. The brain is an example of a membrane-limited compartment. For this organ in the rat,  $pa = 0.013 \text{ min}^{-1}$ ,  $k_{2i} = 0.005 \text{ min}^{-1}$ , and  $(pa/(pa + k_{2i})) = 0.72$  [34]. Thus, brain exposure to cisplatin is 72% of that experienced by the arterial plasma.

Much recent research on anticancer drug therapy involves the use of regional drug administration [35]. The purpose of regional administration is to increase drug exposure at the tumor site relative to systemic exposure. Examples of regional chemotherapy include intra-arterial administration, which is used to increase drug exposure to a specific site such as the liver or brain; and intracavitary administration, which allows increased drug exposure to tissues in, or adjacent to, a body cavity.

A major therapeutic concern with intracavitary administration of anticancer drugs is the concentration of a free drug that penetrates to a given depth in the tissues adjacent to the cavity (i.e., the tissue concentration gradient) [9,36,37,38]. Similar concerns arise for intratissue administration. Following intracavitary administration, the drug diffuses into the tissues that are adjacent to the cavity. For a reactive drug such as cisplatin, the diffusion continues until the molecules either penetrate capillary walls and are carried off by the blood or react to form metabolites [9]. For such a system at steady state, when the concentration in the tissue ( $C$ ) is much greater than that in the plasma ( $C_p$ ), the tissue concentration profile decreases exponentially from the concentration in the cavity ( $C_C$ ) [9,37]. This behavior is shown diagrammatically for a tissue adjacent to the peritoneal cavity in Figure 7. Mathematically, the gradient is described by Eq. (7).

$$C/C_C = e^{-x[(pa + k_{2i})/D]^{1/2}} \quad (7)$$

where:

- $C, C_C$  = drug concentrations in tissue and cavity, respectively
- $x$  = distance into the tissue from the cavity surface
- $D$  = intratissue diffusivity

The meanings of  $pa$  and  $k_{2i}$  are the same as discussed above. In Eq. (7), the characteristic diffusion length is given by the value  $[D/(pa + k_{2i})]^{1/2}$  [33]. This length represents the linear depth of penetration into the tissue where the drug concentration is approximately 37% of its concentration at the point of tissue contact [37]. For the brain, where  $D$  has been estimated as  $1.9 \times 10^{-6} \text{cm}^2 \text{sec}^{-1}$  [34], the model predicts that the concentration of free cisplatin will drop tenfold over a distance of 2 mm and 100-fold over 4 mm.

Both cisplatin and its mobile metabolite can move freely between compartments, and both are readily excreted in the urine. Fixed metabolite is released from compartments only as a result of macromolecular catabolism, a process that is slow compared to metabolite formation. As a result of the relative rates of these processes, fixed Pt becomes the dominant species in all tissues within a few hours following cisplatin administration. This behavior means that the concentration of Pt within a compartment can be used in conjunction with the compartment's fixed metabolite formation rate

constant to estimate that compartment's exposure to cisplatin. If mobile metabolite formation is ignored and measurements are taken before significant protein catabolism occurs, then the total tissue Pt concentration,  $C_T$ , is equal to  $k_{2t}(AUC_T)$ , and the tissue exposure,  $AUC_T$ , is given by  $C_T/k_{2t}$ . As mentioned above, if the reaction rate constant,  $k_{2t}$ , is small compared to the appropriate mass transport parameter,  $q$  or  $pa$ , then  $AUC_T \approx AUC_P$  and the exposure to the tissue is approximately equal to that of the arterial plasma. Gut, for example, is a tissue where  $k_{2t}$  is relatively low compared to  $q$ . In the rat, the respective values are  $0.014 \text{ min}^{-1}$  and  $0.48 \text{ min}^{-1}$ . During the one to eight-hour period following iv administration of 4 mg/kg cisplatin to the rat, the average Pt concentration in the gut was found to be  $2 \mu\text{g/g}$  [12]. Based on this concentration, gut exposure to cisplatin is estimated to be  $143 \mu\text{g min/g}$ . From model simulations for the same drug dose [12], the cisplatin exposure received by rat plasma ( $AUC_P$ ) is estimated to be approximately  $150 \mu\text{g min/g}$ .

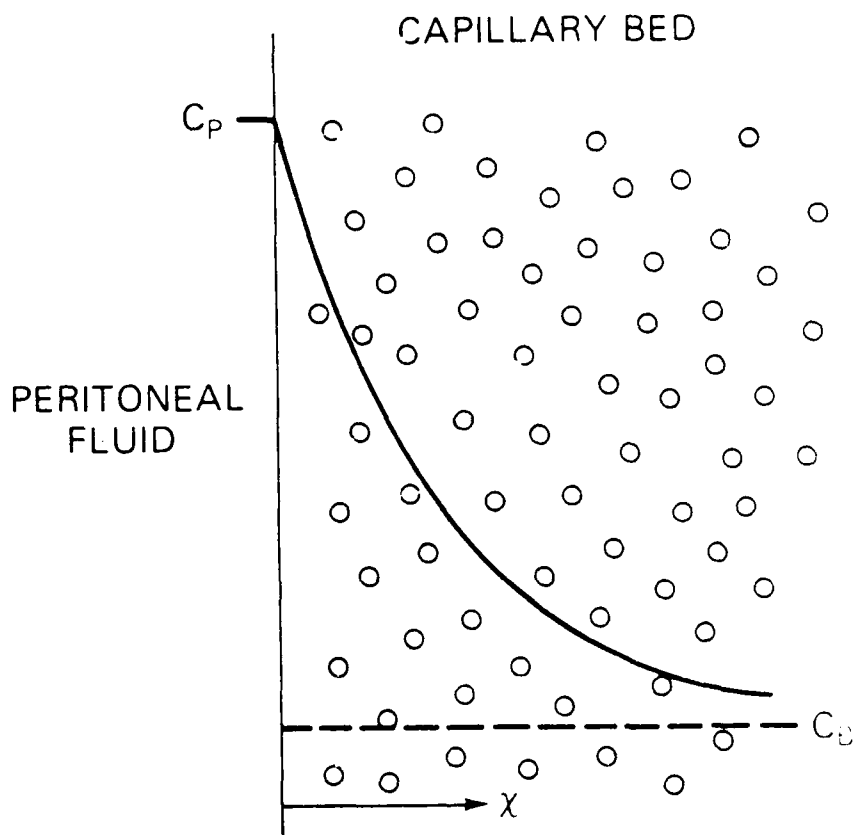


Figure 7. Conceptual model for diffusion between peritoneal fluid and blood. The solute diffuses through tissue and either reacts to form metabolites or transfers between extracellular fluid and blood in a spatially distributed capillary network. (Adapted from Dedrick et al., [37])

#### **Development of a pharmacodynamic model for cisplatin**

Present evidence indicates that the specific cellular site or target responsible for the pharmacologic activity of cisplatin is DNA [39,40,41] and that the binding between the Pt atom and

the DNA molecule is very tight or irreversible [42,43,44,45]. Although a variety of complexes between cisplatin and DNA have been identified [41,46,47], intrastrand adducts with Pt covalently linking two adjacent guanines (G-G) or an adenine and an adjacent guanine (A-G) have been reported to account for a major portion of the DNA-bound Pt [46,48,49] and to correlate most directly with the drug's antitumor activity [46,50]. One possible explanation for the prevalence of these particular adducts is that they may be recognized and/or repaired by cells inefficiently and therefore accumulate in DNA to a greater extent than do other adducts [51]. It has been suggested that cisplatin's antitumor activity may result from the accumulation of Pt-containing intrastrand adducts within cells [51].

If adduct formation results from the direct interaction of cisplatin with DNA, then the extent of adduct formation within a given compartment presumably is related to the cisplatin exposure received by that compartment. Because the present pharmacokinetic model can be used to simulate drug-concentration vs. time profiles and to estimate drug exposures for each compartment, it should be possible to extend the model to simulate cisplatin's pharmacodynamic activity. The development of such a pharmacodynamic model is deterred by our lack of knowledge regarding the biochemical mechanisms and kinetics of formation and repair of the different classes of adducts. For example, the mechanistic steps involved in the bidentate bonding between Pt and DNA may be critical to the kinetics of formation of the intrastrand adducts. Once the critical biochemical and kinetic information becomes available, incorporation of the appropriate equations into the present model should be straightforward.

### ***Pharmacokinetics of cisplatin analogs***

The therapeutic successes obtained by cisplatin have stimulated considerable interest in the development of analogous Pt(II)-containing antineoplastic agents [24,52,53,54]. Analogs that maintain the basic structural characteristics of cisplatin (i.e., two *cis* groups that are bound firmly to the Pt atom and the other two groups that are more labile) logically might be expected to undergo reactions fundamentally similar to those of cisplatin. If this is true, then the model developed for cisplatin should provide a coherent mechanism for comparing and classifying these analogs according to their kinetic characteristics and in guiding the development of other analogs with desired kinetic properties. As the nature of the substituents surrounding the Pt(II) is changed, the values of some of the kinetic parameters are expected to vary. Those parameters most likely to be altered include renal clearance and the fixed and mobile metabolite formation rate constants. There is little reason to expect any significant alterations in the anatomic and physiologic parameters or in the rate of release of Pt once it is bound as fixed metabolite. Values for equilibrium distribution coefficients might change, depending on the characteristics of the substituents attached to the Pt. If we make the simplifying assumption that any changes in the distribution coefficients are of marginal importance,

then the fixed metabolite formation rate constants and the renal clearances become the dominant parameters. Consider the following example.

Carboplatin, a therapeutically promising analog, is structurally similar to cisplatin except that cyclobutanedicarboxylate, a bidentate ligand, replaces the two chloride ions of the original drug. This ligand produces a chelate effect that decreases carboplatin's reactivity compared to that of cisplatin [24]. On incubation in dilute rat plasma and liver and kidney homogenates, carboplatin binds to macromolecules at only about one-tenth the rate of cisplatin [24]. The renal clearance of both drugs (and presumably their mobile metabolites) is approximately GFR. Because the rate of formation of fixed Pt is much lower for carboplatin than cisplatin, the model predicts that urinary excretion will be more extensive for carboplatin than for cisplatin. In addition, tissue-Pt concentrations following carboplatin administration should be substantially lower than those found following an equal dose of cisplatin. Both of these predictions have been confirmed experimentally. The cumulative urinary Pt excreted in the first 4 h following iv dosing in the rat has been found to be twofold greater for carboplatin than for cisplatin [24]. In these same studies, when carboplatin was administered to rats at approximately a sevenfold higher dose than cisplatin, the two drugs produced similar Pt levels in liver. In kidney, Pt levels were about twice as high in the carboplatin dosed animals as in those receiving cisplatin. As a result of the kinetic differences between these two drugs, carboplatin tends to be less toxic than cisplatin [27,52] but therapeutically, carboplatin must be administered in doses that are approximately five times those of cisplatin [27,55].

In addition to allowing a general analysis of the type shown above, the model presumably can be adapted and used to simulate quantitatively the disposition of cisplatin analogs and their metabolites. Such simulations are currently underway for carboplatin.

## DISCUSSION

Physiological pharmacokinetic models are constructed so that their parameters are defined in terms of actual physical and chemical entities. For example, the volumes assigned to compartments represent the actual sizes of tissues or other anatomical structures, and each reaction rate constant is associated with a specific identifiable process. The significance of this approach is that the parameters remain identifiable and still have meaning even if taken from the context of the model. In other words, the information contained within the model's parameters is applicable to problems and situations other than those that fit precisely within the framework of the original model.

In the present paper, we have illustrated how the information contained within a physiological model can be applied in different ways to improve our understanding of the kinetics and pharmacology of a drug, and to direct us towards new areas of study. To facilitate the discussion, a model developed originally to describe the pharmacokinetics of cisplatin and its metabolites was used

as the focal point of the presentation. The applications that were chosen for discussion were selected because of their special relevance to cisplatin. However, they are only examples of the possible uses of physiological models. The utility and versatility of a particular model depends on its structure and the nature of its parameters.

#### REFERENCES

- 1 Collins, J.M. and Dedrick, R.L. (1982) Pharmacokinetics of anticancer drugs. In: B.A. Chabner (Ed.), *Pharmacologic Principles of Cancer Treatment*, W.B. Saunders, Inc., Philadelphia, PA, pp. 77-99.
- 2 O'Flaherty, E.J. (1981) *Toxicants and Drugs: Kinetics and Dynamics*, John Wiley & Sons, Inc., New York, NY.
- 3 Wagner, J.G. (1971) *Biopharmaceutics and Relevant Pharmacokinetics*, 1st Ed., Drug Intelligence Publications, Hamilton, IL.
- 4 Evans, W.E., Schentag, J.J., and Jusko, W.J. (1986) *Applied Pharmacokinetics: Principles of Therapeutic Drug Monitoring*, 2nd Edition, Applied Therapeutics, Inc., Spokane, WA.
- 5 Bischoff, K.B. (1975) Some fundamental considerations of the applications of pharmacokinetics to cancer chemotherapy. *Cancer Chemotherapy Reports* 59, 777-793.
- 6 Gerlowski, L.E. and Jain, R.K. (1983) Physiologically based pharmacokinetic modeling: Principles and applications. *J. Pharm. Sci.* 72, 1103-1127.
- 7 Lutz, R.J., Dedrick, R.L. and Zaharko, D.S. (1980) Physiological pharmacokinetics: An *in vivo* approach to membrane transport. *Pharmacol. Ther.* 11, 559-592.
- 8 Dedrick, R.L. (1975) Pharmacokinetic and pharmacodynamic considerations for chronic hemodialysis. *Kidney International* 7 (Suppl 2), S7-S15.
- 9 Dedrick, R.L. (1986) Interspecies scaling of regional drug delivery. *J. Pharm. Sci.* 75, 1047-1052.
- 10 Dedrick, R.L. (1973) Animal scale-up. *J. Pharmacokinet. Biopharm.* 1, 435-461.
- 11 Dedrick, R.L. and Bischoff, K.B. (1980) Species similarities in pharmacokinetics. *Fed. Proc.* 39, 54-59.
- 12 Farris, F.F., King, F.G., Dedrick, R.L., and Litterst, C.L. (1985) Physiological model for pharmacokinetics of *cis*-dichlorodiammineplatinum(II) (DDP) in the tumored rat. *J. Pharmacokinet. Biopharm.* 13, 13-39.
- 13 King, F.G., Dedrick, R.L., and Farris, F.F. (1986) Physiological pharmacokinetic modeling of *cis*-dichlorodiammineplatinum(II) (DDP) in several species. *J. Pharmacokinet. Biopharm.* 14, 131-155.
- 14 Chen, H-S.G. and Gross, J.F. (1979) Estimation of tissues to-plasma partition coefficients used in physiological pharmacokinetic models. *J. Pharmacokinet. Biopharm.* 7, 117-125.

- 15 Lin, J.H., Sugiyama, Y., Awazu, S., and Hanano, M. (1982) *In vitro* and *in vivo* evaluation of the tissue-to-blood partition coefficient for physiological pharmacokinetic models. *J. Pharmacokinet. Biopharm.* 10, 637-647.
- 16 Edwards, N.A. (1975) Scaling of renal functions in mammals. *Comp. Biochem. Physiol.* 52A, 63-66.
- 17 Munro, H.N. (1969) Evolution of protein metabolism in mammals. In: H.N. Munro (Ed.), *Mammalian Protein Metabolism*, Vol. III, Academic Press, New York, NY. pp. 158-173.
- 18 Munro, H.N. and Downie, E.D. (1964) Relationship of liver composition to intensity of protein metabolism in different mammals. *Nature* 203, 603-604.
- 19 Litterst, C.L. (1984) Plasma pharmacokinetics, urinary excretion, and tissue distribution of platinum following i.v. administration of cyclobutanedicarboxylatoplatinum-II and *cis*-platinum to rabbits. In: M.P. Hacker, E.B. Douple, and I.H. Krakoff (Eds.), *Platinum Coordination Complexes in Cancer Chemotherapy*, Martinus Nijhoff Pub., Boston, MA, pp. 71-81.
- 20 Himmelstein, K.J., Patton, T.F., Belt, R.J., Taylor, S., Repta, A.J., and Sternson, L.A. (1981) Clinical kinetics of intact cisplatin and some related species. *Clin. Pharmacol. Therap.* 29, 658-664.
- 21 Pretorius, R.G., Petrilli, E.S., Kean, C., Ford, L.C., Hoeschele, J.D., and Lagasse, L.D. (1981) Comparison of the iv and ip routes of administration of cisplatin in dogs. *Cancer Treat. Rep.* 65, 1055-1062.
- 22 Daley-Yates, P.T. and McBrien, D.C. H. (1984) Cisplatin metabolites in plasma, a study of their pharmacokinetics and importance in the nephrotoxic and antitumor activity of cisplatin. *Biochem. Pharmacol.* 33, 3063-3070.
- 23 Gibaldi, M. and Perrier, D. (1982) *Pharmacokinetics*, 2nd Ed., Marcel Dekker, Inc., New York, NY. pp. 319-327.
- 24 Siddik, Z.H., Dible, S.E., Boxall, F.E., and Harrap, K. R. (1986) Renal pharmacokinetics and toxicity of cisplatin and carboplatin in animals. In: D.C.H. McBrien and R.F. Slater (Eds.), *Biochemical Mechanisms of Platinum Antitumor Drugs*, IRL Press Ltd., Oxford, England, pp. 171-191.
- 25 Jensen, D. (1976) *The Principles of Physiology*, Appleton-Centurn-Crofts, New York, NY, p. 529.
- 26 Waterlow, J.C., Garlick, P.J., and Millward, D.J. (1978) *Protein Turnover in Mammalian Tissues and in the Whole Body*, North-Holland Publishing Co., Amsterdam, The Netherlands, pp. 443-477.
- 27 Dailey-Yates, P.T. (1986) The metabolites of platinum antitumor drugs and their biological significance. In: D.C.H. McBrien and T.F. Slater (Eds.), *Biochemical Mechanisms of Platinum Antitumor Drugs*, IRL Press Ltd., Oxford, England, pp. 121-139.
- 28 Riley, C.M., Sternson, L.A., and Repta, A.J. (1982) Assessment of cisplatin reactivity with peptides and proteins using reverse-phase high-performance liquid chromatography and flameless atomic absorption spectroscopy. *Anal. Biochem.* 124, 167-179.

- 29 Waymouth, C. (1982) Methods for obtaining cells in suspension from animal tissues. In: T.G. Pretlow, II, and T.P. Pretlow (Eds.), Cell Separation: Methods and Selected Applications, Vol. 1, Academic Press, New York, NY, pp. 1-29.
- 30 Lin, J.H., Sugiyama, Y., Awazu, S., and Hanano, M. (1982) Physiological pharmacokinetics of ethoxybenzamide based on biochemical data obtained *in vitro* as well as on physiological data. J. Pharmacokinet. Biopharm. 10, 649-61.
- 31 Melius, P. and Friendman, M.E. (1977) Complexes of platinum with polypeptides and proteins. Inorg. Perspectives Biol. Med. 1, 1-18.
- 32 Riley, C.M., Sternson, L.A., Repta, A.J., and Slyter, S.A. (1982) Reactivity of *cis*-dichlorodiammineplatinum(II) (cisplatin) toward selected nucleophiles. Polyhedron 1, 201-202.
- 33 Dedrick, R., Morrison, P. King, F., and Farris, F. (1986) Plasma and tissue binding of cisplatin relevant to regional chemotherapy. In: Abstracts of the 5th NCI-EORTC Symposium on New Drugs in Cancer Therapy. Amsterdam, The Netherlands, Oct. 22-24.
- 34 Morrison, P.F. and Dedrick, R.L. (1986) Transport of cisplatin in rat brain following microinfusion: An analysis. J. Pharm. Sci. 75, 120-128.
- 35 Howell, S.B. (Ed.) (1984) Intra-arterial and Intracavitary Cancer Chemotherapy, Martinus Nijhoff, Pub., Boston, MA.
- 36 Collins, J.M. (1984) Pharmacokinetic rationale for intracavitary therapy. In: S.B. Howell (Ed.), Intra-arterial and Intracavitary Cancer Chemotherapy, Martinus Nijhoff Pub., Boston, MA, pp. 41-51.
- 37 Dedrick, R.L., Flessner, M.F., Collins, J.M., and Schultz, J.S. (1982) Is the peritoneum a membrane? Am. Soc. Artificial Int. Organs J. 5, 1-8.
- 38 Flessner, M.F., Dedrick, R.L., and Schultz, J.S. (1984) A distributed model of peritoneal-plasma transport: Theoretical considerations. Am. J. Physiol. 246, R597-R607.
- 39 Munchhausen, L.L. and Rahn, R.O. (1975) Biological and chemical effects of *cis*-dichlorodiammineplatinum(II) on DNA. Cancer Chemother. Rep. 59, 643-646.
- 40 Roberts, J.J. and Pera, M.F., Jr. (1983) DNA as a target for anticancer coordination compounds. In: S.J. Lippard (Ed.), Platinum, Gold, and Other Metal Chemotherapeutic Agents, American Chemical Society, Washington, DC, pp. 3-25.
- 41 Zwellung, L.A. and Kohn, K.W. (1979) Mechanism of action of *cis*-dichlorodiammineplatinum(II). Cancer Treat. Rep. 63, 1439-1444.
- 42 Hoeschele, J.D., Johnson, N.P., Rahn, R.O., and Brown, D.H. (1978) Comparative distribution/binding studies of <sup>195m</sup>Pt-labeled dichlorodiammineplatinum(II), DDP, in the rat with emphasis on the localization in DNA. Biochimie 60, 1054.
- 43 Johnson, N.P., Hoeschele, J.D., and Rahn, R.O. (1980) Kinetic analysis of the *in vitro* binding of radioactive *cis*- and *trans*-dichlorodiammineplatinum(II) to DNA. Chem. Biol. Interact. 30, 151-169.

- 44 Litterst, C.L., Poirier, M.C., and Reed, E. (1988) Factors influencing the formation and persistence of platinum-DNA adducts in tissues of rats treated with cisplatin. In: M. Hacker, J.S. Lazo and T. Tritton (Eds.), *Organ Directed Toxicities of Anticancer Drugs*, Martinus Nijhoff Pub., Boston, MA, pp. 159-171.
- 45 Plooy, A.C.M., van Dijk, M., and Lohman, P.H.M. (1984) Induction and repair of DNA cross-links in Chinese hamster ovary cells treated with various platinum coordination compounds in relation to platinum binding to DNA, cytotoxicity, mutagenicity, and antitumor activity. *Cancer Res.* 44, 2043-2051.
- 46 Plooy, A.C.M., Fichtinger-Schepman, A.M.J., Schutte, H.H., van Dijk, M., and Lohman, P.H.M. (1985) The quantitative detection of various Pt-DNA-adducts in Chinese hamster ovary cells treated with cisplatin: Application of immuno-chemical techniques. *Carcinogenesis (London)* 6, 561-566.
- 47 Zwelling, L.A., Anderson, T., and Kohn, K.W. (1979) DNA-Protein and DNA inter-strand cross-linking by *cis*- and *trans*-platinum(II) diamminedichloride in L1210 mouse leukemia cells and relation to cytotoxicity. *Cancer Res.* 39, 365-369.
- 48 Eastman, A. (1986) Multiple mechanisms of *cis*-diamminedichloroplatinum(II) resistance in a murine leukemia L1210 line. *Proc. Am. Assoc. Cancer Res.* 27, 291.
- 49 Pinto, A.L. and Lippard, S.J. (1985) Binding of the antitumor drug *cis*-diamminedichloroplatinum(II) (cisplatin) to DNA. *Biochem. Biophys. Acta* 780, 167-180.
- 50 Lippard, S.J., Ushay, H.M., Merkel, C.M., and Poirier, M.C. (1983) Use of antibodies to probe the stereochemistry of antitumor platinum drug binding to DNA. *Biochemistry* 22, 5165-5168.
- 51 Ciccarelli, R.B., Solomon, M.J., Varshavsky, A., and Lippard, S.J. (1985) *In vivo* effects of *cis*- and *trans*-diamminedichloroplatinum(II) on 5V40 chromosomes: Differential repair, DNA-protein cross-linking, and inhibition of replication. *Biochemistry* 24, 7533-7540.
- 52 Calvert, A.H. (1986) Clinical applications of platinum metal complexes. In: D.C.H. McBrien and T.F. Slater (Eds.), *Biochemical Mechanisms of Platinum Antitumor Drugs*, IRL Press Ltd., Oxford, England, pp. 307-315.
- 53 Cleare, M.J., Hydes, P.C., Malerbi, B.W., and Watkins, D.M. (1978) Anti-tumor platinum complexes: Relationships between chemical properties and activity. *Biochimie* 60, 835-850.
- 54 Harrison, R., McAuliffe, C.A., Zaki, A., Baer, J., Sharma, H., Smith, A., Jackson, H., and Fox, B.W. (1983) A comparative study of the distribution in the male rat of platinum-labelled *cis*-dichlorodiammineplatinum(II), *cis-trans*-dichlorodihydroxy-bis-(isopropylamine) platinum(II), and *cis*-dichloro-bis-cyclopropylamineplatinum(II). *Cancer Chemother. Pharmacol.* 10, 90-95.
- 55 Harding, B.J., Foster, B.J., and Leyland-Jones, B. (1986) Carboplatin (CBDCA): Current status and future plans. In: *Abstracts of the 5th NCI-EORTC Symposium on New Drugs in Cancer Therapy*. Amsterdam, The Netherlands, October 22-24.

**SESSION III**

**Bioeffects Modeling**

**Dr. Rory B. Conolly, Chairman**

## BIOLOGICALLY MOTIVATED TWO-STAGE MODEL FOR CANCER RISK ASSESSMENT

Suresh H. Moolgavkar

*Fred Hutchinson Cancer Research Center, Seattle, WA*

### SUMMARY

A model for carcinogenesis is presented that incorporates two features: (1) transition of target stem cells into cancer cells via an intermediate stage in two irreversible steps, and (2) growth and differentiation of normal target and intermediate cells. Implications of the model for initiation-promotion and environmental carcinogenesis are considered.

### INTRODUCTION

Because human epidemiologic evidence regarding the carcinogenic potential of exposure to low levels of environmental agents is rarely available, the assessment of cancer risks associated with such exposure poses two fundamental and difficult problems. First, risk to humans must be inferred from animal bioassay experiments in which animals of a given species are exposed to the agent under investigation. This poses the "mouse to man" problem; that is, the problem of extrapolation of risk from one species to another. Second, the bioassay is carried out at high doses of the agent because experiments at low doses require large numbers of animals for adequate statistical power. This leads to the second problem, that of low-dose extrapolation of risk.

A rational approach to the rather formidable challenge posed by quantitative cancer risk assessment is the separation of risk assessment into several components. A biologically based model for carcinogenesis is one such component. This model relates fundamental biological processes at the cellular level to the incidence of tumors of specific tissues in human or animal populations. The parameters of the model should be clearly interpretable in biological terms and capable of being made functions of the dose of the environmental agent under study. To relate the parameters of the model to the specific agent under investigation, however, it is necessary to know the dose of the active metabolite responsible for the carcinogenic action in the tissue of interest. Thus, before the carcinogenesis model can be used, either direct measurements of the metabolite in question must be made in the tissue of interest or a pharmacokinetic model must be used to infer the tissue level of the metabolite from knowledge of the level of the agent in the environment. Physiologically based pharmacokinetic modeling is another component of a rational risk assessment strategy [1,2,3,4]. The ultimate goal of the analysis is, of course, to study the dosimetry of the carcinogenic response in terms of the environmental exposure to the agent of interest. The purpose of this paper is to present a biologically based mathematical model for carcinogenesis and to study its implications for exposure

to environmental agents. The paper by Conolly *et al.* [5] will illustrate how this model can be combined with a pharmacokinetic model for risk assessment.

#### THE ARMITAGE-DOLL MODEL AND ITS ROLE IN CANCER RISK ASSESSMENT

One of the most widely used models of carcinogenesis was proposed by Armitage and Doll [6] to explain the observation that the age-specific incidence rates of many human carcinomas increase roughly with a power of age. This multistage model views carcinogenesis as the end result of progressive deterioration of a normal cell via a number of intermediate stages to malignancy. The waiting time for the cell to go from one stage to the next is assumed to be exponentially distributed, and the action of environmental agents is modeled by allowing the parameters of the waiting times (also called the transition rates) to be functions, usually linear, of dose.

The Armitage-Doll model is flawed biologically because it does not take explicit account of cell division and differentiation, which we know are important in carcinogenesis. In addition, the stages postulated by the model are mathematical abstractions and have no biological interpretation. Within the framework of the Armitage-Doll model, initiators are often considered to be "early" stage carcinogens whereas promoters are considered to be "late" stage carcinogens. It is not easy to reconcile this view of initiation-promotion with the results of the so-called IPI (initiator-promotor-initiator) protocol [7,8].

Even if the Armitage-Doll model is accepted at face value, the current statistical use of the model is seriously flawed. For risk assessment, the Armitage-Doll model is often used in the form [9]

$$P(d,t) = 1 - \exp[-g(d)H(t)]$$

where

$P(d,t)$  = the probability of a carcinogenic response by time  $t$ ,

$g(d)$  = a polynomial in dose, and

$H(t)$  = a power of time.

This formulation crucially depends upon the adequacy of a couple of approximations [10,11]. These approximations are likely to be poor when the probability of tumor is high. This is typically the case in animal experiments; thus, the formula above is inappropriate in precisely those situations in which it is most widely used (i.e., the analysis of experimental data). A second problem is that when the approximations hold, the Armitage-Doll model implies that the polynomial  $g(d)$  is a product of linear terms. In the application of this formula, however,  $g(d)$  is treated as a general polynomial. For a critical review of the current methodology in cancer risk assessment, see Freedman and Zeisel [8].

## TWO-MUTATION MODEL

### *Biological considerations*

Recent advances in cancer research provide strong evidence that there are two distinct classes of cancer genes. The first class of genes, the oncogenes, was discovered by work on the acutely transforming retroviruses, such as the Rous Sarcoma Virus. The protein product of a single gene present in the genome of this virus, the *src* gene, is capable of producing malignant transformation. It was later shown that normal vertebrate cells contain oncogenes, the inappropriate activation of which can lead to malignant transformation.

The other class of genes, the antioncogenes, was discovered by a study of some human hereditary cancers. As the name implies, when these genes function normally they prevent malignant transformation. Thus, in contrast to the oncogenes, antioncogenes lead to malignancy when they are inappropriately inactivated [12]. Evidence for the existence of antioncogenes arises from a study of human cancers that occur in two forms, one that is sporadic and one that appears to be transmitted in families in an autosomal dominant fashion on pedigree analysis. Examples of such tumors are the childhood tumors, *retinoblastoma* and *Wilms' tumor*; and the adult tumor, *carcinoma of the colon*. The chromosomal location of the genes responsible for the hereditary cases is known for *retinoblastoma* and for *Wilms' tumor*. Cytogenetic analysis reveals that, in many cases of hereditary *retinoblastoma* and *Wilms' tumor*, the respective genes are deleted. Thus, it is the inactivation (absence) of these genes that leads to malignancy. Further, although every cell in the affected tissue has the inactivated antioncogenes, only a few of the cells go on to develop malignancy (in *retinoblastoma*, for example, the typical gene carrier develops 3 to 4 tumors), indicating that inheritance of the oncogene is not sufficient and that at least one more event must occur for malignant transformation.

The working hypothesis that oncogene activation is the final common pathway in malignant transformation may be incorporated into a 2-stage model for carcinogenesis by using a genetic regulatory schema proposed by Comings [13]. According to this schema, all cells contain tissue-specific genes capable of coding for transforming factors that can release the cell from normal growth constraints. These oncogenes are expressed during histogenesis and tissue renewal; their expression is controlled by diploid pairs of antioncogenes (regulatory genes). Malignant transformation of a cell occurs when the oncogenes are turned on to inappropriately high levels. According to the model of Comings [13], this occurs with inactivation of the appropriate pair of antioncogenes. Thus, the crucial feature of the model necessary for a mathematical development is the recognition of carcinogenesis as the end result of two critical, specific, irreversible, rate-limiting, and hereditary (at the level of the cell) genomic events. The first event, which may be either germinal

(in the hereditary cases) or somatic, leads to partial abrogation of cellular control, so that a stem cell that has sustained it has a small growth advantage over the surrounding cells. Such a cell may be thought of as an "initiated" cell, and over a period of time will give rise to a clone of initiated cells – a premalignant lesion. The second event, which is always somatic, leads to total abrogation of growth control (i.e., malignant transformation). For more details, see Moolgavkar and Knudson [14] and Moolgavkar [7,15].

A deficiency of early multistage models of carcinogenesis is that they did not take explicit account of cell division and differentiation, although it is abundantly clear that these play an important role in carcinogenesis. The model presented here explicitly ties mutations to cell division and takes account of the growth of tissues. Figure 1 is a schematic representation of the model. For concreteness, the two rare genomic events in the model may be thought of as mutations at homologous loci, as described above. A model in which mutations occur at the antioncogene (regulator gene) loci is biologically attractive. However, the specific nature of the rare events is not important to the mathematical development. Thus, the mathematical model is more general than the biological model described above. For a discussion of the various biological possibilities for the two rare events, see Knudson [16].

The two-stage model has been shown to be consistent with a large body of biological and epidemiological data in a series of papers. The focus here will be on the implications of the model for environmental carcinogenesis, and the concepts of initiation and promotion within the framework of the model in particular. Before doing so, a brief mathematical development is given.

### **Mathematical development [17,18]**

For the analyses of human epidemiologic and animal experimental data, two important quantities must be derived from the model. These are the hazard (or incidence) function, which is the rate at which malignant tumors appear in a previously tumor-free tissue, and the probability of tumor by time  $t$ . More precisely, let  $T$  represent the time to appearance of the first tumor in a tissue. Then  $h(t)$ , the hazard function, is defined by

$$h(t) = \lim_{\Delta t \rightarrow 0} \left[ \frac{1}{\Delta t} \text{Prob} (t \leq T < t + \Delta t | T \geq t) \right]$$

Let  $P(t)$  represent the probability of a malignant tumor by time  $t$ . Then  $P(t)$  and  $h(t)$  are related by the equation

$$P(t) = 1 - \exp \left[ - \int_0^t h(s) ds \right]$$

The following assumptions are necessary for the mathematical development.

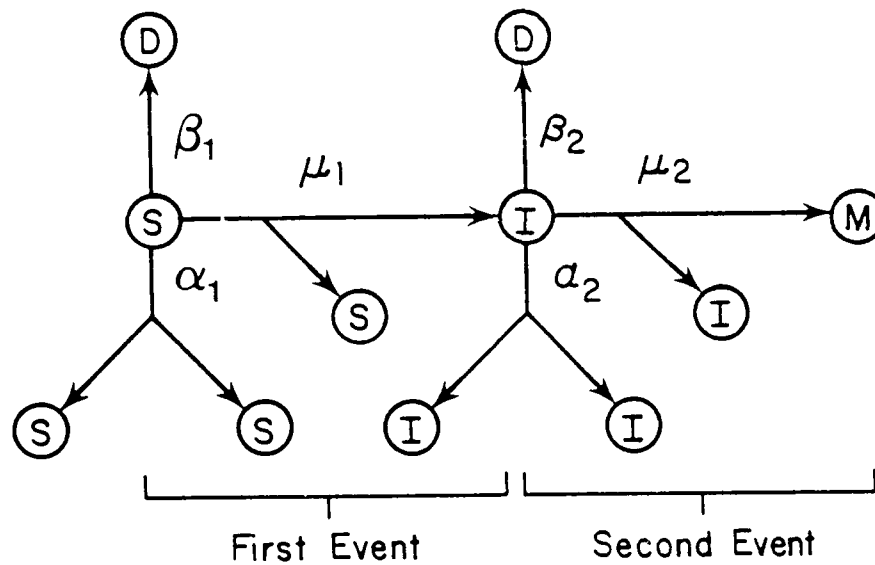


Figure 1. Two-stage model for carcinogenesis (from Moolgavkar and Knudson [14]). S = normal stem cell; I = intermediate cell; D = dead or differentiated cell; M = malignant cell.  $\alpha_1$  = rate (per cell per year) of cell division of normal cells;  $\beta_1$  = rate (per cell per year) of death or differentiation of normal cells;  $\mu_1$  = rate (per cell per year) of division into one normal and one intermediate cell;  $\alpha_2$ ,  $\beta_2$ , and  $\mu_2$  are defined similarly. Note that the mutation rate per cell division for normal and intermediate cells is given by  $\mu_1/(\alpha_1 + \mu_1)$  and  $\mu_2/(\alpha_2 + \mu_2)$ , respectively. The rate is to be thought of as the effective mutation rate; i.e., it takes into account host defenses such as immune surveillance that may destroy the malignant cell. Cells in the intermediate stage have a slight proliferative advantage over their neighbors owing to defective control of cell division. The essential role of promoters is to increase this advantage, i.e., to increase  $\alpha_2 - \beta_2$ .

- Cancers are clonal (i.e., malignant tumors arise from a single malignant progenitor cell).
- Each susceptible stem cell in a tissue becomes malignantly transformed independently of the other susceptible stem cells.
- Let  $t$  represent time. Then in the small interval  $(t, t + \Delta t)$ , a normal susceptible cell divides into two normal susceptible cells with probability  $\alpha_1(t)\Delta t + o(\Delta t)$ ; it dies or differentiates with probability  $\beta_1(t)\Delta t + o(\Delta t)$ ; it divides into one normal cell and one intermediate cell (a cell that has sustained the first genomic event or mutation) with probability  $\mu_1(t)\Delta t + o(\Delta t)$ ; and the probability of more than one event occurring is  $o(\Delta t)$ .
- Likewise at time  $t$ , an intermediate cell divides into two intermediate cells, dies (or differentiates), or divides into one intermediate and one malignant cell with rate parameters  $\alpha_2(t)$ ,  $\beta_2(t)$ , and  $\mu_2(t)$ , respectively. Once a malignant cell is generated, a malignant tumor arises with probability 1; further, the time required for a malignant cell to develop into a detectable tumor is assumed to be a constant. Thus, all the quantities derived must be translated by a constant factor along the time axis.

A schematic representation of the model is given in Figure 1. Mutation rates per cell division are of biological interest; these rates for the first and second mutation are  $\mu_1(t) / [\alpha_1(t) + \mu_1(t)]$  and  $\mu_2(t) / [\alpha_2(t) + \mu_2(t)]$ , respectively. Locus-specific mutation rates are quite small and are typically in the range  $10^{-8} - 10^{-6}$  per cell division. Since  $\mu_i(t)$ ,  $i = 1, 2$  is much smaller than  $\alpha_i(t)$ ,  $i = 1, 2$ , an excellent approximation to the mutation rate per cell division is given by the expression  $\mu_i(t) / \alpha_i(t)$ ,  $i = 1, 2$ .

Let  $X(t)$ ,  $Y(t)$ ,  $Z(t)$  represent, respectively, the number of normal, intermediate, and malignant cells at time  $t$ . Let  $\psi(x, y, z; t)$  be the probability generating function at time  $t$  starting with a single normal cell at time 0. Then

$$\psi(x, y, z; t) = \sum_{i, j, k} \text{Prob}[X(t)=i, Y(t)=j, Z(t)=k | X(0)=1, Y(0)=0, Z(0)=0] x^i y^j z^k$$

The Kolmogorov forward differential equation for  $\psi$  is easily derived:

$$\psi'(t) = \partial\psi/\partial t = \{\mu_1(t)xy + \alpha_1(t)x^2 + \beta_1(t) - [\alpha_1(t) + \beta_1(t) + \mu_1(t)]x\} \partial\psi/\partial x$$

$$+ \{\mu_2(t)yz + \alpha_2(t)y^2 + \beta_2(t) - [\alpha_2(t) + \beta_2(t) + \mu_2(t)]y\} \partial\psi/\partial y$$

with the initial condition  $\psi(0) = x$ , where the dependence of  $\psi$  and  $\psi'$  on  $x, y, z$  has been suppressed for notational convenience.

In terms of  $\psi(t)$  and  $\psi'(t)$ ,  $h(t)$  is given by

$$h(t) = -\psi'(1, 1, 0; t) / \psi(1, 1, 0; t)$$

From Kolmogorov's equation we have

$$\psi'(1, 1, 0; t) = -\mu_2(t) \frac{\partial\psi}{\partial y}(1, 1, 0; t)$$

Noting that

$$\frac{\partial\psi}{\partial y}(1, 1, 0; t) / \psi(1, 1, 0; t) = E[Y(t) | Z(t)=0]$$

we have

$$h(t) = \mu_2(t) E[Y(t) | Z(t)=0]$$

In this expression,  $E[Y(t) | Z(t)=0]$  is the expected number of intermediate cells at time  $t$  conditional on there being no malignant cell at time  $t$ .

Computation of  $h(t)$  is much simplified if the conditional expectation of  $Y(t)$  can be replaced by the unconditional expectation, that is, if the approximation  $E[Y(t) | Z(t) = 0] \approx E[Y(t)]$  is good. The Kolmogorov equation leads immediately to the following system of differential equations for the expectations of the number of normal, intermediate, and malignant cells at time  $t$ .

$$\frac{dE[X(t)]}{dt} = [\alpha_1(t) - \beta_1(t)] E[X(t)]$$

$$\frac{dE[Y(t)]}{dt} = [\alpha_2(t) - \beta_2(t)] E[Y(t)] + \mu_1(t) E[X(t)]$$

$$\frac{dE[Z(t)]}{dt} = \mu_2(t) E[Y(t)]$$

Solving these equations and using the approximation referred to above leads immediately to

$$h(t) \approx \mu_2(t) E[Y(t)] = \mu_2(t) \int_0^t \{ \mu_1(s) E[X(s)] \exp \int_s^t [\alpha_2(u) - \beta_2(u)] du \} ds$$

where

$$E[X(s)] = \exp \int_0^s [\alpha_1(u) - \beta_1(u)] du$$

When the parameters  $\alpha_2$ ,  $\beta_2$ ,  $\mu_2$ , are constant, the above expression for  $h(t)$  reduces to

$$h(t) \approx \mu_1 \mu_2 \int_0^t E[X(s)] \exp [(\alpha_2 - \beta_2)(t-s)] ds$$

A parallel development can be given for a model in which the growth of normal tissue is treated as being deterministic. Precisely, let  $X(s)$  represent the number of susceptible stem cells in a tissue at time  $s$ , and let  $\mu_1(s)$  be the "rate" of first mutation. We assume that intermediate cells are generated from normal ones as a nonhomogeneous Poisson process with intensity  $\mu_1(s)X(s)$ : in a small time interval  $\Delta s$ , the probability that an intermediate cell arises by mutation of a normal cell is given by  $\mu_1(s)X(s)\Delta s + o(\Delta s)$ . The probability that more than one intermediate cell will arise in this fashion is  $o(\Delta s)$ . The rules governing the birth, death, and mutation of intermediate cells to malignant cells are the same as those for the completely stochastic model with parameters  $\alpha_2(t)$ ,  $\beta_2(t)$ ,

$\mu_2(t)$ . If the approximation  $E[Y(t) | Z(t)] \approx E[Y(t)]$  is good, this model leads to an approximate hazard function

$$h(t) \approx \mu_2(t) \int_0^t \{ \mu_1(s) X(s) \exp \int_s^t [\alpha_2(u) - \beta_2(u)] du \} ds$$

and with constant parameters

$$h(t) \approx \mu_1 \mu_2 \int_0^t X(s) \exp [(\alpha_2 - \beta_2)(t-s)] ds$$

It is in this form that the model has been applied to human epidemiologic data. When the parameters of the model are constant, the mutation rates  $\mu_1$  and  $\mu_2$  are multiplicative factors that are important in determining the overall incidence rates of the cancer in question, but not the shape of the incidence curve. The shape of the incidence curve is determined by the growth curve of the normal tissue and cellular kinetics of intermediate cells. It is crucial to note that the expressions for the hazard function presented here depend upon the adequacy of an approximation. When the probability of tumor is low, as in human cancer, this approximation is excellent. However, in animal experiments in which a large number of animals develop tumors, the approximation is likely to be poor and the hazard function is considerably more complicated. This issue is addressed in a recent paper [18]. For an application of the model to human epidemiologic data, see Moolgavkar and Knudson [14].

The mathematical formulation that models the growth of normal cells deterministically is much easier to work with than the completely stochastic version. As indicated above, if the focus of interest is the incidence function in human cancers, then both formulations of the model yield identical expressions. However, in many animal experiments, more information is available. For example, in hepatocarcinogenesis experiments, data are often available on the number and size of enzyme altered foci (pre-malignant lesions). The completely stochastic model does not readily yield mathematical expressions for such quantities. In contrast, the model with the growth of normal cells deterministically yields tractable expressions [23].

#### ENVIRONMENTAL CARCINOGENESIS: INITIATION AND PROMOTION

The early experimental observation of Berenblum and Shubik that the *sequence* in which certain chemicals were applied to mouse skin was critical to the subsequent appearance of tumors led to the concepts of initiation and promotion. Promoters were agents that, when applied after, but not before, an initiator, led to the appearance of tumors. Such a temporal sequence is not observable in human carcinogenesis, of course. Nevertheless, the terms initiation and promotion are used, rather loosely, in human epidemiology. As mentioned earlier within the framework of the Armitage-Doll

model, initiators are often thought of as early stage carcinogens, whereas promoters are thought of as late stage carcinogens.

Later experimental work showed that the idealized scenario of initiation followed by promotion was not strictly correct. Application of an agent classically considered to be a promoter followed by an initiator also increased the yield of tumors, albeit to a small extent. More recently, experiments with the IPI protocol have shown that a second application of an initiator after initiation-promotion leads to a higher yield of *malignant* tumors than initiation-promotion alone, which yields mainly benign tumors [20,21]. Some of the earlier experimental literature is difficult to interpret because, although cancer is the end point of interest, many of the experiments were stopped after the appearance of benign tumors.

Within the context of the model presented here, agents could affect the incidence of cancer in one or both of two ways: (1) by affecting the mutation rates, and (2) by affecting the kinetics of cell division and differentiation. Consider first an agent that increases the mutation rates, but has no influence on cell kinetics. The main effect of acute (short-term) exposure to such an agent will be to increase the number of normal cells that sustain the first mutation and become intermediate (or initiated) cells. Thus, such an agent will act as an initiator. However, if the nature of the two mutational events is the same, there is non-negligible probability that at least one of the cells will suffer both mutations and become malignant with prolonged exposure. Thus, the agent would be viewed as a complete carcinogen even though it has no promoting activity (see below for a discussion of promotion within the framework of the model). This scenario does not allow for the concept of a pure initiator. That is, any initiating agent applied for a long enough period of time will lead to malignant tumors. There are two circumstances under which an agent could be a pure initiator: (1) if metabolic activation of the agent is necessary and the intermediate cells have lost their ability for metabolic activation, and (2) if the nature of the two genomic events is different. For example, the first genomic event could be a point mutation and the second event a deletion.

If the two genomic events are mutations on homologous chromosomal loci, then it is possible to postulate the existence of agents that increase the rate of the second event without increasing the rate of the first. Homozygosity at the critical locus could be brought about by mitotic recombination or by deletion of a chromosome followed by duplication of the homologous chromosome. Any agent that facilitates such events could be called a completer. There is good evidence that such events play an important part in bringing about homozygosity in retinoblastoma. Bloom's syndrome, a rare recessive condition in humans, is characterized by chromosomal fragility leading to an increased frequency of sister chromatid and homologous chromosomal exchanges. Afflicted persons are predisposed to leukemia and to other cancers. It has been suggested [7,14] that Bloom's syndrome is

a "completer" syndrome, that is, it predisposes to malignancy by increasing the rate of second genomic event without affecting the first.

Within the framework of the model, a second class of agents could affect cancer incidence by modifying the kinetics of cell division and differentiation. This class of agents includes the promoters, and a definition of promotion within the context of the model is given below. Two broad possibilities need to be considered. First, an agent may increase or decrease both division and differentiation rates (of normal or intermediate cells or both) equally, thus leaving the size of the tissue unaffected. However, such an agent would increase or decrease the appropriate mutation rate ( $\mu_1$  and  $\mu_2$ ). Since  $\mu_1$  and  $\mu_2$  are mutation rates per unit time, and because it is the mutation rate per cell division that is constant,  $\mu_1$  and  $\mu_2$  must increase (or decrease) as the rate of cell division increases (or decreases). For example, an agent may increase both  $\alpha_2$  and  $\beta_2$  in such a way that  $(\alpha_2 - \beta_2)$  remains constant. Such an agent would increase  $\mu_2$  and therefore may be indistinguishable insofar as the quantitative implication of the model is concerned from an agent that interacts directly with DNA to increase  $\mu_2$ .<sup>1</sup> Examples of agents that behave in this fashion may be provided by hormones. The epithelium of the breast in the adult female, for instance, turns over in response to hormonal stimulation during the menstrual cycle. An interesting hypothesis, for which the epidemiologic evidence is equivocal, is that risk of breast cancer is related directly to the level of sex hormones in the blood. Presumably, women with higher hormone levels have a higher cellular turnover of the breast epithelium.

Second, an agent may differentially increase or decrease the cell division and differentiation rates. In this case there will be net change in the size of the normal or intermediate tissue. As discussed above, a consequence of a change in the rate of cell division is a change in the appropriate mutation rate per unit time. A small increase or decrease in  $\alpha_1 - \beta_1$ , that is, a small change in the net rate of growth of normal tissue, has only a small impact on the incidence of malignant tumors. However, a small change in  $\alpha_2 - \beta_2$ , that is, a small change in the net rate of growth of intermediate cells, has a rather profound effect on the incidence of malignant tumors.

The essential feature of promotion is to cause an expansion of clones of intermediate cells; that is, promotion increases  $\alpha_2 - \beta_2$ , either by increasing  $\alpha_2$  or by decreasing  $\beta_2$  or both. This may be adopted as the definition of promotion within the framework of the model. Thus, the effect of promotion is to increase the population of those cells that are the targets of the second mutation leading to malignancy. This increases the probability that one of the cells will sustain the second

---

<sup>1</sup> There is a mathematical subtlety involved here, however. We saw that with a certain approximation, the incidence rate predicted by the model depends only on  $(\alpha_2 - \beta_2)$  and not on the parameters  $\alpha_2$  and  $\beta_2$  individually. However, when the approximation is poor (i.e., when tumors are common), the exact expression for the incidence must be used, and this expression depends on  $\alpha_2$  as well as  $(\alpha_2 - \beta_2)$ . Thus, in theory, an agent that increases  $\alpha_2$  while keeping  $(\alpha_2 - \beta_2)$  constant can be distinguished from an agent that directly increases  $\mu_2$  in situations in which the probability of tumors is high. See Moolgavkar et al. [18] for further details.

mutation and become malignant. According to this model, the salient feature of promotion is the growth of intermediate tissue; however, a promoter may well have other actions such as causing hyperplasia of the normal tissue.

In summary, brief exposure of a tissue to a mutagenic agent will cause a small number of cells to sustain the first locus-specific mutation on the path to cancer. Application of a promoter will now lead to an expansion of clones of these intermediate cells leading to premalignant tumors, such as the papillomas in the mouse skin painting experiments and the enzyme-altered foci in the rat hepatocarcinogenesis experiments. A few of these intermediate cells may sustain the second locus-specific mutation and become malignant. If, at this stage, an active mutagen is again applied (IPI protocol), the probability of the second locus-specific mutation is greatly increased, leading to an increased yield of malignant tumors. For a more detailed discussion of intermediate lesions, see Moolgavkar and Knudson [14].

In human epidemiology and carcinogenesis experiments, it is often of interest to study the evolution of cancer risk for different patterns of exposure. A precise analytical description of risk with a time-dependent dose pattern is rather difficult and is discussed in a recent paper [18]. A qualitative description of some simple situations is to be found in Moolgavkar [7,15].

## CONCLUSION

The model I have described here has been shown to be consistent with epidemiologic and experimental data on carcinogenesis [7,14]. For cancer risk assessment, the model is flexible enough to accommodate agents that directly affect mutation rates and agents that affect the rates of cell division and differentiation, and its use for this purpose has been advocated recently [21,22]. The model needs much more validation, however, before the results of fitting it can be accepted without reservation. Although the parameters of the model are interpretable in biological terms, actual measurements of these parameters, especially as functions of the dose of an environmental agent, would appear to be very difficult. Additionally, precise information from the model depends upon knowledge of quantities such as the number and growth characteristics of normal stem cells, which again appear to be difficult to obtain. Nevertheless, the virtue of the model for risk assessment is that it focuses attention on some key biological variables that ultimately may be measurable.

## ACKNOWLEDGMENT

Supported by USPHS Grant CA-39949 from NIH

## REFERENCES

1. Dedrick, R. L. (1985) Application of model systems in pharmacokinetics in risk quantitation and regulatory policy, Banbury Report No. 19, Cold Spring Harbor Laboratory, NY, Lb. 187-199

2. Hoel, D.G. Kaplan, N.L. and Anderson, M.W. (1983) Implication of nonlinear kinetics on risk estimation in carcinogenesis. *Science*, 219, 1032-1037.
3. Krewski, D., Murdoch, D.J. and Dewanji, A. (1986) Statistical modeling and extrapolation of carcinogenesis data. In: S.H. Moolgavkar and R.L. Prentice (Eds.), *Modern Statistical Methods in Chronic Disease Epidemiology*, John Wiley, New York.
4. Murdoch, D.J., Krewski, D. and Crump, K.S. (1987) Mathematical models of carcinogenesis, In: J.R. Thompson, B.W. Brown and M. Dekker (Eds.), *Cancer Modeling*, Marcel Dekker, New York.
5. Conolly, R.B. Reitz, R.H., Clewell, H.J. III and Andersen, M.E. (1987) Pharmacokinetics, biochemical mechanism and mutation accumulation: A comprehensive model of chemical carcinogenesis. *Toxicol. Lett.* 43, 189-200.
6. Armitage, P. and Doll, R. (1954) The age distribution of cancer and a multistage theory of carcinogenesis. *Br. J. Cancer* 8, 1-12.
7. Moolgavkar, S.H. (1986) Carcinogenesis modeling: from molecular biology to epidemiology. *Annu. Rev. Public Hlth.* 7, 151-169.
8. Freedman, D.A. and Zeisel, H. (In Press) From mouse to man: the quantitative assessment of cancer risks. *Stat. Sci.*
9. Brown K.G. and Hoel, D.G. (1954) Statistical modeling of animal bioassay data with variable dosing regimens: example - vinyl chloride. *Risk Anal.* 6, 155-166.
10. Moolgavkar, S.H. (1978) The multistage theory of carcinogenesis and the age distribution of cancer in man. *J. Natl. Cancer Inst.*, 61, 49-52.
11. Moolgavkar, S.H. and Dewanji, A. (In Press) Biologically based models for cancer risk assessment: a cautionary note. *Risk Anal.*
12. Knudson, A.G. (1985) Hereditary cancer, oncogenes, and antioncogenes. *Cancer Res.* 45, 1437-1443.
13. Cornings, D.E. (1973) A general theory of carcinogenesis. *Pro. Natl. Acad. Sci. USA*, 70, 3324-3328.
14. Moolgavkar, S.H. and Knudson, A.G. Jr. (1981) Mutation and cancer: a model for human carcinogenesis. *J. Natl. Cancer Inst.* 66, 1037-1052.
15. Moolgavkar, S.H. (1986) Hormones and multistage carcinogenesis. *Cancer Surv.* 5, 635-648.
16. Knudson, A.G. (1987) A two-mutation model for human cancer. In: G. Klein (Ed.), *Advances in Viral Oncology*, Vol. 7, Raven Press, New York, pp. 1-17.
17. Moolgavkar, S.H. and Venzon, D.J. (1979) Two-event models for carcinogenesis: incidence curves for childhood and adult tumors. *Math. Biosci.* 47, 55-77.
18. Moolgavkar, S.H., Dewanji, A. and Venzon, D.J. (In Press) A stochastic two-stage model for cancer risk assessment I: the hazard function and the probability of tumor, *Risk Anal.*

19. Hennings, H., Shores, R., Wenk, M.L., Spangler, E.F., Tarone, R. and Yuspa, S.H. (1983) Malignant conversion of mouse skin tumors is increased by tumor initiators and unaffected by tumor promoters. *Nature* 304, 67-69.
20. Scherer, E., Feringa, A.W. and Emmelot, P. (1984) Induction of neoplastic foci within islands of precancerous liver cells in the rat. In: M. Borzsonyi, N.E. Day, K. Lapis and H. Yamasaki (Eds.), *Models, Mechanisms and Ethiology of Tumor Promotion*, IARC Scientific Publications No. 56, Lyon.
21. Thorslund, T.W., Brown, C.C. and Charnley, G. (1987) Biologically motivated cancer risk models. *Risk Anal.* 7, 109-119.
22. Wilson, J.D. (1986) Time for a change. *Risk Anal.* 6, 111-112.
23. Dewanji, A., Venzon, D.J. and Moolgavkar, S.H. (In Press) A stochastic two-stage model for cancer risk assessment. II. The number and size of premalignant clones. *Risk Anal.*

## CELL GROWTH DYNAMICS IN LONG-TERM BLADDER CARCINOGENESIS

Samuel M. Cohen and Leon B. Ellwein

*Department of Pathology and Microbiology and the Eppley Institute for Research on Cancer and Allied Diseases, University of Nebraska Medical Center, Omaha, NE*

### SUMMARY

A biologically based probabilistic model of the carcinogenic process has been developed based on a two-stage theory of carcinogenesis. The model has been validated utilizing experimental urinary bladder carcinogenesis studies in the rat, with an emphasis on quantification of cell dynamics. Critical parameters tracked through this process include mitotic rates, cell loss and birth rates, and irreversible cellular transitions from normal to initiated to transformed states. Analyses demonstrate the sensitivity of tumor incidence to the timing and magnitude of changes to these cellular variables. Modeling has been applied to genotoxic compounds, such as N-[4-(5-nitro-2-furyl)-2-thiazolyl]-formamide, and non-genotoxic compounds, such as sodium saccharin. For the latter compounds, complex administration regimens have been studied, including two-generation experiments, initiation-promotion experiments, and sodium saccharin administration following ulceration and regenerative hyperplasia. Modeling indicates that the effects of such compounds can be explained entirely on the basis of cytotoxicity and consequent hyperplasia. Quantitative modeling based on biological processes has the potential for direct application to carcinogenic risk assessment.

### INTRODUCTION

Cancer is an increasingly common problem in our society, and considerable evidence suggests that a large proportion of cancers in humans are due to exposure to a variety of chemicals, natural and man-made [1]. Epidemiologic research has demonstrated clearly the carcinogenic effects of a relatively small number of chemical agents, but among those implicated are several associated with the development of cancer of the urinary bladder, including cigarette smoking [1]. The association of chemicals with the development of urinary bladder carcinogenesis has been well-known in human populations since the discovery by Rehn in 1895 that workers in the German aniline dye industry had a markedly increased risk of developing cancer of the urinary bladder [2, 3]. A number of chemicals are well documented as human bladder carcinogens, including 2-naphthylamine, 4-aminobiphenyl, benzidine, other benzidine dyes [2, 3], and cyclophosphamide [4]. In addition, there is considerable evidence from a variety of animal experiments that these compounds cause bladder cancer in other species, such as the dog, rat, or mouse, depending on the test agent [2, 3, 4].

Epidemiologic studies are the most reliable but least acceptable method of identifying chemicals hazardous to humans. It is better to identify potential carcinogens in experimental systems

and avoid human exposure entirely. Included among the chemicals administered to experimental animals, primarily rats and mice, are many that have been identified as carcinogens and subsequently prevented from entering the market, thereby avoiding human exposure [2, 3]. For the urinary bladder, this list includes a variety of nitrosamines, nitrofurans, and numerous benzidine dyes. These compounds satisfy unquestionably the classical criteria for designation as a carcinogen. For other compounds, evaluation is less clear-cut, particularly when a compound has been observed to cause tumors in one or both sexes in one or more species of experimental animals, but extensive human exposure has not produced significant evidence of carcinogenicity. The most notorious example of such a compound is sodium saccharin [5, 6]. In these cases, the responsibility of regulatory agencies is to make an informed estimate of the risk to society from exposure to these chemicals, both in absolute and relative terms, and to determine whether the compound should be taken off the market. Extrapolation from animal experiments to human conditions forms the scientific basis for these quantitative risk assessments, an exercise generally fraught with assumptions, both explicit and implicit.

Quantitative risk assessment for regulatory purposes relies heavily upon a variety of mathematical models for extrapolating low-dose response from high-dose experiments [7]. Unfortunately, these models were chosen more for their mathematical tractability than for their biological soundness. In contrast to these mathematically based extrapolation models, we concentrated on modeling the carcinogenic process at a level that takes explicit account of biological change as reflected in cellular parameters [8]. We have implemented this simulation model on a computer and validated it using data from experiments on the bladder carcinogen N-[4-(5-nitro-2-furyl)-2-thiazolyl]-formamide (FANFT), a classical mutagenic carcinogen, and sodium saccharin, a non-mutagenic (non-genotoxic) chemical. We believe that quantitative extrapolation from animal experiments to humans is placed on a firmer foundation when based on a mathematical model of the carcinogenic process, as theorized after decades of experimental study.

#### **BIOLOGICAL-BASED MODELING OF CARCINOGENESIS**

Chemical carcinogenesis has been shown to be an extremely complex, dynamic process with numerous means of enhancement or inhibition. In establishing the relationship between the effects of chemicals in animals and humans, it is necessary to quantitate differences in exposure levels, in the pharmacokinetics and metabolism of the chemical, in the interaction of active metabolites with cellular targets, and in the cellular response to the stimulus. Control mechanisms of the target tissue and the organism as a whole also must be taken into account. Pharmacokinetic modeling is addressed by others at this meeting, focusing on species differences in the delivery of the chemical to the target organ. Although this is an extremely critical component in our quantitative understanding

of the carcinogenic response to an administered chemical, it does not address the biological response of the target organ.

Our efforts are directed toward quantitative study of the biological response of the target organ at the cellular level and the appearance of tumors. The chemicals with which we have worked thus far generally show a good correlation between the human and the test species, usually the male rat, in the amount of the administered dose reaching the target site. Obviously, combining the pharmacokinetic and cellular response models would be a further refinement of the overall quantitative assessment process.

The theoretical foundation for our model is illustrated in Figure 1. Several assumptions have been made with respect to the carcinogenic process as presented in our model. We assume that the carcinogenic process is effective only in the stem-cell-equivalent population of a tissue. It is assumed that exposure of fully differentiated or committed cells to a chemical carcinogen will not have an impact on the production of tumors, since these cells eventually die and are not propagated. On the other hand, control mechanisms influencing cell proliferation might readily involve differentiated and/or committed cells which would, in turn, influence the proliferative rates of the stem cell population. We assume that the carcinogenic process entails two specific and irreversible events. The first we refer to as initiation, which involves the transition, or conversion of a normal stem cell to an *initiated stem cell*. The second event is referred to as transformation and involves the conversion of initiated cells into fully malignant cells. Cells that are present in benign proliferations, such as hyperplastic nodules or papillomas, are part of the initiated cell population and not part of the transformed, malignant cell population. Further, we have assumed that each of these two events can occur only during the active part of the cell cycle, not when the cell is at rest, and that the two events occur in a probabilistic fashion. That is, every time a normal stem cell goes through the cell cycle, there is a certain probability ( $P_i$ ), generally extremely low under usual circumstances, of being converted from a normal to an initiated cell. Likewise, every time an initiated cell goes through the cell cycle, it has a certain probability ( $P_T$ ), again very low, of undergoing transformation.

Within this framework, it is apparent that the major variables of concern in assessing the potential for carcinogenicity are the number of normal stem cells at any given time, the rate at which they proliferate (including birth and death rates), and the probability during each cell cycle of a cell's being converted from normal to initiated. Similar variables are needed to represent the likelihood of cells moving from the initiated to the transformed state. Considering the variety of protocols and exposure regimens that have been employed in experimental studies, it is readily apparent that these variables will change over time. Cancer is a dynamic process, and the time-varying nature of these

cellular variables must be reflected in the model if it is to be a valid representation of the carcinogenic process and accurately predict tumor response as a function of these variables.

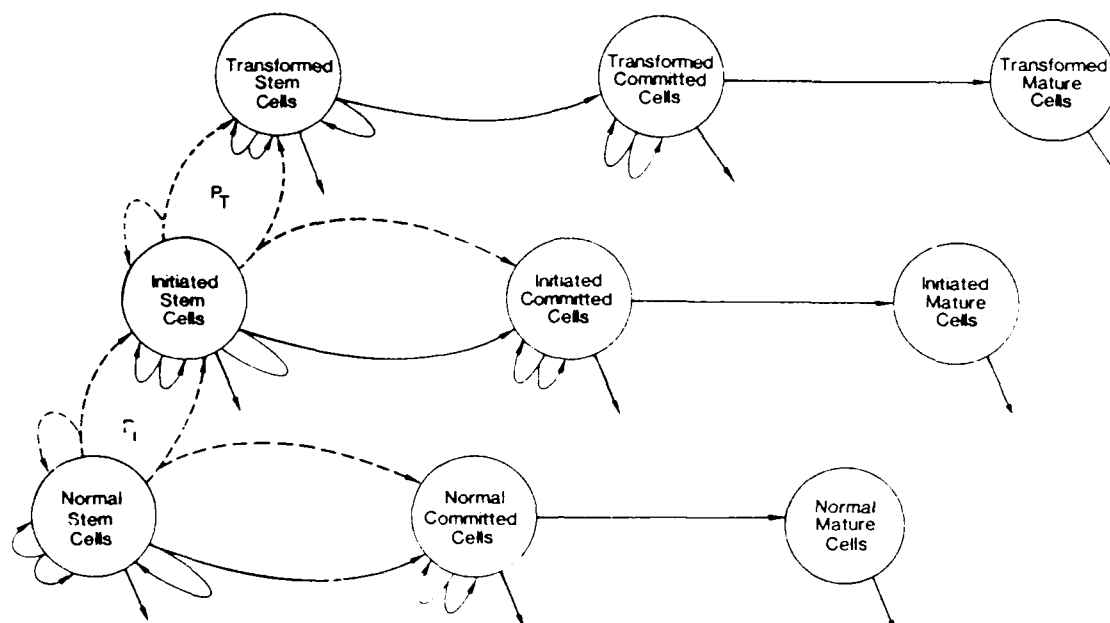


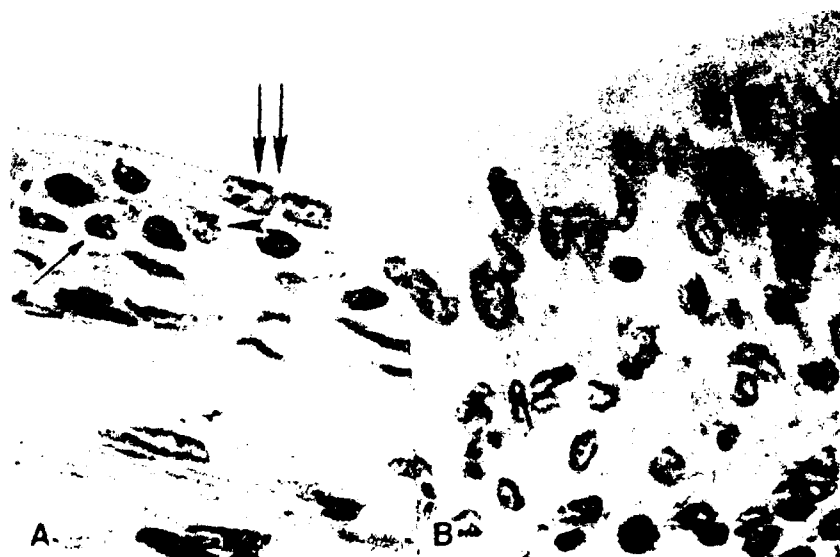
Figure 1. Diagrammatic representation of the two-stage model of carcinogenesis. The circles on the left portion of the diagram represent the stem cell states which lead to development of malignancy beginning in the lower left-hand corner with normal cells, which can undergo a change to initiated cells, which in turn can undergo a change to transformed (malignant) cells. The circle to the right of the stem cell states represent cells committed to differentiation and ultimately death. (Reprinted from Greenfield et al. [8].)

#### **N-[4-(5-nitro-2-furyl)-2-thiazolyl]-formamide (FANFT), a classical genotoxic carcinogen**

FANFT is a nitrofurant antibiotic that induces essentially a 100% incidence of bladder cancer in rats, mice, hamsters, and dogs when fed in the diet, but is without activity in the guinea pig [9]. It has all of the properties of a classical carcinogen: it is strongly mutagenic in a variety of *in vitro* test systems [10], it is metabolically activated to a reactive electrophile [11, 12], and it interacts with DNA with the formation of adducts [10, 11, 12]. The amount of 2-amino-4-(5-nitro-2-furyl)thiazolyl (ANFT) excreted in the urine is roughly proportional to the administered dose. ANFT is the proximate metabolite of FANFT [13], which is further metabolically activated in the bladder mucosa to a metabolite that reacts with DNA [14]. Numerous experiments have been performed in male Fischer rats evaluating the effect of varying the length of administration of a constant dietary dose [15, 16, 17] of FANFT and of administering variable doses for a constant length of time [18, 19]. The prevalence of bladder tumors in each of these groups was examined at several time points during the 2-year experimental period. The time-series nature of this data was of pivotal importance in the

validation of our model, including determining the influence of values for the unobservable cell conversion probabilities [8].

It is critical in understanding and modeling the biology of the cancer process to have some knowledge of the changes that occur in histopathology during the induction of cancer. The normal urinary bladder epithelium in most adult species, including rats, mice, and humans, is mitotically quiescent [2, 20, 21]; in experimental animals, labeling indices 1 h after a pulse of  $^3\text{H}$ -thymidine are in the range of 0.1%. When FANFT is administered in the diet at a level of 0.2%, there is a rapid increase in labeling index [20] with a concomitant increase in the size and number of urothelial cells [18]. The labeling index increases to greater than 2%, a more than 20-fold increase compared to controls [20]. The hyperplasia that results from FANFT administration gradually increases in severity [15] until the normal three-cell layers of the bladder epithelium are increased to 8 to 10 cell layers by 8 weeks of administration. At that time, nodular and papillary hyperplasia begin to appear. These are focal lesions (Figure 2) with a marked increase in cell proliferation rates and cell number. The autoradiographic determinations of labeling index and histopathology estimates of cell number are the bases upon which the cell kinetic parameters of the model are established.



**Figure 2.** The histopathology of progressive proliferative states during urinary bladder carcinogenesis in the rat.

- A. Normal bladder epithelium with three cell layers, including the basal (stem) cells (single arrow), intermediate (committed) cells (arrowhead), and large superficial, umbrella (mature) cells (double arrows).
- B. Mildly hyperplastic epithelium with an increasing number of cells and increased size of cells following administration of FANFT.



Figure 2. C. Moderate simple hyperplasia following 6 weeks of FANFT administration.



Figure 2. D. Nodular hyperplasia following 10 weeks of FANFT administration.



Figure 2. E. Papillary hyperplasia following 10 weeks of FANFT administration

The results of applying the model to experiments utilizing a constant dose of FANFT over a variable period of administration are illustrated in Figure 3. By taking into account the extent to which FANFT increases cell number (hyperplasia) and proliferation rates at this dose, it was determined that FANFT must also increase markedly the initiation probability ( $P_i$ ). The transformation probability ( $P_T$ ), however, does not appear to be affected by the administration of FANFT; modeling trials where  $P_T$  also was increased resulted in the induction of visible tumors faster than that actually found in the animal experiments. Changes in  $P_i$  are expected in response to FANFT administration, since FANFT is a strongly genotoxic compound and both  $P_i$  and  $P_T$  are, by definition, representative of genetic events such as mutations. The reason that  $P_T$  is not increased during the carcinogenic process of FANFT may be related to a difference in the metabolic capabilities of initiated cells compared to normal cells [22]. It should be noted that inferences regarding  $P_i$  and  $P_T$  were possible from these experiments only because the serial sacrifice schedule provided data beyond that available from the more common single-time-point sacrifices.

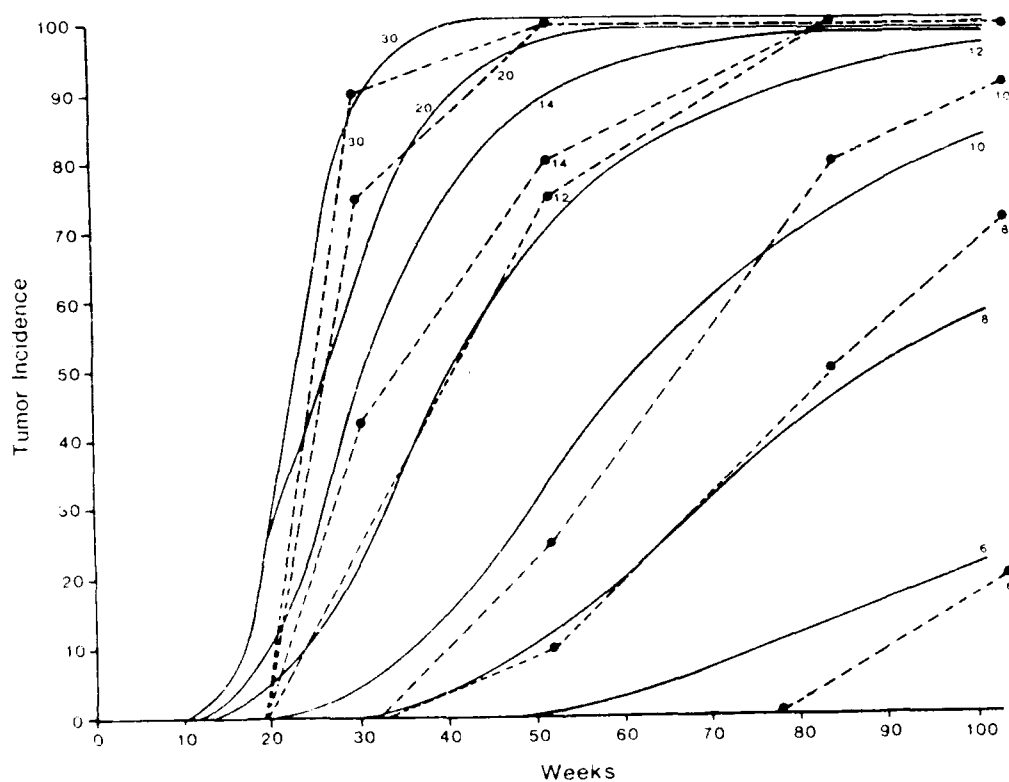


Figure 3. The incidence of bladder tumors following the administration of FANFT for 6 to 30 weeks at a dose of 0.2% of the diet. The solid lines represent the results of computer modeling, whereas the dashed lines represent actual experimental results. (Reprinted from Greenfield et al. [8].)

To demonstrate the usefulness of this model in extrapolations to lower doses, it was applied to the analysis of experiments evaluating the dose response of FANFT with 1- and 2-year sacrifices [18,

20]. The results of these experiments are tabulated in Tables 1 and 2. FANFT doses ranged from 0.0005% to 0.2% of the diet. As seen in Table 1, the response to FANFT is high at dietary levels of 0.05% and above, with minimal effect at 0.01%, and no effect at the lower doses. These tumor incidences paralleled changes in cellular dynamics seen early in the administration of FANFT. At the higher doses, there is a dose-responsive increase in the labeling index and an increase in cell number as evidenced by hyperplasia at doses of 0.05% and above. Although no tumors or hyperplasia are seen at doses as low as 0.005% of the diet, ANFT is generated in the urine at this dose, which is likely to be associated with DNA adduct formation (i.e.,  $P_i$  is likely to remain elevated). It is critical that these changes in cell number and proliferation rates are taken into account, along with possible dose-related changes in  $P_i$ , in attempting to reconcile the lack of tumors at the lower doses. As was shown, the reduction in cell kinetics associated with reduced FANFT doses is sufficient to account for the reduction in tumor incidence even when  $P_i$  is kept elevated at a constant level. Further evidence for the complementary effects of cytotoxicity and genotoxicity were provided in a co-carcinogenesis experiment administering FANFT at a level of 0.005% of the diet concurrently with sodium saccharin in the diet at a level of 5% for 2 years [23]. Sodium saccharin causes a mild increase in cell proliferation and hyperplasia without a genotoxic effect [24, 25]. The combination of a slight genotoxic effect provided by the low levels of FANFT in the diet, combined with the cell proliferation effects of sodium saccharin, led to the induction of tumors, whereas each compound by itself did not induce tumors.

TABLE 1. EFFECT OF DOSE ON THE URINARY BLADDER CARCINOGENICITY OF FANFT IN F-344 MALE RATS

Dose of FANFT	Bladder Tumor Incidences <sup>a,b</sup>					
	1 year <sup>c</sup>			2 years <sup>d</sup>		
	No. of Rats	Rats with Papilloma (%)	Rats with Carcinoma (%)	No. of Rats	Rats with Papilloma (%)	Rats with Carcinoma (%)
0.2	—	—	—	36	0	36 (100)
0.1	16	7 (44)	9 (56)	39	0	39 (100)
0.05	14	9 (64)	4 (29)	39	2 (5)	34 (87)
0.01	15	1 (7)	0	40	1 (2.5)	0
0.005	16	0	0	40	0	0
0.001	15	0	0	40	0	0
0.0005	16	0	0	—	—	—
0.0	20	0	0	39	0	0

<sup>a</sup> Each rat was tabulated only once. If it had a papilloma and carcinoma, it was tabulated as carcinoma.

<sup>b</sup> Weanling rats were fed the respective diets for 30 weeks followed by control diet for 22 (1-year study) or 74 (2-year study) weeks.

<sup>c</sup> Data are from Arai et al. [18].

<sup>d</sup> Data are from Arai et al. [19].

TABLE 2. EFFECTS OF FANFT ON THE RAT URINARY BLADDER

	Dose of FANFT (%)	No. of Rats	Simple Hyperplasia			Papillary or Nodular Hyperplasia	Labeling Index (%) <sup>a</sup>
			Total	Slight	Marked		
At 4 weeks	0.2	11	10 <sup>b</sup>	10 <sup>b</sup>	0	0	2.37 ± 1.40 <sup>b</sup>
	0.1	11	6 <sup>b</sup>	6 <sup>b</sup>	0	0	1.12 ± 0.54 <sup>b</sup>
	0.05	10	0	0	0	0	0.37 ± 0.13 <sup>b</sup>
	0.01	10	0	0	0	0	0.17 ± 0.09
	0.005	10	0	0	0	0	0.12 ± 0.07
	0.001	10	0	0	0	0	0.13 ± 0.06
	0	15	0	0	0	0	0.10 ± 0.05
At 10 weeks	0.2	6	6 <sup>b</sup>	2	4 <sup>b</sup>	2	2.02 ± 0.84 <sup>b</sup>
	0.1	6	6 <sup>b</sup>	3 <sup>b</sup>	3 <sup>b</sup>	1	2.21 ± 0.74 <sup>b</sup>
	0.05	10	9 <sup>b</sup>	9 <sup>b</sup>	0	0	0.84 ± 0.36 <sup>b</sup>
	0.01	10	0	0	0	0	0.11 ± 0.05
	0.005	10	0	0	0	0	0.08 ± 0.06
	0.001	10	0	0	0	0	0.08 ± 0.06
	0	10	0	0	0	0	0.10 ± 0.07

<sup>a</sup> Mean ± S.D.<sup>b</sup> Significantly different from control (0% FANFT) at  $p < 0.05$  by the Fisher exact or Student's *t*-test.  
Data are from Hasegawa et al. [20]

By taking into account the lack of effect of FANFT on cell number and cell proliferation at the lower doses, we are provided with a more complete interpretation of the experimental findings and a more realistic basis upon which to estimate the response to FANFT at low doses. Also, as became evident in these FANFT dose-response experiments, dose-response effects on cell proliferation and cell number are likely to be different from dose-response effects on *P*. Cell number and proliferation rates take into account cytotoxic, regenerative, and mitogenic effects which occur secondary to administration of the carcinogen, only some of which may be related to effects on DNA. In contrast, *P* is likely a reflection only of genotoxic effects. In evaluating the dose-response effects of compounds such as FANFT, it is important that cell kinetic information along with pharmacodynamic and DNA adduct data be considered explicitly in explaining the shape of the dose response curve, particularly as it pertains to extrapolation to lower doses.

### ***Sodium saccharin, a non-genotoxic chemical***

Sodium saccharin is a chemical with none of the properties of classical carcinogens, such as FANFT, and yet it is of considerable importance because of its widespread use by human populations [6, 26]. In contrast to classical carcinogens, saccharin is not mutagenic in most *in vitro* assay systems [6, 27]. It is not metabolized to a reactive electrophile – it is actually anionic in its structure [6, 28, 29], and it does not form adducts with DNA [30]. In addition, it does not appear to bind to cell surface receptors (Garland, Williamson, and Cohen, unpublished observations). Saccharin is a prototype of a broad class of compounds referred to as non-genotoxic, which have been found to be carcinogenic in various experimental models, particularly at high doses [6, 31, 32, 33].

If saccharin is administered at high doses in the diet to rats beginning after weaning, the incidence of bladder tumors is not significant. Summarizing over a large number of experiments, the incidence is less than 1% in males and considerably less than that in females [6, 24, 31, 34]. If saccharin administration is begun prior to conception in the mother and father ( $F_0$  generation), continued in the mother during gestation and lactation, and then to the offspring ( $F_1$  generation) for their lifetime, a significant incidence of bladder tumors occurs in the male rat [6, 31, 33]. This protocol has been referred to as the two-generation experiment. It has emphasized the importance of exposure of the rat bladder to a chemical stimulus during the *in utero* and/or early neonatal time period. Model-based interpretations of these results are dealt with below.

The aforementioned experiments involve the administration of saccharin alone. There also have been numerous complex experimental protocols involving the concurrent or subsequent administration of saccharin with other test compounds. Many of these have followed the classical initiation-promotion protocol originally described for mouse skin [35]. When the promoting substance is administered after the initiating substance, whether immediately or after a delay period, tumors are induced in the test tissue. In contrast, administration of the promoting substance first, followed by the initiator, does not result in tumors. In our experiments, we have utilized FANFT as the initiating substance and sodium saccharin in the diet at high doses (usually 5% by weight) as the promoting substance [24, 34, 36, 37]. Saccharin has been demonstrated as a tumor promoter following initiation by FANFT [36], N-butyl-N-(4-hydroxy-butyl)nitrosamine (BBN) [37], and N-methyl-N-nitrosourea (MNU) [34]. These experiments involve the administration of both initiator and promoter substances after weaning and, thus, are one-generation experiments.

In an attempt to demonstrate the relationship of cell proliferation to a tissue's susceptibility to initiation, FANFT was administered to rats with a rapidly proliferating bladder epithelium induced either by freeze ulceration or by intraperitoneal cyclophosphamide injection [16] (Figure 4). Using either method of inducing ulceration and subsequent regenerative hyperplasia, the results were

similar. The ulcers were repaired and the bladder returned to normal based on cell kinetic and

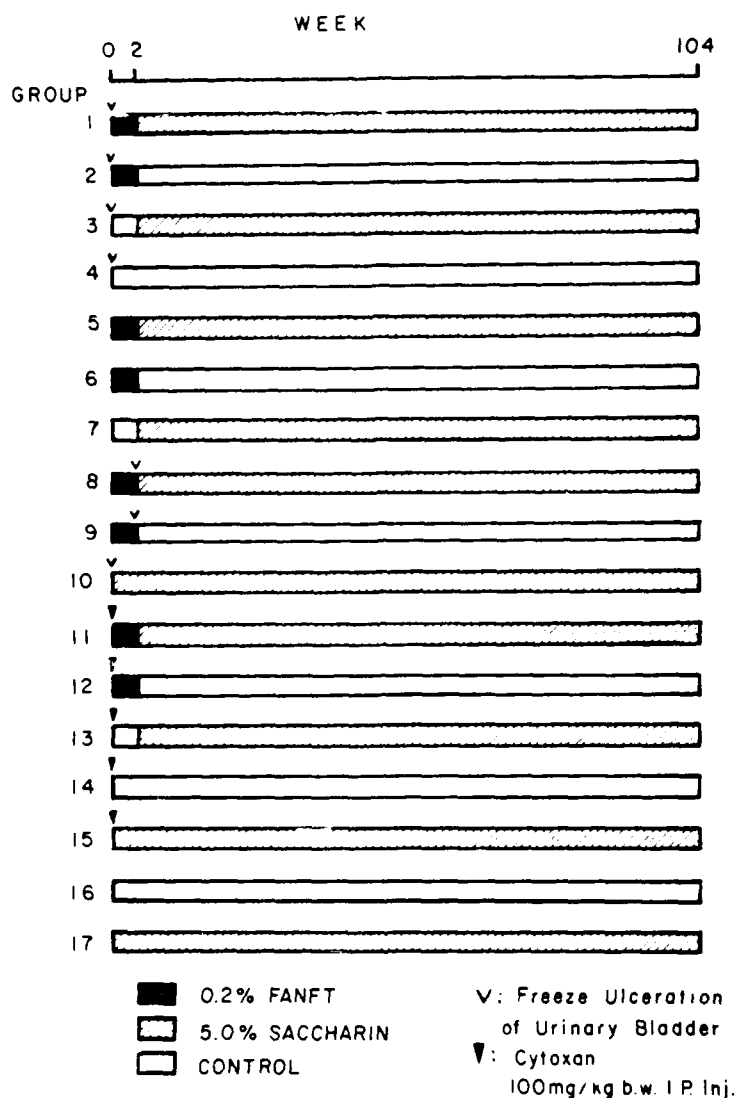


Figure 4. Experimental protocol for evaluation of the administration of saccharin after ulceration of the urinary bladder by either freezing or cytosin (cyclophosphamide) administration. (Reprinted from Cohen et al. [16].)

morphologic criteria within 3 to 4 weeks [38, 39, 40, 41]. In an initial experiment with this protocol [16], rats administered FANFT for 2 weeks following freeze ulceration or cyclophosphamide injection, and then administered sodium saccharin for the remainder of the experiment (2 years), developed bladder tumors (Table 3). Tumors also appeared in the groups administered sodium saccharin after freeze ulceration without FANFT administration, and this occurred whether the saccharin was administered immediately after the ulceration or beginning 2 weeks later during the period of regenerative hyperplasia. To determine whether it was the ulcer and the consequent regenerative hyperplasia or saccharin in the presence of a rapidly proliferating bladder epithelium which was

TABLE 3. LESIONS OF THE URINARY BLADDER

Group	Effective No. of Rats	Simple Hyperplasia	Nodular or Papillary Hyperplasia	Papilloma	Carcinoma
1. U → FANFT → S <sup>a</sup>	23	5 (22) <sup>b</sup>	8 (35)	0	4 (17) <sup>c</sup>
2. U → FANFT	22	7 (23)	1 (5)	0	0
3. U → C → S	20	7 (35)	2 (10)	1 (5)	5 (25) <sup>c,d</sup>
4. U	23	4 (17)	1 (4)	0	0
5. FANFT → S	21	10 (48)	0	0	1 (5)
6. FANFT	19	2 (11)	0		0
7. S	17	7 (41)	1 (6)		0
8. FANFT → U → S	22	5 (23)	4 (18)	1 (5)	8 (36) <sup>c,d</sup>
9. FANFT → U	21	5 (24)	2 (10)	0	2 (10)
10. U → S	21	4 (19)	2 (10)	2 (10)	2 (10) <sup>c</sup>
11. CP → FANFT → S	22	11 (50)	2 (9)	3 (14)	4 (18)
12. CP → FANFT	9	2 (22)	0	0	0
13. CP → Cont → S	17	2 (12)	4 (24)	2 (12)	3 (18) <sup>c,d</sup>
14. CP	7	0	0	1 (14)	0
15. CP → S	17	4 (24)	2 (12)	3 (18)	3 (18) <sup>c,d</sup>
16. C	32	0	0	0	0
17. S	20	6 (30)	0	0	0

<sup>a</sup> U = ulcer; S = sodium saccharin; C = control diet; CP = cyclophosphamide.

<sup>b</sup> Percent of effective number of rats shown in parentheses.

<sup>c</sup>  $p < 0.05$  for incidence of carcinoma and incidence of carcinoma plus papilloma compared to Group 16.

<sup>d</sup>  $p < 0.05$  for incidence of carcinoma plus papilloma compared to Group 5.

Data are from Cohen et al. [16].

primarily responsible for initiation, another series of experiments was designed where sodium saccharin was administered at 5% of the diet beginning at 0, 2, 4, 5, or 18 weeks after freeze ulceration (Table 4) [42]. The hypothesis was that if the ulcer with the subsequent regenerative hyperplasia were pivotal to initiation, all five of these groups should develop bladder tumors, whereas if it were the presence of sodium saccharin during regenerative hyperplasia, tumors should result only in the first two, and possibly the third, groups. Certainly, animals administered sodium saccharin beginning 18 weeks after ulceration were not being exposed to the compound during the rapidly regenerative hyperplasia present after freeze ulceration. As shown in Table 4, all of the five

groups developed similar incidences of bladder tumors, indicating that the ulceration and subsequent regenerative hyperplasia were prime contributors to the initiation process.

TABLE 4. INITIATION OF BLADDER CARCINOGENESIS BY FREEZE ULCERATION

Group	Treatment	Number of Rats	Number of Rats with Bladder Carcinoma
1	U → S	36	11 (31) <sup>c</sup>
2	U → C (2) <sup>b</sup> → S	36	6 (17)
3	U → C (4) → S	40	12 (30)
4	U → C (6) → S	36	7 (19)
5	U → C (8) → S	39	9 (23)
6	S	39	0
7	U → C	39	1 (3)
8	C	39	0

a U = freeze ulceration; S = sodium saccharin, 5% of the diet; C = control diet.

b Numbers in parentheses represent weeks of feeding control diet between the time of ulceration and the beginning of sodium saccharin treatment.

c Numbers in parentheses represent percentages of effective number of rats in the group with carcinoma. Data are from Hasegawa et al. [42.]

Since saccharin does not cause DNA damage, is not mutagenic, and is not metabolically activated like classical carcinogens, how can the various experiments involving saccharin carcinogenesis as described above be explained? Apparently, the cytotoxic effects of sodium saccharin are playing a pivotal role in promoting tumors once the degree of bladder initiation is enhanced through some prior means. Although the cytotoxic mechanism is unclear, repeated observations have indicated that administration of saccharin at high doses in the diet to male rats induces a sustained increase in the proliferative rate of the bladder epithelium, as evidenced by the autoradiographically determined labeling index and by scanning electron microscopic observation [43, 44], and a persistent hyperplasia (increased cell number) [43, 44]. Model analyses [45] demonstrate that these cell kinetic changes are sufficient to explain fully all of the complex experimental protocols in which saccharin is related to carcinogenesis, without having any genotoxic effect on  $P_1$  or  $P_T$ . When saccharin is administered in one-generation experiments, beginning administration after weaning and continuing for 2 years, the mild but sustained increase in cell proliferation and cell number is not enough to result in a significant incidence of tumors. The pre-existing initiated cells subjected to the proliferative effects of saccharin are insufficient in number to produce a transformed cell when only background transformation probabilities are acting. In contrast, after administration of FANFT, the pool of initiated cells is large and the sustained non-

genotoxic stimulus provided to these cells by continuous saccharin administration results in the production of transformed cells and visible tumors.

The interpretation of the ulcer-saccharin experiment can follow similar lines. Model analyses predict that by the time of ulceration, a few stem cells have already been initiated by spontaneous mutations. Thus, any subsequent event that provides for a dramatic further increase in their number can permanently increase the latent potential for tumorigenesis. One can speculate that the ulcer is increasing the initiated cell pool by putting normal stem cells in contact with an endogenous urine carcinogen (thereby increasing  $P_1$ ), or perhaps more plausibly, that the regenerative hyperplasia provides for a dramatic multiplication in the initiated cell population, as it does in the normal cell population, and that the initiated cell micro-foci are less likely than the normal cell hyperplasia to regress. Tumors are expected if this significant population of initiated cells is then continually subjected to even a mild proliferative stimulus, such as produced by high doses of sodium saccharin. Without the explosive cell kinetic effects of ulceration, an insufficient number of initiated cells are available at the start of saccharin administration. Further, if increased proliferation rates following ulceration are not sustained above normal levels, tumors do not appear.

In the two-generation experiment involving saccharin administration beginning before conception, continuing through gestation and lactation, and then for the lifetime of the offspring, the same conjectural effect of saccharin is supported by model analyses. Exposure to saccharin during the development period is of significance if, as conjectured, saccharin stimulates the mitotic rate of initiated cells as it does normal cells and, of pivotal significance here, if it increases the likelihood that two initiated stem cells will be produced at each mitotic event rather than one stem and one committed cell (i.e., the birth rate of initiated stem cells is increased). Based on recent studies in our laboratory, it has been shown that the fetal bladder epithelium is an actively proliferating tissue with a labeling index of approximately 10% through the time of birth. Immediately after birth, the labeling index decreases rapidly so that by 7 days of age the labeling index is approximately 1.5%. It declines further so that by 3 weeks of age the labeling index is approximately 0.1%, essentially at the level of the adult bladder epithelium. In concert with this steady decrease in mitotic rate (labeling index is a direct reflection of mitotic rate) is an increase in the likelihood that, at each mitotic event, one of the two daughter cells is not a stem, but a committed cell (i.e., the birth rate also decreases). This concurrent decrease in birth rate is consistent with the growth in the stem cell population during the neonatal period. Since mitotic and birth rates are already very high in the fetal bladder, no additional effect of saccharin on these rates would be expected. However, in the 3 weeks after birth, proliferation could be influenced so that it would decline at a rate slower than the normal neonatal epithelium. Again, any preferential effect on initiated cells (both mitotic and birth rates) would be particularly significant, because even under normal conditions, model analyses predict that most

animals will have at least one spontaneously generated initiated cell, providing a seed for any proliferative stimulus. Indeed, our modeling indicates that little is gained by starting saccharin before birth in the two-generation feeding protocols. It also predicts that stopping saccharin administration after the neonatal period will not produce tumors. In a recent study reported from the IRDC [33], it was demonstrated that this is likely to be the case. Rats administered saccharin at high doses through the full two-generation protocol had essentially the same incidence as a comparably dosed group of animals that began saccharin administration at birth. Their experiment also demonstrated that administration only through the *in utero* and neonatal time period was insufficient for the development of tumors later on. Based on our modeling and these experimental results (unpublished observations), it is clear that saccharin administration is critical in the 3-week period after birth, but the increased proliferation rate must be sustained essentially for the lifetime of the animal for tumors to appear.

This series of experiments and associated model analyses demonstrate the importance of taking into account the entire lifetime of the animal [45]. It is insufficient to assume that at the time of weaning, or even at birth, there are no spontaneously initiated cells in the bladder epithelium. Although the expected number is likely to be small, their presence has important consequences for modeling and prediction of experimental results. It is particularly important to take into account any influence on proliferation rates and cell accumulations that occur in the *in utero* and/or neonatal time period because this could generate a markedly increased number of initiated cells by the time of weaning. The spontaneous generation of transformed cells (malignant tumors) or initiated cells (one step removed from tumors) has important implications in the interpretation of experiments and extrapolation to low-dose exposures. The importance of these spontaneous events is already recognized in tissues where they are evident experimentally, such as the liver in mice [46].

#### **EXTRAPOLATION FROM ANIMAL EXPERIMENTS INVOLVING HIGH DOSE ADMINISTRATION TO LOW DOSE EXPOSURE IN HUMANS**

In all of the saccharin experiments described above, the administered dose was extremely high, usually at dietary levels of 5% or above. In no *in vivo* study has there been a positive response of any kind, short-term or long-term, at administered doses of less than 1% [6, 33, 44, 47, 48]. In addition, it has been recently demonstrated with saccharin [49] and related moderately strong organic acids [50, 51, 52] such as ascorbate, citrate, and erythorbate, that the form in which the chemical is administered is critical to the development of the biological endpoint, lesions in the bladder. For example, administration of saccharin as a sodium salt at a dietary level of 5% resulted in an increase in labeling index after 10 weeks. Potassium saccharin at 5% of the diet induced an elevated labeling index after 10 weeks [49], but at a level less than that observed with sodium saccharin. Calcium saccharin and acid saccharin did not induce a significant increase in labeling index compared to the

control group. Our initial hypothesis to explain this phenomenon was that a difference in solubility resulted in a difference in gastrointestinal absorption with a consequent difference in excretion of saccharin in the urine, the target organ dose. However, in an experiment in which the levels of saccharin in the urine were measured following administration of these different salt forms, similar levels of excretion occurred in each group regardless of the salt form administered (Table 5). There were marked differences, however, in urinary concentrations of sodium, potassium, hydrogen, calcium, and other ions, as well as differences in volume, which may be related to the mechanism of action of saccharin. Detailed chemical studies, including NMR and infrared spectroscopy, have demonstrated that none of these variations in ions has any effect on the ionic structure of saccharin within the extreme ranges seen in the urine following administration of the different salt forms [29]. In addition, studies have demonstrated that identical levels of ascorbate in the urine give significantly different results depending on the level of sodium and hydrogen ions present in the urine [51]. Based on a wide variety of *in vivo* and *in vitro* studies, there is increasing evidence that the effects on the bladder epithelium following administration of sodium saccharin and related compounds is related to the urinary ionic milieu rather than to the saccharin ion itself.

**TABLE 5. PROLIFERATIVE FINDINGS IN THE RAT URINARY BLADDER EPITHELIUM**

Group	Autoradiography		Urine Chemistries <sup>a</sup>			
	N	Labeling Index (%) <sup>a</sup>	Saccharin (mmol/mL)	pH	Na <sup>+</sup> (meq/L)	CA <sup>++</sup> (meq/L)
Sodium saccharin	5	0.55 ± 0.20 <sup>b</sup>	0.17 ± 0.04	7.2	291 ± 19	24.8 ± 9.6
Potassium saccharin	6	0.18 ± 0.09 <sup>c</sup>	0.14 ± 0.04	6.8	153 ± 39	23.9 ± 1.8
Calcium saccharin	6	0.12 ± 0.11	0.14 ± 0.03	5.7	158 ± 24	41.2 ± 0.5
Acid saccharin	6	0.07 ± 0.04	0.19 ± 0.02	5.5	139 ± 45	51.6 ± 6.7
Control	6	0.06 ± 0.04	0	7.1	158 ± 14	34.5 ± 5.8

<sup>a</sup> Mean ± S.D.

<sup>b</sup> Significantly different from the other groups at  $p < 0.01$  by Student's *t*-test.

<sup>c</sup> Significantly different from control groups at  $p < 0.05$  by Student's *t*-test.

Data are from Hasegawa and Cohen [49].

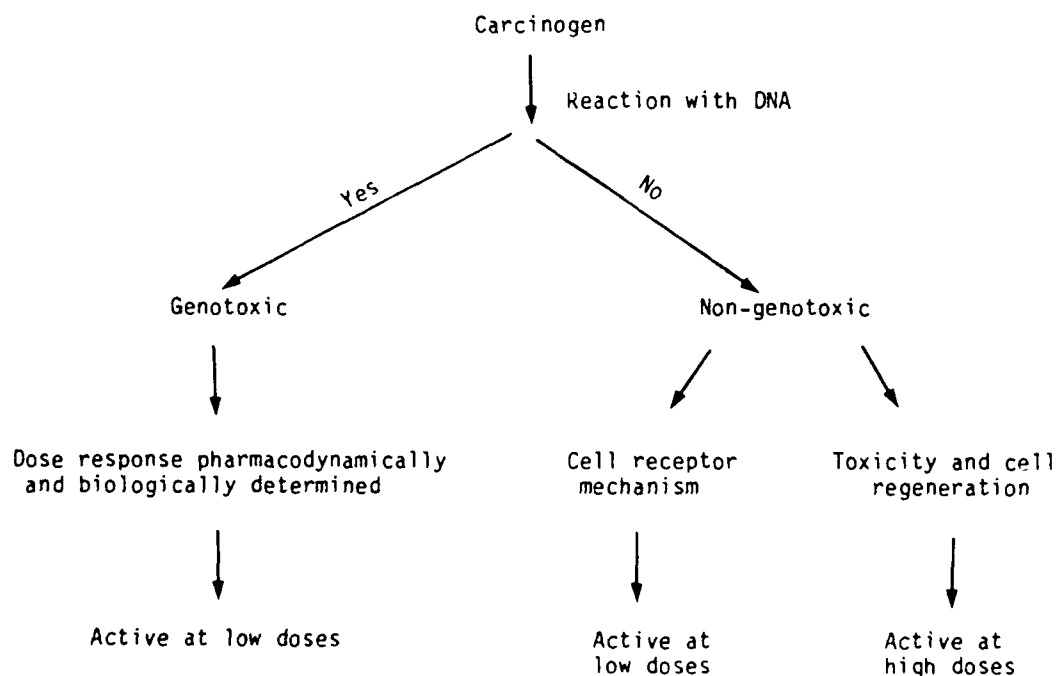
Based on the above biological experiments and model analyses, predictions about low dose effect and extrapolations from rats to humans can be related to biological interpretations rather than simple (or complex) mathematical exercises [53]. Our modeling, supported by animal experiments, would indicate that administering high doses of sodium saccharin in the diet to male rats increases the proliferation rate and cell number in the bladder epithelium, which if sustained over sufficiently long periods of time, can result in a significant tumor incidence. However, until a dose is reached where there is a significant increase in cell proliferation rates or cell number, no other biological

response is anticipated because there is no evidence of interaction with DNA, even at the higher doses. It appears as though a dose of sodium saccharin below 1% of the diet is insufficient to cause a cellular response, and we postulate, therefore, that it is impossible to generate a tumor response below that dose. In addition, based on experiments with a variety of salt forms, it is apparent that whether it is saccharin or the urinary milieu that is important in the induction of bladder epithelium proliferation, the ionic changes in the urine following sodium saccharin administration are critical to the effects seen following such administration. These factors include a relatively high pH, high sodium concentration, and high volume. In extrapolating risk from rat studies to humans, these physiological differences also must be taken into account. In addition, a lack of effect in other species [6, 54, 55] including mouse, hamster, and non-human primate, must be considered in the evaluation.

It is clear from our modeling and that of several other investigators that current approaches to quantitative risk assessment are not based on sound biological foundations. In general, quantitative risk assessment is viewed as a mathematical exercise, extrapolating the results at high doses in animal experiments with high incidence rates [7] to predict results in humans exposed to low doses with vanishingly small incidence rates [53]. These mathematical formulations, whether multi-stage or otherwise, are not grounded in biological thinking, and thus provide no insight into the biology of the system under study. They do not take into explicit account the pharmacokinetics of the administered compound, metabolic activation, interaction with cells, and most importantly, biological response of the target tissue. In the studies described in this paper, such purely mathematical models have no way of addressing biological sensitivity to differences in time of agent administration, such as post-weaning versus *in utero* versus neonatal administration, and certainly do not address such issues as differences in the response to the same test substance, such as saccharin, when it is administered in different salt forms with subsequent different urinary physiology. Even in studies involving classical genotoxic carcinogens, such as FANFT, our modeling and experimental results indicate that it is essential to interpret the observed dose response not only in term of the agent's interaction with DNA, but also by taking into account its effects in target cell proliferation and accumulation. Without taking into account the absence of non-genotoxic influences at lower doses, risk would be overestimated in low dose extrapolations from high dose data. Similar examples are certainly present in other model systems involving other tissues and other species.

Based on contributions by a wide variety of investigators, it is becoming apparent that there are several classes of carcinogens that must be evaluated differently with respect to risk assessment, both in quantitative and biological terms. Figure 5 represents a diagrammatic scheme of such evaluations. If a compound is determined to be carcinogenic in an animal experiment, additional studies are necessary to determine whether this carcinogen reacts with DNA or not. If it does, it is referred to as a genotoxic compound, and if it does not, it is referred to as a non-genotoxic

compound. Genotoxic compounds can be evaluated further with respect to low dose extrapolation based on the pharmacokinetics of the compound in the test species and the likely pharmacokinetics that one could anticipate in the human, as well as differences between the test species and the human in the metabolism of the compound. Determination of DNA adduct levels, even at doses well below those that would be anticipated to result in detectable tumor incidences in large, long-term animal experiments, should considerably improve our ability to extrapolate more realistically the risk to low doses and between species. Although it may not always hold, it is anticipated that genotoxic compounds will result in some DNA adduct formation, even at extremely low doses. If the pharmacokinetics and metabolism indicate a threshold effect for DNA adduct formation, a threshold effect would be anticipated for the biological response in term of tumors. However, it would appear that, in most instances, genotoxic compounds do not have a threshold effect.



**Figure 5. Mechanistic alternatives with genotoxic and non-genotoxic carcinogens.**

Non-genotoxic compounds, on the other hand, appear to operate by more than one mechanism. Compounds such as the phorbol esters and dioxin appear to operate via specific cellular receptors [56, 57]. Since receptors generally have very specific structural requirements and have high affinities to very low compound levels, it is anticipated that these compounds would also be biologically active at low doses and may not experience a no-effect threshold. Again, it would be essential to determine whether there is a cellular response to the receptor binding at low doses.

Other non-genotoxic compounds appear to act entirely without specificity with respect to DNA activation or cellular receptors. Certainly one such example is sodium saccharin; other compounds

are described in the literature, including such non-specific substances as foreign objects in the bladder lumen [2, 3] or thin films placed subcutaneously [58]. Foreign objects appear to act completely by non-chemical means related to a generalized irritative response. Compounds such as saccharin, and numerous others that have been positive in various long-term animal carcinogenesis experiments, appear to act through a cytotoxic effect on the target tissue, sometimes extremely subtle, which results in an increased cell turnover rate in the target tissue [32]. This increased cell turnover rate can be evidenced by either increased synthesis of new cells and/or decreased differentiation and death of cells. Since these compounds act by mechanisms related to toxicity at high doses, one would predict that administration of compounds at sub-toxic levels would not result in tumor formation. This obviously implies the presence of a threshold phenomenon.

An example of such an effect has been illustrated recently with the chemical melamine [59, 60]. Melamine administered to rats at high doses results in the production of urinary calculi, which results in the development of bladder tumors [2, 3, 61]. It is well-known that the formation of urinary calculi, no matter what the substance, produce tumors in rats and mice. This effect occurs also with glass and stainless steel beads, and with cholesterol and paraffin pellets. Obviously, if melamine itself is not causing the bladder tumors, but is acting indirectly by the production of calculi, it does not appear reasonable to extrapolate risk to low doses using any of the commonly employed dose-response models. Below a threshold dose, based on the solubility product of melamine, no calculi would be formed and therefore no tumors would result. A similar argument can be made for other substances that result in bladder calculi such as uric acid [62] or phthalates [63]. Numerous other examples, not only in the bladder system but also in other target tissues [64], are well-known and clearly imply the presence of a threshold effect.

The approach to modeling and risk assessment advocated here is one that begins with a biological underpinning of the phenomena being studied. In chemical carcinogenesis, an experimentally validated and generally accepted paradigm exists, the so-called two-stage theory of carcinogenesis. Although the biological processes and mechanisms may be complex, precluding the use of classical mathematical formulations in modeling, and require data beyond that commonly available from the traditional dose-response experiment, biologically based modeling and analysis is the only risk assessment alternative available if we are interested in reflecting the numerous subtleties inherent in studying the relationship between chemicals and carcinogenesis. Modern technological capabilities [65] should provide us with the means to approach the risk assessment problem better in the future with increasingly scientific acumen.

## ACKNOWLEDGMENTS

We gratefully acknowledge the contributions of the many individuals who have contributed to the research in our laboratory described in this paper. Also we thank Jan Leemkuil for her assistance with the preparation of this manuscript. Research reported in this manuscript has been supported by grants from the Department of Health, State of Nebraska; the National Cancer Institute, CA32513, CA28015, and CA36727; and the International Life Sciences Institute - Nutrition Foundation.

## REFERENCES

- 1 American Cancer Society (1987) Cancer Facts and Figures - 1987. American Cancer Society Inc., New York.
- 2 Clayson, D.B. and Cooper, E.H. (1970) Cancer of the urinary tract. *Adv. Cancer Res.* 13, 271.
- 3 Price, J.M. (1971) Etiology of bladder cancer. *Benign and Malignant Tumors of the Urinary Bladder*. Medical Examination Publ. Co., Inc., Flushing, NY, p. 189.
- 4 IARC Working Group. (1975) Cyclophosphamide. *IARC Monogr.* 26, 165-202.
- 5 Hoover, R. and Hartge, P. (1982) Non-nutritive sweeteners and bladder cancer. *Am. J. Publ. Hlth.* 72, 382-383.
- 6 Office of Technology Assessment (1977) Cancer Testing Technology and Saccharin, U.S. Government Printing Office. Washington, DC.
- 7 Zeise, L., Wilson, R., and Crouch, E.A.C. (1987) Dose-response relationships for carcinogens: A review. *Environ. Hlth. Perspect.* 73, 259-308.
- 8 Greenfield, R.E., Ellwein, L.B., and Cohen, S.M. (1984) A general probabilistic model of carcinogenesis: Analysis of experimental urinary bladder cancer. *Carcinogenesis* 5, 437-445.
- 9 Cohen, S.M. (1978) Toxicity and carcinogenicity of nitrofurans. *Carcinogenesis: A Comprehensive Survey*. Vol. 4 (Nitrofurans), Raven Press, New York, p. 171.
- 10 Klemenic, J.M. and Wang, C.Y. (1978) Mutagenicity of nitrofurans. *Carcinogenesis: A Comprehensive Survey*, Vol. 4 (Nitrofurans), Raven Press, New York, p. 99.
- 11 Swaminathan, S. and Lower, G.M. Jr. (1978) Biotransformation and excretion of nitrofurans. *Carcinogenesis: A Comprehensive Survey*, Vol. 4 (Nitrofurans), Raven Press, New York, p. 59.
- 12 Zenser, T.V., Palmier, M.O., Mattammal, M.B., Bolla, R.I., and Davis, B.B. (1983) Comparative effects of prostaglandin H synthase-catalyzed binding of two 5-nitrofurans urinary bladder carcinogens. *J. Pharmacol. Exp. Ther.* 227, 139-143.
- 13 Spry, L., Lakshmi, V.M., Zenser, T., and Davis, B. (1986) Metabolism and excretion of nitrofurothiazole bladder carcinogens. *J. Pharmacol. Exp. Ther.* 238, 457-462.
- 14 Mattammal, M.B., Zenser, T.V., and Davis, B.B. (1981) Prostaglandin hydroperoxidase-mediated 2-amino-4-(5-nitro-2-furyl) [<sup>14</sup>C]thiazole metabolism and nucleic acid binding. *Cancer Res.* 41, 4961-4966.

- 15 Cohen, S.M., Jacobs, J.B., Arai, M., Johansson, S., and Friedell, G.H. (1976) Early lesions in experimental bladder cancer: Experimental design and light microscopic findings. *Cancer Res.* 36, 2508-2511.
- 16 Cohen, S.M., Murasaki, G., Fukushima, S., and Greenfield, R.E. (1982) Effect of regenerative hyperplasia on the urinary bladder: carcinogenicity of sodium saccharin and N-[4-(5-nitro-2-furyl)-2-thiazolyl]formamide. *Cancer Res.* 42, 65-71.
- 17 Jacobs, J.B., Arai, M., Cohen, S.M., and Friedell, G.H. (1977) A long-term study of reversible and progressive urinary bladder cancer lesions in rats fed N-[4-(5-nitro-2-furyl)-2-thiazolyl]-formamide. *Cancer Res.* 37, 2817-2821.
- 18 Arai, M., Cohen, S.M., Jacobs, J.B., and Friedell, G.H. (1979) Effect of dose on urinary bladder carcinogenesis induced in F-344 rats by N-[4-(5-nitro-2-furyl)-2-thiazolyl]formamide. *J. Nat. Cancer Inst.* 62, 1013-1016.
- 19 Arai, M., St. John, M., Fukushima, S., Friedell, G.H., and Cohen, S.M. (1983) Long-term dose response study of N-[4-(5-nitro-2-furyl)-2-thiazolyl]formamide-induced urinary bladder carcinogenesis. *Cancer Lett.* 18, 261-269.
- 20 Hasegawa, R., Cohen, S.M., St. John, M., Cario, M., and Ellwein, L.B. (1986) Effect of dose on the induction of urothelial proliferation by N-[4-(5-nitro-2-furyl)-2-thiazolyl]formamide and its relationship to bladder carcinogenesis in the rat. *Carcinogenesis* 7, 633-636.
- 21 Tiltman, A.J. and Friedell, G.H. (1972) Effect of feeding N-[4-(5-nitro-2-furyl)-2-thiazolyl]-formamide on mitotic activity of rat urinary bladder epithelium. *J. Nat. Cancer Inst.* 48, 125-129.
- 22 Farber, E. (1984) Cellular biochemistry of the stepwise development of cancer with chemicals: G.H.A. Clowes Memorial Lecture. *Cancer Res.* 44, 5463-5474.
- 23 Murasaki, G. and Cohen, S.M. (1983) Co-carcinogenicity of sodium saccharin and N-[4-(5-nitro-2-furyl)-2-thiazolyl]formamide for the urinary bladder. *Carcinogenesis* 4, 97-99.
- 24 Cohen, S.M., Murasaki, G., Ellwein, L.B., and Greenfield, R.E. (1983) Tumor promotion in bladder carcinogenesis. *Mechanisms of Tumor Promotion*, Vol. I, CRC Press, Boca Raton, FL, p. 131.
- 25 Cohen, S.M., Ellwein, L.B., and Johansson, S.L. (1987) Bladder tumor promotion. *Banbury Report* 25, 55-67.
- 26 Morgan, R.W. and Wong, O. (1985) A review of epidemiological studies on artificial sweeteners and bladder cancer. *Fd. Chem. Toxic.* 23, 529-533.
- 27 Ashby, J. (1985) The genotoxicity of sodium saccharin and sodium chloride in relation to their cancer-promoting properties. *Fd. Chem. Toxic.* 23, 507-519.
- 28 Renwick, A.G. (1985) The disposition of saccharin in animals and man - a review. *Fd. Chem. Toxic.* 23, 429-435.
- 29 Williamson, D.S., Nagel, D.L., Markin, R.S., and Cohen, S.M. (1987) Effect of pH and ions on the electronic structure of saccharin. *Fd. Chem. Toxic.* 25, 211-218.

- 30 Lutz, W.K. and Schlatter, C. (1977) Saccharin does not bind to DNA of liver or bladder in the rat. *Chem.-Biol. Interact.* 19, 253-257.
- 31 Arnold, D.L., Moodie, C.A., Grice, H.C., Charbonneau, S.M., Stavric, B., Collins, B.F., McGuire, P.F., Zawadzka, Z.Z., and Munro, I.C. (1980) Long-term toxicity of ortho-toluene sulfonamide and sodium saccharin in the rat. *Toxicol. Appl. Pharmacol.* 52, 113-152.
- 32 Butterworth, B.E. and Slaga, T.J. (Eds.) (1987) Nongenotoxic mechanisms in carcinogenesis. Banbury Report 25.
- 33 Schoenig, G.P., Goldenthal, E.I., Geil, R.G., Frith, C.H., Richter, W.R., and Carlborg, F.W. (1985) Evaluation of the dose response and *in utero* exposure to saccharin in the rat. *Fd. Chem. Toxic.* 23, 475-490.
- 34 Hicks, R.M. and Chowaniec, J. (1977) The importance of synergy between weak carcinogens in the induction of bladder cancer in experimental animals and humans. *Cancer Res.* 37, 2943-2949.
- 35 Boutwell, R.K. (1964) Some biological aspects of skin carcinogenesis. *Progr. Exptl. Tumor Res.* 4, 207-250.
- 36 Cohen, S.M. (1985) Multi-stage carcinogenesis in the urinary bladder. *Fd. Chem. Toxic.* 23, 521-528.
- 37 Ito, N., Fukushima, S., Shirai, T., and Nakanishi, K. (1983) Effects of promoters of N-butyl-N-(4-hydroxybutyl)nitrosamine-induced urinary bladder carcinogenesis in the rat. *Environ. Hlth. Perspect.* 50, 61-69.
- 38 Fukushima, S., Cohen, S.M., Arai, M., Jacobs, J.B., and Friedell, G.H. (1981) Scanning electron microscopic examination of reversible hyperplasia of the rat urinary bladder. *Am. J. Pathol.* 102, 373-380.
- 39 Fukushima, S., Arai, M., Cohen, S.M., Jacobs, J.B., and Friedell, G.H. (1981) Scanning electron microscopy of cyclophosphamide-induced hyperplasia of the rat urinary bladder. *Lab. Invest.* 44, 89-96.
- 40 Murasaki, G. and Cohen, S.M. (1983) Effect of sodium saccharin on urinary bladder epithelial regenerative hyperplasia following freeze ulceration. *Cancer Res.* 43, 182-187.
- 41 Shirai, T., Cohen, S.M., Fukushima, S., Hananouchi, M., and Ito, N. (1978) Reversible papillary hyperplasia of the rat urinary bladder. *Am. J. Pathol.* 91, 33-48.
- 42 Hasegawa, R., Greenfield, R.E., Murasaki, G., Suzuki, T., and Cohen, S.M. (1985) Initiation of urinary bladder carcinogenesis in rats by freeze ulceration with sodium saccharin promotion. *Cancer Res.* 45, 1469-1473.
- 43 Fukushima, S. and Cohen, S.M. (1980) Saccharin-induced hyperpiasia of the rat urinary bladder. *Cancer Res.* 40, 734-736.
- 44 Murasaki, G. and Cohen, S.M. (1981) Effect of dose of sodium saccharin on the induction of rat urinary bladder proliferation. *Cancer Res.* 41, 942-944.

- 45 Ellwein, L.B. and Cohen, S.M. (In Press) A cellular dynamics model of experimental bladder cancer: Analysis of the effect of sodium saccharin in the rat. *Risk Anal.*
- 46 Newberne, P.M., Suphakarn, V., Punyarit, P., and DeCamargo, J. (1987) Nongenotoxic mouse liver carcinogens. *Banbury Report* 25, 165-178.
- 47 Nakanishi, K., Hagiwara, A., Shibata, M., Imaida, K., Tatematsu, M., and Ito, N. (1980) Dose response of saccharin in induction of urinary bladder hyperplasias in Fischer 344 rats pretreated with N-butyl-N-(4-hydroxy-butyl)nitrosamine. *J. Nat. Cancer Inst.* 65, 1005-1010.
- 48 West, R.W., Sheldon, W.G., Gaylor, D.W., Haskin, M.G., Delongchamp, R.R., and Kadlubar, F. F. (1986) The effects of saccharin on the development of neoplastic lesions initiated with N-methyl-N-nitrosourea in the rat urothelium. *Fund. Appl. Toxicol.* 7, 585-600.
- 49 Hasegawa, R. and Cohen, S.N. (1986) The effect of different salts of saccharin on the rat urinary bladder. *Cancer Lett.* 30, 261-268.
- 50 Fukushima, S., Kurata, Y., Shibata, M.-A., Ikawa, E., and Ito, N. (1984) Promotion by ascorbic acid, sodium erythorbate and ethoxyquin of neoplastic lesions in rats initiated with N-butyl-N-(4-hydroxybutyl) nitrosamine. *Cancer Lett.* 23, 29-37.
- 51 Fukushima, S., Thamavit, W., Kurata, Y., and Ito, N. (1986) Sodium citrate: A promoter of bladder carcinogenesis. *Jpn. J. Cancer Res. (Gann).* 77, 1-4.
- 52 Fukushima, S., Shibata, M.-A., Shirai, T., Tamano, S., and Ito, N. (1986) Roles of urinary sodium ion concentration and pH in promotion by ascorbic acid of urinary bladder carcinogenesis in rats. *Cancer Res.* 46, 1623-1626.
- 53 Carlborg, F.W. (1985) A cancer risk assessment for saccharin. *Fd. Chem. Toxic.* 23, 499-506.
- 54 Fukushima, S., Arai, M., Nakanowatari, J., Hibino, T., Okuda, M., and Ito, N. (1983) Differences in susceptibility to sodium saccharin among various strains of rats and other animal species. *Gann.* 74, 8-20.
- 55 IARC Working Group. (1980) Saccharin. *IARC Monogr.* 22, 111-170.
- 56 Ashendel, C.L. (1985) The phorbol ester receptor: A phospholipid-regulated protein kinase. *Biochem. Biophys. Acta* 822, 219-242.
- 57 Boreiko, C.J. (1987) Modulation of transformed focus formation in cultures of C3H/10T1/2 cells. *Banbury Report* 25, 287-296.
- 58 Brand, K.G. (1987) Solid state carcinogenesis. *Banbury Report* 25, 205-213.
- 59 Melnick, R.L., Boorman, G.A., Haseman, J.K., Montali, R.J., and Huff, J. (1984) Urolithiasis and bladder carcinogenicity of melamine in rodents. *Toxicol. Appl. Pharmacol.* 72, 292-303.
- 60 Tennant, R.W. (1987) Some implications and limitation of *in vitro* genetic toxicity data in regulatory decisions. *Banbury Report* 25, 339-353.
- 61 Clayson, D.B. (1974) Bladder carcinogenesis in rats and mice: Possibility of artifacts. *J. Nat. Cancer Inst.* 52, 1685-1689.

- 62 Shirai, T., Ikawa, E., Fukushima, S., Masui, T., and Ito, N. (1986) Uracil-induced urolithiasis and the development of reversible papillomatosis in the urinary bladder of F-344 rats. *Cancer Res.* 46, 2062-2067.
- 63 Heck, H.D'A. and Tyl, R.W. (1985) The induction of bladder stones by terphthalic acid, dimethyl terphthalate, and melamine (2,4,6-triamino-s-thiazine) and its relevance to risk assessment. *Regulat. Toxicol. Pharmacol.* 5, 294-313.
- 64 Maeura, Y., Weisburger, J.H., and Williams, G.M. (1984) Dose-dependent reduction of N-2-fluorenylacetamide-induced liver cancer and enhancement of bladder cancer in rats by butylated hydroxytoluene. *Cancer Res.* 44, 1604-1610.
- 65 Reynolds, S.H., Stowers, S.J., Patterson, R.M., Maronpt, R.R., Aaronson, S.A., and Anderson, M.W. (1987) Activated oncogenes in B<sub>6</sub>C<sub>3</sub>F<sub>1</sub> mouse liver tumors: implications for risk assessment. *Science* 237, 1309-1316.

**MODELING OF RECEPTOR-MEDIATED PHARMACODYNAMICS OF PREDNISONE IN THE RAT**

**William J. Jusko**

**Department of Pharmaceutics, State University of New York, Buffalo, NY 14260**

**Manuscript Not Submitted**

## A PHARMACODYNAMIC MODEL FOR SOMAN IN THE RAT

Donald M. Maxwell, Constantine P. Vlahacos, and David E. Lenz

*United States Army Medical Research Institute of Chemical Defense, Aberdeen Proving Ground, MD*

### SUMMARY

A pharmacodynamic model for inhibition of acetylcholinesterase (AChE) by soman was developed to describe the intertissue differences in AChE inhibition, the dose response of AChE to inhibition by soman, and the effect of differences in xenobiotic metabolism on soman toxicity. Based on the principles of physiological pharmacokinetics, this pharmacodynamic model consisted of a set of mass balance equations that included parameters for blood flow, tissue volumes, soman metabolism, tissue/plasma partition coefficients, initial AChE levels, and the rate constant for AChE inhibition. Sensitivity analysis of the model revealed that variation of the soman metabolism parameter in plasma was the most important determinant of variation in the inhibition of brain AChE by soman.

### INTRODUCTION

Soman (pinacolymethylphosphonofluoridate) is one of the organophosphorus agents whose toxicity in mammals is believed to be due to its irreversible inhibition of acetylcholinesterase (AChE; EC 3.1.1.7), an enzyme that terminates the action of the neurotransmitter acetylcholine by catalyzing its hydrolysis [1,2]. The increase of acetylcholine at cholinergic synapses resulting from inhibition of AChE, particularly in brain, produces a variety of pharmacological effects, which culminate in convulsions and death by respiratory failure [3,4].

The kinetics of the *in vitro* reaction of soman with purified mammalian AChE has been described in detail [5,6], but the *in vivo* kinetics of AChE inhibition by soman are poorly understood because of additional factors – detoxification, blood flow, agent distribution – that are involved. In addition to its reaction with AChE, soman reacts with three other enzymes – diisopropylfluorophosphatase (DFPase; EC 3.8.2.1), carboxylesterase (CaE; EC 3.1.1.1), and butyrylcholinesterase (BuChE; EC 3.1.1.8). DFPase catalyzes the hydrolysis of soman [7], whereas CaE and BuChE react irreversibly with soman in a manner analogous to its reaction with AChE [8]. The inhibition of CaE and BuChE by organophosphorus agents produces no toxic effect [9,10], and these reactions are important only as potential detoxification reactions since they stoichiometrically reduce the amount of soman available to inhibit AChE. The importance of CaE as a detoxification reaction has been demonstrated by the potentiation of soman toxicity in CaE-inhibited animals [11,12]. Reactions of soman with BuChE are probably not significant means of detoxification since inhibition

of BuChE does not potentiate soman toxicity [11], and BuChE levels in mammals are one-thousandth the levels of CaE [13].

An additional complication in studying the reactions of soman with multiple enzymes is soman's chirality. Soman contains two asymmetric centers and exists usually as equal amounts of four stereoisomers. The rates of reaction of these stereoisomers with mammalian AChE, CaE, and DFPase differ [14,15,16], but the major differences are attributable to the phosphorus chiral center with only small differences due to the carbon chiral center (Table 1). The P(+) isomers are rapidly hydrolyzed by DFPase *in vitro* and have short *in vivo* half-lives. These P(+) isomers are also poor *in vitro* inhibitors of AChE and are relatively nontoxic *in vivo*. The P(-) isomers are slowly hydrolyzed *in vitro* by DFPase and have longer *in vivo* half-lives than P(+) isomers. P(-) isomers are excellent *in vitro* inhibitors of AChE and are highly toxic *in vivo*.

TABLE 1. RATES OF REACTIONAL STEREOISOMERS

Soman Stereoisomer	Relative Toxic Dose <sup>a</sup>	Relative Reactivity with AChE <sup>b</sup>	Relative Hydrolysis by DFPase <sup>c</sup>	Relative Reactivity with CaE <sup>d</sup>
C(-) P(-)	1.0	36,000	1.0	1.0
C(+) P(-)	2.6	56,000	2.2	1.0
C(-) P(+)	59.2	1	800.0	75.5
C(+) P(+)	171.1	1	2300.0	134.9

<sup>a</sup> LD<sub>50</sub> in mice from Benschop et al. [14].

<sup>b</sup> Inhibition of electric eel AChE from Benschop et al. [14].

<sup>c</sup> Hydrolysis of soman by rat plasma from Benschop et al. [19].

<sup>d</sup> Inhibition of mouse plasma CaE from Clement et al. [16].

Although models have been developed to measure the concentration of soman stereoisomers in biological samples [15,17], *in vivo* pharmacokinetic studies of soman have been hindered by the rapid detoxification of soman and the lack of sensitivity of the analytical procedures. Less than 1% of an administered dose of soman is detected as unchanged soman 1-2 min after iv injection in mice or rats [15,17,18]. Lack of analytical sensitivity has necessitated pharmacokinetic studies with administered soman doses of 3-6 LD<sub>50</sub> in animals that are artificially ventilated and atropinized to prevent respiratory failure and death.

Several models to describe various aspects of the pharmacokinetics or pharmacodynamics of soman have been developed by investigators. The pharmacokinetics of 3-6 LD<sub>50</sub> doses of soman have been described by a three-compartment open model that is nonlinear with dose [19]. A schematic four-compartment pharmacodynamic model for soman, which incorporates AChE, agent detoxification, blood flow, and transport has been used to describe qualitatively interagent and

intertissue differences in AChE inhibition [20]. A quantitative one-compartment pharmacodynamic model was developed to describe the competing *in vivo* reactions of AChE, DFPase, and CaE with organophosphorus agents [21]. A multiple regression model has been used to quantitate the relative importance of blood flow and tissue levels of AChE, BuChE, CaE, and DFPase on the kinetics of cholinesterase inhibition by soman in rats [13]. In our current investigations, we attempted to combine the significant features of each of these models into a comprehensive model of the pharmacokinetics/pharmacodynamics of soman.

In this paper our specific goals are to (1) describe the variation of *in vivo* AChE inhibition by soman with respect to time after administration, dose, and level of xenobiotic metabolism; (2) present a pharmacodynamic model of AChE inhibition based on the mass-balance principles of physiological pharmacokinetics [22,23]; (3) test the pharmacodynamic model by comparing experimental and model-predicted values of AChE inhibition; and (4) analyze the sensitivity of predicted AChE inhibition to changes in model parameters.

## **MATERIALS AND METHODS**

### ***Animals***

Male Sprague-Dawley rats (230-250 g) were obtained from Charles River Laboratories, Wilmington, MA. The rats were housed in temperature-controlled animal quarters that were maintained on a 12-h alternating light/dark cycle with artificial light provided between 0600 and 1800. All experiments were carried out between 0800 and 1200. Laboratory rat chow and water were available *ad libitum*.

### ***Materials***

Soman was obtained from Chemical Research, Development and Engineering Center, Aberdeen Proving Ground, MD, and was 98.6% pure when analyzed by  $^{31}\text{P}$  nuclear magnetic resonance spectroscopy. [ $^{14}\text{C}$ ] Acetyl- $\beta$ -methylcholine was synthesized by Amersham, Arlington Heights, IL. Triton X-100 and sucrose were purchased from Sigma Chemical Co., St. Louis, MO. All other chemicals were reagent grade and used as supplied.

### ***Injection procedures and tissue preparation***

Soman was diluted in isotonic saline for administration to rats by i.m. injection in the right hind limb or i.v. injection in the tail vein. Injection volume was 1 mL/kg for either injection route. Control rats received saline injections. Tissue samples and heparinized blood for AChE and CaE analyses were taken from halothane-anesthetized rats that were exsanguinated via cardiac puncture and perfused with 150 mL of saline prior to tissue excision. Tissues were prepared for AChE and CaE analyses by homogenization in nine volumes of isotonic saline containing 1% Triton X-100. Tissue homogenates

were centrifuged at 15,000 x g for 10 min. The resultant supernatants were analyzed for AChE and CaE activity.

#### **Enzyme analysis**

AChE activity was assayed by the method of Siakotos et al. [24] using [ $^{14}\text{C}$ ] acetyl- $\beta$ -methylcholine, a specific substrate for AChE. CaE was assayed by the method of Ecobichon [25] using  $\alpha$ -naphthylacetate as brain membrane AChE substrate. Soman hydrolysis by DFPase was assayed by the method of Maxwell et al. [13].

#### **Kinetic constants**

The *in vitro* bimolecular rate constants describing the reaction of soman with CaE and AChE were determined for rat liver microsomal CaE and rat brain membrane AChE. Rat liver microsomes were prepared by the method of Little [26], and rat brain membranes were prepared by the method of Yamamura and Snyder [27]. These preparations were further solubilized with 0.5% Triton X-100 and centrifuged at 100,000 x g for 30 min to yield liver microsomal CaE and brain membrane AChE. The reaction of soman with these enzymes was determined by following the inhibition of CaE or AChE at pH 7.4 and 37°C. Soman (12.5  $\mu\text{L}$ ) was added to each enzyme preparation (112.5  $\mu\text{L}$ ) and samples (255  $\mu\text{L}$ ) were taken at different time intervals to measure enzyme activity. Inhibition was stopped by dilution, and enzyme activity was immediately determined as previously described. Bimolecular rate constants were calculated by the method of Reiner and Aldridge [28] with at least three soman concentrations for at least four incubation times. The kinetic constants for DFPase-catalyzed hydrolysis of soman in rat plasma were measured at pH 7.4 and 37°C. The maximal velocity ( $V_{\text{max}}$ ) and Michaelis constant ( $K_M$ ) were calculated by nonlinear regression of the hyperbolic function for Michaelis-Menten enzyme kinetics described by Webb [29].

#### **Acute toxicity**

LD<sub>50</sub> values were calculated by probit analysis [30] of deaths occurring within 24 h following administration of soman at 5 different doses with 6 animals per dose.

#### **Physiological pharmacodynamic model**

A flow-limited physiological pharmacokinetic model based on a standard flow scheme (Figure 1) was used to develop the pharmacodynamic model. Each tissue compartment was assumed to be well mixed and homogeneous, and compartments were assumed to be interconnected only through the circulatory system. In each tissue compartment it was further assumed that soman could bind reversibly to tissue, bind irreversibly to AChE and CaE, and undergo hydrolysis by DFPase. The system of mass-balance equations for this pharmacodynamic model was as follows.

Blood

$$\begin{aligned}
d[S]_{Pl}/dt = & (Q_{Br}[S]_{Br}/R_{Br} + Q_{Li}[S]_{Li}/R_{Li} + Q_{Kid}[S]_{Kid}/R_{Kid} + Q_{Mu}[S]_{Mu}/R_{Mu} \\
& + Q_{Dia}[S]_{Dia}/R_{Dia} + Q_H[S]_H/R_H + Q_{Car}[S]_{Car}/R_{Car})/V_{Pl} \\
& - [S]_{Pl}(k_{AChE}[AChE]_{Pl} + k_{CaE}[CaE]_{Pl} + k_{Pl}) \\
& - Q_{Pl}[S]_{Pl}/V_{Pl} + D/2)g(t) \\
d[AChE]_{Pl}/dt = & -k_{AChE}[AChE]_{Pl}[S]_{Pl} \\
d[CaE]_{Pl}/dt = & -k_{CaE}[CaE]_{Pl}[S]_{Pl}
\end{aligned}$$

Other tissues

$$\begin{aligned}
d[S]_i/dt = & Q_i([S]_{Pl} - [S]_i/R_i)/V_i - [S]_i(k_{AChE}[AChE]_i + k_{CaE}[CaE]_i + k_i) \\
d[AChE]_i/dt = & -k_{AChE}[AChE]_i[S]_i \\
d[CaE]_i/dt = & -k_{CaE}[CaE]_i[S]_i
\end{aligned}$$

[S] = soman concentration (M); [AChE] = AChE concentration (M); [CaE] = CaE concentration (M);  
Q = plasma flow through tissue (L/min); V = volume of tissue (L); R = tissue/plasma partition  
coefficient (dimensionless);  $k_{AChE}$  = bimolecular rate constant for reaction of soman and AChE  
(M<sup>-1</sup>min<sup>-1</sup>);  $k_{CaE}$  = bimolecular rate constant for reaction of soman and CaE (M<sup>-1</sup>min<sup>-1</sup>);  $k$  = observed  
first-order rate constant for DFPase-catalyzed hydrolysis of soman (min<sup>-1</sup>);  $t$  = time (min);  
D/2 = administered dose of soman corrected for amount of P(-) isomers (moles);  $g(t)$  = function  
describing introduction of soman into blood; Pl = plasma; Br = brain; Li = liver; Kid = kidney;  
Mu = muscle; Dia = diaphragm; H = heart; Car = carcass; and  $i$  = any tissue except blood.

Solutions of this system of differential equations were obtained by use of GEAR software [31]  
from the International Mathematical and Statistical Libraries, Houston, TX.

### Model testing

The agreement between pharmacodynamic model predictions and experimental data was  
tested by comparing tissue AChE levels predicted by the model with AChE levels measured in rats  
receiving soman. The theoretical predictions of AChE activity were considered to agree with

experimental values if they were within one standard deviation of the mean of the experimental AChE measurements.

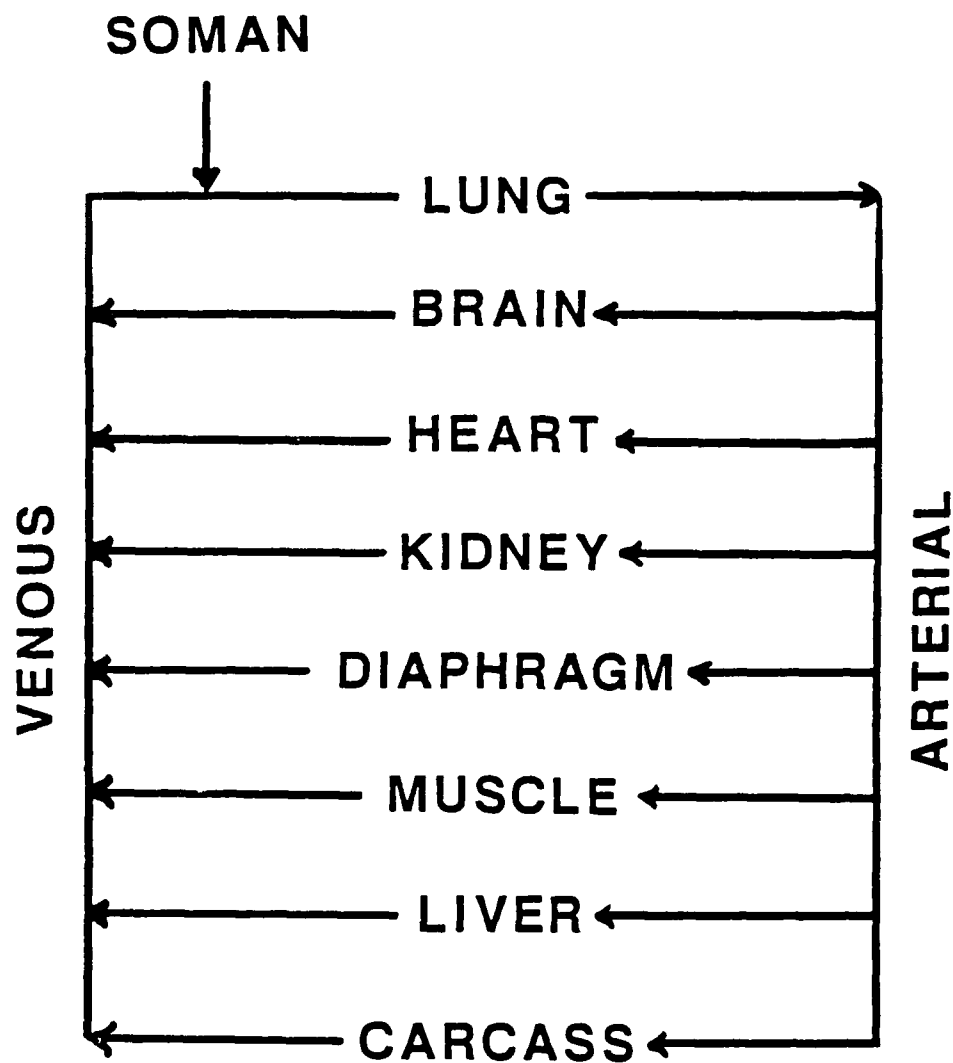


Figure 1. Flow diagram of a physiological pharmacodynamic model for soman.

#### ***Sensitivity analysis***

The sensitivity of the predicted model response to the variation of model parameters was measured by incremental sensitivity analysis [32]. Parameters were varied one at a time by a chosen increment, and computer simulation was used to generate the model response to these incremented values.

#### ***Data analysis***

Significant differences in the mean values of experimental data were identified by the Tukey honestly significant difference test [33]. Differences were considered significant if  $p < 0.05$ .

## RESULTS

The *in vitro* characterization of the fast reactions of P(-) isomers of soman with AChE and CaE is shown in Figure 2. By carefully choosing soman concentrations and short reaction times, interference by competing reactions of P(+) isomers with AChE and CaE was avoided. The reactions of soman with AChE and CaE are irreversible and stoichiometric and are followed by measuring inhibition of enzyme activity vs. time after addition of different soman concentrations. The bimolecular rate constant describing the reaction of soman with AChE ( $3.7 \times 10^7 \text{ M}^{-1} \text{ min}^{-1}$ ) was about tenfold greater than the bimolecular rate constant for the reaction of soman and CaE ( $4.1 \times 10^6 \text{ M}^{-1} \text{ min}^{-1}$ ).

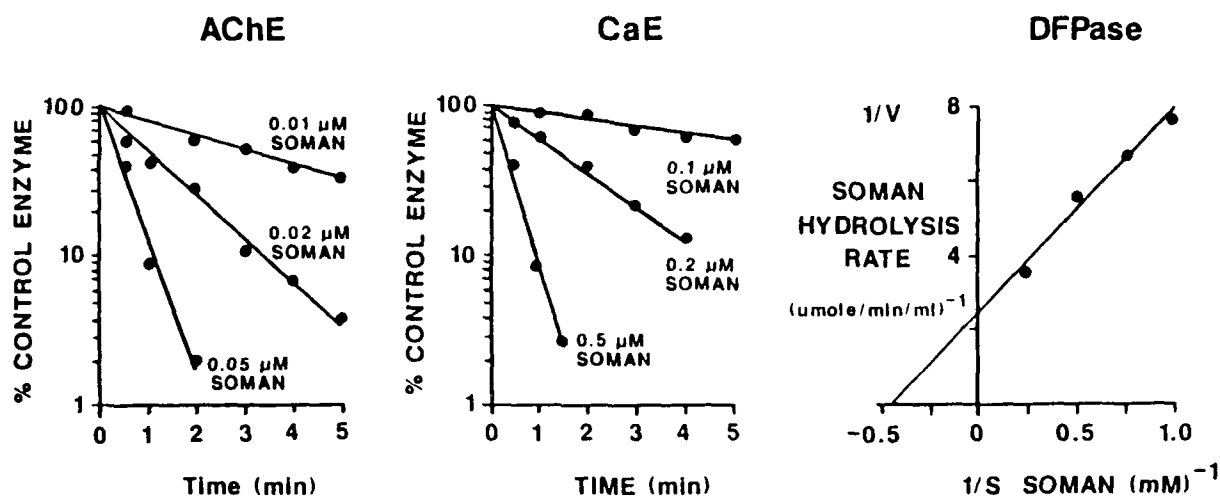


Figure 2. The reactions of soman with AChE, CaE, and DFPase from rats. Reactions were measured at pH 7.4 and 37°C. The bimolecular rate constants for enzyme inhibition by soman were determined to be  $3.5 (\pm 0.5) \times 10^7 \text{ M}^{-1} \text{ min}^{-1}$  for rat brain AChE and  $5.0 (\pm 0.6) \times 10^6 \text{ M}^{-1} \text{ min}^{-1}$  for rat liver CaE. The maximal velocity ( $V_{\text{max}}$ ) and Michaelis constant ( $K_M$ ) for hydrolysis of soman by rat plasma DFPase were determined to be  $0.44 (\pm 0.08) \mu\text{mole}^{-1} \text{ min}^{-1} \text{ mL}^{-1}$  plasma for  $V_{\text{max}}$  and  $1.07 (\pm 0.14) \text{ mM}$  for  $K_M$ . All determinations were done in triplicate. Kinetic constants are expressed as mean values with standard deviation in parentheses.

Soman is a substrate for DFPase, and its enzyme-catalyzed hydrolysis was followed by the production of acid resulting from this reaction. These hydrolysis rates characterized the DFPase activity with the toxic (P-) isomers of soman, since they were measured after the initial rapid degradation of (P+) isomers was complete. A double reciprocal plot (Figure 2) of the rate of soman hydrolysis by rat plasma vs. initial soman concentration demonstrated typical Michaelis-Menten kinetics.  $V_{\text{max}}$  ( $0.44 \mu\text{mole}/\text{min}/\text{mLplasma}$ ) and  $K_M$  ( $2.17 \text{ mM}$ ) for this reaction were calculated by nonlinear regression. DFPase activity in liver, lung, or kidney was greater than DFPase activity in plasma of rats. DFPase activities in these tissues (liver =  $2.51 \mu\text{mole}/\text{min}/\text{g}$ ; lung =  $0.95 \mu\text{mole}/\text{min}/\text{g}$ ; and kidney =  $2.84 \mu\text{mole}/\text{min}/\text{g}$ ) were determined at 5 mM soman concentration and assumed to estimate  $V_{\text{max}}$  for these tissues.

The maximal levels of AChE inhibition in tissues after a 1 LD<sub>50</sub> dose of soman administered by iv, im, or inhalation routes are shown in Figure 3. Although the administered LD<sub>50</sub> of soman varies twofold between i.v., i.m., and inhalation routes, these equitoxic doses of soman produced similar patterns of AChE inhibition, regardless of the route of administration. The times of maximal brain AChE inhibition varied from 2 min after iv administered to 30 min after im administration. AChE inhibition occurred too rapidly after iv dosing to permit measurement of the time course of AChE inhibition in different tissues. Therefore, the im route of administration was chosen for subsequent experiments.

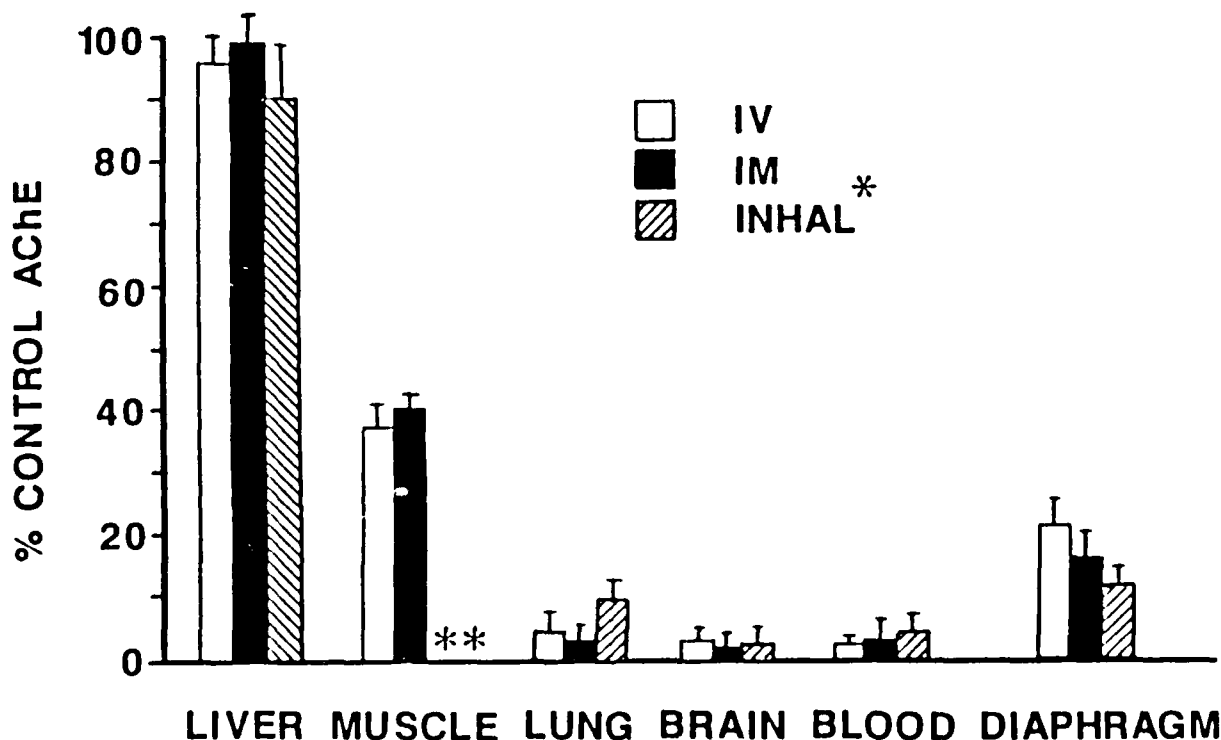


Figure 3. Maximal inhibition of AChE by 1 LD<sub>50</sub> of soman in rats. Doses of soman were 63 µg/kg (i.v.), 107 µg/kg (i.m.), and 128 µg/kg (inhalation). AChE levels were measured 2 min (i.v.), 30 min (i.m.), and 30 min (inhalation) after soman. Values are  $\bar{X} \pm SD$  (n = 6). (\*) Inhalation data were taken from Aas et al. [35] with LD<sub>50</sub> calculated from lethal vapor concentration  $\times$  time  $\times$  alveolar ventilation. (\*\*) No data available.

The time course of *in vivo* AChE inhibition in tissues of rats after an im dose of soman is shown in Figure 4. The maximal level of AChE inhibition as well as the time course of AChE inhibition varied dramatically between tissues. Maximal observed inhibition of AChE activity was achieved in all tissues by 16 min. This suggests that soman is completely absorbed from the im injection site in 16 min. If we assume complete absorption (98%) after six absorption half-lives, then each half-life is 2.7 min. The equivalent first-order absorption rate constant is  $0.693/2.7 \text{ min} = 0.26 \text{ min}^{-1}$ , which was used for subsequent modeling of im absorption of soman. An attempt to model the tissue pattern of AChE inhibition was made using a physiological pharmacodynamic model incorporating the model

parameters in Table 2. The levels of AChE predicted by the pharmacodynamic model are compared to experimental values in Figure 4. Since the predicted AChE values are within the error limits of the experimental values for most time points, the model performed sufficiently well to encourage further testing.

TABLE 2. MODEL AChE PARAMETERS

Tissue	Volume (mL) <sup>a</sup>	Plasma Flow (mL/min) <sup>a</sup>	Initial AChE (nmole) <sup>b</sup>	Initial CaE (nmole) <sup>b</sup>	DFPase $V_{max}/K_m$ (min <sup>-1</sup> ) <sup>c</sup>	Tissue/Plasma Partition Coefficient <sup>d</sup>
Brain	2.91	1.5	0.110	1.6	0	1.0
Lung	1.55	42.3	0.003	20.0	0.44	8.0
Muscle	127.5	11.2	0.843	65	0	2.0
Diaphragm	0.75	0.27	0.004	0.4	0	2.0
Kidney	2.10	6.4	0.001	34.6	1.31	3.0
Heart	0.71	0.8	0.003	1.4	0	2.0
Liver	10.1	8.0	0.009	459.8	1.16	1.0
Plasma	9.8	42.3	0.011	41.1	0.20	—
Carcass	94.6	14.4	0	1200	0	1.0

a. Data taken from Gerlowski and Jain [23] and Maxwell *et al.* [13].

b. Data taken from Maxwell *et al.* [13].

c. Rate constant ( $k$ ) for hydrolysis of soman by DFPase. Calculated from  $V_{max}/K_m$  since *in vivo* concentrations are much less than  $K_m$  of DFPase.

d. Calculated from tissue/plasma ratio of radiolabeled soman during elimination phase. Data taken from Reynolds *et al.* [18].

The *in vivo* dose response of rat brain AChE to inhibition by soman is shown in Figure 5. The levels of AChE inhibition resulting from administration of different soman doses were predicted by use of the pharmacodynamic model and compared to the experimental values. The predicted AChE levels in brain agreed with the experimental values across the range of soman doses.

The sensitivity of the pharmacodynamic response of the model to changes in model parameters was analyzed by incremental sensitivity analysis. Formal differential sensitivity analysis was not possible because of the complexity and size of the system of equations that constitute the pharmacodynamic model. AChE inhibition in brain was chosen as the model response upon which to evaluate the effects of parameter variation because of the important central role of brain AChE in the toxicological response to soman. Table 3 contains the results of the analysis of the sensitivity of brain AChE to 10% increases in a variety of model parameters. The magnitude of change of brain AChE inhibition to equal variation in each parameter defined the relative importance of each parameter in generating a model response. Plasma CaE produced the greatest change in brain AChE (+4.7%) inhibition followed by plasma flow to brain (-3.2%). Except for small effects of 10% changes in brain

values of AChE, CaE, and R, all other tissue parameters produced no effect ( $<0.1\%$ ) on the predicted level of inhibition of brain AChE. The effect of changes in the bimolecular rate constants for reaction of soman with AChE and CaE were roughly equal but in opposite directions. Since bimolecular rate constants do not normally vary and plasma flow to brain is maintained at constant levels in animals under normal circumstances, this analysis suggests that plasma CaE is the most likely parameter to produce variation in inhibition of brain AChE by soman.

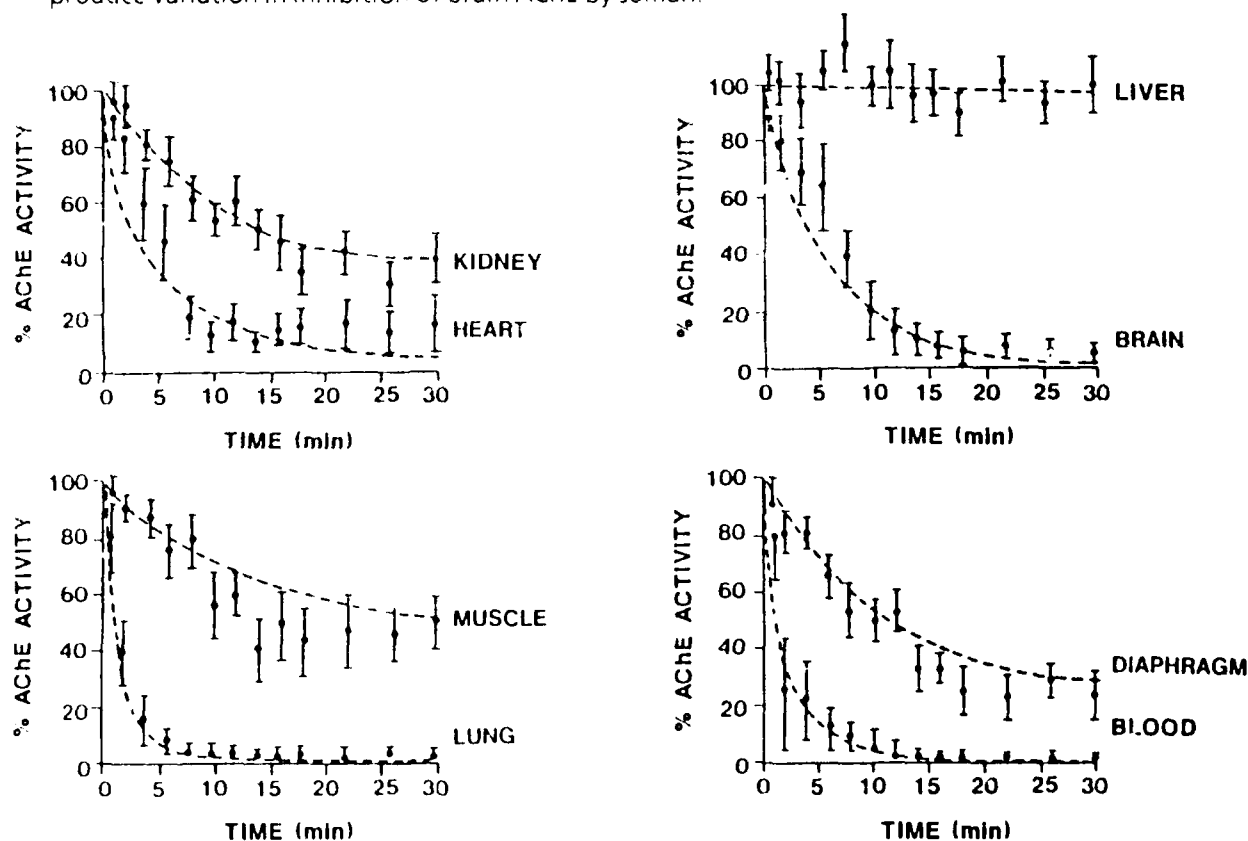


Figure 4. Time course of AChE inhibition in rat tissues after 90 µg/kg soman, im. Points represent  $\bar{X} \pm SD$  ( $n = 6$ ) for experimental values. The curves (—) represent model predictions.

The  $LD_{50}$  of soman increases in rats as they age from 30 days to 60 days and then decreases by 50% as rats age to 120 days (Table 4). The importance of plasma CaE, established by sensitivity analysis, suggested that plasma CaE could contribute to this variation in soman toxicity. To test this hypothesis using our pharmacodynamic model, parameters were scaled for the change in size of rats as they age except for the concentration of plasma CaE, which was experimentally determined. These altered model parameters were then used to predict the level of soman required to cause 99% inhibition of brain AChE to simulate an  $LD_{50}$  dose. The agreement between the predicted and measured  $LD_{50}$  values shown in Table 4 supports the hypothesis that changes in plasma CaE make an important contribution to the change of soman  $LD_{50}$  in aging rats.

TABLE 3. SENSITIVITY OF BRAIN AChE INHIBITION TO CHANGES IN MODEL PARAMETERS

Parameter	% Change in Brain AChE Inhibition When Model Parameter Is Increased 10% <sup>a</sup>			
	Brain	Plasma	Lung	Liver
[AChE]	+0.8	<0.1	<0.1	<0.1
[CaE]	+1.4	+4.7	<0.1	<0.1
Q	-3.2	<0.1	<0.1	<0.1
R	-0.4	<0.1	<0.1	<0.1
k for DFPase		<0.1	<0.1	<0.1
k <sub>AChE</sub> <sup>b</sup>		-2.7		
k <sub>CaE</sub> <sup>b</sup>		+3.9		

a. Model predictions of percent change in brain AChE inhibition at 30 min after im administration of 50 µg/kg soman.

b. General model parameters that do not vary with tissue.

TABLE 4. PREDICTION OF CHANGES IN SOMAN TOXICITY IN AGING RATS

Age (days)	Experimental Soman LD <sub>50</sub> (µg/kg) <sup>a</sup>	Model Parameters		Predicted Soman LD <sub>50</sub> (µg/kg) <sup>d</sup>
		Weight (g) <sup>b</sup>	Plasma Cae (nmole/mL) <sup>c</sup>	
30	87 <sup>e</sup> (78-99)	110	3.6 ± 0.2	90
60	117 (105-134)	281	4.2 ± 0.3	111
90	68 <sup>e</sup> (62-76)	451	2.5 ± 0.1	72
120	59 <sup>e,f</sup> (52-68)	494	1.0 ± 0.1	52

a. LD<sub>50</sub> of soman administered im with 95% confidence limits in parentheses.

b. Used to scale parameters for pharmacodynamic model predictions.

c. Values are X ± SD (n = 6).

d. LD<sub>50</sub> predicted from dose of soman necessary to inhibit 99% of brain AChE.

e. Significantly different from 60-day-old rat.

f. Significantly different from 30-day-old rat.

## DISCUSSION

The validity of the pharmacodynamic model that we have developed to describe the *in vivo* inhibition of AChE was supported by several types of observations. There was good agreement between the model predictions and experimental data for the *in vivo* time course of AChE inhibition by soman in a variety of tissues (Figure 4), the dose response of maximal AChE inhibition in brain (Figure 5), and the effect of changes in soman metabolism on soman toxicity in aging rats (Table 4). In addition, the relative importance of various model parameters on model response determined by sensitivity analysis (Table 3) agrees with the conclusions resulting from other research methods. For example, the importance of plasma CaE in determining the availability of soman to inhibit brain AChE, which was suggested by sensitivity analysis, is also suggested by pharmacological investigations. When plasma CaE is selectively inhibited by cresylbenzodioxaphosphorin oxide at a dose that does not inhibit AChE, the dose of soman inhibits brain AChE as well as to produce lethality is reduced [11,12]. The importance of blood flow on the inhibition of AChE has been suggested previously by multiple linear regression of the factors that produce differences in cholinesterase inhibition among tissues. Intertissue variation in blood flow was found to be the most important factor in explaining the intertissue differences in the rates of *in vivo* inhibition of cholinesterase by soman [13].

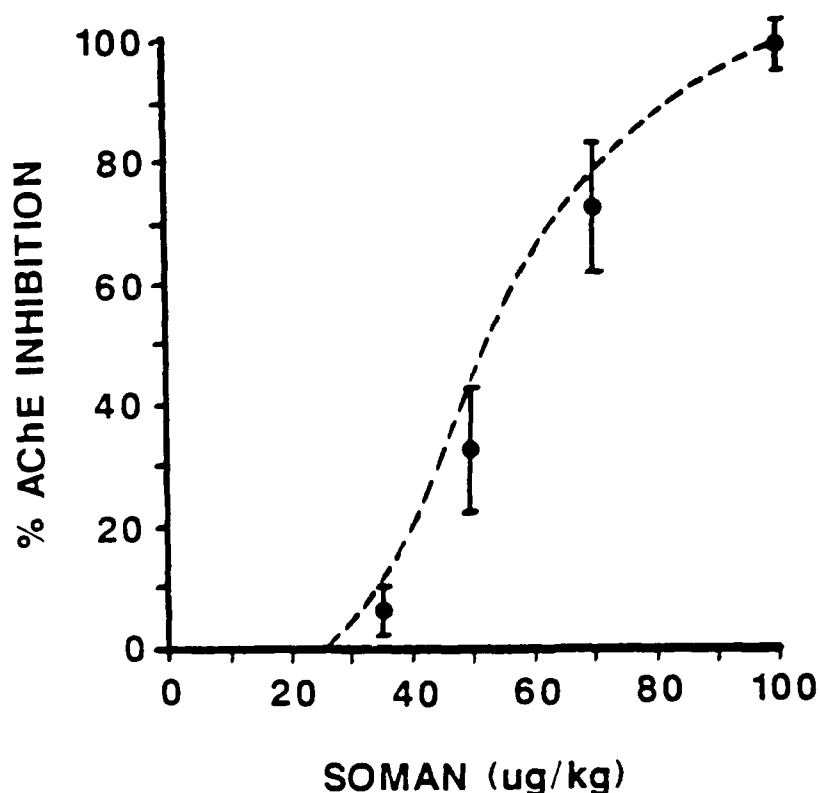


Figure 5. Dose response of brain AChE to inhibition by soman in rats. AChE inhibition was measured 30 min after soman was administered im. Points represent  $\bar{X} \pm SD$  ( $n = 6$ ) for experimental values. Curve (---) represents model predictions.

Although our model was designed to predict AChE inhibition by soman, its structure is such that the same system of equations also predicts pharmacokinetics of soman. At the doses of soman used in our pharmacodynamic studies ( $\leq 1$  LD<sub>50</sub>), experimental measurements of soman concentration are complicated by soman's rapid metabolism. At higher doses (3-6 LD<sub>50</sub>) measurements of soman concentration for pharmacokinetic analysis are performed more easily in order to maintain the versatility of the model to describe either the pharmacodynamics or pharmacokinetics of soman over a wide dose range, the complexity of the model has not been minimized to create a parsimonious model describing only the current pharmacodynamic data. Sensitivity analysis indicated that such parameters as tissue/plasma partition coefficients ( $R$ ) and DEPase ( $k$ ) could be removed from the model without significantly affecting model response. However, at higher doses of soman, these parameters may be important in explaining such phenomena as tissue depots for soman [34] and terminal soman elimination processes [19].

Since the patterns of maximal AChE inhibition in tissues after equitoxic doses of soman are similar (Figure 3), it may be possible to use our pharmacodynamic model as a general model for systemic exposure to soman by merely varying the dosing function. Testing this concept would require the accumulation of data bases for other exposure routes similar to the im administration data that were used to develop the present model. In addition to using the model for describing exposure to soman by other routes, the model has the potential for describing soman exposure in other species if model parameters for those species can be obtained.

#### ACKNOWLEDGMENTS

The authors thank Karen Brecht, Karen Fox-Talbot, and Maj. James Little for their generous technical assistance.

#### REFERENCES

1. Karczmar, A.G. (1970) History of the research with anticholinesterase agents. In: A.G. Karczmar (Ed.), *Anticholinesterase Agents*, Vol. 1, *International Encyclopedia of Pharmacology and Therapeutics*, Sec. 13. Pergamon Press, Oxford.
2. Taylor, P. (1985) Anticholinesterase agents. In: A.G. Gilman, L.S. Goodman, T.W. Rall, and F. Murad (Eds.), *The Pharmacological Basis of Therapeutics*. MacMillan, New York, pp. 115-129.
3. Enimblecombe, R.W. (1977) Drugs acting on central cholinergic mechanisms and affecting respiration. *Pharmacol. Ther.* 3, 65-74.
4. Metcalf, L.L. (1971) Organophosphorus pesticides. *Pharmacology. Prog. Med. Chem.* 8, 1-21.
5. Andersen, R.A., Aaraas, L., Gaare, G., and Fonnum, F. (1977) Inhibition of acetylcholinesterase from different species by organophosphorus compounds, carbamates, and methylsulphonylfluoride. *Gen. Pharmacol.* 8, 331-334.

- 6 Gray, P.J. and Dawson, R.M. (1987) Kinetic constants for the inhibition of eel and rabbit brain acetylcholinesterase by some organophosphates and carbamates of military significance. *Toxicol. Appl. Pharmacol.* 91, 140-144.
- 7 Gay, D.D. and Hoskins, F.C.G. (1979) Stereospecificity and active site requirements in a diisopropylphosphorofluoridate-hydrolyzing enzyme. *Biochem. Pharmacol.* 28, 1259-1261.
- 8 Ooms, A.J.J. and Breebaart-Hansen, J.C.A.E. (1965) The reaction of organophosphorus compounds with hydrolytic enzymes: The inhibition of horse liver aliesterase. *Biochem. Pharmacol.* 14, 1727-1738.
- 9 Junge, W. and Krisch, K. (1975) The carboxylesterases/amidases of mammalian liver and their possible significance. *CRC Crit. Rev. Toxicol.* 3, 371-434.
- 10 Koelle, G.B., Davis, R., Dilibreto, E.J., and Koelle, W.A. (1974) Selective, near-total, irreversible inactivation of peripheral pseudocholinesterase and acetylcholinesterase in cats *in vivo*. *Biochem. Pharmacol.* 23, 175-188.
- 11 Clement, J.G. (1984) Role of aliesterase in organophosphate poisoning. *Fund. Appl. Toxicol.* 4, S96-S105.
- 12 Maxwell, D.M., Brecht, K. M., and O'Neill, B.L. (1987) The effect of carboxylesterase inhibition on interspecies differences in soman toxicity. *Toxicol. Letters* 39, 35-42.
- 13 Maxwell, D.M., Lenz, D.E., Groff, W.A., Kaminskis, A., and Froehlich, H. (1987) The effects of blood flow and detoxification on *in vivo* cholinesterase inhibition by soman in rats. *Toxicol. Appl. Pharmacol.* 88, 66-76.
- 14 Benschop, H., Koenigs, C.A.G., Van Genderen, J., and De Jong, L.P.A. (1984) Isolation, *in vitro* activity, and acute toxicity in mice of the four stereoisomers of soman. *Fund. Appl. Toxicol.* 4, S84-S95.
- 15 Nordgren, I., Lundgren, G., Puu, G., and Holmstedt, B. (1984) Stereoselectivity of enzymes involved in toxicity and detoxification of soman. *Arch. Toxicol.* 55, 70-75.
- 16 Clement, J.G., Benschop, H.P., De Jong, L.P.A., and Wolthuis, O.L. (1987) Stereoisomers of soman (pinacolylmethylphosphonofluoridate): Inhibition of serum carboxylic ester hydrolases and potentiation of their toxicity by CBDP(2-(2-methylphenoxy)-4H-1,3,2-benzodioxaphosphorin-2-oxide) in mice. *Toxicol. Appl. Pharmacol.* 89, 141-143.
- 17 Benschop, H.P., Berends, F., and De Jong, L.P.A. (1981) GLC-analysis and pharmacokinetics of the four stereoisomers of soman. *Fund. Appl. Toxicol.* 1, 177-182.
- 18 Reynolds, M.L., Little, P.J., Thomas, B.F., Bagley, R.B., and Martin, B.R. (1985) Relationship between the biodisposition of [<sup>3</sup>H] soman and its pharmacological effects in mice. *Toxicol. Appl. Pharmacol.* 80, 409-420.
- 19 Benschop, H.P., Bijleveld, E.C., De Jong, L.P.A., Van Der Wiel, H.J., and Van Helden, H.P.M. (1987) Toxicokinetics of the four stereoisomers of the nerve agent soman in atropinized rats - influence of a soman simulator. *Toxicol. Appl. Pharmacol.* 90, 490-500.
- 20 Bajgar, J., Tulach, J., Jakl, A., and Patocka, J. (1971) Differences in anticholinesterase action of some organophosphorus compounds *in vivo*. *Acta. Biol. Med. Germ.* 27, 171-178.

- 21 Green, A.L. (1958) The kinetic basis of organophosphate poisoning and its treatment. *Biochem. Pharmacol.* 1, 115-128.
- 22 Gibaldi, M. and Perrier, D. (1982) *Pharmacokinetics*, 2nd edition. Marcel Dekker, New York, pp. 355-384.
- 23 Gerlowski, L.E. and Jain, R.K. (1983) Physiologically based pharmacokinetic modeling: Principles and applications. *J. Pharm. Sci.* 72, 1103-1127.
- 24 Siakotos, A.N., Filbert, M., and Hester, R. (1969) A specific radioisotopic assay for acetylcholinesterase and pseudo-cholinesterase in brain and plasma. *Biochem. Med.* 3, 1-12.
- 25 Ecobichon, D.J. (1970) Characterization of the esterases of canine serum. *Can. J. Biochem.* 48, 1359-1367.
- 26 Little, J.S. (1977) Isolation and characterization of plasma membranes from the livers of control and *streptococcus pneumoniae*-infected rats. *Infect. Immunity* 16, 628-636.
- 27 Yamamura, H.I. and Snyder, S.H. (1974) Muscarinic cholinergic binding in rat brain. *Proc. Nat. Acad. Sci. U.S.A.* 71, 1725-1729.
- 28 Reiner, E. and Aldridge, W.N. (1967) Effect of pH on inhibition and spontaneous reactivation of acetylcholinesterase treated with esters of phosphoric acids and of carbamic acids. *Biochem. J.* 105, 171-179.
- 29 Webb, J.L. (1963) *Enzyme and Metabolic Inhibitors*. Academic Press, New York, pp. 149-192.
- 30 Finney, D.J. (1971) *Probit Analysis*, 3rd edition. Cambridge University Press, Cambridge, pp. 50-124.
- 31 Hindmarsh, A.C. (1974) GEAR: Ordinary differential equation system solver. Lawrence Livermore Laboratory Report UCID-3001, Rev. 3.
- 32 Carson, E.R., Cobelli, C. and Finkelstein, L. (1983) *The Mathematical Modeling of Metabolic and Endocrine Systems*. John Wiley and Sons, New York, pp. 227-230.
- 33 Winer, B.J. (1971) *Statistical Principles in Experimental Design*, 2nd edition. McGraw-Hill, New York, pp. 196-201.
- 34 Van Helden, H.P.M. and Wolhuis, O.L. (1983) Evidence for an intramuscular depot of the cholinesterase inhibitor soman in the rat. *Eur. J. Pharmacol.* 89, 271-274.
- 35 Aas, P., Sterri, S.H., Hjermstad, H.P., and Fonnum, F. (1985) A method for generating toxic vapors of soman: Toxicity of soman by inhalation in rats. *Toxicol. Appl. Pharmacol.* 80, 437-445.

## PHARMACOKINETICS, BIOCHEMICAL MECHANISM AND MUTATION ACCUMULATION: A COMPREHENSIVE MODEL OF CHEMICAL CARCINOGENESIS

Rory B. Conolly<sup>a</sup>, Richard H. Reitz<sup>b</sup>, Harvey J. Clewell, III<sup>c</sup>, and Melvin E. Andersen<sup>c</sup>

<sup>a</sup>*Northrop Services Inc. – Environmental Sciences, Dayton, OH*, <sup>b</sup>*Mammalian and Environmental Toxicology, 1803 Building, Dow Chemical Company, Midland, MI*, <sup>c</sup>*Armstrong Aerospace Medical Research Laboratory, Toxic Hazards Division, Wright-Patterson AFB, OH*

### SUMMARY

Chemical carcinogenesis is a process beginning with carcinogen absorption and ending with development of a malignant tumor. Individual elements of this process have been studied intensively but no comprehensive model has been developed. This report describes a comprehensive model which incorporates carcinogen pharmacokinetics, biochemical mechanism of action, and the resultant mutation of normal cells to malignancy. Model parameters correspond to specific physiological and biochemical structures and processes. The model was encoded in a simulation language and used to examine biochemical and cellular effects of exposure to an initiator and a promoter. With laboratory validation, the model should be useful for interpretation and design of studies on carcinogenic mechanisms and for risk assessment.

### INTRODUCTION

Although much is known about how chemicals cause cancer, no comprehensive model of chemical carcinogenesis has been proposed. A comprehensive model must encompass three related processes: (1) the pharmacokinetic behavior of the carcinogen, (2) the reaction(s) in the target tissue of the carcinogen or its metabolite(s) with cellular macromolecules, and (3) the effect of these reactions on the malignant transformation of normal cells. Work in the laboratories of Bischoff [1], Dedrick [2], and Andersen [3,4] on physiologically based pharmacokinetics and Moolgavkar [5,6] on the 2-stage cancer model (MVK model) has provided much of the theoretical and practical underpinning needed for such a comprehensive model. This report shows how physiologically based pharmacokinetics and the MVK description of cancer can be linked realistically to form a comprehensive simulation model of chemical carcinogenesis.

### STRUCTURE OF THE COMPREHENSIVE CANCER MODEL

#### *Physiologically based pharmacokinetics*

A chemical carcinogen external to the body is absorbed and then distributed to target tissues where it may be converted to reactive metabolite(s). A physiologically based pharmacokinetic (PB-PK) model based on Ramsey and Andersen [3] is incorporated into the comprehensive cancer model and used to simulate these events (Figure 1, Part I). This approach allows the target tissue

concentration of parent compound and the rate of its metabolism to be estimated both during and after exposure.

### ***Two-stage cancer model***

A simple yet versatile 2-stage model for cancer has been developed by Moolgavkar and Venzon [5] and Moolgavkar and Knudson [6] and is used in the work described here (Figure 1, Part III). The MVK model succeeds where less realistic 2-stage descriptions fail in accounting for complex tumor incidence curves including those for human female breast cancer [7] and retinoblastoma [6]. In the MVK model, normal cells progress to initiated and then malignant genotypes (0, 1, or 2 specific mutations, respectively). The rate at which mutations accumulate in a tissue is a function of a relatively small number of biologically realistic parameters. These are the numbers of normal and initiated cells, the rates at which these cells replicate and die, and the probabilities that critical mutations will occur during their replication. Specification of the relationship between these parameters and tumor incidence is a fundamental contribution of the MVK model. It allows phenomenological definitions of, for example, initiation and promotion, to be replaced with explicit definitions based on molecular and cellular effects. Appendix 1 contains the differential equations for the MVK model.

### ***Linking pharmacokinetic behavior to tumor formation***

The main goal of this work was to develop realistic linkages between the target tissue concentration of a carcinogen and the MVK birth and mutation rate parameters. Given the maturity of the PB-PK and MVK descriptions, these linkages are all that is needed to obtain a model encompassing chemical carcinogenesis from *in vivo* exposure through development of a malignant tumor. For the purposes of this discussion we define such a linkage to be the biochemical mechanism of the carcinogen. Linkages for two hypothetical carcinogens, an initiator and a promoter, are described.

### ***Initiation - carcinogens that form DNA adducts***

Within the framework of the MVK cancer process, a carcinogenic initiator increases the probabilities that normal and initiated cells mutate during replication; that is,  $\mu_1$  and  $\mu_2$  are increased (Figure 1, Parts II and III; Appendix 1). We described a hypothetical initiator that is metabolized in the liver. The metabolite either forms adducts with DNA nucleotides or undergoes first-order elimination. The adducts are repaired by a first-order process. The following differential equation specifies the change in the amount of nucleotide adducts ( $A_{ANU}$  [μmol]) as a function of their time-dependent rates of formation and repair.

$$dA_{ANU}/dt = k_{MNU}A_{MANU} - k_{RNU}A_{ANU} \quad (1)$$

The formation of adducts is described by a second-order rate constant ( $k_{MNU}$  [1/h/ $\mu\text{mol}$ ]), the amounts of reactive metabolite ( $A_M$  [ $\mu\text{mol}$ ]), and of nucleotides ( $A_{NU}$  [ $\mu\text{mol}$ ]). The rate of adduct repair is given by the product of a first-order rate constant ( $k_{RNU}$  [1/h]) and the amount of adducts ( $A_{ANU}$  [ $\mu\text{mol}$ ]). Equation (1) is used to calculate the fraction ( $F_{AD}$ ) of all nucleotides that have adducts. This fraction is then multiplied by a term ( $\mu_{max}$ ) defining the maximum possible increase in transition probabilities  $\mu_1$  and  $\mu_2$  due to the particular DNA-damaging agent. In effect,  $\mu_{max}$  reflects the mutational potency of the adducts. The resulting increase ( $F_{AD}\mu_{max}$ ) is added to both  $\mu_1$  and  $\mu_2$  (Appendix 1, Equations 4 and 5). The birth and death rate parameters  $\alpha_0$ ,  $\beta_0$ ,  $\alpha_1$ , and  $\beta_1$ , however (Appendix 1), are not affected. Both the normal-to-initiated cell and initiated-to-malignant cell transitions are consequently more likely during and for some time after exposure to the DNA-damaging agent. Although the specific chemical discussed here is hypothetical, this mechanism of action is well-supported by the literature [8,9,10,11].

### Promoters

In the MVK scheme, a promoter can be defined as an agent that selectively increases the birth rate of initiated cells, or equivalently, decreases their death rate. We described a hypothetical promoter that increases the birth rate of initiated cells while leaving their death rate unchanged. Normal cells are unaffected. Equation (2) describes the essential features of this mechanism.

$$P_{KBN1} = F_{PRE}K_{BMAX} \quad (2)$$

The promoter binds reversibly to a receptor within the cells of a target tissue. The fractional occupancy of the receptor ( $F_{PRE}$ ) is multiplied by  $K_{BMAX}$ , the maximum possible increase in initiated cell birth rate.  $P_{KBN1}$ , the increase in birth rate of initiated cells due to the promoter, is added to  $\alpha_1$  (Appendix 1). This mechanism of promotion, only one of several possible that could have been portrayed, is consistent with the experimental observation that cells in preneoplastic foci (intermediate cells in the MVK scheme) grow faster than normal cells [12] and with postulated biochemical mechanisms for promotion by 2,3,7,8-tetrachlorodibenzo-*p*-dioxin [13] and phorbol esters [11].

### Computer simulation

The comprehensive model was encoded as a series of time-dependent differential equations. Step-wise numerical integration of these equations allows model behavior to be examined. This computed behavior will simulate the behavior expected *in vivo* to the degree that the model structure is isomorphic with relevant *in vivo* physiological and biochemical structures and processes. For example, PB-PK models succeed to the extent that their encoded structure is a sufficient

description of the physiological and biochemical determinants of pharmacokinetic behavior in the species on which the model is based.

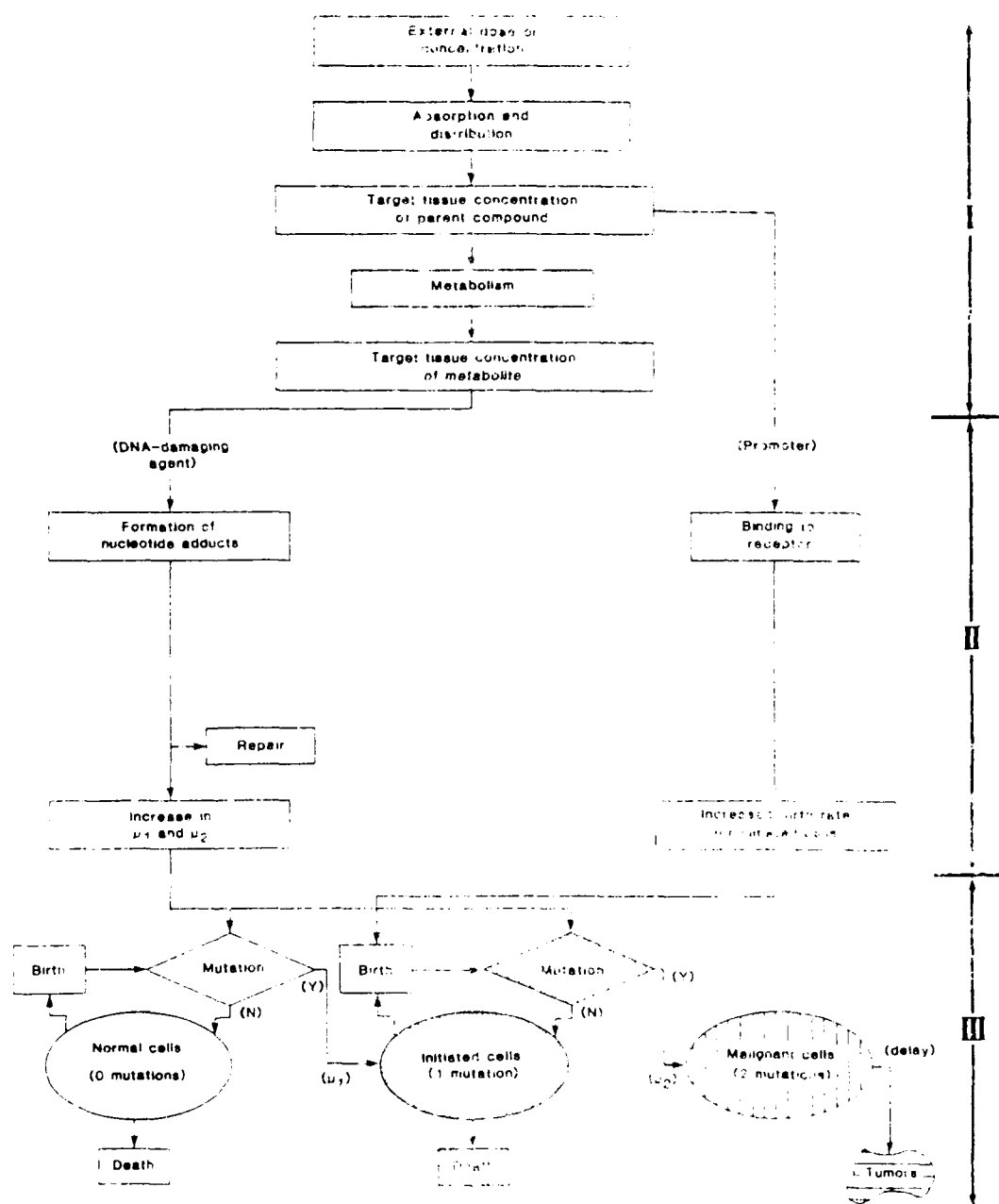


Figure 1. Schematic of the comprehensive cancer model. Part I is a physiologically based description of the processes controlling carcinogen pharmacokinetics. Its main role is converting external carcinogen dose to a realistic target tissue concentration of either the parent compound or relevant metabolite(s). In Part II, representative biochemical mechanisms are described for DNA-damaging agents and promoters. Part III is a 2-stage cancer process where cells are either normal, intermediate, or malignant (0, 1, and 2 mutations, respectively). The interface between Parts II and III specifies how carcinogens acting by different mechanisms affect the cell growth and mutation parameters of the cancer process.

The simulations described here were for a 250-g rat. Physiological parameters controlling carcinogen disposition throughout the organism were set to realistic values as described by Ramsey and Andersen [3]. The liver was the target organ for carcinogens, and specific hepatic parameter values were obtained whenever possible. Hepatocyte volume was set at  $5.608 \times 10^{-12}$  L/cell [14], and the total number of hepatocytes per liver was calculated based on the liver being 4% of body weight. Hepatocyte basal birth and death rates were set at  $1.7 \times 10^{-4}$  events/cell/h based on microautoradiography data collected by R.H. Reitz [unpublished data]. The number of nucleotides per hepatocyte was calculated based on  $2.9 \times 10^9$  base pairs per human cell [15]. The basal transition probabilities  $\mu_1$  and  $\mu_2$  were  $1.0 \times 10^{-6}$  per cell generation [16,17].

While the initiator and promoter described in this work were hypothetical with respect to their carcinogenic actions, they were both configured to have the pharmacokinetic behavior of chloroform. This was accomplished by using the actual partition coefficients and Michaelis-Menten metabolic parameters for chloroform in the Fisher 344 rat [M.L. Gargas, personal communication].

The model was written in SIMUSOLV (Mitchell & Gauthier Assoc., Concord, MA), a Fortran-based continuous simulation language with optimization capabilities, and run on a VAX 8530 (Digital Equipment Corp., Maynard, MA).

#### BEHAVIOR OF THE COMPREHENSIVE MODEL

A number of physiologically based simulations of pharmacokinetic behavior have been published [1,2,3,4]. The ability of the MVK model to simulate tumor incidence has been similarly well described [6,7,18,19]. The simulations depicted in Figures 2 and 3 were, therefore, chosen to illustrate aspects of the biochemical mechanisms linking the pharmacokinetic portion of the comprehensive model with the MVK cancer process. The simulation portrayed in Figure 4 emphasizes the comprehensive nature of the model by showing tumor prevalence in an experimental cohort as a function of daily carcinogen exposure.

##### *Initiation - carcinogens that form DNA adducts*

The relationship between metabolism of the hypothetical DNA-damaging agent and concentration of DNA adducts was examined for an inhalation exposure regimen of 6 h/day, 5 days/week, for 2 weeks (Figure 2). The rate of carcinogen metabolism was used as an index of tissue exposure because it is a better predictor of intensity of effect than, for example, the concentration external to the organism [20]. The daily rise and fall in rate of metabolism is clearly seen as is the corresponding fluctuation in concentration of DNA adducts. When the rate of DNA repair was  $0.01 \text{ h}^{-1}$  (upper curve), DNA adducts accumulated during the week and were not completely repaired during

the weekend. With the repair rate set at  $0.05 \text{ h}^{-1}$  (lower curve), adduct accumulation during the week was diminished and repair was nearly complete on the weekend.

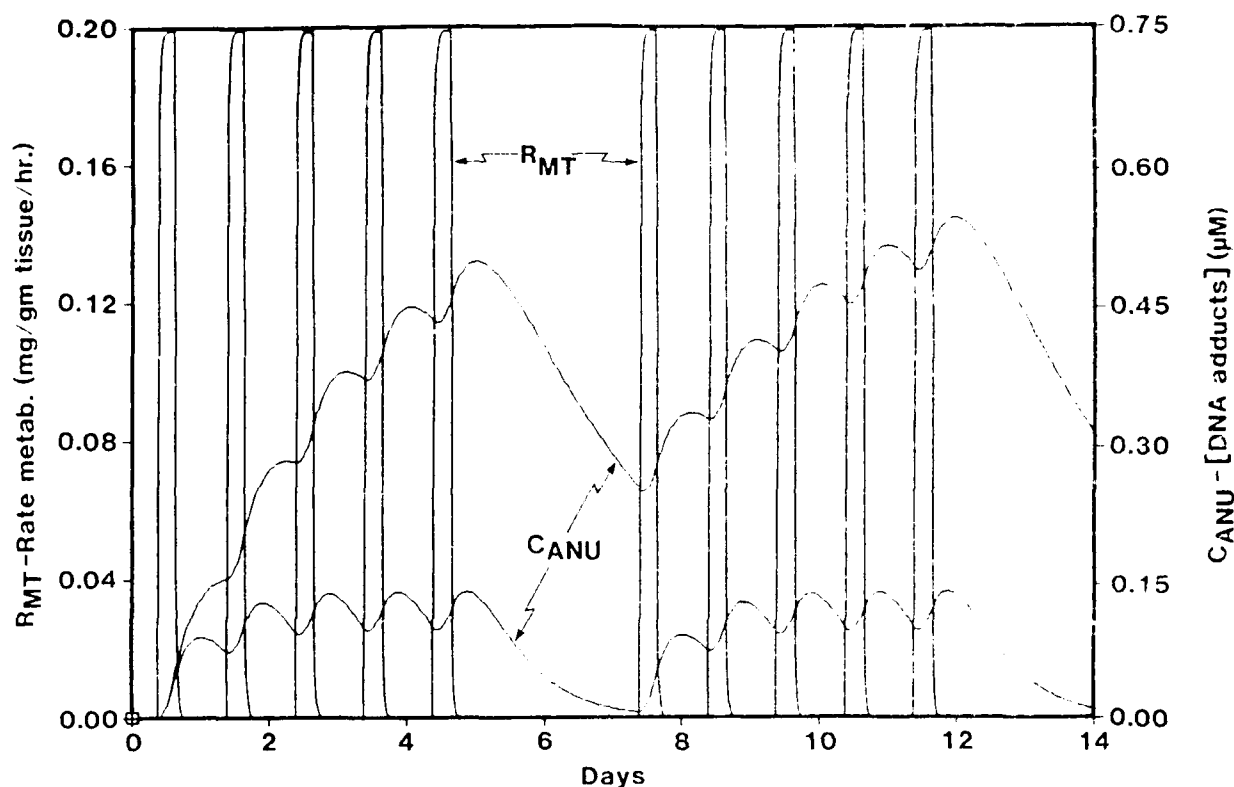


Figure 2. Kinetics and DNA-binding behaviors for a hypothetical DNA-damaging agent. The relationship between the rate of carcinogen metabolism ( $R_{MT}$ ) and the concentration of DNA adducts ( $C_{ANU}$ ) is shown when all parameter values are held constant except the rate of DNA repair. The simulated exposure regimen was 6 h/day, 5 days/week for 2 weeks. The rate of repair was  $0.01 \text{ h}^{-1}$  (upper curve) or  $0.05 \text{ h}^{-1}$ .

### Promoters

Simulations were also conducted for the interaction of the hypothetical promoter with its cellular receptor and the consequence of this interaction for the growth of initiated cells (Figure 3). The exposure regimen was 2 years at 6 h/day, 5 days/week. An interval late in the experiment (Day 700 through Day 712) is depicted because effects on initiated cells can be depicted more clearly once a significant population of these cells has developed. Daily spikes in the fraction of receptor molecules occupied by promoter mirror the daily 6-h exposure to promoter (Figure 3a). Each spike of receptor occupancy is followed by a corresponding increase in the birth rate of initiated cells (Figure 3b). Finally, the number of initiated cells increases in proportion to the increase in birth rate (Figure 3c).

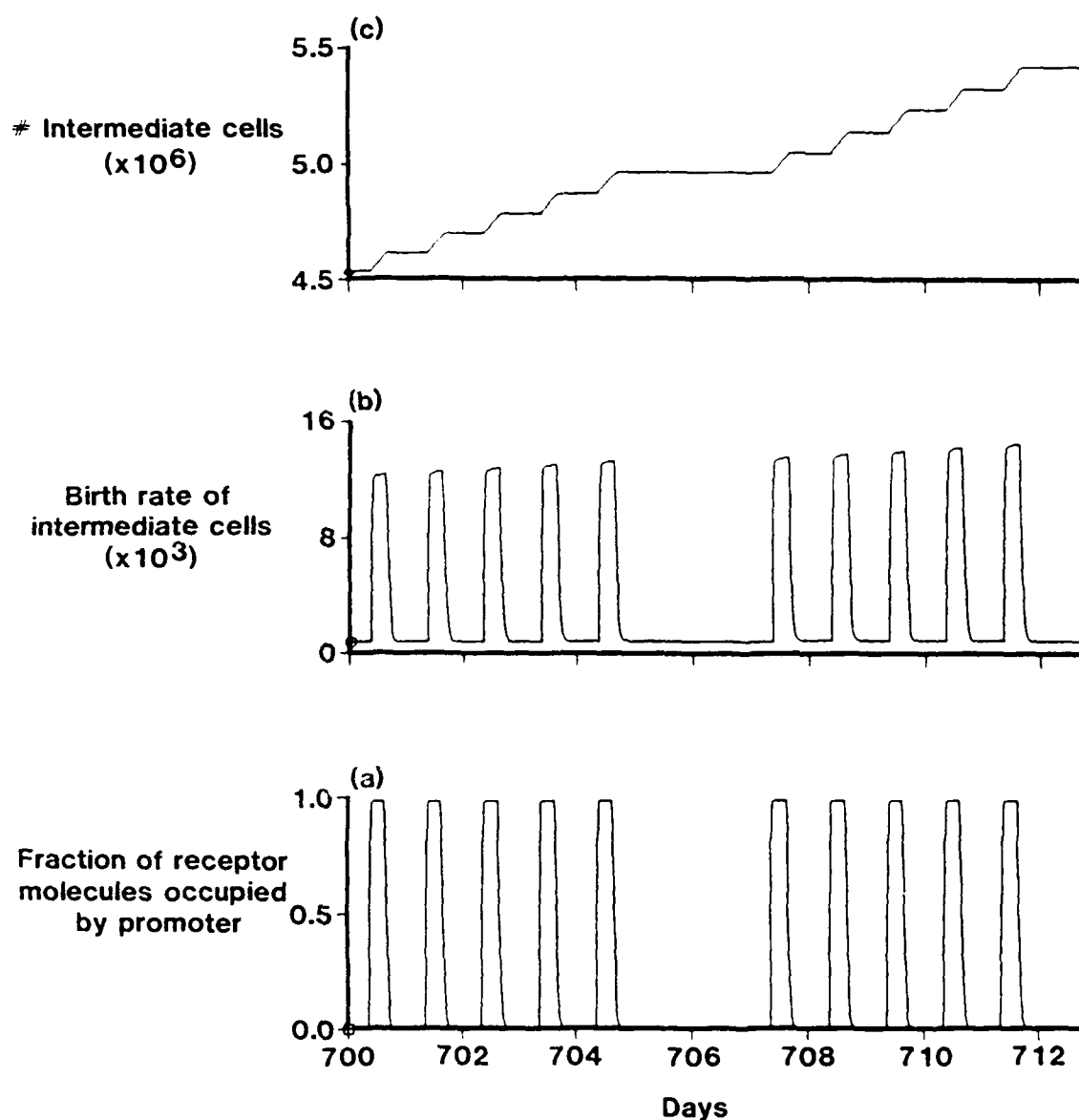


Figure 3. Interaction of a hypothetical promoter with its receptor and the effect on initiated cells. The exposure regimen was 6 h/day, 5 days/week for 2 years. Daily spikes in the fraction of receptor molecules occupied by promoter mirror a daily 6-h exposure to promoter (3a). Each spike of receptor occupancy is accompanied by a corresponding spike in the birth rate of initiated cells above the basal rate (3b) and by an increase in the number of initiated cells (3c).

#### Tumor prevalence

Simulated tumor prevalence curves for an experimental cohort of 100 rats were generated for the hypothetical DNA-damaging agent and promoter (Figure 4). Prevalence, the proportion of animals with one or more tumors, is the product of the probability of tumor (Appendix 2) and the size of the cohort. The exposure regimen was 6 h/day, 5 days/week for 2 years. Exposure concentrations

and model parameter values were set to provide a tumor prevalence close to 100% for each agent at 2 years. Background prevalence, due solely to the regular turnover of normal and initiated cells, totaled about 0.8% at 2 years (Figure 4, curve A). Tumor prevalence initially rises more slowly with the promoter than with the initiator (Figure 4, curves B and C, respectively). This happens because the promoter has a minimal effect on tumor development until a relatively large population of initiated cells has developed while the initiator acts on both the normal and initiated cell populations (Figure 1, Part III).

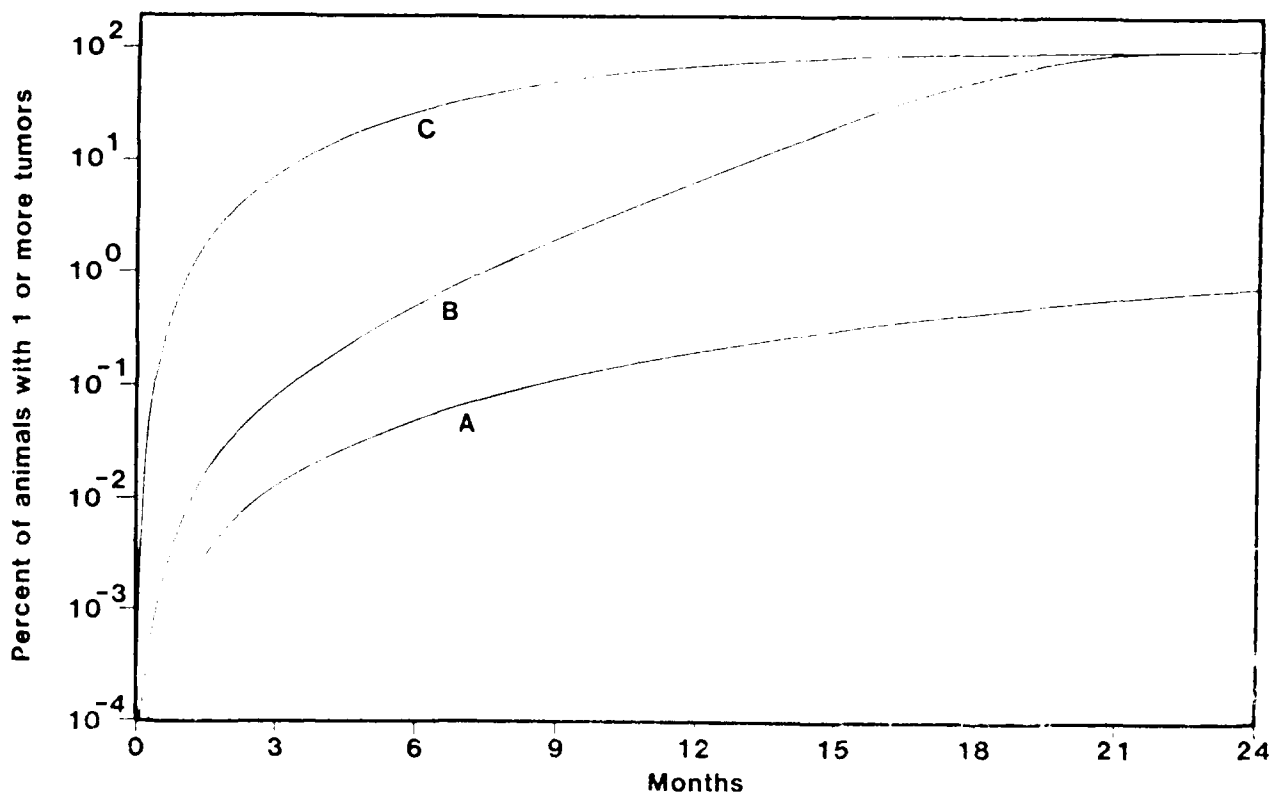


Figure 4. Tumor prevalence curves for a DNA-damaging agent and a promoter. The exposure regimen was 6 h/day, 5 days/week for 2 years. Prevalence elicited by each agent at 2 years was close to 100%, allowing a comparison of the shapes of the curves. Curve A is the background prevalence (about 0.8%). Curves B and C are for a promoter and DNA-damaging agent, respectively.

## DISCUSSION

The computer simulations depicted in Figures 2 through 4 provide a functional illustration of how tissue concentrations of hypothetical carcinogenic agents plausibly can be linked to the critical parameters of the MVK model. Details of linkages for real initiators and promoters may differ somewhat from those described here but would still fit into the overall framework of the model.

This comprehensive simulation model is "biologically structured"; that is, model parameters correspond to real structures and processes in the species on which the model is based. These include,

for example, the volumes of specific tissues and their respective blood flows, partition coefficients describing the equilibrium distribution of carcinogen between blood and tissues and blood and air, and rates of cell death, replication, and mutation in the target tissue. This approach to model design means that, in principle, correct values for model parameters can be obtained by experimentation. For example, DNA adduct formation and repair can be quantitated [21] as can occupancy of cytosolic receptors by promoters [11]. Initiated cells may be assayed by histopathology [22,23] or flow cytometry [24]. An assay for these cells could be used to describe their growth rate and to infer the rate at which normal cells mutate to the initiated state. Tumor prevalence data, preferably obtained at several time points during a bioassay, would allow estimation of the rate at which initiated cells progress to overt malignancy and of the time between first appearance of a malignant cell and the clinical observation of a tumor. In addition, model validation must include the collection of data on how physiological and biochemical parameters change with age. For example, the pharmacokinetics of ethylenediamine change with age in the Fischer 344 rat [25], and age-related changes in percentage of body fat dramatically affect the pharmacokinetic behavior of polychlorinated biphenyls (PCBs) in Sprague-Dawley rats [26].

Once model parameter values are set with laboratory data, they are no longer free to float. Consequently, the ability of a biologically structured and well-validated model to simulate real-world behavior becomes a rigorous test of the model structure. Failure indicates that either model structure is wrong or the data set being simulated is faulty.

This report describes a comprehensive, biologically structured model for chemical carcinogenesis. Use of the model for computer simulation studies allows the behavior of intermediate steps in the carcinogenic process as well as tumor development to be examined. With appropriate laboratory validation, models like the one described here should prove useful in risk assessment for chemical carcinogens and for the design and interpretation of experimental studies of carcinogenic mechanisms.

## APPENDIX 1

These equations describe the numbers (actually, the expectations; see Appendix 2) of normal, initiated, and malignant cells in the target tissue.

$$dA_{N0}/dt = A_{N0}(\alpha_0 - \beta_0) \quad (3)$$

$$dA_{N1}/dt = A_{N1}(\alpha_1 - \beta_1) + \mu_1\alpha_0A_{N0} \quad (4)$$

$$d(N1 \rightarrow N2)/dt = \mu_2\alpha_1A_{N1} \quad (5)$$

Turnover rates for normal and initiated cells (Equations 3 and 4) are related to birth ( $\alpha_0$ ,  $\alpha_1$ ) and death ( $\beta_0$ ,  $\beta_1$ ) rate parameters (events/cell/h) and the numbers of cells ( $A_{N0}$ ,  $A_{N1}$ , respectively). The

term  $\mu_1 a_0 A_{N0}$  in equation (4) describes the rate at which normal cells mutate to the initiated genotype with  $\mu_1$  (mutations/division) being probability of mutation per cell division. Integration of these equations gives the numbers of cells at any point in time.

Equation (5) is different from Equations (3) and (4). It only tracks the formation of malignant cells from initiated cells, not the growth of malignant cells *per se*. In these simulations, malignant cells were treated as though they were tumors. In reality, a clinically evident tumor would not be detected until some time after the appearance of its parental malignant cell. Moolgavkar *et al.* [7], for example, assumed that tumors of the human female breast become clinically evident 5 years after a malignant cell arises. The assumption in this work of equivalence between malignant cells and tumors is sufficient for illustrating qualitative aspects of model behavior. An appropriate delay would, however, have to be described if the model were being used predictively or for simulation of real data.

## APPENDIX 2

### *Expectation and probability of tumor*

The computer simulations depicted in Figures 2 through 4 describe behaviors expected for a target tissue in an "average rat." This means that the value of any simulated behavior (e.g., the number of initiated cells at a given point in time) is actually the average number of initiated cells per cohort member for an infinitely large cohort. Such average values are called "expectations." The numbers of normal, initiated, and malignant cells described in Appendix 1 are in reality the expectations for these cell types. With respect to malignant cells, an expectation of 0.001 means that there are, on the average, 0.001 malignant cells in the target tissue for all the rats in the cohort. This begs the question: How many rats have 1 or more tumors (or conversely, how many are tumor free)? To answer this question, an assumption must be made about the distribution of tumors across the cohort. For this work, it was assumed that the distribution is Poisson. The probability of an individual member of the cohort having 1 or more tumors is then calculated by the expression

$$P_{TUM} = 1 - e^{-AN_2} \quad (6)$$

where  $A_{N2}$  is the expectation of malignant cells. Moolgavkar *et al.* [27] have described a closed-form solution for the true probability of tumor, and Moolgavkar [personal communication] has stated that the Poisson overestimates the true probability when prevalence is greater than about 30%. Ongoing work in our laboratory is evaluating the extent of this discrepancy, and future versions of the model will be modified appropriately.

## REFERENCES

- 1 Bischoff, K.B. and Brown, R.G. (1966) Drug distribution in mammals. *Chem. Eng.Prog. Symp. Ser.* 62, 33-45.
- 2 Matthews, H.B. and Dedrick, R.L. (1984) Pharmacokinetics of PCBs. *Ann. Rev. Pharmacol. Toxicol.* 24, 85-103.
- 3 Ramsey, J.R. and Andersen, M.E. (1984) A physiological model for the inhalation pharmacokinetics of inhaled styrene in rat. and humans. *Toxicol. Appl. Pharmacol.* 73, 159-175.
- 4 Andersen, M.E., Clewell, H.J., III, Gargas, M.J., Smith, F.A. and Reitz, R.H. (1987) Physiologically based pharmacokinetics and the risk assessment process for methylene chloride. *Toxicol. Appl. Pharmacol.* 87, 185-205.
- 5 Moolgavkar, S.H. and Venzon, D.J. (1979) Two-event models for carcinogenesis: incidence curves for childhood and adult tumors. *Math. Biosci.* 47, 55-77.
- 6 Moolgavkar, S.H. and Knudson, A.G., Jr. (1981) Mutation and cancer: a model for human carcinogenesis. *J.Natl.Cancer Inst.* 66, 1037-1052.
- 7 Moolgavkar, S.H., Day, N.E. and Stevens, R.G. (1980) Two-stage model for carcinogenesis: Epidemiology of breast cancer in females. *J.Natl. Cancer Inst.* 65, 559-569.
- 8 McCann, J., Choi, E., Yamasaki, E. and Ames, B.N. (1975) Detection of carcinogens as mutagens in the salmonella/microsome test: assay of 300 chemicals. *Proc. Natl. Acad. Sci.* 72, 5135-5139.
- 9 Barrett, J.C., Tsutsui, T. and Ts'o, P.O.P. (1978) Neoplastic transformation induced by a direct perturbation of DNA. *Nature* 274, 229-232.
- 10 Reddy, E.P. (1983) Nucleotide sequence analysis of the T24 human bladder carcinoma oncogene. *Science* 220, 1061-1063.
- 11 Weinstein, I.B. (1981) Current concepts and controversies in chemical carcinogenesis. *J. Supramol. Struct. Cell. Biochem.* 17, 99-120.
- 12 Emmelot, P. and Scherer, E. (1980) The first relevant cell stage in rat liver carcinogenesis. A quantitative approach. *Biochim. Biophys. Acta* 605, 247-304.
- 13 Gasiewicz, T.A. and Rucci, G. (1984) Cytosolic receptor for 2,3,7,8-tetrachlorodibenzo-*p*-dioxin. Evidence for a homologous nature among various mammalian species. *Molec. Pharmacol.* 26, 90-98.
- 14 de la Iglesia, F.A., McGuire, E.J. and Feuer, G. (1975) Coumarin- and 4-methylcoumarin-induced changes in the hepatic endoplasmic reticulum studied by quantitative stereology. *Toxicology* 4, 305-314.
- 15 Darnell, J., Lodish, H. and Baltimore, D. (1986) *Molecular Cell Biology*, Scientific American Books, New York, p. 138.
- 16 Elmore, E., Kakunaga, T. and Barrett, J.C. (1983) Comparison of spontaneous mutation rates of normal and chemically transformed human skin fibroblasts. *Cancer Res.* 43, 1650-1655.

- 17 Tsutsui, T., Crawford, B.D. and Ts'o, P.O.P. (1981) Comparison between mutagenesis in normal and transformed Syrian hamster fibroblasts. Difference in the temporal order of Hprt gene replication. *Mutat. Res.* 80, 357-371.
- 18 Moolgavkar, S.H. (1983) Model for human carcinogenesis: Action of environmental agents. *Environ. Hlth. Perspect.* 50, 285-291.
- 19 Moolgavkar, S.H. (1986) Carcinogenesis modeling: From molecular biology to epidemiology. *Ann. Rev. Public Hlth.* 7, 151-169.
- 20 Andersen, M.E. (1987) Tissue dosimetry in risk assessment, or What's the problem here anyway. In: *Drinking Water and Health, Vol. 8: Pharmacokinetics in Risk Assessment*, National Academy Press, Washington, D.C., pp. 8-23.
- 21 Freidberg, E.C. (1985) DNA Repair. W H. Freeman and Co., New York, pp. 23-40.
- 22 Peraino, C., Carnes, B.A. and Stevens, F.J. (1986) Evidence for growth among foci with different phenotypes in the population of altered hepatocyte foci induced by a single neonatal treatment with carcinogen. *Carcinogenesis* 7, 191-192.
- 23 Rushmore, T.H., Sharma, R.N.S., Roomi, M.W., Harris, L., Satoh, K., Sato, K., Murray R.K. and Farber, E. (1987) Identification of a characteristic cytosolic polypeptide of rat neoplastic hepatocyte nodules as placental glutathione S-transferase. *Biochem. Biophys. Res. Commun.* 143, 98-103.
- 24 Digernes, V. (1983) Chemical liver carcinogenesis: Monitoring of the process by flow cytometric DNA measurements. *Environ. Hlth. Perspect.* 50, 195-200.
- 25 Yang, R.S., Tallant, M.J. and McKelvy, J.A. (1984) Age-dependent pharmacokinetic changes of ethylenediamine in Fisher-344 rats parallel to a two-year chronic toxicity study. *Fund. Appl. Toxicol.* 4, 663-670.
- 26 Lutz, R.J., Dedrick, R.L., Matthews, H.B., Elmg, T.E. and Anderson, M.W. (1977) A preliminary pharmacokinetic model for several chlorinated biphenyls in the rat. *Drug Metab. Disp.* 5, 386-396.
- 27 Moolgavkar, S.H., Dewanji, A. and Venzon, D.J. (in Press) A stochastic two-stage model for cancer risk assessment I: The hazard function and the probability of tumor. *Risk Anal*

**SESSION IV**

**EMERGING TECHNIQUES**

**Major Michael J. Parnell, USAF, Chairman**

## FLOW CYTOMETRIC ANALYSIS OF THE CELLULAR TOXICITY OF TRIBUTYLtin

Robert M. Zucker<sup>a</sup>, Kenneth H. Elstein<sup>a</sup>, Robert E. Easterling<sup>b</sup>, and Edward J. Massaro<sup>b</sup>

<sup>a</sup>*Northrop Services, Inc. - Environmental Sciences, Research Triangle Park, NC, and*

<sup>b</sup>*Health Effects Research Laboratory, U.S. Environmental Protection Agency, Research Triangle Park, NC*

### SUMMARY

Flow cytometric and light/fluorescence microscopic analyses indicate that tributyltin (TBT) alters the plasma membrane/cytoplasm complex of the murine erythroleukemic cell (MELC) in a dose-dependent and time-dependent manner. The flow cytometric parameter axial light loss, a measure of cell volume, decreases in cells exposed to 5  $\mu$ M TBT relative to control cells or cells exposed to 50  $\mu$ M TBT. The flow cytometric parameter 90° light scatter, a function of refractive index and a measure of protein content, increases as a function of TBT concentration above 0.5  $\mu$ M. Following exposure to TBT concentrations greater than 0.5  $\mu$ M, but less than 50  $\mu$ M, DNA distribution across the cell cycle cannot be resolved adequately by flow cytometry. Also, the cells become resistant to solubilization of the cell membrane/cytoplasm complex by nonionic detergents.

Relative to logarithmically growing cells, MELC in the stationary phase of the growth cycle and butyric acid-differentiated cells exhibit decreased plasma membrane permeability resulting in increased carboxyfluorescein (CF) retention derived from the intracellular hydrolysis of carboxyfluorescein diacetate (CFDA). Similarly, cells exposed to TBT concentrations below 50  $\mu$ M exhibit increased cellular CF retention. Viability in terms of CFDA hydrolysis/CF retention and propidium iodide (PI) exclusion is not decreased by exposure to TBT concentrations below 1  $\mu$ M. At doses between 5 and 50  $\mu$ M, however, cells exhibit both CF and PI fluorescence simultaneously and are programmed for death. At TBT concentrations greater than 1.0  $\mu$ M, MELC plasma membrane potential, measured with the cyanine dye, 3,3'-diethyloxycarbocyanine iodide (DiOC6) decreases at the same time that the uptake of PI is observed. In conjunction with other data, the concentration-dependent increase in CF fluorescence, resistance to detergent-mediated solubilization of the plasma membrane/cytoplasm complex, and increase in 90° light scatter suggest fixation (protein denaturation, cross-linking, etc.) as a mechanism of the toxic action of TBT.

### INTRODUCTION

Organotins (e.g., tributyltin) have potent fungicidal, insecticidal, and molluscicidal properties and are neurotoxic in humans and other species [1-4]. Triorganotin compounds are membrane-active molecules. They function as ionophores facilitating halide/hydroxyl exchange across cell/mitochondrial membranes and lowering the intracellular pH and anion concentration of the

cytoplasm/mitochondrial matrix [5-11]. They also inhibit  $(\text{Na}^+, \text{K}^+)\text{-ATPase}$  activity and oxidative phosphorylation, induce changes in the shape of erythrocytes, and cause hemolysis in a concentration-dependent manner [12-14]. Concentrations of tributyltin (TBT) below  $1\ \mu\text{M}$  have been shown to affect components of the immune system *in vitro* [15-17].

Membrane integrity is employed as an index of cell viability: An intact membrane selectively excludes both acidic (e.g., propidium iodide [PI]) and basic (e.g., trypan blue) dyes [18]. Cell viability also can be determined with vital stains such as esters of fluorescein or carboxyfluorescein (e.g., carboxyfluorescein diacetate [CFDA]) [19-20]. These molecules are lipophilic and nonfluorescent. They cross the cell membrane and are hydrolyzed by intracellular esterases to fluorescent, negatively charged molecules (CFDA  $\rightarrow$  carboxyfluorescein [CF]) that are retained (incompletely) by cells with an intact plasma membrane. Viability also can be determined by flow cytometric analysis of light scattering parameters. Cells with damaged membranes or dead cells scatter more light than live cells [21].

Employing flow cytometry, we have observed previously that exposure of murine erythroleukemic cells (MELC) to micromolar concentrations of TBT results in increased cellular CF fluorescence in a concentration (C)-  $\times$  time (T)-dependent manner below a critical  $\text{C} \times \text{T}$  product value (CPV). Above this value, cellular CF fluorescence is decreased, PI uptake is observed, resistance to detergent ( $\text{NP}_{40}$ )-mediated cytolysis develops, and 2-dimensional crystallization of  $(\text{Na}^+, \text{K}^+)\text{-ATPase}$  molecules in microsomal membrane preparations is inhibited, a process requiring protein mobility [22, 23]. These observations suggest that TBT acts via fixation (i.e., protein denaturation, cross-linking, etc.) of the cell membrane/cytoplasm complex and are supported by light scatter data obtained from ethanol-fixed MELC. Ethanol-fixed MELC scatter more light than unfixed cells.

Optimal resolution of the cell cycle by flow cytometry is best achieved with "clean" nuclei. Such nuclei are prepared by detergent lysis. The cells are treated with Nonidet P<sub>40</sub> ( $\text{NP}_{40}$ ) or Triton X-100 to solubilize the cell membrane/cytoplasm complex, and the isolated nuclei are stained with a DNA-binding fluorescent dye (e.g., PI) [24].

We have investigated the effects of TBT exposure on the flow cytometric parameters of MELC and nuclei isolated therefrom. We have observed that exposure of MELC to TBT results in increased cellular CF fluorescence and  $90^\circ$  scatter (a parameter related to internal structure/refractive index) and a decrease in axial light loss (a parameter related to cell volume) in a concentration/time-dependent manner. Nuclei prepared from MELC exposed to TBT concentrations greater than  $0.5\ \mu\text{M}$  exhibit excessive green fluorescence following treatment with the fluorescent protein stain fluorescein isothiocyanate (FITC). The excessive FITC fluorescence emanates from adherent protoplasmic remnants (tags) resistant to detergent solubilization. In addition, we have observed

that, compared to logarithmically growing MELC, stationary phase cells and those differentiated by the butyric acid method [25] exhibit increased CF retention. It has been reported that the cell membrane of stationary phase and differentiated cells is less permeable/fluid than that of log phase cells [26-29]. Taken together, these data suggest fixation as a mode of the toxic action for TBT.

## **METHODS**

### ***Cells***

MELC (T3CL2: obtained from Dr. Clyde Hutchison, University of North Carolina, Chapel Hill) were grown in suspension culture in RPMI 1640 (GIBCO, Grand Island, NY) supplemented with 10% fetal bovine serum (FBS) and 25 mM Hepes (H3375: Sigma, St. Louis, MO). Cell density was monitored with a Coulter Counter (Model ZBI: Coulter Electronics, Inc., Hialeah, FL) and the cells were passed at 2- to 3-day intervals to maintain logarithmic growth. Unless stated otherwise, all experiments were performed on cells in the logarithmic phase of growth.

### ***Tributyltin exposure***

TBT concentrations up to 50  $\mu$ M were investigated. Duration of exposure was 4 or 16 h. TBT (methoxide, 97% pure: catalogue No. 22,924-5, Aldrich, Milwaukee, WI) was diluted 1:10,000 with ethanol prior to addition to logarithmically growing MELC. The ethanol concentration of the culture medium was 1%, which had no effect on cell viability as measured by the CFDA/PI assay. Subsequent treatments were performed on aliquots of cells removed from the cultures.

### ***Viability assay***

Viability was determined employing a modification of the CFDA/PI assay of Goodall and Johnson [20]. Viable cells take up CFDA and exclude PI. Prior to use, a stock solution of CFDA (Molecular Probes, Eugene, OR), 2 mg/ml acetone, was diluted 1:50 with phosphate-buffered saline (PBS) and added to approximately  $2.5 \times 10^5$  MELC/ml of growth medium to a final concentration of 3.6  $\mu$ g/ml. The cells were incubated for 10 min at 37°C, chilled on ice for 10 min, and PI (Sigma P5264) was added from a 50- $\mu$ g/ml (PBS) stock solution to a final concentration of 4.5  $\mu$ g/ml. The cells were maintained at 0°C during flow cytometric analysis. The green fluorescence of CF, derived from CFDA by intracellular esterase-catalyzed hydrolysis, and the red fluorescence of PI, resulting from its intercalation into the helical structure of nucleic acids, were measured.

### ***Flow cytometry***

Flow cytometric measurements were made with an Ortho Flow Cytometer (Model 50 H) equipped with an analytical flow cell (30 H), a 5 W Coherent argon (blue) laser (Innova 90-5) emitting at 488 nm at 200 mW, and a 0.8 mW helium-neon (HeNe: red) laser emitting at 633 nm. The flow rate was maintained at less than 200 cells/sec. The data from 10,000 cells/nuclei were collected and stored

in an Ortho 2150 computer system. To visualize the viable cells only, the gain of the red signal was adjusted to place the PI-staining cells in channel 1000. The cytogram regions of the CF-staining cells were electronically isolated (gated) to quantify green fluorescence. Compensation circuitry was used to eliminate fluorescence enhancement due to green/red fluorescence overlap resulting from the optical configuration of the instrument. Four parameters, obtained simultaneously, were investigated: green (CF) fluorescence, red (PI) fluorescence, 90° light scatter, and axial light loss.

The red laser was used to obtain the axial light loss signal, a measure of cell volume. The 90° scatter signal, a measure of internal structure/refractive index and FITC-labeled protein content, were obtained with the blue laser. A 645-nm Schott long-pass filter was used to prevent 90° red light scatter from the HeNe laser from entering the PI (red) fluorescence channel.

#### ***Membrane potential***

DiOC6 (Kodak, Rochester, NY), a dye excited by the blue laser, was employed to measure relative membrane potential. MELC were exposed to TBT concentrations between 0.5 and 50  $\mu$ M. Cells suspended in growth medium ( $2.5 \times 10^5$  cells/ml) were then exposed to 50 nM DiOC6 for 30 min at 37°C, chilled to 0°C on ice, and analyzed at 0°C [30,31].

#### ***DNA cell cycle analysis***

Nuclei were prepared by incubating  $1 \times 10^6$  cells/ml of 0.2% NP<sub>40</sub> in PBS containing 0.5 mg/ml RNase (Sigma R4875) for 15 min at 25°C [22,24]. The nuclei were chilled on ice to 0°C, and 50  $\mu$ g/ml PI and 1.5  $\mu$ g/ml FITC (Sigma F7250) were added to stain nucleic acids and proteins, respectively. PI and FITC fluorescence were measured with the argon laser.

#### ***Ethanol fixation***

Washed cells ( $1 \times 10^6$ ) were suspended in 1 ml of cold (-20°C) 95% ethanol and incubated for 30 min on ice followed by the addition of 1 ml of a cocktail containing 0.1 mM EDTA, 0.1% NP<sub>40</sub>, and 0.5 mg/ml RNAase, incubation for 15 min at room temperature, and the addition of 50  $\mu$ g/ml PI.

#### ***Cell differentiation***

MELC were differentiated by incubation with 1 mM butyric acid (Sigma B2503) or 1.5% DMSO (Sigma D5879) for 72 h [32]. Following dilution with medium supplemented with 10% FBS, the cells were counted and their volume distribution was obtained with a Coulter Counter interfaced with a Coulter Channelyzer (Model 20) [27,32]. Viability was determined by the CFDA/PI assay as described.

### Cell density studies

Cells were grown to concentrations of  $2.9 \times 10^5$ ,  $1.1 \times 10^6$ , and  $1.7 \times 10^6$  cells/ml over 1, 2 and 5 days, respectively, and designated as logarithmic, early stationary phase, and late stationary phase, respectively.

### RESULTS

Axial light loss (cell volume) of MELC decreases non-vectorially as a function of TBT concentration (Figure 1) while  $90^\circ$  light scatter increases with concentration above  $0.5 \mu\text{M}$  up to  $50 \mu\text{M}$ , the highest concentration investigated (Figure 2). The combined data of Figures 1 and 2 are displayed in the form of contour maps in Figure 3. The concentration-dependent increase in the complexity of the maps (which is not completely illustrated for purposes of clarity) is an index of toxicity. The interactions of TBT with the cell are time-dependent as well as concentration-dependent (Figures 4 through 6). For example, at  $0.5 \mu\text{M}$  TBT, only minimal differences in axial light loss and  $90^\circ$  scatter are observed after 4 h of exposure. However, after 16 h, axial light loss is decreased (Figures 4,6),  $90^\circ$  light scatter is increased (Figures 5,6), and the data resemble those of the  $5\text{-}\mu\text{M}$  dose at 4 h (compare Figures 1 with 4, and 2 with 5).

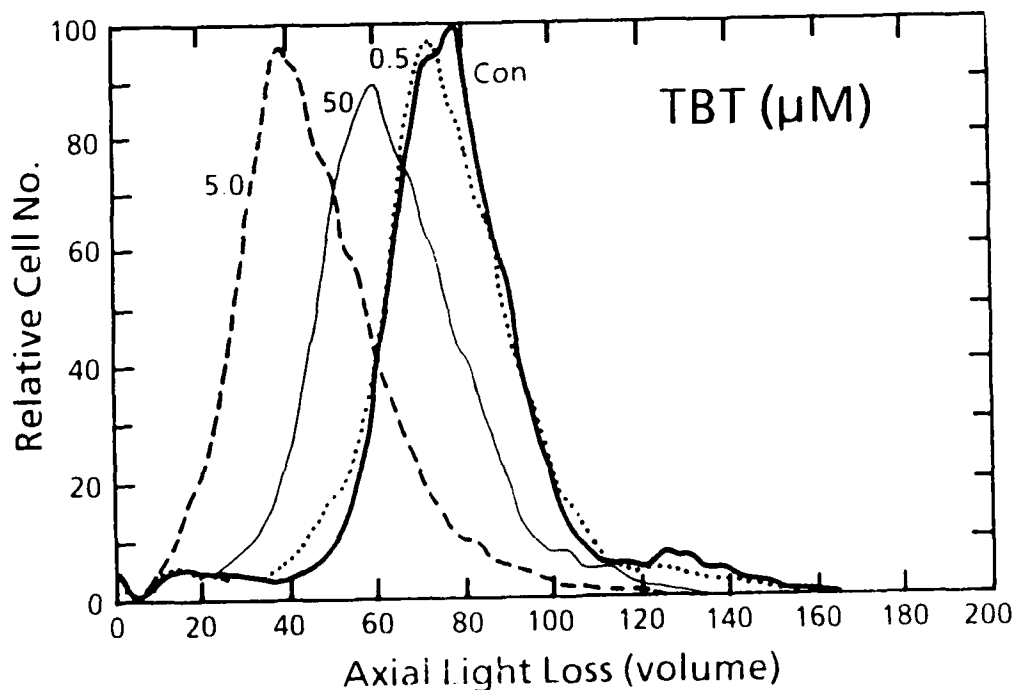


Figure 1. Axial light loss (histogram) of MELC as a function of TBT concentration. Exposure was for 4 h. The decrease in axial light loss (cell volume) is a non-vectorial function of TBT concentration. The decrease in cell volume is believed to be the consequence of TBT-mediated  $\text{Cl}^-/\text{OH}^-$  exchange. The smaller decrease in volume at  $50 \mu\text{M}$  TBT compared to  $5 \mu\text{M}$  appears to be a function of rate of fixation which increases with concentration.

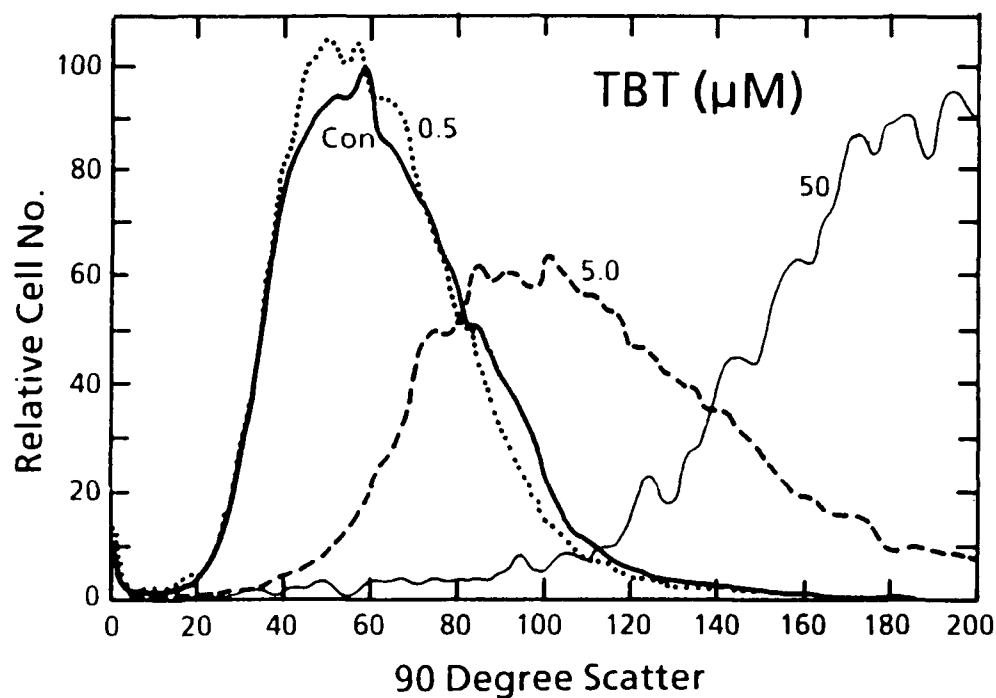


Figure 2. 90° light scatter (histogram) of MELC as a function of TBT concentration. Exposure was for 4 h. 90° scatter increases as the concentration of TBT increases above 0.5 μM.

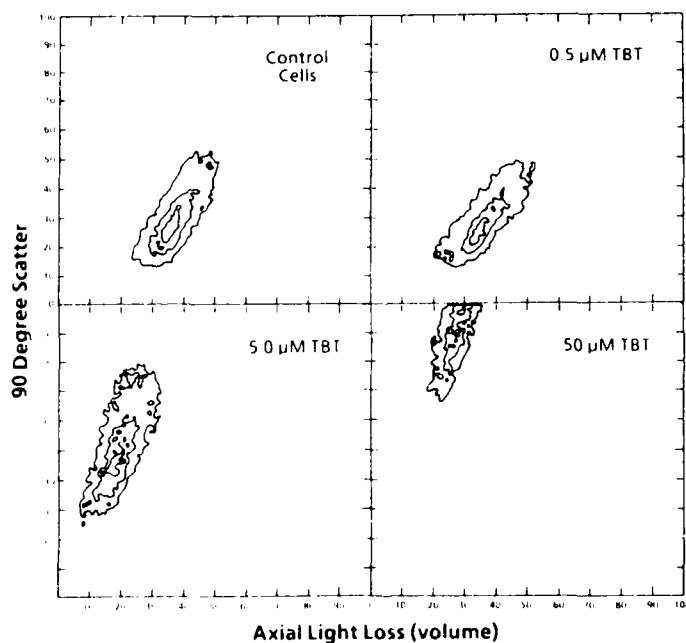


Figure 3. The data of Figures 1 and 2 are plotted together in a contour format (cytogram) in which relative cell number is displayed as a series of stacked plateaus outlined by concentric lines denoting surfaces generated by data points, each of which is defined by the intersection of the values of its axial light loss (x-axis) and 90° light scatter (y-axis) parameters.

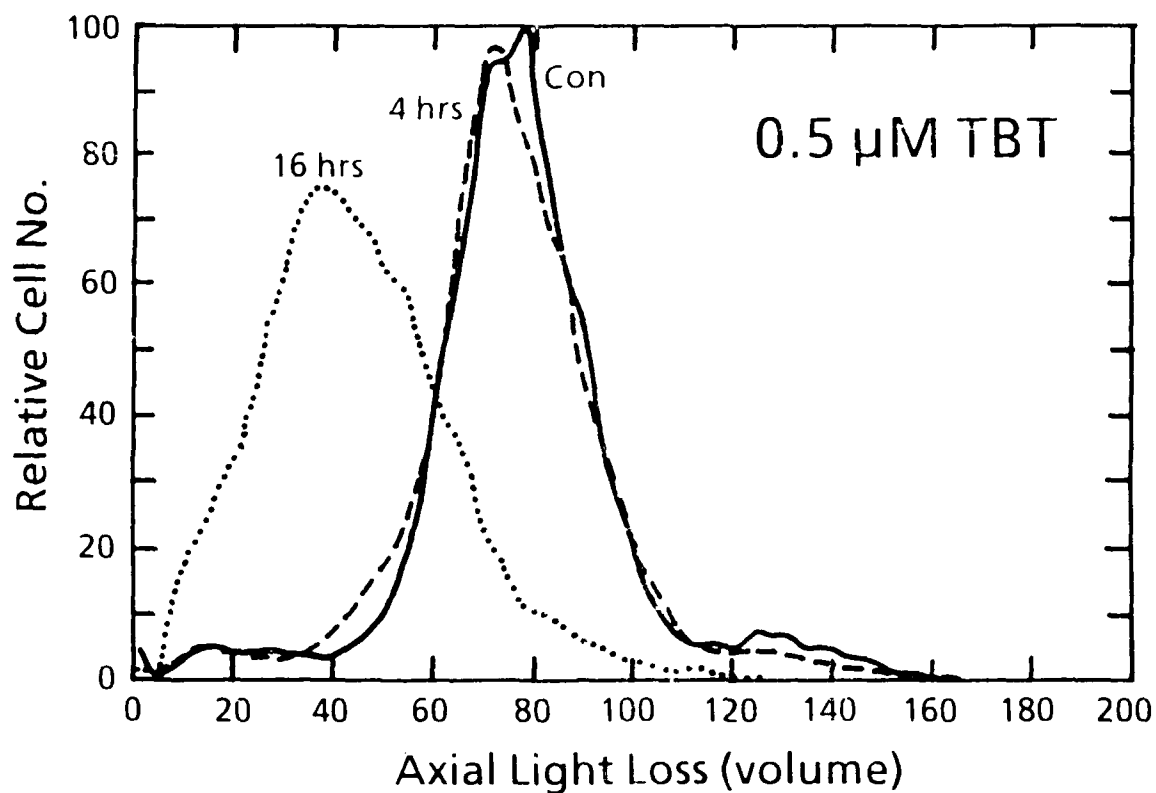


Figure 4. The time-dependence of axial light loss (histogram) at a single concentration of TBT. MELC were exposed to 0.5 μM TBT for 4 or 16 h at 37°C. Exposure for 16 h resembles that for 4 h at 5 μM TBT (refer to Figure 1).

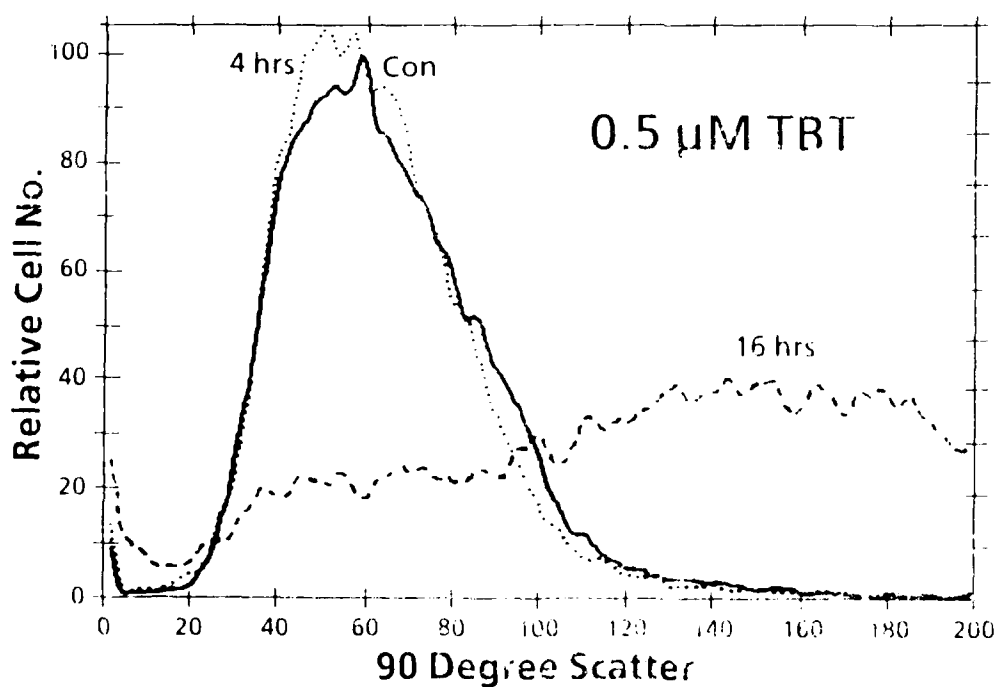


Figure 5. The time-dependence of 90° scatter (histogram) at a single concentration of TBT. MELC were exposed to 0.5 μM TBT for 4 h or 16 h at 37°C. Exposure for 4 h produces minimal effects while the effects of exposure for 16 h resemble those of exposure for 4 h at 5 μM TBT.

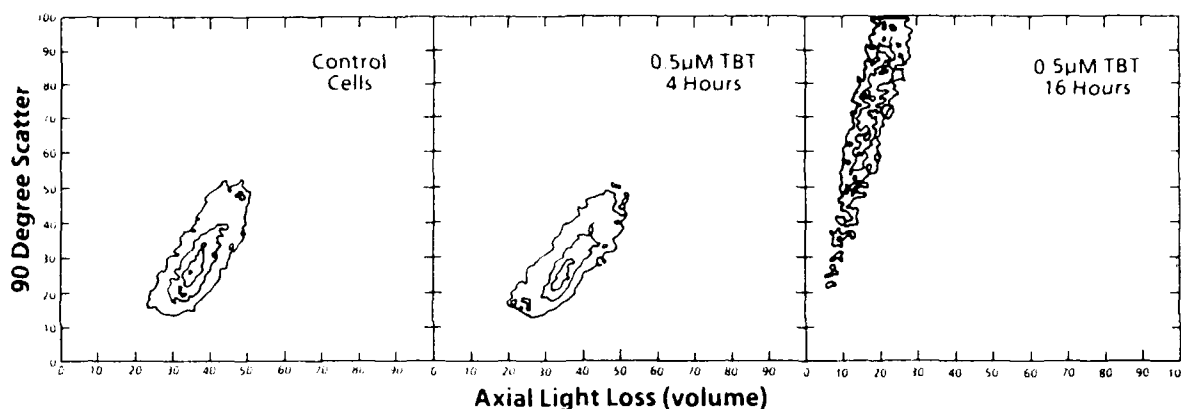


Figure 6. Fig. 6: Cytograms of 90° scatter (y-axis) versus axial light loss (x-axis) obtained from MELC exposed to 0.5  $\mu$ M TBT for 4 or 16 h. Note the increased complexity of the 16-h contour map, which denotes increased toxicity.

Flow cytometric analysis of the cell cycle is best accomplished with "clean" nuclei prepared by removal of the cell membrane/cytoplasm complex via nonionic detergent solubilization. Treatment of control MELC and cells exposed to 0.5  $\mu$ M TBT for 4 h with NP<sub>40</sub>, as described above, produces "clean" nuclei exhibiting baseline (control-equivalent) axial light loss and 90° scatter signals. However, at TBT concentrations above 0.5  $\mu$ M, the nuclei exhibit increased 90° light scatter and axial light loss (Figure 7). Light microscopy reveals that, at 50  $\mu$ M TBT, the majority of cells are intact. In effect, the cell membrane/cytoplasm complex is resistant to NP<sub>40</sub>-mediated solubilization. At 5  $\mu$ M TBT, the cell membrane/cytoplasm complex of the majority of cells appears to be only partially solubilized and the nuclei are pycnotic.

The G<sub>1</sub> peak of histograms of DNA distribution across the cell cycle obtained from nuclei prepared from cells exposed to 5 and 50  $\mu$ M TBT for 4 h exhibit a higher coefficient of variation (CV) than that of nuclei prepared from cells exposed to 0.5  $\mu$ M TBT or control conditions. However, nuclear preparations from cells exposed to 50  $\mu$ M TBT exhibit a lower CV than that of cells exposed to 5  $\mu$ M TBT. This suggests that the pycnotic condition of the nuclei of MELC exposed to 5.0  $\mu$ M TBT for 4 h is responsible, at least in part, for the higher CV (Figure 8).

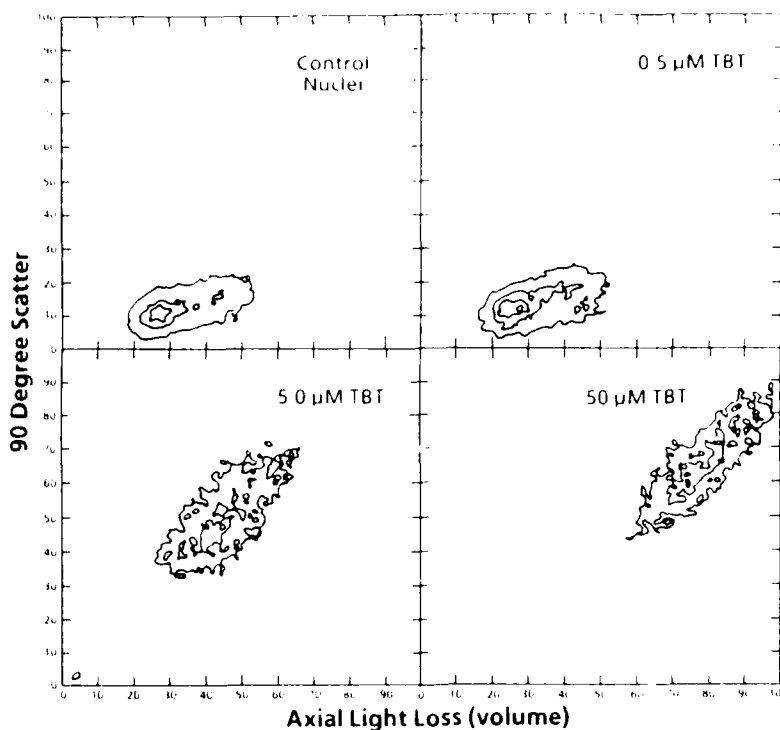


Figure 7. Cytofluorograms of 90° light scatter versus axial light loss of nuclei prepared from MELC exposed for 4 h to 0.5  $\mu$ M, 5  $\mu$ M, or 50  $\mu$ M TBT. Both flow cytometric parameters increase as a function of TBT concentration above 0.5  $\mu$ M.

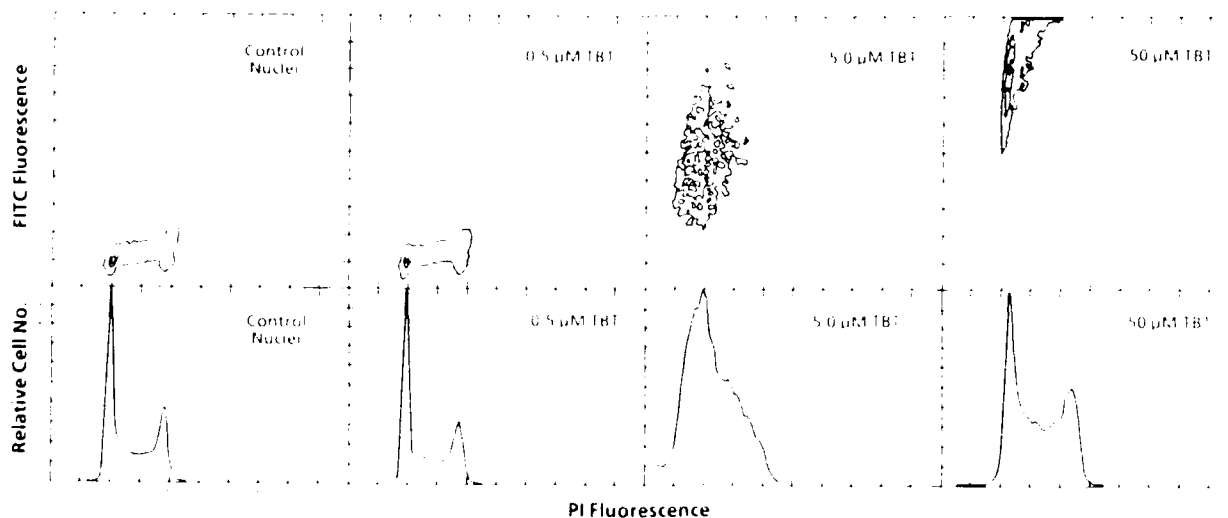


Figure 8. Cytofluorograms of nuclear FITC (protein) fluorescence versus PI (DNA) fluorescence and corresponding histograms of relative number of nuclei versus PI fluorescence. Control nuclei were prepared from untreated MELC. All other nuclei were prepared from cells exposed to TBT (0.5, 5.0 or 50.0  $\mu$ M) for 4 h.

FITC (protein) fluorescence of nuclei prepared from MELC exposed to TBT concentrations greater than 0.5  $\mu\text{M}$  (Figure 8) is increased due to retention of cytoplasmic tags (at 5.0  $\mu\text{M}$ ) or resistance to detergent-mediated solubilization of the cell membrane/cytoplasm complex (at 50  $\mu\text{M}$ ). The light microscopic appearance of MELC exposed to 50  $\mu\text{M}$  TBT for 4 h is similar to that of ethanol-fixed cells. In addition, in experiments in which the 90° light scatter of unfixed cells and nuclei prepared from unfixed cells was compared to that of ethanol-fixed cells, the fixed cells scattered more light than the unfixed cells, which scattered more light than the nuclei (Figure 9). The 90° scatter signal obtained from TBT-exposed cells falls between that of unfixed and ethanol-fixed cells, the exact position being dependent on the concentration of TBT (Figure 2) and the length of exposure (Figure 5). The 90° scatter signal of nuclei prepared from TBT-exposed cells is greater than that of nuclei prepared from unfixed/TBT-exposed ( $\leq 0.5 \mu\text{M}$ ) cells (Figure 7).

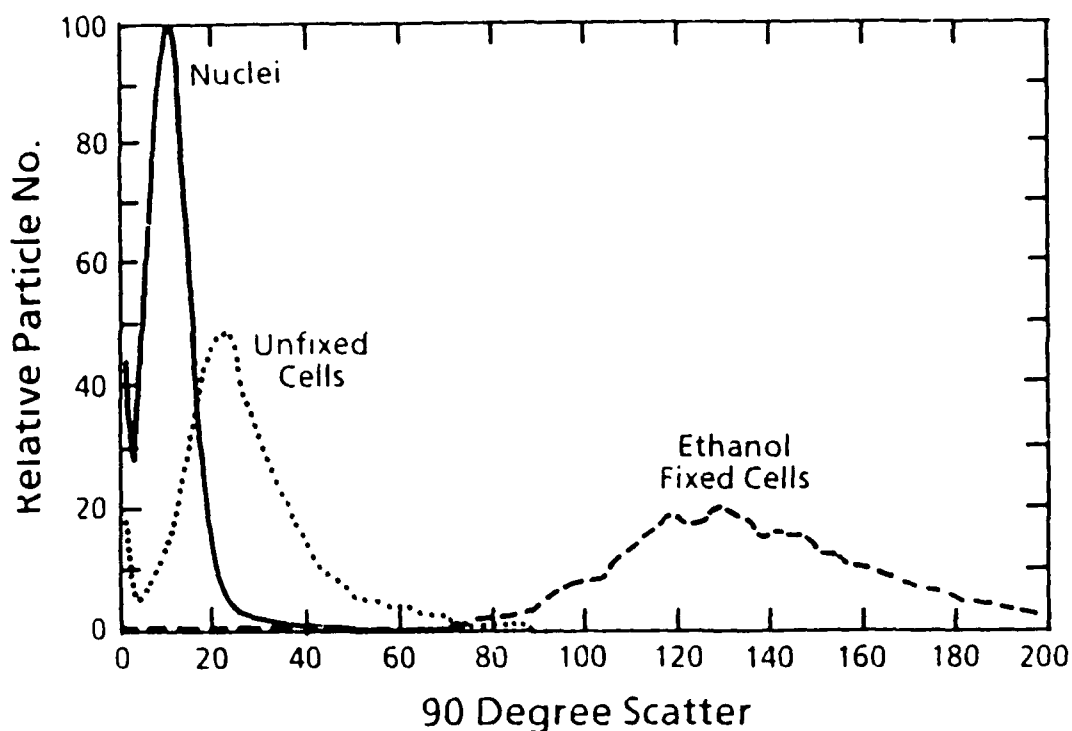


Figure 9. Comparison of the 90° light scatter of unfixed cells, nuclei prepared from unfixed MELC, and ethanol (95%)-fixed cells. Fixed cells have a greater refractive index (90° scatter signal) than unfixed cells, which have a greater refractive index than unfixed nuclei.

DiOC6 has been reported to be useful for obtaining a relative measure of plasma membrane potential [30,31]. Exposure of MELC to TBT (1.0, 2.5, or 5.0  $\mu\text{M}$ ) results in a concentration-dependent decrease in plasma membrane potential (control mean =  $29.1 \pm 13.3$  units; 1.0  $\mu\text{M}$  mean =  $23.4 \pm 12.8$  units; 2.5  $\mu\text{M}$  mean =  $13.0 \pm 11.3$  units; 5.0  $\mu\text{M}$  mean =  $7.9 \pm 2.7$  units). Corresponding to this decrease, 90° light scatter increased (control mean =  $17.0 \pm 7.1$  units; 1.0  $\mu\text{M}$  mean =  $17.0 \pm 7.1$  units; 2.5  $\mu\text{M}$

mean =  $23.1 \pm 13.3$  units; 5.0  $\mu\text{M}$  mean =  $34.1 \pm 11.2$  units) and forward blue scatter (a measure of cell volume) decreased (control mean =  $21.4 \pm 5.1$  units; 1.0  $\mu\text{M}$  mean =  $18.5 \pm 4.6$  units; 2.5  $\mu\text{M}$  mean =  $17.3 \pm 5.4$  units; 5.0  $\mu\text{M}$  mean =  $16.4 \pm 4.1$  units) (Figure 10). These data, along with those of viability (PI exclusion), are summarized in Figure 11: as viability (PI exclusion) decreases, the potential across the cell membrane (DiOC6 fluorescence) decreases and 90° light scatter increases. Tables 1 and 2 summarize the concentration-dependent (4-h exposure) effects of TBT on biophysical and morphological parameters of MELC and MELC nuclei.

Two other conditions in which the cell membrane is known to be altered, namely the stationary phase compared to the logarithmic phase of the cell growth curve and the differentiated compared to the undifferentiated state of the MELC, were investigated [25-30]. Equal numbers ( $2.4 \times 10^5$  cells) of normal logarithmically growing MELC (density =  $2.9 \times 10^5$  cells/ml) were compared to early stationary (density =  $1.1 \times 10^6$  cells/ml) and late stationary phase (density =  $1.7 \times 10^6$  cells/ml) cells. Greater CF retention was observed in late stationary phase compared to early stationary phase cells, which exhibited greater CF retention than logarithmically growing cells (Figure 12).

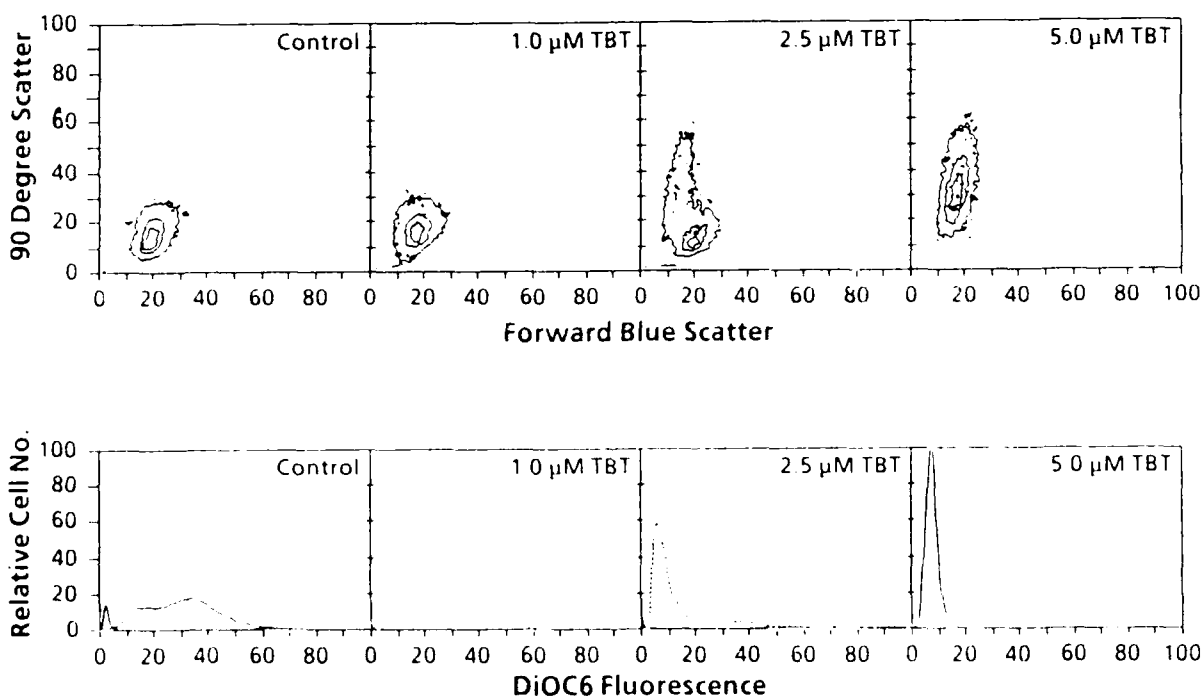


Figure 10. Cytograms of 90° scatter versus forward blue scatter and corresponding histograms of DiOC6 fluorescence obtained from MELC exposed to 1.0, 2.5, or 5.0  $\mu\text{M}$  TBT for 4 h. As TBT concentration increases, 90° light scatter increases and DiOC6 fluorescence (relative membrane potential) decreases.

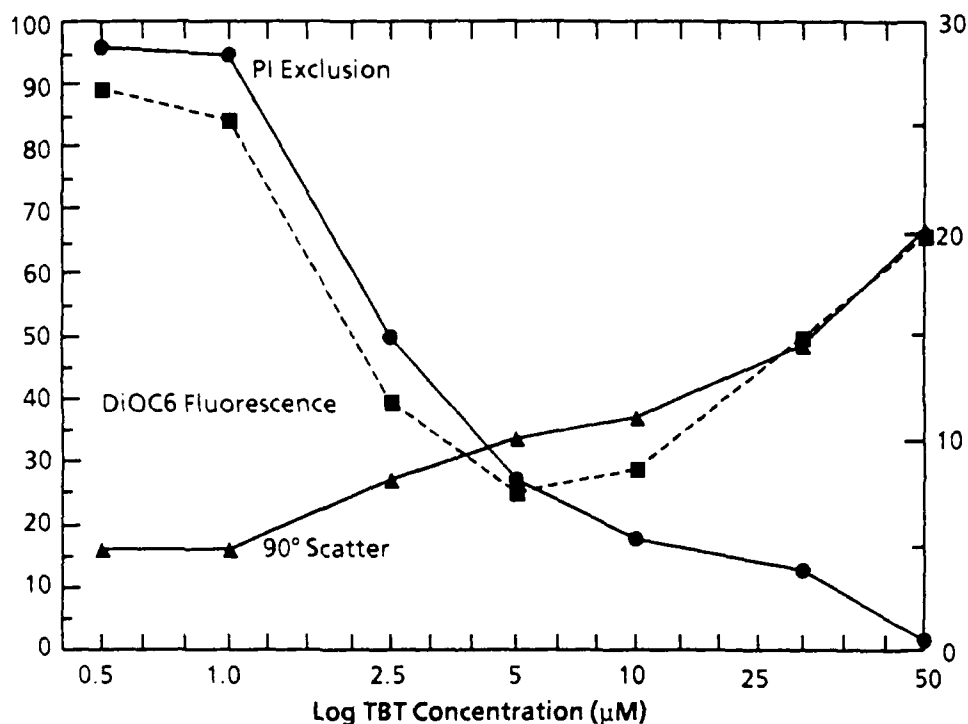


Figure 11. Summary plot of mean 90° light scatter, mean DiOC6 fluorescence, and the percentage of MELC excluding PI as a function of TBT concentration.

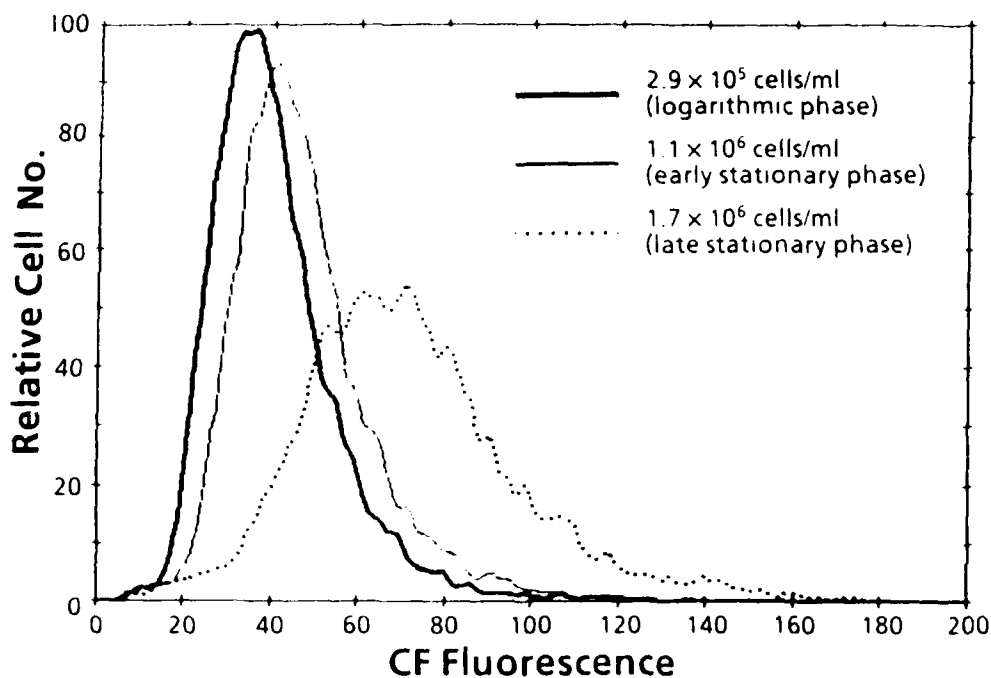


Figure 12. Comparison of the cellular CF fluorescence of logarithmically growing cells (density =  $2.9 \times 10^5$  cells/ml), early stationary phase cells (density =  $1.1 \times 10^6$  cells/ml), and late stationary phase cells (density =  $1.7 \times 10^6$  cells/ml). CF fluorescence was measured in viable cells only (cells excluding PI).

TABLE 1: Changes in cellular parameters. Summary of the concentration-dependent (4-h exposure) effects of TBT on biophysical and morphological parameters of MELC. CF retention data are derived from a previous study [22].

TBT Dose ( $\mu$ M)	PI Exclusion (Viability)	Carboxy-fluorescein Retention	DiOC <sub>6</sub> Fluorescence (Membrane Potential)	Axial Light Loss (Cellular Volume)	90° Light Scatter (Internal Structure)	Microscopy
0.5	No loss of viability	Increased retention	Decreased cell membrane potential	No change	No change	No PI fluorescence
5.0	Large decrease in viability	Increased retention	Further decrease	Large decrease	Increased	Simultaneous PI and CF fluorescence
50.0	Further decrease	Decreased retention (< control)	Increased, but < control	< control > 5.0 $\mu$ M dose	Further increase	Simultaneous PI and CF fluorescence

TABLE 2: Changes in Nuclear Parameters. Summary of the concentration-dependent (4-h exposure) effects of TBT on biophysical and morphological parameters of MELC nuclei.

TBT Dose ( $\mu$ M)	DNA Histogram (Cell Cycle Effects)	FITC Fluorescence (Protein)	Axial Light Loss (Nuclear Volume)	90° Light Scatter (Internal Structure)	Microscopy (NP <sub>40</sub> Lysis)
0.5	Normal distribution	No change	No change	No change	"Clean" nuclei
5.0	increased C.V. of G <sub>1</sub> peak. Perturbed distribution	Increased	Increased	Increased	Cytoplasmic tags Pycnosis
50.0	Improved distribution C.V. of G <sub>1</sub> peak > control, but < 5.0 $\mu$ M dose.	Further increase	Further increase	Further increase	Intact ("fixed") cells (no lysis)

MELC were differentiated by exposure to 1 mM butyric acid (BA) or 1.5% DMSO for 3 days [32]. Such treatment results in a decrease in cell volume and alteration of the nature of the plasma membrane [25-28,32]. Mean cellular CF fluorescence is decreased in DMSO-treated cells and increased in BA-treated cells (Figure 13). The decreased CF fluorescence of DMSO-treated cells can be explained as a consequence of increased plasma membrane permeability resulting from the treatment with the reagent [25]. The increased retention of CF by the BA-treated cells is consistent with previously reported observations of decreased MELC plasma membrane permeability following BA-mediated differentiation [25,27,28].

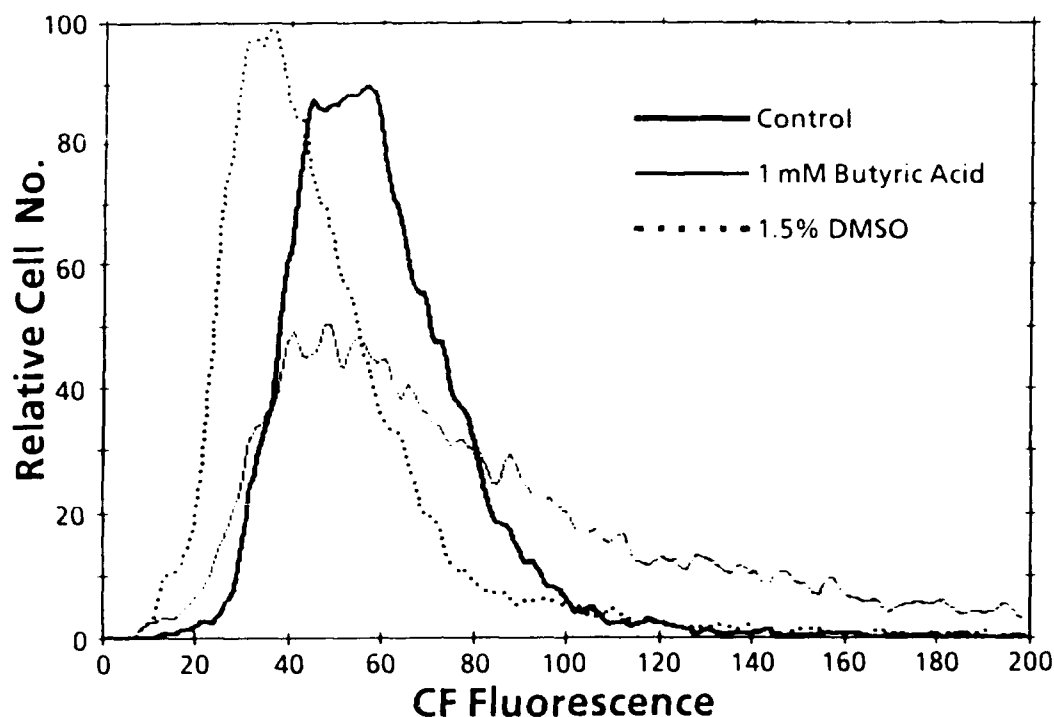


Figure 13. Comparison of cellular CF fluorescence of MELC differentiated by exposure to 1.5% DMSO or 1 mM BA for 3 days. Differentiation by either method results in a decrease in cell volume and rate of growth. CF fluorescence was measured in viable cells only (cells excluding PI).

## DISCUSSION

The cell interfaces with its environment via the plasma membrane and interacts with its environment via membrane and transmembrane processes. Therefore, alteration of the composition/structure of the plasma membrane can result in altered cell function. The ability to detect subtle changes in the condition of the membrane may be of considerable value in predicting the response of cells to toxic insult.

TBT is a lipophilic, membrane-active molecule [11,14]. To gain insight into its mechanism of action, we have investigated its effects on flow cytometric parameters of the MELC. The MELC was

selected for study primarily because of the large literature on its biology, its capacity to be differentiated, and its ability to grow in suspension culture, thereby reducing possible membrane damage resulting from harvesting techniques.

TBT is a potent inhibitor of  $(\text{Na}^+, \text{K}^+)\text{-ATPase}$  activity [12], and facilitates halide/hydroxyl exchange across the cell membrane [5-8]. By flow cytometric analysis, we have observed that exposure to TBT can result in decreased cell volume (decreased axial light loss) and increased  $90^\circ$  scatter. Increased  $90^\circ$  scatter also is a consequence of fixation (Figure 9). These findings, together with our observation that TBT-treated cells become resistant to detergent-mediated lysis and solubilization of the cell membrane/cytoplasm complex [22], suggest fixation (protein denaturation, cross-linking, etc.) as a significant mechanism of the toxic action of TBT.

The decreased cell volume (axial light loss) observed following exposure (for 4 h) to  $5\ \mu\text{M}$  compared to  $50\ \mu\text{M}$  TBT (Figures 1,3) appears to be related to the rate/degree of fixation of the cell membrane/cytoplasm complex. At the higher concentration, TBT apparently "hard fixes" the complex. Due to a relatively slow rate of fixation at the lower concentration, the decrease in cell volume may be the result of TBT-mediated  $\text{Cl}^-/\text{OH}^-$  exchange [5] and/or autolytic processes. In any case, TBT-mediated decrease in cell volume is manifested as a non-vectorial function of concentration.

The occurrence of nuclear pycnosis following exposure to  $5\ \mu\text{M}$ , as opposed to  $50\ \mu\text{M}$ , TBT supports the hypothesis of slow/incomplete fixation at the lower concentration. In addition, we have observed that the quantity of light scattered in the  $90^\circ$  direction by MELC decreases in the following order: ethanol (95%) fixation/exposure to  $50\ \mu\text{M}$  TBT for 4 h > exposure to  $5\ \mu\text{M}$  TBT for 4 h > untreated (control) cells > nuclei prepared from control cells. The rate and degree of fixation impinge upon the density (fluidity) of the cell. Fixation increases cell density and increased density increases refractive index and, therefore,  $90^\circ$  scatter. In addition, by altering protein-protein interactions, the lipid-protein interactions, etc., fixation alters the solubility properties of the cell membrane/cytoplasm complex. "Hard-fixed" cells, such as those exposed to 95% ethanol for 30 min or  $50\ \mu\text{M}$  TBT for 4 h (or longer), become resistant to detergent-mediated cytolysis/solubilization of the cell membrane/cytoplasm complex.

We have observed that FITC (protein) fluorescence and  $90^\circ$  light scatter of nuclei prepared from MELC exposed to TBT increase as a function of the product of TBT concentration ( $C$ ) times duration ( $T$ ) of exposure [23]. Likewise, the CV of the  $G_1$  peak of DNA histograms increases. Light and fluorescence microscopy reveal that, above a critical value of the product of  $C \times T$  (CPV), detergent-mediated solubilization of the cell membrane/cytoplasm complex is blocked; in effect, the cell is fixed. Below the CPV, a range of  $C \times T$  product values exists that allows varying degrees of detergent-

mediated cytolysis/solubilization of the cell membrane/cytoplasm complex resulting in preparations of nuclei containing varying quantities of nuclei-adherent cytoplasmic remnants [22]. Thus, the increase in the nuclear axial light loss signal (volume), 90° light scatter (internal structure), FITC fluorescence (protein content), and CV of the G<sub>1</sub> peak of DNA histograms (Figures 7,8) correlate with resistance of the cell to detergent-mediated cytolysis. The broadening of the CV of the G<sub>1</sub> peak of DNA histograms suggests variability of PI and/or RNase uptake or reduced RNase efficiency (e.g., reduced substrate accessibility as a consequence of physicochemical alterations/pycnosis) and is consistent with a fixation mode of action of TBT. It is to be emphasized that exposure to 5  $\mu$ M TBT for 4 h yields the poorest resolution of DNA distribution (Figure 8) and results in nuclear pycnosis, phenomena consistent with cell injury. Better resolution is obtained from cells exposed to 50  $\mu$ M TBT for 4 h, which hard fixes the cell (simulating alcohol fixation), while exposure to 0.5  $\mu$ M TBT yields resolution comparable to that of control nuclei [22].

MELC membrane potential (relative potential referenced to DiOC6 fluorescence) decreases as a function of TBT concentration (4-h exposure) up to 5.0  $\mu$ M. The percentage of cells excluding PI also decreases in parallel with membrane potential (Figure 11). Both membrane potential and PI exclusivity remain relatively constant up to 1.0  $\mu$ M TBT and decrease precipitously at higher concentrations. At TBT concentrations greater than 5.0  $\mu$ M, DiOC6 fluorescence increases. However, microscopic observation reveals that the fluorescence was pale and diffusely uniform throughout the cytoplasm, as opposed to the bright, multifocal fluorescence characteristic of control cells and cells treated with TBT at lower concentrations. This indiscriminate uptake of DiOC6/PI denotes that the cell is programmed for death and indicates irreversible damage following exposure for 4 h to concentrations of TBT greater than or equal to 1.0  $\mu$ M.

Numerous substances, including organic and inorganic metal compounds, can interfere with membrane molecular structure/interactions/function and subsequently perturb membrane integrity and the functioning of the cell. Disruption of membrane integrity allows PI to enter the cell, and uptake of PI is indicative of irreversible cell damage. In the CFDA/PI viability assay, PI uptake can occur in cells exhibiting CF fluorescence so long as intracellular esterase activity is preserved and sufficient integrity of the cell membrane/cytoplasm complex exists to retard CF efflux. This results in cells exhibiting both red nuclei and green cytoplasmic fluorescence (unpublished data). This phenomenon is observed in cells exposed to concentrations of 2.5 and 5.0  $\mu$ M TBT for 4 h. At 50  $\mu$ M TBT, the cell is hard fixed, the nucleus is stained with PI, and the cytoplasm exhibits minimal CF fluorescence [23]. Since the CFDA/PI assay is a standard method for assessing viability, investigators should be aware that, under certain conditions, the cell can absorb both dyes and exhibit simultaneous red and green fluorescence.

In summary, we have reported that exposure to TBT results in increased resistance of the MELC to detergent-mediated cytolysis [22], inhibition of 2-dimensional crystallization of (Na<sup>+</sup>,K<sup>+</sup>)-ATPase in microsomal membrane preparations, and increased impedance of cellular CF efflux below the CPV [23]. In addition, above the CPV, TBT exposure increases 90° light scatter and decreases axial light loss, PI enters the cell, and membrane potential decreases. These data suggest fixation, the denaturation and cross-linking of proteins of the cell membrane/cytoplasm complex, as a mechanism of the toxic action of TBT.

## REFERENCES

1. Krigman, M.R. and Silverman, A.P. (1984) General toxicology of tin and its organic compounds. *Neurotoxicology* 5(2), 129-140.
2. Schweinfurth, H. (1985) Toxicology of tributyltin compounds. *Tin and Its Uses*, 143, 9-12.
3. Aldridge, W.N., Verschoyle, R.D., Thompson, C.A., and Brown, A.W. (1987) The toxicity and neuropathology of dimethyltin and methyldiethyltin in rats. *Neuropathol. Appl. Neurobiol.* 13, 55-69.
4. Brock, T.O. and O'Callaghan, J.P. (1987) Quantitative changes in the synaptic vesicle proteins synapsin I and p38 and the astrocyte-specific glial fibrillary acidic protein are associated with chemical-induced injury to the rat central nervous system. *J. Neurosci.* 7(4), 931-942.
5. Selwyn, M.J., Dawson, A.P., Stockdale, M., and Gains, N. (1970) Chloride-hydroxide exchange across the mitochondrial, erythrocyte, and artificial lipid membranes by trialkyl- and triphenyltin-compounds. *Eur. J. Biochem.* 14, 120-126.
6. Selwyn, M.J. (1976) Triorganotin compounds as ionophores and inhibitors of ion-translocating ATPases. In: J.J. Zuckerman (Ed.), *Organotin Compounds: New Chemistry and Applications*, American Chemical Society, Washington, D.C., pp. 204-226.
7. Tosteson, M.T. and Wieth, J.O. (1979) Tributyltin-mediated exchange diffusion of halides in lipid bilayers. *J. Gen. Physiol.* 73, 789-800.
8. Wieth, J.O. and Tosteson, M.T. (1979) Organotin-mediated exchange diffusion of anions in human red cells. *J. Gen. Physiol.* 73, 765-788.
9. Gray, B.H., Porvaznik, M., and Lee, L.H. (1986) Cyanide stimulation of tri-*n*-butyltin-mediated hemolysis. *J. Appl. Toxicol.* 6, 263-269.
10. Gray, B.H., Porvaznik, M., Lee, L.H., and Fleming, C. (1985) Inhibition of tributyltin-mediated hemolysis by mercapto compounds. *J. Appl. Toxicol.* 6, 363-370.
11. Snoeij, N.J., Van Iersel, A.A.J., Penninks, A.H., and Seinen, W. (1986) Triorganotin-induced cytotoxicity to rat thymus, bone marrow, and red blood cells as determined by several *in vitro* assays. *Toxicology* 39, 71-83.
12. Stockdale, M., Dawson, A.P., and Selwyn, M.J. (1970) Effects of trialkyltin and triphenyltin compounds on mitochondrial respiration. *Eur. J. Biochem.* 15, 342-351.

13. Johnson, T.L. and Knowles, C.O. (1983) Effects of organotins on rat platelets. *Toxicology* 29, 39-48.
14. Porvaznik, M., Gray, B.H., Mattie, D., Jackson, A.G., and Omlor, R.E. (1986) The ultrastructural localization of tri-*n*-butyltin in human erythrocyte membranes during shape transformation leading to hemolysis. *Lab. Invest.* 54, 254-267.
15. Snoeij, N.J., Punt, P.M., Penninks, A.H., and Seinen, W. (1986) Effects of tri-*n*-butyltin chloride on energy metabolism, macromolecular synthesis, precursor uptake and cyclic AMP production in isolated rat thymocytes. *Biochim. Biophys. Acta* 852, 234-243.
16. Awakawa, Y. and Wada, O. (1984) Inhibition of neutrophil chemotaxis by organotin compounds. *Biochem. Biophys. Res. Commun.* 123, 543-548.
17. Pace, C.S. and Tarvin, J.T. (1983) pH modulation of glucose-induced electrical activity in B-cells: involvement of Na/H and HCO<sub>3</sub>/Cl antiporters. *J. Membrane Biol.* 73, 39-49.
18. Shapiro, H.M. (1985) *Practical Flow Cytometry*. Alan R. Liss, Inc., New York, pp. 94-96, 129-130.
19. Rotman, B. and Papermaster, B.W. (1966) Membrane properties of living cells as studied by enzymatic hydrolysis of fluorogenic esters. *Proc. Natl. Acad. Sci.* 55, 134-141.
20. Goodall, H. and Johnson, M.H. (1982) Use of carboxyfluorescein diacetate to study formation of permeable channels between mouse blastomeres. *Nature* 295, 524-526.
21. Penttila, A., McDowell, E., and Trump, B. (1977) Optical properties of normal and injured cells. *J. Histochem. Cytochem.* 25, 9-20.
22. Zucker, R.M., Elstein, K.H., Easterling, R.E., and Massaro, E.J. (In Press) Metal-induced alteration of the cell membrane/cytoplasm complex studied by flow cytometry and detergent lysis. *Toxicology*.
23. Zucker, R.M., Elstein, K.H., Easterling, R.E., and Massaro, E.J. (In Press) Effects of tributyltin on biomembranes: alteration of flow cytometric parameters and inhibition of (Na<sup>+</sup>, K<sup>+</sup>)-ATPase two-dimensional crystallization. *Toxicol. Appl. Pharmacol.*
24. Thornethwaite, J.J., Sugarbaker, E.O., and Temple, W.J. (1980) Preparation of tissues for DNA flow cytometric analysis. *Cytometry* 1, 225-237.
25. Lyman, G.H., Preisler, H.D., and Papahadjopoulos, D. (1976) Membrane action of DMSO and other chemical inducers of Friend leukemic cell differentiation. *Nature* 262, 360.
26. Marks, P.A. and Rifkind, R.A. (1978) Erythroleukemic differentiation. *Ann. Rev. Biochem.* 47, 409.
27. Loritz, F., Bernstein, A., and Miller, R.C. (1977) Early and late volume changes during erythroid differentiation of cultured Friend leukemic cells. *J. Cell Physiol.* 91, 423.
28. Tapiero, H., Fourcade, A., and Billar, C. (1980) Membrane dynamics of Friend leukemic cells II: changes associated with cell differentiation. *Cell Differentiation* 9, 211.
29. Watson, J.O. (1980) Enzyme kinetic studies in cell populations using fluorogenic substrates and flow cytometric techniques. *Cytometry* 1, 143-151.

30. Dwyer, T.M. and Cuchens, M. (1987) Membrane potential measurements by flow cytometry. *J. Electrophysiol. Tech.* 14, 43-57.
31. Shapiro, H.M. ( 1985) *Practical Flow Cytometry*. Alan R. Liss, Inc., New York, pp. 141-153.
32. Zucker, R.M., Wu, N.C., Mitrani, A., and Silverman, M. (1975) Cell volume decrease during Friend leukemic cell differentiation. *J. Histochem. Cytochem.* 27, 413-416.

## FLOW CYTOMETRY TECHNIQUES IN RADIATION BIOLOGY

Kenneth F. McCarthy and Martha L. Hale

*Radiation Biochemistry Department, Armed Forces Radiobiology Research Institute, Bethesda, MD  
(U.S.A.)*

### SUMMARY

Hematopoietic stem cells (HSC) are present in the marrow at a concentration of approximately 2 to 3 HSC per 1,000 nucleated marrow cells. In the past, only clonogenic assays requiring 8 to 13 days and 10 irradiated recipient rodents were available for assaying HSC. Because of the importance of HSC in the post-irradiation syndrome, we have developed a new rapid method based on flow cytometry not only to assay but also to purify and characterize HSC. This new method makes extensive use of monoclonal antibodies conjugated to fluorescent phycobiliproteins through the sulfhydryls of the hinge region of the IgG molecule. An optical bench arrangement with a dye laser and an argon laser was used for dual excitation of the phycobiliprotein-monoclonal antibody conjugates and various cellular and DNA probes. Using 4',6-diamidino-2-phenylindole dihydrochloride (DAPI) exclusion to identify viable cells, it was possible to follow regeneration of postirradiated rat marrow HSC.

### INTRODUCTION

Considerable evidence exists that all blood cells are derived from HSC. These cells are of interest to radiobiologists because they are highly sensitive to low doses of ionizing radiation [1]. In the rodent HSC, as measured by the CFU-S assay, is characterized by a  $D_0$  of 0.8-1.0 Gy. As such, doses greater than 9 Gy effectively sterilize the HSC compartment. If not rescued by bone marrow grafting, the lethally irradiated individual will eventually die, primarily from bleeding and sepsis, due to the inability to replenish blood cells from HSC. Therefore, it is of importance to understand how radiation damages these HSC in order to prevent this damage or to devise methods by which the damaged HSC may be replaced in the irradiated individual.

The major difficulty in studying directly the interaction of ionizing radiation with the HSC is the scarcity of these cells in the marrow and the lack of a distinguishing feature necessary for their accurate and rapid identification. In the rat, HSC comprise less than 0.3% of the total marrow hematopoietic cells [2,3]. In the past, efforts to isolate the HSC used physical techniques such as density gradient centrifugation in isotonic media, sedimentation velocity, elutriation, electrophoresis, nylon wool filtration, and plastic adherence. These techniques usually result in purification of less than 10-fold, which is well short of the 300-fold-plus purification necessary to generate a pure HSC population. For this reason this laboratory and others [4] have made extensive

use of the techniques of flow cytometry and/or fluorescence-activated cell sorting [5] for the isolation and identification of HSC.

## MATERIALS AND METHODS

### *Flow cytometry and sorting*

Flow cytometry measurements and cell sorts were performed on a dual laser Becton Dickinson FACS II cell sorter interfaced to a Consort 40 computer system. The optical bench arrangement for the dual lasers is shown in Figure 1.

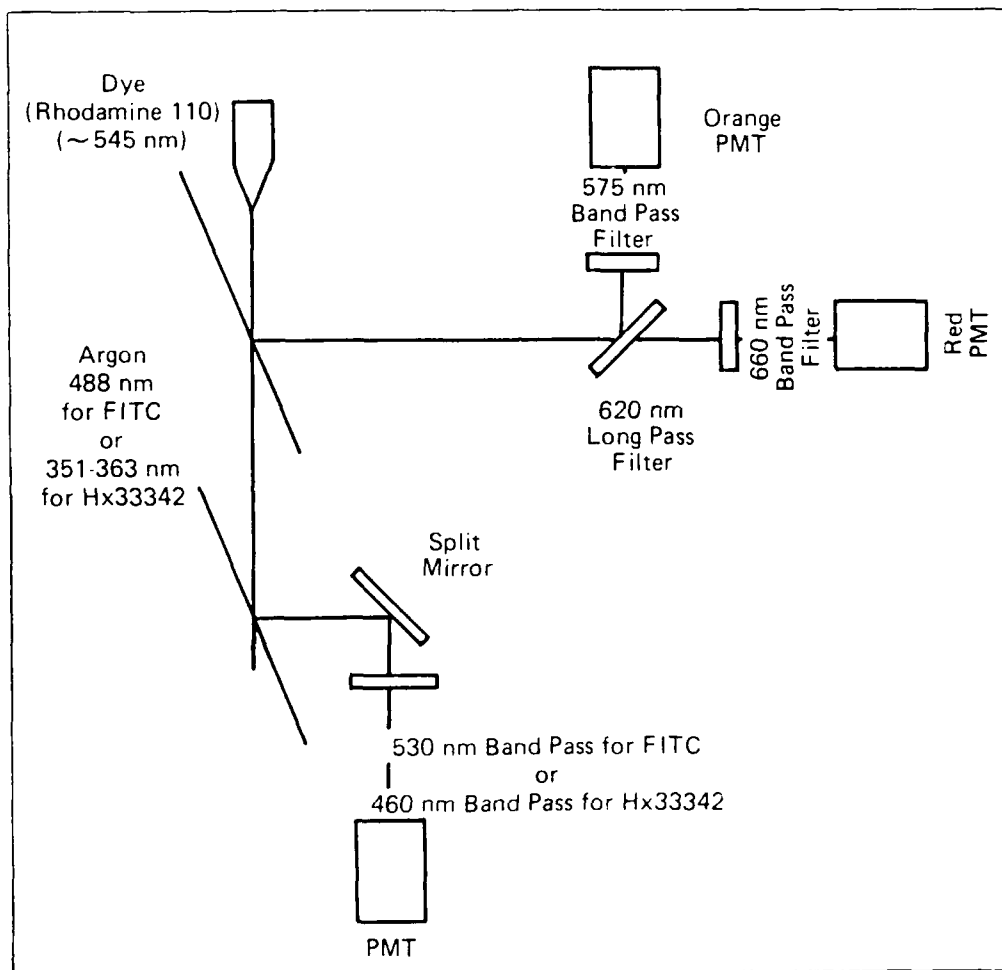
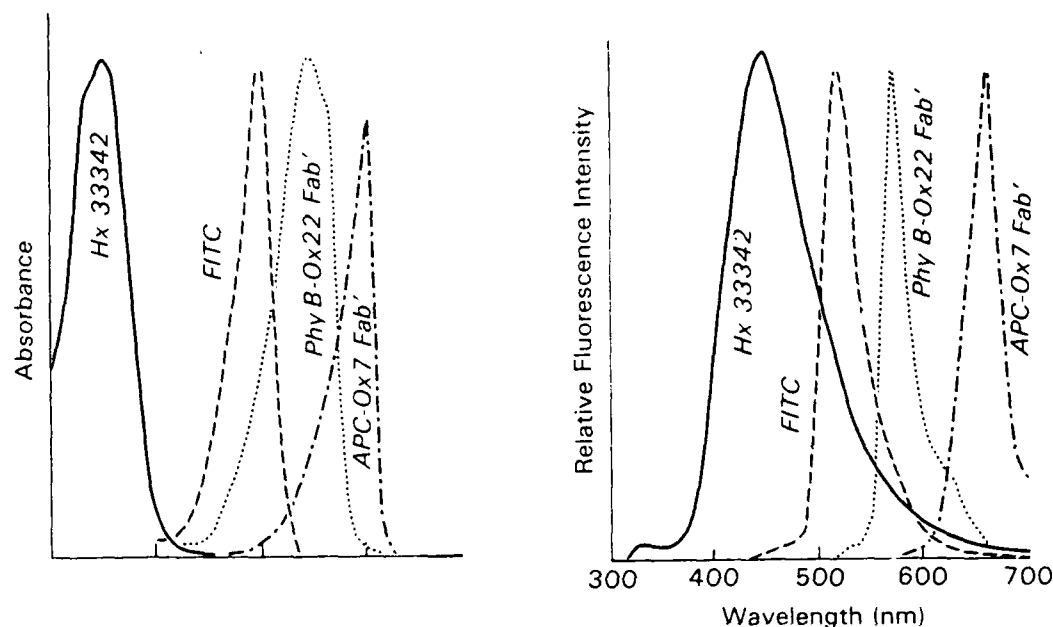


Figure 1. Optical bench arrangement of four parameter light activated cell sorter.

### *Phycobiliproteins*

Studies of the isolation and characterization of HSC have made extensive use of a new class of fluorescent proteins referred to as phycobiliproteins [6]. These fluorescent proteins are isolated from cyanobacteria (blue-green algae) and red algae. They show maximum absorbance in the 470 to 650

nm region, and fluorescence emission bands begin in the orange (550 nm) and extend into the far red. The molar fluorescence intensity of phycoerythrins is up to 20 times that of fluorescein isothiocyanate (FITC). Several different proteins are included in the phycobiliprotein family. We have used primarily phycoerythrin B (PhyB) and allophycocyanin (APC). The excitation and emission spectra of these two phycobiliproteins are shown in Figure 2.



**Figure 2.** Excitation and emission spectra of several compounds. Hx33342 is a DNA specific dye used to generate cell cycle DNA histograms. Absorption and emission fluorescence spectra were determined on a model SLM-8000 fluorescence spectrophotometer. Spectra are normalized at peak amplitude and are uncorrected.

#### ***Lasers and optical bench arrangement***

Because both phycoerythrin R (PhyR) and FITC have an absorbance maximum between 490 and 496 nm but emit at different wavelengths (in green and orange, respectively), most dual parameter immunofluorescence work is performed using the strong 488.0 nm spectral line of the argon laser to excite both PhyR- and FITC-conjugated monoclonal antibodies bound to cell surface determinants. However, we have chosen to label two different monoclonals with two different phycobiliproteins rather than one phycobiliprotein and FITC [3]. We have found that excitation for both APC and PhyB can be performed effectively with the krypton laser tuned to the 530.9-nm spectral line, by an argon laser tuned to the 528.7-nm spectral line, or by a dye laser (rhodamine 110) tuned to approximately 545-nm spectral line. Further, we have shown that APC can also be excited with the 488.0 argon laser spectral line, allowing 3 parameter immunofluorescence studies (APC, PhyB, and FITC) to be performed with a single laser. However, it was determined that the best results are obtained when the dye laser is used as the primary laser and the argon laser (tuned to the 488-nm or UV spectral lines) is used as the delayed or secondary laser. This optical bench arrangement allowed us to not

only identify the HSC with the dye laser but also to analyze and characterize the HSC with the argon laser.

### ***Conjugation of monoclonal antibodies to phycobiliproteins***

It was found previously [2] that incubation of marrow cells with the monoclonal antibody Ox7 restricted the generation of splenic hematopoietic colonies (see *HSC assays*), presumably due to initiation of *in vivo* cellular cytotoxic events by the Fc region of the bound IgG molecule. This problem can be avoided by digesting the monoclonal antibody with pepsin, which produces the F(ab')<sub>2</sub> fragment. The F(ab')<sub>2</sub> fragment is then reduced with Cleland's reagent, and the Fab' with its free sulfhydryl is linked through a thioether bond to the maleimide-phycobiliprotein conjugate. Although time-consuming, this technique has proven to be a reliable method of conjugating monoclonal IgG to phycobiliproteins. The following monoclonal antibodies have all been conjugated to either PhyR, PhyB, or APC using this technique: W3/13, Ox22, Ox7, W3/25, Ox19, Ox8, and My10 [2,3]. These conjugates generate a more intense signal than can be achieved using the sandwich technique, which uses FITC-antimouse IgG antibody as the second antibody. There are other benefits of this technique. The Fab'-phycobiliproteins conjugates (greater than a year) have a long shelf life when stored at 4°C in 0.01% sodium azide. There is an absence of binding to Fc receptors, it is stable when shipped through the mail, and it is easy to perform 3 parameter immunofluorescence studies by using FITC-antimouse IgG Fc specific antibody as the second reagent in the sandwich technique [7].

A variation of the conjugation technique described above is as follows. Maleimidobutyl biocytin (MMB) is substituted for the maleimide-phycobiliprotein, the result being biotinylation of the free Fab' sulfhydryl group. Following incubation of cells with the biotinylated-Fab' antibody, avidin conjugated to either FITC or phycobiliprotein is added [3]. Unfortunately, this technique does not work with all monoclonal antibodies. For example, it works well with Ox8 but not with W3/13 or Ox22.

### ***Animals***

Lewis rats (male, 6 to 8 weeks old) were obtained from Charles River Labs (Kingston, NY) and were quarantined on arrival and screened for evidence of disease before being released from quarantine. They were maintained in an AAALAC-accredited facility in plastic Micro-isolator cages on hardwood chip contact bedding and were provided with commercial rodent chow and acidified tap water *ad libitum*. The rats were on a 12-h light/dark full spectrum with no twilight. Total body irradiation (TBR) was delivered with an opposing <sup>60</sup>Co radiation source as described previously [3]. Rats were euthanized by exsanguination while under methoxyfurane inhalation anesthesia. Irradiated rats were given 1 mg/mL tetracycline in their drinking water. Rats were cared for according

to principles enunciated in the Guide for the Care and Use of Laboratory Animals Resources, National Research Council.

### **HSC assays**

Three different HSC assays were used to measure the degree of HSC purification. They were the CFU-S assay [2], the 30-day survival of lethally irradiated recipient rats [3], and the intrathymic injection of histocompatible, T-cell allotype disparate donor stem cells [7]. The CFU-S assay was performed as follows: irradiated rats (9 Gy  $^{60}\text{Co}$  TBR, 0.4 Gy/min) were grafted by intravenous injection of bone marrow cellular suspensions or purified HSC. In the rat, approximately 3 to 10% of the stem cells seed the spleen [2], proliferate, and form discrete colonies of hematopoietic cells. The number of colonies formed is proportional to the number of HSC injected. This clonogenic assay is time-consuming: 11 to 13 days, as well as a large number of irradiated recipient animals, are required to perform this assay. The second assay involves grafting of HSC in order to protect lethally irradiated rats from the lethal effects of irradiation. Rats receive a dose of 9.5 Gy  $^{60}\text{Co}$  TBR, 0.4 Gy/min. The rats are then grafted with either normal marrow or purified HSC. The ratio number of normal marrow cells or purified HSC required to rescue the lethally irradiated rat is used to calculate the degree of purification of HSC. This assay is generally considered to be a more accurate assay for HSC than the CFU-S assay, which appears to measure committed as well as multipotent HSC [8]. The third assay used was the direct injection of either normal or purified Lewis rat HSC into the thymus of sublethally irradiated (8 Gy  $^{60}\text{Co}$  TBR, 0.4 Gy/min) Norway Black Rat (NBR) recipient rats [9]. After an extended incubation period, the HSC proliferate and differentiate into thymocytes. The number of newly generated thymocytes is measured by the use of the allogeneic system designated as RT 7. Lewis rats express the RT 7.1 antigen on thymocytes while the histocompatible NBR rats express the RT 7.2 antigen. Using the monoclonal antibodies BC-84 and 8G6.1, which recognize RT 7.1 and RT 7.2, respectively, the number of donor thymocytes (from Lewis marrow cells) that appear 18 days postinjection is a linear function of the number of cells injected. This assay establishes the origin of the newly formed thymocytes. Further, the thymus is an avascular organ and this minimizes the escape of the injected HSC into the circulation. The main advantage of this assay is its sensitivity, as it is 50 times more sensitive than the CFU-S assay [10].

### **Cell preparation and staining**

Rat marrow cells were prepared as described previously [3]. Staining with fluorescein diacetate (FDA) was performed according to the Hale and McCarthy method [11]. Cells were tagged with FITC-wheat germ lectin (FITC-WGA) according to the method of Visser et al. [12]. DAPI (1 mg/mL in distilled water) and propidium iodide (PI) (1 mg/mL in ethanol) were added to a cell suspension at a final concentration of 10  $\mu\text{g/mL}$  and 20  $\mu\text{g/mL}$ , respectively.

## RESULTS

### *HSC characterization and isolation*

The ideal solution to measuring the concentration of marrow HSC is to develop a monoclonal antibody to a membrane antigenic determinant expressed only on the HSC and no other marrow cell. Conjugation of this antibody with the appropriate fluorochrome would then allow fluorochrome-tagged HSC to be identified and separated from the remainder of the marrow by cell sorting. Unfortunately, no such unique HSC antigen has been identified to date. In order to isolate the HSC, it was necessary to label marrow hematopoietic cells with a "cocktail" of fluorochrome-conjugated monoclonal antibodies and/or lectins and to identify the HSC by pattern recognition. A partial list of monoclonals used and their specificities is presented in Table 1.

TABLE 1. MONOCLONAL ANTIBODIES RECOGNIZING DETERMINANTS ON RAT LYMPHOCYTES

Monoclonal Antibody <sup>a</sup>	Antigenic Determinant Recognized	Cell Population Recognized
Ox2	Glycoprotein on thymocyte membrane	B-cells, neuronal endothelial cells, thymocytes, dendritic cells
Ox3	Polymorphic determinant on rat 1a	B-cells, some epithelial cells, dendritic cells
Ox4	Polymorphic determinant on rat 1a	B-cells, 20% of thymocytes
Ox6	Monomorphic determinant on rat 1a	B-cells, 20% of thymocytes
Ox7	Rat thy 1.1 antigen	Thymocytes, stem cells, neuronal cells, immature B-cells
Ox8	Glycoprotein determinant on thymocyte membranes	Cytotoxic, suppressor T-cells, NK, thymocytes
Ox12	Rat kappa chains	B-cells
Ox17	$\alpha$ -chain rat 1a-antigen	B-cells
Ox18	Monomorphic determinant rat class I MHC	Class I MHC (RT-1A)
Ox19	Glycoprotein on thymocytes	Thymocytes, peripheral T-cells
Ox22	High molecular weight form of leukocyte common antigen	B-cells, some T-cells
W3/13	Sialoglycoprotein of rat thymocytes	Thymocytes, peripheral T-cells, granulocytes
W3/25	Glycoprotein on helper T-cells	Helper T-cells, thymocytes

The combination of conjugated antibodies that proved to be optimum for HSC identification was APC-Ox7 Fab', PhyB-Ox22 Fab', and FITC-W3/13 IgG. A correlated dual parameter plot of marrow cells tagged with the above mentioned antibodies and excited with a dye laser (rhodamine 110) tuned to 545 nm is shown in Figure 3. The HSC was found exclusively in the Ox7 upper 20% positive, Ox22 negative window [3,7]. The purification of HSC as measured by the CFU-S assay, survival following lethal irradiation, and intrathymic injection are presented in Table 2. There is a discrepancy between the CFU-S assay and the other two assays for measuring HSC purification. We believe this is due in part to an obligatory step of HSC lodgement in bone marrow before it can express itself in the spleen as a CFU-S assay [13]. Further, a more complex, dual laser, 3 parameter immunofluorescence study using a second argon laser tuned to 488 nm and FITC-W3/13 as the third antibody showed that the Ox7 upper 20% positive, Ox22 negative cells to be primarily W3/13 dim (80 to 90%) and the remainder W3/13 positive (data not shown).

**TABLE 2. ASSAYS FOR ANALYZING PURIFICATION OF STEM CELL POPULATIONS**

Route of Injection	Assay System	Stem Cell Purification
i.v.	CFU-S	100
i.v.	Irradiated recipient survival	350
i.v.	Intrathymic adoptive transfer	282

Using the sandwich technique [7], it was possible to further characterize the HSC as being Ox8, W3/25, Ox6 and Ox17 negative; possibly Ox19 dim; and Ox18 very bright. The specificities of these monoclonal antibodies are given in Table 1. The optical bench arrangement shown in Figure 1 can also be used to characterize HSC with respect to lectin receptor sites and various intracellular enzyme systems. For example, the rat HSC binds FITC-WGA and is apparently characterized by a high cytoplasmic concentration of nonspecific esterases as measured by FDA uptake as shown in Figures 4 and 5.

#### ***Comparison of dose survival curves generated by the CFU-S and FACS assays***

HSC were assayed in irradiated rats by both the CFU-S and FACS procedures. These two assay systems generated different results as shown in Figure 6 and reported previously [14]. One of several possible explanations for this discrepancy might be nonspecific tagging of dead and dying cells with the phycobiliprotein-monoclonal antibody conjugates so that these dead cells are scored as HSC by the FACS procedure, leading to overestimation of the concentration of viable HSC in the marrow of postirradiated rats. Therefore, a new technique was devised for determining and enumerating viable marrow cells, including HSC, in the immediate postirradiated marrow.

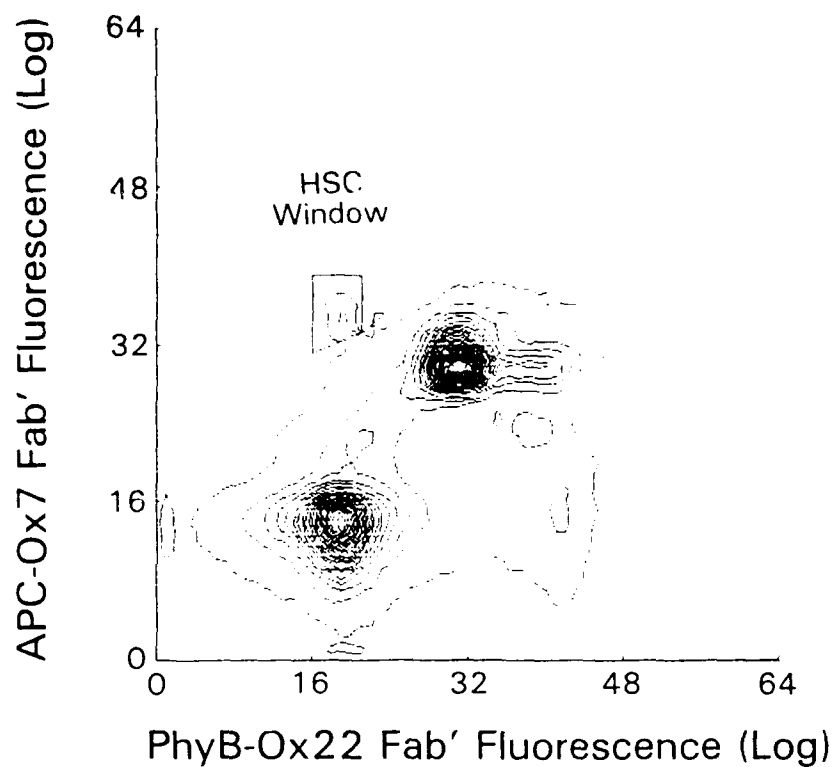


Figure 3. Contour plot of rat marrow cells labeled with PhyB-Ox22 Fab' and APC-Ox7 Fab'. HSC were found only within the Ox7 upper 20% positive, Ox22 negative window and cells within this window accounted for 0.265% of the total marrow cell population.

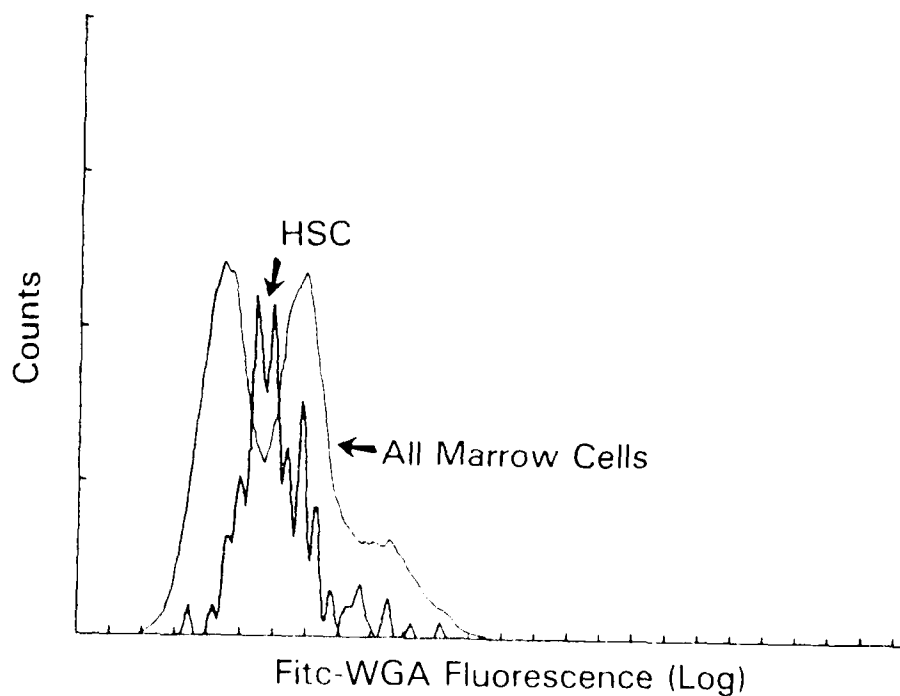


Figure 4. Relative fluorescence distribution of marrow cells and HSC incubated with FITC-wheat germ agglutinin.

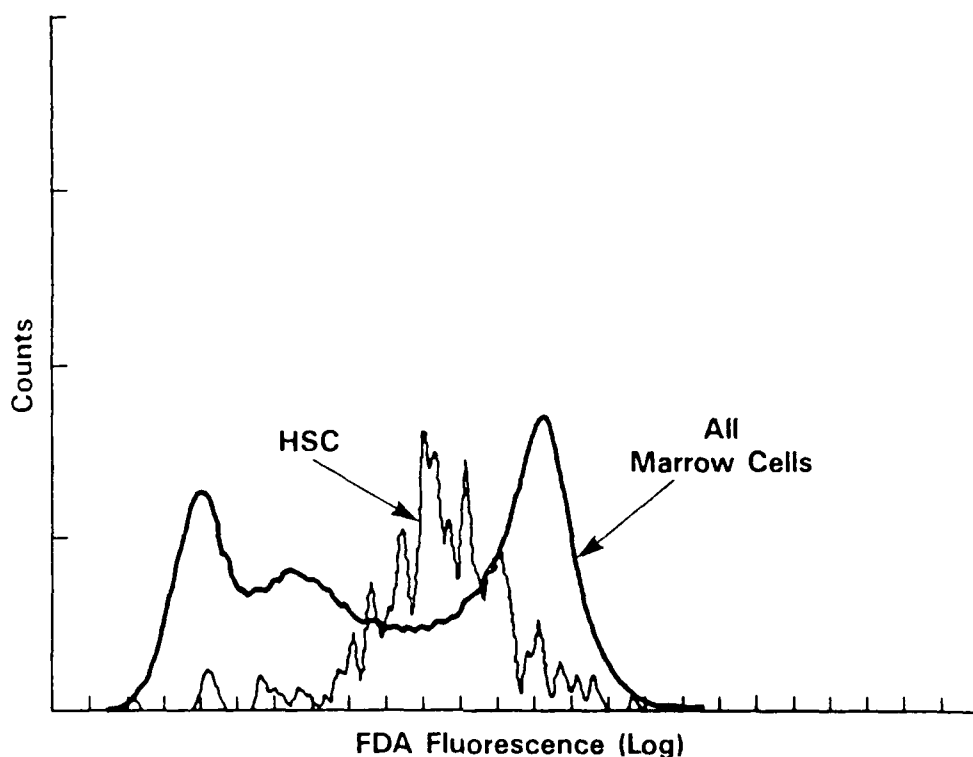
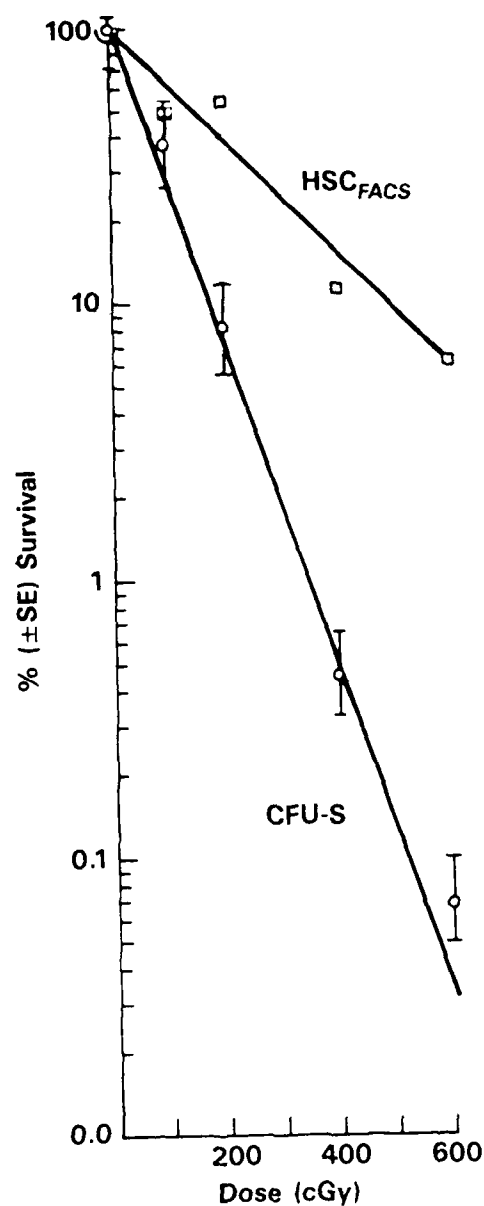


Figure 5. Relative fluorescence distribution of marrow cells and HSC incubated with FDA.

#### ***DAPI staining of dead cells***

The most commonly used fluorescent probe in flow cytometry for staining and gating out dead cells from immunofluorescence histograms is PI. It is an intercalating DNA dye with an absorbance maximum in the yellow and an emission maximum in the orange-red (for a more comprehensive discussion of DNA stains, see [15]). Dead cells are labeled with PI by including it in the last cell wash at concentration of 20  $\mu\text{g/mL}$ . Live cells exclude the PI while dead cells take up the stain. The result is an intensive orange-red nuclear fluorescence emanating from the dead cells. Although the fluorescence of PI overlaps that of PhyB and PhyR, PI can be used to gate out dead cells in two and three parameter immunofluorescence studies. The orange-red fluorescence of the PI stained dead cells is an order of magnitude brighter than the immunofluorescence from the PhyB- or PhyR-antibody tagged viable cells and does not interfere with or alter the immunofluorescence histograms of viable cells. However, the immunofluorescence histograms of dead and dying cells cannot be determined in the presence of PI, for the PI fluorescence cannot be separated from the PhyB or the PhyR fluorescence. In order to determine the phenotype of dead cells it was necessary to use a fluorescent probe whose emission spectrum did not overlap that of FITC, Phy, or APC. Such a fluorescent probe is DAPI.



**Figure 6.** Radiation dose-response curves for HSC as measured by FACS and CFU-S assays.

DAPI is a non-intercalating DNA-specific stain with an absorption maximum in the UV and an emission maximum in the blue [15]. Like Hx33342, DAPI can be excited with the argon laser tuned to the UV and the resulting fluorescence can be detected using the 460 nm PMT (Figure 1). In order to demonstrate that DAPI stains only dead cells, 20  $\mu$ g PI and 10  $\mu$ g DAPI were added to a 1-mL solution of  $5 \times 10^6$  rat marrow cells. The cells were allowed to incubate for 30 min at 4°C and then analyzed on the FACS. The PI stained cells were excited with the dye laser and their fluorescence measured with the orange PMT, while DAPI stained cells were excited with the UV laser and their fluorescence recorded on the violet-blue PMT. The correlated PI and DAPI fluorescences are plotted in Figure 7. Clearly, marrow cells that stain with PI (i.e., dead cells) also stain with DAPI. Viable cells that do not

stain with PI also exclude DAPI. Therefore, substituting DAPI for PI as a cell viability stain allows not only dead cells to be gated "out" of two parameter immunofluorescence work but also makes it possible to gate "on" dead cells for the analysis of both the rate and phenotype of dying cells in the postirradiated rat marrow. Such a study is shown in Figure 8, where the phenotypes of viable and dead cells are presented as a function of time postirradiation. The first cells to die immediately postirradiation appear to be blast cells and erythrocytic precursors, followed by lymphocytes at 1 to 3 days postirradiation and granulocytes at 4 to 5 days postirradiation. Further information on the dead cell fraction in the total marrow population and the dead cell fraction within the Ox7 upper 20% positive, Ox22 negative window or HSC window is given in Table 3.

TABLE 3. PERCENT DEAD CELLS INCLUDING HSC IN POSTIRRADIATED RAT MARROW

EXP.	Total Cells/ Femur $\times 10^{-7}$	% Total Cells DAPI	HSC/ $10^5$ Cells	% HSC DAPI	Corrected HSC/ $10^5$ Cells	HSC/Femur
Control <sup>a</sup>						
1	3.20	0.8	307	2.0	301	96,320
2	4.80	0.5	408	0.2	407	195,360
Irradiated <sup>b</sup>						
3 h						
1	2.30	23.3	1,071	63.4	392	90,409
2	1.75	24.6	1,104	67.8	355	62,210
6 h						
2	1.30	26.9	347	24.2	263	34,193
2	1.10	23.9	416	23.8	317	34,869
24 h						
1	0.80	4.7	463	14.7	395	31,595
2	0.55	11.7	277	22.0	216	11,883
30 h						
1	0.55	12.8	252	7.9	232	12,765
2	0.32	17.6	250	16.0	210	6,720
3 days						
1	2.70	19.3	078	2.6	75	20,512
2	2.47	—	—	—	—	—
5 days						
1	2.95	17.6	117	17.9	96	28,336
2	2.40	31.2	122	45.1	67	16,074

<sup>a</sup> Each experiment consisted of two rats.

<sup>b</sup> Experiment performed on rats receiving 2Gy  $^{60}\text{Co}$  TBR, dose rate 0.4 Gy/min.

## DISCUSSION

New techniques were developed for the identification of rat HSC in normal marrow by flow cytometry using a modified FACS-II instrument. When these techniques were used to monitor the concentration and regeneration of HSC in the postirradiated rat, discrepancies between the CFU-S assay and the FACS assay for determining the relative size of the postirradiation HSC compartment became obvious. The results presented in the present study indicate that part of the difference between these two assays can be explained by the presence of dead and dying cells in the Ox7 upper 20% positive, Ox22 negative window or the HSC window. If these cells are either dead HSC or nonspecifically phycobiliprotein-antibody tagged dead cells, then the number of surviving HSC as determined by the FACS assay would be overestimated. However, the total difference between the phenotypic FACS assay and the clonogenic CFU-S assay cannot be fully accounted for by the presence

of dead and dying cells in the HSC window. It is conceivable that the difference that remains between the two assays after subtracting out these dead and dying cells from the total number of cells found within the HSC window represents damaged irradiated HSC that do not express themselves in the CFU-S assay [14].

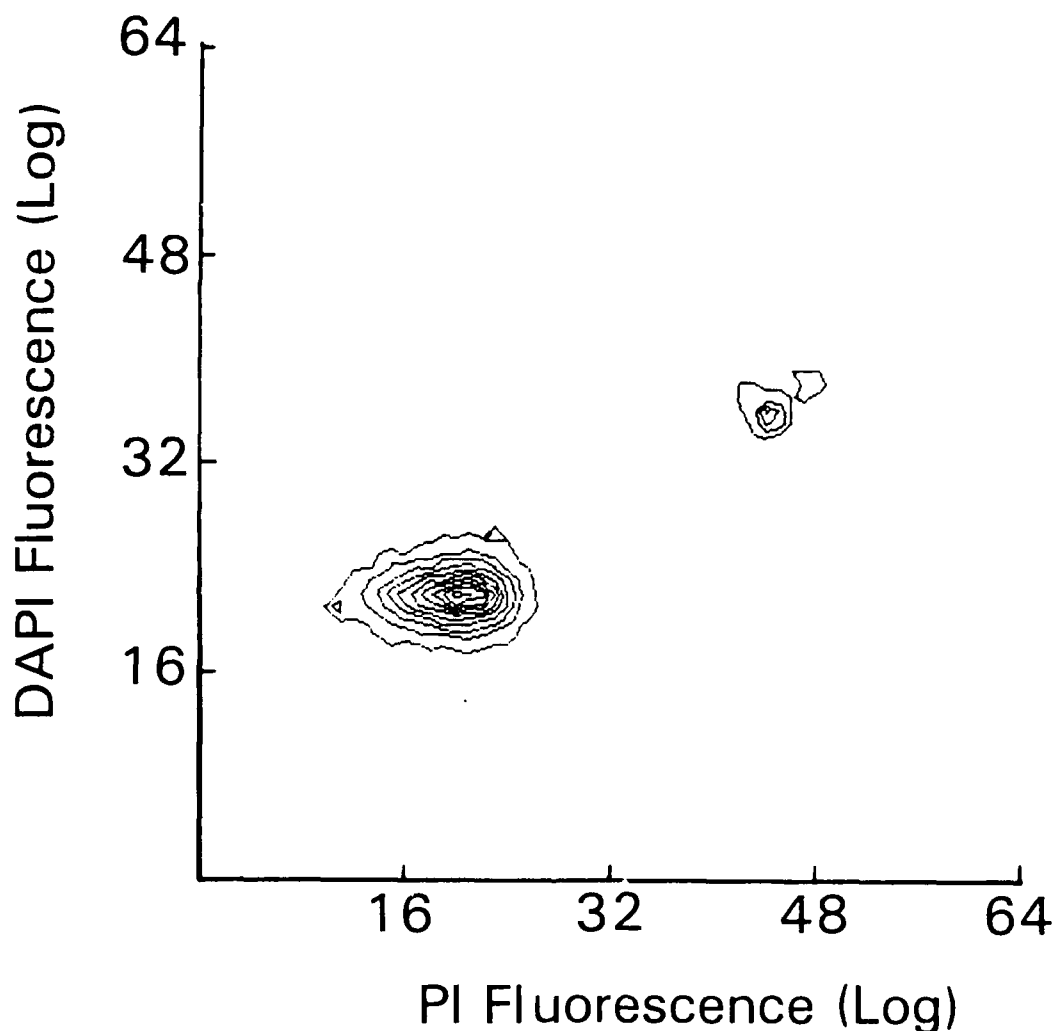
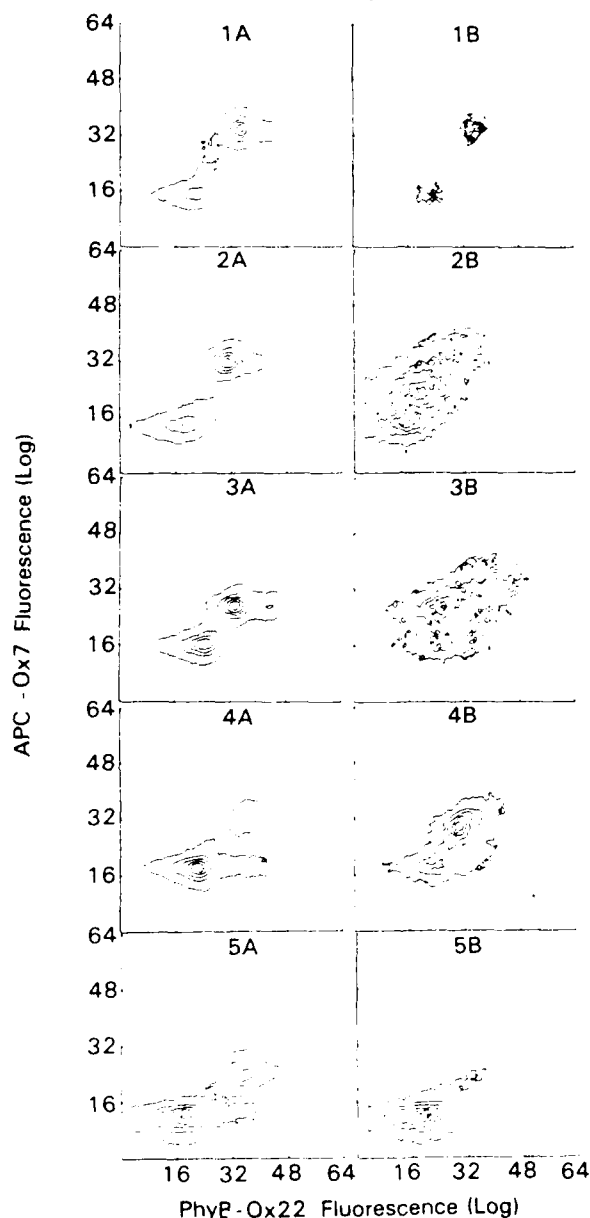


Figure 7. Contour plot of rat marrow cells labeled with PI and DAPI.

The present optical bench arrangement and computer support limit us to four parameter cellular measurements, which are a forward light scatter measurement, two immunofluorescence measurements, and a DAPI-DNA fluorescence measurement. Therefore, enumeration of dead cells could be undertaken only in the Ox7 upper 20% positive, Ox22 negative window and not in the Ox7 upper 20% positive, Ox22 negative, W3/13 dim window. There is the possibility, although slight, that in a three parameter immunofluorescence analysis of the postirradiated HSC compartment, dead

cells would not appear in the Ox7 upper 20% positive, Ox22 negative, W3/13 dim window. To perform this experiment, a five parameter flow cytometer would be needed.



**Figure 8.** Contour plots of viable (A) and dead (B) cells labeled with APC-Ox7 Fab', PhyB-Ox22 Fab', and DAPI. DAPI fluorescence was determined with the delayed or second laser and is not shown. Viable cells are DAPI negative while dead cells are DAPI positive. Time sequence from top to bottom is as follows: (1) normal marrow, (2) 3 h postirradiation, (3) 1 day postirradiation, (4) 3 days postirradiation, (5) and 5 days postirradiation. Contour maps were drawn as a percent of peak amplitude at increments of 5%, 25%, 45%, 65%, and 85%. Radiation was 2 Gy TBR  $^{60}\text{Co}$  at a dose rate of 0.04 Gy/min.

The above limitations notwithstanding, the present FACS assay of postirradiation rat marrow indicates that at least 30 h is required for removal of dead and dying HSC from the marrow. At this time the initial regeneration of the HSC compartment can be observed by both the FACS (Table 3) and

the CFU-S assays [16]. HSC removal, therefore, begins while there is still extensive cell death occurring in the marrow lymphocyte and granulocyte compartments. What influence this continued hematopoietic cell death has on the stromal tissues that support hematopoiesis and on regenerating HSC is an important question to be addressed if we wish to improve therapies for rapid recovery of the postirradiated marrow.

#### ACKNOWLEDGMENTS

This research was supported by the Armed Forces Radiobiology Research Institute, Defense Nuclear Agency, under Research Work Unit B3012. Views presented in this paper are those of the authors; no endorsement by the Defense Nuclear Agency has been given or should be inferred. Research was conducted according to the principles enunciated in the "Guide for Care and Use of Laboratory Animals" prepared by the Institute of Laboratory Animal Resources, National Research Council.

#### REFERENCES

- 1 Till, J.E. and McCulloch, E.A. (1961) A direct measurement of the radiation sensitivity of normal mouse bone marrow cells. *Radiat. Res.* 14, 213-222.
- 2 McCarthy, K.F., Hale, M.L., and Fehnel, P.L. (1985) Rat colony-forming unit is Ox7 positive, W3/13 positive, Ox1 positive, and Ox22 negative. *Exp. Hematol.* 13, 847-854.
- 3 McCarthy, K.F., Hale, M.L., and Fehnel, P.L. (1987) Purification and analysis of rat hematopoietic stem cells by flow cytometry. *Cytometry* 8, 296-305.
- 4 van der Engh, G. and Visser, J. (1984) Flow cytometry in experimental hematology. In: S.J. Baum (Ed.), *Current Methodology in Experimental Hematology*, Karger, New York, pp. 42-62.
- 5 Herzenberg, L.A., Sweet, R.G., and Herzenberg, L.A. (1976) Fluorescence-activated cell sorting. *Scien. Amer.* 234, 108-117.
- 6 Glazer, A.N. and Stryer, M.P. (1984) Phycofluor probes. *TIBS* 9, 423-427.
- 7 Hale, M.L., Griener, D.L., and McCarthy, K.F. (1987) Characterization of rat prothymocyte with monoclonal antibodies recognizing rat lymphocyte membrane antigenic determinants. *Cell. Immunol.* 107, 188-200.
- 8 Magli, M.C., Iscove, N.N., and Odartchenko, N. (1982) Transient nature of early hematopoietic spleen colonies. *Nature* 295, 527-529.
- 9 Griener, D.L., Goldschneider, I., and Lubaroff, D.M. (1984) Identification of thymocyte progenitors in the hematopoietic tissues of the rat. I. A quantitative assay system for thymocyte regeneration. *Thymus* 6, 181-199.

- 10 Goldschneider, I., Komschlies, K.L., and Greiner, D.L. (1986) Studies of thymocytopoiesis in rats and mice. I. Kinetics of appearance of thymocytes using a direct intrathymic adoptive transfer assay for thymocyte precursors. *J. Exp. Med.* 163, 1-17.
- 11 Hale, M.L. and McCarthy, K.F. (1984) Effect of sublethal ionizing radiation on rat peyer's patch lymphocytes. *Radiat. Res.* 99, 151-164.
- 12 Visser, J.W., Bauman, J.G.J., Mulder, A.H., Eliason, J.F., and de Leeuw, A.M. (1984) Isolation of murine pluripotent hematopoietic stem cells. *J. Exp. Med.* 59, 1576-1590.
- 13 Van Zant, G. (1984) Studies of hematopoietic stem cells spared by 5-fluorouracil. *J. Exp. Med.* 159, 679-690.
- 14 McCarthy, K.F. and Hale, M.L. (In Press) Measurement of the radiosensitivity of rat marrow by flow cytometry. *Pharm. Ther.*
- 15 Shapiro, H.M. (1985) *Practical Flow Cytometry*. Alan R. Liss, New York, pp. 84-154.
- 16 McCarthy, K.F. and Hale, M.L. (In Press) Flow cytometry techniques for the study of irradiated hematopoietic stem cells. In: D. McCormack, C.E. Swenberg, and H. Bucker (Eds.), *Terrestrial Space Radiation and Its Biological Effects*. Plenum Publishing Corp, New York.
- 17 Mason, D.W., Arthur, R.P., De Iman, M.J., Green, J.R., Spickett, G.P., and Thomas, M.L. (1983) Functions of rat t-lymphocyte subsets isolated by means of monoclonal antibodies. *Immunological Rev.* 74, 57-82.

## MODELING THE TISSUE SOLUBILITIES AND METABOLIC RATE CONSTANT OF HALOGENATED METHANES, ETHANES, AND ETHYLENES

Michael L. Gargas<sup>a</sup>, Paul G. Seybold<sup>b</sup>, and Melvin E. Andersen<sup>a</sup>

<sup>a</sup>Armstrong Aerospace Medical Research Laboratory, Toxic Hazards Division, Wright-Patterson Air Force Base, OH, and <sup>b</sup>Departments of Chemistry and Biological Chemistry, Wright State University, Dayton, OH

### SUMMARY

Experimental solvent:air and tissue:air partition coefficients for 25 halogenated methanes, ethanes, and ethylenes in saline solution; olive oil; and rat blood, muscle, liver, and fat tissues have been examined using theoretical molecular modeling techniques. The metabolic rate constant,  $V_{max}$ , was also investigated by these techniques for 19 chlorinated compounds in this group. Two graph theoretical approaches (the distance method of Wiener and the connectivity index method of Randic, Kier, and Hall) and an approach utilizing *ad hoc* molecular descriptors were employed. Satisfactory regression models for solubility were obtained with both the Randic-Kier-Hall approach and the *ad hoc* descriptors approach. Fluorine substituents decrease tissue solubilities, whereas both chlorine and bromine substituents increase tissue solubilities, with the relative influence being  $Cl < Br$ . Tissue solubilities can also be represented conveniently in terms of contributions from oil and saline solubilities, a procedure reinforced by factor analysis of the data. Equations derived by these methods adequately estimated the solubilities for 8 additional compounds. No approach could successfully model  $V_{max}$  for all 19 compounds, but a subset of 16 compounds was modeled using the connectivity indices. The equation is limited in its use but indicated future modeling directions for  $V_{max}$ .

### INTRODUCTION

Lower molecular weight halogenated hydrocarbons are employed commercially as solvents, degreasing agents, chemical intermediates, refrigerants, and fire retardants. However, many exhibit toxic effects and some are suspected carcinogens. Moreover, the halogenated methanes, ethanes, and ethylenes are widely distributed in the environment, a matter of concern because of their potential toxicities. The environmental problem posed by these compounds may be especially severe in indoor settings, both because many people spend a considerable portion of their time indoors, and because chemicals "offgassed" from construction and other materials cannot readily escape [1].

Halogenated hydrocarbons are metabolized in the body to potentially harmful intermediates and end products [2,3] and an understanding of their toxicological effects requires that their tissue distributions, metabolic pathways, and rates of metabolism be known. Over the past several years, Andersen and co-workers have developed a physiological model for the distribution and metabolism

of inhaled gases and vapors [4,5,6,7]. The model is based on rates of gas uptake, tissue volumes, and tissue:air partition coefficients ("solubilities"), and can be employed to assess the time-dependent distributions and Michaelis-Menten kinetic rate constants for metabolism of a variety of chemicals. An important aspect of the model is that information obtained for a chemical in one species (e.g., rats) can be extrapolated to other species (e.g., humans) using standard allometric methods [8].

In its present form, the model relies on measured values of the tissue:air partition coefficients and kinetic constants of chemical metabolism. Such measurements can represent a considerable effort. It was, therefore, of interest to see if the partition coefficients and kinetic constants could be estimated in some way for halogenated hydrocarbons with reasonable reliability. With such estimates the model could be used to predict the behavior of heretofore untested compounds. We have previously estimated several of the physical properties of these compounds using molecular structure-property relations [9]. Here we describe the estimation of tissue:air partition coefficients and the rate constant,  $V_{max}$ , using quantitative structure-property relations (QSPR) based on molecular structure.

## METHODS

The first task in a study such as this is to find appropriate descriptors of molecular structure [10]. Three general modeling schemes were examined for description of the present tissue partition coefficients and  $V_{max}$ . The first two schemes, utilizing the approaches of Wiener [11,12], Randic [13], and Kier and Hall [14,15] fall within the purview of chemical graph theory [16]. The third scheme employs a collection of molecular descriptors chosen on an *ad hoc* basis.

### Wiener's method

Wiener [11,12] estimated a number of physical and chemical properties of alkanes using parameters based on the distances (in terms of bonds) between atoms in molecules. The Wiener index  $w$  is the sum of all unique atom-atom paths in the hydrogen-suppressed graph<sup>1</sup> of a molecule, the reduced index  $w_r = w/N^2$ , where  $N$  is the number of atoms, excluding hydrogens, in the molecule. The index  $p$  is the sum of all paths of length 3. The  $f$  index of Platt [17], equal to the number of adjacent bonds to each bond, summed over all bonds (again excluding those to hydrogen atoms), was also included in the Wiener approach.

In its usual form the Wiener scheme does not account for the presence of *hetero* (i.e., non-carbon) atoms. Barysz et al. [18] have proposed a parameterization of the Wiener scheme that accounts for such atoms. Using the atom and bond parameters of Barysz et al. [18], valence Wiener indices  $w^v$  and  $w_r^v = w^v/N^2$ , analogous to the usual Wiener indices  $w$  and  $w_r$ , have been calculated.

---

<sup>1</sup> The graph of a compound refers to its molecular skeleton in which the vertices are atoms and the edges are bonds. In a hydrogen-suppressed graph, hydrogen atoms are ignored.

### Randic, Kier, and Hall's method

In the Randic [13] scheme each atom in the hydrogen-suppressed graph of a molecule is assigned a "valence"  $\delta$ , equal to the number of bonds to it. The connectivity index  $\chi$  is then defined as the sum over all bonds  $i-j$  as

$$\chi = \sum 1 / (\delta_i \delta_j)^{1/2} \quad (1)$$

Kier and Hall [14,15] extended this concept to include higher and lower connectivity indices  ${}^m\chi$ , as analogous sums over atoms, bonds, and larger structural subunits. For example, the zeroth-order index  ${}^0\chi$  is a sum over all nonhydrogen atoms.

$${}^0\chi = \sum (1 / \delta_i)^{1/2} \quad (2)$$

The high-order indices  ${}^3\chi_c$ ,  ${}^4\chi_c$ , and  ${}^4\chi_{pc}$ , entail similar sums over clusters of 3 bonds, clusters of 4 bonds, and path-cluster substructures of 4 bonds, respectively, appearing in the hydrogen-suppressed graphs of the molecules (Figure 1).

## SUBSTRUCTURES OF HIGH-ORDER INDICES

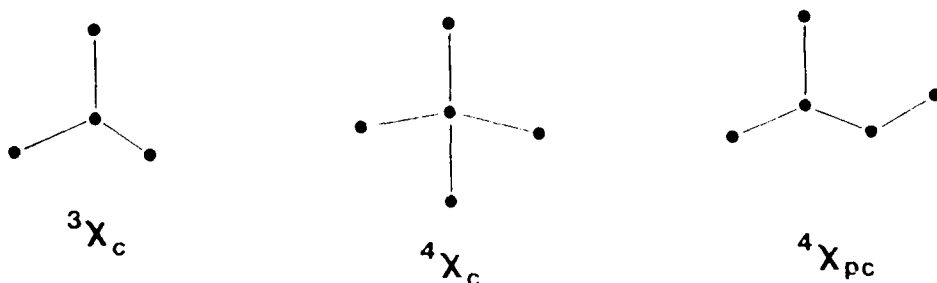


Figure 1. Substructures contributing to the connectivity indices  ${}^3\chi_c$ ,  ${}^4\chi_c$ , and  ${}^4\chi_{pc}$ .

Heteroatoms and multiple bonds were accounted for by Kier and Hall [15] by assigning valences  $\delta^v$  to each atom according to the formula

$$\delta^v = \frac{Z^v - h}{Z - Z^v - 1} \quad (3)$$

in which  $Z$  is the total number of electrons of the atom,  $Z^v$  is the number of valence electrons, and  $h$  is the number of attached hydrogen atoms. Eq. (3) reduces to the usual Randic assignments for saturated carbon atoms; for halogens it assigns  $\delta^v = 7$  to F,  $\delta^v = 7/9$  to Cl, and  $\delta^v = 7/27$  to Br. Using

these values  $\chi_s^m$ , analogous to the indices  $\chi_s^m$ , can be defined. The valence structure index  $\chi_s^v$  is defined as

$$\chi_s^v = 1 / (\delta_1^v \delta_2^v \cdots \delta_N^v)^{1/2} \quad (4)$$

and includes all nonhydrogen atoms of the molecule.

### **Ad Hoc descriptors**

Many quantitative structure-property relationships (QSPR) rely on molecular descriptors chosen on an *ad hoc* basis. Such descriptors may refer to global molecular features such as molecular weights, or to more specific features such as the presence of certain atoms, functional groups, or other entities. Descriptors investigated in this study included number of carbon atoms ( $N_C$ ); number of trigonal ( $N_{C3}$ ) and tetrahedral carbons ( $N_{C4}$ ); numbers of fluorine ( $N_F$ ), chlorine ( $N_{Cl}$ ), and bromine ( $N_{Br}$ ) atoms; and the polar hydrogen factor  $Q_H$  defined by Di Paolo et al. [19]. The factor  $Q_H$  accounts for the polarizing effects of C-H bonds of halogens located on the same and adjacent carbons. As suggested by Di Paolo et al. [19], bond values lower than 0.50 were neglected in calculating  $Q_H$ . Fiserova-Bergerova et al. [20] have previously used  $Q_H$  and  $\chi$  together to model oil/gas partition coefficients.

### **Experimental data**

Rat tissue:air partition coefficients  $P_i$  at 37°C for blood, liver, muscle, and fat, as well as 0.9% saline solution:air and olive oil:air  $P_i$  values at 37°C were determined using a vial equilibration procedure [21,22] for 25 halogenated methanes, ethanes, and ethylenes (Table 1). The kinetic constants,  $V_{max}$ ,  $K_m$ , and any first order processes,  $K_f$ , were determined for the chlorinated series of methanes, ethanes, and ethylenes including penta- and hexachloroethane (Table 2) by gas uptake [23] or exhaled breath techniques [24].

Regression analyses and factor analysis were performed using the SAS Statistical Analysis System<sup>2</sup> software package on the Wright State University IBM 3083E computer. For the regressions a restriction of at least five observations per modeling parameter was imposed for statistical purposes.

### **RESULTS**

Experimental data for the partition coefficients are given in Table 1, the kinetic constants in Table 2, and the molecular structure parameters employed for all 27 compounds are summarized in

<sup>2</sup> SAS Institute Inc. Box 8000, Cary, NC 27512

TABLE 1. LIQUID AND RAT TISSUE: AIR PARTITION COEFFICIENTS AT 37°C<sup>a</sup>

Compound Number	Chemical	Saline	Olive Oil	Blood	Liver	Muscle	Fat
1	Methyl chloride	0.88 ± 0.08	8.57 ± 2.18	2.47 ± 0.16	3.47 ± 0.25	0.97 ± 0.38	13.5 ± 0.4
2	Dichloromethane	5.96 ± 0.71	131 ± 7	19.4 ± 0.8	14.2 ± 1.2	7.92 ± 1.77	120 ± 6
3	Chloroform	3.38 ± 0.09	402 ± 12	20.8 ± 0.1	21.1 ± 1.5	13.9 ± 1.9	203 ± 5
4	Carbon tetrachloride	0.35 ± 0.03	374 ± 11	4.52 ± 0.35	14.2 ± 0.97	4.54 ± 0.59	359 ± 11
5	Vinyl Chloride	0.43 ± 0.04	24.4 ± 3.7	1.68 ± 0.18	1.60 ± 0.17	2.20 ± 0.45	20.0 ± 0.7
6	1,1-Dichloroethylene	0.35 ± 0.07	64.3 ± 3.4	5.00 ± 0.19	4.42 ± 0.30	2.05 ± 0.31	68.6 ± 2.1
7	cis 1,2-Dichloroethylene	3.25 ± 0.12	278 ± 6	21.6 ± 2.0	15.3 ± 1.1	6.09 ± 1.02	227 ± 11
8	trans-1,2-Dichloroethylene	1.41 ± 0.04	178 ± 6	9.58 ± 0.94	8.96 ± 0.61	3.52 ± 0.54	148 ± 11
9	Trichloroethylene	0.83 ± 0.30	553 ± 46	21.9 ± 1.4	27.2 ± 3.4	10.1 ± 2.7	554 ± 21
10	Tetrachloroethylene	0.79 ± 0.06	2134 ± 159	18.9 ± 1.1	70.3 ± 9.0	20.0 ± 2.5	1638 ± 91
11	Chloroethane	1.09 ± 0.06	38.9 ± 3.1	4.08 ± 0.39	3.61 ± 0.32	3.22 ± 0.68	38.6 ± 0.7
12	1,1-Dichloroethane	2.45 ± 0.04	186 ± 6.7	11.2 ± 0.1	10.8 ± 0.5	5.12 ± 0.48	164 ± 4.0
13	1,2-Dichloroethane	11.4 ± 0.1	366 ± 8	30.4 ± 1.2	35.7 ± 1.6	23.4 ± 1.4	344 ± 5
14	1,1,1-Trichloroethane	0.75 ± 0.07	295 ± 22	5.76 ± 0.50	8.6 ± 0.9	3.15 ± 0.33	263 ± 12
15	1,1,2-Trichloroethane	13.3 ± 0.3	1776 ± 26	58.0 ± 1.1	73.0 ± 0.8	22.9 ± 0.8	1438 ± 58
16	1,1,2,2-Tetrachloroethane	23.4 ± 2.0	6358 ± 402	142 ± 6	196 ± 12	101 ± 10	3767 ± 93
17	1,1,1,2-Tetrachloroethane	3.53 ± 0.23	2686 ± 51	41.7 ± 0.97	88.2 ± 1.8	39.5 ± 2.5	2148 ± 82
18	Difluoromethane	1.31 ± 0.05	4.76 ± 0.75	1.60 ± 0.10	2.75 ± 0.39	1.44 ± 0.25	1.43 ± 0.31
19	Fluorochloromethane	3.08 ± 0.07	22.3 ± 1.4	5.08 ± 0.06	3.44 ± 0.27	2.46 ± 0.52	15.4 ± 1.0

(continued)

TABLE 1. (Continued)

Compound Number	Chemical	Saline	Olive Oil	Blood	Liver	Muscle	Fat
20	Bromochloromethane	8.65 ± 0.28	361 ± 9	41.5 ± 0.9	29.2 ± 0.5	11.1 ± 1.8	325 ± 3
21	Dibromomethane	14.4 ± 0.4	957 ± 39	74.1 ± 1.5	68.1 ± 1.4	40.5 ± 2.0	792 ± 14
22	1,1,1-Trifluoro-2-chloro-2-bromoethane	0.50 ± 0.05	198 ± 4	5.26 ± 0.13	7.62 ± 1.20	4.46 ± 0.29	182 ± 5
23	Vinyl bromide	0.44 ± 0.06	56.0 ± 1.5	4.05 ± 0.16	3.33 ± 0.38	2.26 ± 0.13	49.2 ± 1.2
24	1-Bromo-2-chloroethane	8.91 ± 0.56	569 ± 23	52.7 ± 3.5	42.8 ± 3.3	25.4 ± 3.1	959 ± 39
25	1,1,1-Trifluoro-2-chloroethane	0.42 ± 0.04	24.0 ± 2.48	1.27 ± 0.06	1.84 ± 0.14	1.23 ± 0.14	21.2 ± 0.6

\* All values are mean ± standard error of the mean (n = 3-15). Large sample sizes were occasionally required to minimize standard errors and occurred most frequently with muscle tissue.

TABLE 2. METABOLIC KINETIC CONSTANTS

Compound Number	Chemical	$V_{max}$ (mg/h) <sup>a</sup>	$V_{max}$ ( $\mu$ Moles/h)	$K_m$ (mg/L)	$K_m$ ( $\mu$ M)	$K_f$ (h <sup>-1</sup> ) <sup>a</sup>
1	Methyl chloride	6.0	111.8	1.0	19.8	0
2	Dichloromethane	4.0	47.1	0.4	4.71	2.0
3	Chloroform	7.0	58.6	0.25	2.09	0
4	Carbon tetrachloride	0.4	2.6	0.25	1.63	0
5	Vinyl chloride	2.5	40.0	0.1	1.60	1.0
6	1,1-Dichloroethylene	7.5	77.4	0.1	1.03	0
7	<i>cis</i> -1,2-Dichloroethylene <sup>b</sup>	3.0	30.9	0.5	5.16	0
8	<i>trans</i> -1,2-Dichloroethylene <sup>b</sup>	3.0	30.9	0.1	1.03	0
9	Trichloroethylene	11.0	83.7	0.25	1.90	0
10	Tetrachloroethylene	0	0	—	—	0.3
11	Chloroethane	4.0	62.0	0.1	1.55	1.0
12	1,1-Dichloroethane <sup>c</sup>	7.5	75.8	0.2	2.02	0
13	1,2-Dichloroethane	3.15	31.8	0.25	2.53	0
14	1,1,1-Trichloroethane	0	0	—	—	5.0
15	1,1,2-Trichloroethane	7.7	57.7	0.78	5.85	0
16	1,1,2,2-Tetrachloroethane	12.0	71.5	0.8	4.77	0
17	1,1,1,2-Tetrachloroethane	6.5	38.7	0.92	5.48	0
26	Pentachloroethane	9.2	45.5	0.9	4.45	0
27	Hexachloroethane	2.0	8.4	0.8	3.38	0

\*  $V_{max}$  and  $K_f$  are scaled to a 1.0-kg rat.

<sup>b</sup> Values were determined using a suicide inhibition model (Andersen et al. [28]).

<sup>c</sup> Values were determined using a glutathione depletion model (D'Sousa et al. [29]).

Tables 3 and 4. Table 5 shows the correlations among the  $\log(P_i)$  values themselves. As expected, the correlations are strongest among the more fatty media, such as fat and liver tissues and olive oil. The blood value  $\log(P_{blood})$  correlate modestly with values for the other tissues and with both  $\log(P_{oil})$  and  $\log(P_{saline})$ .

The Wiener indices proved to be inadequate for modeling of the present tissue solubilities. Most regressions, even including three parameters, yielded coefficients of determination below  $r^2 = 0.5$  ( $r$  is the correlation coefficient). The single exception was  $\log(P_{oil})$  where  $r^2 = 0.524$ .

TABLE 3. WIENER PATH INDICES

Compound Number	$w$	$w_r$	$w^v$	$w^v_r$	$P$	$f$
1	1	0.2500	1.000	0.2500	0	0
2	4	0.4444	2.706	0.3007	0	2
3	9	0.5625	5.118	0.3199	0	6
4	16	0.6400	8.236	0.3294	0	12
5	4	0.4444	2.353	0.2614	0	2
6	9	0.5625	4.912	0.3070	0	6
7	10	0.6250	5.412	0.3383	1	4
8	10	0.6250	5.412	0.3383	1	4
9	18	0.7200	9.177	0.3671	2	8
10	29	0.8056	14.148	0.3930	4	12
11	4	0.4444	3.353	0.3726	0	2
12	9	0.5625	6.412	0.4008	0	6
13	10	0.6250	7.412	0.4633	1	4
14	18	0.7200	12.177	0.4871	2	8
15	16	0.6400	10.177	0.4071	0	12
16	29	0.8056	18.648	0.5180	4	12
17	28	0.7778	17.648	0.4902	3	14
18	4	0.4444	3.334	0.3704	0	2
19	4	0.4444	3.020	0.3356	0	2
20	4	0.4444	2.524	0.2804	0	2
21	4	0.4444	2.342	0.2602	0	2
22	42	0.8571	29.643	0.6050	6	18
23	4	0.4444	2.171	0.2412	0	2
24	10	0.6250	7.048	0.4405	1	4
25	28	0.7778	21.416	0.5949	3	14
26	42	0.8571	28.825	0.5883	6	18
27	58	0.9063	34.708	0.5423	9	24

TABLE 2. METABOLIC KINETIC CONSTANTS

Compound Number	Chemical	$V_{max}$ (mg/h) <sup>a</sup>	$V_{max}$ ( $\mu$ Moles/h)	$K_m$ (mg/L)	$K_m$ ( $\mu$ M)	$K_f$ (h <sup>-1</sup> ) <sup>a</sup>
1	Methyl chloride	6.0	111.8	1.0	19.8	0
2	Dichloromethane	4.0	47.1	0.4	4.71	2.0
3	Chloroform	7.0	58.6	0.25	2.09	0
4	Carbon tetrachloride	0.4	2.6	0.25	1.63	0
5	Vinyl chloride	2.5	40.0	0.1	1.60	1.0
6	1,1-Dichloroethylene	7.5	77.4	0.1	1.03	0
7	<i>cis</i> -1,2-Dichloroethylene <sup>b</sup>	3.0	30.9	0.5	5.16	0
8	<i>trans</i> -1,2-Dichloroethylene <sup>b</sup>	3.0	30.9	0.1	1.03	0
9	Trichloroethylene	11.0	83.7	0.25	1.90	0
10	Tetrachloroethylene	0	0	—	—	0.3
11	Chloroethane	4.0	62.0	0.1	1.55	1.0
12	1,1-Dichloroethane <sup>c</sup>	7.5	75.8	0.2	2.02	0
13	1,2-Dichloroethane	3.15	31.8	0.25	2.53	0
14	1,1,1-Trichloroethane	0	0	—	—	5.0
15	1,1,2-Trichloroethane	7.7	57.7	0.78	5.85	0
16	1,1,2,2-Tetrachloroethane	12.0	71.5	0.8	4.77	0
17	1,1,1,2-Tetrachloroethane	6.5	38.7	0.92	5.48	0
26	Pentachloroethane	9.2	45.5	0.9	4.45	0
27	Hexachloroethane	2.0	8.4	0.8	3.38	0

<sup>a</sup>  $V_{max}$  and  $K_f$  are scaled to a 1.0-kg rat

<sup>b</sup> Values were determined using a suicide inhibition model (Andersen et al. [28]).

<sup>c</sup> Values were determined using a glutathione depletion model (D'Sousa et al. [29]).

Tables 3 and 4. Table 5 shows the correlations among the  $\log(P_i)$  values themselves. As expected, the correlations are strongest among the more fatty media, such as fat and liver tissues and olive oil. The blood value  $\log(P_{blood})$  correlate modestly with values for the other tissues and with both  $\log(P_{oil})$  and  $\log(P_{saline})$ .

The Wiener indices proved to be inadequate for modeling of the present tissue solubilities. Most regressions, even including three parameters, yielded coefficients of determination below  $r^2 = 0.5$  ( $r$  is the correlation coefficient). The single exception was  $\log(P_{oil})$  where  $r^2 = 0.524$ .

TABLE 3. WIENER PATH INDICES

Compound Number	$w$	$w_r$	$w^v$	$w^v_r$	$P$	$f$
1	1	0.2500	1.000	0.2500	0	0
2	4	0.4444	2.706	0.3007	0	2
3	9	0.5625	5.118	0.3199	0	6
4	16	0.6400	8.236	0.3294	0	12
5	4	0.4444	2.353	0.2614	0	2
6	9	0.5625	4.912	0.3070	0	6
7	10	0.6250	5.412	0.3383	1	4
8	10	0.6250	5.412	0.3383	1	4
9	18	0.7200	9.177	0.3671	2	8
10	29	0.8056	14.148	0.3930	4	12
11	4	0.4444	3.353	0.3726	0	2
12	9	0.5625	6.412	0.4008	0	6
13	10	0.6250	7.412	0.4633	1	4
14	18	0.7200	12.177	0.4871	2	8
15	16	0.6400	10.177	0.4071	0	12
16	29	0.8056	18.648	0.5180	4	12
17	28	0.7778	17.648	0.4902	3	14
18	4	0.4444	3.334	0.3704	0	2
19	4	0.4444	3.020	0.3356	0	2
20	4	0.4444	2.524	0.2804	0	2
21	4	0.4444	2.342	0.2602	0	2
22	42	0.8571	29.643	0.6050	6	18
23	4	0.4444	2.171	0.2412	0	2
24	10	0.6250	7.048	0.4405	1	4
25	28	0.7778	21.416	0.5949	3	14
26	42	0.8571	28.825	0.5883	6	18
27	58	0.9063	34.708	0.5423	9	24

TABLE 4. CONNECTIVITY INDICES AND POLAR HYDROGEN FACTOR

Compound Number	$^1\chi$	$^0\chi^v$	$^1\chi^v$	$\chi^v_s$	$^3\chi^v_c$	$^4\chi^v_c$	$^4\chi^v_{pc}$	$Q_H$
1	1.0000	2.1339	1.1339	1.1339	0.0000	0.0000	0.0000	0.00
2	1.4142	2.9749	1.6036	0.9091	0.0000	0.0000	0.0000	1.64
3	1.7321	3.9791	1.9640	0.8417	0.8417	0.0000	0.0000	1.23
4	2.0000	5.0356	2.2678	1.4638	2.9157	1.4638	0.0000	0.00
5	1.4142	2.4184	1.0629	0.4629	0.0000	0.0000	0.0000	0.00
6	1.7321	3.4749	1.4874	0.4546	0.4546	0.0000	0.0000	0.00
7	1.9142	3.4225	1.6426	0.4286	0.0000	0.0000	0.0000	1.02
8	1.9142	3.4225	1.6426	0.4286	0.0000	0.0000	0.0000	1.02
9	2.2701	4.4790	2.0772	0.4208	0.3712	0.0000	0.4208	0.61
10	2.6427	5.5356	2.5178	0.4133	0.6429	0.0000	1.4579	0.00
11	1.4142	2.8410	1.5089	0.8018	0.0000	0.0000	0.0000	0.00
12	1.7321	2.8451	1.8867	0.7423	0.7423	0.0000	0.0000	0.82
13	1.9142	3.6820	2.1036	0.6429	0.0000	0.0000	0.0000	2.04
14	2.2701	4.6861	2.5193	0.5952	0.5249	0.0000	0.5952	2.14
15	2.0000	4.9017	2.2008	0.7289	2.6575	0.7289	0.0000	0.00
16	2.6427	5.6903	2.9519	0.5510	0.8571	0.0000	1.9438	2.04
17	2.5607	5.7427	2.8562	0.5844	2.0926	0.5154	1.0309	1.42
18	1.4142	1.4630	0.5345	0.1010	0.0000	0.0000	0.0000	1.72
19	1.4142	2.2190	1.0690	0.3030	0.0000	0.0000	0.0000	1.68
20	1.4142	3.8050	2.1905	1.5747	0.0000	0.0000	0.0000	1.70
21	1.4142	4.6350	2.7775	2.7274	0.0000	0.0000	0.0000	1.76
22	2.9434	5.0309	2.6442	0.0347	0.7936	0.0156	1.1122	1.24
23	1.4142	3.2484	1.5421	0.8018	0.0000	0.0000	0.0000	0.00
24	1.9142	4.5121	2.6905	1.1135	0.0000	0.0000	0.0000	2.08
25	2.5607	3.4749	1.7223	0.0216	0.1785	0.0191	0.1718	1.60
26	2.9434	6.7468	3.2988	0.5411	2.5713	0.4208	3.7876	1.12
27	3.2500	7.8034	3.6516	0.5313	3.3864	0.7289	5.8315	0.00

TABLE 5. CORRELATIONS AMONG THE LOG (P<sub>i</sub>) VALUES

	Saline	Oil	Blood	Liver	Muscle	Fat
Saline	1.000					
Oil	0.535	1.000				
Blood	0.839	0.871	1.000			
Liver	0.716	0.939	0.944	1.000		
Muscle	0.767	0.910	0.945	0.962	1.000	
Fat	0.504	0.985	0.859	0.915	0.880	1.000

A much better account of the tissue solubilities was provided by the following connectivity indices.

$$\begin{aligned}
 \text{LOG}(P_{\text{saline}}) = & 2.422 (\pm 0.334) {}^1\chi^v - 1.444 (\pm 0.234) {}^0\chi^v - 0.032 (\pm 0.088) (1/\chi^v_s) - \\
 & 2.06 (\pm 0.83) (1/{}^1\chi) + 0.256 (\pm 0.159) {}^4\chi^v_{pc} + 2.433 (\pm 0.862) \quad (5) \\
 r^2 = & 0.7825 \quad s = 0.3019
 \end{aligned}$$

$$\begin{aligned}
 \text{LOG}(P_{\text{oil}}) = & 0.840 (\pm 0.082) {}^1\chi^v - 0.031 (\pm 0.004) 1/\chi^v_s - 1.909 (\pm 0.360) (1/{}^1\chi) - \\
 & 0.229 (\pm 0.114) {}^4\chi^v_c + 1.919 (\pm 0.349) \quad (6) \\
 r^2 = & 0.9575 \quad s = 0.1779
 \end{aligned}$$

$$\begin{aligned}
 \text{LOG}(P_{\text{blood}}) = & 0.811 (\pm 0.082) {}^1\chi^v - 0.023 (\pm 0.005) (1/\chi^v_s) - 0.262 (\pm 0.062) {}^3\chi^v_c - \\
 & 0.269 (\pm 0.158) \quad (7) \\
 r^2 = & 0.8552 \quad s = 0.2309
 \end{aligned}$$

$$\begin{aligned}
 \text{LOG}(P_{\text{liver}}) = & 1.072 (\pm 0.137) {}^1\chi^v - 0.021 (\pm 0.004) (1/\chi^v_s) + 0.647 (\pm 0.272) (1/{}^1\chi^v) - \\
 & 0.304 (\pm 0.140) {}^4\chi^v_c - 1.212 (\pm 0.415) \quad (8) \\
 r^2 = & 0.8796 \quad s = 0.2208
 \end{aligned}$$

$$\begin{aligned}
\text{LOG}(P_{\text{muscle}}) = & 0.995 (\pm 0.132) {}^1\chi^v - 0.018 (\pm 0.004) (1/\chi_s^v) - 0.424 (\pm 0.134) {}^4\chi^v c + \\
& 0.602 (\pm 0.260) (1/{}^1\chi^v) - 1.334 (\pm 0.397) \\
r^2 = & 0.8707 \quad s = 0.2112
\end{aligned}
\tag{9}$$

$$\begin{aligned}
\text{LOG}(P_{\text{fat}}) = & 0.734 (\pm 0.096) {}^1\chi^v - 0.029 (\pm 0.003) (\chi_s^v) - 1.570 (\pm 0.284) (1/{}^1\chi^v) - \\
& 0.559 (\pm 0.167) (1/{}^1\chi^v) - 0.098 (\pm 0.038) {}^3\chi^v c + 2.213 (\pm 0.365) \\
r^2 = & 0.9779 \quad s = 0.1348
\end{aligned}
\tag{10}$$

where  $s$  is the root-mean-square-error of the fit and the values in parentheses are the standard errors of the coefficients. In all cases,  $n = 25$  and  $p < 0.0001$ . It is apparent that solubilities in oil and fat are best fit by these parameters, and the solubilities in the more aqueous media, saline solution and blood, are least well described. The first-order valence connectivity index  ${}^1\chi^v$  and the inverse of the valence structure index  $\chi_s^v$  appear to be consistently important structural descriptors.

Regression results obtained using the *ad hoc* molecular descriptors were as follows.

$$\begin{aligned}
\text{LOG}(P_{\text{saline}}) = & 0.611 (\pm 0.048) Q_H - 0.360 (\pm 0.038) N_F - 0.091 (\pm 0.042) N_{C3} - \\
& 0.150 (\pm 0.072) \\
r^2 = & 0.9315 \quad s = 0.1612
\end{aligned}
\tag{11}$$

$$\begin{aligned}
\text{LOG}(P_{\text{oil}}) = & 0.572 (\pm 0.025) N_{Cl} + 0.954 (\pm 0.058) N_{Br} + 0.308 (\pm 0.033) Q_H + \\
& 0.385 (\pm 0.054) N_C - 0.158 (\pm 0.031) N_F + 0.058 (\pm 0.109) \\
r^2 = & 0.915 \quad s = 0.1205
\end{aligned}
\tag{12}$$

$$\begin{aligned}
\text{LOG}(P_{\text{blood}}) = & 0.443 (\pm 0.042) Q_H - 0.303 (\pm 0.039) N_F + 0.225 (\pm 0.032) N_{Cl} + \\
& 0.510 (\pm 0.074) N_{Br} + 0.155 (\pm 0.069) N_C - 0.104 (\pm 0.139) \\
r^2 = & 0.9420 \quad s = 0.1537
\end{aligned}
\tag{13}$$

$$\begin{aligned} \text{LOG}(P_{\text{liver}}) = & 0.366 (\pm 0.036) N_{Cl} + 0.588 (\pm 0.085) N_{Br} + 0.345 (\pm 0.048) Q_H - \\ & 0.179 (\pm 0.045) N_F - 0.007 (\pm 0.099) \end{aligned} \quad (14)$$

$$r^2 = 0.9225 \quad s = 0.1771$$

$$\begin{aligned} \text{LOG}(P_{\text{muscle}}) = & 0.379 (\pm 0.050) Q_H + 0.278 (\pm 0.038) N_{Cl} + 0.536 (\pm 0.088) N_{Br} - \\ & 0.190 (\pm 0.047) N_F + 0.169 (\pm 0.082) N_C - 0.439 (\pm 0.166) \end{aligned} \quad (15)$$

$$r^2 = 0.9077 \quad s = 0.1831$$

$$\begin{aligned} \text{LOG}(P_{\text{fat}}) = & 0.563 (\pm 0.028) N_{Cl} + 1.028 (\pm 0.065) N_{Br} + 0.467 (\pm 0.060) N_C + \\ & 0.270 (\pm 0.036) Q_H - 0.199 (\pm 0.034) N_F - 0.097 (\pm 0.121) \end{aligned} \quad (16)$$

$$r^2 = 0.9781 \quad s = 0.1341$$

where  $n = 25$  and  $p < 0.0001$  for all cases. It is apparent that all partition coefficients, including those for saline solution and blood, are reasonably well represented by these descriptors. The halogens exert a consistent influence on the solubilities: Fluorine decreases the solubility (as indicated by its negative coefficient) in all tissues, whereas both *Cl* and *Br* increase solubility, *Br* more than *Cl*. The polar hydrogen factor  $Q_H$  was an important descriptor for all tissues and solvents examined, in all cases corresponding to increased solubility, the effect being more prominent in the more aqueous media, saline and blood.

Combination of the most relevant descriptors from the previous models yielded the following regression equations.

$$\begin{aligned} \text{LOG}(P_{\text{saline}}) = & 0.527 (\pm 0.042) Q_H - 0.381 (\pm 0.030) N_F - 0.156 (\pm 0.037) N_{C3} - \\ & 0.296 (\pm 0.091) {}^4\chi^v_c + 0.130 (\pm 0.048) {}^4\chi^v_{pc} - 0.022 (\pm 0.069) \end{aligned} \quad (17)$$

$$r^2 = 0.9636 \quad s = 0.1235$$

$$\begin{aligned} \text{LOG}(P_{\text{oil}}) = & 0.997 (\pm 0.065) {}^1\chi^v + 0.237 (\pm 0.041) N_{Cl} - 0.013 (\pm 0.004) (1/\chi^v_s) - \\ & 0.212 (\pm 0.057) {}^3\chi^v_c + 0.074 (\pm 0.118) \end{aligned} \quad (18)$$

$$r^2=0.9613 \quad s=0.1698$$

$$\begin{aligned} \text{LOG}(P_{\text{blood}}) = & 0.541 (\pm 0.051) \chi^v - 0.026 (\pm 0.003) (1/\chi_s^v) + 0.269 (\pm 0.036) Q_H - \\ & 0.436 (\pm 0.091) \chi_{pc}^v + 0.063 (\pm 0.026) N_{Cl} - 0.218 (\pm 0.081) \end{aligned} \quad (19)$$

$$r^2=0.9632 \quad s=0.1224$$

$$\begin{aligned} \text{LOG}(P_{\text{liver}}) = & 0.685 (\pm 0.120) \chi^v + 0.232 (\pm 0.049) Q_H - 0.020 (\pm 0.003) (1/\chi_s^v) + \\ & 0.298 (\pm 0.216) (1/\chi^v) + 0.104 (\pm 0.032) N_{Cl} - 0.726 (\pm 0.324) \end{aligned} \quad (20)$$

$$r^2=0.9386 \quad s=0.1617$$

$$\begin{aligned} \text{LOG}(P_{\text{muscle}}) = & 0.399 (\pm 0.071) \chi^v + 0.295 (\pm 0.042) Q_H - 0.007 (\pm 0.008) (1/\chi_s^v) + \\ & 0.259 (\pm 0.073) \chi_{pc}^v - 0.194 (\pm 0.093) N_F - 0.217 (\pm 0.119) \end{aligned} \quad (21)$$

$$r^2=0.9429 \quad s=0.1441$$

$$\begin{aligned} \text{LOG}(P_{\text{fat}}) = & 1.037 (\pm 0.048) \chi^v - 0.199 (\pm 0.029) N_F - 0.177 (\pm 0.042) \chi_c^v + \\ & 0.022 (\pm 0.035) Q_H + 0.183 (\pm 0.027) N_{Cl} - 0.0036 (\pm 0.079) \end{aligned} \quad (22)$$

$$r^2=0.9854 \quad s=0.1097$$

where  $n = 25$  and  $p < 0.0001$  in all cases. Plots of  $\log(P_i)$  values calculated from these equations vs. experimental values are shown in Figures 2-7.

Sato and Nakajima [25] demonstrated an empirical relationship between the logarithms of the blood:air, oil:air, and water:air partition coefficients:

$$\text{Log}(P_{\text{blood}}) = a \log(P_{\text{oil}}) + b \log(P_{\text{water}}) + c$$

$$n=20 \quad r^2=0.935 \quad s=0.675$$

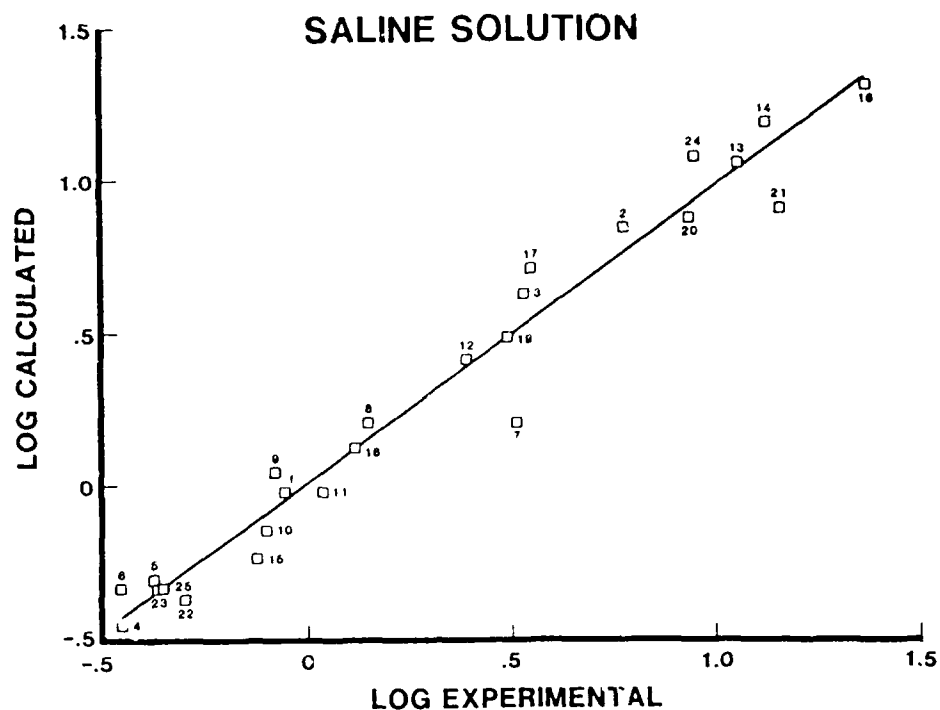


Figure 2. Relationship between calculated and experimental  $\log(P_{\text{saline}})$  values. The identifying numbers correspond to the compound number in Table 1 and will also be used in Figures 3-11. The calculated values were obtained using Eq. 17.

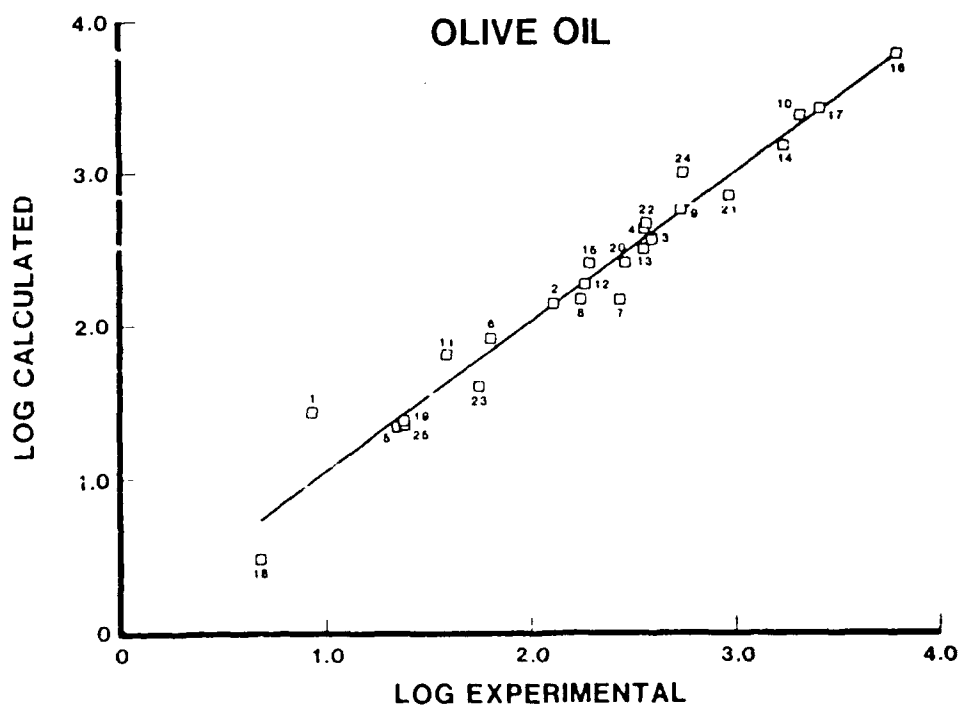


Figure 3. Relationship between calculated (Eq. 18) and experimental  $\log(P_{\text{oil}})$  values.

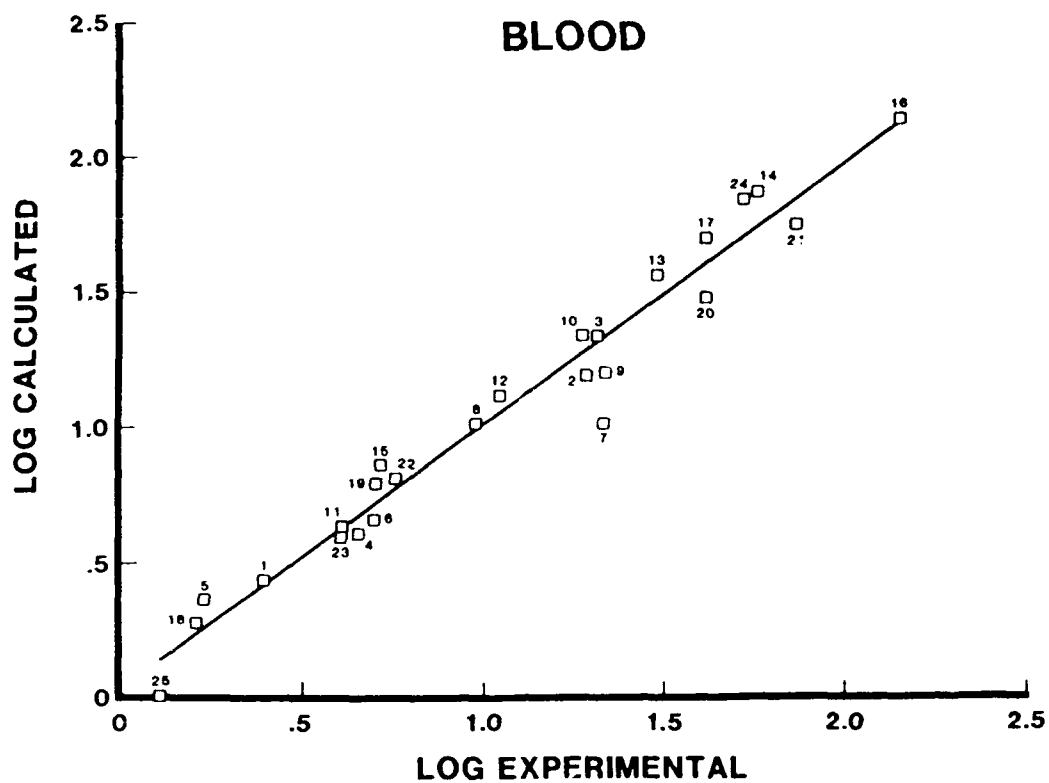


Figure 4. Relationship between calculated (Eq. 19) and experimental log ( $P_{blood}$ ) values.

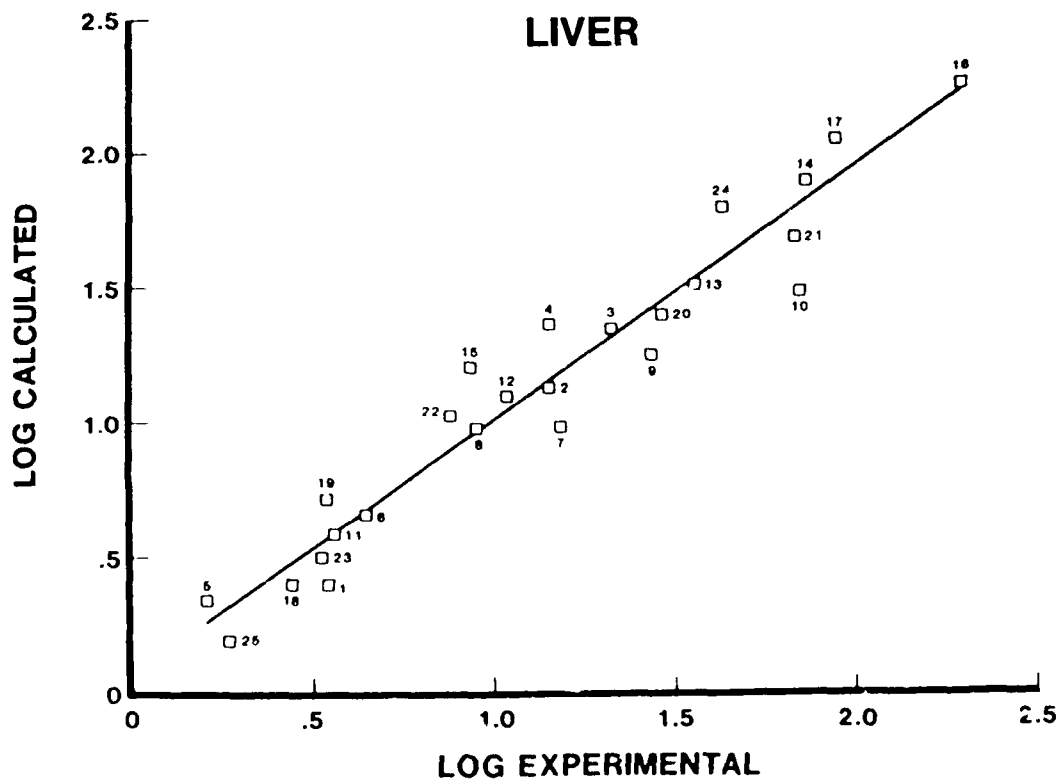


Figure 5. Relationship between calculated (Eq. 20) and experimental log ( $P_{liver}$ ) values.

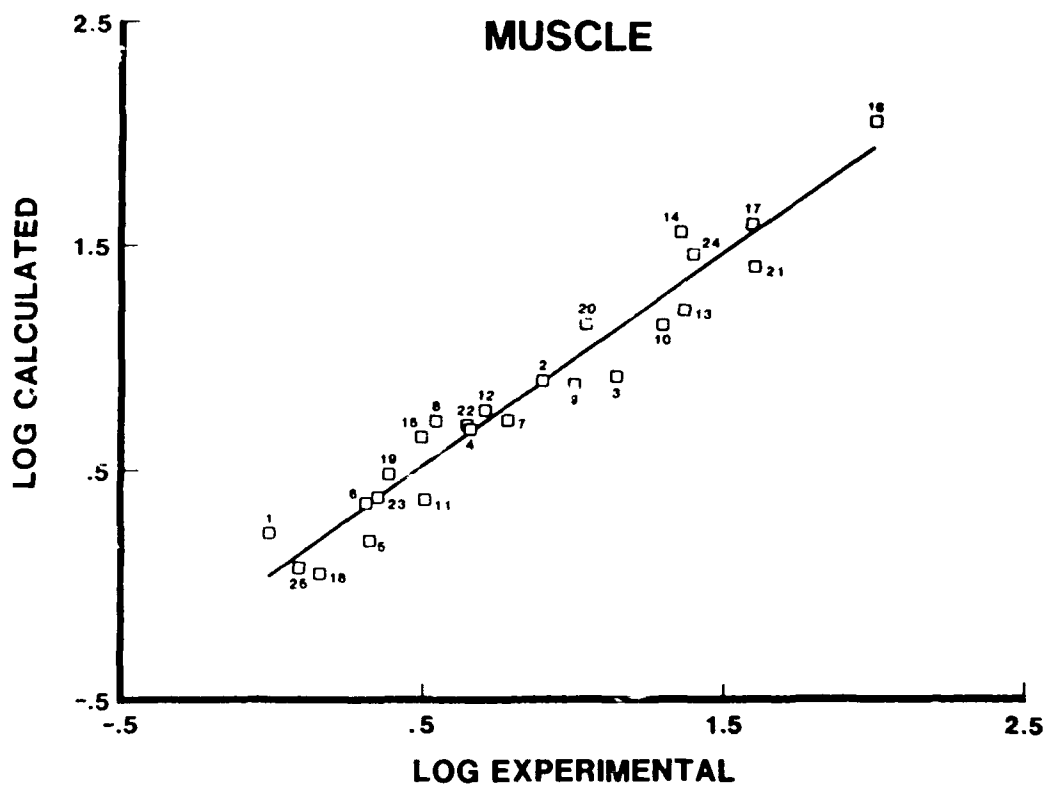


Figure 6. Relationship between calculated (Eq. 21) and experimental  $\log(P_{muscle})$  values.

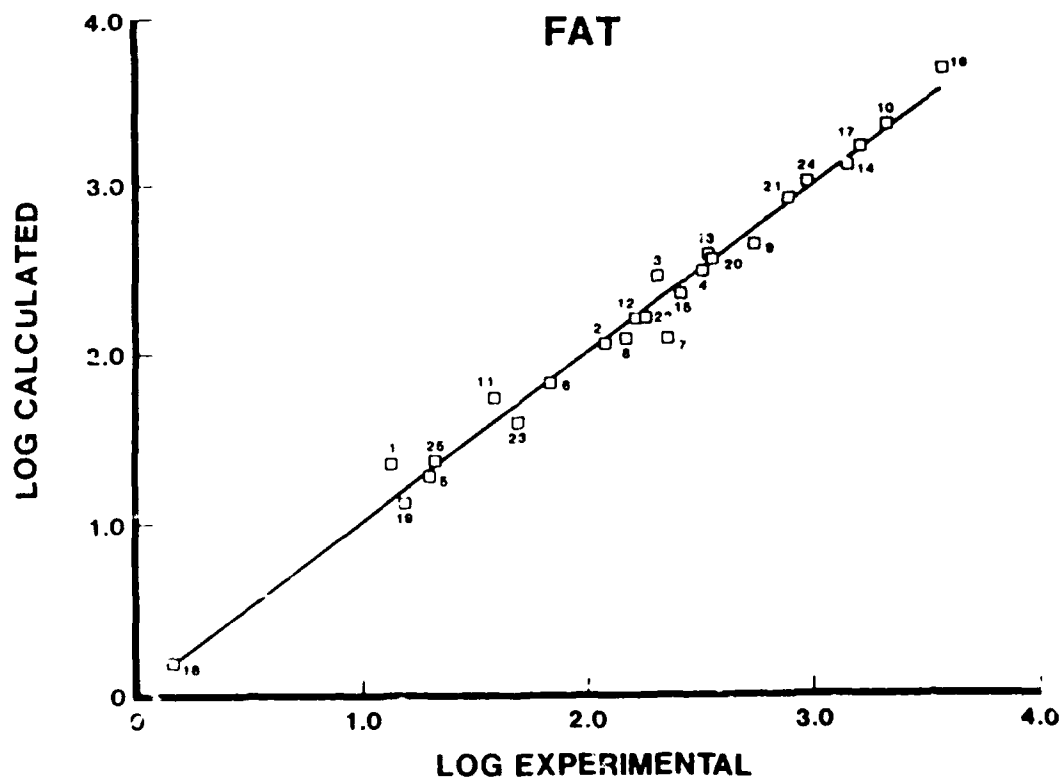


Figure 7. Relationship between calculated (Eq. 22) and experimental  $\log(P_{fat})$  values.

where  $a$ ,  $b$ , and  $c$  are constant. (They imply that  $a = b$ .) Consequently, it was of interest to see if the present blood:air and other partition coefficients could be equally well represented in terms of combinations of oil:air and saline:air partition coefficients. The results were as follows.

$$\begin{aligned} \text{LOG}(P_{\text{blood}}) &= 0.426 (\pm 0.039) \text{LOG}(P_{\text{oil}}) + 0.515 (\pm 0.054) \text{LOG}(P_{\text{saline}}) - \\ &0.070 (\pm 0.086) \end{aligned} \quad (23)$$

$$r^2 = 0.9536 \quad s = 0.1277$$

$$\begin{aligned} \text{LOG}(P_{\text{liver}}) &= 0.574 (\pm 0.044) \text{LOG}(P_{\text{oil}}) + 0.302 (\pm 0.060) \text{LOG}(P_{\text{saline}}) - \\ &0.278 (\pm 0.096) \end{aligned} \quad (24)$$

$$r^2 = 0.9450 \quad s = 0.1423$$

$$\begin{aligned} \text{LOG}(P_{\text{muscle}}) &= 0.477 (\pm 0.043) \text{LOG}(P_{\text{oil}}) + 0.365 (\pm 0.058) \text{LOG}(P_{\text{saline}}) - \\ &0.374 (\pm 0.094) \end{aligned} \quad (25)$$

$$r^2 = 0.9382 \quad s = 0.1393$$

$$\begin{aligned} \text{LOG}(P_{\text{fat}}) &= 1.027 (\pm 0.045) \text{LOG}(P_{\text{oil}}) - 0.046 (\pm 0.061) \text{LOG}(P_{\text{saline}}) - \\ &0.119 (\pm 0.098) \end{aligned} \quad (26)$$

$$r^2 = 0.9701 \quad s = 0.1457$$

where  $n = 25$  and  $p < 0.0001$  for all cases. The relationship is seen to hold well for all tissues. For rat blood it is apparent that the coefficients of  $\log(P_{\text{oil}})$  and  $\log(P_{\text{saline}})$  are roughly equal. Plots of calculated  $\log(P_i)$  values obtained from these equations vs. the experimental values are shown in Figures 8 - 11.

To examine the inherent dimensionality of the tissue solubility data, factor analysis was performed using the correlations in Table 5. Results of the initial principal components analysis are shown in Table 6. A single factor accounts for 87% of the variance in the solubility data, and two factors account for almost 98%, a reasonable limit when the probable accuracy of the partition data is considered. Thus, we conclude that the tissue solubilities can be represented in terms of two dimensions. Since principal components analysis does not necessarily locate the simplest factor structure, further orthogonal (VARIMAX) and oblique (PROMAX) rotations were performed. The results after oblique rotation are shown in Table 7 and Figure 12. It is evident that two factors are attained that can sensibly be described as an oily or fatty dimension and an aqueous/saline dimension. The tissues are seen to load on these dimensions according to their relative degrees of

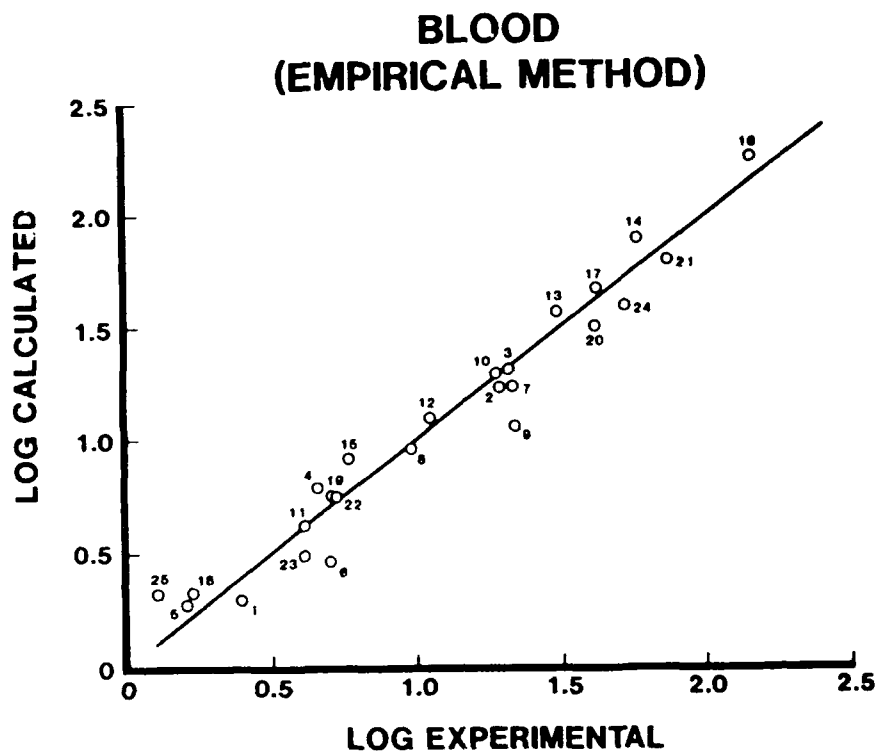


Figure 8. Relationship between calculated and experimental  $\log(P_{blood})$  values. The calculated values were obtained using the empirically derived Eq. 23 in which  $\log(P_{blood})$  was defined as a linear combination of  $\log(P_{oil})$  and  $\log(P_{saline})$ .

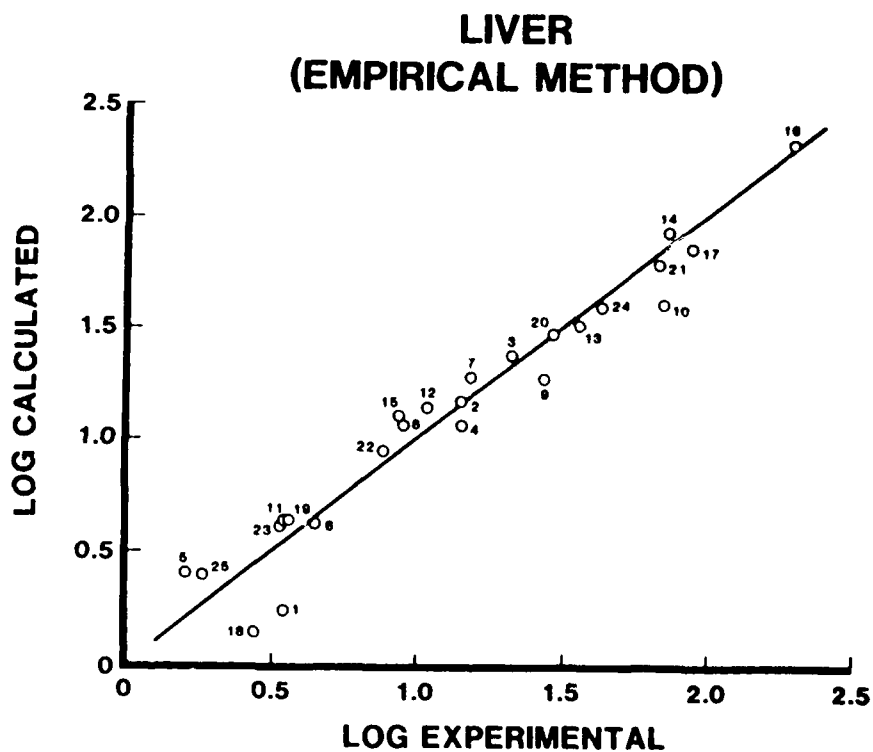


Figure 9. Relationship between calculated (Eq. 24) and experimental  $\log(P_{liver})$  values using an empirical approach.

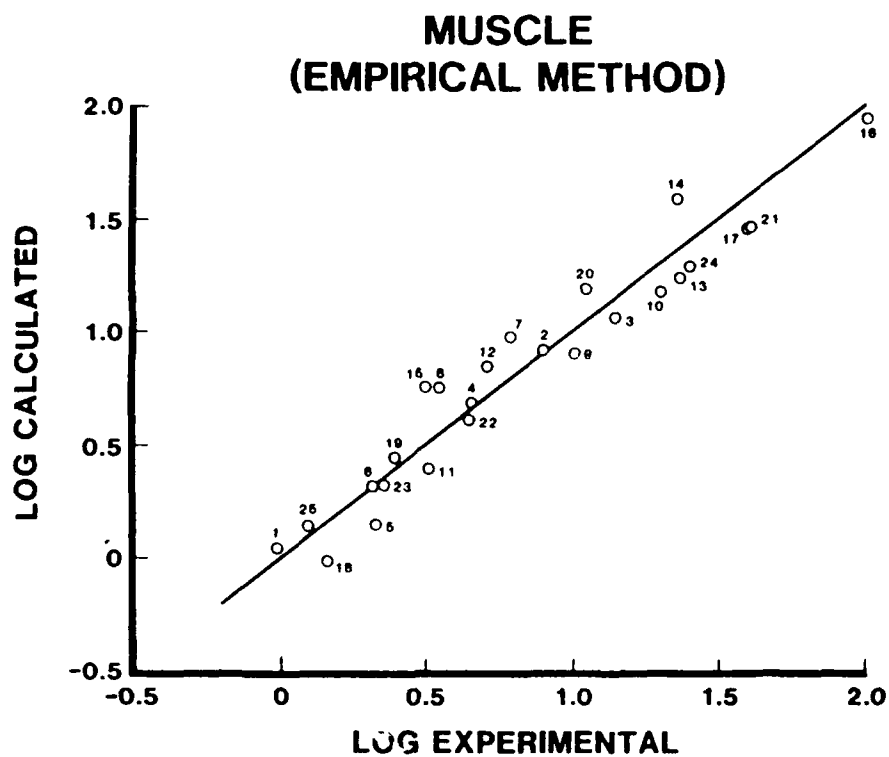


Figure 10. Relationship between calculated (Eq. 25) and experimental  $\log (P_{muscle})$  values using an empirical approach.

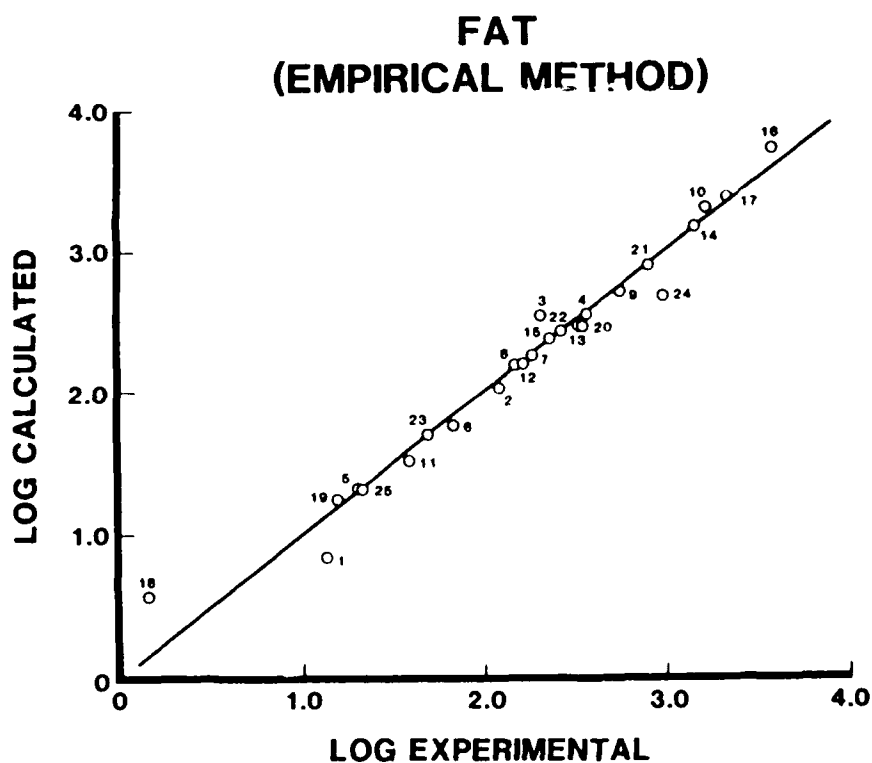


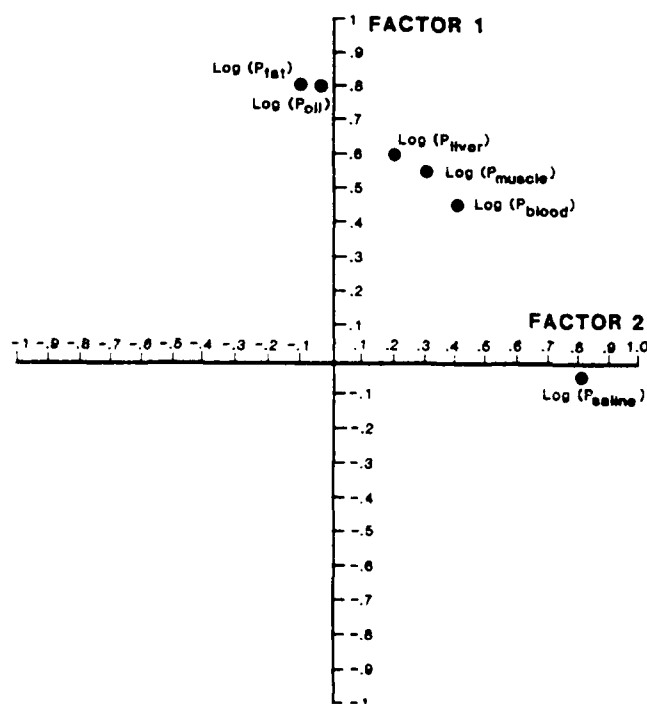
Figure 11. Relationship between calculated (Eq. 26) and experimental  $\log (P_{fat})$  values using an empirical approach.

TABLE 6. RESULTS OF THE PRINCIPAL COMPONENTS ANALYSIS

Factor	Eigenvalue	Cumulative % Variance
1	5.221	87.0%
2	0.643	97.7%
3	0.064	98.8%
4	0.036	99.4%
5	0.026	99.8%
6	0.011	100.0%

TABLE 7. FACTOR ANALYSIS RESULTS AFTER OBLIQUE ROTATION

	Factor 1	Factor 2
LOG (P <sub>saline</sub> )	-0.064	0.923
LOG (P <sub>oil</sub> )	0.805	-0.033
LOG (P <sub>blood</sub> )	0.449	0.418
LOG (P <sub>liver</sub> )	0.616	0.227
LOG (P <sub>muscle</sub> )	0.542	0.311
LOG (P <sub>fat</sub> )	0.823	-0.071

Figure 12. Results of oblique factor analysis of the tissue partition data. The correlation of the two factors is  $r = 0.614$ .

"oiliness" and "aqueousness" in a satisfactory manner. Blood, for example, loads almost equally on the two factors, whereas fat loads almost entirely on the first (fatty) factor. Thus, the empirical representation above in Eqs. 23-26 is well supported, and even suggested, by the factor analysis.

To test the predictive ability of the equations, the partition coefficients for 8 additional compounds were determined experimentally and compared to the values predicted using the equations from the combined indices (Eqs. 17-22) and the empirical approach (Eqs. 23-26). Overall, the equations provided an adequate estimation of the experimental solubilities (Table 8). In most cases, the estimated values were within a factor of 2 or 3 of the experimental values. Notable exceptions to this were the estimations for the olive oil:air and fat:air coefficients for hexachloroethane using the combined indices equations. In this case, the predicted values were approximately fivefold too high. This was also true for the saline:air estimation for allyl chloride.

The three molecular modeling approaches all failed to model the  $\log(V_{max})$  values for the 19-compound data set (Table 2). Preliminary results obtained on a 10-compound subset of these chemicals (Gargas et al. [26] indicated that compounds with no apparent  $V_{max}$  could not be modeled as well as the well-metabolized chemical, methyl chloride. There is evidence that methyl chloride metabolism is primarily glutathione-mediated and not catalyzed by cytochrome P-450, which is believed to be responsible for the metabolism of the other 18 compounds (Gargas, unpublished observations). The data set was reduced to 16 compounds (eliminating methyl chloride, tetrachloroethylene, and 1,1,1-trichloroethane), and the three modeling approaches were repeated. Both the Wiener and *ad hoc* approaches failed to model  $\log(V_{max})$  adequately. The connectivity indices were more successful, resulting in the following equation.

$$\begin{aligned} \text{LOG}(V_{max}) = & -1.676 (\pm 0.049) {}^4\chi_c^v + 0.424 (\pm 0.110) {}^3\chi_c^v \\ & - 0.134 (\pm 0.045) {}^4\chi_{pc}^v + 1.622 (\pm 0.049) \end{aligned} \quad (27)$$

$$r^2 = 0.9047 \quad s = 0.1355 \quad n = 16 \quad p < 0.0001$$

This equation relies completely on the higher-ordered valence connectivity indices. It should be pointed out that 6 of the 16 compounds used to develop this equation have values of zero for these three indices (Table 4), and thus all have predicted values equal to the intercept. A plot of calculated vs. experimental values (Figure 13) shows a clustering of points between  $\log(V_{max})$  of 1.5 – 2.0. Even though the equation appears adequate ( $r^2 = 0.9047$ ), it should be considered very limited in its predictive ability since the correlation is dominated by the outlying compounds 4 and 27.

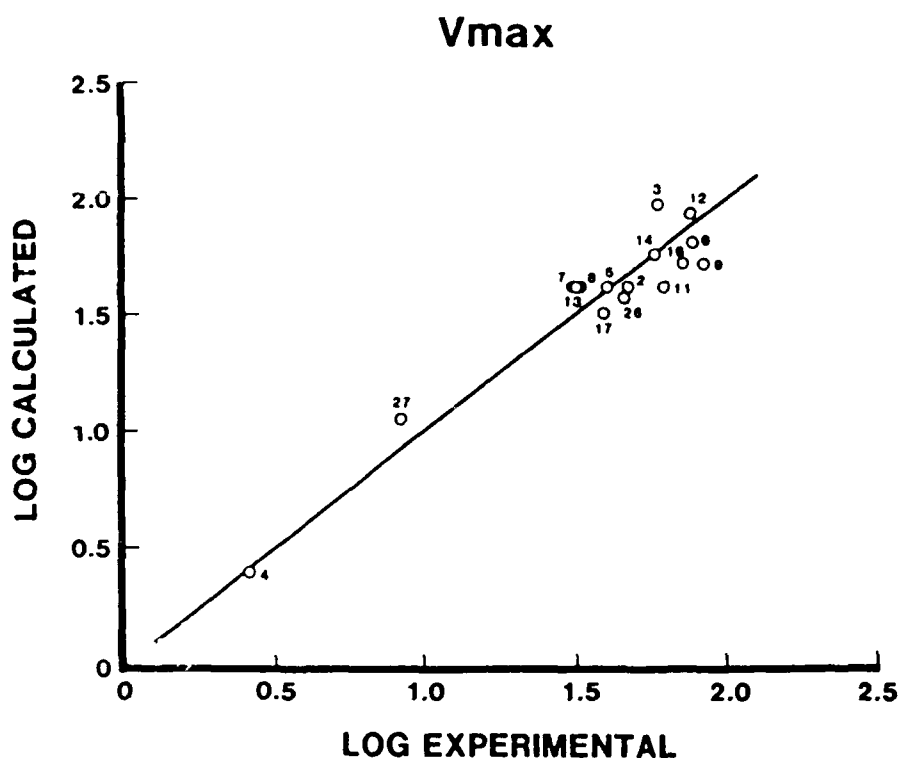


Figure 13. Relationship between calculated (Eq. 27) and experimental  $\log(V_{max})$  values. The identifying numbers correspond to the compound number in Table 2.

## DISCUSSION

These results demonstrate the feasibility of modeling the tissue solubilities of halogenated  $C_1$  and  $C_2$  hydrocarbons. Both the connectivity indices and the *ad hoc* structural descriptors yield adequate representations of the tissue solubilities, the latter being superior in this application. A combination of the two approaches provided a still more accurate representation and account satisfactorily for the solubilities of those halogenated compounds in both aqueous and lipid-rich media. For the present compounds and properties the Wiener approach was not satisfactory, probably because the presently available indices do not adequately account for the important electronic differences among the halogen atoms.

The connectivity indices do not, unfortunately, permit simple physical interpretations. The first-order valence connectivity index  $^1\chi^v$  in some way represents both structural and electronic features of a compound, although not in a simple way. The indices  $^3\chi^v_c$  and  $^4\chi^v_c$  represent multiple substitution patterns of the halogens on carbons in these compounds. The index  $^4\chi_{pc}$  has been associated with flexibility in polymers (Kier and Hall [15]), but more likely  $^4\chi^v_{pc}$  in this study represents a significant halogen substitution pattern.

The results obtained using the *ad hoc* structural descriptors, Eqs. 11-16, are more readily interpreted. Fluorine substituents reduce solubility in all tissues and solvents, the effect being greatest in the more aqueous media, saline solution and blood. Conversely, chlorine and bromine substituents increase solubility in all media, and these influences are most evident in the lipophilic media regressions, where the coefficients of  $N_{Cl}$  are consistently about half those of  $N_{Br}$ . The order  $F < Cl < Br$  is the order of increasing atomic polarizabilities (and decreasing electronegativities), suggesting, at least for  $Cl$  and  $Br$ , that these atoms increase solubility via dispersion interactions with the medium.

The polar hydrogen factor  $Q_H$  is an important descriptor, in particular with respect to solubility in aqueous media. In fact, addition of  $Q_H$  to the connectivity indices greatly improves their performance, to the extent that solubilities in all media become reasonably well described ( $r^2 \geq 0.93$ ). It is tempting to speculate that  $Q_H$  accounts to some extent for hydrogen bonding between the halocarbon and water. Di Paolo et al. [19] employed this factor in their analyses of halocarbon anesthetics.

The representation of tissue solubilities in terms of oil:air and saline:air solubilities has an appealing, heuristic simplicity. Moreover, the approach is reinforced further by the results of factor analysis (Table 5) that show that two factors account for almost 98% of the variance in the solubility data. After oblique rotation these factors could be identified as an oil/fat solubility dimension and an aqueous/saline solubility dimension (Table 7 and Figure 12). This method allows an additional means, separate from the molecular modeling approach, for estimating tissue solubilities for chemicals within the present class of compounds. Once a tissue has been characterized in this way, determination of a compound's oil:air and saline:air partition coefficients would allow estimation of the compound's solubility in the tissue of interest. Recently, Abraham et al. [27] have characterized a number of tissues using water and oil Ostwald coefficients in a manner similar to the present study.

The equations from the combined indices and the empirical approach performed adequately in estimating solubilities for chemicals outside the basis set (Table 8). This test set of chemicals contains three propanes and a three-carbon allyl compound. No compounds containing these basic structures were present in the data set used to develop the equations. Even though the estimated values were reasonable, care should be taken when estimating values for chemicals whose structures lie outside those of the basis set.

The modeling of  $\log(V_{max})$  by higher-order valence connectivity indices is more an indication for future efforts than a means of estimating this rate constant for untested chemicals. Eq. 27 is limited in that it cannot model compounds with  $V_{max}$  values that are zero or near zero and could only be developed after the data set was reduced. The value of this equation lies in the knowledge that

these higher order indices represent significant substitution patterns present in the substructures of these compounds and in some way also encode electronic information. This would indicate that  $V_{max}$  may be dependent on steric constraints and on more specific electronic information such as charge distributions. Successful future modeling of  $V_{max}$  may require parameters that account for these types of information.

## REFERENCES

- 1 Ember, L. (1985) Toxic chemical levels higher indoors than out. Chem. Engr. News, June 24, 21-22.
- 2 Henschler, D. (1985) Halogenated alkenes and alkynes. In: M.W. Anders (Ed.), Bioactivation of Foreign Compounds. Academic Press, New York, pp. 317-346.
- 3 Anders, M.W. and Pohl, L.R. (1985) Halogenated alkanes. In: M.W. Anders (Ed.), Bioactivation of Foreign Compounds. Academic Press, New York pp. 283-315.
- 4 Andersen, M.E. (1981) Pharmacokinetic of inhaled gases and vapors. Neurobehav. Toxicol. Teratol. 3, 383-389.
- 5 Andersen, M.E. (1981) A physiologically based toxicokinetic description of the metabolism of inhaled gases and vapors. Analysis at steady state. Toxicol. Appl. Pharmacol. 60, 509-526.
- 6 Ramsey, J.C. and Andersen, M.E. (1984) A physiologically based description of the inhalation pharmacokinetics of styrene monomer in rats and humans. Toxicol. Appl. Pharmacol. 73, 159-175.
- 7 Andersen, M.E., Gargas, M.L., and Ramsey, J.C. (1984) Inhalation pharmacokinetics: Evaluating systemic extraction, total *in vivo* metabolism, and the time course of enzyme induction for inhaled styrene in rats based on arterial blood: inhaled air concentration ratios. Toxicol. Appl. Pharmacol. 73, 176-187.
- 8 Dedrick, R.L. (1973) Animal scale-up. J. Pharmacol. Biopharm. 1, 435-561.
- 9 Seybold, P.G., May, M.A., and Gargas, M.L. (1986) On the physical properties of halogenated hydrocarbons. Acta. Pharm. Jugosl. 36, 253-265.
- 10 Seybold, P.G., May, M.A., and Bagal, V.A. (1987) Molecular structure property relationships. J. Chem. Educ. 64, 575-581.
- 11 Weiner, H. (1947) Structural determination of paraffin boiling points. J. Amer. Chem Soc. 69, 17-20.
- 12 Weiner, H. (1948) Relation of the physical properties of the isomeric alkanes to molecular structure. J. Phys. Chem. 52, 1082-1089.
- 13 Randic, M. (1975) On characterization of molecular branching. J. Amer. Chem. Soc. 97, 6609-6615.
- 14 Kier, L. B. and Hall, L.H. (1976) Molecular Connectivity in Chemistry and Drug Research. Academic Press, New York, NY.

- 15 Kier, L. B. and Hall, L.H. (1983) General definition of valence delta-values for molecular connectivity. *J. Pharm. Sci.* 72, 1170-1173.
- 16 Trinajstić, N. (1984) *Chemical Graph Theory*. CRC Press, Boca Raton, FL.
- 17 Platt, J.R. (1952) Prediction of isomeric differences in paraffin properties. *J. Phys. Chem.* 56, 328-336.
- 18 Barysz, M., Jashari, G., Lall, R.S., Srivastava, V.K., and Trinajstić, N. (1983) On the distance matrix of molecules containing heteroatoms. In: R.B. King (Ed.), *Chemical Applications of Topology and Graph Theory*, Elsevier, Amsterdam, pp. 222-230.
- 19 DiPaolo, T., Kier, L.B., and Hall, L.H. (1979) Molecular connectivity study of halocarbon anesthetics. *J. Pharm. Sci.* 68, 39-42.
- 20 Fiserova-Bergerova, V., Tichy, M., and DiCarlo, F.J. (1984) Effects of biosolubility on pulmonary uptake and disposition of gases and vapors of lipophilic chemicals. *Drug Metab. Revs.* 15, 1033-1070.
- 21 Sato, A. and Nakajima, T. (1979) Partition coefficients of some aromatic hydrocarbons and ketones in water, blood, and oil. *Brit. J. Ind. Med.* 36, 231-234.
- 22 Gargas, M.L., Clewell, H.J. III, and Andersen, M.E. (1986) Metabolism of inhaled dihalomethanes *in vivo*: Differentiation of kinetic constants of two independent pathways. *Toxicol. Appl. Pharmacol.* 82, 211-223.
- 23 Gargas, M.L., Andersen, M.E. and Clewell, H.J. III. (1986) A physiologically based simulation approach for determining metabolic constants from gas uptake data. *Toxicol. Appl. Pharmacol.* 86, 341-352.
- 24 Gargas, M.L. and Andersen, M.E. (1988) A gas phase technique for determining the kinetic constants of chemical metabolism in the rat. *The Toxicologist* 8, paper no. 445.
- 25 Sato, A. and Nakajima, T. (1979) A structure-activity relationship of some chlorinated hydrocarbons. *Arch. Environ. Health*, March/April, 69-75.
- 26 Gargas, M.L., Andersen, M.E., and Seybold, P.G. (1987) Modeling the tissue solubilities and kinetic parameters of halocarbons. Presented at the American Industrial Hygiene Conference, May 31 - June 5, Montreal, Canada.
- 27 Abraham, M.H., Kamlet, M.J., Taft, R.W., Doherty, R.M., and Weathersby, P.K. (1985) Solubility properties in polymers and biological media. 2. The correlation of the solubilities of nonelectrolytes in biological tissues and fluids. *J. Med. Chem.* 28, 865-870.
- 28 Andersen, M.E., Gargas, M.L., and Clewell, H.J. III. (1986) Suicide inactivation of microsomal oxidation by *cis*- and *trans*-dichloroethylene (C-DCE and T-DCE) in male Fischer 344 rats *in vivo*. *The Toxicologist* 6, abstract no. 47.
- 29 D'Sousa, R.W., Francis, W.R. and Andersen, M.E. (In Press) A physiological model for tissue glutathione depletion and increased resynthesis following ethylene dichloride exposure. *J. Pharmacol. Exp. Therap.*

- 30 Medinsky, M.A., Bechtold, W.E., Birnbaum, L.S., Chico, D.M., Gerlack, R.L., and Hendersen, R.F. (1987) Uptake of vinylidene fluoride (VDF) in rats simulated by a physiological model. The Toxicologist 7, paper no. 125.

# COMPUTATIONAL APPROACHES TO THE IDENTIFICATION OF SUSPECT TOXIC MOLECULES

Peter Politzer

*Department of Chemistry, University of New Orleans Lakefront, New Orleans, LA 70148 (U.S.A.)*

## SUMMARY

We have presented computational approaches that can be used for the relatively rapid identification of suspect toxigens, including carcinogens, in two different classes of compounds: (a) halogenated olefins and epoxides, and (b) substituted dibenzo-*p*-dioxins. A common element in these approaches is the key role played by the molecular electrostatic potential. It is applied in two different ways, however; it is used to assess the reactivity of a specific site in the case of the epoxides, and for the dibenzo-*p*-dioxins the focus is on the overall pattern of negative regions above the molecular plane. While we are continuing to develop and refine both types of analysis, especially that related to the dibenzo-*p*-dioxins, the results obtained so far are encouraging, and indicate that these can be regarded as useful screening techniques for identifying compounds that require further and more exhaustive investigation.

## INTRODUCTION

Certain classes of chemicals (e.g., polynuclear aromatic hydrocarbons, halogenated hydrocarbons, dibenzo-*p*-dioxins) are found on a relatively large scale in our environment. Not all of the individual compounds of these types pose a serious health threat. Since some do, however, there is a need for fast but reliable techniques for assessing the relative degrees of hazard associated with specific members of these classes. One possible approach involves animal testing. This is a lengthy and expensive undertaking, however, and the results are very sensitive to the conditions of the testing procedure.

Accordingly, one of our objectives has been to develop effective alternatives that complement current laboratory approaches, and thus avoid the unrealistic prospect of having to apply the latter to hundreds of compounds. We need to formulate rapid and reliable computational procedures for assessing and predicting degrees of toxicity so that the likely hazard associated with a compound can be estimated in a matter of hours. Animal testing, which requires an extended period of time, could then be focused only on those compounds that already have been shown to be suspect.

We have shown, for two different classes of chemicals, that the molecular electrostatic potential provides a basis for the initial assessment of toxicity. This is the potential  $V(r)$  that is created in the space around a molecule by its nuclei and electrons; it is through this potential that the molecule is "seen" or "felt" by any other systems in its vicinity. The value of  $V(r)$  at any point  $r$  is given rigorously by Eq. (1):

$$V(\mathbf{r}) = \sum_A \frac{Z_A}{|\mathbf{r}_A - \mathbf{r}|} - \int \frac{\rho(\mathbf{r}') d\mathbf{r}'}{|\mathbf{r}' - \mathbf{r}|} \quad (1)$$

where  $Z_A$  is the charge on nucleus  $A$ , located at  $\mathbf{r}_A$ , and  $\rho(\mathbf{r})$  is the electronic density function of the molecule, which we obtain from the computed molecular wave function.

The first term on the right side of Eq. (1) gives the contribution of the nuclei, which is positive; the second represents the effect of the electrons, which is negative. Thus, when an electrophile approaches the molecule, its initial tendency is to go to those regions where  $V(\mathbf{r})$  has its most negative values, since it is there that the effects of the molecule's electrons predominate. A knowledge of the electrostatic potential around a molecule is therefore of considerable assistance in interpreting its reactive behavior and in predicting the sites on the molecule at which interactions are most likely to occur [1, 2, 3].

A second important application of the electrostatic potential is in the area of "recognition" processes such as occur in enzyme-substrate or drug-receptor interactions. In such a process, the initial step is one of recognition: the receptor "recognizes" that an approaching molecule has certain key features that will promote their mutual interaction. Such recognition is believed to take place typically when the molecule and the receptor are at a relatively large separation; it precedes the formation of any covalent bonds.

Since the electrostatic potential of a molecule is a physically meaningful representation of how it is perceived by a system in its vicinity, it is reasonable to look to  $V(\mathbf{r})$  in seeking the key features that determine whether or not a recognition process involving the molecule and a particular cellular receptor will occur. The potential has indeed proven to be an effective means for analyzing and elucidating recognition processes; in a number of cases (which are reviewed in Politzer *et al.* [4]), the affinity of a given molecule for a specific receptor has been shown to depend upon the degree to which the potential of the former possesses certain characteristics that have been established as being required for effective interaction with that receptor.

An important feature of the electrostatic potential is that it is a real physical property, which can be determined experimentally by diffraction methods as well as computationally [3]. At present, however, the latter approach is by far the more widely used.

We used the electrostatic potential to determine the susceptibilities of certain molecular sites toward electrophilic attack and to identify general patterns of positive and negative potential that promote interaction with a specific cellular receptor. Each approach has been found to be effective for assessing the likely toxicities of individual members of a particular class of compounds.

### ***Halogenated olefins and their epoxides***

The halogenated olefins and their epoxides are a widely occurring and commercially important class of chemicals. They are used in the manufacture of textiles and plastics, as solvents, pesticides, dry-cleaning fluids, refrigerants, flame retardants, degreasing agents, and as intermediates in syntheses. At least a dozen halogenated olefins have been identified in drinking water [5, 6]. (For a detailed discussion of the occurrence of halogenated olefins and epoxides in the environment, see Woo *et al.* [7].)

Many of these compounds are known to be carcinogenic. Perhaps the most notorious is vinyl chloride, which has been shown to cause liver angiosarcomas, lung adenocarcinomas, and other tumors in animals [8, 9], and has been strongly implicated in liver, lung, and lymphatic cancers in humans [10, 11]. Other halogenated olefins and epoxides are also known to be carcinogens; some of these include epichlorohydrin, *cis*- and *trans*-1-chloropropylene oxide, *cis*- and *trans*-1,3-dichloropropylene oxide, vinylidene fluoride and vinylidene chloride, vinyl bromide, ethylene oxide and propylene oxide, and others [7, 12, 13, 14, 15].

There appear to be at least four important factors involved in the carcinogenic behavior of halogenated olefins and epoxides.

#### **(1) Ease of epoxidation of the olefin.**

The initial step in the metabolism of many halogenated olefins is epoxidation, which occurs through the action of microsomal monooxygenases [7, 13, 14, 16, 17, 18]. It is the resulting epoxides that are believed to be responsible for the carcinogenicities of a number of these compounds [7, 14, 19, 20]. If this metabolic epoxidation involves interaction with an electrophilic oxygen species [21], then it should proceed more readily as the electrostatic potential in the olefinic double-bond region becomes more strongly negative. For the chlorinated ethylenes, we have shown that this potential becomes more negative as the number of chlorines decreases [22], which parallels a general increase in reactivity of these molecules toward electrophiles that has been observed experimentally [23, 24, 25, 26].

#### **(2) Tendency of the epoxide to undergo oxygen protonation.**

Protonation of an epoxide oxygen is known to weaken the C-O bonds and facilitate the opening of the epoxide ring [27, 28, 29, 30]. We have further evidence of this in terms of C-O force constants and bond lengths [31, 32, 33]. For example, protonation of the epoxide oxygen typically lengthens the C-O bonds by about 0.07 Å.

Supporting the expectation that the halogenated olefin epoxides are protonated in the environment of interest is the fact that there do exist subcellular regions with high proton activities [34, 35, 36]. The nuclear membrane, in which the enzymatic reactions of DNA replication occur,

contains certain redox systems that are believed to produce high local proton activities [36, 37, 38], including the cytochrome P-450 system that epoxidizes olefins [39].

(3) Reactivity of the protonated epoxide.

The epoxide needs to be sufficiently reactive to undergo the interaction(s) involved in the carcinogenic process. However, too great a degree of activity leads to a high likelihood of its reacting with other cellular species before reaching the key site(s) at which the carcinogenic process would be initiated. (This happens in the case of the *syn* and *anti* 7,8-dihydrodiol-9,10-epoxides of benzo[a]pyrene; the *syn* is chemically more active while the *anti* is more carcinogenic [40, 41, 42, 43].) The concept that there is some zone of intermediate reactivity which is optimum for initiating the carcinogenic process has been expressed earlier [33, 44, 45, 46, 47].

(4) Nature of the critical cellular adduct that is formed.

If and when the potentially carcinogenic cellular interaction occurs, presumably involving DNA, it can be expected that the properties and behavior of the product will help to determine the subsequent course of events. Recently, the primary *in vivo* DNA alkylation product of vinyl chloride has been shown to be the 7-N-(2-oxoethyl) derivative of guanine [48, 49]. The carcinogenicity of vinyl chloride has been attributed to the formation of this derivative. Its NMR spectrum was interpreted as indicating that it may exist in equilibrium with a cyclic hemiacetal [48]; this would affect the hydrogen bonding between guanine and cytosine, and could lead to miscoding [50, 51, 52] and replicational and transcriptional errors [48, 53]. We have carried out computational analyses of systems designed to model the oxoethyl derivative and the hemiacetal [54]; we estimate the equilibrium to be very far in the direction of the former.

Since the carcinogenic process appears to involve a number of separate steps, it must be anticipated that it will not be possible to establish a direct correlation between the carcinogenicity and any single molecular property or parameter. However, we have found a criterion that does permit us to separate epoxides into the two general categories of (1) likely to be carcinogenic, and (2) likely to be inactive or only weakly carcinogenic. This criterion, which will now be discussed in detail, appears to be related to the second of the four factors mentioned above (i.e., the tendency of the epoxide to undergo oxygen protonation).

### Computational approach

As was pointed out above, it is the metabolically produced epoxides that are believed to be the carcinogenic forms of the halogenated olefins. Accordingly, our computational analyses have focused upon epoxides. For each one that we have studied, the first step was to calculate its optimized geometry. This was done even in those instances when an experimentally determined structure was available, in order to ensure consistency in comparing the results for different molecules. An *ab initio* self-consistent-field (SCF) molecular orbital procedure was used at the STO-3G

level; this basis set has been shown to be effective for structure calculations [55]. Once the geometry had been obtained, the molecular electrostatic potential was computed, in terms of the STO-5G basis set. We have found this to yield good results for properties related to the electronic charge distribution, as is  $V(r)$ .

### *Oxygen potentials as a criterion for epoxide carcinogenicity*

#### *Protonation and oxygen potentials*

Epoxides typically have negative electrostatic potentials in the neighborhood of the oxygen [56, 57]. There are generally two local minima (points at which the most negative values are found) that can be viewed as reflecting the oxygen's lone pairs. Table 1 compares the calculated proton affinities of several epoxides (oxygen protonation) with the single most negative value of  $V(r)$  in the vicinity of each oxygen, denoted  $V_{\min}$ . The excellent correlation between  $V_{\min}$  and the proton affinity demonstrates that  $V_{\min}$  is a good indicator of the relative ease of protonation of these molecules.

TABLE 1. COMPARISON OF CALCULATED PROTON AFFINITIES AND  $V_{\min}$  VALUES <sup>a,b</sup>

Name of Molecule	Structure	Proton Affinity (Oxygen)	$V_{\min}$ (Oxygen)
Propylene Oxide		239	- 53.4
Ethylene Oxide		232	- 51.3
Epichlorohydrin		226	- 43.1
Chlorooxirane		217	- 38.1
<i>trans</i> -Dichlorooxirane		204	- 23.1

<sup>a</sup> The proton affinities and the  $V_{\min}$  values were computed at the STO-3G and STO-5G levels, respectively. All are in kcal/mole.

<sup>b</sup> The data in this table are taken from Politzer et al. [47].

Since protonation is an important factor in facilitating epoxide reactions, as discussed below, we have computed  $V_{\min}$  for a large number of epoxides. The results are presented in Table 2. The magnitudes of the oxygen minima clearly can be related to the nature of the substituent on the epoxide ring. Thus, the substitution of a halogen on ethylene oxide causes  $V_{\min}$  to become less negative, presumably due to the halogen attracting electronic charge away from the oxygen. The effect increases with the degree of halogenation and is stronger when the substitution is directly on the ring than when it involves an exocyclic carbon. Chlorine affects the oxygen potential more than does fluorine, despite the latter's greater intrinsic electronegativity. This again demonstrates the anomalous nature of fluorine [58, 59], which can be interpreted in terms of Huheey's concept of charge capacity [60, 61, 62]: the ability of fluorine to accommodate additional electronic charge diminishes relatively rapidly, despite the strong initial attraction. Finally, Table 2 shows that aliphatic hydrocarbon groups cause  $V_{\min}$  to become slightly more negative than it is in ethylene oxide, which is consistent with the weakly electron-releasing natures of these groups [27, 63].

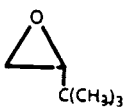
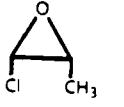
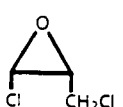
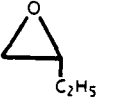
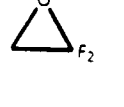
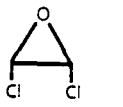
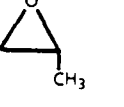
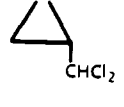
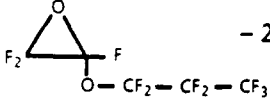
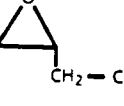
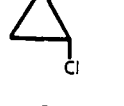
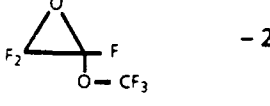

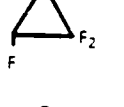
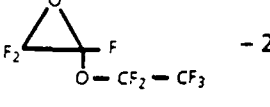
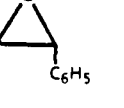
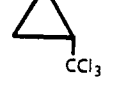
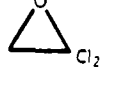
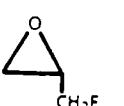
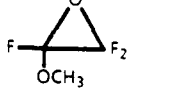
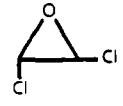
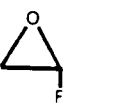
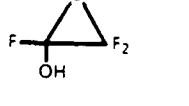
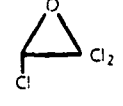
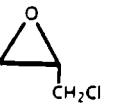
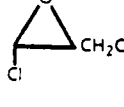
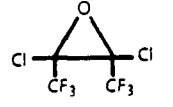
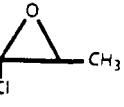
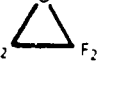
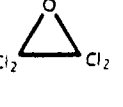
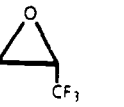
#### ***Enzyme inhibition***

Since  $V_{\min}$  directly reflects the electron-withdrawing or -releasing powers of substituents on epoxide rings, it seemed reasonable to explore its use in developing a quantitative measure of the abilities of epoxides to inhibit epoxide hydrase, an enzyme that catalyzes the hydrolysis of epoxides. This inhibition is often due to the inhibitor competing as an alternate substrate [64, 65, 66], and thus should depend upon factors similar to those believed to determine the extents of interaction of epoxides with epoxide hydrase; these include the electron-withdrawing or -releasing tendencies of substituents on the epoxide ring and steric compatibility [66].  $V_{\min}$  is a measure of the former; to take steric effects into account, we used Taft's steric substituent parameter  $E_s$  [67, 68]. In confirmation of this reasoning, we were indeed able to demonstrate a good correlation between epoxide hydrase inhibition and the quantity  $V_{\min}/E_s$  [56]; the correlation coefficient is 0.94.

#### ***A Criterion for the Identification of Suspect Carcinogens***

We have found that there is a general relationship between the electrostatic potential and carcinogenicity for hydrocarbon and halogenated hydrocarbon epoxides. More specifically, we have shown that carcinogenicity is associated with a relatively strong negative potential in the neighborhood of the epoxide oxygen [56].

TABLE 2. CALCULATED  $V_{\min}$  VALUES (KCAL/MOLE) FOR SOME EPOXIDES<sup>a</sup>

Molecule	$V_{\min}$ (Oxygen)	Molecule	$V_{\min}$ (Oxygen)	Molecule	$V_{\min}$ (Oxygen)
1. 	-54.0	12. 	-40.3	22. 	-28.4
2. 	-53.9	13. 	-39.9	23. 	-27.7
3. 	-53.4	14. 	-39.8	24. 	-27.6
4. 	-53.2	15. 	-38.1	25. 	-26.7
5. 	-51.3	16. 	-34.8	26. 	-26.6
6. 	-51.2	17. 	-34.2	27. 	-26.5
7. 	-47.7	18. 	-33.2	28. 	-23.1
8. 	-46.5	19. 	-33.1	29. 	-17.1
9. 	-43.1	20. 	-31.5	30. 	-15.6
10. 	-40.8	21. 	-29.5	31. 	-9.2
11. 	-40.7				

<sup>a</sup> The data in this table are taken in part from Politzer and Laurence [57].

When the epoxides are ranked in order of their  $V_{min}$  values, the established carcinogens (as shown by laboratory studies) are found to have the more negative  $V_{min}$ ; the inactive or weakly active ones have less negative values. The threshold potential, in terms of our STO-5G computational level, is approximately -30 kcal/mole. (This would probably change somewhat if another basis set were used, which simply means that it is necessary to be consistent with respect to the basis set.)


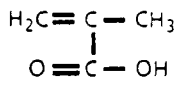
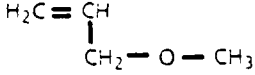
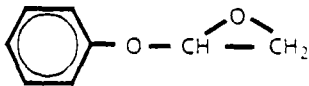
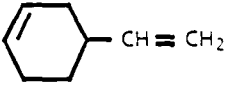
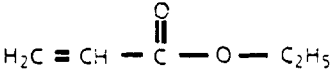
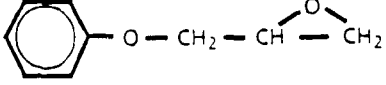
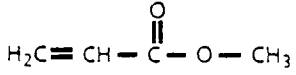
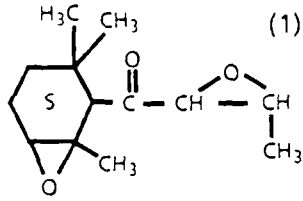
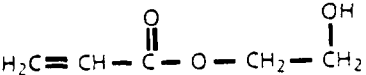
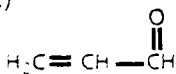
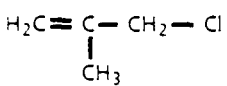
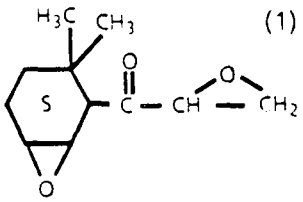
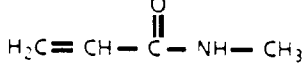
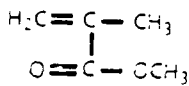
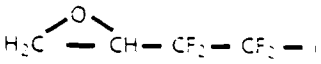
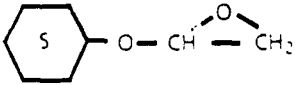
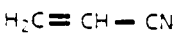

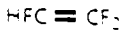

These observations provide a useful predictive capability for the identification of suspect carcinogens. If the electrostatic potential near the oxygen of a halogenated hydrocarbon epoxide reaches values more negative than roughly -30 kcal/mole, then the molecule should be regarded as reasonably likely to be carcinogenic. In the practical application of this criterion, it is an important advantage that the magnitude of  $V_{min}$  follows well-defined patterns related to the natures of the substituents on the epoxide ring, as pointed out earlier. Once these patterns have been discerned through computational analyses of a larger number of molecules (Table 2),  $V_{min}$  often can be estimated for other systems to within 1-2 kcal/mole, without the necessity for further calculation. For example, for the epoxide of 3-chloro-2-methylpropene, our prediction was that  $V_{min}$  would be between -42 and -45 kcal/mole; its computed value turned out to be -42.9 kcal/mole.

We suggest that the apparent association of carcinogenicity with a strongly negative oxygen potential reflects the importance of protonation at that site. This was mentioned earlier as one of four factors that appears to be involved in the carcinogenic behavior of halogenated olefins and epoxides. However, while a strongly negative  $V_{min}$  seems to be a prerequisite for carcinogenicity, its magnitude does not indicate the degree of activity. For example, vinyl chloride is certainly more carcinogenic than either ethylene or ethylene oxide [7], yet  $V_{min}$  for chlorooxirane (the active metabolite of vinyl chloride) is -38.1 kcal/mole, compared to -51.3 kcal/mole for ethylene oxide (Table 2). In order to be able to estimate the relative carcinogenicities of the epoxides, it is necessary to be able to take quantitative account of their overall reactivities. We are currently addressing this problem [69].

#### ***Application of the $V_{min}$ criterion***

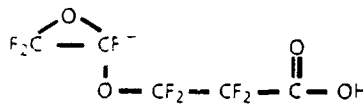
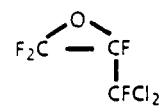
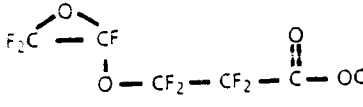
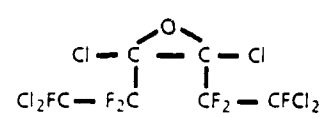
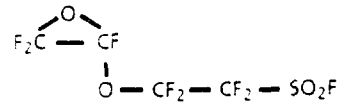
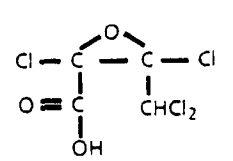
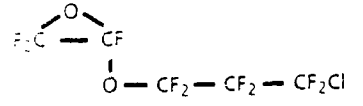
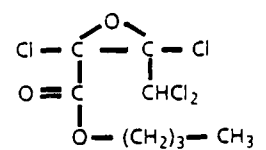
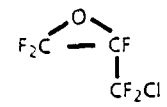
We have applied our electrostatic potential criterion for carcinogenicity, involving  $V_{min}$ , to a number of compounds that the Environmental Protection Agency requested us to analyze. These were not limited to the categories of halogenated olefins and their epoxides, although all of them are either epoxides of some sort or contain double bonds that can presumably form epoxides metabolically. Out of a total of 21 compounds, we found 23 to be suspect carcinogens (Table 3), for which further evaluation is suggested.

TABLE 3. CALCULATED AND ESTIMATED  $V_{\min}$  VALUES FOR OLEFINS AND EPOXIDES AS REQUESTED BY ENVIRONMENTAL PROTECTION AGENCY. FOR OLEFINS,  $V_{\min}$  IS FOR THE CORRESPONDING EPOXIDE.<sup>a</sup>

Molecule	$V_{\min}$ (kcal/mole)	Molecule	$V_{\min}$ (kcal/mole)
 <chem>S1CCCCC1OCC2OC2</chem>	- 54b (est.)	 <chem>CC(C)(O)C=CO</chem>	- 46.3 (calc.)
 <chem>CC(C)=COC</chem>	- 53.3 (calc.)	 <chem>c1ccccc1C2OC2</chem>	- 45.7 (calc.)
 <chem>C1=CCCCC1</chem>	- 53.3 (calc.)	 <chem>CCOC(=O)C=C</chem>	- 44.8 (calc.)
 <chem>c1ccccc1C2OC2</chem>	- 53 (est.)	 <chem>COC(=O)C=C</chem>	- 44.2 (calc.)
 <chem>CC1(C)C2OC2C(=O)C1(C)C</chem>	(1) - 51 (est.) (2) - 49 (est.)	 <chem>OC(CO)COC(=O)C=C</chem>	- 43.4 (calc.)
 <chem>CC(C)=CC</chem>	- 49.6 (calc.)	 <chem>CC(C)=CCl</chem>	- 42.9 (calc.)
 <chem>CC(C)=CC</chem>	(1) - 49 (est.) (2) - 47 (est.)	 <chem>CNC(=O)C=C</chem>	- 39.9 (calc.)
 <chem>CC(C)=CC</chem>	- 48.9 (calc.)	 <chem>CC(F)(F)C(F)(F)C</chem>	- 39 (est.)
 <chem>c1ccccc1C2OC2</chem>	- 47 (est.)	 <chem>C#NC=C</chem>	- 35.9 (calc.)
 <chem>CC(C)=CC</chem>	- 46.5 (calc.)	 <chem>CC(F)(F)=F</chem>	- 34.8 (calc.)
		 <chem>CC(F)=F</chem>	- 29.5 (calc.)

(continued)

TABLE 3. (Continued).

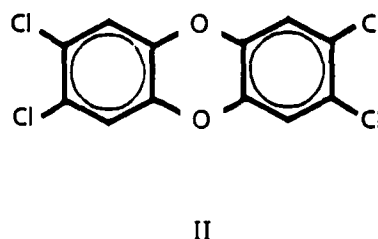
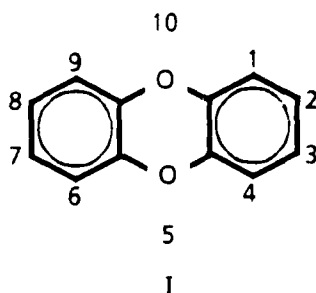
Molecule	$V_{\min}$ (kcal/mole)	Molecule	$V_{\min}$ (kcal/mole)
	- 25.5 (calc.)		- 21.8 (calc.)
	- 25 (est.)		- 16 (est.)
	- 25 (est.)		- 16 (est.)
	- 25 (est.)		- 16 (est.)
	- 24.4 (calc.)		

<sup>a</sup> Beside each  $V_{\min}$  is indicated whether it was calculated directly (at the STO-5G level) or estimated on the basis of the patterns that have been observed.

<sup>b</sup> Threshold Value: - 30 kcal/mole.

### Dibenzo-*p*-dioxins

Dibenzo-*p*-dioxin (I) is the parent compound for a large number of derivatives, with halogens and other substituents at various positions. These exhibit varying degrees of toxicity, ranging from virtually none to very high, the latter being exemplified by the notorious 2,3,7,8-tetrachlorodibenzo-*p*-dioxin (TCDD, II).



These compounds are formed as trace contaminants in the manufacture of herbicides, insecticides, fungicides, and disinfectants. They are also produced in very small amounts in combustion processes, including the burning of wood.

The toxic responses produced by the dibenzo-*p*-dioxins include, to varying degrees, gastric and liver lesions, hepatomegaly, loss of lymphoid tissue, urinary tract hyperplasia, acute loss of weight, and chloracne [70, 71]. Relatively few of these compounds have been tested for carcinogenicity; however, TCDD (II) has been shown to be a highly potent carcinogen in mice and rats [72, 73], and it has also been found to act as a tumor promoter [74]. A mixture of two hexachlorodibenzo-*p*-dioxins was observed to be carcinogenic in rats and mice [75], whereas the 2,7-dichloro derivative is only marginally active [76] and unsubstituted dibenzo-*p*-dioxin is noncarcinogenic [77].

In addition to the various degrees of toxicity exhibited by the dibenzo-*p*-dioxins, certain other biochemical responses are elicited as well. One of these is the induction of aryl hydrocarbon hydroxylase (AHH) activity [78, 79]. This enzyme is responsible for the hydroxylation and epoxidation of polycyclic aromatic hydrocarbons [39]. An excellent correlation between the toxicities of the dibenzo-*p*-dioxins and their potencies in inducing AHH activity has been found [71, 78, 79, 80, 81, 82]; for example, the highly toxic TCDD is also an extremely strong AHH-inducer.

These observations suggest that some mechanistic feature(s) may be common to both the toxic and the AHH-inducing activities of these compounds. Indeed, it is now believed that both the toxicity and the AHH induction involve initial binding of the molecule to the same cytosolic receptor [71, 83, 84]. Both the toxicities and the AHH-inducing potencies have been found to correlate well with binding affinities to this receptor.

Certain structural features of the dibenzo-*p*-dioxins have been identified as being associated with high degrees of toxic potency, AHH induction and binding to the cytosolic receptor [71, 79]. These are as follows.

1. The molecule should be essentially planar and rectangular, with dimensions that are roughly 3 Å x 10 Å.
2. At least three of the four lateral positions (2, 3, 7, and 8) should have halogen substituents. The activity is greater if all four of these positions are halogenated.
3. The activity induced by halogen substituents decreases in going from bromine to chlorine to fluorine.
4. For activity, at least one ring position should remain unsubstituted.

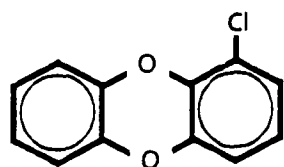
It was later suggested that the need for an unsubstituted position reflects a steric requirement of the receptor for an unhindered region of space [85, 86]. It was further proposed that AHH induction may

require activation of the receptor by an interaction between a negative center on the molecule (e.g., a chlorine), and an electrophilic site on the receptor.

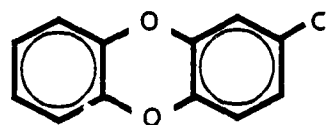
In view of the evidence indicating that the toxic effects produced by dibenzo-*p*-dioxins are related to their binding to a cytosolic receptor, our work has focused upon this interaction. We treat this as involving a recognition process, and accordingly seek patterns in the electrostatic potentials of the dibenzo-*p*-dioxins that can be related to their degrees of toxicity.

#### Computational approach

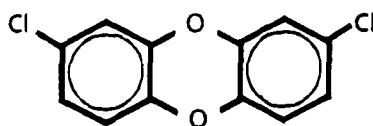
We have computed the SCF STO-5G electrostatic potentials of molecules I through XIII [87, 88]. The structure of TCDD (II) has been determined crystallographically [89], and this was used as the model for the other systems, with appropriate modifications: chlorines were replaced by X (X = H, CH<sub>3</sub>, or F), with C-C-X angles set at 120°. C-H and C-F bond lengths were taken to be 1.08 Å and 1.35 Å, respectively [90, 91], while the -CH<sub>3</sub> geometries were taken from an optimized toluene structure [92]. For each molecule,  $V(r)$  was calculated at 1.75 Å above the molecular plane, since this is what a receptor would encounter; 1.75 Å is the van der Waals radius of chlorine [93], which is the largest atom found in these molecules.  $V(r)$  was also computed in the perpendicular plane through the oxygens to determine the effects of various degrees of substitution upon the negative potentials near the oxygens.



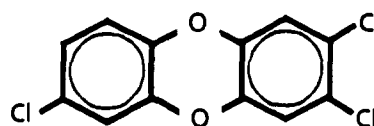
III



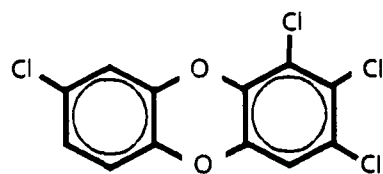
IV



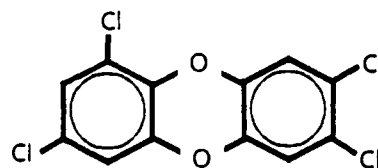
V



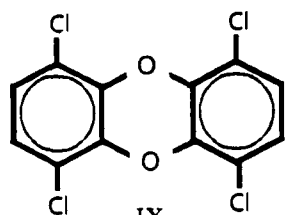
VI



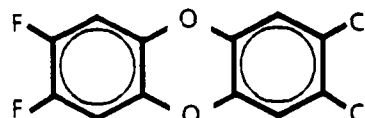
VII



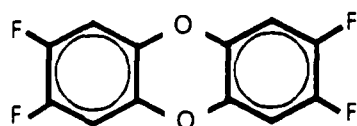
VIII



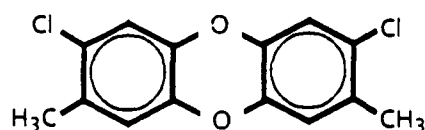
IX



X



XI



XII

#### ***Electrostatic potentials of dibenzo-*p*-dioxins as a criterion for toxicity***

Table 4 presents the most negative values (the local minima) of  $V(r)$  in the plane 1.75 Å above each of the molecules I through XII, as well as the minima near the oxygens, obtained from the perpendicular plots. (Figures showing the calculated electrostatic potentials of I, II, IV, and IX through XII are given by Murray et al. [87] and Murray and Politzer [88].)

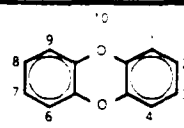
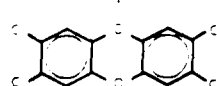
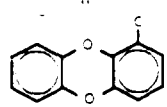
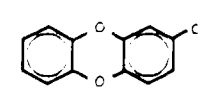
Only the parent, unsubstituted molecule (I) has negative regions above the aromatic rings; these can be interpreted as being due to the  $\pi$  electrons. Molecule I also has strong negative potentials near each oxygen, with minima above and below the molecular plane that can be attributed to its lone pairs; this is typical of what has been found for oxygens in other systems. (See Table 2 and Politzer and Laurence [57].) These potentials extend well beyond the plane 1.75 Å above the molecule.

It is notable that the electron-withdrawing effect of just one chlorine substituent suffices to eliminate the negative regions above the aromatic rings, even for the ring that does not bear the chlorine (see results for III and IV in Table 4). The introduction of chlorines also produces a significant weakening of the oxygen negative potentials; the  $V(r)$  minima go from -50.7 kcal/mole for the

unsubstituted system I to -28.9 kcal/mole for the tetrachloro derivative II. The spatial extents of these negative regions also decrease; thus, whereas they still extend beyond the 1.75 Å plane in the dichlorinated molecule (V), the substitution of a third chlorine, in VI, reduces their sizes to the point that no negative potentials remain at 1.75 Å (Table 4). (IX appears to be an exception to these trends; however, its anomalously strong oxygen potentials are due to the proximity of the chlorines and the consequent overlapping of the oxygen and chlorine negative regions.)

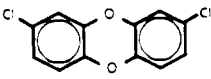
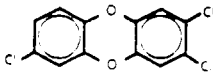
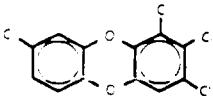
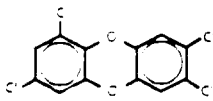
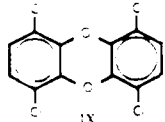
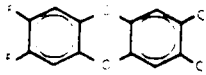
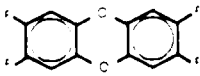
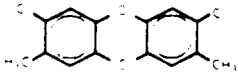
Table 4 shows that there are invariably negative potentials above the chlorine and fluorine substituents. These become weaker as the number of halogens increases, reflecting the fact that each is receiving a smaller share of the polarizable electronic charge. This is a phenomenon that we have observed in other systems in the past [22, 88]. The data in Table 4 again bring out the fact that chlorine is better able to accommodate additional electronic charge than is fluorine. This can be seen, for example, by comparing the results for II and XI. Even more striking is the observation that the chlorines in X are more negative than their counterparts in either II or VI, showing that they compete more successfully for the polarizable electronic charge against two fluorines than against even only one chlorine (as in VI).

TABLE 4. CALCULATED ELECTROSTATIC POTENTIAL MINIMA OF SOME DIBENZO-*p*-DIOXINS.

Molecule	$V(r)$ minima at 1.75 Å above molecular plane (kcal/mole)	$V(r)$ minima near oxygen, in perpendicular plane (kcal/mole)
 I	- 11.6 (O) <sup>a</sup> - 5.8 (aromatic rings) <sup>a</sup>	- 50.7 <sup>a</sup>
 II	- 12.9 (Cl) <sup>a</sup>	- 28.9 <sup>a</sup>
 III	- 20.5 (Cl) - 7.2 [O(5)]	- 50.4 [(O(10))] - 45.5 [O(5)]
 IV	- 18.6 (Cl) - 7.3 [O(10)] - 6.8 [O(5)]	- 45.5 [O(10)] - 44.0 [O(5)]

(continued)

TABLE 4. (continued).

Molecule	V(r) minima at 1.75 Å above molecular plane (kcal/mole)	V(r) minima near oxygens, in perpendicular plane (kcal/mole)
 V	- 16.4 (Cl) - 3.3 [O(10)] - 2.1 [O(5)]	- 39.4 [O(10)] - 38.7 [O(5)]
 VI	- 14.9 [Cl(2)] - 14.8 [Cl(3)] - 14.4 [Cl(7)]	- 34.2 [O(10)] - 35.5 [O(5)]
 VII	- 12.5 [Cl(1)] - 13.5 [Cl(2)] - 11.4 [Cl(3)] - 13.4 [Cl(8)]	- 34.6 [O(10)] - 29.6 [O(5)]
 VIII	- 13.7 [Cl(2)] - 13.3 [Cl(3)] - 10.5 [Cl(7)] - 11.3 [Cl(9)]	- 34.5 [O(10)] - 29.6 [O(5)]
 IX	- 14.8 (Cl)	- 40.1
 X	- 15.1 (Cl) - 3.2 (F)	- 34.7
 XI	- 5.3 (F) - 3.6 (O)	- 40.6
 XII	- 16.8 (Cl) - 5.2 [O(10)] - 3.4 [O(5)]	- 42.8 [O(10)] - 41.1 [O(5)]

Among the molecules that have been included in this study, I, III through V, IX, XI, and XII are biologically relatively inactive [71, 78]. Table 4 shows that it is also these molecules that have the strongest and most extensive negative potentials associated with the oxygens. We have accordingly suggested that biological activity on the part of the substituted dibenzo-*p*-dioxins may require that the negative potentials above the oxygens be considerably weaker than in the parent molecule, I [87, 88].

We have also pointed out that the presence of relatively strong negative potentials above most or all of the two lateral regions of the molecule (positions 2, 3 and 7, 8) appears to be linked to biological activity [87, 88]. Thus, molecules VI through VIII, all of which show some degree of activity [71, 78], have negative potentials of between -10 and -15 kcal/mole above one lateral region and half of the other (Table 4), while in the highly active TCDD (II), the potentials are in this range above all of both lateral regions. In contrast, most of the inactive or very weakly active molecules do not have even one lateral region that is completely negative; the exception is XI, but its lateral potentials are very weak.

On the other hand, it should not be inferred that the degree of biological activity necessarily becomes greater as the lateral regions become more negative. In II, VI, and VIII, activity increases [79, 85] as the lateral potentials become less negative. This suggests that there may be some intermediate range of values that correspond to a high level of activity.

In conclusion, our studies have focused attention upon the electrostatic potentials above the lateral regions and the oxygens of the substituted dibenzo-*p*-dioxins [87, 88]. Biological activity appears to require negative potentials above all or most of the lateral regions, with an apparent optimum range of magnitudes in the neighborhood of -13 kcal/mole (when computed with the STO-5G basis set). A second requirement seems to be a very significant weakening of the negative potentials associated with the oxygens.

#### ACKNOWLEDGMENTS

We express our appreciation to the U.S. Environmental Protection Agency for partial funding of this work under assistance agreement CR808866-01-0 and cooperative agreement CR-813013-01-0 to Peter Politzer. The contents do not necessarily reflect the views and policies of the Environmental Protection Agency, nor does mention of trade names or commercial products constitute endorsement or recommendation for use. We are also grateful for the financial support provided by the University of New Orleans Computer Research Center.

## REFERENCES

1. Scrocco, E. and Tomasi, J. (1978) Electronic molecular structure, reactivity and intermolecular forces: an euristic interpretation by means of electrostatic molecular potential. *Adv. Quantum Chem.* 11, 115-193.
2. Politzer, P. and Daiker, K.C. (1981) Models for chemical reactivity. In: B.M. Deb (Ed.), *The Force Concept in Chemistry*. Van Nostrand-Reinhold, New York, pp. 294-387.
3. Politzer, P. and Truhlar, D.G. (Eds.) (1981) *Chemical Applications of Atomic and Molecular Electrostatic Potentials*. Plenum Press, New York.
4. Politzer, P., Laurence, P.R. and Jayasuriya, K. (1985) Molecular electrostatic potentials: an effective tool for the elucidation of biochemical phenomena. *Environ. Health Persp.* 61, 191-202.
5. Environmental Protection Agency, Science Advisory Board. (1975) *Assessment of Health Risk From Organics in Drinking Water*, Washington, DC, April 30.
6. Keith, L.H., Garrison, A.W., Allen, F.R., Carter, M.H., Floyd, T.L., Pope, J.D. and Thurston, A.D., Jr. (1976) *Identification and Analysis of Organic Pollutants in Water*. Ann Arbor Science Publishers, Ann Arbor, Michigan, ch. 22.
7. Woo, Y.-T., Lai, D., Arcos, J.C. and Argus, M.F. (1984) *Chemical Induction of Cancer*. Vol IIIB. Academic Press, New York, sect. 5.2.2.1.
8. Viola, P.L., Biogotti, A. and Caputo, A. (1971) Oncogenic response of rat skin, lungs and bones to vinyl chloride. *Cancer Res.* 31, 516-522.
9. Maltoni, C. (1977) Recent findings on the carcinogenicity of chlorinated olefins. *Environ. Health Perspect.* 21, 1-5.
10. Waxweiler, R.J., Stringer, W., Wagoner, J.K., Jones, J., Falk, H. and Carter, C. (1976) Neoplastic risk among workers exposed to vinyl chloride. *Ann. N.Y. Acad. Sci.* 271, 40-48.
11. Rawls, R. (1980) Studies update vinyl chloride hazards. *Chem. Eng. News*. April 7, pp. 27-28.
12. International Agency for Research on Cancer (1976) *IARC Monographs on the Evaluation of Carcinogenic Risk of Chemicals*. Lyon, France, pp. 1-306.
13. Bartsch, H., Malaveille, C., Barbin, A. and Planche, G. (1979) Mutagenic and alkylating metabolites. *Arch. Toxicol.* 41, 249-279.
14. Bult, H.M., Laib, R.J. and Filser, J.G. (1982) Reactive metabolites and carcinogenicity of halogenated ethylenes. *Biochem. Pharmacol.* 31, 1-4.
15. Van Durren, B.L., Kline, S.A., Melchionne, S. and Seidman, I. (1983) Chemical structure and carcinogenicity relationships of some chloroalkene oxides and their parent olefins. *Cancer Res.* 43, 159-162.
16. Van Duuren, B.L. (1975) Possible mechanism of carcinogenic action of vinyl chloride. *Ann. N.Y. Acad. Sci.* 246, 258-267.

17. Rannug, U, Gothe, R. and Wachtmeister, C.A. (1976) The mutagenicity of chloroethylene oxide, chloro-acetaldehyde, 2-chloroethanol and chloroacetic acid, conceivable metabolites of vinyl chloride. *Chem-Biol. Interact.* 12, 251-263.
18. Leibman, D.C. and Ortiz, E. (1977) Metabolism of halogenated ethylenes. *Environ. Health Perspect.* 21, 91-97.
19. Osterman-Golkar, S., Hultmark, D., Segerback, D., Calleman, C.J. and Gothe, R. (1977) Alkylation of DNA and proteins in mice exposed to vinyl chloride. *Biochem. Biophys. Res. Commun.* 76, 259-266.
20. Banerjee, S. and Van Duuren, B.L. (1978) Covalent binding of carcinogen trichloroethylene to hepatic microsomal proteins and to exogenous DNA *in vitro*. *Cancer Res.* 38, 776-780.
21. Pudzianowski, A.T. and Loew, G.H. (1980) Quantum chemical studies of model cytochrome P-450 hydrocarbon oxidation mechanisms. 1. A MINDO/3 study of hydroxylation and epoxidation pathways for methene and ethylene. *J. Amer. Chem. Soc.* 102, 5443-5449.
22. Politzer, P. and Hedges, W.L. (1982) A study of the reactive properties of the chlorinated ethylenes. *Int. J. Quantum Chem. Quantum Biol. Symp.* 9, 307-309.
23. Williamson, D.G. and Cvetanovic, R.J. (1968) Rates of reactions of ozone with chlorinated and conjugated olefins. *J. Amer. Chem. Soc.* 90, 4248-4253.
24. Griesbaum, K., Kibar, R. and Pfeffer, B. (1975) Synthese und stabilität von 2,3-dichloroxiranen. *Liebigs Ann. Chem.* 214-224.
25. Bonse, G. and Henschler, D. (1976) Chemical reactivity, biotransformation, and toxicity of polychlorinated aliphatic compounds. *CRC Crit. Revs. Toxicol.* 395-409.
26. Ikeda, M. and Ohtsuji, H. (1972) Comparative study of the excretion of Fujiwara reaction-positive substances in urine of humans and rodents given trichloro- or tetrachloro-derivatives of ethane and ethylene. *Br. J. Ind. Med.* 29, 99-104.
27. Morrison, R.T. and Boyd, R.N. (1973) *Organic Chemistry*, 3rd Ed., Allyn and Bacon Pub, Boston.
28. Politzer, P., Daiker, K.C., Estes, V.M. and Baughman, M. (1978) Epoxide-nucleophile interactions: acid-catalyzed reaction of ethylene with water. *Int. J. Quantum Chem. Quantum Biol. Symp.* 5, 291-299.
29. Politzer, P. and Estes, V.M. (1979) The catalytic effect of hydrogen bonding upon epoxide ring opening. In: B. Pullman (Ed.), *Catalysis in Chemistry and Biochemistry. Theory and Experiment*. Reidel Pub, Dordrecht, Holland, pp. 305-321.
30. Ferrell, J.E., Jr. and Loew, G.H. (1979) Mechanistic studies of arene oxide and diol epoxide rearrangement and hydrolysis reactions. *J. Am. Chem. Soc.* 101, 1358-1368.
31. Politzer, P. and Proctor, T.R. (1982) Calculated properties of some possible vinyl chloride metabolites. *Int. J. Quantum Chem.* 22, 1271-1279.
32. Laurence, P.R. and Politzer, P. (1984) Some reactive properties of chlorooxirane, a likely carcinogenic metabolite of vinyl chloride. *Int. J. Quantum Chem.* 25, 493-503.

33. Laurence, P.R., Proctor, T.R. and Politzer, P. (1984) Reactive properties of *trans*-dichlorooxirane in relation to the contrasting carcinogenicities of vinyl chloride and *trans*-dichloroethylene. *Int. J. Quantum Chem.* 26, 425-438.
34. McLaren, A.D. (1960) Enzyme action in structurally restricted systems. *Enzymologia.* 21, 356-364.
35. Sols, A. and Marco, R. (1970) Concentrations of metabolites and binding sites. Implications in metabolic regulation. *Curr. Top. Cell. Reg.* 2, 227-273.
36. Welch, G.R. and Berry, M.N. (1983) Long-range energy continua in the living cell: protochemical considerations. *Coherent Excitations in Biological Systems.* Springer-Verlay Pub., New York, p. 95-116.
37. Depierre, J.W. and Ernster, L. (1977) Enzyme topology of intracellular membranes. *Annu. Rev. Biochem.* 46, 201-262.
38. Kell, D.B. (1979) On the functional proton current pathway of electron transport phosphorylation - an electronic view. *Biochim. Biophys. Acta.* 549, 55-99.
39. Guengerich, F.P. and Macdonald, T.L. (1984) Chemical mechanisms of catalysis by cytochromes P-450: a unified view. *Accts. Chem. Res.* 17, 9-16.
40. Whalen, D.L. and Ross, A.M. (1978) Stereoelectronic factors in the solvolysis of bay region diol epoxides of polycyclic aromatic hydrocarbons. *J. Am. Chem. Soc.* 100(16), 5218-5221.
41. Politzer, P., Daiker, K.C., Estes, V.M. and Baughman, M. (1979) The role of hydrogen bonding in some diol epoxides. *Int. J. Quantum Chem. Quantum Biol. Symp.* 6, 47-53.
42. Politzer, P. and Trefonas, P., III (1980) An analysis of the reactivities of epoxide rings in some cyclic hydrocarbons. In: B. Pullman, P.O.P. Ts'o and H. Gelboin (Eds.), *Carcinogenesis: Fundamental Mechanisms and Environmental Effects*, Dordrecht, Holland, D. Reidel Pub., pp. 67-79.
43. Harvey, R.G. (1981) Activated metabolites of carcinogenic hydrocarbons. *Acc. Chem. Res.* 14, 218-226.
44. Woo, Y.-T., Arcos, J.C. and Lai, D. (1985) *Handbook of Carcinogenic Testing.* Noyes Pub. Co., Park Ridge, New Jersey.
45. Jones, R.B. and Mackrodt, W.C. (1982) Structure-mutagenicity relationships for chlorinated ethylenes: a model based on the stability of the metabolically derived epoxides. *Biochem. Pharmacol.* 31(22), 3710-3712.
46. Jones, R.B. and Mackrodt, W.C. (1983) Structure-genotoxicity relationships for aliphatic epoxides. *Biochem. Pharmacol.* 32(15), 2359-2362.
47. Politzer, P., Laurence, P.R. and Jayasuriya, K. (1985) Halogenated olefins and their epoxides: factors underlying carcinogenic activity. In: R. Rein (Ed.), *Molecular Basis of Cancer, Part A: Macromolecular Structure, Carcinogens, and Oncogenes.* Alan R. Liss, Inc. Publ, New York, pp. 227-237.

48. Sherer, E., Van Der Laken, C.J., Gwinner, L.M., Laib, R.J. and Emmelot, P. (1981) Modification of deoxyguanosine by chloroethylene oxide. *Carcinogenesis* 2, 671-677.
49. Laib, R.J., Gwinner, L.M. and Bolt, H.M. (1981) DNA alkylation by vinyl chloride metabolites: ethenol derivatives of 7-alkylation of guanine. *Chem.-Biol. Interact.* 37, 219-231.
50. Zajdela, F., Croisy, A., Barbin, A., Malaveille, C., Tomatis, L. and Bartsch, H. (1980) Carcinogenicity of chloroethylene oxide, an ultimate reactive metabolite of vinyl chloride, and bis(chloromethyl)ether after subcutaneous administration and in initiation-promotion experiments in mice. *Cancer Res.* 40, 352-356.
51. Hathway, D.E. and Kolar, G.F. (1980) Mechanisms of reaction between ultimate chemical carcinogens and nucleic acid. *Chem. Soc. Revs.* 9, 241-264.
52. Barbin, A., Bartsch, H., Leconte, P. and Radman, M. (1981) Studies on the miscoding properties of 1,N<sup>6</sup>-ethenoadenine and 3, N<sup>4</sup>-ethenocytosine, DNA reaction products of vinyl chloride metabolites, during *in vitro* DNA synthesis. *Nucl. Acids Res.* 9, 375-387.
53. Spengler, S. and Singer, B. (1981) Transcriptional errors and ambiguity resulting from the presence of 1,N<sup>6</sup>-ethenoadenosine or 3-N<sup>4</sup>-etheno-cytidine in polyribonucleotides. *Nucl. Acids. Res.* 9, 365-373.
54. Politzer, P., Bar-Adon, R. and Zilles, B.A. (1986) The structure and properties of 7-(2-oxoethyl)-guanine: a model for a key DNA alkylation product of vinyl chloride. In: B. Singer and H. Bartsch (Eds.), *The Role of Cyclic Nucleic Acid Adducts in Carcinogenesis and Mutagenesis*, International Agency for Research on Cancer Scientific Publication, Lyon, France, pp. 37-43.
55. Pople, J.A. (1977) *Applications of Electronic Structure Theory*. Vol. 4, Plenum Press, New York, ch. 1.
56. Politzer, P. and Laurence, P.R. (1984) Relationships between the electrostatic potential, epoxide hydase inhibition and carcinogenicity for some hydrocarbon and halogenated hydrocarbon epoxides. *Carcinogenesis* 5(6), 845-848.
57. Politzer, P. and Laurence, P.R. (1984) Halogenated hydrocarbon epoxides: factors underlying biological activity. *Int. J. Quantum Chem. Quantum Biol. Symp.* 11, 155-166.
58. Politzer, P. (1969) Anomalous properties of fluorine. *J. Am. Chem. Soc.* 91, 6235-6237.
59. Politzer, P. and Timberlake, J.W. (1972) Anomalous properties of halogen substituents. *J. Org. Chem.* 37, 3557-3559.
60. Huheey, J.E. (1965) The electronegativity of groups. *J. Phys. Chem.* 69, 3284-3291.
61. Evans, R.S. and Huheey, J.E. (1973) The meaning and definition of "charge" in molecules. *Chem. Phys. Lett.* 19, 114-116.
62. Politzer, P. (1977) Physical aspects of main-group homonuclear bonding. In: *Homoatomic Rings, Chains, and Macromolecules of Main-Group Elements*, Elsevier Scientific Pub., Amsterdam, ch. 4.
63. Lowry, T.H. and Richardson, K.S. (1981) *Mechanism and Theory in Organic Chemistry*, 2nd Ed., Harper & Row, New York, sect. 2.2

64. Oesch, F., Kaubisch, N., Jerina, D.M. and Daly, J.W. (1971) Hepatic epoxide hydrase structure-activity relationships for substrates and inhibitors. *Biochem.* 10, 4858-4866.
65. Oesch, F. (1974) Purification and specificity of a hman microsomal epoxide hydratase. *Biochem. J.* 139, 77-88.
66. Hanzlik, R.P. and Walsh, J.S.A. (1980) Halogenated epoxides and related compounds in inhibitors of epoxide hydrase. *Arch. Biochem. Biophys.* 204, 255-263.
67. Taft, R.W., Jr. (1956). *Steric Effects in Organic Chemistry*. Wiley Pub., New York, Pub. 556, p. 556..
68. Unger, S.H. and Hansch, C. (1976) Quantitative models for steric effects. *Prog. Phys. Org. Chem.* 12, 91-118.
69. Politzer, P. and Murray, J.S. (1987) Halogenated hydrocarbon epoxides: some predictive methods for carcinogenic activity based on electronic mechanisms. *Molecular Toxicology* 1, 1-15.
70. Windholz, M. (Ed.) (1983) *The Merck Index*, 10th Ed., Merck & Co., Rathway, NJ, #8957.
71. Poland, A. and Knutson, J.C. (1982) 2,3,7,8-tetrachlorodibenzo-*p*-dioxin and related halogenated aromatic hydrocarbons: examination of the mechanism of toxicity. *Ann. Rev. Pharmacol. Toxicol.* 22, 517-554.
72. Kociba, R.J., Keyes, D.G., Beyer, J.E., Carreon, R.M., Wade, C.E., Henber, D.A., Kalnins, R.P., Frauson, L.E., Park, C.N., Barnard, S.D., Hummel, R.A. and Humiston, C.G. (1978) Results of a two-year chronic toxicity and oncogenicity study of 2,3,7,8-tetrachlorodibenzo-*p*-dioxin in rats. *Toxicol. Appl. Pharmacol.* 46, 279-303.
73. Holmes, P.A., Rust, J.H., Richter, W.R. and Shefner, A.M. (1978) Conference on Health Effects of Halogenated Aromatic Hydrocarbons. New York Acad. Sci.
74. Pitot, H.C., Goldsworthy, T., Campbell, H.A. and Poland, A. (1980) Quantitative evaluation of the promotion by 2,3,7,8-tetrachlorodibenzo-*p*-dioxin of hepatocarcinogenesis from diethylnitrosamine. *Cancer Res.* 40, 3616-3620.
75. National Cancer Institute Carcinogenesis Technical report. (1980) Ser. 198 and 212, NTP 80-12, 80-13, Washington, DC.
76. National Cancer Institute Carcinogenesis Technical Report. (1979) Ser. 123, Washington, DC.
77. National Cancer Institute Carcinogenesis Technical Report. (1977) Ser. 122, Washington, DC.
78. Poland, A. and Glover, E. (1973) Chlorinated dibenzo-*p*-dioxins. Potent inducers of 8-aminolevulinic acid synthetase and aryl hydrocarbon hydroxylase. II. Structure-activity relation. *Mol. Pharmacol.* 9, 736-747.
79. Kende, A.S., Wade, J.J., Ridge, D. and Poland, A. (1974) Synthesis and transform carbon-13 nuclear magnetic resonance spectroscopy of new toxic polyhalodibenzo-*p*-dioxins. *J. Org. Chem.* 39, 931-937.

80. McKinney, J.D., Chae, K., Gupta, B.N., Moore, J.A. and Goldstein, J.A. (1976) Toxicological assessment of hexachlorobiphenyl isomers and 2,3,7,8-tetrachloro-dibenzofuran in chicks. 1. Relationship of chemical parameters. *Toxicol. Appl. Pharmacol.* 36, 65-80.
81. Moore, J.A., McConnell, E.E., Dalgard, D.W. and Harris, M.W. (1979) Comparative toxicity of three halogenated dibenzofurans in guinea pigs, mice, and rhesus monkeys. *Ann. N.Y. Acad. Sci.* 320, 151-163.
82. Knutson, J. and Poland, A. (1981) *Halogenated Hydrocarbons*. Pergamon Press, New York, p. 187.
83. Poland, A., Greenlee, W.F. and Kende, A.S. (1979) Studies on the mechanism of action of the chlorinated dibenzo-*p*-dioxins and related compounds. *Ann. N.Y. Acad. Sci.* 320, 214-230.
84. Goldstein, J.A. (1980) *Halogenated Biphenyls, Terphenyls, Naphthalenes, Dibenzodioxins and Related Products*. Elsevier, New York, pp. 151-190.
85. Cheney, B.V. and Tolly, T. (1979) Electronic factors affecting receptor binding of dibenzo-*p*-dioxins and dibenzofurans. *Int. J. Quantum Chem.* 16, 87-110.
86. Cheney, B.V. (1982) Structural factors affecting aryl hydrocarbon hydroxylase induction by dibenzo-*p*-dioxins and dibenzofurans. *Int. J. Quantum Chem.* 21, 445-463.
87. Murray, J.S., Zilles, B.A., Jayasuriya, K. and Politzer, P. (1986) Comparative analysis of the electrostatic potentials of dibenzofuran and some dibenzo-*p*-dioxins. *J. Am. Chem. Soc.* 108, 915-918.
88. Murray, J.S. and Politzer, P. (1987) Electrostatic potentials of some dibenzo-*p*-dioxins in relation to their biological activities. *Theoret. Chim. Acta.* 72, 507-517.
89. Boer, F.P., Remoortere, F.P., North, P.P. and Newman, M.A. (1972) The crystal and molecular structure of 2,3,7,8-tetrachlorodibenzo-*p*-dioxin. *Acta Cryst.* B28, 1023-1029.
90. Huheey, J.E. (1972) *Inorganic Chemistry*. Harper & Row, New York, p. 699.
91. Harmony, M.D., Laurie, V.W., Kuczkowski, R.L., Schwendeman, R.H., Ramsay, D.A., Lovas, F.J., Lafferty, W.J. and Maki, A.G. (1979) Molecular structures of gas-phase polyatomic molecules determined by spectroscopic methods. *J. Phys. Chem. Ref. Data.* 8, 619-721.
92. Politzer, P., Jayasuriya, K., Sjöberg, P. and Laurence, P.R. (1985) Properties of some intermediate stages in the nitration of benzene and toluene. *J. Am. Chem. Soc.* 107, 1174-1177.
93. Bondi, A. (1964) Van der Waals volumes and radii. *J. Physical Chem.* 68, 441-451.

## QSAR APPROACHES TO PREDICTING TOXICITY

William J. Dunn, III

*Department of Medicinal Chemistry and Pharmacognosy, University of Illinois at Chicago,  
833 S. Wood, Chicago, IL*

### SUMMARY

Due to the demands of time and the high cost of testing compounds for toxicity in test animals, it would be an advantage to be able to estimate the toxic response of chemical agents using theoretical approaches. Predicting whether a compound will be toxic or nontoxic is a classification problem and the methods of studying quantitative structure activity relationships (QSAR) can be used for this purpose [Hansch, C. (1969) *Accounts of Chem. Res.*, 2, 232]. It should be recognized, however, that formulating the QSAR problem as one of active vs. inactive makes it different from classical QSAR problems. This requires that methods be applied that can predict the category of a compound to be used, i.e., so-called methods of pattern recognition [Varmuza 1983] being required. There are several methods of pattern recognition that can be used with some being more suitable than others. The nature of this unique QSAR problem, the appropriate methods to apply, and some of the pitfalls of applying QSAR techniques to predicting toxicity are discussed.

### INTRODUCTION

Classification problems are common in chemistry and pharmacology. An integral part of the training of chemists and pharmacologists is experience in recognizing spectral patterns and relating them to chemical structure. Pharmacologists are trained to recognize certain response patterns that result when an organism is stimulated with organic compounds and to correlate these patterns with a type of biological activity. A logical extension of these classification exercises is that of associating a chemical structure with a type of biological activity. It is straightforward for a trained pharmacologist to examine the two-dimensional structure of a compound and estimate whether it will stimulate or block the response of an important receptor. QSAR approaches to predicting toxicity involve making this a quantitative estimation in the sense that the prediction will have a statistical basis.

### MATERIALS AND METHODS

#### *Pattern Recognition*

As discussed above, pattern recognition is a retrospective technique in the sense that its application requires that prior knowledge of the activity or response of substances similar to the unknown be available. This knowledge is used in a quantitative way to classify the unknown into one

of the known classes. The quantitative rules used in the classification process are mathematical models derived from information in the chemical structures of the compounds.

Any user or potential user of pattern recognition methods should be aware of the levels of information that can be extracted from a classification analysis. These have been discussed as the four levels of pattern recognition [1]. The first, or lowest, level of information that can be obtained is whether a compound is a member of one of the defined classes. This assumes that it is known in advance that an unknown must be a member of one of the known groups. At the next level, or level 2, it is possible to classify a compound into one of several defined classes with the additional information that it is none of the defined classes. This allowed result is increased information of level 1. At level 3, an unknown is classified into one of the defined classes and a level of activity (very active, moderately active, or weakly active) is estimated. In analytical chemistry the analogous problem is classification and calibration. Level 4 is an extension of level 3 in that several types of activity are known for the training compounds and this is used to estimate several levels of activity for an unknown in a post classification step. For the problem of using QSAR as a method for estimating toxicity, this is the desired level of pattern recognition.

All methods of pattern recognition begin with a data table as shown in Figure 1. The compounds in Figure 1 are those of known pharmacological response, i.e., active vs. inactive, agonist vs. antagonist, substrate vs. inhibitor, etc. These compounds are the defined classes or training sets. Those of unknown response are the test compounds.

Compound	Biological Activity					Chemical Descriptors							
	1	2	.	j	.	m	1	2	3	.	.	i	.
1													Class 1
2													
3													
.													Class 2
.													
k													
.													Test set
n													

Figure 1. Data table for a classification problem.

Here, there are  $p$  chemical variables for  $n$  compounds. The compound index is  $k$  and the variable index is  $i$ . The elements ( $X_{ki}$ ) of the data table or matrix are chemical structure descriptors, or variables, which are in some way relevant to the classification problem. The objective of pattern recognition methods is to derive models or classification rules from the chemical data that will classify the unknown or test compounds.

The classification rules are derived in the following way. An orthogonal coordinate system is defined with the axes of the system being that of the chemical descriptors. This is called the descriptor or pattern space. The data for the training compounds are projected into the pattern space with the result that each compound is represented by a point. In the ideal case, the classes will cluster in different regions of descriptor space. This is shown for two classes in Figure 2. Here, pattern space is three-dimensional for illustrative convenience. In most cases, more than three variables are necessary for resolution of class structure due to the complexity, or multivariate nature, of QSAR problems in general.

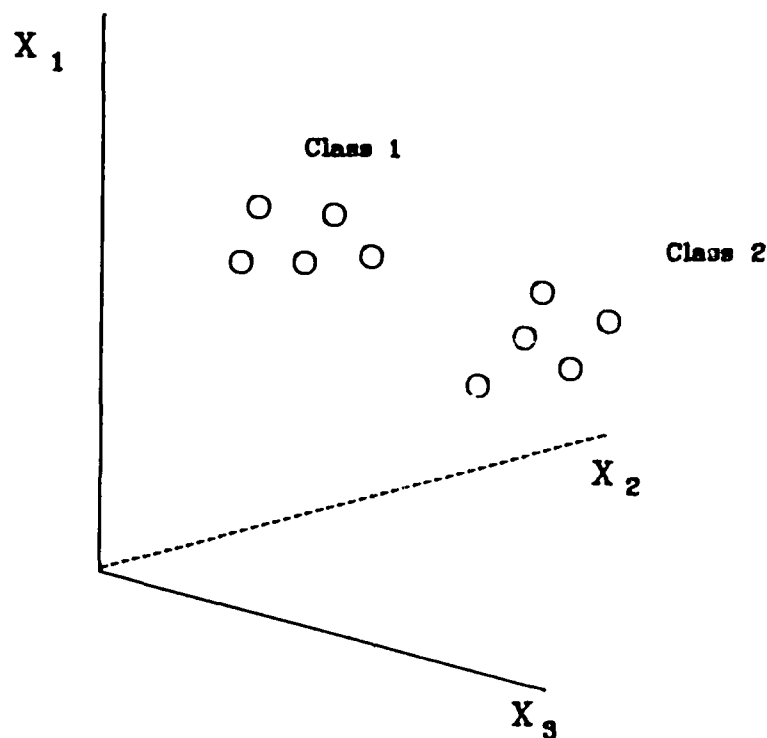


Figure 2. The projection of two classes into pattern space.

In the next step of a classification study, it is necessary to define the regions of pattern space where the training classes cluster. This is done in different ways depending on the method of classification used. The methods are basically of three different types: (1) hyperplane methods, (2) distance methods, and (3) class modeling methods.

The hyperplane methods derive the equation of a line, plane, or hyperplane that will separate the pattern space into regions where the two classes will have the greatest probability to be found. This is called a discrimination function and it is the basis of linear discriminant analysis and the linear learning machine. This is illustrated in Figure 3 in which the classes are separated by a line.

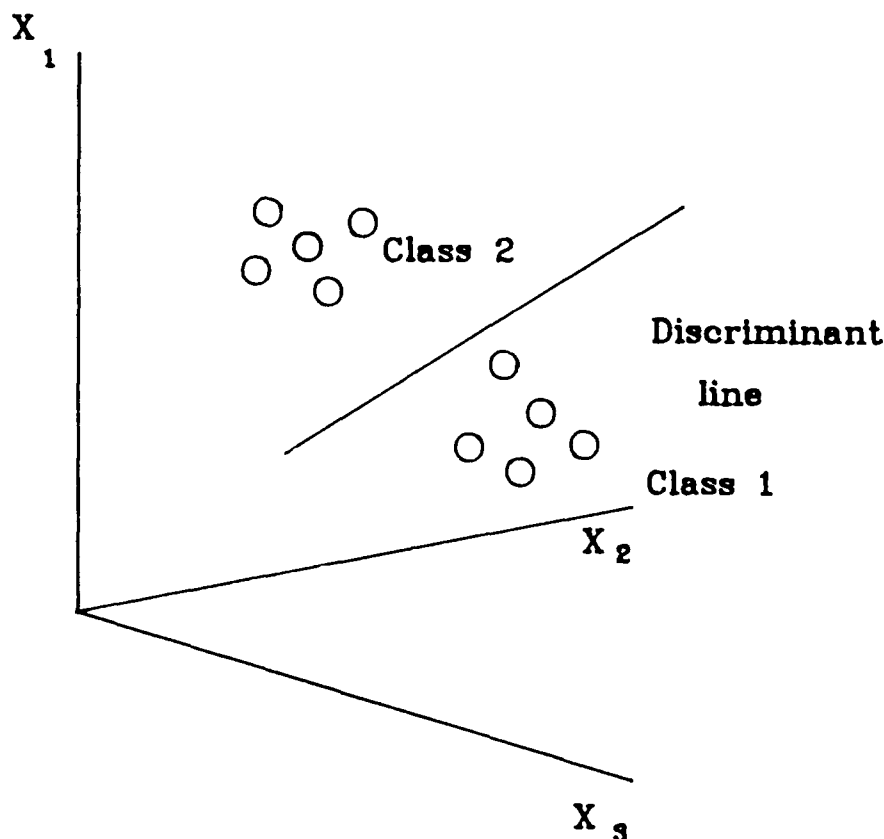


Figure 3. The separation of two classes by a discriminant line.

One limitation of this method is that it is sensitive to the number of descriptors,  $p$ , relative to the number of compounds,  $n$ , in a class. The  $n/p$  ratio should be as large as possible in order for the discriminant function to be highly stable numerically. A ratio of 5/1 is an acceptable minimum for these techniques. Another limitation is that it must be known in advance that the unknowns are members of one of the defined classes. This means that these methods operate at level 1 because any compound will be on one side or the other of the discriminant line or plane. Seldom in QSAR work is this condition satisfied. Generally, these and other limitations make hyperplane methods of very limited use in QSAR work, especially for predicting toxicity. This point will be addressed later.

Distance methods classify compounds on the basis of their Euclidean distance to those of known class assignment. This is the basis of the  $k$ -Nearest Neighbor [2] method, or  $k$ -NN, where  $k$  is the number of nearest neighbors selected by the analyst. Usually  $k$  is a small odd number. The  $k$ -NN

method is illustrated in Figure 4 where the class structure is determined by each compound's three nearest neighbors. The k-NN method has the advantage of operating at level 2.

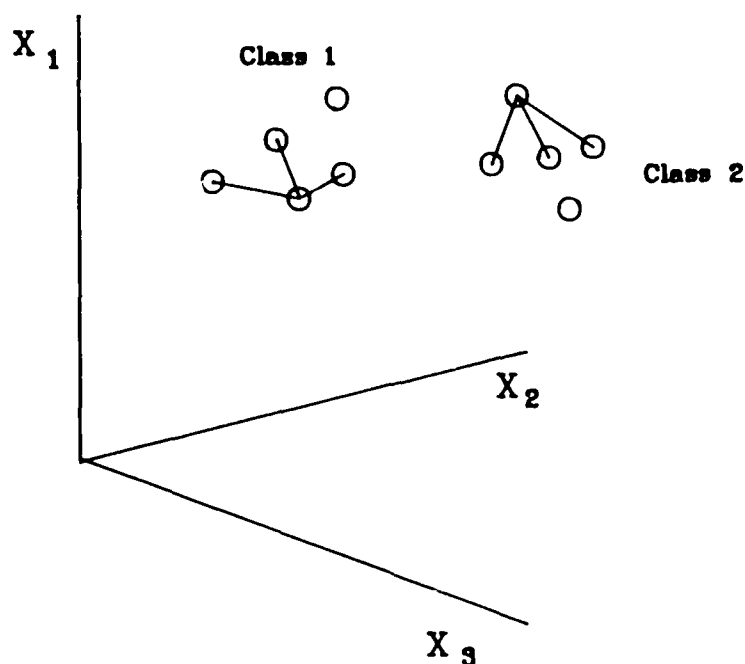


Figure 4. k-NN identification of class structure.

Class modeling methods are the method of choice for QSAR studies. An example of this group of techniques is the SIMCA method [1,2,3] of pattern recognition. This is the method of choice for QSAR studies as it operates at level 4 as discussed above. This method models the variation in the chemical data for a class of compounds with principal components models. A geometric interpretation of this approach is shown in Figure 5 in which the variation in the data for one of the classes is approximated by a plane, or a two-component principal components model. A residual standard deviation above and below the plane can be obtained from the fit of the training set data to the models. This defines a volume in pattern space where members of a class have the most probable position. Unknown compounds are classified into one of the defined classes or the unknowns may be outside of the defined classes.

Since compounds of similar type of activity cluster into regions of pattern space, it is logical to expect compounds of similar level of activity to cluster inside of class. Therefore, a compound's position in the class cluster may be used to estimate its level of activity. This is the basis for SIMCA operating at level 4. It is the only method that can give this type of information, thus making it desirable for QSAR approaches to predicting toxicity.

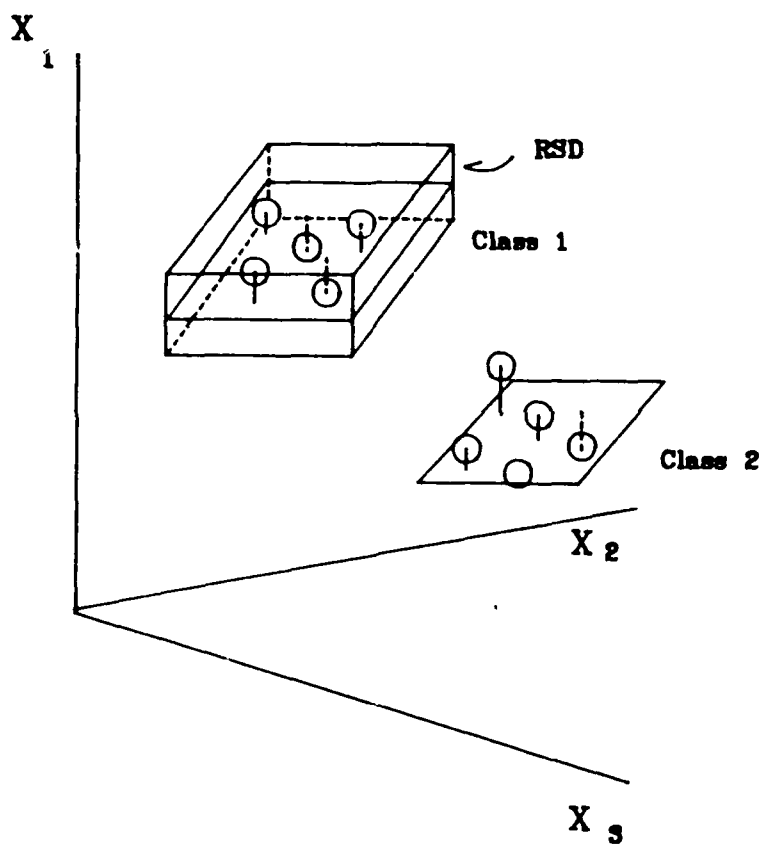


Figure 5. SIMCA representation of two classes.

#### ***The toxic vs. nontoxic classification problem***

The problem of predicting whether a compound is toxic or nontoxic is a unique classification problem. This is due to the type of data structure that can be observed in classification studies. In Figure 2, the two classes are shown to cluster into well-defined data swarms in different regions of descriptor space. This is referred to as symmetric data structure [4]. This is due to the underlying assumption that the members of each class are chemically and pharmacologically similar. This implies that they can in some way be described as chemically similar and elicit their response by the same mechanism of action.

Can this assumption generally be made in the case where the training sets are toxic and nontoxic compounds? The answer is probably not. This is due to the fact that the toxic class of compounds represents a well-defined class and the nontoxic compounds are nonmembers of the toxic class. Figure 6 illustrates this geometrically and is an example of what we term asymmetric data structure [4]. This is to say that the physicochemical requirements for class membership are rather rigid. If these limits are exceeded, the structure activity relationship for the active class breaks down and nonactivity results. This is equivalent to moving away from the active class in any direction in

Figure 6 to give nonactive compounds that are not a chemically or pharmacologically homogenous class.

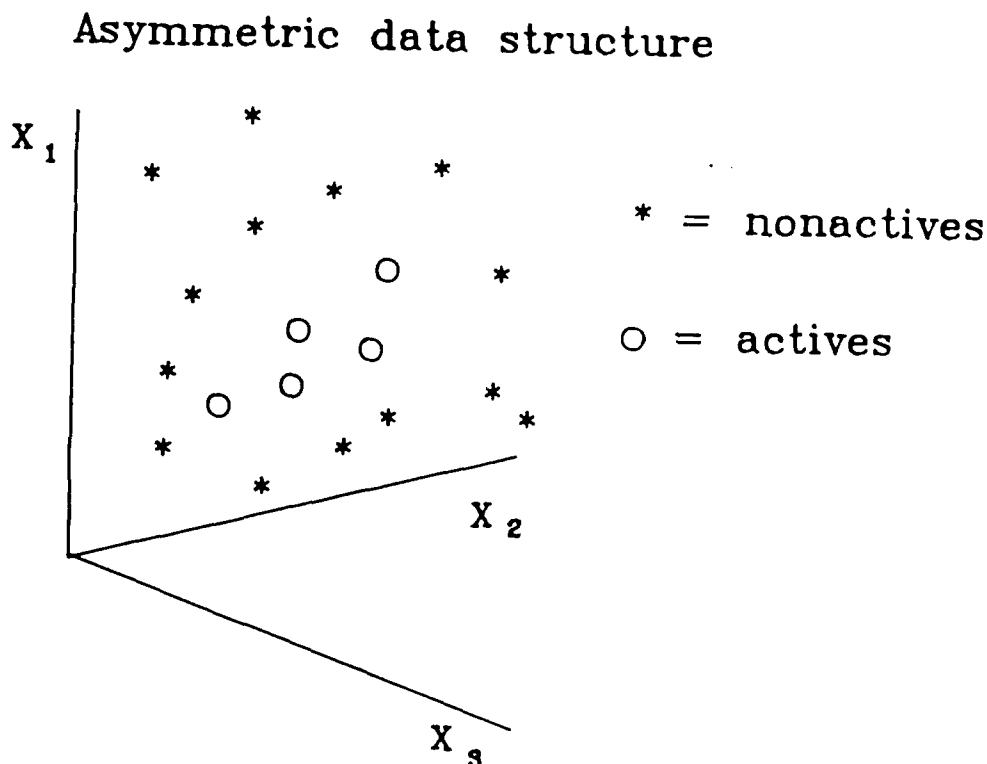


Figure 6. Asymmetric data structure in which the active compounds form a well-defined cluster and the nonactive class members are randomly scattered around this class.

The effect of this in classification studies is that a general class model for nonactivity, or nontoxicity, cannot be derived. A classification result in which the unknown is a nonmember of the active class does not lead to the result that the compound is nonactive, but rather is a nonmember of the active class. In this case, the unknown could be a member of a class of unobserved toxic agents. This result has been observed in several cases [4].

## RESULTS

Pattern recognition methods have been applied to the problem of predicting toxicity with mixed success [5]. The above discussion of symmetric and asymmetric data structure gives a clue as to the reasons for mixed success and leads to the conclusion that in order to get optimal results the method should be sensitive to the problem of asymmetric data structure. Reference to Figure 3 shows that the class discrimination methods cannot lead to a reliable classification result in such cases. A method that operates at least at level 2 is required and the k-NN neighbor will operate at this level

and could give reliable results. However, the SIMCA method is the one of choice since it is the only method operating at level 4.

The most important factor in obtaining reliable classification results lies in the nature of the training data, however, and this issue has only recently been addressed. In order to obtain highly predictable models for classification, the training set data must result from some systematic experimental design. The training sets must be representative of the chemical classes of compounds for which toxicity models are to be developed and must span as broad a chemical and pharmacological spectrum as possible. If they are not to be tested on the systems on which their ultimate toxicity is to be manifest, they should then be tested in model systems that mimic as closely as possible the biological systems on which toxic response estimates are to be made. This will reduce the uncertainty in extrapolations that must be made. There must be a departure from the random selection of compounds for testing that presently exists in order for generally reliable predictions to be made.

#### REFERENCES

- 1 Albano, A., Dunn, W.J., III, Edlund, U., Johansson, E., Norden, R., Sjöström, M., and Wold, S. (1978) Four levels of pattern recognition. *Anal. Chim. Acta Comput. Techn. Optim.*, 2, 429
- 2 Varmuza, K. (1983) *Pattern Recognition in Chemistry*, Springer Verlag, Berlin, 1980; Wold S and Dunn, W. J. III, *J. Chem. Info. Comp. Sci.*, 23, 6.
- 3 Dunn, W. J., III, and Wold, S. (1980) Structure-activity analyzed by pattern recognition. *J. Med. Chem.*, 23, 595.
- 4 Dunn, W. J., III, and Wold, S. (In Press) *Comprehensive Medicinal Chemistry*, Pergamon Press, Oxford England, Vol. 4, Chapter 19.2.

**SESSION V**

**QUANTITATIVE METHODS FOR BEHAVIORAL TOXICOLOGY**

**Major James R. Cooper, Chairman**

## QUANTITATIVE PERSPECTIVES ON BEHAVIORAL TOXICOLOGY

Bernard Weiss

*Department of Biophysics and Environmental Health Sciences Center, University of Rochester Medical Center, Rochester, NY*

### SUMMARY

Behavioral endpoints offer special challenges to toxicology. One arises from the sometimes conflicting ways in which adverse effects may be expressed. For example, both increases and decreases in response rates of schedule-controlled performance may be produced by a specific agent, depending on the specific schedule. Interpretations of such an outcome depend upon a close analysis of the experimental circumstances and the behavioral findings. Another arises from the many disparate variables that can influence a particular outcome. Accurate measures of sensory thresholds, for instance, depend upon precise means for delivering stimuli and upon appropriate psychophysical procedures. Such examples emphasize that quantification in behavioral toxicology is more than a matter of attaching numbers to some arbitrarily selected measure. Instead, meaningful quantification first requires that the investigator understand in principle the sources of the measures to which the numbers are being attached. This is especially critical when the measures are being used not for the relatively straightforward purpose of hazard identification, but for the more subtle aim of risk assessment and dose-response (effect) extrapolation. For these aims, behavioral microanalyses, based on the coordination of multiple measures in individual subjects, usually provide the most robust guides.

### INTRODUCTION

Toxicology is beginning to emerge as a quantitative science, but its roots remain firmly embedded in pathology, a mostly descriptive, qualitative discipline. By tradition, toxicity was defined by tissue damage or by death. Even the LD<sub>50</sub>, that most venerable measure of lethal potency, is basically more qualitative than quantitative because it offers few specific guides to modes or mechanisms of death.

A conspicuous force impelling toxicology toward more advanced quantification is risk assessment. Many scientists view this activity with skepticism, largely because it often presses extrapolation uncomfortably beyond the tangible data, while others approach it with extreme caution. Its influence, however, is a healthy counterpoise to certain traditional practices in toxicology (e.g., its reliance on pathology as an endpoint). One product of the new agenda is exploration of alternative approaches to the design of experiments and the analysis of experimental data [1] in ways that foster enhanced precision in the measurement of responses at low dose levels.

And, in a manner not expected from its statistical origins, risk assessment also has incited questioning about the biological, rather than statistical, significance of research findings. For example, a growing emphasis on pharmacokinetics is one outcome of the debates about the adequacy of various carcinogenic risk estimates and models based on rodent experiments [2]. Behavioral toxicology is another beneficiary of such questioning because it has prompted debates about the contribution and relevance of different approaches.

Quantification, however, can be a deceptive term. Most articles published in the major professional journals present some variant of statistical analysis, typically in the form of asserting the probability of differences between control and treated groups or between control and specified dose levels. Does that make a study inherently quantitative? Some of us would argue against such an assumption; data of low reproducibility, sensitivity, or precision are not useful guides either to mechanisms or to protective measures. Nor are data of dubious validity; that is, data that fail to reflect the state, action, or process asserted to be under study in a particular experiment.

Process is a key word in how we apply quantification in toxicology, and behavior may be the best archetype. Two features of behavior are especially pertinent. First, for many of the substances that arouse questions about neurotoxicity, the onset is frequently progressive, first detectable only as subtle behavioral impairment that later assumes more visible and severe manifestations. One of the earliest indications of methylmercury toxicity is paresthesia, a subjective complaint that almost never is quantified, and which is succeeded by increasingly devastating signs of nervous system damage.

Second, because of their noninvasive nature, behavioral measurements facilitate continuous monitoring of the progression of toxicity and, under appropriate conditions, recovery of function. Reversibility of impairment, and the ability to specify the exposure conditions under which it remains possible, is a critical public health consideration. By some definitions, reversible changes in function do not pose significant problems in health protection. For example, acute low-level ozone exposure, at levels that interfere with function but that produce no currently detectable lung damage, would be considered a minor health hazard. If this is a doubtful model for the lung, it deserves even more skepticism when applied to behavior. Allegedly reversible changes in function often appear on a substrate of pathology. Clinically, for example, patients may seem to recover from strokes despite the verified presence of lesions. On an experimental level, a substantial body of research shows that staged lesions, defined as lesions cumulated in small increments, usually result in much less behavioral disruption than a lesion of equivalent size produced all at once [3]. For this reason, repeated episodes of presumed reversible toxicity may actually be correlated with a gradually enlarging lesion that, for behaviors other than that under test, could prove critical. Monkeys exposed twice to courses of

acrylamide showed no permanent impairment of somatosensory acuity but, at sacrifice, revealed extensive damage to the visual system [4].

To exploit the advantages of behavioral measures and their relationships to other endpoints, experimenters should adopt approaches different from those prevailing in some other aspects of toxicology and even different from some of the approaches currently preferred by many investigators of behavioral toxicity. It may mean devising experiments in which toxicity is traced individually in the experimental populations rather than across groups. Even for circumstances in which the primary concern is lodged in acute effects, as would be the anesthetic actions of volatile solvents, progression is a salient feature. Gross ataxia is a clear consequence of excessive acute exposure, but blunted judgment and impaired speed of reactions appear at lower exposures and could represent a greater threat to workplace safety simply because steps to intervene would be delayed.

### ***Sources of concern***

One of the prods to the growth of behavioral toxicology is the array of chemicals linked to nervous system toxicity. Anger and Johnson [5] estimated that 25% of commercial and industrial chemicals may influence nervous system status. Of the nearly 13,000 chemicals produced in excess of one million pounds annually, about 10,000 lack adequate information about toxicity. If the figure given by Anger and Johnson accurately classifies these agents, then about 2,500 widely used chemicals may induce behavioral and neurological changes. The problems with volatile organic solvents, discussed above, illustrate one facet of these concerns. Short Term Exposure Limits (STELs), specified by the American Conference of Governmental Industrial Hygienists (ACGIH), deal explicitly with such possibilities. Concentrations that may "impair self-rescue" or "increase accident proneness" refer to behavioral consequences. Moreover, arguments for a syndrome induced by chronic organic solvent exposure have been advanced by Scandinavian investigators whose evidence is based primarily on psychological test results [6].

Most insecticides act by interfering with neurotransmitter function in the target organisms, and, because mammalian nervous systems use corresponding neurotransmitters, they also pose an immediate threat to humans exposed acutely. Some, however, may reveal their toxicity only after a prolonged latency. Organophosphorous-induced delayed neuropathy (OPIDN; [7]) is a syndrome actually recognized since 1930, when it disabled thousands of victims, mostly in the southern United States. The Environmental Protection Agency has proposed specific tests for organophosphorous insecticide neurotoxicity as part of a more general scheme to screen potential neurotoxicants.

Many metals are toxic to nervous system tissue. Both elemental mercury and certain organic mercurials produce distinctive neurotoxic syndromes. Methylmercury, shown to be far more dangerous to the fetus than the adult in epidemics of poisoning [8], is now under investigation as a

developmental neurotoxicant in populations that consume substantial quantities of fish that contain methylmercury. But, instead of relying on clinical criteria such as cases of cerebral palsy or mental retardation as evidence of risk, these newer studies use psychological tests aimed at much lower exposure levels that produce no visible signs of adverse effects. Excessive manganese exposure induces a syndrome comprising both behavioral and neurological disorders ranging in severity from gross dystonias to subtle impairment of performance on psychological tests of coordination and memory [9]. And the elimination of lead from gasoline is based primarily on its reduction of psychological test scores [10]. In fact, the most recent data, from a surprising range of populations, indicate that exposure levels believed only a short time ago to exact no excess risk pose unacceptable hazards (e.g., Bellinger et al. [11]) as defined by small, but socially significant reductions in measures of intellectual development.

Other agents, not part of any toxicologically circumscribed groups, have also aroused questions about behavioral toxicity. Carbon monoxide clearly impairs nervous system function at high concentrations, and, for that reason, has been investigated for more subtle effects at lower concentrations, such as those prevailing in heavy vehicle traffic. Certain food additives, such as food dyes, are implicated in adverse behavioral responses in children [12]. Parkinsonism is currently speculated to arise from an as yet unidentified environmental agent, a speculation prompted by the recent outbreak of that disorder among drug abusers who injected themselves with illicit drugs containing the agent, 1-methyl-4-phenyl-1,2,3,6-tetrahydropyridine [13].

With so many classes of substances posing neurotoxic hazards, both the scientific and regulatory implications of human exposure require exploration. But science and regulation are not disparate issues, of course. The higher the quality of the underlying science, the firmer the logic of the corresponding regulatory decisions. This principle is universally accepted, but its translation into practice is highly variable.

### ***Choice of endpoint***

Like other kinds of endpoints, behavioral responses are seen to fulfill two roles in the risk assessment process. The first of these, hazard identification, offers few difficulties because it is the first phase of the risk assessment process. Detection of nervous system activity can be accomplished in many different ways, ranging from simple observational techniques, to instrumented measures of activity and coordination, to neuropathology. Beyond this phase lies the much more difficult task of establishing dose-response (or dose-effect) relationships with endpoints more suitable for extrapolation to exposure levels typical of the natural environment.

Although behavioral toxicology seems now to be reaching beyond the elementary stages of identification and to be investing more of its resources in questions such as similarities and

differences between neurotoxic agents that require multiple measures and endpoints, even this phase of the discipline's development is inadequate for risk assessment. For those purposes, the science needs to apply tools sensitive to the early phases of most neurotoxic processes. Otherwise, crucial decisions will tend to be encumbered by huge uncertainties coupled with either inflated or insufficient risk estimates.

In some quarters, subjective complaints and slight reductions in performance are trivial endpoints, and incipient toxicity is too vague an attribute to engage the serious attention of toxicologists. In certain settings, however, the implications of such effects are overwhelming. At this workshop, we heard of a simulated space shuttle mission during which failure of the crew to carry out a critical step of a response sequence was attributed to headaches and poor sleep. These symptoms were traced to a programmed contaminant leak. What might have been the consequences of such incipient dysfunction during an actual mission? What is the significance of a 10% rise in reaction time in a fighter pilot? Or a slight distortion of judgment on the part of naval officer exposed to a low concentration of neurotoxic fumes from a fire?

Once a decision is taken to undertake the advanced phases of risk assessment, the question becomes, what to measure. Behavior science is a rigorous, highly quantitative discipline. Some of its roots lie in psychophysics, while some derive from psychometrics, or the methodology of psychological testing. Psychologists were among the first life scientists to adopt computers as research tools [14]. With that kind of history, it was natural for behavior scientists to bring special quantitative perspectives to toxicology.

Advancing behavioral science in its own context calls on one set of specialized skills. Selecting appropriate endpoints for toxicological evaluation is another matter. Behavior is so extraordinarily multifaceted that an investigator can choose from an almost unlimited variety of possibilities in pursuing a particular question. Such a selection is narrowed considerably, however, once the investigator examines the nature of the agent(s) to be studied. It is further narrowed by focusing on endpoints that are important functionally, whose principles are understood, and whose components permit individual manipulation and analysis.

For the current symposium, aspects of behavior, representing broad areas, have been selected as examples of what rigorous experimental measurement, control, and analysis can contribute to toxicology. They include motor function, sensory function, complex performance (including learning and adaptation), and what have been termed naturalistic behaviors. None of these areas are what they seem superficially, which is where the challenge lies.

Many attempts to ascertain the presence of neurotoxicity have relied on conventional clinical examinations. Typically, the clinical examination aims at a diagnosis and searches for evidence of

disease. It usually yields only a yes-no decision that might be modified by a statement that the degree of disability is mild or advanced. Although the neurotoxic properties of the agents chlordecone and methyl n-butyl ketone were first detected by alert clinicians to whom exposed workers complained of neurobehavioral symptoms, few would assert that the clinical examination is suitable for the steps beyond hazard identification. Moreover, no one, at least in public, is willing to assert that humans should serve in such a role.

Consider the intrinsic limitations of the clinical neurological examination. To measure grip strength, the patient may be asked to squeeze the examiner's hand or fingers. To measure balance, the patient may be asked to stand on one leg. To measure coordination, the patient may be asked to touch the examiner's finger. To measure tremor, the patient is asked to extend a hand while the examiner tries to evaluate tremor frequency and amplitude. To measure somatosensory acuity, the patient may be asked to respond to a pin prick. All are designed to allow the examiner to judge the presence or absence of overt disease.

Rating scales, which require an observer or subject to estimate the magnitude of some variable or effect, provide a kind of primitive quantification in both clinical and experimental settings. Such scales have been developed for movement disorders such as Parkinsonism and tardive dyskinesia, for example, and for psychiatric disorders such as schizophrenia. Although these scales may be useful for screening untested therapies, they lack the properties necessary to conduct parametric statistical analyses. A rating scale score of 4.0 does not imply twice the efficacy of a score of 2.0, for instance (i.e., ratings form ordinal scales).

In some experimental studies, rating scales may be used to denote degree of severity and are often relied on by pathologists to convey an estimate of damage. They also have been used to signify degree of behavioral impairment. Observational batteries may attempt a finer resolution than simply presence or absence of a response, such as sensitivity to toe pinch in rodents, by requiring the observer to attach a numerical rating to the intensity of the response. A serious problem with all rating scales is reproducibility. Only rarely do investigators try to ascertain whether different observers coincide in ratings of the same event or state. Without dependable agreement, ratings can be worse than useless; they can be misleading.

Suppose, however, that an investigator has chosen endpoints that can be measured reliably. Several collections of tests have been proposed to serve as screening batteries for the detection, in animals, of neurotoxic potential. They typically include measures of motor function such as the rotarod, measures of spontaneous activity such as the residential maze or open field, measures of sensory sensitivity such as the startle response to a loud sound, and measures of learning such as

passive avoidance. All of these techniques provide counts or times or amplitudes. Do these fulfill the quantitative requirements of extrapolation modeling?

Part of the answer lies in how the experimenter approaches the problem. Such batteries, usually designed for rodents, would not be claimed to offer a direct translation into human terms. Could they be used, however, to calculate values such as No Observed Effect Levels (NOEL), which, in other contexts, have been converted into standards such as Acceptable Daily Intakes (ADIs)? Two features should prompt hesitation: their recognized lack of sensitivity, and the usual experimental design in which they are placed. The typical design is based on group comparisons. Even if groups are surveyed more than once to determine the consequences of chronic dosing or the enduring effects of earlier exposure, the response of individuals is masked. Group means or other collective values constitute the basis for statistical analysis. If the toxicity of a particular agent tends to be cumulative, say, or the response progressive, variations among groups, when multiplied by inherent interindividual variation in those factors, could be great enough to bury even powerful effects. If, however, the statistical analyses recognize these issues and make provision for tracing the responses of individual subjects, we probably will achieve a much more precise notion of the latency to and rate of development of toxicity [15].

Statistical analyses, however, are only a mechanism for exploiting data. If an experiment is not designed and conducted to yield appropriate data, it cannot be rescued by statistical manipulation. Particularly for behavioral endpoints, tracing the progress of toxicity, especially its onset, or detecting modifications of performance at low exposure levels, requires stable baselines. Some investigators argue that the long training periods often needed to attain such stability in animal studies make them too costly and lengthy. Apart from the question of how useful it is to acquire gross and variable data to respond to difficult and subtle problems, is the view about cost a valid one? As the participants in this symposium demonstrate, precision in measurement and flexibility of experimental control need not, especially because of the availability of computer technology, incur huge costs.

Finally, and probably the most important message to emerge from this workshop, precise measures in a few animals may be a more valid basis for extrapolation than crude measures in many animals. Newland's elegant analyses of tremor, and its modification in monkeys exposed to various agents, should dissipate any lingering confidence in the neurological examination or in the rotarod as a basis for estimating the risk of incipient motor disorders arising from toxic exposure. Maurissen's *description of psychophysical procedures*, the ways in which they are applied to assess sensory function, and the widespread misunderstanding of their bases, demonstrates how much of the current literature is probably untrustworthy. To select only one point, how reliable are many of the current statements about vibration sensitivity in humans exposed to neurotoxicants when almost always investigators have failed to specify the major parameters, amplitude, and frequency of the

stimulus? Rice's tutorial on schedules of reinforcement shows how this feature of operant behavior research, because of its extraordinary flexibility, can be used to frame experimentally almost any question about complex performance. For example, Wood and Cox [16], basing their inferential procedures on schedule-controlled performance in rats, were able to approximate the TLM for toluene without exceeding the bounds of their experimental data. Cory-Slechta et al. [17] relied on schedule-controlled performance to show that rats exposed to low levels of lead exhibited behavioral changes at blood lead values in the range found by Zeilinger et al. [11] to retard intellectual development. The paper by Evans, although devoted to activity and appetitive behaviors, follows the same tradition by showing the degree to which behavioral data can be amplified by a focus on fine-grained analyses in individual subjects.

The participants in this section of the workshop adopted the point of view that extrapolation is the predominant issue in both human and animal testing. But extrapolation is not a unitary issue. One facet is its traditional implication of prediction, currently framed in terms of risk, and the part that sustains most of the efforts on its behalf. The other part is less direct. It is extrapolation for the purpose of mechanistic identification. Behavior is the outcome of manifold processes in the nervous system. The coordination of behavioral, physiological, and biochemical variables to yield a complete portrait of integrated nervous system processes is an aim, not just of neuroscience in general, but also of neurotoxicology. It seems wholly sensible that a grasp of how this integration takes place is better served by precise, detailed, and coordinated analyses of behavior, morphology, physiology, and neurochemistry than by exquisite microanalyses at one level (biochemistry) supplemented by coarse analyses at another level (behavior), a frequent and incoherent blend. The physiologically based pharmacokinetic models pioneered by Andersen and his colleagues [2], for instance, deserve to be accompanied by behavioral endpoints of at least equal quantitative stature.

## ACKNOWLEDGMENTS

Preparation supported by grants ES01247, ES01248, and ES03054 from the National Institute of Environmental Health Sciences.

## REFERENCES

- 1 Crump, K.S. (1984) A new method for determining allowable daily intakes. *Fund. Appl. Toxicol.* 4, 854-871.
- 2 Andersen, M.E., Clewell, H.J., Gargas, M.L., Smith, F.A., and Reitz, R.H. (1987) Physiologically based pharmacokinetics and the risk assessment process for methylene chloride. *Toxicol. Appl. Pharmacol.* 87, 185-205.
- 3 Finger, S. (1978) *Recovery from Brain Damage*. Plenum Press, New York.

- 4 Eskin, T.A., Lapham, L.W., Maurissen, J.P.J., and Merigan, W.H. (1985) Acrylamide effects on the macaque visual system. *Invest. Ophthalmol. Vis. Sci.* 26, 317-329.
- 5 Anger, W.K. and Johnson, B.L. (1985) Chemicals affecting behavior. In: J. O'Donoghue (Ed.), *Neurotoxicity of Industrial and Commercial Chemicals*. CRC Press, Boca Raton, FL, pp. 51-148.
- 6 Chronic Effects of Organic Solvents on the Central Nervous System and Diagnostic Criteria. (1985) World Health Organization, Copenhagen.
- 7 Cranmer, J.M. and Hixson, E.J. (1984) *Delayed Neurotoxicity*. Intox Press, Little Rock, Arkansas.
- 8 Clarkson, T.W., Cox, C., Marsh, D.O., Myers, G.J., Al-Tikriti, S.K., Amin-Zaki, L., and Daubagh, A.R. (1981) Dose-response relationships for adult and prenatal exposures to methylmercury. In: G.G. Berg and H.D. Maillie (Eds.), *Measurement of Risks*, Plenum Press, New York. pp. 111-130.
- 9 Roels, H., Lauwerys, R., Buchet, J.-P., Genet, P., Sarhan, M.J., Hanotiau, I., deFays, M., Bernard, A., and Stanescu, D. (1987) Epidemiological survey among workers exposed to manganese: effects on lung, central nervous system, and some biological indices. *Amer. J. Indust. Med.* 11, 307-327.
- 10 Environmental Protection Agency. (1986) *Air Quality Criteria for Lead*. Vol. 1, Research Triangle Park, NC, U.S. Environmental Protection Agency.
- 11 Bellinger, D., Leviton, A., Waternaux, C., Needleman, H., and Rabinowitz, M. (1987) Longitudinal analyses of prenatal and postnatal lead exposure and early cognitive development. *New Engl. J. Med.* 316, 1037-1043.
- 12 Weiss, B. (1986) Food additives as a source of behavioral disturbances in children. *Neurotoxicology* 7, 197-208.
- 13 Ballard, P.A., Tetrud, J.W., and Langston, J.W. (1985) Permanent Parkinsonism due to 1-methyl-4-phenyl-1,2,3,6-tetrahydropyridine. *Neurology* 35, 949-956.
- 14 Weiss, B. (1973) *Digital Computers in the Behavioral Laboratory*. Appleton-Century-Crofts, New York.
- 15 Cox, C. and Cory-Slechta, D.A. (1987) Analysis of longitudinal "time series" data in toxicology. *Fund. Appl. Toxicol.* 8, 159-169.
- 16 Wood, R.W. and Cox, C.C. (1986) A repeated-measures approach to the detection of the minimal acute effects of toluene. *Toxicologist* 6, 221.
- 17 Cory-Slechta, D.A., Weiss, B., and Cox, C. (1985) Performance and exposure indices of rats exposed to low concentrations of lead. *Toxicol. Appl. Pharmacol.* 78, 291-299.

## QUANTIFICATION OF MOTOR FUNCTION IN TOXICOLOGY

M. Christopher Newland

*Department of Psychology, Auburn University, Auburn, AL*

### SUMMARY

Disturbances of movement and other motor functions can result from exposure to toxicants and drugs. Sometimes, as with acute exposure to ethanol or solvents, these effects disappear when exposure ends. Other times, as with manganese, haloperidol, or chronic ethanol, motor disturbances are irreversible and may even lie undetected until after exposure has ended. Motor disturbances can take on many guises, including tremor, difficulty in positioning, fatigue, or rigidity. Techniques for measuring these different endpoints in primates will be addressed. One preparation that enables the simultaneous monitoring of positioning, tremor, and operant behavior in nonhuman primates is described, and tactics for obtaining spectral estimates of tremor from a positioning task are outlined. The spectra obtained from this preparation are reliable and valid: They are stable over a period of a year, they correspond to spectra obtained from accelerometers, and are altered by acute administration of ethanol or oxotremorine. These two drugs had opposite effects on tremor but affected bar positioning in a similar manner.

### INTRODUCTION

Motor disturbances result from exposure to many classes of substances including metals, solvents, gases, pesticides, and drugs. These disturbances reflect damage to a wide variety of structures ranging from peripheral axons to regions deep within the central nervous system. The association between toxicant exposure and dysfunction can be specific both to the structure of the chemical and to the site of action. For example, the toxicity associated with 2,5-hexanedione (2,5-HD) exemplifies both structural and biological specificity. Substances such as *n*-hexane or methyl *n*-butyl ketone, which are metabolized to 2,5-HD produce a characteristic dying-back neuropathy in axons that is so specific that it may serve as a model for other neurological diseases [1,2]. Another sign of motor dysfunction, tremor, is characteristic and indeed diagnostic, of excessive exposure to some substances, such as inorganic mercury and the pesticide chlordecone, and is associated with exposure to a number of other substances. Because tremor has been so commonly associated with chlordecone, that syndrome became known among workers as the "Kepone shakes" [3].

Of the many possible motor signs and symptoms that have been reported, a few appear with some regularity. Anger [4] summarized the criteria used by the American Conference of Governmental Industrial Hygienists (ACGIH) in setting threshold limit values on 588 chemicals. Fourteen different motor effects were cited for 89 substances (about half of those cited for neurotoxic effects) and an additional 8 substances produced "Weariness/Fatigue/Lethargy." Four

complaints dominated the category of motor effects: (1) tremor was mentioned most frequently, being cited for 19 different substances; (2) convulsions and spasms were cited for 18 substances; (3) weakness for 12 (this category grows to 20 if fatigue is included); and (4) incoordination was cited for 10 substances.

These data demonstrate the importance of assessing motor function in any battery to be used in the workplace and such efforts have been reported [5,6,7,8,9]. Tests of motor function also form an important part of test batteries used in initial screening of compounds with animals. When these tests have been validated and their reliability has been assessed they can provide an important guide to research [10,11,12].

Endeavors to quantify and characterize motor dysfunction induced by exposure to drugs or toxic substances yield many benefits. Of course, specificity of symptoms and signs assist greatly in diagnosis and guide an industrial hygienist or occupational physician more directly to a source of exposure. But there are more fundamental implications of specificity as well. Once neurotoxic damage is characterized precisely, it is possible to compare that damage with known neurological syndromes; to the extent that the damage corresponds to the clinical syndrome, a model is possible. For example, 2,5-HD-induced toxicity is a model of axonopathies in general and the basal ganglia damage associated with the pyridine neurotoxicant 1-methyl phenyl tetrahydropyridine (MPTP) provides a close model of Parkinson's disease [13,14].

Some procedures designed to quantify motor dysfunction are described below. The measurement of tremor will be described first and in some detail because this sign appears so frequently and because it is often poorly characterized. Since the frequency, or rate, of tremor contains information about its character and its source, this form of quantification will be described in some detail. Next, one approach to experimentally examining disruptions in movement and positioning will be discussed in order to raise some of the issues that should be considered in their quantification.

## **TREMOR**

The single word "tremor" actually refers not to a unitary disorder or neurological sign, but rather to a variety of phenomena. Several types of tremor have been described though the definitions have sometimes overlapped. A recent taxonomy clarified the different definitions by categorizing tremor on the basis of the conditions under which it appears [15]. These categories include resting, postural, and movement tremor (the latter breaks down into initial, transition, and terminal tremor). The terms are relatively simple and almost self-explanatory, making this taxonomy useful in the clinical examination.

Quantifying tremor by describing its magnitude and the shape of its waveform is as important as specifying the conditions under which it appears. The magnitude and frequency of the dominant

frequency of tremor, as well as the shape of its spectral profile of tremor, all provide important clues to its causes [16]. Techniques for describing and quantifying tremor with spectral analysis will be described, and representative data describing tremor in human and animals will be presented.

Spectral analytic techniques provide precise, quantitative descriptions of tremor, an advantage not only in describing this disorder but also in assessing its underlying cause. These techniques break movement down into a set of discrete frequency components corresponding to different rates, or frequencies, of movement. Thus, slow movements correspond to low-frequency changes and fast movements with high-frequency changes. The general approach is analogous to breaking white light down into different frequencies (or wavelengths) using a prism.

Two examples from the literature illustrate the importance of providing spectral descriptions of tremor. The tremor resulting from mercury vapor exposure is sometimes described as having a 6 Hertz (Hz, or cycles/sec) frequency of oscillation [17], a characterization that suggests a single peak in the spectrum. However, spectral analyses have revealed patients whose spectrum does not contain a single peak but rather a wide lobe representing an increase in the variance of the spectrum [7,18,19]. Such a waveform would not be detectable without spectral analysis.

A second example illustrates a situation in which the power spectrum is notable not by the presence of power in a frequency band, but by its absence. Freund et al. [20] present spectra from a muscular dystrophy patient pressing on a strain gauge. Unlike normal people or patients with Parkinson's disease whose spectrum typically contains a single, dominant peak, this patient's spectrum was characterized by the presence of many peaks between 0 and 4 Hz and in the 14-32 Hz band. Most striking was the absence of power between 6 and 14 Hz, the band typically containing most of the power in healthy subjects. Such a pattern, which would be difficult to describe without spectral analyses, is consistent with the myopathic damage of muscular dystrophy.

## **SPECTRAL ANALYSIS**

### ***The Fourier transform***

Spectral analyses involve some rather complex mathematical transformations to the signal under analysis, but the techniques are hardly new. Fourier's theorem, on which these analyses are based, was introduced in 1822 and published in 1878. An algorithm, called the Fast Fourier Transform (FFT) for computing Fourier transforms rapidly on digital computers, was introduced more than 20 years ago [21]. With the development of faster computers, inexpensive memory, and improved software, it is possible to perform spectral analyses with greater facility than ever before.

The Fourier transform is an analytic tool that converts a signal, which is obtained in time (called the time-domain signal), into a sum of sine (or sometimes cosine) waves in which the sine terms oscillate at different frequencies. Each sine term is described by three parameters: (1) magnitude, (2) phase, and (3) frequency. The Fourier transform is usually expressed as magnitude and phase as a

function of frequency. The description based upon frequencies of oscillation is called the frequency-domain signal. The Fourier transform does not remove information from a signal; the frequency-domain characterization is merely a different way of describing a waveform and the original waveform can be recovered from the transform.

Perhaps the claim that the original signal is recoverable from its Fourier representation can be made believable with an illustration of how a time-domain waveform is reconstructed from its Fourier representation. Any periodic waveform can be described using Fourier techniques. The right side of Figure 1 shows a rectangular wave and its representation as a sum of sine terms. The bar graphs on the left depict the magnitude of the Fourier components used to reconstruct the rectangular wave. The complete transform of the rectangular wave contains an infinite number of components but in practice only a finite number of terms are required to reconstruct adequately the time-domain signal.

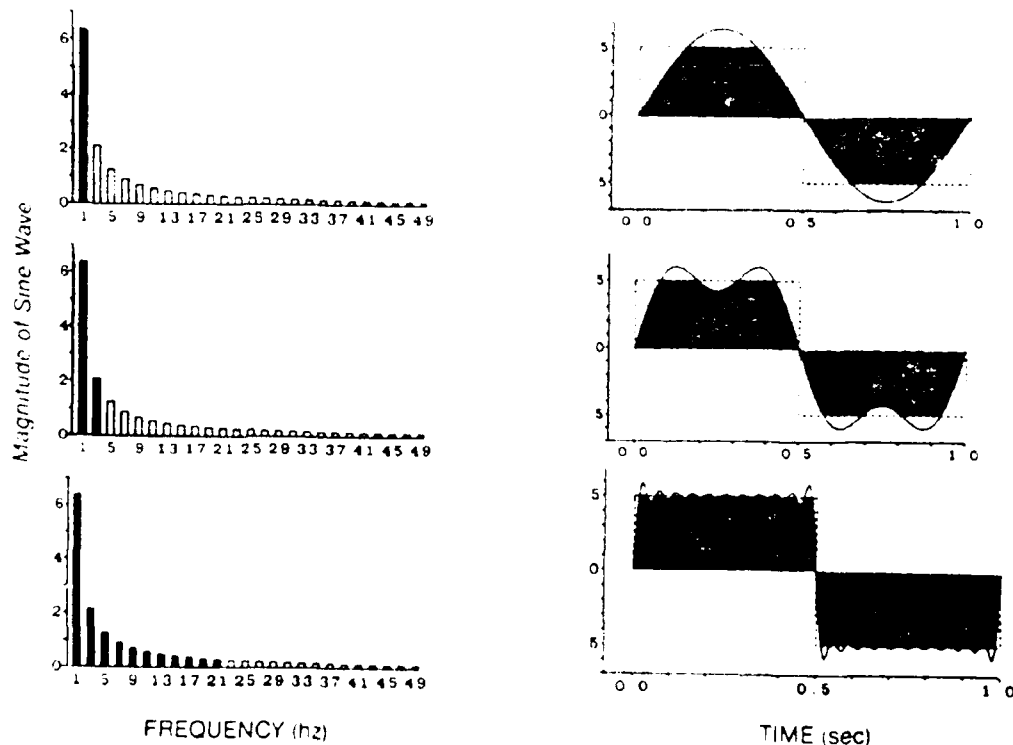


Figure 1. The first 25 non-zero components of the Fourier series (left) used to reproduce a rectangular wave (right) and the reproduction of the rectangular wave using 1, 2, and 11 terms. The shaded bars on the left indicate which terms were used to fit the rectangular wave on the right. The shaded portion on the right shows the area that is common to the original signal and its Fourier reconstruction. Adding high-frequency terms improves the fit at rapid changes in the time signal, such as during the onset and offset, and reduces the ripple seen when the signal is constant.

The Fourier components in the left column of Figure 1 correspond to the magnitude of the sine-waves used to estimate of the rectangular wave in the right column. The first row contains an

approximation based upon the first sine term (of magnitude 6.37) and this single term provides only a fair estimate of the rectangular wave. The next sine wave has a magnitude of 2.12 and contributes to the reconstruction by improving the rise and fall time of the reconstructed signal. The use of 11 sine terms provides an even closer approximation of the rectangular wave, mostly by improving the fit at the abrupt changes of magnitude.

### ***The power spectrum***

Figure 1 illustrates the use of the Fourier transform, but tremor analyses typically use power spectral analyses, a form of spectral analysis that uses the square of the time-domain signal. The spectral density function that results from this analysis describes the amount of power in each frequency band and is analogous to the more familiar probability density function. A power spectrum describes the frequency content of the time-domain signal in a form that facilitates comparisons of spectral content within and across spectra. This is because the power within different frequency bands combine additively, and the power within each band can be compared meaningfully with the total power in the signal. Power spectra lack phase information so the original time-domain signal cannot be reconstructed from the power spectrum, but phase is rarely of interest in tremor analyses.

Readers familiar with analysis of variance (ANOVA) techniques will recognize the general approach to power spectral analysis, since the two approaches are very similar. Both power spectral analysis and the ANOVA break down the total sum of squares into a sum of orthogonal (i.e., independent) elements. Indeed, the Fourier series provides a sum of sine or cosine waves that is the best approximation (in the least mean square sense) of the time signal [22]. The total sum of squares with power spectral analysis is the sum of squared deviations from the mean of the time-domain signal, while with ANOVA it is the sum of squared deviations from the grand mean in the experiment. Thus, the principal difference between the two analyses lies in the way that the total sum of squares is partitioned: the power spectrum breaks the sum of squares into a sum of trigonometric functions while the ANOVA usually breaks it down into a sum of linear contrasts.

Power spectra hold many advantages over Fourier transforms. The area under the spectral density function equals the total power, or variance, in the time-domain signal. (Identically, with the ANOVA the sum of the squares for each condition, including error, equals the total sum of squares in the experiment.) The power in each frequency band divided by the total sum of squares is the proportion of the variance accounted for by that term.

The square root of the total power (the root-mean-square or RMS value) is sometimes used as a rough indicator of tremor. RMS power provides no frequency information but it does describe the

total dispersion about the mean in the original units, just as the mean and the standard deviation (which is identical to RMS power) are in common units.

Table 1 illustrates some of these relationships for the first 6 terms of the sinusoidal approximation of rectangular wave illustrated in Figure 1. For this example, let the units of the original displacement be centimeters. Column 2 is the magnitude of the sine wave in centimeters, and column 3 contains the corresponding spectral density in  $\text{cm}^2/\text{Hz}$ . The spectral density is  $1/2$  the square of the magnitude of the sine term (within rounding error). A technicality of the Fourier transform requires division by 2 after squaring the term: the transform is defined over the domain of  $-\infty$  to  $+\infty$  but only non-negative frequencies, or  $1/2$  of this domain, are used. Total power ( $\text{cm}^2$ ) in a frequency band is the area and equals the spectral density times the bandwidth in Hertz. In this example, the density equals the total power since the bandwidth is 1 Hz. Column 4 is the percent of the total variance accounted for by each term. The total variance of 25 is simply the area of the rectangular wave in Figure 1.

In Figure 1, the fundamental frequency of 1 Hz accounts for 81% of the variance in the time signal (see Table 1). Higher frequencies account for progressively smaller proportions of the variance.

**TABLE 1. VALUES OF THE FIRST FIVE SINE WAVES USED TO APPROXIMATE A RECTANGULAR WAVE WITH A MAGNITUDE OF  $\pm 5$  CM AND VARIANCE OF  $25 \text{ CM}^2$ <sup>a</sup>**

Frequency (Hz)	Magnitude of Fourier Term (cm)	Spectral Density ( $\text{cm}^2/\text{Hz}$ )	% Variance
1	6.37	20.3	81.2
3	2.12	2.25	9.0
5	1.27	0.81	3.2
7	0.91	0.41	1.6
9	0.71	0.25	1.0

<sup>a</sup> The results describe a rectangular wave of magnitude 5 for 0.512 sec,  $-5$  for 0.512 sec, for a total epoch of 1.024 sec. Sampling occurred at 100 Hz. Thus, the resolution is 0.977 Hz and the upper frequency limit is 50 Hz. Frequencies in column 1 are rounded to the nearest hertz for simplicity and to emphasize the correspondence to Fig. 1.

#### LIMITATIONS AND RESTRICTIONS OF SPECTRAL ANALYSES

Many software packages are available for performing spectral analyses. These packages eliminate tedious calculations and can handle large data sets. However, limitations of spectral analyses must always be remembered when using them because the software does not always perform these checks for the user. Moreover, software has errors and documentation contains ambiguities so it is crucial to test the package in use as well as the specific application.

There are several sampling and statistical considerations that must be incorporated into any spectral analysis, and these are rarely handled adequately by the software package. The limitations imposed by digital sampling of a finite, analog signal include (1) a lower limit on the resolution imposed by the length of the series, (2) an upper limit on the highest frequency that can be resolved unambiguously, and (3) artifactual errors due to the finite length of the time series. The first two statistical considerations are that the signal under analysis must be stable and representative of all other signals. Formally these properties are called stationarity and ergodicity. The third statistical consideration applies to the error of the spectral estimate and tactics for deriving confidence intervals of the estimates will be described below. These considerations have been detailed in many texts [22,24,25] so they will only be highlighted here.

### **Resolution**

The lowest frequency that can be estimated in a finite duration is determined by the duration of sampling. At least one full cycle must be present in the signal under analysis so the lowest frequency that can be measured (called the fundamental frequency) is simply the inverse of the signal duration. The resolution of other estimates is directly related to the fundamental frequency because all frequencies are integer multiples of it. For example, if sampling is taken over 10 sec then 0.1 Hz wave can be estimated and estimates every 0.1 Hz are possible. If only a 0.5-sec epoch is used then 2 Hz represents the lowest limit and the resolution. One important outcome of Fourier's theorem is that as long as multiples of the fundamental frequency are used, each magnitude estimate is orthogonal to, that is, independent of, other magnitude estimates. This result greatly eases the statistical evaluation of spectral estimates.

### **Aliasing**

Ignoring the lower frequency limit will lead to non-independent estimates, a problem that complicates statistical analyses. If the upper limit is ignored, however, then the estimates will be wrong. The highest frequency that can be estimated (sometimes called the Nyquist frequency) is 1/2 of the sampling frequency. There must be at least two points in each cycle to provide an unambiguous estimate. This upper limit results from a process called aliasing, a concept that is best illustrated graphically.

The top row of Figure 2 shows two signals at different frequencies, one at 40 Hz and one at 60 Hz. The middle row shows which points would be sampled if sampling were to occur at 100 Hz. The bottom portion of the figure shows the digital representation of the two waveforms, connected by broken lines to emphasize the pattern. Note that in the bottom row, one digital representation is simply the mirror image of the other; they can be distinguished in phase (when the signal begins) but not in frequency. The digital representation of the 60-Hz signal occurs at the same frequency as that

for the 40-Hz signal; the 60-Hz signal takes an alias of 40 Hz. A Fourier transform of these signals would reveal a single peak at 40 Hz representing a contribution from both the 40- and the 60-Hz signal.

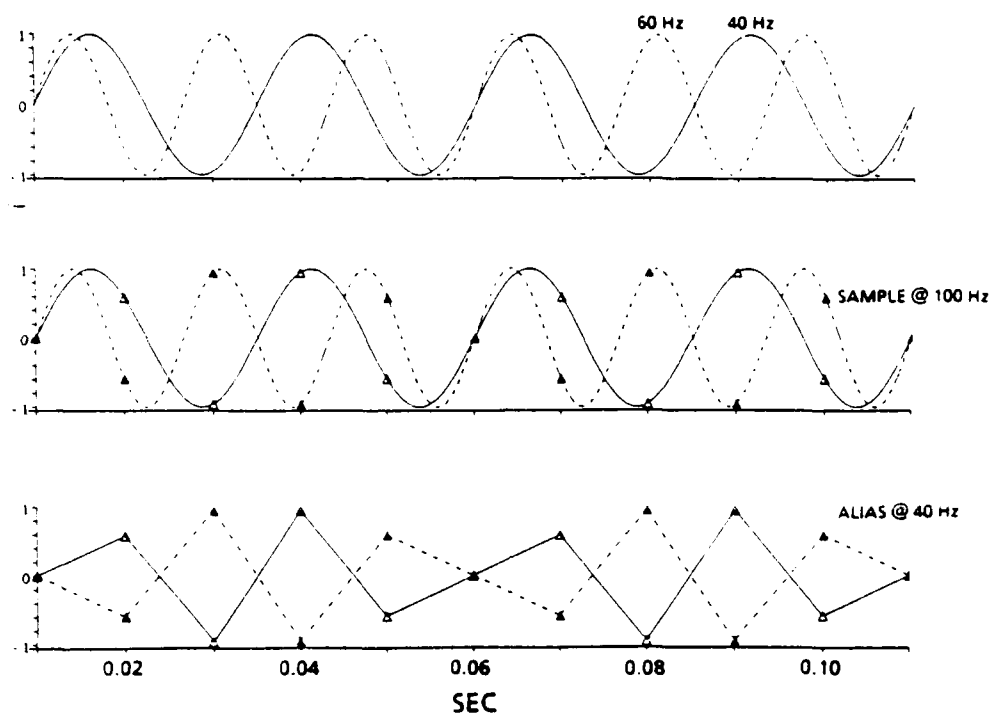


Figure 2. A 60-Hz signal induces a 40-Hz alias when sampled at 50-Hz. The top row shows a 60-Hz (solid line) and a 40-Hz (dashed line) signal. The middle row shows where samples would be taken if digital sampling occurred at 50 Hz. The bottom row shows the digital representation, connected by lines to facilitate comparison, of the analog signal in row 1. The digital representation of both time signals appears at 40 Hz.

Aliasing is the artifactual appearance of unwanted, high-frequency signals at a frequency somewhere in the band under investigation. Once the analog signal is digitized it is contaminated and no amount of processing will distinguish real frequencies from aliased higher frequencies. These higher frequencies can derive from 60-Hz power supplies, fluorescent lights, or any of the other sources of electrical contamination found in laboratory or industrial settings. Aliasing can be prevented by removing all frequencies higher than the Nyquist frequency with a low-pass filter. Alternatively, the sampling frequency can be increased so that all frequencies are accurately represented. It is important to emphasize that filtering must be accomplished before digitizing: once the signal is digitized it is too late.

### **Windowing**

Infinite signals are impractical so all time signals consist of an onset and offset (i.e., they occur within a temporal window). If the first or last samples are non-zero then an instantaneous rise or fall time occurs at the endpoints. The resulting sampling interval is called a "boxcar" window. As was evident in the example in Figure 1, an infinite number of frequencies are required to describe such an instantaneous change. Analytically, it can also be shown that if the signal contains an instantaneous onset or offset, then the estimate at each frequency "leaks" into estimates at adjacent frequencies and thereby contaminates them. The amount of leakage is related to the magnitude of the estimate.

Leakage can be reduced by any of several smoothing operations. These entail calculating a moving average of the frequency spectrum or, equivalently, tapering the ends of the time signal. The topic is a complicated one and has been discussed at length by others [24, 25, 26, 27, 28].

Hanning and Hamming are two smoothing techniques that have often been applied to spectral data to reduce artifacts induced by frequency leakage. In the frequency domain, these techniques entail calculating a three-point moving average in which the center point is more heavily weighted than the two adjacent points. For example, with Hanning the power estimate  $g_k$  at frequency  $f_k$  is  $0.25 \times g(f_{k-1}) + 0.5 \times g(f_k) + 0.25 \times g(f_{k+1})$ . With Hamming, the multipliers for frequencies  $f_{k-1}$ ,  $f_k$ , and  $f_{k+1}$  are 0.23, 0.54, and 0.23, respectively. Hamming windows provide less leakage than Hanning.

In the time-domain, such smoothing appears as a gradually rising taper starting at the onset of the signal and increasing to the midpoint of the sampling epoch. It then forms a gradual decline from the midpoint to the offset of the signal. As these windows remove some power from the signal, a conversion factor must be applied to the power spectrum after windowing to restore the estimate to the correct magnitude. This conversion factor is 1.56 for Hanning and 1.85 for Hamming [27].

### **Confidence intervals and smoothing**

The standard error of an estimate derived from a single time signal is equal to the estimate itself. This is true regardless of the duration of sampling. Duration determines the frequency resolution of a spectral estimate, but increasing it does not affect the ratio of signal to noise. To improve the signal-to-noise ratio or, equivalently, to reduce the standard error of the estimate, it is necessary to combine estimates by ensemble averaging or frequency smoothing. Frequency smoothing applies when the signal duration is very long and it involves averaging over a band of frequencies to obtain a central estimate. Ensemble averaging smooths the data by a more familiar route: many short signals are taken, transformed, and the resultant spectra averaged together. When analyzing tremor, ensemble averaging is preferable to frequency smoothing; power spectra

from many short signals can be averaged together and fatigue, which would introduce nonstationarity, is avoided.

Bendat and Piersol [24,25] have shown that when spectra are log-transformed before averaging, the average is normally distributed and the normalized standard error of the estimate equals the square root of  $[2/(\text{number of spectra in the ensemble})]$ . This formulation is useful if there are limitations on the amount of data that can be analyzed. Of course, direct computation of the standard error is preferable if it is possible to keep spectra of every signal.

### **Software errors**

Software contains errors and must be tested. Two initial tests should be conducted on spectral analytic packages. First, generate a waveform containing known magnitudes and frequencies. A Fourier transform should reproduce these frequencies and magnitude within the errors imposed by digitizing and rounding. The power spectrum should produce magnitudes that are about one-half of the square of the magnitudes in the Fourier transform. A final check is provided by the fact that the integral of the power spectrum equals the variance in the time-domain signal. Since the variance and the area under the power curve are produced by separate analytic paths, the comparison provides an excellent check both on the package and on the specific application.

### **TRANSDUCERS FOR DETECTING TREMOR**

Quantification of tremor in human and non-human subjects has been accomplished using a variety of transducers to convert the mechanical energy of tremor to electrical energy that, in turn, can be digitized. Some of these transducers are listed in Table 2 (see also [29]).

An accelerometer attached to the tremoring limb is the simplest, most direct, and common measure of tremor in human applications. There are many advantages to acceleration-based measures over others. At the relevant frequencies of 6 to 8 Hz, small deviations in position appear as large deviations in acceleration. Acceleration emphasizes those frequencies of greatest interest in detecting tremor, namely those over about 4 Hz, while displacement-based measures emphasize slower movements.

Force transducers also have seen much use with both human and animal subjects. These devices are based upon the principle that displacement of an ideal spring is proportional to the applied force. Deflection, therefore, provides a measure of force within the linear range of the spring. In experiments with load cells or strain gauges, a subject is required to maintain a force within a specified band and tremor appears as deviations about a central position. In the animal experiments, the major endpoint studied has been the accuracy of performance or measures of

response topography [30], but spectral analyses of the tremor produced by these devices have also been reported [31].

TABLE 2. REPRESENTATIVE TRANSDUCERS USED TO DETECT TREMOR

Form of Energy	Transducer	Typical Application	Physical Units	Sample References
Acceleration	Accelerometer	Attach to limb	cm/sec/sec g millii-g	[8,42,47,48,49]
Force	Load cell strain gauge	(1) Press with hand, finger or paw	Dynes Newtons Pounds	[31,32,33,34,36,37,43]
		(2) Set rodent and platform on device	Grams <sup>a</sup>	
Displacement	Potentiometer Rotary transformer	Move with a limb	Centimeters	[19,50]
	Magnet in electric field	Attach magnet to limb	Centimeters	[51]
	Platform on speaker coil	Place mouse on platform	Pen deflections	[52]
Frequency	Strobe light	Tune of tremor frequency	Hertz	[53]

<sup>a</sup> Grams, units of mass, are usually reported but dynes or Newtons are the appropriate unit of force.

Force measures also have been applied in rodent studies of the pharmacology and toxicology of tremor by placing a platform containing a rat upon a load cell and analyzing the spectral content of the entire system (rat and platform). For example, Tilson and his colleagues report on tremor produced by a number of substances [32,33,34]. Lehtinen and Gothoni [35] describe a similar system, except that an accelerometer is the transducer. These authors also outline a technique for assessing, and eliminating, the contribution of the measurement system to the measurement itself.

Because load cells measure force, which is proportional to mass and acceleration, it might be thought that the tremor recorded from these devices will resemble that found in an accelerometer [36]. However, the spectra from force transducers contain more low-frequency power than those obtained from accelerometers. There are important physical and procedural differences in the application of these devices that could account for these differences. Accelerometers are used by strapping the transducer to the limb and asking the subject to hold this limb against gravity while load cells are used and by asking the subject to press down upon an isometric transducer. Accelerometer measures are relatively uncontaminated by the mass of the accelerometer, which is

constant and relatively small in most accelerometers. Load cells, however, measure a combination of both mass and acceleration.

The physical demands of the task also can account for some of the differences between force and acceleration transducers. The act of pressing on a load cell with one's finger could filter high-frequency data because of the soft padding on the end of the finger. The net force exerted by the limb accelerometer experiments is upward, while in load cell experiments it is an algebraic sum of the force required to hold the limb up and the force required to meet the demands of the experiment. The magnitude and frequency of tremor is related to the force applied; therefore, such procedural differences can greatly influence the results [37].

Displacement transducers of various types also have been applied to assessing tremor. While these have been more frequently used with non-human subjects, they also have been used with humans [19]. Table 2 lists several examples of displacement devices.

#### ***Physical properties of the transducer***

Whatever the transducer, it is important to demonstrate both that it is sensitive and that its physical properties do not contaminate the signal. One potentially serious source of contamination is resonance—a property of all physical systems. A chamber with a 300-gram rat will resonate when hit lightly. Such a pulse is a simple test of the resonant frequency of the measuring system and should be performed. If the resonant frequency is in the band being measured (0 to 30 Hz for tremor), then it can inflate the frequency estimate at the resonant frequency and diminish the estimate at other frequencies.

A second physical property to be considered is damping. The measurement device should be equally sensitive to all frequencies between 0 and 50 Hz, and any deviations should be accounted for in the analysis. Otherwise, the resulting spectrum will be distorted. Both resonance and frequency-dependent damping can be avoided by computing a transfer function of the system and using this to remove the system's influence [35] or by designing the system with the appropriate physical characteristics.

#### ***Selecting a transducer***

Many considerations influence the choice of a transducer. If human tremor is the sole interest then an accelerometer is the simplest and most direct transducer. Accelerometers provide data that can be analyzed and expressed in units that are directly comparable to the tremor literature. They also have excellent signal-to-noise properties and are quite sensitive. Displacement devices, load cells, or force-joysticks are useful if collateral measures such as tracking, coordination, reaction time, or positioning are desired. Load cells or force-sticks also offer a measure of strength.

The species under study, of course, is also a critical consideration. Humans can be told how to perform a task and they will not destroy the transducer, so an accelerometer taped to the back of the hand is well suited to human investigation. However, monkeys are saboteurs and their behavior must be shaped, so the durability of the mechanism and the ease of training are crucial considerations in these experiments.

### **NORMAL HUMAN TREMOR**

A comprehensive description of tremor includes the spectral density function over the entire band of relevant frequencies. Such a profile often has one narrow band of frequencies that contains most of the power, but multiple peaks are not uncommon [38]. Summary measures typically include the total RMS power in the spectrum, the dominant frequency, and the spectral density at the dominant frequency.

In a series of studies, Marsden et al. [38,39,40] described the variability in the velocity spectrum of normal human finger tremor. The spectral profile of normal humans is consistent over at least 16 months [38], reflecting great stability in the frequencies of the spectral peaks. However, the magnitudes of these peaks can vary several-fold when measured at different times. Essential tremor may have a less stable profile than normal tremor [41]. Fatigue can significantly alter the spectrum so care must be taken to allow the subject to rest between trials and to avoid long trials. While the dominant and non-dominant hands of some subjects may show different spectral profiles, more often than not the two hands are similar [40].

There are insufficient published data from experiments in which normal human tremor is assessed with accelerometers to provide a guide to the dominant frequency, its magnitude, and the variability of these values. Table 3 provides some estimates taken from papers in which data were obtained from groups of humans. Data from the finger, hand, arm, and foot are reported. For comparison, descriptions of essential and Parkinsonian tremor are also provided in Table 3.

### **Frequency**

Clinical observations often result in a numerical estimate of the frequency of oscillation (e.g., about 7 Hz for an extended hand resisting gravity), but this estimate is not based upon direct measurement and more likely reflects a "fast", "normal", or "slow", judgment and certainly reflects the dominant frequency. Detecting multiple peaks, harmonics, or the absence of expected frequencies that can point to underlying syndromes is impossible without spectral analytic techniques. These techniques not only enable the investigator to describe the waveform in a quantitative manner but also facilitate comparisons among individuals, exposure conditions, and published studies.

TABLE 3. DESCRIPTION OF HUMAN POSTURAL TREMOR FROM SELECTED EXPERIMENTS THAT USE ACCELEROMETERS<sup>a</sup>

Limb	Characteristics of Spectral Peak								Reference
	Total Power (milli-g) <sup>2</sup>		Frequency (Hz)		Power (milli-g) <sup>2</sup> /Hz		RMS Power (milli-g)		
	Mean	Range	Mean	Range	Mean	Range	Mean	Range	
Normal hand	1369.	445–2400	6.0	4.9–7.1	543.	180–992	23.	3–31	[8]
Normal hand	NA	NA	7.0	5.8–8.3	611. <sup>b</sup>	2–1225	17. <sup>b</sup>	1–35	[42]
Normal hand	3370.	1170–11160	7.2 <sup>b</sup>	6–8.3	570. <sup>c</sup>	NA	24. <sup>c</sup>		[43]
Parkinson, hand	93000.	27000–279000	5.7 <sup>b</sup>	4.5–6.9	28000. <sup>c</sup>	NA	167. <sup>c</sup>		[43]
Essential tremor, hand	195000.	45000–604000	7.2 <sup>b</sup>	5.7–8.6	108000. <sup>c</sup>	NA	329. <sup>c</sup>		[43]
Normal finger	73.	16–162	6.4	3.2–9.3	11.	2–20	3.	1–5	[48]
Normal ankle	12.	4–49	7.5 <sup>b</sup>	6.0–9.0	23. <sup>c</sup>	NA	4. <sup>c</sup>	NA	[49]
Normal forearm	NA	NA	3.3	3.0–3.7	1. <sup>c</sup>	NA	1.	NA	[54]

a. Selected experiments from which sufficient information could be extracted. In these papers the value "1 g<sup>2</sup> × 10<sup>-3</sup>" is assumed to be 001 g<sup>2</sup> and is listed as 1000 (milli-g)<sup>2</sup>. An entry of "NA" means that the data was not available.

b. The midrange was used since no estimate of central tendency was available.

c. Population statistics were unavailable so values from figures describing representative subjects are used.

Table 3 shows that when tremor is measured with an accelerometer attached to an outstretched hand, the frequency corresponding to peak acceleration in adults with no known neurological symptoms is  $7 \pm 1.25$  Hz (mean  $\pm$  1 standard deviation). This value begins a decline to a mean of about 6 Hz at 70 years of age [38,42]. A peak at 6 to 8 Hz has been replicated many times under different circumstances (e.g., [7,8,36]) and so it represents a benchmark against which syndromes involving tremor can be compared. The frequency corresponding to the peak in a velocity spectrum usually does not depend upon the hand being measured [40] and is quite stable over time [38].

Not all subjects have a pronounced peak, and some have two [38]. Marsden et al. [38] reported the lack of a pronounced peak in 5% of adults tested and in 60% of children less than 16 years old. The presence of multiple peaks complicates analyses that include only the dominant frequency.

## Magnitude

As with measures of the dominant frequency, precise quantification of the magnitude of tremor also facilitates comparisons and provides more meaningful data than are available from ordinal assessments. Amplitude of the dominant peak(s) or total RMS power measures can be obtained from power spectra. Such information can assist greatly in comparing an individual record with what might be expected from a normal population.

The most common physical units in the measure of tremor are some multiple of the acceleration due to gravity, *g* (981 cm/sec/sec), and the most convenient form, although not the most commonly used, is the milli-*g* (0.981 cm/sec/sec). Table 3 shows that the spectral peak for normal human finger tremor has an RMS value of about 1 to 5 milli-*g*, while that for hand tremor is 1 to 35 milli-*g*, and ankle tremor is about 5 milli-*g*. In patients with essential tremor, the peak acceleration is 10 to 100 times that observed in normal humans (e.g., [41,43]). That is, it can range from about 40 to over 400 milli-*g*. To put these numbers into perspective, at about 7 milli-*g* tremor becomes noticeable and at about 30 milli-*g* it is "socially embarrassing" [42].

The stability of the dominant frequency contrasts with the 30-fold variation in the range of magnitudes. The threefold difference between the highest peak and the bulk of the distribution of magnitudes suggests a skewed distribution and that applying a log transform or, equivalently, converting the data to decibels, may be appropriate before statistical analysis.

RMS units are sometimes used to describe the spectral content of tremor. The units of RMS power are that of *g*/Hz or milli-*g*/Hz (and here 1000 milli-*g* = 1 *g*). RMS units have more direct physical meaning since they are in the same units as the original signal and therefore may be easier to grasp. However, RMS power cannot be integrated to obtain the total variance in the signal.

The displacement that corresponds to RMS acceleration can be calculated. Displacement is the second integral (in time) of acceleration and the calculation yields the following relationship between RMS acceleration (in milli-*g*) and RMS displacement (in centimeters):

$$d = \frac{(0.981) a}{(2\pi f)^2} = \frac{.025 a}{f^2}$$

where: *d* = displacement in centimeters

*a* = acceleration in milli-*g* (and 1 milli-*g* is 0.981 cm/sec/sec)

*f* = frequency in Hz (1/sec)

Note the inverse dependence upon the square of the frequency. Applying this formula to the normative data presented above indicates that 1 to 5 milli-*g* (RMS) of tremor results in about 0.0005 to 0.015 cm (RMS) displacement at 7 Hz. The RMS displacement in essential tremor can range from

about 0.02 to over 0.2 cm at 7 Hz. Because of the dependence upon frequency these numbers increase at the lower frequencies that dominate in most tremor disorders. Thus, 400 milli-g RMS corresponds to 0.2 cm of displacement at 7 Hz but 0.8 cm displacement at 3.5 Hz.

The use of milli-g and centimeters provide convenient approximation formulas. A value of 1 milli-g is approximately 1 cm/sec/sec of acceleration. To convert from milli-g to cm at the 7 Hz normal peak, it is necessary only to multiply by 0.0005 (i.e., move the decimal point three places to the left and divide by 2).

Many papers describe power with the ambiguous notation of  $1 \text{ g}^2 \cdot 10^{-3}$ , a notation that is interpreted correctly as .001  $\text{g}^2$  or 1000 milli- $\text{g}^2$ . However, a number like  $1 \text{ g} \cdot 10^{-3}$  has mistakenly been abbreviated as 1 (milli-g) $^2$ . This is wrong. Just as there are one million square millimeters in a square meter, there are one million square milli-g in a square g. If all computations are performed in milli-g rather than in units of g multiplied by a power of 10, the units are more straightforward and confusion is less likely to occur.

#### **ASSESSING TREMOR WITH A DISPLACEMENT TRANSDUCER**

An example of assessing tremor with a displacement transducer will be presented to illustrate the application of some of the above techniques.

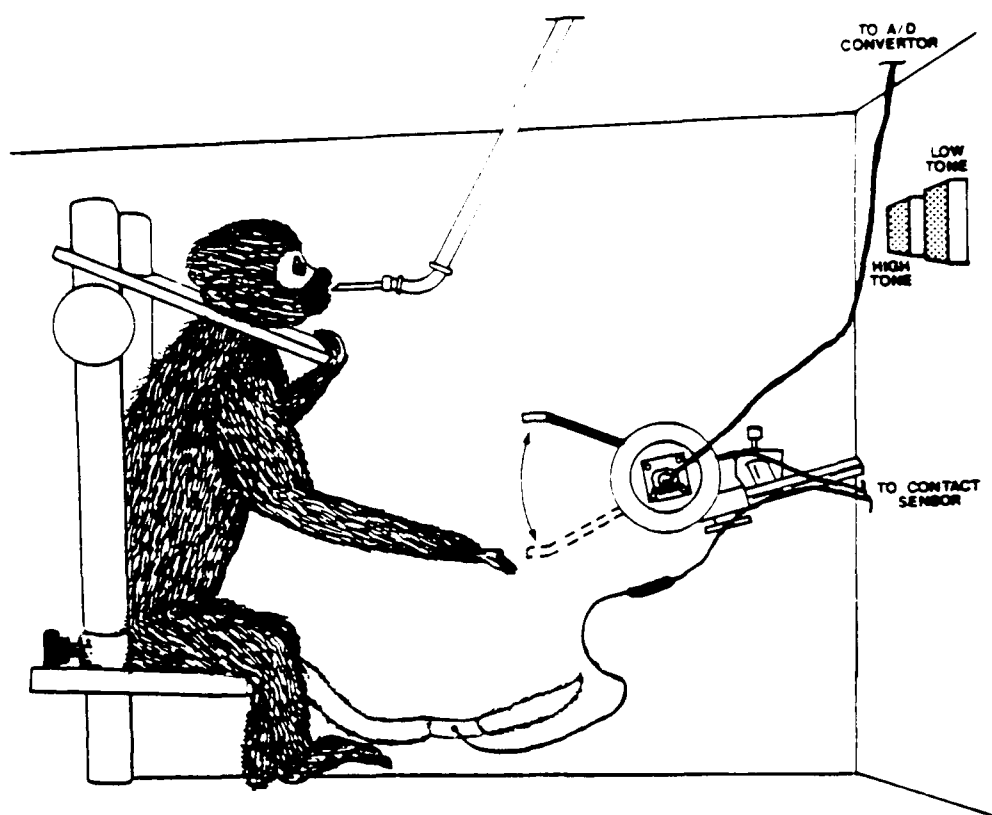
##### ***Transducer***

Figure 3 illustrates a displacement device used in studies of the pharmacology and toxicology of motor function in squirrel monkeys. It was designed to detect the hallmark characteristics of Parkinson's disease: tremor, bradykinesia, and rigidity. An additional advantage is that training squirrel monkeys to manipulate this device is relatively easy. Squirrel monkeys grab anything that is placed within arm's reach. After training the animals to drink from the spout, it was only necessary to place the lever in front of them, and they grabbed it immediately.

The lever is attached to a rotary variable differential transformer (RVDT). The mechanical properties of the bar are excellent. The bar, counterweight, and insulation has a mass of only 1.3 grams. It is sensitive to a wide range of frequencies, from 0 Hz to well over 100 Hz. When tapped, it resonates at less about 0.5 Hz and, slightly, at a frequency much greater than 100 Hz, values that are well outside of the frequency bands of interest in detecting tremor.

##### ***Signal processing***

Figure 4 illustrates how data from the RVDT was used to assess tremor induced by oxotremorine. The doses presented were selected because of the different spectral profiles that they produced.



**Figure 3.** An illustration of a squirrel monkey and the response bar. The bar is insulated everywhere except on the handle to restrict the response topography. A contact sensor attached to the monkey's tail and the bar registers when the bar is gripped. Bar position is digitally converted and stored for later analysis. When the bar is held in range a low-frequency tone sounds. Every completed response results in a high-frequency tone burst and, on a random-ratio 2 schedule of reinforcement, a squirt of fruit juice.

To remove higher frequencies that can induce a low-frequency alias, bar position was analog-filtered (low-pass beginning at 50 Hz) before sampling at 100 Hz, a rate that accurately samples frequencies of 0 to 50 Hz and at which 60-Hz contamination takes a 40-Hz alias. The data were then digitally filtered from 25 Hz and higher and subsequently down-sampled to a 50-Hz sampling rate (by using only every other point). These tactics removed frequencies above 25 Hz and allowed adequate description of frequencies of 0 to 25 Hz.

Row 1 contains the position signal as is seen from the RVDT. Slow undulations are most clearly visible in this representation, while rapid changes in position are barely visible because they correspond to such small displacements. Row 2 shows the first derivative, or velocity. Undulations are still visible but rapid changes in position are clearer. Row 3 shows the second derivative, or acceleration. This signal resembles what an accelerometer would produce and the units correspond to those sometimes used in the investigation of tremor.

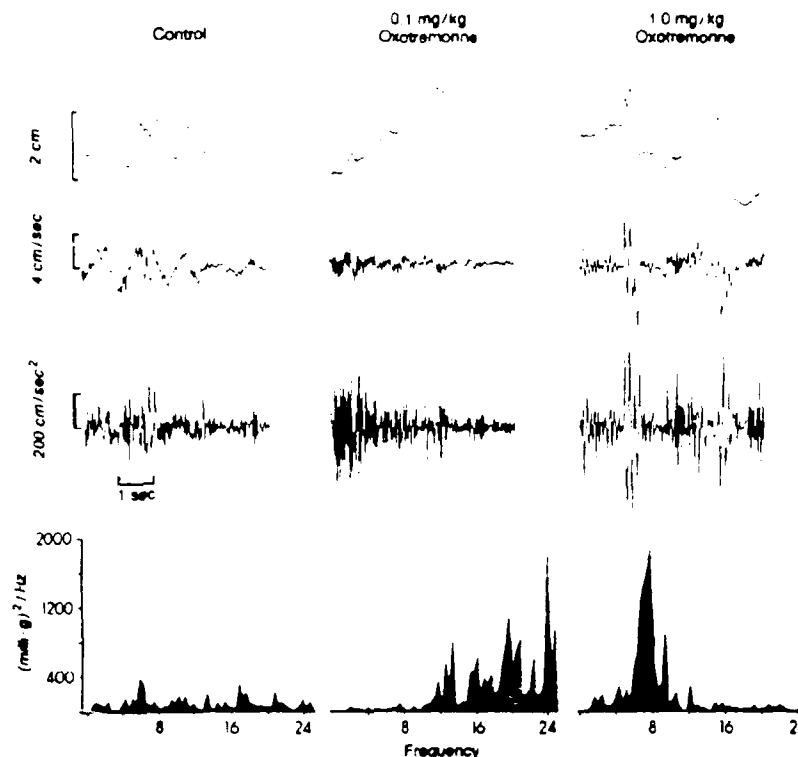


Figure 4. Representative signals taken from a squirrel monkey using the displacement transducer illustrated in Figure 3. Each column contains data from a different dosing condition. The first row shows displacement of the bar through the 5.12-sec sampling interval. The second row shows the first derivative (velocity) of row 1 and the third shows the second derivative of row 1 in units of acceleration. The bottom row is the power spectrum of the acceleration signal in row 3. 0.1 mg/kg of oxotremorine elevated power in the higher frequencies and reduced power at lower frequencies. 1.0 mg/kg resulted in a single, pronounced mode at about 6 Hz.

Row 4 shows the Fourier transform of the signal in row 3. During control sessions there was not much tremor but two peaks seem to be present. At the lowest dose of oxotremorine, a broadband, high-frequency tremor is visible and at the highest dose of oxotremorine a pronounced peak appeared at about 7 Hz.

### Drug effects

To compare the effects of oxotremorine and ethanol, ensemble averages of control and drug sessions were computed. Thus, individual spectra from all control sessions (one such spectrum is displayed in row 4 of column 1 of Figure 4) were transformed and averaged together to produce an estimate of the control profile for that subject. This was repeated for all spectra collected under similar dosing conditions. Confidence intervals were calculated from the standard error of this average. The combined spectrum from a drug condition was compared with the control spectrum for that subject in two steps to assess drug effects, and an overall chi-square test was performed on the two spectra to determine if they differed [24,25]. If they differed, individual frequencies were

compared by determining if their 95% confidence intervals overlapped. Finally, for graphical presentation the spectra were converted back to the original units by taking the antilog at each frequency.

Two drugs that affect tremor in different directions have been assessed with this device (Figure 5). While this was partly a validation exercise, it also provided some basic, and previously unquantitative, data bearing on the effects of these substances on tremor. A dose of 0.56 mg/kg (i.m.) of oxotremorine increased tremor, particularly in the 8-10 Hz band. Ethanol reduces tremor when administered acutely although spectral data describing this effect have not been published. In Figure 5 it is clear that ethanol produced a uniform reduction in the whole spectrum at 1 gram/kg.

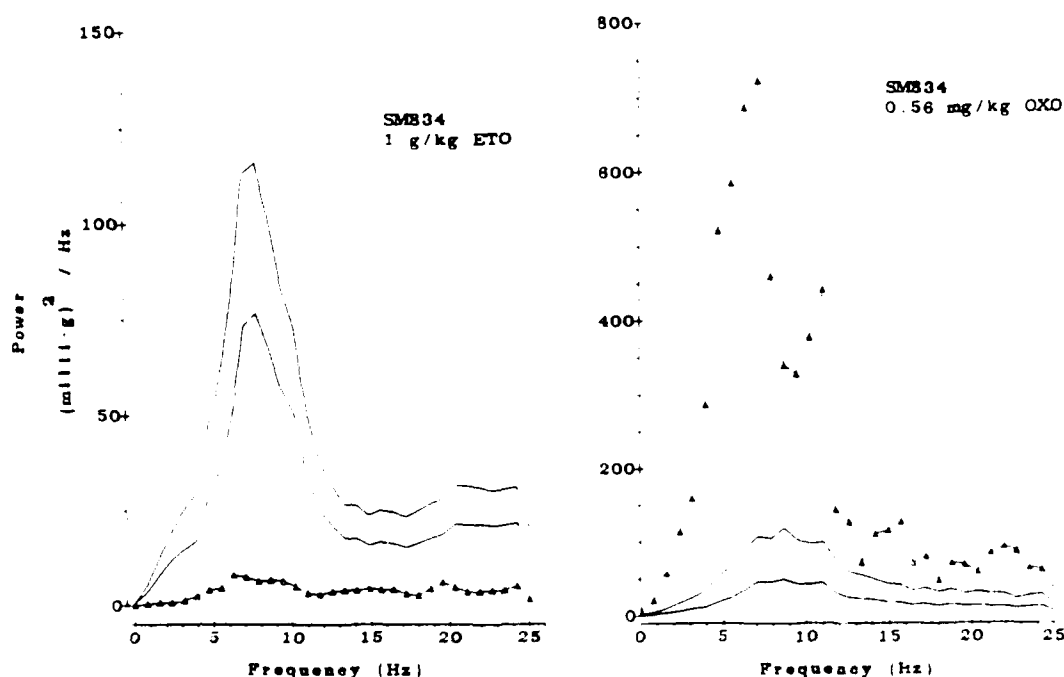


Figure 5. Power spectra from squirrel monkey SM834 after 1 gram/kg of ethanol (p.o.) or 0.56 mg/kg (i.m.) of oxotremorine. In each panel, the mean spectrum from the drug condition (triangles) is compared with upper and lower 95% confidence intervals (lines) of spectra taken from days preceding drug administration. Filled symbols indicate points that are significantly different from control. Note the change of scale on the ordinates. The control sessions for the oxotremorine and ethanol curves were taken from sessions separated by about one year but the profile and magnitude almost match.

Figure 6 shows time records and power spectra from a human with noticeable caffeine-induced tremor using the RVDT and an accelerometer. The major peak in both spectra is at precisely the same location and has the same magnitude. There is more power in the spectrum taken from the RVDT, probably due to noise introduced by differentiating the displacement signal and, in part, because this device seems to support more movement than the accelerometer.

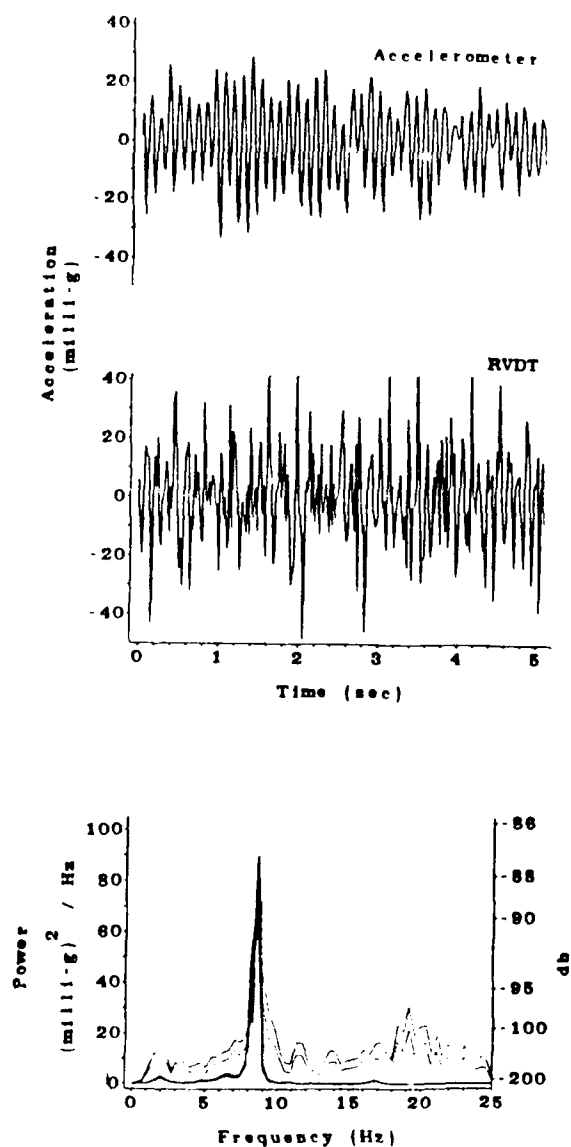


Figure 6. Hold-time distributions (at 2" resolution) after 0.56 mg/kg (i.m.) of oxotremorine and 1.0 gram/kg of ethanol (p.o.) (triangles) compared with 95% confidence intervals from control sessions (dotted lines). Both drugs increased the proportion of short-holds (less than 2" in length) and other subcriterion holds while decreasing the proportion of holds that met the reinforcement criterion of 8 sec.

#### DISCRIMINATIVE MOTOR FUNCTION

Other complaints described by Anger [4], like incoordination and performance changes, may fall under the category of discriminative motor function. Less attention will be devoted to this topic since a superb and recent paper [30] reviews experimental procedures that provide precise quantification of drug effects on multiple biophysical parameters of motor function. In these experiments, a rat or monkey is trained to press on a load cell for a reinforcer [44,45]. In some

experiments, the animal is trained to press and release in a manner analogous to lever pressing, except that there is little displacement and only changes in applied force. In other experiments, the animal is trained to maintain an appropriate level of force within a band for a specified period of time. The accuracy of this performance is sensitive to a variety of drugs. Application of multivariate techniques have revealed distinctions among major drug classes, such as neuroleptics, barbiturates, and benzodiazepines [46]. This literature confirms that the effects of xenobiotics depend critically upon the reinforcement contingencies maintaining response. Part of the reason for this dependency must lie in the different response topographies selected by the reinforcement contingencies.

The approach described in Fowler's review [30] has direct application in neurotoxicology. The squirrel monkey experiments described above represent one such application with the important difference that the transducer measures displacement, not force. These experiments were designed to assess simultaneously multiple aspects of motor function, including tremor. Indeed, the principal design consideration was the ability to assess positioning accuracy and smoothness of movement.

Figure 7 presents representative data describing the effects of ethanol and oxotremorine on response duration. Duration was part of the reinforcement contingency; the animals had to hold the bar for 8 sec to obtain a reinforcer. Despite the dramatic differences in the drugs' effect on tremor (Figure 5), their effects on bar-holding were similar. At the same dose that substantially altered tremor, both drugs increased the number of short-duration holds, both in the very short category (less than 2 sec) and in the sub-criterion category (between 2 and 8 sec).

Figure 7 is presented to demonstrate that investigating several endpoints enables meaningful comparisons to be made quite directly. Specific and nonspecific effects of substances can be isolated in such experiments. Hence, these designs make efficient use of precious species such as primates. While some training is required to achieve these endpoints, the payoff in specificity and sensitivity is great.

## SUMMARY

Motor aspects of behavior can be quantified and the effort is worthwhile. Quantifying tremor provides spectral information that facilitates comparisons among different exposure conditions or with known compounds, as well as clues about mechanisms. Quantification of other response measures such as response topography and pattern provides valuable information about subtle effects of substances at doses below which overt signs begin to appear. By including different schedules of reinforcement in the experimental design, different response topographies appear in behavior and these differences can be exploited to examine different effects of chemical exposure

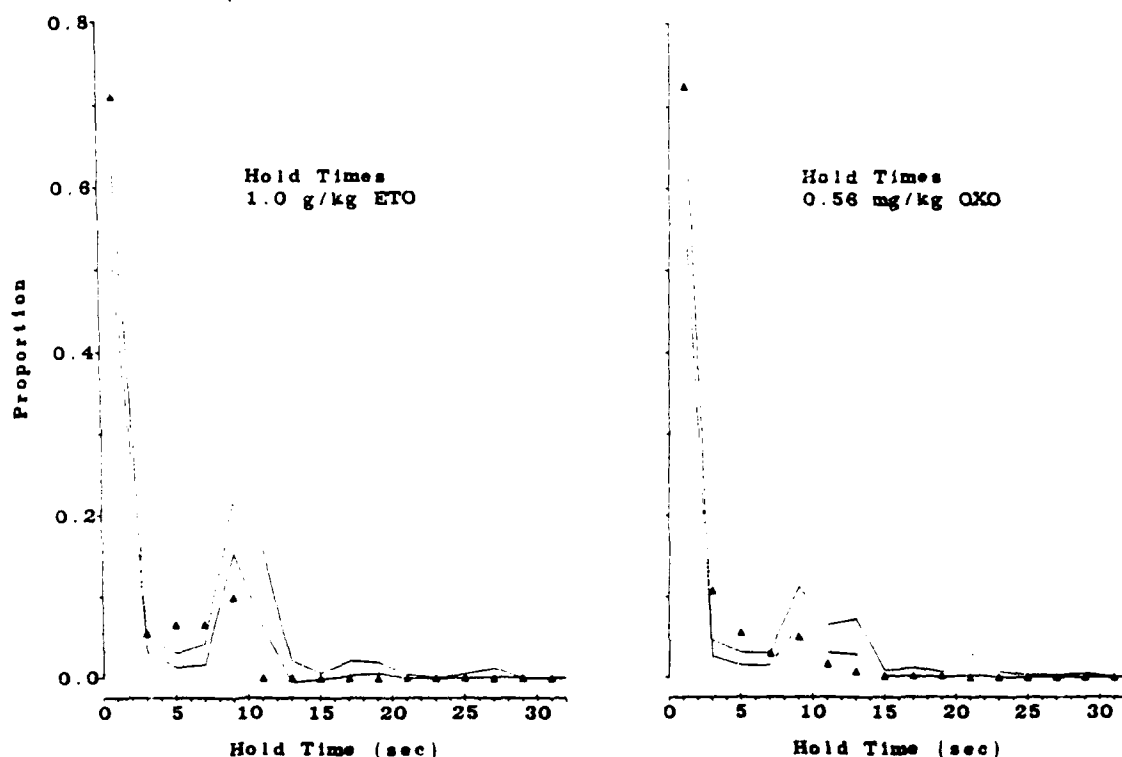


Figure 7. Hold-time distributions (at 2" resolution) after 0.56 mg/kg (i.m.) of oxotremorine and 1.0 gram/kg of ethanol (p.o.) (triangles) compared with 95% confidence intervals from control sessions (dotted lines). Both drugs increased the proportion of short-holds (less than 2" in length) and other subcriterion holds while decreasing the proportion of holds that met the reinforcement criterion of 8 sec.

#### ACKNOWLEDGMENTS

Special thanks to Rhea Eskew and William Stine for many helpful comments on an earlier version of the manuscript and to Bernard Weiss for encouragement and support. The paper was written while the author was at the Environmental Health Sciences Center, in the University of Rochester School of Medicine and Dentistry. Supported by AA05188, ES01247, ES01248 to the University of Rochester.

#### REFERENCES

- 1 DiVencenzo, G.D., Hamilton, M.L., Kaplan, C.J., and Dedinas, J. (1980) Characterization of the metabolites of methyl *n*-butyl ketone. In: P.S. Spencer and H.H. Schaumburg (Eds.), *Experimental and Clinical Neurotoxicology*. Williams and Wilkins, Baltimore, pp. 846-855.
- 2 Spencer, P.S., Couri, D., and Schaumburg, H.H. (1980) *n*-Hexane and methyl *n*-butyl ketone. In: P.S. Spencer and H.H. Schaumburg (Eds.), *Experimental and Clinical Neurotoxicology*. Williams and Wilkins, Baltimore, pp. 456-475.
- 3 Taylor, J.R., Selhorst, J.B., and Calabrese, V.P. (1980) Chlordecone. In: P.S. Spencer and H.H. Schaumburg (Eds.), *Experimental and Clinical Neurotoxicology*. Williams and Wilkins, Baltimore, pp. 407-421.

- 4 Anger, W.K. (1984) Neurobehavioral testing of chemicals: impact on recommended standards. *Neurobehav. Toxicol. Teratol.* 6, 147-153.
- 5 Anger, W.K. (1985) Neurobehavioral tests used in NIOSH supported worksite studies, 1973-1983. *Neurobehav. Toxicol. Teratol.* 7, 359-368.
- 6 Bleeker, M.L. (1984) Clinical neurotoxicology: Detection of neurobehavioral and neurological impairments occurring in the workplace and the environment. *Arch. Env. Health* 39, 213-217.
- 7 Fawer, R.F., De Ribaupierre, Y., Guillemin, M.P., Berode, M., and Lob, M. (1983) Measurement of hand tremor induced by industrial exposure to metallic mercury. *Brit. J. Ind. Med.* 40, 204-208.
- 8 Roels, H., Malchaire, J., Van Wambeke, J.P., and Buchet, J.P. (1983) Development of a quantitative test for hand tremor measurement. *J. Occupational Health* 25, 481-487.
- 9 Roels, H., Lauwerys, R., Buchet, J.P., Genet, P., Sarhan, M.J., Hanotiau, I., de Fays, M., and Bernard, A. (1987) Epidemiological survey among workers exposed to manganese: Effects on lung, central nervous system, and some biological indices. *Am. J. Ind. Med.* 11, 307-327.
- 10 Pryor, G.T., Uyeno, E.T., Tilson, H.A., Mitchell, C.L. (1983) Assessment of chemicals using a battery of neurobehavioral tests: a comparative study. *Neurobehav. Toxicol. Teratol.* 5, 91-117.
- 11 Tilson, H.A., Mitchell, C.L., and Cabe, P.A. (1979) Screening for neurobehavioral toxicity: The need for and examples of validation of testing procedures. *Neurobehav. Toxicol. Teratol.* 1, 137-148.
- 12 Tilson, H.A., Cabe, P.A., and Burne, T.A. (1980) Behavioral procedures for the assessment of neurotoxicity. In: P.S. Spencer and H.H. Schaumburg (Eds.), *Experimental and Clinical Neurotoxicology*. Williams and Wilkins, Baltimore, pp. 758-766.
- 13 Ballard, P.A., Tetrad, J.W., and Langston, J.W. (1985) Permanent human Parkinsonism due to 1-methyl-4-phenyl-1,2,3,6-tetrahydropyridine (MPTP). *Neurology* 35, 949-956.
- 14 Langston, J.W., Ballard, P., Tetrad, J.W., and Irwin, I. (1983) Chronic Parkinsonism in humans due to a produce of meperidine-analog synthesis. *Science* 219, 979-980.
- 15 Findley, L.J. and Capildeo, R. (1984) *Movement Disorders: Tremor*. Oxford University Press, New York.
- 16 Gresty, M.A. and Findley, L.J. (1984) Definition, analysis and genesis of tremor. In: L.J. Findley and R. Capildeo (Eds.), *Movement Disorders: Tremor*. Oxford University Press, New York, pp. 15-26.
- 17 Rondot, P., Jedynak, C.P., and Ferrey, G. (1978) Pathological tremors: nosological correlates. In: J.E. Desmedt (Ed.), *Physiological Tremor, Pathological Tremors, and Clonus*. S. Karger, New York.
- 18 Wood, R.W., Weiss, A.B., and Weiss, B. (1973) Hand tremor induced by industrial exposure to mercury. *Arch. Environ. Health.* 26, 249-252.

- 19 Freund, H.J., Hefter, H., Homberg, V., and Reiners, K. (1984) Differential diagnosis of motor disorders by tremor analysis. In: L.J. Findley and R. Capildeo (Eds.), *Movement Disorders: Tremor*. Oxford University Press, New York, pp. 27-36.
- 20 Langolf, G.D., Chaffin, D.B., Henderson, R., and Whittle, H.P. (1978) Evaluation of workers exposed to elemental mercury using quantitative tests of tremor and neuromuscular functions. *Am. Ind. Hyg. Assoc. J.* 39, 976-984.
- 21 Cooley, J.W. and Tukey, J.W. (1965) An algorithm for the machine calculation of complex Fourier series. *Mathematics of Computation* 19, 297.
- 22 Cheng, D.K. (1959) *Analysis of Linear Systems*. Addison-Wesley, Reading, MA.
- 23 Jenkins, G.M. and Watts, D.G. (1968) *Spectral Analysis and its Applications*. Holden-Day, San Francisco.
- 24 Bendat, J.S. and Piersol, A.G. (1971) *Random Data: Analysis and Measurement Procedures*. Wiley-Interscience, New York.
- 25 Bendat, J.S. and Piersol, A.G. (1986) *Random Data: Analysis and Measurement Procedures*. Wiley-Interscience, New York.
- 26 Otnes, R.K. and Enochson, L. (1972) *Digital Time Series Analysis*. John Wiley and Sons, New York.
- 27 Harris, F.J. (1978) On the use of windows for harmonic analysis with the discrete Fourier transform. *Proceedings of the IEEE* 66, 51-83.
- 28 Nuttall, A.H. (1981) Some windows with very good sidelobe behavior. *IEEE Transactions on Acoustics, Speech, and Signal Processing*. ASSP- 29, 84-91.
- 29 Ko, W.H. (1986) Solid-state physical transducers for biomedical research. *IEEE Transactions on Biomedical Engineering*. BME-33, 153-162.
- 30 Fowler, S.C. (1987) Force and duration of operant response and dependent variables in behavioral pharmacology. In: T. Thompson and P.B. Dews (Eds.), *Advances in Behavioral Pharmacology*. Erlbaum, New York.
- 31 Fowler, S.C., Morgenstern, C., and Notterman, J.M. (1972) Spectral analysis of variations in force during a bar-pressing time discrimination. *Science* 176, 1126-1127.
- 32 Gerhart, J.M., Hong, J.S., and Tilson, H.A. (1983) Studies on the possible sites of chlordecone-induced tremor in rats. *Toxicol. Appl. Pharmacol.* 70, 382-389.
- 33 Gerhart, J.M., Hong, J.S., Uphouse, L.L., and Tilson, H.A. (1982) Chlordecone-induced tremor: Quantification and pharmacological analysis. *Toxicol. Appl. Pharmacol.* 66, 234-243.
- 34 Herr, D.W., Hong, J.S., Tilson, H.A. (1985) DDT-Induced tremor in rats: Effects of pharmacological agents. *Psychopharmacology* 86, 426-431.
- 35 Lehtinen, M.S. and Gothoni, P.R. (1985) A system for measuring tremor intensity in rats. *IEEE Transactions on Biomedical Engineering* 8, BME-32.

- 36 Albers, J.W., Potvin, A.R., Tourtellotte, W.W., Pew, R.W., and Striobey, K.F. (1973) Quantification of hand tremor in the clinical neurological examination. *IEEE Transactions on Biomedical Engineering*. BME-20, 27-37.
- 37 Sutton, G.G. and Sykes, K. (1967) The variation of hand tremor with force in healthy subjects. *J. Physiol.* 191, 699-711.
- 38 Marsden, C.D., Meadows, J.C., Lange, G.W., and Watson, R.S. (1969) Variations in human physiological finger tremor, with particular reference to changes with age. *Electroenceph. Clin. Neurophysiol.* 27, 169-178.
- 39 Marsden, C.D., Meadows, J.C., Lange, G.W., and Watson, R.S. (1969) The role of ballistocardiac impulse in the genesis of physiological tremor. *Brain* 92, 647-662.
- 40 Marsden, C.D., Meadows, J.C., Lange, G.W., and Watson, R.S. (1969) The relation between physiological tremor of the two hands in healthy subjects. *Electroenceph. Clin. Neurophysiol.* 27, 179-185.
- 41 Cleeves, L. and Findley, L.J. (1987) Variability on amplitude of untreated essential tremor. *Neurol. Neurosurg. Psychiatry* 50, 704-708.
- 42 Wade, P., Gresty, M.A., and Findley, L.J. (1982) A normative study of postural tremor of the hand. *Arch. Neurol.* 39, 358-362.
- 43 Homberg, V., Heftner, H., Reiners, K., and Freund, H.J. (1987) Differential effects of changes in mechanical limb properties on physiological and pathological tremor. *J. Neurol. Neurosurg. Psychiatry* 50, 568-579.
- 44 Ando, K., Johanson, C.E., Seiden, L.S., and Schuster, C.R. (1985) Sensitive changes to dopaminergic agents in fine motor control of rhesus monkeys after repeated methamphetamine administration. *Pharmacol. Biochem. Behav.* 22, 737-743.
- 45 Johanson, C.E., Aigner, T.G., Seiden, L.S., and Schuster, C.R. (1979) The effects of methamphetamine on fine motor control in rhesus monkeys. *Pharmacol. Biochem. Behav.* 11, 273-278.
- 46 Walker, C.H., Faustman, W.O., Fowler, S.C., and Kazar, D.B. (1981) A multivariate analysis of some operant variables used in behavioral pharmacology. *Psychopharmacology* 74, 182-186.
- 47 Randall, J.E. and Stiles, R.N. (1963) Power spectral analysis of finger acceleration tremor. *J. Appl. Physiol.* 19, 357-360.
- 48 Wyatt, R.H. (1968) A study of power spectra analysis of normal finger tremors. *IEEE Transactions on Bio-Medical Engineering*. BME-15, 33-45.
- 49 Pozos, R.S., Iazzo, P.A., and Petry, R.W. (1982) Physiological action tremor of the ankle. *J. Appl. Physiol.* 52, 226-230.
- 50 Newland, M.C. and Weiss, B. (1986) Effects of oxotremorine on tremor and operant behavior in squirrel monkeys. *The Toxicologist* 6, 215.
- 51 Tang, A.H. and Alway, C.D. (1969) An improved method for recording static tremors in monkeys. *J. Appl. Physiol.* 27, 561-563.

- 52 Remington, G. and Anisman, H. (1976) A simple method for quantifying tremor in rodents. *Pharmacol. Biochem. Behav.* 4, 721-732.
- 53 Isokawa, M. and Komisaruk, B.R. (1985) Tuning the power spectrum of physiological finger tremor frequency with flickering light. *J. Neurosci. Res.* 14, 373-380.
- 54 Fox, J.R. and Randall, J.E. (1970) Relationship between forearm tremor and the biceps electromyogram. *J. Appl. Physiol.* 29, 103-108.

# QUANTITATIVE SENSORY ASSESSMENT IN TOXICOLOGY AND OCCUPATIONAL MEDICINE: APPLICATIONS, THEORY, AND CRITICAL APPRAISAL

Jacques P. J. Maurissen

*The Dow Chemical Company, Mammalian and Environmental Toxicology Research Laboratory,  
Midland, MI*

## SUMMARY

Sensory systems are affected by a number of chemicals. Their functions can be quantitatively assessed with psychophysical methods. Psychophysics is the scientific study of the relationship between the physical dimension(s) of a stimulus and the behavioral response it generates. First, the unique contribution of psychophysics to toxicology is illustrated with a few examples taken from the fields of audition, vision, and somatosensory sensitivity. Then, a brief survey of the evolution of psychophysics is presented and followed by a review of its basic scientific foundations. Psychophysical evaluation is accomplished by delivering quantified stimuli in a prespecified order and by requesting a standardized response from the subject. Psychophysical methods specify the sequence of presentation of stimuli, and include the method of limits, the method of constant stimuli, as well as the adjustment and tracking methods. The response paradigms specify the standardized response the subject has to make to stimuli presented according to a specific format. The three major response paradigms are the yes-no, forced-choice, and rating paradigms. Sensory processes can be studied in humans as well as in animals by several techniques, such as classical conditioning, operant behavior, and reflex modulation.

A critical review of the application of psychophysical methods and response paradigms is developed. Several examples illustrate the potential confusion brought about by unorthodox use of psychophysical terminology and methodology. Finally, a few suggestions are given for the evaluation of sensory processes in humans.

## INTRODUCTION

Sensory systems provide the interface between the living organism and the external milieu, and represent targets of pathological processes affecting the nervous system in animals and humans. Endogenous diseases as well as exogenous events (physical or chemical) can alter the structure and function of sensory receptors, afferent pathways, and primary projection areas in the brain. It is important to evaluate the integrity of sensory systems from a functional point of view. Solely relying on a morphological approach presents some inherent problems. A morphopathological evaluation is destructive and does not usually lend itself to repeated measures in the same organism. Sophisticated morphological techniques (e.g., electron microscopy) can also generate data difficult to interpret.

Perturbation of sensory functions may not be detected by simple clinical observation. More elaborate techniques are necessary. In this context, psychophysics provides exquisite and robust tools to quantify sensory functions in animals and humans.

The intent of this paper is fourfold.

1. Illustrate the contribution of psychophysical (i.e., sensory) studies to toxicology with a few examples.
2. Recount briefly the salient events forging the history of psychophysics and define its scope.
3. Acquaint the reader with the (often misunderstood) methods, paradigms, and techniques for the assessment of sensory functions in humans and animals.
4. Evaluate critically the methodology used in human sensory studies as applied to toxicology and occupational medicine.

#### **NEUROTOXICANTS AND SENSORY FUNCTIONS: SELECTED EXAMPLES**

A large number of chemicals affect sensory organs and functions [1,2,3]. Some overviews have focused more specifically on the psychophysical approach to chemically induced auditory [4], visual [5], somatosensory [6,7], and olfactory disorders [8]. The intent of this section is not to review this literature exhaustively, but to show some examples of the unique contributions of psychophysics to toxicology.

##### ***Audition***

The ototoxic effects of toluene were unknown until Pryor et al. described them in 1983 [9]. The authors exposed rats to 1400 and 1200 ppm of toluene, 14 h/day, 7 days/week for 5 weeks. Rats were trained to avoid an electrical shock delivered to the floor by climbing a pole suspended from the ceiling of the cage. The aversive stimulus was preceded by a tone. Climbing the pole during this warning tone terminated the trial and reflected detection of the auditory stimulus. Both intensity and frequency of the tone were varied. Comparison of the conditioned avoidance performance of the control and exposed groups revealed that toluene impaired hearing markedly at 12, 16, and 20 kHz, and slightly at 8 kHz. No difference in hearing was found between control and exposed rats at 4 kHz.

These data showed for the first time that toluene preferentially affected hearing at higher frequencies in the rat, and left the low frequencies practically untouched. Subsequently, electrophysiological techniques revealed that the latency of the eighth nerve component of the brainstem auditory-evoked response was prolonged in toluene-exposed rats at high frequencies in comparison to control animals [10].

### ***Vision***

The effects of acrylamide on visual functions were first described by Merigan et al. [11]. Macaque monkeys faced two oscilloscopes with evenly illuminated displays. One of two types of stimuli appeared randomly on either scope, while the other scope was blank: A fine grating or a flickering unpatterned stimulus was used to measure visual acuity or flicker fusion, respectively. In both cases, the monkeys received some fruit juice after pressing the button corresponding to the scope presenting the stimulus.

Four monkeys were trained in both visual modalities. Three of them were administered oral doses of acrylamide (10 mg/kg/day, 5 days a week) until they showed overt signs of intoxication. Each monkey was used as its own control, and one served as a time-matched control. By the end of dosing (7 to 9 weeks after the first dose), visual acuity and flicker fusion were reduced in dosed monkeys. After termination of dosing, flicker fusion recovered quickly and completely. Visual acuity substantially improved, but had not completely recovered by 19 to 20 weeks after the end of dosing.

Morphological examination of a monkey euthanized at the end of the dosing period indicated that the described loss of function was accompanied by distal axonal swelling in the optic tract and lateral geniculate nucleus [12,13].

### ***Somatosensory sensitivity***

Acrylamide causes central-peripheral distal axonopathy. Since sensory signs and symptoms usually dominate the clinical manifestations of intoxication with this chemical, Maurissen et al. [14] developed a system to assess quantitatively the effects of acrylamide on vibration and electrical sensitivity in monkeys, and to follow the functional recovery after cessation of intoxication.

Six monkeys were trained to report detection of a vibratory or electrical stimulus applied to the fingertip. After baseline data were obtained, four monkeys were dosed orally with 10 mg/kg of acrylamide 5 days/week until the appearance of overt toxic signs. Each monkey served as its own control. The other two monkeys were used as time-matched controls. Fine visuomotor coordination and body weights diminished during dosing, but had recovered within 5 to 8 weeks. Vibration sensitivity also decreased during the same period, but remained impaired much longer, outlasting all the other effects. Electrical sensitivity had been unaffected during the whole study. These data indicate that vibration sensitivity can trace the time course of acrylamide intoxication, and they provide unique information on the clinical status of the peripheral nervous system that could not be inferred from the other observations made here.

Morphological analysis of sural nerve biopsies in two exposed monkeys revealed that the extent of the damage considerably differed between the 2 animals (25% of nerve fibers vs. an

occasional nerve fiber affected), while their sensitivity to vibration was reduced in a comparable manner. These data emphasize the importance and complementarity of a functional approach to sensory analysis. In this study, a morphological approach alone could have given a distorted conception of the clinical status of the subject.

### **BRIEF HISTORICAL SURVEY**

The study of sense organs evolved from developments occurring mainly in the field of physiology during the 19th century. In the early 1800s, special attention began to focus on the peripheral nervous system and the sense organs. Theodore Schwann, from the University of Liège, discovered the myelin sheath [15]. Bell [16] demonstrated that the anterior root of the spinal cord was motor in function, while Magendie [17] described the sensory function of the posterior roots.

The formulation of the doctrine of specific energies, which states that a given nerve generates only one type of sensation, gave an impetus to sensory physiology during the 19th century [18]. Ernst Heinrich Weber (1795-1878), professor of anatomy and physiology in Leipzig, began the study of the innervation of the skin and special sense organs in humans, and investigated two-point discrimination, as well as perception of weight and temperature [19,20]. But it was Gustav Theodor Fechner (1801-1887) who really formalized the study of sense organs in his "Elemente der Psychophysik" in 1860 [21]. In this book, he also described psychophysical methods still in use today.

More recently, signal detection theory elaborated a theoretical framework that directly benefited psychophysics. It was developed in the 1950s by engineers who drew upon statistical decision theory and electronic communications. Signal detection theory provides a means of analyzing detection problems. It has broadened the scope of the psychophysical approach [22], and its major contribution has been to isolate the system's intrinsic discriminative capabilities from factors affecting the translation of these discriminations into decisions. In other words, it has allowed the experimenter to tease apart true sensory events from nonsensory events that can significantly contaminate the results of sensory testing. Signal detection theory has distinguished between three main experimental situations in which detection tasks can be performed (yes-no, forced-choice, and rating paradigms). These paradigms will be described later.

### **OBJECT OF PSYCHOPHYSICS: MEASURING THE "UNMEASURABLE"**

Psychophysics is the scientific study of the relationship between a physical dimension of a stimulus and the behavioral response it generates. To describe the psychological aspect of the word "psychophysics," the term "behavioral response" is used here instead of "sensation" to avoid introspectionistic and mental dimensions, which hamper the scientific approach. Operational

definitions are indispensable to scientific endeavor. Stevens [23] has best captured the true nature of the psychophysical approach:

"What we can get at in the study of living things are the responses of organisms, not some hyperphysical mental stuff, which, by definition, eludes objective test. Consequently, verifiable statements about sensation become statements about responses – about differential reactions of organisms. ( . . . ) I know nothing about your sensations except what your behavior tells me." (p. 386)

The realm of psychophysics is still commonly misunderstood nowadays, and a recurrent fallacy is that "sensations" can only be studied in humans due to their intimate nature, a mistake made by Claude Bernard himself [24]. It is, however, more surprising to read a similar statement in a more recent publication [25]:

"Resort to animal experimentation instead of man, eliminates one whole area of response, namely, the organoleptic or sensory response . . . ." (pp. 18-19)

Basically, psychophysical evaluation is accomplished by delivering stimuli in a prespecified order (psychophysical methods) and by requesting from the subject (human or nonhuman) a codified response to the stimuli presented according to a specific format (response paradigm).

## **PSYCHOPHYSICAL METHODS**

Psychophysical methods, established by Fechner [21], describe the sequence of presentation of stimuli. Associated with each stimulus is a response probability. The function that relates these two parameters is usually characterized as ogival and is called the psychometric function. More details on psychophysical methods can be found in a number of textbooks [26-30].

### ***Method of limits***

The method of limits consists of an equal number of presentations of ascending and descending stimulus levels. In the descending series, the first stimulus magnitude exceeds the detection level and is decreased until the first report of "no detection" by the observer. In an ascending series, the first stimulus magnitude is situated below the detection threshold and is increased until the first detection response is given (Figure 1). In each series, the midpoint between the last two levels is calculated, and the threshold consists of the average of these midpoints.

Two types of errors have been reported with this method in humans. One is the error of habituation, in which the observer has a tendency to repeat the preceding response, and the other is the error of anticipation, in which the observer prematurely changes the response from "detection" to "no detection" (or vice-versa) in view of the number of stimuli already presented in this series. Starting each series at a different stimulus level is therefore mandatory.

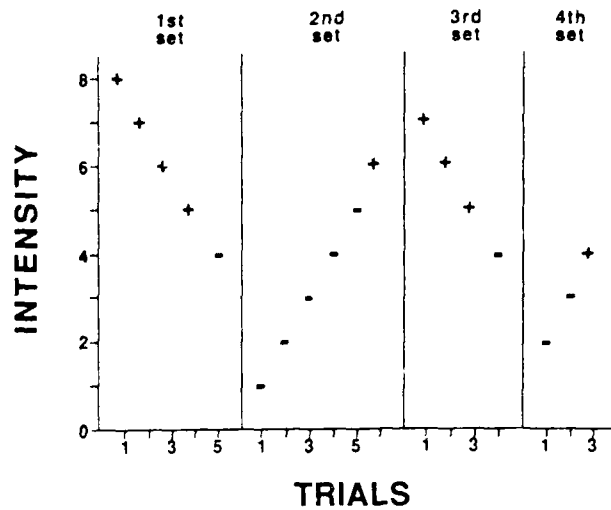


Figure 1. Stimulus sequence in the method of limits. The + sign means "correct response" and the - sign means "incorrect response."

#### Method of constant stimuli

This method obviates some of the errors potentially associated with the method of limits. Stimuli are delivered in a random order to prevent the observer from anticipating the magnitude of the following stimulus. Every stimulus of each set is presented for the same number of times (Figure 2).

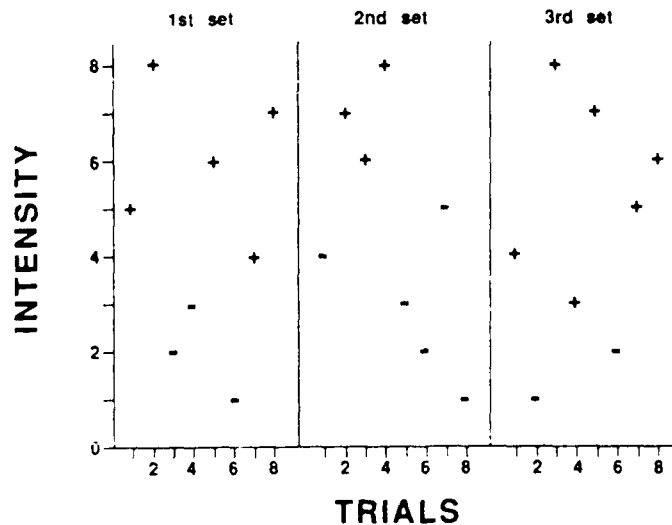


Figure 2. Stimulus sequence in the method of constant stimuli. The + sign means "correct response", and the - sign means "incorrect response."

The percentage of correct responses to each stimulus level is calculated, a psychometric function is derived, and the level corresponding to some predetermined correct response rate represents the threshold. This method, however, has an important disadvantage: Every stimulus level must be tested many times before a threshold can be determined with a reasonable level of accuracy.

### Method of adjustment

The method of adjustment or of average error is a variant of the method of limits. The observer, most often an active participant, has direct control over the attribute of the stimulus under evaluation [31], and is requested to adjust the stimulus level to reach some criterion (e.g., to make the stimulus just detectable). One of the advantages of this method is that it provides a rapid way of obtaining thresholds. This is especially interesting when one is measuring a quickly changing threshold. However, test results can easily be biased by the subject.

### Tracking methods

**Simple up-down rule.** The simple up-down rule is a variation of the method of limits. The order of stimulus presentation depends directly on the subject's performance. If the observer detects the presence of the stimulus, its intensity is decreased at the next trial. If the observer does not detect the stimulus, its intensity is increased at the next trial [32]. Going from a "detection" to a "no detection" (or vice-versa) defines a reversal (Figure 3). With this up-down rule, all the observations are hovering about and converging on the stimulus level that is detected on 50% of the trials. The threshold is an estimate of this stimulus level and is calculated by averaging all the stimulus intensities [33] or the stimulus intensities associated with each reversal [34]. This simple up-down rule has the advantage of maximizing the presentation of stimuli in the neighborhood of the threshold, and typically requires less time than the method of limits or of constant stimuli.

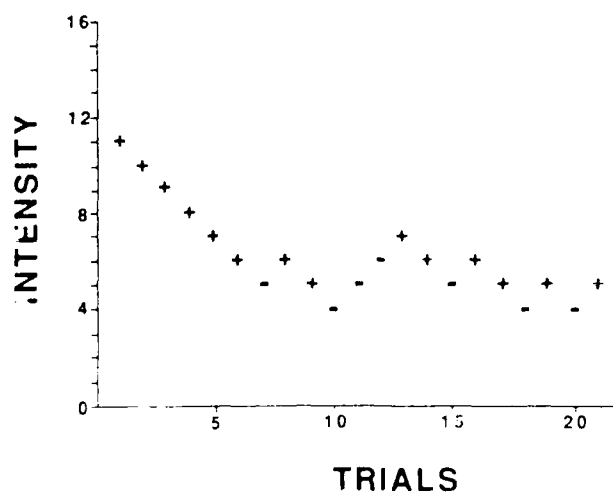


Figure 3. Stimulus sequence in the simple up-down rule: one correct response (+) decreases the stimulus intensity at the next trial, while one incorrect response (-) increases it.

**Up-down transformed rule.** The up-down transformed rule (UDTR) is a generalization of the simple up-down rule, and it aggregates responses around a stimulus level correctly detected in a pre-specified percentage of the trials, usually other than 50%. Figure 4 illustrates an example of a transformed rule. Two consecutive correct responses will decrease the stimulus level at the next trial,

while only one incorrect response is needed to increase the stimulus level at the next trial. Table 1 (panel A) shows that, with this rule, the series of responses will converge from any start point to a stimulus level correctly detected in 70.7% of the cases. The average stimulus level at steady-state represents the threshold. Panels B and C (Table 1) illustrate two additional strategies. More details on these procedures can be obtained from Wetherill and Levitt [34].

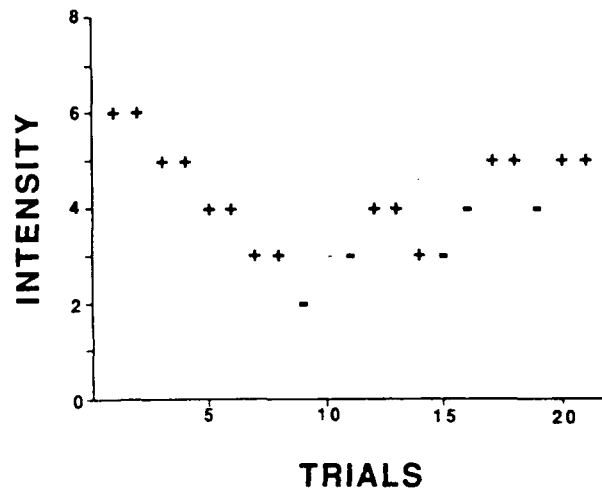


Figure 4. Stimulus sequence in an up-down transformed rule: two correct responses in a row (+ +) drives the intensity down at the next trial, while one incorrect response (-) drives it up.

**Parameter estimation by sequential testing.** The parameter estimation by sequential testing (PEST) method is also a variant of the up-down rule. It automatically determines each stimulus level to obtain information about the location of the threshold as efficiently as possible. Stimulus step size is variable and the testing session ends when a selected criterion has been met, that is, when some predetermined minimum step size has been reached. By the end of the session, the threshold is represented by the last stimulus level tested. Such a technique uses precise rules to determine step size and number of trials needed to calculate a threshold. This method can reduce the total number of trials to achieve some predetermined criterional stability. PEST was developed by Taylor and Creelman [35] and has been revisited on several occasions since [36-41].

TABLE 1. UP-DOWN TRANSFORMED RULES

Up-Down Transformed Rules for Stimulus Sequence	Symbolic Representation	Probability of Changing Level <sup>a</sup>	Condition of Convergence <sup>b</sup>	Probability of Correct Response at Convergence
A 2 consecutive correct responses → decreased level	+ + ↓	$p^2$	$p^2 = 1 - p + p(1 - p)$	$p = 0.707$
1 incorrect response				
→ increased level				
B 3 consecutive correct responses → decreased level	+ + + ↓	$p^3$	$p^3 = 1 - p + p(1 - p) + p^2(1 - p)$	$p = 0.794$
1 incorrect response				
→ increased level				
C 4 consecutive correct responses → decreased level	+ + + + ↓	$p^4$	$p^4 = 1 - p + p(1 - p) + p^2(1 - p) + p^3(1 - p)$	$p = 0.841$
1 incorrect response				
→ increased level				

<sup>a</sup>  $p$  = probability of a correct response<sup>b</sup> The series converges or stabilizes at the level where the sum of the probabilities of a decrease equals the sum of the probabilities of an increase

## RESPONSE PARADIGMS

While psychophysical methods only specify the rules governing a change in stimulus level, response paradigms define the type of response requested from the observer to some signals presented according to a specified format (i.e., one or several stimuli presented in each trial). The three major paradigms will be briefly mentioned here.

### *Yes-no paradigm*

In the yes-no paradigm, the subject has to decide at each presentation whether an observation interval contains a signal (i.e., stimulus) or not ("yes" or "no"). No other response is accepted in the simple detection task. To minimize bias, the number of trials without a signal (also called "catch" or "blank" trials) should approximate the number of trials with a signal ("test" or "stimulus" trials). It is advisable to let the subject know whether the response was correct or not. From these two stimulus and response alternatives (presence/absence vs. "yes"/"no"), one can build a stimulus-response matrix, in which entries in each cell contain conditional probabilities (Figure 5).

		STIMULUS	
		s	n
RESPONSE	S	$P(S s)$ hit	$P(S n)$ false positive
	N	$P(N s)$ miss	$P(N n)$ correct rejection

Figure 5. Stimulus-response matrix in a yes-no paradigm. Actual presence or absence of the signal is denoted by "s" or "n," while "S" and "N" refer to the reported presence or absence of a signal by the observer.

With the yes-no paradigm, the criterion used by the subject to report the presence or the absence of the stimulus can vary widely among observers and even within observers over time. Several factors will affect this criterion. Two of these are the probability of signal presentation (i.e., the proportion of trials with and without a signal), and the payoff matrix, which assigns rewards and penalties associated with right and wrong decisions. These two nonsensory factors are under the direct control of the experimenter and directly manipulate the observer's response. A high probability of stimulus presentation will favor "yes" responses [42], and will result in an increased proportion of false positives ("yes" responses in the absence of a stimulus). As a consequence, it will artificially drive the "threshold" to lower values if no correction is applied. Table 2 illustrates how

false positives can affect sensory thresholds. The raw percentage of "yes" responses is corrected for 3 false positive rates, using a correction described by Blackwell [43]. The thresholds are calculated here by linear interpolation between two points (for the sake of simplicity) and set as the stimulus level corresponding to the 50% detection point. Alternative ways of dealing with false positives have been proposed by the signal detection theory ([22], pp. 86-116).

**TABLE 2. CALCULATION OF THE 50% THRESHOLD IN THE YES-NO PROCEDURE AS A FUNCTION OF FALSE-POSITIVE RATES**

Stimulus Intensity Level	Raw Percentage of "Yes" Responses (Hits)	Percentage of "Yes" Responses Corrected for False Positives (FP) <sup>a</sup>		
		10% FP	20% FP	30% FP
6	100	100	100	100
5	70	67	63	57
4	60	56	50	43
3	40	33	25	14
2	10	0		
1	0			
Intensity Level Corresponding to 50% of "Yes" Responses				
	3.5	3.7	4.0	4.5

<sup>a</sup> Correction according to Blackwell ([43], p 309)

### **Forced-choice paradigm**

In the forced-choice paradigm, the subject is presented with several intervals or alternatives, and has to indicate which one contains the stimulus. If no signal is clearly perceived, guessing is required. Abstaining from making a choice is not allowed. It is recommended that feedback be given to the subject [44]. When two alternatives are used, they may be distributed in the spatial or temporal domains and are referred to as (spatial) two-alternative forced-choice and two-interval forced-choice paradigms, respectively.

In a two-interval forced choice, for example, the signal is presented during the first or the second interval with the same probability. With this paradigm, the point of no detection will necessarily correspond to 50% of correct answers. The threshold is defined as the stimulus level corresponding to some response probability or discriminability, usually to the midpoint of the psychometric function, that is, to the 75% correct response rate for the two-alternative and two-interval forced-choice paradigms [35,38,40,45-55]

### ***Rating paradigm***

This paradigm is a variation of the yes-no paradigm, and is designed for humans. One signal per trial is presented to the observer who is instructed to report, on a several-point scale, the likelihood that the signal or no signal was presented.

### **TECHNIQUES FOR ANIMAL STUDIES**

The basic psychophysical methods and response paradigms developed for a human observer are germane to those designed for lower order animals. Sensory capacities of nonverbal subjects can be assessed by several techniques: classical conditioning, operant behavior, and reflex modulation.

#### ***Classical conditioning***

In 1927, Pavlov published a new method for the investigation of reflexes [56]. By pairing a stimulus that had no observable effects (neutral stimulus), with another stimulus capable of eliciting a response or reflex (unconditioned stimulus), Pavlov was able to induce the same response by presenting the once neutral (now conditioned) stimulus alone. This method of pairing is called classical or Pavlovian conditioning.

This principle underlies the "method of contrast" also developed by Pavlov to differentiate a conditioned stimulus, which was always accompanied by an unconditioned stimulus and a response, from a neighboring neutral stimulus never followed by the unconditional stimulus or response. Differential responding entailed sensory differentiation.

An example of the application of classical conditioning in psychophysics can be seen in Northmore and Muntz [57], who measured the sensitivity of fish to moving and stationary bars of light and to diffuse light. An electrical shock served as the unconditional stimulus. Its effect was to produce a consistent increase in the activity of the fish. By pairing neutral and unconditional stimuli a certain number of times, the neutral (now conditioned) stimulus alone produced the increased swimming activity and was evidence of detection. In a similar manner, Otis et al. [58] induced decreased respiration and heart rates by electrical stimulation in goldfish to assess detection of a change in illumination.

Passe [59] used a classical conditioning technique, called autoshaping, to evaluate the absolute visual sensitivity in pigeons. In this experiment, the pigeons were food-deprived to reach 80% of their free-feeding body weights. A response key was illuminated and followed by grain delivery. After an adequate number of trials, the pigeons reliably pecked the key only when it was illuminated, even though pecking the key was not required for grain delivery. The intensity of the key illumination was varied, and pecking the key when it was illuminated indicated detection of the light.

Hearing also can be studied with classical conditioning techniques. Jamison [60] used ammonia as the unconditional stimulus to decrease heart rate in rats. After pairing a tone with ammonia presentation, the tone alone reduced heart rate. Detection of the stimulus was evidenced by a change in heart rate.

Overall, there are limitations to the classical conditioning approach: total number of trials per day, necessity for reconditioning due to loss of the conditioned reflex, and problem of defining a criterional response change, to name a few.

## **OPERANT BEHAVIOR**

In 1938, Skinner elaborated on Thorndike's "law of effect," systematized an approach to learned motivated behavior, and developed the methods of experimental analysis of behavior [61]. He explained behavior by its consequences: previous consequences model current performance. Because an operant (i.e., any response that modifies the environment) can be placed under the differential control of a stimulus, new possibilities for sensory research emerged. Several procedures have been designed to analyze sensory processes in animals, and they use one or more response manipulanda. The major drawback of this method lies in the training required to place a behavior under stimulus control.

**Go/no-go procedure.** This procedure is the operant version of the yes-no paradigm. The animal is trained to give a response in the presence of a standard stimulus and to withhold it in its absence or in the presence of a comparison stimulus. Terman and Terman [62] used this procedure to evaluate rats' discriminative capabilities for auditory intensity. By pressing a bar, the rats turned on a tone. After the tone, a 3-sec choice interval was presented. Rats received a reward (or reinforcement) if:

1. they pressed the bar during the choice interval following presentation of the tone at standard intensity,
2. they did not press the bar during the choice interval following presentation of a tone at a different intensity.

Aversive stimuli can also control such a behavior. Clack and Herman [63] tested monkeys' auditory thresholds by shock avoidance conditioning and generated data comparable to those obtained with positive reinforcement.

**Forced-choice paradigm.** The forced-choice paradigm also has been used successfully in animal sensory research. Typically, two stimuli are presented. They can be spatially or temporally spaced, and each stimulus is associated with one response manipulandum or one interval

For example, Yager and Thorpe [48] tested color vision in goldfish in the following manner: The fish first swam to the back of the tank, made an observing response by pressing a key that illuminated both choice keys, swam toward the choice keys, and struck one of them. On the average, every third correct response was reinforced. A correction procedure prevented the formation of a position habit.

**Conditioned suppression procedure.** In 1941, Estes and Skinner described the "conditioned emotional response" [64]: When a signal that terminates with a shock is superposed over a steady rate of an operant, it acquires suppressing properties. The suppression is measured by the ratio of the response rates before vs. during the signal and reflects detection of the stimulus. However, it was not until later that this procedure was exploited in psychophysics [65-66].

Using this procedure, Sidman et al. [65] studied hearing and vision in animals. Mice were trained to lick a tube and received a drop of milk after a variable number of licks. This schedule of reinforcement generates a sustained rate of licking sufficiently stable so that the interfering effects of random signals announcing an electrical shock can be evaluated. These warning stimuli have a fixed duration and develop conditioned suppression (i.e., the rate of licking is drastically reduced during the warning stimuli and therefore indicates detection).

Excellent reviews of animal psychophysics can be found in Blough and Blough [67], Stebbins [68], and Blough and Young [69].

### ***Reflex modulation***

Hoffman and Ison [70] defined reflex modulation or reflex modification as:

"... the phenomenon whereby the reflex elicited by one stimulus is modified by the prior presentation, withdrawal, or change of another (usually weaker) stimulus."

As early as 1863, Sechenov showed that stimulation of the frog's brain inhibited reflexes to painful cutaneous stimuli [71]. One of the first applications of reflex modification to sensory analysis goes back to Yerkes [72]. He established that ringing a bell before tapping the frog's head modified the flexor jerk reflex, and concluded that frogs can hear.

More recently, the technique has been refined and applied by several laboratories to assess sensory processes. For example, Young and Fechter [73] investigated animal audiometry and used reflex modulation with the method of constant stimuli. They tested rats and guinea pigs with 115 dBA white noise startle bursts of 20-msec duration. On control trials, the startle-eliciting stimulus was presented alone. On prestimulus trials, a pure-tone stimulus of varying intensity and frequency preceded the startle-eliciting stimulus by 100 msec. For each test session, an average startle amplitude was calculated at each prestimulus intensity and frequency, and expressed as a percentage

of average startle amplitude during control trials. A psychometric function relating relative startle amplitude to prestimulus intensity was generated for each tested frequency. The data calculated for rats and guinea pigs with reflex modulation are comparable to those collected with operant techniques on rats by Kelly and Masterton [74] and on guinea pigs by Prosen et al. [75].

One of the problems of reflex modulation consists in the definition of a response change that can evidence sensory detection. More details on this technique can be found in Hoffman and Ison [70], Ison and Hoffman [76], Hoffman [77], and Fechter and Young [78].

### CRITICAL EVALUATION OF HUMAN PSYCHOPHYSICAL STUDIES

Psychophysics grew roots in the middle of the 19th century, and its methods have been refined, analyzed and criticized since. Overlooking more than 100 years of scientific advancement in psychophysics, as well as neglecting the framework of signal detection theory, have fostered confusion in the application of psychophysical methods in human toxicology and occupational medicine. In the next few paragraphs, this point will be illustrated.

#### **Nonclassical terminology**

It has been implied that the "method of constant stimuli" means that the stimulus is always present, when, in fact, it signifies that discrete, prespecified stimuli are generated randomly, as described earlier:

"Some methods use *constant stimuli* instead of discrete stimulus presentation. In these procedures the stimulus is always present ..." ([79], p. 9)

The forced-choice paradigm also has been erroneously defined as follows:

"In the forced choice method the examinee knows when the stimulus may have been presented, but does not necessarily know it was. In this procedure during a fixed time interval, which is usually defined by a light clue, the observer is required to indicate whether or not the stimulus was present." ([79], p. 8)

This is, in fact, the accepted definition of the yes-no paradigm, which is diametrically opposite to the forced-choice paradigm.

Similarly, giving a choice between two intervals and also allowing the observer to abstain from making a choice has been erroneously referred to as a forced-choice paradigm (in a commercially available operating manual). By definition, abstention is not allowed in a forced-choice situation.

The "method of limits" has been contrasted with the "forced-choice paradigm" although these two pertain to two entirely different domains, as explained above. The former refers to a method of stimulus presentation, and the latter to a response paradigm. The method of limits conceivably can be used in a forced-choice situation. What some authors really meant by "method of

limits" was the "yes-no paradigm" used in conjunction with the method of limits. Such confusion also has been perpetuated in some brochures and operating manuals for commercially available devices.

### ***Nonconventional procedures***

Some authors do not describe the psychophysical method or the response paradigm used in their studies [80]. Sometimes, modified or new methods are adopted for which no or almost no literature exists, or for which no clear rationale is given. For example, Arezzo et al. [81] used the following up-down transformed rule to test sensation: If stimuli are correctly identified on 2 out of 3 trials, the stimulus level is decreased; if errors are made on 2 out of 3 trials, the stimulus level is increased.

Binomial analysis of this strategy and of the simple up-down procedure (Table 3, panels A and B) shows that both rules converge on the exact same stimulus level (i.e., the level corresponding to the 50% correct response rate). Therefore, both procedures give the same estimate, but, by definition, it will take between 2 and 3 times longer to get the same answer with the transformed strategy described above (Table 3, panel B), compared to the simple up-down rule (Table 3, panel A). Advantages of this up-down transformed procedure are elusive.

### ***Unorthodox threshold definition***

Sosenko et al. [82] and Arezzo et al. [81] used the modified up-down rule (described in Table 3, panel B) in conjunction with the two-alternative forced-choice paradigm. They calculated the sensitivity threshold as the stimulus level corresponding to a 50% correct response rate (i.e., chance detection). Such a threshold definition is unusual in a two-alternative forced choice because it corresponds to a stimulus level that cannot be detected by definition. There is no single point on the abscissa of the psychometric function that corresponds to the 50% correct response rate, but rather an infinity of points encompassing all potential levels that the subject could not detect (Figure 6). This criterion would be equivalent to estimating the stimulus level corresponding to 0% detection in a yes-no paradigm.

TABLE 3. UP-DOWN RULES

Up-Down Rules for Stimulus Sequence	Symbolic Representation	Probability of Changing Level <sup>a</sup>	Condition of Convergence <sup>b</sup>	Probability of Correct Response at Convergence
A. correct response				
→ decreased level	+ ↓	p	p = 1-p	p = 0.5
incorrect response				
→ increased level	- ↑	1-p		
B. 2 out of 3 correct responses				
→ decreased level	+ + ↓ + - + ↓ - + + ↓	p <sup>2</sup> p <sup>2</sup> (1-p) p <sup>2</sup> (1-p)	2p <sup>2</sup> (1-p) + p <sup>2</sup> = 2p(1-p) <sup>2</sup> + (1-p) <sup>2</sup>	p = 0.5
2 out of 3 incorrect response				
→ increased level	- - ↑ - + - ↑ + - - ↑	(1-p) <sup>2</sup> p(1-p) <sup>2</sup> p(1-p) <sup>2</sup>	6p <sup>2</sup> - 4p <sup>3</sup> - 1 = 0	

<sup>a</sup> p = probability of a correct response<sup>b</sup> The series converges or stabilizes at the level where the sum of the probabilities of a decreased equals the sum of the probabilities of an increase

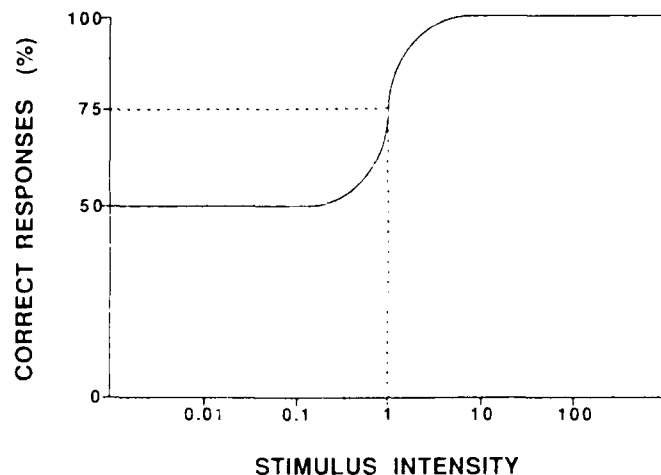


Figure 6. Psychometric function relating detection probability to stimulus intensity in a two-alternative forced-choice paradigm.

A similar approach has already been criticized by Rose et al. [47] who stated:

"... it makes no sense to use the yes-no rule in a forced-choice situation since there is not just one point, but a continuum of stimulus values for which the forced-choice psychometric function has the value of 0.5." (p. 200)

by Kershaw [83] who wrote:

"In a few papers other UDTR rules are used with the 2IFC procedure. (...) It is difficult to see what interpretation can be made of the threshold estimates that they obtain. If the Up-and-Down rule is used in 2IFC experiments, then levels will drift towards low stimulus levels for which there is little or no chance of detecting the stimulus." (p. 36)

by Penner [51] who made the following statement about the forced-choice paradigm:

"Obviously, it is necessary to track stimulus levels for which a unique detection probability exists. Since infinitely many stimulus levels result in 100% and 50% detection, these levels are of no interest as a dependent variable. We cannot compare thresholds obtained in various conditions if these thresholds are not unique. We must restrict our measures to stimulus levels that have a unique detection probability associated with them." (p. 115)

and by Levine and Shefner [52] who wrote about the forced-choice paradigm:

"As 50% is the score expected for an invisible stimulus, it cannot be taken as the threshold." (p. 17)

#### **Limited number of trials**

Care should be taken to use an adequate number of trials to ensure threshold reliability and validity. On the basis of statistical analysis, Dixon and Mood [84] recommended a sample size of 40 to 50 trials for the up-down method. Shelton et al. [38] showed that neither PEST nor the transformed

up-down rule will converge on a threshold with only 10 trials and recommend running 40 to 60 trials to evaluate a threshold with the up-down transformed rule. However, some authors conclude their tests after a total of 5 incorrect responses and report their thresholds as the average of 8 values [82].

Some authors have used only 20% of catch trials per session [85]. As discussed earlier, such a practice will most likely underestimate the actual threshold in the absence of correction.

### ***Nontraditional units***

Physical parameters of stimuli should be fully characterized and calibrated so that similar conditions can be replicated in a different setting. Vibration sensitivity amplitude thresholds have been expressed in inappropriate and/or erroneous units, such as "Biothesiometer units," or more simply, "units" [82,86], "volts" [85,87-93], "volts square" [94] and even in "Hertz" [95].

In the field of vision, it is not unusual to see light flash intensity characterized only in terms of a device setting on a specified photostimulator rather than in appropriate optical units [96]. The experimenter should measure the stimulus of interest rather than an attribute generated before or during the production of this stimulus. For example, Bleecker [88] and Anger et al. [91] studied vibration sensitivity, but they measured the voltage applied to the vibrator rather than the actual vibration amplitude. With the same device, the former reported a threshold of 3.67 volts in normal subjects of 31 to 40 years of age, while the latter recorded 8.8 volts in a referent group with an average age of 36 years. As a test score of about 7 volts should be considered as significantly elevated according to the nomograms furnished by the manufacturer, a value of 8.8 volts would certainly have to be considered as highly pathological although it characterizes a control group. More likely, this difference may be related to lack of calibration of the 2 units.

## **CONCLUSION AND RECOMMENDATIONS**

Psychophysical studies have helped characterize the toxic potential of chemicals to sensory functions in a quantitative and noninvasive manner. Extrapolation of psychophysical observations from one species to another is facilitated because sensory pathways are phylogenetically old structures, and very similar methods can be used across species.

This psychophysical approach has appealed to many, and a large number of studies have flourished. On several occasions, however, sensory testing in humans has presented deficiencies not usually present in most animal studies. Therefore, it is suggested that major methodological features developed for sensory assessment in animals (including signal detection theory approach) be taken into consideration in human sensory analysis. The following recommendations should be considered:

1. Minimize relations between the tester and the testee during sensory evaluation.

2. Automate stimulus delivery and response recording.
3. Standardize instructions.
4. Preestablish rigid objective rules to define all the test events (i.e., response, stimulus sequence, ...), and to accept or reject data points.
5. Choose appropriate units of measurement that will allow for comparison between different studies.
6. Describe all relevant physical dimensions of stimuli, and perform frequent calibrations.
7. Insert catch trials (whenever appropriate) in adequate proportions to correct sensory data.
8. Use appropriate number of trials.
9. Give feedback on subject's performance.
10. Use correction procedures to prevent position habits, whenever applicable.

All these factors will minimize errors and potential unconscious bias on the part of the subject and/or test administrator, and will increase the reliability, accuracy, and validity of the data collected.

#### REFERENCES

1. Merigan, W.H. and Weiss, B. (Eds.) (1980) *Neurotoxicity of the Visual System*. Raven Press, New York, NY.
2. Hayes, A.W. (Ed.) (1985) *Toxicology of the Eye, Ear, and Other Special Senses*. Raven Press, New York, NY.
3. Miller, J.J. (1985) *Handbook of Ototoxicity*. CRC Press, Boca Raton, FL.
4. Stebbins, W.C. (1982) Concerning the need for more sophisticated animal models in sensory behavioral toxicology. *Environ. Health Perspect.* 44, 77-85.
5. Merigan, W.H. (1979) Effects of toxicants on visual systems. *Neurobehav. Toxicol.* 1 (Suppl. 1), 15-22.
6. Maurissen, J.P.J. (1979) Effects of toxicants on the somatosensory system. *Neurobehav. Toxicol.* 1 (Suppl. 1), 23-31.
7. Maurissen, J.P.J. (1985) Psychophysical testing in human populations exposed to neurotoxicants. *Neurobehav. Toxicol. Teratol.* 7, 309-317.
8. Halpern, B.P. (1982) Environmental factors affecting chemoreceptors: An overview. *Environ. Health Perspect.* 44, 101-105.

- 9 Pryor, G.T., Dickinson, J., Howd, R.A., and Rebert, C.S. (1983) Transient cognitive deficits and high-frequency hearing loss in weanling rats exposed to toluene. *Neurobehav. Toxicol. Teratol.* 5, 53-57.
- 10 Rebert, C.S., Sorenson, S.S., Howd, R.A., and Pryor, G.T. (1983) Toluene-induced hearing loss in rats evidenced by the brainstem auditory-evoked response. *Neurobehav. Toxicol. Teratol.* 5, 59-62.
- 11 Merigan, W.H., Barkdoll, E. and Maurissen, J.P.J. (1982) Acrylamide-induced visual impairment in primates. *Toxicol. Appl. Pharmacol.* 62, 342-345.
- 12 Merigan, W.H., Barkdoll, E., Maurissen, J.P.J., Eskin, T.A., and Lapham, L.W. (1985) Acrylamide effects on the Macaque visual system. I. Psychophysics and electrophysiology. *Invest. Ophthalmol. Vis. Sci.* 26, 309-316.
- 13 Eskin, T.A., Lapham, L.W., Maurissen, J.P.J., and Merigan, W.H. (1985) Acrylamide effects on the Macaque visual system, II. Retinogeniculate morphology. *Invest. Ophthalmol. Vis. Sci.* 26, 317-329.
- 14 Maurissen, J.P.J., Weiss, B., and Davis, H.T. (1983) Somatosensory thresholds in monkeys exposed to acrylamide. *Toxicol. Appl. Pharmacol.* 71, 266-279.
- 15 Schwann, T. (1839) *Mikroskopische Untersuchungen über die Uebereinstimmung in der Struktur und dem Wachsthum der Thiere und Pflanzen.* Sander, Berlin, Germany.
- 16 Bell, C. (1811) *Idea of a New Anatomy of the Brain.* Strahan and Preston, London, England.
- 17 Magendie, F. (1822) Expériences sur les fonctions des racines des nerfs rachidiens. *J. Physiol. Exp. Pathol.* 2, 276-279, 366-371.
- 18 Müller, J. (1826) *Zur vergleichenden Physiologie des Gesichtssinnes des Menschen und der thiere.* C. Knobloch, Leipzig, Germany.
- 19 Weber, E.H. (1834) *De Pulsu, Resorptione, Auditu et Tactu. Annotationes Anatomicae et Physiologicae,* C.F. Koehler, Lipsiae, Germany.
- 20 Weber, E.H. (1846) Der tastsinn und das gemeingefühl. In: R. Wagner (Ed.), *Handwörterbuch der Physiologie*, Vol. 3, Vieweg, Braunschweig, Germany, pp. 481-588.
- 21 Fechner, G.T. (1860) *Elemente der Psychophysik.* Breitkopf und Härtel, Leipzig, Germany. 2 Vols.
- 22 Green, D.M. and Swets, J.A. (1974) *Signal Detection Theory and Psychophysics.* Robert E. Krieger Publishing Co., Huntington, NY.
- 23 Stevens, S.S. (1958) Measurement and man. *Science* 127, 383-389.
- 24 Bernard, C. (1856) *Introduction à l'Etude de la Médecine Expérimentale* Editions Pierre Beltond, Paris, France, 1966, p. 212.
- 25 Stokinger, H.E. (1974) Behavioral toxicology in the development of threshold limit values. In: C. Xintaras, B.L. Johnson, I. de Groot (Eds.), *Behavioral Toxicology. Early Detection of Occupational Hazards*, HEW Publication No. (NIOSH) 74-126.

- 26 Guilford, J.P. (1954) *Psychometric Methods*. McGraw-Hill Book Company, New York, NY.
- 27 Corso, J.F. (1957) *The Experimental Psychology of Sensory Behavior*. Rinehart and Winston, New York, NY.
- 28 D'Amato, M.R. (1970) *Experimental Psychology: Methodology, Psychophysics, and Learning*. McGraw-Hill Book Company, New York, NY.
- 29 Scharf, B. (1975) *Experimental Sensory Psychology*. Scott, Foresman and Co., Glenview, Illinois.
- 30 Gescheider, G.A. (1976) *Psychophysics. Methods and Theory*. Lawrence Erlbaum Associates, Hillsdale, NJ.
- 31 Békésy, G. von. (1947) A new audiometer. *Acta Otolaryngol.* 35, 411-422.
- 32 Cornsweet, T.N. (1962) The staircase-method in psychophysics. *Am. J. Psychol.* 75, 485-491.
- 33 Brownlee, K.A., Hodges, Jr. J.L., and Rosenblatt, M. (1953) The up-and-down method with small samples. *J. Amer. Stat. Assoc.* 48, 262-277.
- 34 Wetherill, G.B. and Levitt, H. (1965) Sequential estimation of points on a psychometric function. *Br. J. Math. Stat. Psychol.* 18, 1-10.
- 35 Taylor, M.M. and Creelman, C.D. (1967) PEST: Efficient estimates on probability functions. *J. Acoust. Soc. Am.* 41, 782-787.
- 36 Findlay, J.M. (1978) Estimates on probability functions: A more virulent PEST. *Percept. Psychophys.* 23, 181-185.
- 37 Pentland, A. (1980) Maximum likelihood estimation: The best PEST. *Percept. Psychophys.* 28, 377-379.
- 38 Shelton, B.R., Picardi, M.C., and Green, D.M. (1982) Comparison of three adaptive psychophysical procedures. *J. Acoust. Soc. Am.* 71, 1527-1533.
- 39 Watson, A.B. and Pelli, D.G. (1983) QUEST: A Bayesian adaptive psychometric method. *Percept. Psychophys.* 33, 113-120.
- 40 Madigan, R. and Williams, D. (1987) Maximum-likelihood psychometric procedures in two-alternative forced-choice: Evaluation and recommendations. *Percept. Psychophys.* 42, 240-249.
- 41 Relkin, E.M. and Pelli, D.G. (1987) Probe tone thresholds in the auditory nerve measured by two-interval forced-choice procedures. *J. Acoust. Soc. Am.* 82, 1679-1691.
- 42 Elsmore, T.F. (1972) Duration discrimination: Effects of probability of stimulus presentation. *J. Exp. Anal. Behav.* 18, 465-469.
- 43 Blackwell, H.R. (1952) The influence of data collection procedures upon psychophysical measurement of two sensory functions. *J. Exp. Psychol.* 44, 306-315.
- 44 Lukaszewski, J.S. and Elliott, D.N. (1962) Auditory threshold as a function of forced-choice technique, feedback, and motivation. *J. Acoust. Soc. Am.* 34, 223-228.

- 45 Wilson, M., Stamm, J.S. and Pribram, K.H. (1960) Deficits in roughness discrimination after posterior parietal lesions in monkeys. *J. Comp. Physiol. Psychol.* 53, 535-539.
- 46 Campbell, R.A. (1963) Detection of a noise signal of varying duration. *J. Acoust. Soc. Am.* 35, 1732-1737.
- 47 Rose, R.M., Teller, D.Y., and Rendleman, P. (1970) Statistical properties of staircase estimates. *Percept. Psychophys.* 8, 199-204.
- 48 Yager, D. and Thorpe, S. (1970) Investigations of goldfish color vision. In: W.C. Stebbins (Ed.), *Animal Psychophysics: The Design and Conduct of Sensory Experiments*, Appleton-Century-Crofts, New York, NY, pp. 259-275.
- 49 Pfingst, B.E., Hienz, R., and Miller, J. (1975) Reaction-time procedure for measurement of hearing. II. Threshold functions. *J. Acoust. Soc. Am.* 57, 431-436.
- 50 Dyck, P.J., Zimmerman, I.R., O'Brien, P.C., Ness, A., Caskey, P.E., Karnes, J., and Bushek, W. (1978) Introduction of automated systems to evaluate touch-pressure, vibration, and thermal cutaneous sensation in man. *Ann. Neurol.* 4, 502-510.
- 51 Penner, M.J. (1978) Psychophysical methods and the minicomputer. In: M.S. Mayzner and T.R. Dolan (Eds.), *Minicomputers in Sensory and Information-Processing Research*, Lawrence Erlbaum Associates, Publishers, Hillsdale, NJ, pp. 100 and 115.
- 52 Levine, M.W. and Shefner, J.M. (1981) *Fundamentals of Sensation and Perception*. Addison-Wesley Publishing Company, Reading, MA, p. 17.
- 53 McKee, S.P., Klein, S.A., and Teller, D.Y. (1985) Statistical properties of forced-choice psychometric functions: Implications of probit analysis. *Percept. Psychophys.* 37, 286-298.
- 54 Pasternak, T., Flood, D.G., Eskin, T.A., and Merigan, W.H. (1985) Selective damage to large cells in the cat retinogeniculate pathway by 2,5-hexanedione. *J. Neurosci.* 5, 1641-1652.
- 55 Merigan, W.H. and Eskin, T.A. (1985) Spatio-temporal vision of Macaques with severe loss of P<sub>g</sub> retinal ganglion cells. *Vision Res.* 26, 1751-1761.
- 56 Pavlov, I.P. (1927) *Conditioned Reflexes: An Investigation of the Physiological Activity of the Cerebral Cortex*, Translated by G.V. Anrep. Dover Publications, New York, NY, 1960.
- 57 Northmore, D.P.M. and Muntz, W.R.A. (1974) Effects of stimulus size on spectral sensitivity in fish (*Scardinius erythrophthalmus*), measured with a classical conditioning paradigm. *Vision Res.* 14, 503-514.
- 58 Otis, L.S., Cerf, J.A., and Thomas, G.J. (1957) Conditioned inhibition of respiration and heart rate in the goldfish. *Science* 126, 263-264.
- 59 Passe, D.H. (1981) Autoshaping as a psychophysical paradigm: Absolute visual sensitivity in the pigeon. *J. Exp. Anal. Behav.* 36, 133-139.
- 60 Jamison, J.H. (1951) Measurement of auditory intensity thresholds in the rat by conditioning of an autonomic response. *J. Comp. Physiol. Psychol.* 44, 118-125.

- 61 Skinner, B.F. (1938) *The Behavior of Organisms. An Experimental Analysis.* Appleton-Century-Crofts, New York, NY
- 62 Terman, M. and Terman, J.S. (1972) Concurrent variation of response bias and sensitivity in an operant-psychophysical test. *Percept. Psychophys.* 11, 428-432.
- 63 Clack, T.D. and Herman, P.N. (1963) A single-lever psychophysical adjustment procedure for measuring auditory thresholds in the monkey. *J. Audit. Res.* 3, 175-183.
- 64 Estes, W.K. and Skinner, B.F. (1941) Some quantitative properties of anxiety. *J. Exp. Psychol.* 29, 390-400.
- 65 Sidman, M., Ray, B.A., Sidman, R.L., and Klinger, J.M. (1966) Hearing and vision in neurological mutant mice: A method for their evaluation. *Exp. Neurol.* 16, 377-402.
- 66 Smith, J. (1970) Conditioned suppression as an animal psychophysical technique. In: W.C. Stebbins (Ed.), *Animal Psychophysics: The Design and Conduct of Sensory Experiments*, Appleton-Century-Crofts, New York, NY, pp. 125-159.
- 67 Blough, D. and Blough, P. (1977) Animal Psychophysics. In: W.K. Honig and J.E.R. Staddon (Eds.), *Handbook of Operant Behavior*, Prentice-Hall Inc., Englewood Cliffs, NJ, pp. 514-539.
- 68 Stebbins, W.C. (Ed.) (1970) *Animal Psychophysics: The Design and Conduct of Sensory Experiments.* Appleton-Century-Crofts, New York, NY.
- 69 Blough, P.M. and Young, J.S. (1985) Psychophysical assessment of sensory dysfunction in nonhuman subjects. In: A.W. Hayes (Ed.), *Toxicology of the Eye, Ear and Other Special Senses*, Raven Press, New York, pp. 79-90.
- 70 Hoffman, H.S. and Ison, J.R. (1980) Reflex modification in the domain of startle. I. Some empirical findings and their implications for how the nervous system processes sensory input. *Psych. Rev.* 87, 175-189.
- 71 Sechenov, I.M. (1863) *Reflexes of the Brain*, translated by S. Belsky, M.I.T. Press, Cambridge, MA, 1965, p. 14.
- 72 Yerkes, R.M. (1905) The sense of hearing in frogs. *J. Comp. Neurol. Psychol.* 15, 279-304.
- 73 Young, J.S. and Fechter, L.D. (1983) Reflex inhibition procedures for animal audiometry: A technique for assessing ototoxicity. *J. Acoust. Soc. Am.* 73, 1686-1693.
- 74 Kelly, J.B. and Masterton, B. (1977) Auditory sensitivity of the albino rat. *J. Comp. Physiol. Psychol.* 91, 930-936.
- 75 Prosen, C.A., Petersen, M.R., Moody, D.B., and Stebbins, W.C. (1978) Auditory thresholds and kanamycin-induced hearing loss in the guinea pig assessed by a positive reinforcement procedure. *J. Acoust. Soc. Am.* 63, 559-566.
- 76 Ison, J.R. and Hoffman, H.S. (1983) Reflex modification in the domain of startle. II. The anomalous history of a robust and ubiquitous phenomenon. *Psychol. Bull.* 94, 3-17.

- 77 Hoffman, H.S. (1984) Methodological factors in the behavioral analysis of startle. The use of reflex modification procedures and the assessment of threshold. In: R.C. Eaton (Ed.), *Neural Mechanisms of Startle Behavior*, Plenum Publishing Corporation, New York, NY, pp. 267-285.
- 78 Fechter, L.D. and Young, J.S. (1986) Reflexive measures. In: Z. Annau (Ed.), *Neurobehavioral Toxicology*, Johns Hopkins University Press, Baltimore, MD, pp. 23-42.
- 79 Wilber, L.A. (1979) Threshold measurement methods and special considerations. In: W.F. Rintelmann (Ed.), *Hearing Assessment*, University Park Press, Baltimore, MD.
- 80 Lupolover, Y., Safran, A.B., Desangles, D., de Weisse, C., Meyer, J.J., Bousquet, A., and Assimakopoulos, A. (1984) Evaluation of visual function in healthy subjects after administration of Ro 15-1788. *Eur. J. Clin. Pharmacol.* 27, 505-507.
- 81 Arezzo, J.C., Schaumburg, H.H., and Laudadio, C. (1986) Thermal sensitivity tester. Device for quantitative assessment of thermal sense in diabetic neuropathy. *Diabetes* 35, 590-592.
- 82 Sosenko, J.M., Gadia, M.T., Natori, N., Ayyar, D.R., Ramos, L.B. and Skyler, J.S. (1987) Neurofunctional testing for the detection of diabetic peripheral neuropathy. *Arch. Intern. Med.* 147, 1741-1744.
- 83 Kershaw, C.D. (1985) Statistical properties of staircase estimates from two interval forced choice experiments. *Brit. J. Math. Stat. Psychol.* 38, 35-43.
- 84 Dixon, W.J. and Mood, A.M. (1948) A method for obtaining and analyzing sensitivity data. *J. Am. Stat. Assoc.* 43, 109-126.
- 85 Arezzo, J.C. and Schaumburg, H.H. (1980) The use of the Optacon as a screening device. A new technique for detecting sensory loss in individuals exposed to neurotoxins. *J. Occup. Med.* 22, 461-464.
- 86 LeQuesne, P.M. and Fowler, C.J. (1986) A study of pain threshold in diabetics with neuropathic foot lesions. *J. Neurol. Neurosurg. Psychiat.* 49, 1191-1194.
- 87 Kardel, T. and Nielsen, V.K. (1974) Hepatic neuropathy. A clinical and electrophysiological study. *Acta Neurol. Scand.* 50, 513-526.
- 88 Bleecker, M.L. (1983) Optacon - A new screening device for peripheral neuropathies. In: R. Gilioli, M.G. Cassito, and V. Foà (Eds.), *Neurobehavioral Methods in Occupational Health*, Pergamon Press, Elmsford, NY, pp. 41-46.
- 89 Arezzo, J.C., Schaumburg, H.H., and Petersen, C.A. (1983) Rapid screening for peripheral neuropathy: A field study with the Optacon. *Neurology* 33, 626-629.
- 90 Arezzo, J.C., Schaumburg, H.H., and Laudadio, C. (1985) The Vibratron: A simple device for quantitative evaluation of tactile/vibratory sense. *Neurology* 35, (Suppl. 1), 169.
- 91 Anger, W.K., Moody, L., Burg, J., Brightwell, W.S., Taylor, B.J., Russo, J.M., Dickerson, N., Setzer, J.V., Johnson, B.L., and Hicks, K. (1986) Neurobehavioral evaluation of soil and structural fumigators using methyl bromide and sulfuryl fluoride. *Neurotox.* 7, 137-156.
- 92 Svendsgaard, D.J., Soliman, S.A., Soffar, A., and Otto, D.A. (1987) Screening pesticide plant workers for organophosphorus induced delayed neuropathy (OPIDN). *The Toxicologist* 7, 134.

- 93 Lipton, R.B., Galer, B.S., Dutcher, J.P., Portenoy, R.K., Berger, A., Arezzo, J.C., Mizruchi, M., Wiernik, P.H., and Schaumburg, H.H. (1987) Quantitative sensory testing demonstrates that subclinical sensory neuropathy is prevalent in patients with cancer. *Arch. Neurol*, 44, 944-946.
- 94 Nielsen, V.K. (1972) The peripheral nerve function in chronic renal failure, IV. An analysis of the vibratory perception threshold. *Acta Med. Scand.* 191, 287-296.
- 95 Bleecker, M.L. and Moreland, R. Carpal (1984) tunnel syndrome: Comparisons of alterations in vibration threshold versus electrodiagnostic studies. In: *Conference on Medical Screening and Biological Monitoring for the Effects of Exposure in the Workplace*, National Technical Information Service, Springfield, VA, #PB86-242641, p. 27.
- 96 Onofrj, M., Harnois, C., and Bodis-Wollner, I. (1985) The hemispheric distribution of the transient rat VEP: A comparison of flash and pattern stimulation. *Exp. Brain Res.* 59, 427-433.

## QUANTITATION OF NATURALISTIC BEHAVIORS

Hugh L. Evans

*Institute of Environmental Medicine, New York University Medical Center, New York, NY*

### SUMMARY

Naturalistic behaviors are behaviors that organisms exhibit "in nature." Eating, sleeping and sexual behaviors are examples. Since naturalistic behaviors are observed to occur without any apparent training or learning, some people mistakenly believe that all naturalistic behaviors are unlearned, and are thus different from laboratory behaviors. We maintain that naturalistic behaviors can be studied profitably in the toxicological laboratory, using quantitative techniques from behavioral neuroscience. Understanding of toxicity and underlying mechanisms is enhanced when naturalistic behaviors are thought of as responses to stimuli. Stimuli that influence naturalistic behaviors may arise inside the organisms (e.g., physiological signals of hunger) or outside the organisms (e.g., the smell of food or the start of the nocturnal lighting cycle). A practical, noninvasive, automated system can be used to improve upon the cage-side observation currently used to evaluate naturalistic behaviors in toxicity screening. Effects of alkyltins and other neurotoxicants upon eating, drinking, rearing, and the daily cycle of rest-activity will be shown. The rodent's pattern of nocturnal activity has proven to be particularly sensitive to neurotoxicants, and thus deserves additional attention in developing neurobehavioral toxicology.

### INTRODUCTION

Naturalistic behaviors are behaviors that organisms exhibit "in nature." Eating, drinking, sleeping, and moving from place to place are examples. Some people mistakenly believe that all naturalistic behaviors are unlearned, and thus different from laboratory behaviors, since naturalistic behaviors are observed to occur without any apparent training or learning. Actually, naturalistic behaviors such as locomotor activity are subject to many of the same mechanisms that govern all behavior, whether in the laboratory or in the field [1,2]. The thesis of this paper is that naturalistic behaviors can be studied profitably in the toxicological laboratory, using quantitative techniques from behavioral neuroscience.

Ethologists study behavior in natural living situations [3,4]. Adapting ethological methods to the service of toxicology poses several problems: the difficulty in examining a large enough number of animals to yield significant dose-effect data; the limited availability of suitable control and exposed populations in the wild; the dependence on observational scoring of behavior or the difficulty of operating measurement instruments outdoors; and the limited opportunity for experimental control or manipulation of variables needed to identify mechanisms of toxicity.

Laboratory studies of behavior have been questioned for their relevance to "real-world" situations. Indeed, the demonstration of the ecological validity of laboratory measures is as important in behavioral science as in, say, immunology or pharmacotherapy. Behaviors of animals freely moving within a cage represent one of the more "natural" preparations available to toxicologists; compare such a preparation to *in vitro* preparations of cells or tissue slices; invasive physiological preparations requiring sedation, restraint, electrodes, cannulae, etc; and histopathological preparations that are frozen at one instant in time.

Many improvements in housing and care of lab animals have minimized concerns with stresses associated with confinement and experimental manipulations that may render the behavior of laboratory animals unnatural [5]. Animals in the wild commonly experience more severe stresses (diseases, predators and competitors for mates and for food) than their laboratory cousins.

Only a subset of the many systems proposed for neurotoxicity screening (see Tilson [6] for a recent review) are addressed. I will focus on locomotion, rearing, wheel-running and sleep/wakefulness cycles as evidenced in diurnal rhythms in these behaviors. These are the endpoints having received the most attention and for which there has emerged a demonstrable potential for toxicity testing. Toxicologists have sought naturalistic behavior as a convenience, hoping that the unlearned behaviors could reduce the time and expertise needed to prepare animals for study. We now will review methods for which published toxicological data provide evidence of sensitivity, specificity, and validity.

## **NATURAL BEHAVIORS EVALUATED OUTSIDE OF THE LIVING CAGE**

### ***Observational techniques***

Pharmaceutical screening provided the original impetus for using a standardized rating scale to score a battery of simple, unlearned behaviors and reflexes as indices of drug effects upon the nervous system [7]. This technique is useful in pharmaceutical screening because the range of chemicals has already been narrowed to those having a targeted, therapeutic effect. In contrast, I found no publications in which techniques similar to the Irwin screen have successfully evaluated the broader range of compounds which are in consumer and industrial products and for which the target organ is unknown. The Irwin battery is moderately labor intensive, requiring a skilled technician; it is intrusive, requiring manual examination of the animal; and it provides ordinal data, which is less powerful statistically than continuous measures

The Irwin system has been incorporated into a Functional Observational Battery proposed for environmental toxicology by the Environmental Protection Agency [8,9]. This battery also includes

quantitative tests of grip strength and sensory function. Examples of similar neurological exams applied to developing rats have been reported [10].

An advantage of all of the above-mentioned tests is their relative economy of instrumentation and simplicity of procedure. They are non-invasive in that the skin is not broken, electrodes are not attached, and animals are not harnessed. But all are intrusive, requiring the animal to be removed from the home cage and carried to a novel testing arena. Some procedures require that the animal be manipulated by a human observer. Naturally, the test must take place under high enough illumination to permit the observer to see the animal's behavior. Handling and exposure to light tend to suppress the behavior of nocturnal animals such as rodents [3].

#### ***Automated recording of locomotor activity***

Automated recording of animal behavior affords several advantages over human observation: it can be less labor intensive; it is compatible with the automated data recording demanded by Good Laboratory Practice regulations; it reduces human error and differences between individual observers; and it can measure behavior in the dark, when the rodent's full behavioral repertoire is on display. The sensitivity of the rodent's nocturnal behavior will be reviewed below (see *Diurnal rhythms*).

The open field is a quasi-standardized arena that has been widely employed for observing animal behavior. Advantages and disadvantages have been reviewed by Walsn & Cummins [11] and by Reiter & MacPhail [12]. Although it is quite limited as an observational technique, the open field can be automated for improved quantification. An early system recorded rodent behavior on film for subsequent analyses into category and pattern of behavior by a human observer [13]. Although filming provided the opportunity to review behaviors that might have been missed by the unaided eye, it required testing in a lighted environment. The technique did not document consistent effects of exposure to lead or amphetamine [14].

Newer techniques permit the automated measurement of nocturnal behavior. The animal's activity during the dark interrupts infrared lightbeams which are invisible to rodents but can be detected and counted by electronic circuits. Although these systems cannot distinguish as large a variety of behavioral acts as a human observer can, judicious placement of the photobeams can distinguish between walking and rearing, for example.

The sensitivity and specificity of automated open field techniques is well established from published results with toxicants and drugs. Automated tests of spontaneous locomotor activity have been proposed by the U.S. EPA [8] for screening for neurotoxicity. A brief measure of spontaneous motor activity actually equalled more complex tests in sensitivity to chronic exposure to any of eight neurotoxicants [15]. Effects of toluene on continuously measured locomotor activity was reported by

Bushnell *et al.* [16]; effects of organotin by Wenger *et al.* [17], and effects of drugs by Sandberg *et al.* [18].

The limitation of open field devices of this type is the paucity of stimuli to engage the animal's behavior. In short, there is little for a rodent to do in an open field, and, therefore, little upon which to base mechanistic interpretations of its behavior. Even organisms as simple as bacteria do not move through their environment in a strictly random fashion. An attempt to embellish open field tests was the enlargement of the open field in the shape of a figure-eight in order to characterize some effects of trimethyltin [19], lead, and other compounds [10-12].

### ***Effects of handling***

Handling of laboratory animals can be a useful strategy. In screening, the investigator can provoke the animal so as to reveal neurotoxicity that is not apparent with casual observation. This strategy is used to the fullest in mechanistically oriented research in order to assess the organism's full range of sensory function (e.g., Evans, [20]).

However, tests that require frequent, intrusive handling of animals have certain limitations for toxicological screening. First, they are labor-intensive and therefore expensive. Second, the degree of variability between individuals performing the procedure often is an obstacle to sensitivity. Third, health risks to workers due to bites or contact with pathogens or toxicants are increased with each animal handled. Handling animals treated with carcinogens is an undesirable task. Finally, handling and exposure to light tend to suppress the behavior of nocturnal animals such as rodents [3].

Handling and transfer of an animal from the residential cage to an unfamiliar test cage can stimulate behavioral activity that is not representative of the animal's "natural" behavioral pattern [21]. Timing of feeding or other intrusions into the animal's environment also will distort the ongoing pattern of activity (e.g., Evans, [1]). As indicated above, this can be used to advantage if one's goal is to place a specific item of behavior under a magnifying glass so as to demonstrate mechanisms of toxicity. However, research techniques are better suited to that goal than the simpler measures of activity being discussed here.

The effects of handling can distort the picture of toxic effects. An example is provided in Figure 1. Transferring rats from their residential cage to a novel test cage obliterated the natural diurnal rhythm in locomotor activity. The highest activity of both treated and control rats occurred during the lighted portion of the light/dark cycle and lower activity was recorded after the lights were turned off at 1800 h (Figure 1). A large difference in baseline activity usually is associated with the light-dark cycle when rodents are not disturbed (e.g., Figure 2). The results of Figure 1 and similar results by Johnson *et al.* [22] might lead to the conclusion that trimethyltin causes an increase in locomotor activity at all times of day. The results of trimethyltin in two species of undisturbed

animals show that the tin-induced hyperactivity occurs mainly during the natural waking hours (Figure 2). Thus, a comparison of Figures 1 and 2 suggests that in the studies of Johnson *et al.* [22] and Ruppert *et al.* [19], handling washed out the effects of diurnal lighting, which was the variable of interest in the study. Likewise, the practice of inserting rats into a test cage in the light portion of the daily light/dark cycle yields an unusual ("unnatural") diurnal pattern in which the relative amount of nocturnal activity is reduced because of unusually high activity in the first, lighted hours after insertion into the apparatus. Examples of this are provided by material reviewed by Reiter & MacPhail [12] and by Buelke-Sam *et al.* [10].

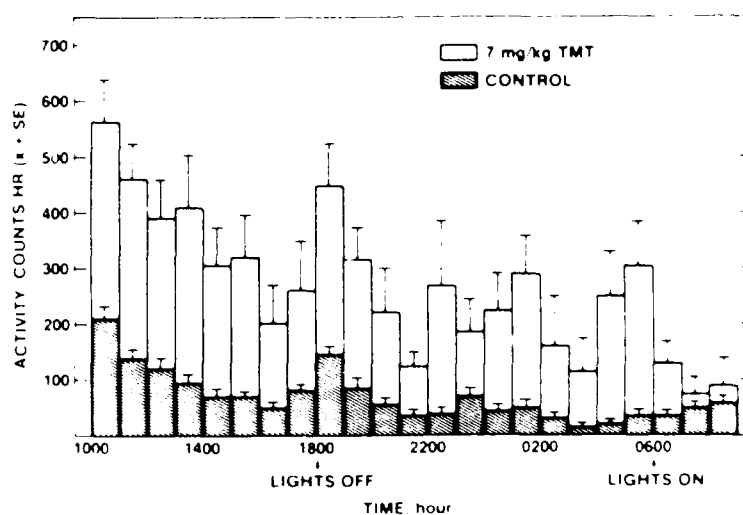


Figure 1. Handling altered the natural diurnal pattern of locomotor activity of rats during a 23-h test in a figure-8 shaped open field. The time of day is shown on the X axis. Both the controls and the group given acute trimethyltin (TMT) were very active after being placed in the maze at 1000 h with the lights on; this activity level exceeded that recorded later when the lights were off during 1800 to 0600 h. From Ruppert *et al.*, [19].

Transferring animals to novel test cages for measurement of spontaneous locomotor activity has not produced convincing evidence of superior sensitivity to toxicants over less intrusive methods. This leads us to nonintrusive methods for evaluating behavior in the home cage

## NONINTRUSIVE QUANTITATION OF HOMECAGE BEHAVIOR

### Cage-side observation

The most frequently used nonintrusive method is cage-side observation. The effects of toxicants upon sleeping, eating, or abnormal movements can be objectively defined and quantified (e.g., Evans *et al.*, [23]). A time-sampling protocol is helpful. Figure 3 provides an example. Mice usually are observed to be inactive (sleeping or resting) in their home cages during the light portion of the daily light-dark cycle (Figure 3, right half). After return to the home cage following sham inhalation exposure to room air, the large majority of mice quickly became inactive (Figure 3, exposed

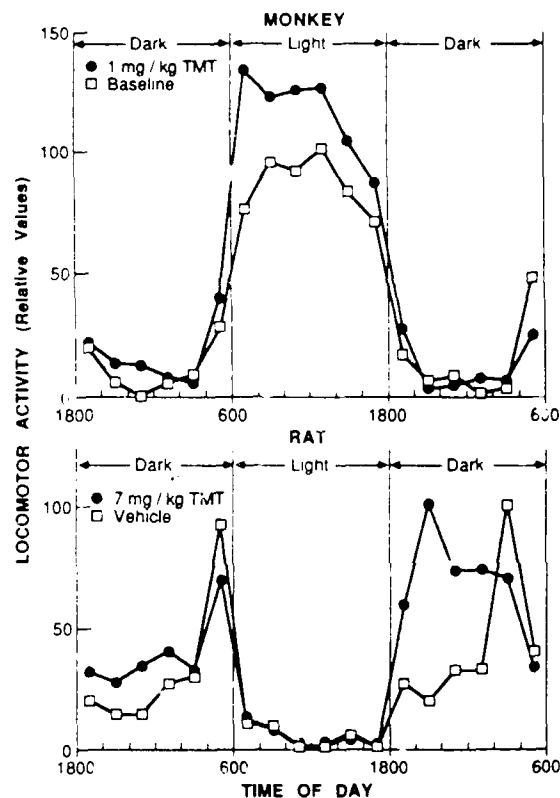


Figure 2. The diurnal pattern of locomotor activity of macaque monkeys and of rats that had not been handled for several days prior to measurement with infrared photobeams in the NYU homecage system. The Y axes show behavioral activity relative to the animal's maximal baseline score (100). Note that each species is characterized by distinct periods of activity and quiescence. Acute trimethyltin (TMT) selectively increased locomotion of each species at the times of day at which activity naturally occurs without significant changes at times when the animals are inactive. TMT was administered orally 2 days before the day shown here. Data for monkeys from Graefe et al. [40]; data on rats from Bushnell & Evans [32]. The data for rats is a detail from a continuous recording shown in Figure 8.

to 0 ppm benzene). After return to the home cage following inhalation exposure to either 300 or 900 ppm benzene, fewer mice were observed to be inactive. The same observational method was able to specify eating and grooming as the behaviors increased by benzene exposure [23]. This method is suited to document toxicant-induced stimulation of behavior, as is frequently produced by organic solvents, since control animals are usually sleeping. Observational methods such as this one are economical and nonintrusive. The disadvantage is that observations must be made in the light when rodents are normally exhibiting little ongoing behavior.

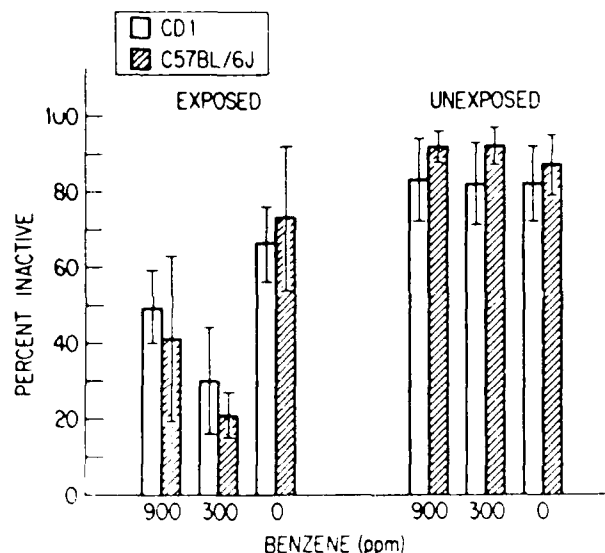


Figure 3. The percentage of mice that was observed to be inactive (lying down and immobile) on days when they had been exposed for 6 h in an inhalation chamber ("exposed") and for the same mice on days when they were not put into the inhalation chamber ("unexposed"). Two strains of mice (CD1 or C57) were observed at the same time of day during the light portion of the light/dark cycle starting 75 min after their return from the inhalation exposure or at the same time on unexposed days. Each bar reflects the mean and SD of 12 cages. From Evans et al.[23].

## AUTOMATIC RECORDING OF HOMECAGE BEHAVIOR

### *Residential mazes*

The residential figure-8 maze overcomes some of the limitations of open-field tests mentioned above. It provides quantitation of locomotor activity in a more complex situation than the open field. The figure-8 maze was intended to resemble the rodent's natural pattern of burrowing. Residential mazes have been used to evaluate toxicant-induced changes in the aggregate activity of groups of rats [12,24]. Such mazes provide an interesting technique for research on social variables, but there is no evidence that grouping of animals, short of inhumane crowding, will significantly increase sensitivity to drugs or toxicants. Although the group of animals residing in a maze increases the number of variables impinging upon the organisms above that of a solitary rodent in an open field, the group's activity is statistically no more powerful than a single observation of one rat. Unfortunately, this inefficient use of animals is both costly and in conflict with efforts to reduce the number of animals used for toxicity screening.

### *Wheel running*

Residential cages with attached running wheels have been a long-established preparation for studying natural exercise and circadian rhythms in rodents. The advantages of wheel running as an endpoint for toxicology are that (1) it is noninvasive, (2) it can be quantified automatically, (3) it

provides an ample baseline in which the rodent voluntarily runs several miles per day, and (4) the exercising animal provides a different model than the sedentary animal. Exercise increases both food consumption and pulmonary ventilation, and thus would increase exposure to toxicants in the food or air [25]. The exercising animal is probably a better model of occupational exposures than are the more commonly used models employing sedentary animals. Procedures to magnify these effects of exercise by forced walking on a treadmill were recently reviewed by Tepper & Weiss [26]. A significant disadvantage of runwheels is that commercially available models do not presently meet minimal cage size regulations [5].

The literature indicates the successful use of wheel running to evaluate inhaled toxicants. Inhaled benzene reduced postexposure running by mice [27], possibly because it increased the occurrence of eating and grooming which are incompatible with running [23]. These effects occurred at concentrations of benzene that had no effect on the spontaneous locomotor activity of sedentary mice having no access to a runwheel [28]. The feasibility of wheel running of mice for documenting the consequences of inhalation exposure to other solvents such as toluene is shown by Figure 4. Two mice clearly indicated the effects of their first exposure to toluene.

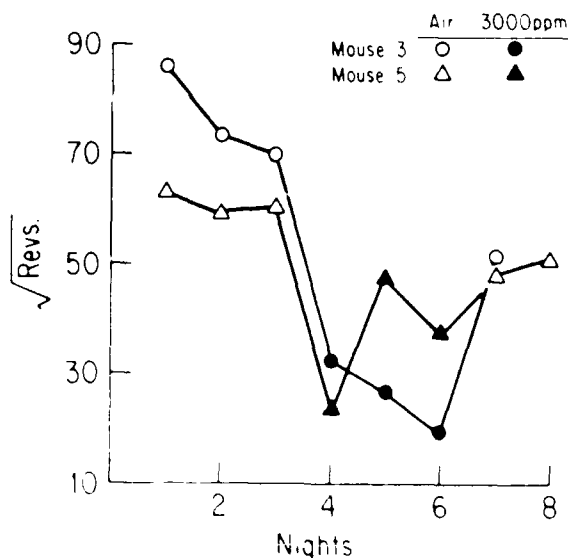


Figure 4. The nocturnal wheel running of two individual mice following 6-h inhalation exposures to air or 3000 ppm toluene. The number of revolutions decreased markedly after the first exposure (night 4). Recovery was incomplete 2 days after the last toluene exposure (nights 7 & 8). Exposure methods were same as those of Dempster et al. [28].

Figure 5 compares wheel running with several other behavioral indices of ozone exposure in the rat. The sensitivity of running was attributed to the enhanced uptake of ozone by exercising rats [26]. Other experiments have demonstrated the ability of running to document the effects of ammonia [2] and of organotin compounds [29].

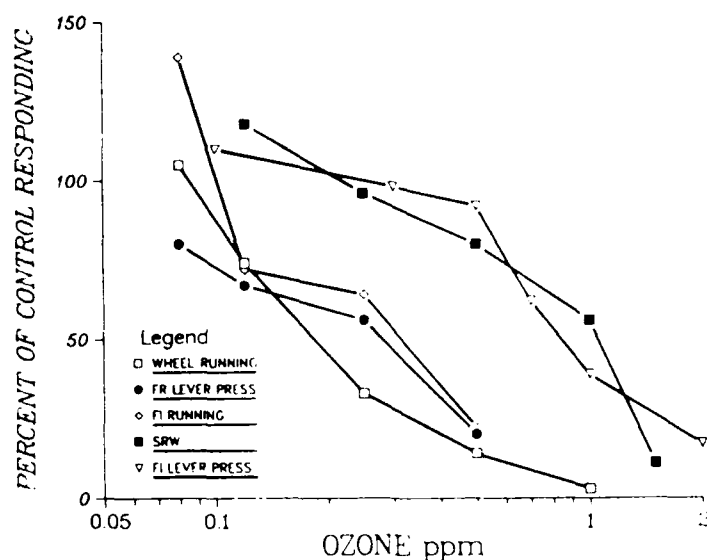


Figure 5. A physically demanding response such as running was more sensitive to ozone than other behavioral responses requiring minimal effort. Wheel running was measured during inhalation exposure. From Tepper & Weiss [26].

#### Standard residential cages

Standard polypropylene mouse cages can be placed inside an automated open field for long-term studies of motor activity [30]. The activity of an individual mouse can thus be studied for several weeks of preexposure baseline and postexposure data collection. Wenger *et al.* [30] found trimethyltin to decrease total activity of mice while the diurnal pattern, measured in 6 h epochs, was preserved. The finding of hypoactivity in TMT-treated mice differs from the hyperactivity reported by several laboratories with TMT-treated rats; the difference is probably attributed to species differences between rats and mice rather than to the characteristics of the activity system used by Wenger *et al.* [30]

#### The NYU homecage system

The research described thus far had established the practicality and sensitivity of automated recording of rodent locomotor activity. In order to capitalize upon these findings, a new system was designed to improve neurotoxicity testing in the following ways: (1) to require less than half of the lab space that normally is required for preparations such as runwheel cages or residential mazes; (2) to economize by using standard sized, commercially available, residential cages of the type readily available wherever caged rodents are studied; (3) to minimize intrusiveness so as to maximize the potential sensitivity of nocturnal behavior; (4) to permit detailed studies of several natural behaviors, e.g., eating, drinking, locomotion, and sleep/activity cycles of individual animals; (5) to increase the precision by employing on-line computer control of environmental lighting and data collection; (6) to increase the number of animals tested simultaneously so as to increase the procedure's statistical

power; and (7) to employ methods that facilitate comparative studies of several animal species (e.g., Figure 2).

The system's validity was demonstrated by experimental manipulation of environmental lighting (Figure 2), food deprivation, and the effects of reference drugs [31]. The system's sensitivity also is shown by the results in Figure 6, which consistently exceed the sensitivity reported in automated measurements with either the figure-8 maze (several studies reported in Buelke-Sam et al., [10] or open field [18].

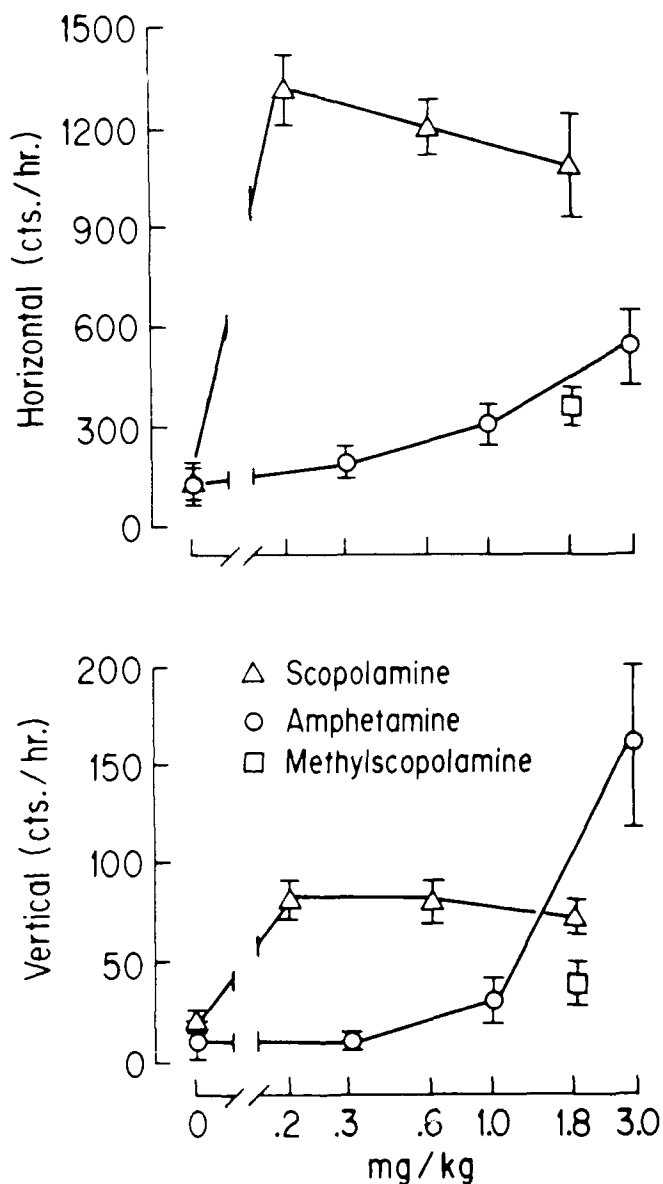


Figure 6. Nocturnal activity in the NYU home cage system is very sensitive to the acute effects of three reference drugs. Data were recorded for 1 h starting 5 to 20 min after ip injection. Doses were calculated as the salt. Normal saline (0 mg/kg). Points represent mean and SEM, N = 20. From Evans et al. [31].

The system's sensitivity to environmental toxicants was shown by studies of organotin compounds, in which nocturnal behavior proved to be sensitive to doses below those required to alter morphological, biochemical, or other behavioral endpoints [31,32,33,34]. Figure 7 illustrates the greater sensitivity to TET of wheel running and vertical activity than traditional endpoints such as body weight, food, and water consumption. Note that the endpoints having low baseline variability were not the most useful indices.

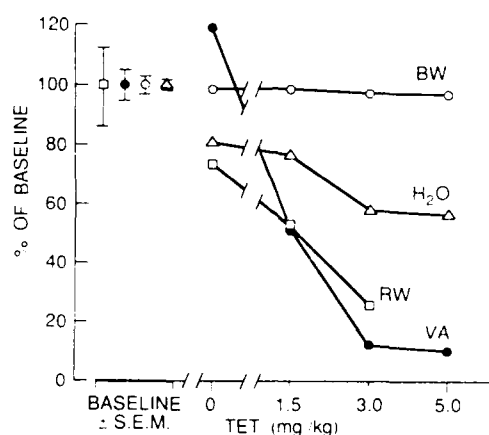


Figure 7. The baseline variability and sensitivity to triethyltin (TET) of several endpoints. Data were recorded on day 2 (48-72 h) after oral exposure to TET as described by Bushnell & Evans [33]. BW = body weight; H<sub>2</sub>O = 24 h total volume of water consumed; RW = 24 h total number of runwheel revolutions by rats residing in cages equipped with runwheels; VA = 24 h total vertical activity (rearing) by rats in the NYU homecage system.

The number of animals tested is an important factor in screening. The current system simultaneously evaluates one rack with 40 rats. Additional multiples of 40 rats can be studied simply by exchanging cages with another rack, depending on whether one wishes to evaluate each rat for one hour, one day, or one week.

### Diurnal rhythms

It is well known that daily rhythms of behavioral and physiological endpoints can reflect health and disease [35,36] as well as the effects of toxicants. Figure 8 indicates the modification of the diurnal pattern of homecage activity following exposure to organotins.

Changes in activity rhythms also have been reported following exposure to lead [12] and carbon monoxide [37]. These and other reports with toxicants suggest that the diurnal pattern of behavior can be a more sensitive index of toxicity than 24 h totals [33,38].

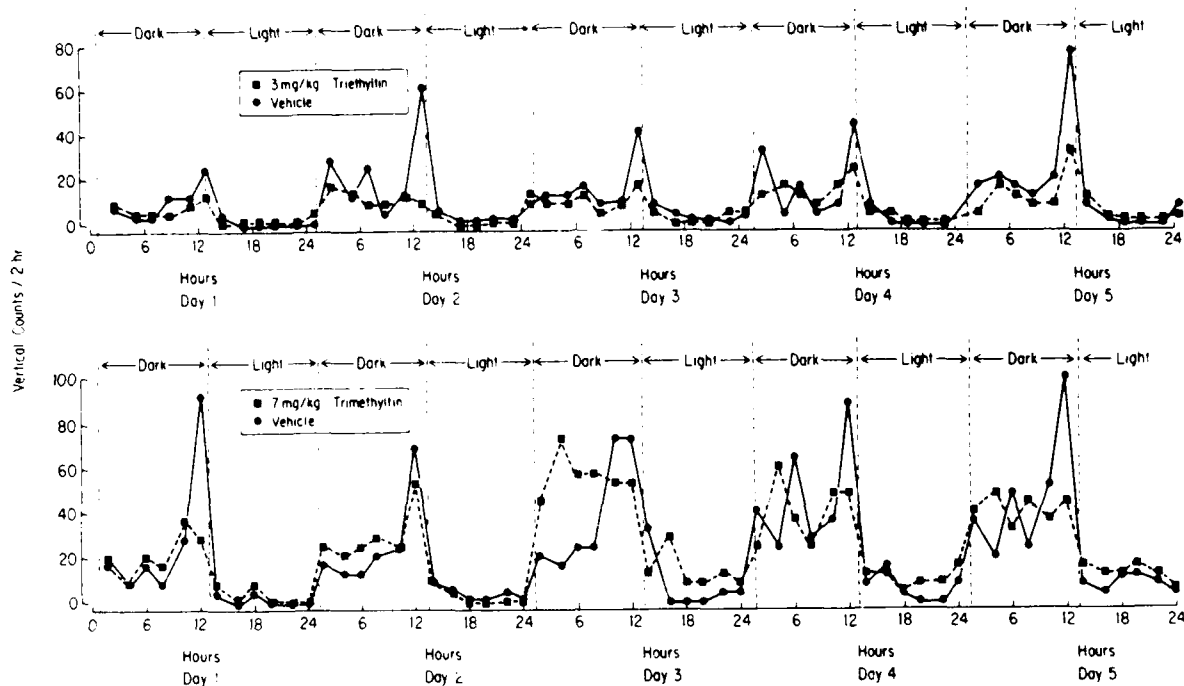


Figure 8. Diurnal patterns in vertical activity (rearing) of rats in the NYU homecage system. Upper panel: effect of acute TET or vehicle (15% ethanol in water),  $N = 10$ . Lower panel: effect of TMT or distilled water,  $N = 5$ . Data recorded in 2-h epochs starting immediately after oral intubation (hour 0, day 1). From Evans et al., [31]. A detail from day 2 after TMT is shown in Figure 2.

## CONCLUSIONS

As we prepare for a future with less emphasis upon the  $LD_{50}$  as an index of toxicity, we must identify new endpoints that are practical, sensitive, and humane. Sufficient data have been published since the review of Reiter and MacPhail [12] to justify the inclusion of automated studies of locomotor behavior in the first tier of toxicity screening. Wheel running and homecage rearing have proven both sensitive and easily quantified. Cage-side observation or a functional observational battery may also fill a need in toxicity testing, but the current toxicological data on observational methods is insufficient to document their validity and sensitivity for toxicity screening.

Several publications indicate that the rodent's nocturnal behavior is more sensitive to toxicants than is behavior in the light [24,32,33,39]. This should be recognized in selection of apparatus and time of day for testing.

An avenue for further research is the possibility that the diurnal pattern of homecage behaviors will be more sensitive and provide new information beyond that provided by the total amount or rate of occurrence of behavior. Behavioral pharmacology provides a precedent indicating that drugs may alter the pattern without altering the total output of behavior. The gain in understanding behavioral mechanisms of toxicity clearly warrants examination of patterns in basic

research; it is not clear whether the gain in sensitivity of examining patterns is sufficient to justify its inclusion in the first tier of toxicity screening.

The effects of chronic exposure have been studied much less than acute effects, for understandable reasons. Many subtle neurotoxic effects are likely to be observed only after chronic exposure. It is thus of great importance to identify practical tests for repeated evaluation of behavioral change. Nonintrusive and automated procedures seem to be the best suited to this important goal.

It has been observed that the effects of chemicals on locomotor activity can vary depending upon the measurement procedure. This is not a failing of activity as a regulatory endpoint; instead it indicates a naive assumption that "behavioral activity" is a unitary endpoint. Animals have evolved with the natural capacity to behave differently depending on whether they have been handled, whether they have access to a running wheel, and whether or not their cages are brightly illuminated. Toxicological tests should make use of the animal's natural tendency to interact with its environment. In this regard, the toxicology of naturalistic behavior requires the same careful attention to procedural variables as is demanded for chemical and morphological analyses.

#### ACKNOWLEDGMENTS

Supported in part by a Center Grant ES-00260 and a Research Grant ES-003641, both from the National Institute of Environmental Health Sciences, U.S. Dept. Health and Human Services.

#### REFERENCES

- 1 Evans, H.L. (1971) Rats' activity: influence of light-dark cycle, food presentation and deprivation. *Physiology & Behavior* 7,455-459.
- 2 Tepper, J.S., Weiss, B. and Wood, R.W. (1985) Alterations in behavior produced by inhaled ozone or ammonia. *Fund. Appl. Toxicol.* 5,1110-1118.
- 3 Barnett, S.A. (1963) *The Rat: A Study in Behavior*. Aldine Publishing Co., Chicago, Ill.
- 4 Davis, J.M. (1982) Ethological approaches to behavioral toxicology. In: C.L. Mitchell, (Ed.) *Nervous System Toxicology*. Raven Press, New York, pp. 29-44.
- 5 U.S.N.I.H. (1985) *Guide for the Care and Use of Laboratory Animals*. U.S. Dept. of Health and Human Services, Bethesda.
- 6 Tilson, H.A. (1987) Behavioral indices of neurotoxicity: what can be measured. *Neurotoxicol. Teratol.* 9,427-443.
- 7 Irwin, S. (1968) Comprehensive observational assessment. *Psychopharmacologia* 13,222-257.
- 8 U.S.E.P.A. (1985) Subpart G, Neurotoxicity, 798.6050 Functional observational battery; 798.6200 Motor activity. *Federal Register* 50: No. 188, 39458-39461.

- 9 Sette, W.F. and Levine, T.E. (1986) Behavior as a regulatory endpoint. In: Z. Annau (Ed.), *Neurobehavioral Toxicology*, Johns Hopkins University Press, Baltimore, pp. 391-403.
- 10 Buelke-Sam, J., Kimmel, C.A. and Adams, J. (1985) Design considerations in screening for behavioral teratogens: Results of the collaborative behavior teratology study. *Neurobehav. Toxicol. Teratol.* 7,537-674.
- 11 Walsh, R.N. and Cummins, R.A. (1976) The open-field test: a critical review. *Psychol. Bull.* 83,482-504.
- 12 Reiter, L.W. and MacPhail, R.C. (1982) Factors influencing motor activity measurements in neurotoxicology. In: C.L. Mitchell (Ed.), *Nervous System Toxicology*, Raven Press, New York, pp. 45-66.
- 13 Norton, S. 1977. Observational techniques for behavioral toxicology. In: H. Zenick and L.W. Reiter (Eds.), *Behavioral Toxicology: An Emerging Discipline*, U.S.E.P.A. Document EPA-600/9-77-042, pp 1-11.
- 14 Mullenix, P. (1977) Altered behavioral patterning in rats postnatally exposed to lead: the use of time-lapse photographic analysis. In: H. Zenick and L.W. Reiter (Eds.), *Behavioral Toxicology: An Emerging Discipline*, U.S.E.P.A. Document EPA-600/9-77-042, pp 1-13.
- 15 Pryor, G.T., Uyeno, E.T., Tilson, H.A. and Mitchell, C.L. (1983) Assessment of chemicals using a battery of neurobehavioral tests: a comparative study. *Neurobehav. Toxicol. Teratol.* 5,91-117.
- 16 Bushnell, P.J., Evans, H.L. and Palmes, E.D. (1985) Effects of toluene inhalation on carbon dioxide production and locomotor activity in mice. *Fundam. Appl. Toxicol.* 5,971-977.
- 17 Wenger, G.R., McMillan, D.E. and Chang, L.W. (1982) Behavioral toxicology of acute trimethyltin exposure in the mouse. *Neurobeh. Toxicol. Teratol.* 4,157-161.
- 18 Sandberg, P.R. Hagenmeyer, S.H. and Henault, M. A. 1985. Automated measurement of multivariate locomotor behavior in rodents. *Neurobehav. Toxicol. Teratol.* 7, 87-94.
- 19 Ruppert, P.H., Walsh, T.J., Reiter, L.W. and Dyer, R.S. (1982) Trimethyltin induced hyperactivity: time course and pattern. *Neurobeh. Toxicol. Teratol.* 4,135-139.
- 20 Evans, H.L. (1982) Assessment of vision in behavioral toxicology. In: C.L. Mitchell (Ed.), *Nervous System Toxicology*. Raven Press, New York, pp. 81-108.
- 21 Campbell, B. A. and Raskin, L.A. (1978) Ontogeny of behavioral arousal: the role of environmental stimuli. *J. Compar. Physiol. Psychol.* 92,176-184.
- 22 Johnson, C.T., Dunn, A., Robinson, C., Walsh, T.J. and Swartzwelder, H.S. (1984) Alterations in regulatory and locomotor behaviors following trimethyltin exposure in the rat: a time and dose analysis. *Neurosci. Letters* 47,99-106.
- 23 Evans, H.L., Dempster, A.M. and Snyder, C.A. (1981) Behavioral changes in mice following benzene inhalation. *Neurobehav. Toxicol. Teratol.* 3,481-485.
- 24 Elsner, J., Looser, R. and Zbinden, G. (1979) Quantitative analysis of rat behavior patterns in a residential maze. *Neurobehav. Toxicol.* 1: Suppl. 1, 163-174.

- 25 Hesseltine, G.R., Wolff, R.K., Hanson, R.L., McClellan, R.O. and Mauderly, J.L. (1985) Comparison of lung burdens of inhaled particles of rats exposed during the day or night. *J. Toxicol. Environ. Hlth.* 16,323-329.
- 26 Tepper, J.S. and Weiss, B. (1986) Determinants of behavioral response with ozone exposure. *J. Appl. Physiol.* 60,868-875.
- 27 Horiuchi, K., Horiuchi, S. and Morioka, S. (1967) Maximum allowable concentration of benzene in an animal experiment. *Osaka City Medical J.* 13,1-8.
- 28 Dempster, A.M., Evans, H.L. and Snyder, C.A. (1984) The temporal relationship between behavioral and hematological effects of inhaled benzene. *Toxicol. Appl. Pharmacol.* 76,195-203.
- 29 Gerber, G.J., Nawiesniak, E., Ratte, S. and O'Shaughnessy, D. (1985) Triethyltin produced decrease and recovery of wheel running and food reinforced lever pressing in rats. *Neurobehav. Toxicol. Teratol.* 7,433-438.
- 30 Wenger, G.R., McMillan, D.E. and Chang, L.W. (1984) Behavioral effects of trimethyltin in two strains of mice. *Toxicol. Appl. Pharmacol.* 73,78-88.
- 31 Evans, H.L., Bushnell, P.J., Taylor, J.D., Monico, A., Teal, J.J. and Pontecorvo, M.J. (1986) A system for assessing toxicity of chemicals by continuous monitoring of homecage behaviors. *Fundam. Appl. Toxicol.* 6,721-732.
- 32 Bushnell, P.J. and Evans, H.L. (1985) Effects of trimethyltin on patterns of homecage behavior in rats. *Toxicol. Appl. Pharmacol.* 79,134-142.
- 33 Bushnell, P.J. and Evans, H.L. (1986) Diurnal patterns in homecage behavior of rats after acute exposure to triethyltin. *Toxicol. Appl. Pharmacol.* 85,346-354.
- 34 Bondy, S.C. and Hall, D.L. (1986) The relation of the neurotoxicity of organic tin and lead compounds to neurotubule disaggregation. *Neurotoxicology* 7, 51-56.
- 35 Brown, F.M. and Graeber, R.C. (1982) *Rhythmic Aspects of Behavior*. Lawrence Erlbaum Assoc., Hillsdale, NJ.
- 36 Moore-Ede, M.C., Sulzman, F.M. and Fuller, C.A. (1982) *The Clocks That Time Us*. Harvard University Press, Cambridge, MA.
- 37 Culver, B. and Norton, S. (1976) Juvenile hyperactivity in rats after acute exposure to carbon monoxide. *Exper. Neurol.* 50,80-98.
- 38 Raslear, T.G. and Kaufman, L.W. (1983) Diisopropyl phosphorofluoridate (DFP) disrupts circadian activity patterns. *Neurobehav. Toxicol. Teratol.* 5,407-411.
- 39 Tilson, H.A., Davis, G.J., McLachlan, J.A. and Lucier, G.W. (1979) The effects of polychlorinated biphenyls given prenatally on the neurobehavioral development of mice. *Environ. Res.* 18,466-474.
- 40 Graefe, J.F., Evans, H.L. and Bushnell, P.J. (1986) Diurnal rhythm of monkey and rat activity after trimethyltin exposure. *The Toxicologist* 6,220.

## QUANTIFICATION OF OPERANT BEHAVIOR

Deborah C. Rice

*Toxicology Research Division, Food Directorate, Health Protection Branch, Health and Welfare  
Canada, Ottawa, Ontario, Canada K1A 0L2*

### SUMMARY

The study of performance on intermittent schedules of reinforcement has proved to be a powerful tool in the fields of experimental psychology and behavioral pharmacology and presently is proving equally valuable in behavioral toxicology. The ability to specify precisely contingencies of reinforcement allows a careful and detailed quantification of performance. Intermittent schedules of reinforcement may be used in behavioral toxicology in a number of ways. A baseline of performance may be established and utilized to monitor acute effects or to track effects of chronic exposure to a toxic agent. Alternatively, schedules of reinforcement may be used in experiments requiring group comparisons, where both terminal performance and acquisition of performance may be of interest. The use of different schedules, generating different rates and patterns of performance, may be compared to elucidate behavioral mechanisms. Use of computers for schedule control and data acquisition allows a detailed analysis of performance, thus increasing the probability of the detection of subtle effects.

### INTRODUCTION

The term "operant behavior" has a very specific and well-defined meaning in experimental psychology. Unfortunately, it often is used in a much narrower sense, particularly in behavioral pharmacology and toxicology. This undoubtedly leads to confusion and misunderstanding, particularly among those not conversant in behavioral methodology and theory.

Operant behavior is movement that operates on (changes) the environment. In general, voluntary movement (as opposed to reflexes) may be considered operant behavior and may include any of a variety of responses, such as pressing a lever, running in a wheel or down an alley, or swimming. Any operant behavior may be conditioned. Operant conditioning is the process by which the frequency or strength of an operant response is modified by its consequences. For example, if depression of a lever by a hungry rat is followed by the presentation of food, the likelihood that the response (lever press) will occur again is increased. That is, the consequences of the behavior come to control the likelihood of the response. Operant conditioning techniques provide an extremely powerful tool with which to ask the subject questions about learning, memory and sensory function, as well as general well-being [1]. Such techniques are ideally suited to answer the questions relevant to behavioral toxicology.

In the natural world, reinforcement does not usually follow every instance of any particular behavior. Rather, behavior is reinforced infrequently or intermittently. An obvious example is the distribution of paychecks, typically on a fixed (regular) interval. In school, children are not praised for every problem solved, but for completing the required set of problems. In the natural environment, reinforcement schedules, or requirements before reinforcement is forthcoming, may be quite complex or even indiscernible. The laboratory allows the experimenter the opportunity to examine performance on simple, precisely specified schedules.

#### DESCRIPTION OF INTERMITTENT SCHEDULES

Intermittent schedules of reinforcement have been studied extensively by experimental psychologists, and performance thus generated is orderly, predictable, and reproducible [2, 3]. On intermittent schedules, reinforcement is based on the number of responses emitted, some temporal requirement for emission of responses, or a combination of these. For example, a fixed ratio (FR) schedule requires that a fixed number of responses be emitted for reinforcement. A fixed interval (FI) schedule, on the other hand, requires that a specified fixed length of time elapse before a response is reinforced. The FR typically generates a high response rate, with a pause at the beginning of each FR. The higher the FR requirement, the longer the initial pause (Figure 1). The FI schedule, on the other hand, generates a scalloped pattern of response, characterized by an initial pause followed by a gradually accelerating rate of response terminating in reinforcement. Other simple schedules include the variable ratio (VR) and the variable interval (VI) schedules. In these, reinforcement is dependent upon a number of responses (VR) or after an interval that varies around some average (VI). Both of these schedules generate a constant rate of response with no post-reinforcement pause; the VR schedule usually generates a higher rate of response than the VI schedule.

The typical manner of visually representing performance on intermittent schedules, and one which has a venerable history, is by means of the cumulative record (see Figure 1). The pattern of response is recorded on a cumulative recorder as the session progresses. A motor drives a strip of paper at a constant speed, and each response moves the pen vertically. Reinforcements are traditionally signalled by a downward deflection of this pen. The pen may be programmed to reset to baseline, at the end of each schedule component, for example, if desired. The behaviorist attuned to reading the cumulative record thus generated is able to discern important patterns of response and may feel deprived of an important source of information if only numbers summarizing the session are available.

The type of response required of the subject is termed the "operant." For performance on intermittent schedules, typically some action by the subject closes a microswitch, which is sensed as a

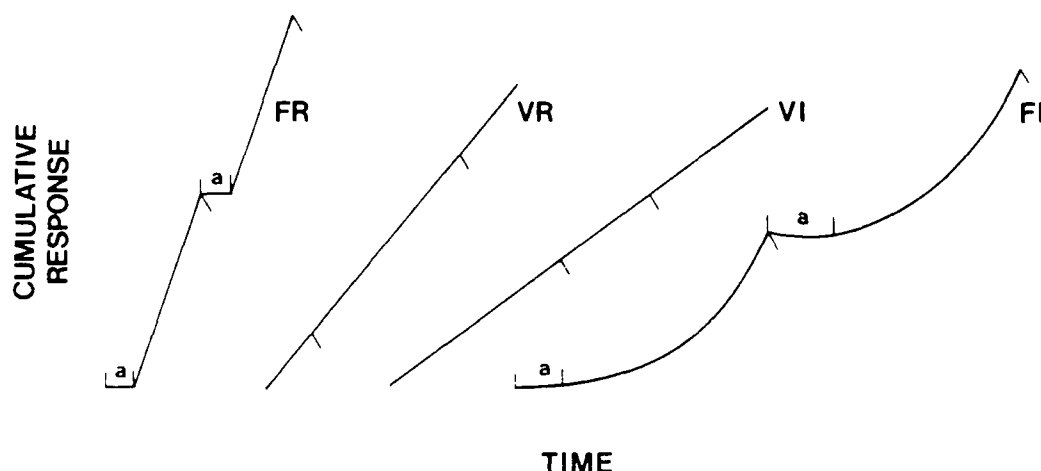


Figure 1. Schematic cumulative records for FR, VR, VI, and FI schedules of reinforcement. Responses are cumulated vertically over time. A greater slope to any line represents a higher rate of response. Reinforcements are signalled by downward deflection of the pen. Each "a" represents a postreinforcement pause, observed under FR and FI schedules.

response and recorded by the equipment controlling the experiment. For rats this is most often pressing a lever; for birds, pecking at a round disk (called a key); and for primates, pulling a knob or pressing a disk. An operant convenient for use with rodents that requires little or no training is the "nose-poke," in which interruption of a photocell beam by insertion of the snout (or sometimes paw) into the food delivery tube serves as the response. Running in an exercise wheel is another convenient operant for a variety of species; a "response" may consist of completing any specified fraction of a revolution. Licking a tube from which the fluid reinforcer will be delivered has been used successfully as an operant, especially with mice. Each lick is sensed by a ground-detecting circuit and recorded as a response.

The grossest measure of performance on intermittent schedules is the average or overall response rate, which is simply the total number of responses divided by the total session time. Such a measure may be considered only a crude summary of performance, however. It is usually desirable to examine the performance in greater detail, differentiating it into component parts. Such an analysis allows a more precise understanding of the manner in which the schedule controls behavior and may also suggest possible behavioral mechanisms affected by the toxic agent.

Analysis of FI performance offers perhaps the best example. FI performance is characterized by a complex pattern of response, which may be examined in a number of ways. The initial pause at the beginning of the interval is typically a function of the interval length; the longer the interval, the longer the pause. After the pause is subtracted, the rate of responding during the remainder of the interval is termed the run rate. A measure that may be sensitive to disruption to toxicant exposure is

the inter-response time (IRT) distribution. This is the actual times between successive responses, from which a frequency distribution of various length IRTs may be generated.

The scalloped pattern of responding under the FI schedule is a consequence of the temporal control over behavior exerted by the schedule, and the characterization of this pattern is therefore of considerable interest. This typically is done in one of two ways (Figure 2). The simplest of these to calculate is the quarter life [4], which is the proportion of the interval required to emit the first one-quarter of the responses in the interval. The index of curvature [5] specifies the deviation from linearity of the shape of the FI "scallop."

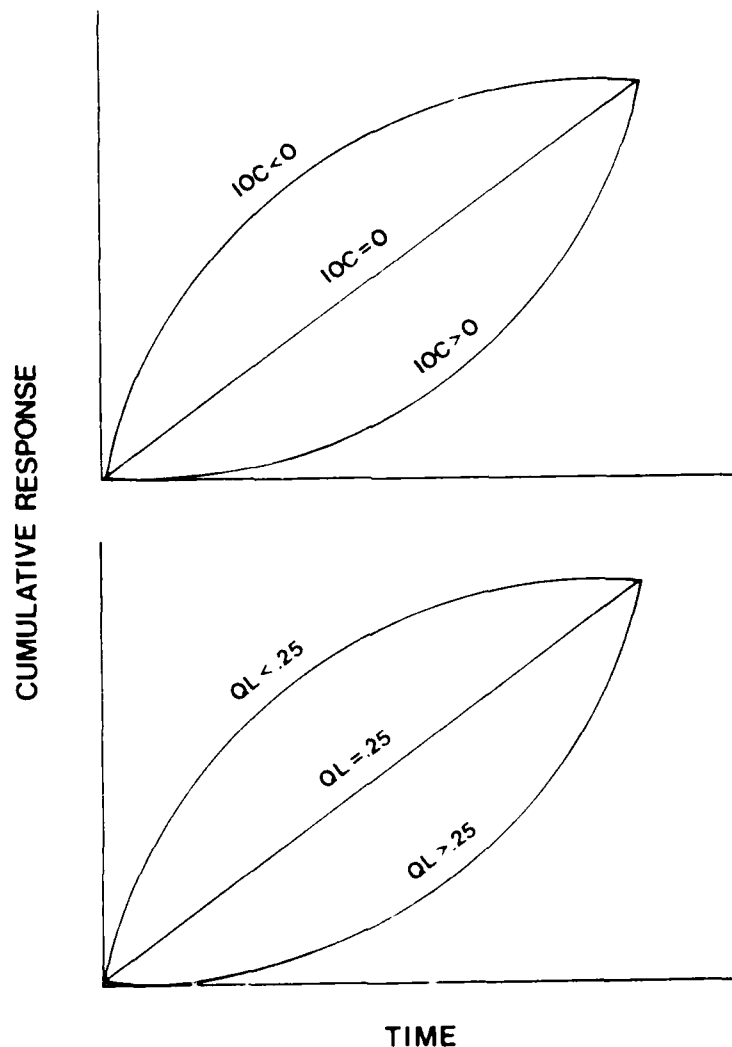


Figure 2. Schematic of the value of the quarter life (QL) (top) or the index of curvature (IOC) (bottom) on an FI schedule of reinforcement. The  $QL = .25$  if the response pattern is linear,  $QL > .25$  if the pattern is positively accelerated (the typical FI response pattern from a trained subject), and  $QL < .25$  if the pattern is negatively accelerated. The  $IOC = 0$  if the response pattern is linear, and  $-1 < IOC < 0$  or  $0 < IOC < 1$  for negatively or positively accelerated patterns respectively.

The FI offers important advantages in the analysis of behavioral effects produced by toxicants. Since only one response is required at the end of a constant specified interval for reinforcement, individual subjects may respond at any rate (except an extremely low one) without affecting the density of reinforcement. Thus rate increases or decreases may be readily detected. In addition, analysis of the temporal distribution of responses during the interval yields information about the ability of the subject to discriminate time.

Another schedule that may be considered to examine temporal discrimination is the differential reinforcement of low rate (DRL) schedule. The DRL specifies a minimum time between successive response (or between a reinforcement and the next response) for reinforcement. For example, a DRL 30-s schedule requires that at least 30 s elapse between the last event (response or reinforcement) and the next response.

Performance also may be maintained on intermittent schedules by the use of negative reinforcement, usually a brief mild electric shock. The most popular of this is continuous or "Sicman" avoidance, in which each response postpones the shock for a prespecified period of time. By spacing successive responses within this time period, the subject may postpone shock indefinitely. Schedules using negative reinforcement are particularly useful as a comparison to behavior generated by positive reinforcement (food or fluid) as a control for anorectic effects.

Simple intermittent schedules such as these may be combined in a variety of ways to produce complex schedules. This allows more than one baseline, which may be differentially sensitive to the effects of a toxicant, to be examined in the same session. The most common way in which simple schedules are combined is termed a multiple schedule. For example, if FR and FI schedules were presented in succession during a test session, the resulting schedule would be a multiple fixed interval fixed ratio (mult FI-FR). Each component of the multiple schedule is independent and occurs in the presence of a different external discriminative stimulus that signals the schedule component in effect. For example, the FI component may be signaled by a green light above the response lever and the FR component by a yellow one. The schedule components typically are presented in an alternating fashion, so that data on the different components can be collected almost simultaneously. Frequently, performance on the FI and FR are contrasted because of the marked difference in the baseline performance on these two schedules and because the FI allows so much variation in performance (see above).

Simple intermittent schedules of reinforcement may be combined in a number of other ways as well [2, 6]. The mixed schedule is identical to the multiple schedule, except that there are no external stimuli signalling which type of schedule component is in effect, the only stimuli available to the subject are the effects of its own behavior in relation to the schedule. In a chain schedule, the subject

is required to complete two or more schedule components sequentially, with reinforcement available upon completion of the entire chain. As in the multiple schedule, each component is signalled by unique discriminative stimuli. The tandem schedule of reinforcement is equivalent to the chain schedule except that no external stimuli indicate which component is in effect.

The use of intermittent schedules of reinforcement offers several advantages to the behavioral toxicologist. Of considerable importance is the fact that the pattern of responding on intermittent schedules is similar across species (Figure 3), including humans under some conditions, thus ensuring that the performance under study has some species generality. An extensive body of literature describes the effects of a wide variety of psychoactive drugs on intermittent schedules of reinforcement [7, 8, 9, 10]. The effects of drugs on particular schedules are also often similar across species [7]. The large body of literature on the effects of drugs of various classes allows comparison of effects produced by a toxicant to those of psychoactive agents whose mechanisms, symptoms, and signs are well or at least partly characterized.

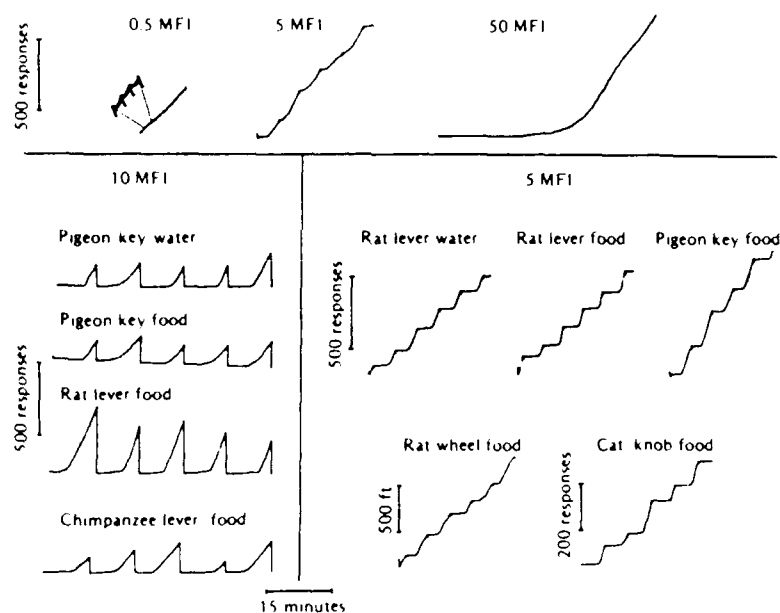


Figure 3. Generality of the pattern of FI responding. Ordinate: cumulative number of responses. Abscissa: time. The upper panel represents an individual pigeon pecking a response key for food on three different FI durations. The general pattern of response persists despite the 100-fold change in schedule parameter. The lower left frame represents performance on an FI-10 min schedule for a number of species and different reinforcers. The end of each FI was signalled by a reset of the pen to baseline. The lower right panel depicts performance on an FI 5-min schedule for different species, type of manipulation, and reinforcer. (From Kelleher and Morse [33].)

Intermittent schedules of reinforcement possess properties that render them ideal candidates with which to explore a variety of experimental questions. They generate performance that is remarkably stable over long periods of time. A baseline of performance may be utilized for within-

subject designs, such as generation of acute dose-effect curves, or assessment of progression of toxicity or reversibility following chronic exposure. Alternatively, intermittent schedules may be used in studies requiring between-group comparisons, such as the assessment of developmental or longitudinal effects. In such instances, acquisition of performance may be of equal or more interest than terminal stable performance. Disruption of performance on intermittent schedules may be the result of a very specific change in the central nervous system, the result of toxicity in other organ systems, or the consequence of aversive properties of the toxic agent itself. Therefore, performance on intermittent schedules may serve as a sensitive indicator of a variety of toxic effects.

The use of laboratory computers in behavioral toxicology has simplified data collection and computation of summary measures, and provides flexibility not possible during the days when the schedule contingencies and data collection were accomplished by means of electromechanical or transistor-based hardware. For example, the computer allows each IRT to be recorded separately, so the entire session may be reconstructed exactly. This allows *post hoc* analyses of interesting observations. For example, IRT distributions often are generated by deciding the resolution of the frequency distribution before the study begins. Typically it is fairly coarse – 1 s or greater. There is not the possibility of performing a more fine-grained analysis later, if examination of the cumulative record indicates this may prove fruitful, because of the limitation in the manner in which the data were collected. Similarly, if changes in response pattern over the course of the session are observed, there may not be the possibility of *post hoc* examination of these changes. The accurate recording of the session also circumvents inaccuracies compelled by other data-gathering strategies. If data are collected in such a way that the session appears as one grand FI, for example, then calculations of quarter life, index of curvature, and even run rate are weighted by intervals with many responses, and those with few responses will not influence the data. This is not a trivial point, since intervals with low and high response rates are a common feature of FI performance. If each FI can be analyzed individually, however, then performance during all intervals can contribute equally to the summary data, if desired. This method of data analysis also provides the opportunity to calculate within-session variability, which may be affected by exposure to a toxicant.

#### SELECTED EXAMPLES IN BEHAVIORAL TOXICOLOGY

Simple intermittent schedules have been utilized quite extensively in behavioral toxicology. For example, the effects of lead on FI performance have been examined in some detail in the monkey. Low doses of lead produced a dose-related decrease in the average IRT [11], without changes in the pause time or the shape of the FI scallop. Examination of the cumulative record revealed a "grainy" pattern of response, atypical of FI performance, for monkeys in the highest dose group [12]. This pattern was the result of bursts of responding with very short IRTs. When IRT distributions were generated based on a fine resolution (100 msec), these monkeys were found to have a predominance

of very short IRTs ( $<0.5$  s) (Figure 4). Such a histogram distribution would not have been planned *a priori* for a long FI (8 min) in the monkey; the manner in which the data were recorded (see above) allowed detailed examination of this unexpected phenomenon. Performance on the FI proved a more sensitive indicator of lead exposure than locomotor activity; increased activity was manifested on FI responding but not locomotion in this group of monkeys [12].

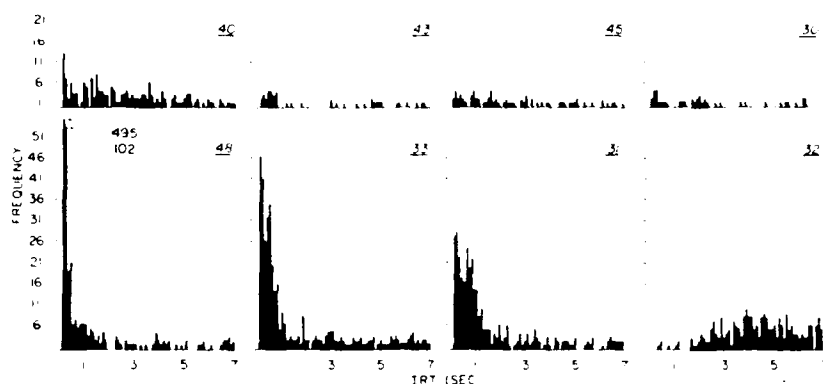


Figure 4. IRT absolute frequency distribution for one session of a fixed interval schedule for control (top) and monkeys treated with lead from birth (bottom). The divisions along the abscissa represent the classes of time between successive responses in 100 msec increments. The lead-treated monkeys in general had a much higher absolute frequency of IRTs, and a distribution skewed toward shorter IRTs (from Rice et al., [12].)

Monkeys exposed to a higher dose of lead exhibited not only a decrease in average IRT (and concomitant increase in run rate), but also a change in the shape of the FI response pattern. This was reflected in both a longer pause time and an increase in the index of curvature [11]. This change in the pattern of FI responding suggests a difference in temporal discrimination between control and treated monkeys not present at lower doses of lead. In addition, the effect on run rate and pause are in the "opposite" direction; the increase in pause time represents a decrease in responding, while the increase in run rate represents an increase. If average response rate had been utilized as the summary measure of FI performance, the actual effects produced by lead would have gone unrecognized. In fact, there may be no change at all in average rate of response in the present experiment (it has not been calculated).

Intermittent schedules may be used to monitor effects other than, or in addition to, direct effects on the central nervous system. The effects of carbon monoxide exposure have been examined in the mouse by comparing performance on an FR schedule with the ability to climb a screen [13]. Effects were found on the FR at lower concentrations and concomitantly lower carboxy-hemoglobin levels than those required to impair the ability to perform the screen-climbing task. In this study, the rate-lowering effect of CO on FR performance (as well as on the screen test) is probably attributable to a generalized disability produced by oxygen deprivation. The decrease in performance therefore represents a secondary effect on the nervous system as a result of the ability of CO to lower the oxygen-carrying capacity of blood, as well as effects on other organ systems (muscle-for example) due to oxygen deprivation. Similarly, Weiss et al. [14] studied the effects of ozone, a chemical known to

produce headache, dizziness, and lung irritation, on FI responding in the rat. The observed rate decrement was interpreted as decreased motivation as a result of the general discomfort produced by ozone (Figure 5).

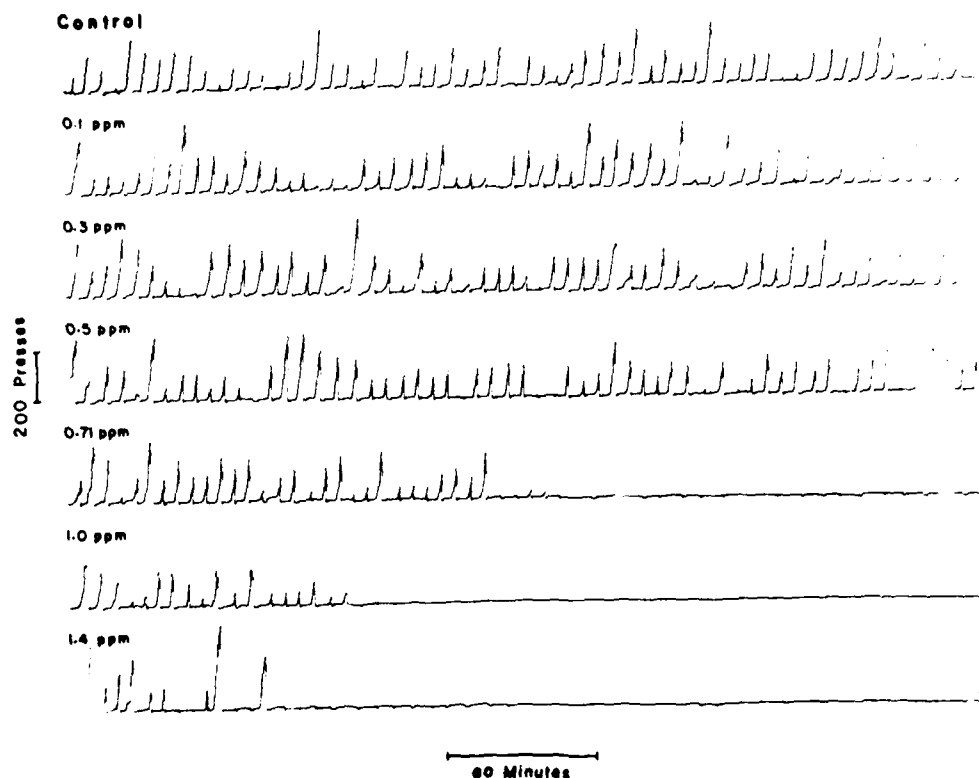


Figure 5. Cumulative records of FI performance of one rat during exposure to various concentrations of ozone exposure. Each lever press stepped the pen upward; the pen reset at the end of each interval. Increasing concentrations of ozone resulted in cessation of responding at a successively earlier point in the session. (From Weiss et al., [14].)

The advantages offered by complex schedules have been recognized and exploited by behavioral toxicologists. Both components of a mult FI-FR schedule proved equally sensitive to the effects of the organic solvent methyl *n*-butyl ketone [15], indicating that this toxicant produced a generalized impairment in performance. In contrast, Colotla et al. [16] demonstrated differential sensitivity of the components of a mult DRL-FR to the organic solvent toluene. Moreover, the effects were in the opposite direction, with toluene producing a rate increase in the DRL component and a decrease in FR response rate (Figure 6). Similarly, differential sensitivity between schedule components was observed with trimethyltin [17]. There was change in the pattern of FI performance, indicated by the quarter life, at a dose insufficient to produce other behavioral changes. At higher doses, FI and FR performances were disrupted differentially, with rate increases on the FI and rate decreases on the FR several days following acute administration. Wood et al. [18] studied the effects of toluene on an unusual multiple schedule using two varieties of a fixed consecutive number (FCN)

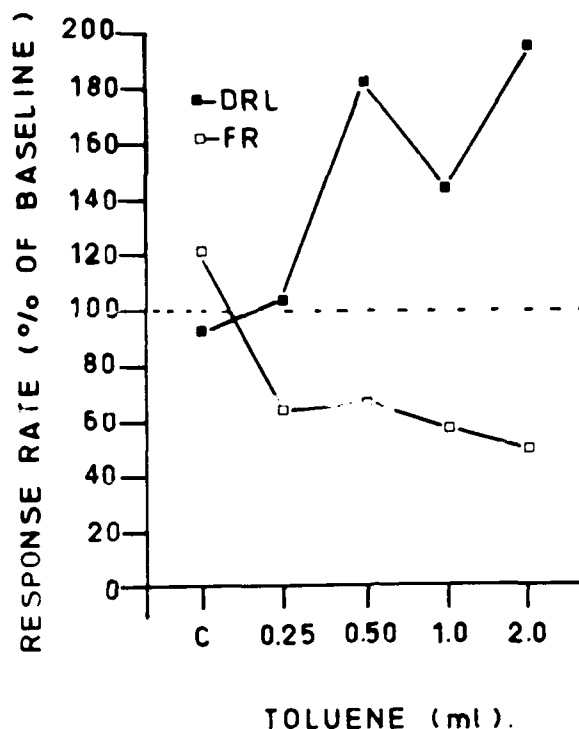


Figure 6. Average response rate for a group of rats responding on a multiple FR-DRL schedule of reinforcement under various concentrations of toluene. Response rate on the DRL component increased markedly, while rate on the FR component decreased. (From Colotla et al., [16].)

schedule. The FCN schedule required a series of 8 consecutive responses on one lever followed by one response on a second lever for reinforcement. Performance was tested under two conditions: (1) with no cues to indicate when the 8 responses had been completed, and (2) with a combination of lights and a tone signaling the completion of the 8 responses. (The former schedule is an example of a chain schedule, and the latter of a tandem.) These two conditions were combined into a multiple schedule, with 10 components under one condition followed by 10 components under the other. The concentration of toluene required to disrupt performance under the no-stimulus condition was considerably less than that required to disrupt performance that was under the control of external discriminative stimuli (Figure 7).

The results from the several studies described in the previous paragraph serve as examples of important principles of the effects of chemicals (including drugs) on behavior. An important determinant of the effect of chemicals on behavior is the schedule requirements. For example, in the study by Wenger et al. [17] discussed above, changes in temporal discrimination on the FI were observed in the absence of other changes. Another important variable in determining drug or toxicant effects may be the rate of responding [19]. Many agents, including stimulants, depressants, and opiates, decrease high rates of responding and increase low rates. This may account for the

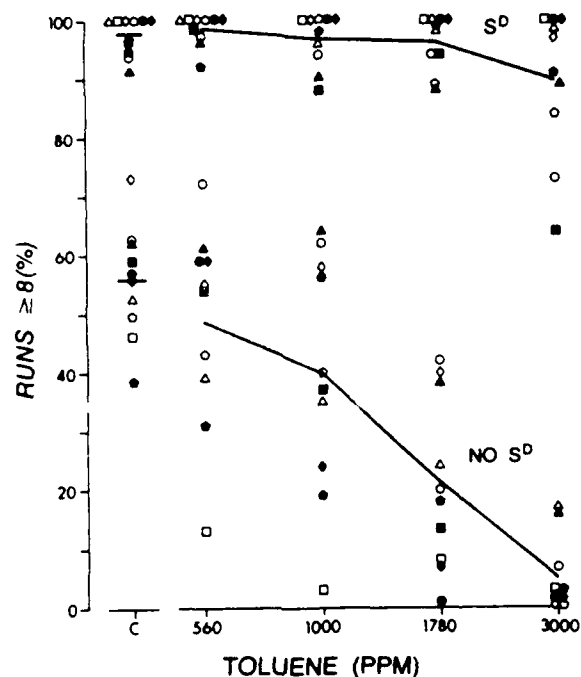
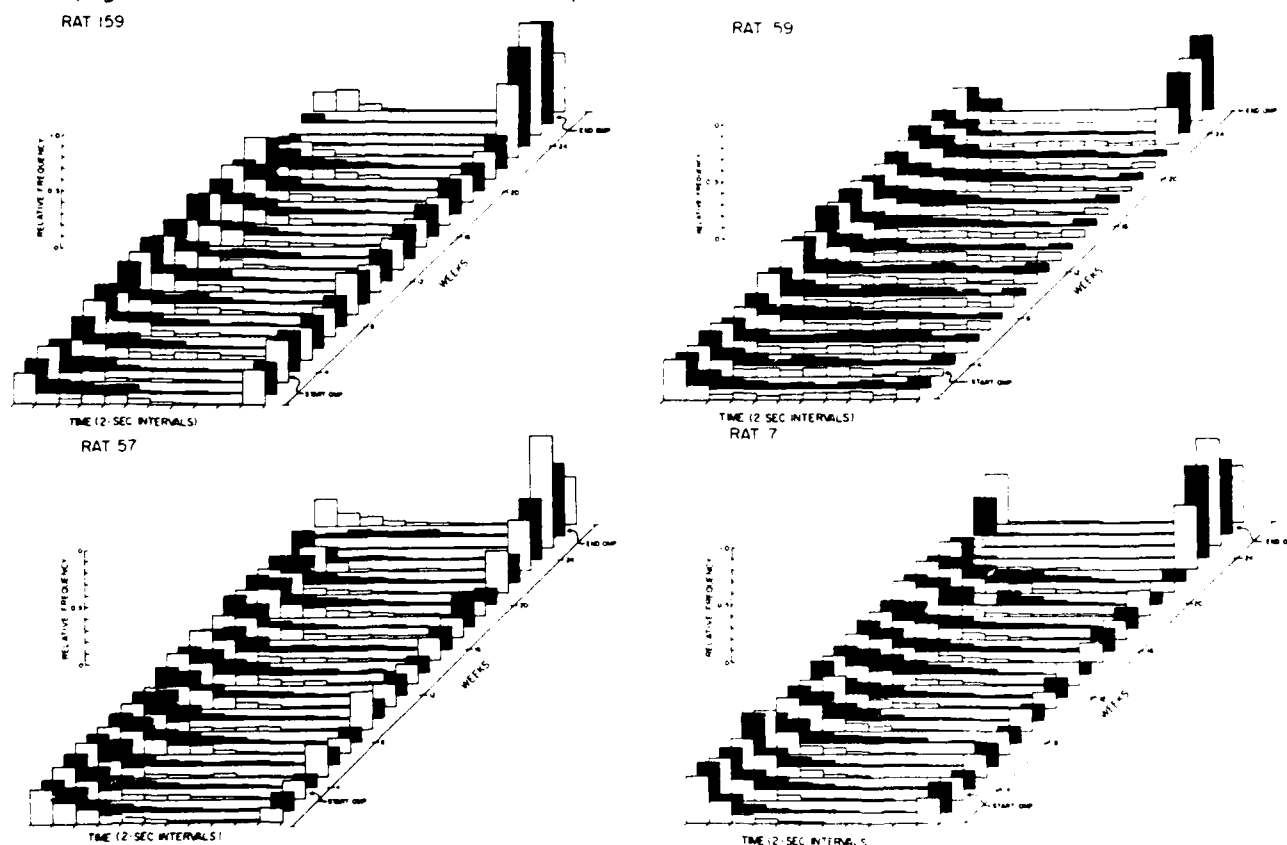


Figure 7. Effects of toluene on rats performing on a multiple fixed consecutive number (signaled)-fixed consecutive number (unsignaled) schedule. Each rat is represented by a unique symbol. The signaled condition (S<sup>D</sup>) produced better performance than the unsignaled (no S<sup>D</sup>). Deficits were apparent at a lower concentration under the unsignaled condition. (From Wood et al., [18].)

results of Colotla et al. [16] described above, for example, in which toluene produced a rate increase on a schedule generating a low rate of response (DRL) and decreased responding on a schedule generating a high rate of response (FR). Another variable of importance may be the extent to which external stimuli control performance (see Laties [20] for review). Substances typically exert less effect on performance under the control of external stimuli than upon performance not under such explicit control. The result of Wood et al. [18] presents an elegant example.

A characteristic of performance on intermittent schedules, as mentioned above, is that the effects of chemicals are often consistent across species. A compelling example of this in toxicology is a comparison of the effects of lead in the rat and the monkey. At low doses, exposure to lead during development produced a dose-related increase in response rate on the FI schedule in both the rat [21, 22] and the monkey [11,12]. In contrast, response rate on the FR decreased in both species as a result of developmental lead exposure [11,23]. In both species, the FI schedule proved more sensitive to disruption by lead exposure than the FR. These differential effects on the two schedules probably reflect both rate dependency and differences in schedule requirements. The fact that lead produced virtually identical effects in two very different species confers confidence concerning the generality and reproducibility of these effects.

One of the important characteristics of intermittent schedules is that, once trained, they generate performance that is stable across long periods of time. Thus they are extremely useful for tracking onset and/or reversibility of behavioral toxicity. (This is in marked contrast to many other simple tests used to determine behavioral toxicity, which may be tested only once or a few times, thus necessitating large numbers of animals if testing at several time points is of interest.) For example, Walsh et al. [24] used continuous avoidance responding to track the toxicity of a low dose of a tributyltin ester. After 5 months of exposure, the stable baseline of performance shifted, manifested by an increase in shock rate, decreased response rate, and a shift in the IRT distribution toward long IRTs (Figure 8). These effects were reversible upon withdrawal of the toxicant. Intermittent schedules



**Figure 8.** Absolute IRT distribution on a free avoidance schedule for rats exposed chronically to a low dose of a tributyltin ester. After approximately 5 months of exposure, the IRT distribution shifted toward a decrease in short IRTs and an increase in longer ones. This was accompanied by an increase in shock frequency. (From Walsh et al., [24].)

have been used to track the effects of chronic administration of pesticides [25]. Parathion was found to affect rate of response on a mult FI-FR in a rate-dependent manner, while chronic exposure to mirex or chlordecone resulted in initial rate increases followed by rate decreases as exposure continued. Behavioral effects were observed in the absence of signs of gross toxicity. Cory-Slechta and Thompson [26] utilized FI responding to assess the reversibility of the response rate increases produced by post-weaning lead exposure in the rat. Withdrawal of lead resulted in the response rate

decreasing to control levels after approximately one month, while the response rate of rats maintained on lead remained elevated.

While the utility of the stable baseline generated by intermittent schedules is well recognized, little attention has focused on the acquisition of performance. We observed apparent differences in the acquisition of DRL performance in monkeys exposed to lead from birth [27], and attempted to quantify them. We compared the increment in the number of reinforcements, and the decrement in the number of nonreinforced responses, between sessions 1 and 2 (which were training sessions on a DRL 5-s schedule), and between sessions 1-5 and 6-10 on the terminal DRL 30-s schedule. Since the DRL reinforces the first response after the specified elapsed time, and responses before this time are not only not reinforced but also reset the time contingency, these two measures are indicative of the degree of acquisition. Treated monkeys were retarded in the acquisition of DRL performance in a dose-dependent manner (Figure 9). These differences were observed in the absence of differences on the more typical measures of DRL performance such as pauses, response rates, or IRT distributions. These results were consistent with performance of these monkeys on other tasks that presumably measure "learning."

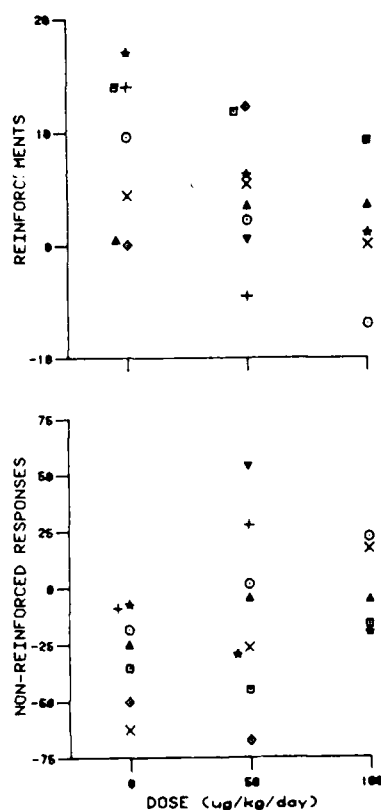


Figure 9. Difference in the number of reinforced (top) and nonreinforced responses between sessions 1 and 2 on a DRL schedule for monkeys exposed to lead from birth. Each symbol represents an individual monkey. Treated monkeys "learned" the DRL more slowly than controls. (From Rice and Gilbert [27].)

One aspect of performance that is typically not analyzed on intermittent schedules (or on other behavior tasks) is variability of performance, either within a session or between sessions. (Within-group variability is discussed in the next section.) Differences in variability of performance between treated and control subjects may prove a sensitive indicator of toxic effect and indeed may be observed in the absence of other effects. In the DRL experiment described above, for example, the variability of performance of monkeys in the treated groups increased over the course of the 60 DRL 30-s sessions, while between-session variability in the control monkeys did not (Figure 10). This effect was observed in the absence of differences in rates, pauses, or IRT distributions. Similarly, increased between-session variability was observed on FR responding on a mult FI-FR schedule as a result of lead exposure, in the absence of any other discernible effect on FR performance [11]. While comparison of between-session variability is relatively straightforward, a computer is almost a necessity for comparison of within-session variability (see above). Each individual schedule component (FI or FR, for example) can be analyzed separately and the within-session variance determined. We observed, for example, that lead produced a within-session increase in the variability of responding on an FI schedule of reinforcement [28].

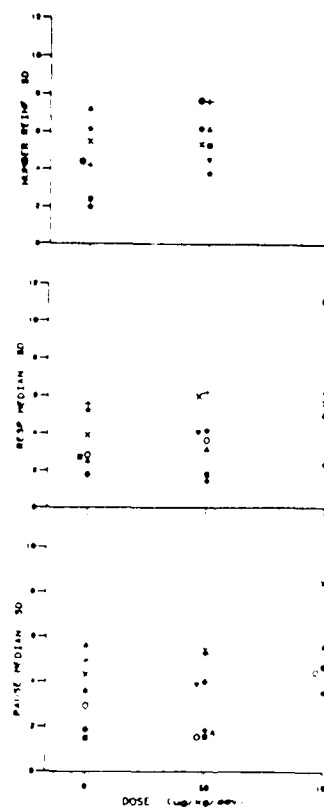


Figure 10. Standard deviation for number of reinforcements (top), response median (center), and pause median (bottom) over sessions 51-60 of a DRL schedule for monkeys exposed to lead from birth. Each symbol represents an individual. Treated monkeys were more variable in their performance across sessions than were controls. Absolute values for these measures did not differ between groups. (From Rice and Gilbert [27].)

## STATISTICAL CONSIDERATIONS

One of the most problematic issues confronting the behavioral toxicologist is choice and availability of appropriate statistical methodology, and statistical analysis of performance on intermittent schedules is no exception. (The relevant issues and problems are in fact not unique to behavioral toxicology, but are common to many areas of toxicology.) A feature shared by many behavioral experiments is that there are relatively small numbers of subjects in each treatment group, and repeated measures are collected from each subject for a number of parameters. The typical statistical method applied to such a design by psychologists is the ANOVA for repeated measures. The ANOVA is powerful in detecting changes over the course of the experiment, but has much less power to detect effects between groups, which is the statistical interest to the behavioral toxicologist. Multivariate statistical analyses typically are not suitable because the number of subjects is too small compared to the number of parameters. It is usually desirable to use statistical techniques more elegant and holistic than large numbers of individual comparisons, which in any case may be too conservative if the  $\alpha$  level is distributed over all components.

Variability in the treated groups may be greater than in the control group due to the presence of responders and nonresponders in the treated groups [29, 30]. This often results in inhomogeneity of variance, thus violating one of the assumptions for parametric statistical analyses. The typical response to this phenomenon is transformation of the data to eliminate heterogeneity of variance, which may in fact mask an important treatment effect. A randomization test has been devised [29] that is sensitive not only to differences in the mean, but also to differences in variance between groups. The relative weight of these factors is specified by constants in the equation. As demonstrated by Good [29], such a test is more powerful than the t-test under conditions commonly encountered in behavioral toxicity data.

A promising approach to the analysis of repeated measures between groups has been the application of curve-fitting techniques to behavioral toxicity data (Cox and Cory-Slechta [31]). They fitted cubic orthogonal polynomials to individual profiles for several sets of real data, including data generated under different schedules, few or relatively large numbers of sessions, and treatment groups consisting of 6 or 12 subjects. They found this curve-fitting analysis, combined with randomization tests, to be more sensitive than repeated-measures, ANOVAs or a multivariate test.

A consideration often overlooked in the analysis of behavioral data is a determination of the power of the study to detect an effect if one were present. Particularly if the study is designed to determine a no-effect level, the power to detect an effect should be calculated after completion of the study. (Ideally, an estimate should be performed before initiation of the study, in order to calculate the required number of subjects. However, limitation of resources usually necessitates

smaller-than-optimal group sizes.) Similarly, the change required for an effect to be detected given the number of subjects, variability of the data, and the chosen  $\alpha$ , may be calculated by such measures as the coefficient of detection [32]. Such calculations may be extremely important in the interpretation of results, particularly if negative results are obtained.

## CONCLUSIONS

The field of behavioral toxicology is a relatively new one, and one that is developing rapidly. Its literature is growing at a tremendous rate, along with the range of new techniques applied to toxicological problems. Many of these techniques enjoy an extensive history, based in experimental psychology, behavioral pharmacology, or the broader areas of neuroscientific research. Performance generated by intermittent schedules of reinforcement has been well characterized for more than 30 years, and the effects of a wide variety of psychoactive agents have been determined. These effects are predictable and reproducible, between laboratories and often across species as well. Schedule-controlled performance therefore provides an extensive background of information against which the effects of a toxic agent may be compared, allowing possible insight into behavioral or biochemical mechanisms. This is in contrast to some of the tests that have been introduced into the behavioral toxicology literature in the last several years, for which the relevant controlling behavioral variables, effects of psychoactive agents, reproducibility, and species generality are unknown.

Intermittent schedules of reinforcement offer unique characteristics that should be utilized in answering a variety of experimental questions. They may be used to determine effects of acute or chronic exposure, examine acquisition and variability of performance, and track progression and reversibility of behavioral toxicity. They are relatively easy to train and are suitable for almost any species. They are therefore ideally suited to serve as the "workhorse" for examination of learned behavior in behavioral toxicology.

## REFERENCES

- 1 Laties, V.G. (1982) Contribution of operant conditioning to behavioral toxicology. In: C.L. Mitchell (Ed.), *Nervous System Toxicology*, Raven Press, New York, pp. 67-80.
- 2 Ferster, C.B. and Skinner, B.F. (1957) *Schedules of Reinforcement*. Prentice-Hall, New Jersey.
- 3 Schoenfeld, W.N. (1970) *The Theory of Reinforcement Schedules*. Appleton-Century-Crofts, New York.
- 4 Herrnstein, R.J. and Morse, W.H. (1957) Effects of pentobarbital on intermittently reinforced behavior. *Science* 125, 929-931.
- 5 Fry, W., Kelleher, R.T., and Cook, L. (1960) A mathematical index of performance on fixed-interval schedules of reinforcement. *J. Exp. Anal. Behav.* 3, 193-199.

- 6 Reynolds, G.S. (1958) A Primer of Operant Conditioning. Scott, Foresman and Co., Glenview, Illinois.
- 7 Kelleher, R.T. and Morse, W.H. (1969) Determinants of the behavioral effects of drugs. In: D.H. Tedeschi and R.E. Tedeschi (Eds.), Importance of Fundamental Principles of Drug Evaluation, Raven Press, New York, pp. 383-405.
- 8 Thompson T. and Schuster, C.R. (1968) Behavioral Pharmacology. Prentice-Hall, New Jersey.
- 9 McKearney, J.W. and Barrett, J.E. (1978) Schedule-controlled behavior and the effects of drugs. In: D.E. Blackman and D.J. Sanger (Eds.), Contemporary Research in Behavioral Pharmacology, Plenum Press, New York, pp. 1-68.
- 10 Iverson, S.D. and Iverson, L.L. (1981) Behavioral Pharmacology. 2nd Ed., Oxford University Press, New York.
- 11 Rice, D.C. (1985), Effects of lead on schedule-controlled behavior in monkeys. In: L.S. Seiden and R.L. Balster (Eds.), Behavioral Pharmacology: The Current Status, Alan R. Liss, New York, pp. 473-486.
- 12 Rice, D.C., Gilbert, S.G., and Willes, R.F. (1979) Neonatal low-level lead exposure in monkeys: locomotor activity, schedule-controlled behavior, and the effects of amphetamine. Toxicol. Appl. Pharmacol. 51, 503-513.
- 13 Knisely, J.S., Rees, D.C., Salay, J.M., Balster, R.L., and Breen, T.J. (1987) Effects of intraperitoneal carbon monoxide on fixed-ratio and screen-test performance in the mouse. Neurotox. Teratol. 9, 221-226.
- 14 Weiss, B., Ferin, J., Merigan, W., Stern, S., and Cox, C. (1981) Modification of rat operant behavior by ozone exposure. Toxicol. Appl. Pharmacol. 58, 244-251.
- 15 Anger, W.K. and Lynch, D.W. (1977) The effect of methyl *n*-butyl ketone on response rates of rats performing on a multiple schedule of reinforcement. Environ. Res. 14, 204-211.
- 16 Colotla, V.A., Bautista, S., Lorenzana-Jimenez M., and Rodriguez, R. (1979) Effects of solvents on schedule-controlled behavior. In: Test Methods for Definition of Effects of Toxic Substances on Behavior and Neuromotor Function, Neurobehav. Toxicol. 1 (Suppl. 1), 113-118.
- 17 Wenger, G.R., McMillan D.E., and Chang, L.W. (1984) Behavioral effects of trimethyltin in two strains of mice II. Multiple fixed ratio, fixed interval. Toxicol. Appl. Pharmacol. 73, 89-96.
- 18 Wood, R.W., Rees D.C., and Laties, V.G. (1983) Behavioral effects of toluene are modulated by stimulus control. Toxicol. Appl. Pharmacol. 68, 462-472.
- 19 Sanger, D.J. and Blackman, D.E. (1976) Theoretical review. Rate-dependent effects of drugs: a review of the literature. Pharmacol. Biochem. Behav. 4, 73-83.
- 20 Laties, V.G. (1975) The role of discriminative stimuli in modulating drug action. Fed. Proc. 34, 1880-1888.
- 21 Cory-Slechta, D.A., Weiss, B., and Cox, C. (1983) Delayed behavioral toxicity of lead with increasing exposure concentration. Toxicol. Appl. Pharmacol., 71, 342-352.

- 22 Cory-Slechta, D.A., Weiss, B., and Cox, C. (1985) Performance and exposure indices of rats exposed to low concentrations of lead. *Toxicol. Appl. Pharmacol.* 78, 291-299.
- 23 Cory-Slechta, D.A. (1986) Prolonged lead exposure and fixed-ratio performances. *Neurobehav. Toxicol. Teratol.* 8, 237-244.
- 24 Walsh, J.M., Curley, M.D., Burch L.S., and Kurlansik, L. (1982) The behavioral toxicity of a tributyltin ester in the rat. *Neurobehav. Toxicol. Teratol.* 4, 241-246.
- 25 McMillan, D.E. (1982) Effects of chronic administration of pesticides on schedule-controlled responding by rats and pigeons. In: J.E. Chambers and J.D. Yarbrough ("Eds."), *Effects of Chronic Exposure to Pesticides of Animal Systems*, Raven Press, New York, pp. 211-226.
- 26 Cory-Slechta, D.A. and Thompson, T. (1979) Behavioral toxicity of chronic postweaning lead exposure in the rat. *Toxicol. Appl. Pharmacol.* 47, 151-159.
- 27 Rice, D.C. and Gilbert, S.G. (1985) Low-level lead exposure from birth produces behavioral toxicity (DRL) in monkeys. *Toxicol. Appl. Pharmacol.* 80, 421-426.
- 28 Rice, D.C. (1983) Nervous system effects of perinatal exposure to lead or methylmercury in monkeys. In: T.W. Clarkson, G. Nordberg and P. Sager (Eds.), *Reproductive and Developmental Toxicity of Metals*, Plenum Press, New York, pp. 517-540.
- 29 Good, P.I. (1979) Detection of a treatment effect when not all experimental subjects will respond to treatment. *Biometrics* 35, 483-489.
- 30 Cox, C. (1981) Detection of treatment effects when only a portion of subjects respond. In: S.A. Miller (Ed.), *Nutrition and Behavior*, The Franklin Institute Press, Philadelphia, pp. 285-289.
- 31 Cox, C. and Cory-Slechta, D.A., (1987) Analysis of longitudinal "time series" data in toxicology. *Fundam. Appl. Toxicol.* 8, 159-169.
- 32 Buelke-Sam, J., Kimmel, K.A., Adams, J., Nelson, C.J., Vorhees, C.V., Wright, D.C., St. Omer, V., Koral, B.A., Butcher, R.E., Geyer, M.A., Holson, J.F., Kutscher C.L., and Wagner, M.J. (1985) Collaborative behavioral toxicology study: Results. *Neurobehav. Toxicol. Teratol.* 7, 591-624.
- 33 Kelleher, R.T. and Morse, W.H. (1968) Determinants of the specificity of the behavioral effects of drugs. *Ergebnisse der Physiologie.* 60, 1-56.

## Closing Remarks

Dr. Melvin E. Andersen

This has been a very ambitious conference. We have been busy for 2½ days and most of the evenings, and I want to give some thanks and then go home and rest. I would also like to thank the people from Northrop Services, our contractor, for organizing a very efficient meeting. There are many people who should be thanked individually. I would like to thank Debbie Ussery-Baumrucker and Lois Doncaster for the administrative work in organizing the meeting. I would also like to thank Jim Stokes for keeping all the computer connectors and the pieces of the computers operational and for keeping the audio and visual equipment in good working order. We have had five very interesting sessions. I want to thank the session chairmen and all the speakers. It has been a particularly articulate group of people, and I can say that because I have sat through every talk. It is probably the first time in 10 years that I have come to a meeting and sat through all the talks. Obviously, that is due in large part to the fact that I am the program chairman, but I thank everybody for making that much easier for me.

I want to remind everyone that this is the first conference at which we have offered you a poster to take home as a remembrance. There are posters here and, if you don't have one, take one because we want to go down in history as being the first conference that offered a free computer to everyone who attended. And last, I look out into the audience and there have been moments during the conference when the audience has been larger, but it has been a very faithful audience. As my last item of business, I would like to thank all of the people who have been faithful in attending these talks and participating in the poster sessions and computer sessions. Thank you very much for helping make this a very successful meeting, and I wish you all a safe journey home or wherever you are going.